Università degli Studi di Ferrara

DOTTORATO DI RICERCA IN
SCIENZE CHIMICHE

CICLO XXX

COORDINATORE Prof. Carlo Alberto Bignozzi

SYNTHESIS OF BIO-ACTIVE MITOCHONDRIA TARGET COMPOUNDS

Settore Scientifico Disciplinare CHIM/06

Dottorando
Dott. Fantinati Anna

Tutore
Prof. Trapella Claudio

Anni 2014/2017

A nonna Mara

Everything is theoretically impossible, until it is done.
-Robert A. Heinlein-

Abstract

Mitochondria are small cytoplasmic organelles remnant of a prokaryotic organism that had become a vital symbiotic partner to the eukaryotic cell early in the evolution.

Mitochondria contain their own DNA, which is maternally inherited. These organelles adopt different shapes depending on the cell type and the metabolic demands of the cell. They have a typical double membrane structure: the smooth outer membrane (OMM) that contains many copies of a transport protein porin, which forms aqueous channels allowing molecules with a maximal molecular weight of 5000 Daltons to penetrate the membrane; the inner membrane (IMM), conspicuously folded, forming tubular or lamellar structures called cristae, which are connected to it by narrow tubular structures, cristae junctions. In between of these two membranes there is the inter-membrane space (IMS). Mitochondria nourish cells by converting energy from carbon sources into ATP (adenosine triphosphate). Additionally, they are important for thermogenesis, calcium and iron homeostasis, intracellular signaling and apoptosis, various metabolic intermediary pathways including metabolism of amino acids, lipids, cholesterol, steroids and nucleotides through oxidative phosphorylation (OXPHOS). The mitochondria are involved in homeostasis, as said before. When the cytoplasmic Ca^{2+} increases above certain levels (>10 μM), a drastically rise of Ca^{2+} in the mitochondria and matrix is verified. Eventually, when the mitochondria is excessing of accumulation of Ca^{2+}, it causes the opening of a non-specific large-conductance channel in the inner mitochondrial membrane, commonly referred to as the permeability transition pore (PTP), that collapses the membrane potential, induces swelling of the inner membrane.

Another main role of mitochondria is the regulation of the programmed cell death mechanism, also called apoptosis. The two main pathways through which this cell death process is initiated are the intrinsic and extrinsic cell death pathways, both converging on caspase activation. p53 is a central protective node and its main function is to prevent the propagation of damaged cells that are potentially mutagenic by orchestrating defense pathways of apoptosis, cell cycle arrest, senescence and DNA repair. P53 is regulated by a protein MDM2 (Murine Double Minute 2).

In the cancerogenesis framework it could be placed the MAGMAS (mitochondria-associated granulocyte macrophage CSF signaling molecule) protein. Magmas is located in the mitochondrial inner membrane and it is highly conserved, it is essential for mitochondrial activity and cell survival. This protein can also be called as Tim 16 or Pam 16. With the cooperation between Tim 14 (Pam 18) and Tim 16 and the formation of

heterodimer, Magmas is able to regulate the carriage of protein precursors in the mitochondrion through transport proteins. Since Magmas is a gene that induces GM-CSF and it is involved in the transport of mitochondrial proteins, some studies have been accomplished to evaluate the effect of the gene expression in healthy and neoplastic tissues.

Ischemia and Reperfusion Injury (IRI) Inhibitors

Ischemia is a restriction in blood supply to tissues, causing a shortage of oxygen and glucose needed for cellular metabolism (to keep tissue alive). Ischemia is generally caused by problems with blood vessels, with resultant damage to or dysfunction of tissue. During ischemia, ATP synthesis is inhibited, and existing ATP is cleaved into ADP and phosphate. Since oxidative phosphorylation is interrupted, proton ions accumulate into mitochondrial matrix and pH quickly decreases.

The final result is a Ca^{2+} accumulation into mitochondria and its inhibited reuptake by ER. So, since ETC still inactive and ROS generated, these are inductors of mPTP opening and also they contribute to the decrease of IMM transmembrane potential, inducing the apoptosis intrinsic pathway.

There are some agents known to inhibit with alternative mechanism mPTP. The most known inhibitor of mitochondrial ATP synthase is Oligomycin, that is a macrolide with a 26 membered lactone ring, isolated from *Streptomyces diastatochromogenes.* On the Olygomicyn structure basis we synthetized some compounds, as potential mPTP inhibitors. Several of those have been obtained from Isatine and 5-Fluoroisatine, maintaining the same scaffold but with different modifications at key positions. Specifically we introduced diverse (poly)cyclic ketones with or without N-alkylation at the isatine nitrogen (a,b,c). In addition, we synthetized a small library of N-benzyl-piperidone derivatives with the general structure (d). We chose these last molecules because of the presence of two spiro centers that gives rigidity to the structure and also for their steric hindrance. They could be potentially interesting as inhibitors as well (Figure 1).

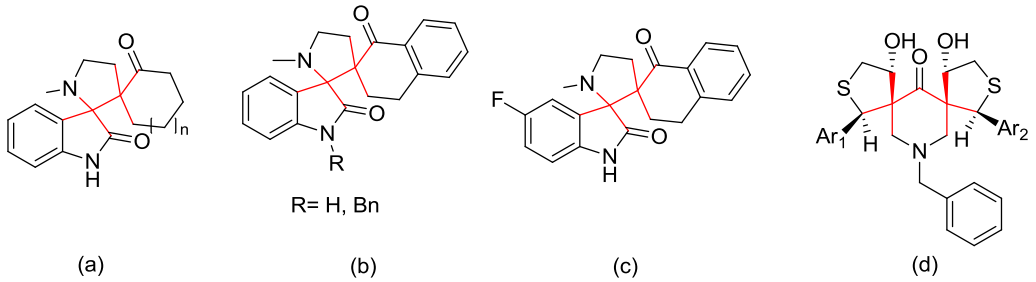

Figure 1.

Some of these products showed a good activity in inhibiting the opening of mPTP.

Nutlins as anti-cancer drugs

Among the different therapeutic strategies evaluated pharmacologically, the attention has been focused on the drug design able to modulate the p53-MDM2 interaction. The structure of this complex p53/MDM2 is known pretty well, as a matter of fact there is a tridimensional structure available with specific interaction sites of the MDM2 hydrophobic pocket. Nutlins, which is the first and more important class of small molecules, are *cis*-imidazoline analogs which inhibit the interaction between MDM2 and tumor suppressor p53. The most important is (-)-Nutlin-3, which is commonly used in anti-cancer studies.

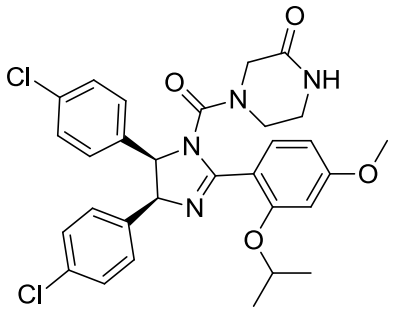

(-)-Nutlin-3

Figure 2: (-)-Nutlin-3 structure.

The aim of this project was to find a synthetic pathway to obtain only (-)-Nutlin-3, because of its activity, as product, instead of the racemic mixture, as mostly reported in literature.

MAGMAS Inhibitors

Magmas complex, located in the mitochondrial inner membrane, is essential for the mitochondrial survival; its inhibition causes cell death.

On the basis of published analysis in literature, the compound **84** seems to be a good Magmas inhibitor, because the concentration of 10 μM is able to completely inhibit the cell proliferation. Another compound that, recently, showed good activity of inhibiting the cell proliferation was the product **89**, that maintain the structure of **84** but with the reduction of the two olefin moiety.

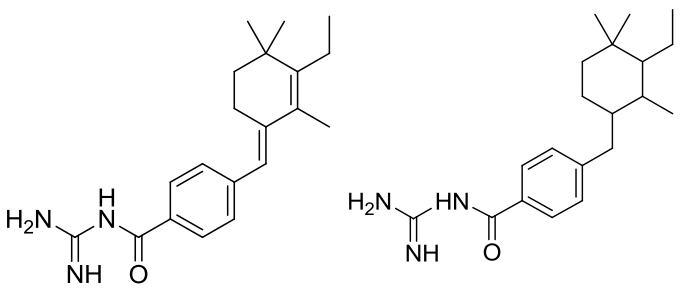

84 **89**

Figure 3: structure of compound 84 and 89.

List of contents

1. Introduction …… 1

1.1 Mitochondria …… 1

1.2 Oxidative phosphorylation mechanism…… 3

1.3 Ca^{2+} homeostasis and mPTP…… 6

1.4 Mitochondria and apoptosis…… 8

1.5 p53 and mitochondria……..... 10

1.6 Interaction p53-MDM2 and cancerogenesis…….. 11

2. Ischemia and reperfusion Injury (IRI) inhibitors……. 15

2.1 Aim and objectives…… 15

2.2 Discussion…….. 18

2.2.1 Synthesis of dispiropyrrolidine derivatives using Isatine…….. 19

2.2.2 Synthesis of dispiropyrrolidine derivatives using 5-fluoro Isatine 20

2.2.3 Reaction mechanism for the synthesis of dispiropyrrolidines 21

2.2.4 Synthesis of dispiropiperidone-tetrahydrothiophene heterocycles 22

2.2.5 Reaction mechanism to synthetize dispiropiperidone-tetrahydrothiophene heterocycles……... 24

2.2.5.1 Aldolic Reaction……. 24

2.2.5.2 Tandem Micheal Reaction…….. 24

2.3 Conclusions and results…….. 26

3. Nutlins as anti-cancer drugs……. 28

3.1 Aim and objectives…… 28

3.2 Discussion…….. 30

3.2.1 Synthesis of racemic Nutlin-3……... 30

3.2.2 Asymmetric synthesis of (-)-Nutlin-3……... 33

3.2.3 Synthesis of a precursor of (-)-Nutlin-3,enantiomerically enriched 34

3.2.4 Co-catalysis DMAP-thiourea…… 35

3.2.5 Preparation of meso-diamine **46**……... 37

3.2.6 Preparation of anhydride **69**…….. 38

3.2.7 Reaction of asymmetric acylation of meso-diamine **46** through DMAP-thiourea co-catalysis…….. 39

3.2.8 Cis-imidazoline ring formation…….. 43

3.2.9 Synthesis of HB-catalyst, thiourea **cat-1**…….. **45**
3.3 Conclusions and results…… 46
4. MAGMAS Inhibitors…….. 48
4.1 Aim and objectives……... 48
4.2 Discussion……. 49
4.2.1 Synthesis of compound **84** (*(E)-N-carbamimidoyl-4-((3-ethyl-2,4,4-trimethylcyclohex-2-en-1-ylidene)methyl)benzamide)*…… 49
4.2.2 Studies of the phosphonium salt…….. 50
4.2.3 SAR study about MAGMAS inhibitors…….. 56
4.2.4 1-amino-4(3H)-quinazolinone/2-aminoquinazoline derivatives as Magmas inhibitors analog…….. 60
4.3 Conclusions and results ……. 62
5. Experimental section…… 67
5.1 Chemicals and methods…….. 67
5.2 IRI inhibitors synthesis…… 68
5.2.1 Synthesis of dispiropyrrolidines using Isatine……. 68
5.2.2 Synthesis of dispiropyrrolidines using 5-fluoro Isatine……... 79
5.2.3 Synthesis of intermediates through a double Aldolic reaction… 89
5.2.4 Synthesis of dispiropiperidone-tetrahydrothiophene derivatives 100
5.3 (-)-Nutlin-3…….. 109
5.4 Magmas Inhibitors…….. 136
5.4.1 Biological Experimental Section…… 156
References …… 158
Abbreviations …….. 161

1. Introduction

Mitochondria are recognized as one of the most important targets for new drug design in cancer, cardiovascular, and neurological diseases.

1.1 Mitochondria

Mitochondria are small cytoplasmic organelles remnant of a prokaryotic organism that had become a vital symbiotic partner to the eukaryotic cell early in the evolution[1].

As an essential step in the process of eukaryotic evolution, the size of the mitochondrial chromosome was drastically reduced, and the behavior of mitochondria within eukaryotic cells radically changed[2].

Mitochondria contain their own DNA, which is maternally inherited. These organelles adopt different shapes depending on the cell type and the metabolic demands of the cell. Their two predominant morphologies are reflected in the Greek name of the organelle – 'mitos' for thread and 'chondros' for grain. Mitochondria are usually 0.5-1 µm in size. They have a typical double membrane structure (figure 1): the smooth outer membrane (OMM) that contains many copies of a transport protein porin, which forms aqueous channels allowing molecules with a maximal molecular weight of 5000 Daltons to penetrate the membrane; the inner membrane (IMM), conspicuously folded, forming tubular or lamellar structures called cristae, which are connected to it by narrow tubular structures, cristae junctions. In between of these two membranes there is the inter-membrane space (IMS).

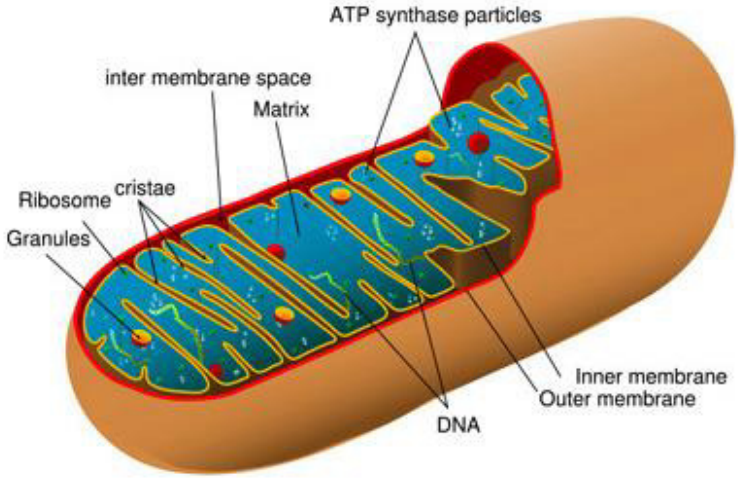

Figure 1: mitochondria structure.

The core of the mitochondria is the matrix that includes a vast number of enzymes that facilitates biological reactions (except glycolysis), such as pyruvate dehydrogenase (PDH),

citrate synthase, carbamoyl phosphate synthetase, pyruvate carboxylase acyl-CoA dehydrogenase and transaminases and it is where the mitochondrial DNA (mtDNA) is located.

Two distinct genetic systems encode mitochondrial proteins: mtDNA and nuclear DNA (nDNA). mtDNA is a small 16.6 kb circle of double stranded DNA that codes for 13 respiratory chain polypeptides of respiratory complexes I, III, IV, and V (only complex II is solely composed of proteins encoded by nuclear genes) and 24 nucleic acids necessary for intra-mitochondrial protein synthesis[3].

Mitochondria are involved in cellular homeostasis. They nourish cells by converting energy from carbon sources into ATP (adenosine triphosphate). Additionally, they are important for thermogenesis, calcium and iron homeostasis, intracellular signaling and apoptosis, various metabolic intermediary pathways including metabolism of amino acids, lipids, cholesterol, steroids and nucleotides through oxidative phosphorylation (OXPHOS).

1.2 Oxidative phosphorylation mechanism

Oxidative phosphorylation is the metabolic pathway in which cells use enzymes to oxidize nutrients, to release energy which is used to produce ATP. In most eukaryotes this takes place inside mitochondria. Pyruvate generated from carbohydrates in glycolysis and fatty acids produced from triglycerides are necessary for the oxidative metabolism. These are selectively imported into the mitochondrial matrix and turned into acetyl CoA by the pyruvate dehydrogenase complex or the β-oxidation pathway. The acetyl group then rules in the citric acid cycle, which produces substrates for OXPHOS, like NADH and $FADH_2$. Electrons generated from NADH are passed along a series of carrier molecules called the electron transport chain (ETC), the products of this process are water and ATP. In this system, protons are pumped from the matrix across the mitochondrial inner membrane through respiratory complexes: I, III, and IV. The protons return to the mitochondrial matrix down their electrochemical gradient through ATP synthase, ATP is synthesized via complex V converting ADP and phosphate using this potential energy (figure 2). Thus the mitochondrion converts energy derived from chemical fuels by an OXPHOS process that is more efficient than anaerobic glycolysis. In the mitochondrion the metabolism of one molecule of glucose produces about 30 molecules of ATP, while only two molecules of ATP are produced by glycolysis in the cytoplasm.

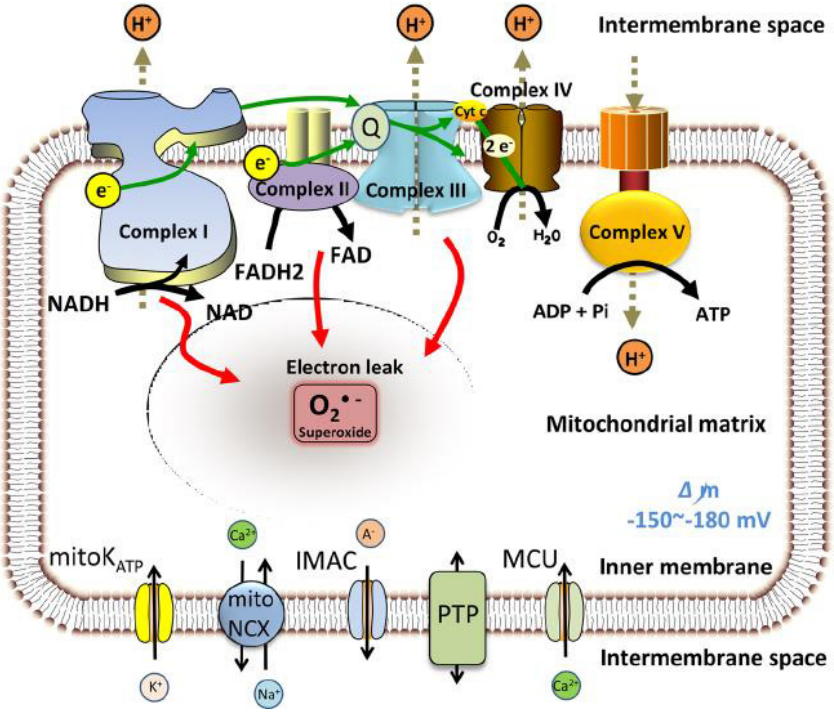

Figure 2: Oxidative phosphorylation and reactive oxygen species (ROS) production in mitochondria .

The diagrams of the mitochondrial inner membrane show key components of the electron transport chain (ETC) above, and channels and transporters (below). Reducing equivalents

nicotinamide adenine dinucleotide (NADH) and flavin adenine dinucleotide ($FADH_2$) produced from the 2 tricarboxylic acid (TCA) cycle feed electrons to the ETC along the mitochondrial inner membrane. The electrons flow through the ETC with the following sequence: two electrons are removed from NADH and transferred to ubiquinone, obtaining ubiquinol, that diffuses within the membrane, while complex I transfers the four protons across the membrane. Then complex II transports electrons from succinate, that is been oxidized, to coenzyme Q. Then the electrons pass through complex III to cytochrome C (Cyt C). Finally, complex IV, cytochrome oxidase, transports electrons from cyt C to O_2, reducing it in H_2O, during which coupled redox reactions drive H^+ across the inner membrane, forming the proton gradient and the negative mitochondrial membrane potential ($\Delta\Psi$ m =−150 to −180 mV). The free energy stored in the proton gradient and $\Delta\Psi$ m, then, drive H^+ through the mitochondrial ATP synthase (complex V), converting ADP to ATP. An estimated 0.1% to 1% of the electrons leak prematurely to O at complexes I, II, or III, resulting 2 in the formation of superoxide (O•−). Multiple important mitochondrial channels located on the inner membrane including mitochondrial 2 K channels (mito-K), the mitochondrial Na^+ /Ca^{2+} exchanger (mito-NCX), the inner membrane anion channel (IMAC), the permeability ATP transition pore (PTP), and the mitochondrial calcium uniporter (MCU) also contribute to the regulation of mitochondrial function, myocardial ROS, and cellular cation homeostasis[4].

Human mitochondrial (mt) ATP synthase, or complex V consists in two functional domains: F_1, situated in the mitochondrial matrix, and Fo, located in the inner mitochondrial membrane.

F_1 is composed of three copies of each of subunits α and β, and one each of subunits γ, δ and ε. F_1 subunits γ, δ and ε constitute the central stalk of complex V. Fo consists of a subunit c-ring and one copy each of subunits a, b, d, F_6 and the oligomycin sensitivity-conferring protein (OSCP)[5] (figure 3). Therefore, F_O is also called C-ring, because it is formed by 10 hydrophobic C subunits organized to form an oligomeric ring that makes up the F_O rotor [6]. The F_1 domain is composed by five different subunits located in the mitochondrial matrix. Three α and three β subunits are alternative placed to form a ring out of a central linear γ subunit. Its main role is the catalysis of the reaction between ADP and phosphate to form ATP. This is due to a rotational catalysis mechanism in three steps, based on a constantly alternate affinity of each one of the three β subunit to ADP and Phosphate, to ATP and to none of them. In this way, firstly a β subunit binds ADP and Phosphate. Secondly it acquires a major affinity to ATP and, hence, it catalyzes the formation of ATP itself. Finally, it loses its affinity to ATP and it releases it into the

matrix. F_O and F_1 domains link together with a lateral bridge, consisting of δ, α and β subunits and thanks to ε one, which connects γ subunit with the c ring. Because of this ATPase structure, protons influx and ATP synthesis are deeply connected.

It is required three conditions to synthetize ATP: a substrate able to be oxidized, as NADH, a ADP molecule and phosphate. Obviously, if the oxidation reaction is inhibited, even the electron and, hence, the proton fluxes are repressed. Thus, ATPase receives no stimulation by the proton motive force to the production of ATP. However, more noticeably, even the ATP synthesis inhibition represses the electron flux. Clearly, both the transport of electrons and the synthesis of ATP have to happen, without even one of the two processes, the flux of electrons is inhibited as much as the ATP synthesis. When Oligomycin A binds the C ring, physically inhibits the return of protons to the matrix through ATPase channel and eventually the outside of the mitochondrion develops such a large positive charge that the electron transport chain can no longer pump protons against the gradient, inhibiting the oxidation reactions.

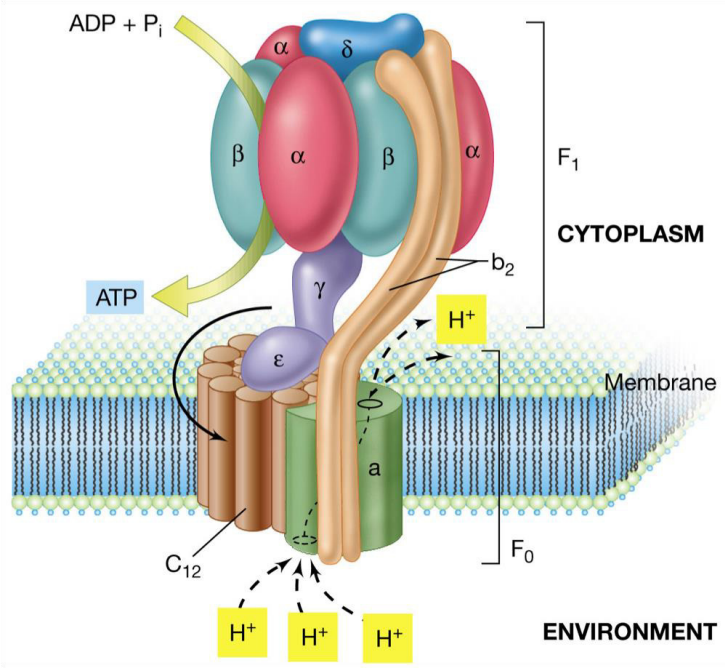

Figure 3: ATP synthase structure and mechanism.

ATPase can promote either ATP synthesis or the opposite reaction, meaning the ATP hydrolysis. When the cell is in hypoxic status, the transfer of electrons to the oxygen can't be accomplished and the oxidative phosphorylation is interrupted. In this condition, ATPase could promote the ATP hydrolysis instead of the synthesis, causing a drastic reduction of ATP levels. However, this process can be inhibited by a small protein (84

aminoacids) IF_1, that binds two molecules of ATP synthase, inhibiting their activity. This inhibitor is active only in its dimerization form (figure 4), which happens when pH decreases under 6.5. In a hypoxic cell, the main source of ATP is the glycolysis and pyruvic acid produced by the anaerobic metabolism, reducing the pH of the cytosol and the mitochondrial matrix. This condition promotes the IF_1 dimerization[7], to inhibit the ATP hydrolysis. When the aerobic metabolism is restored, the production of pyruvic acid slows down, the cytosolic pH increases, the dimer IF_1 becomes unstable and so the inhibition of ATPase is removed[8]. The reactive oxygen species, also, will be regenerated.

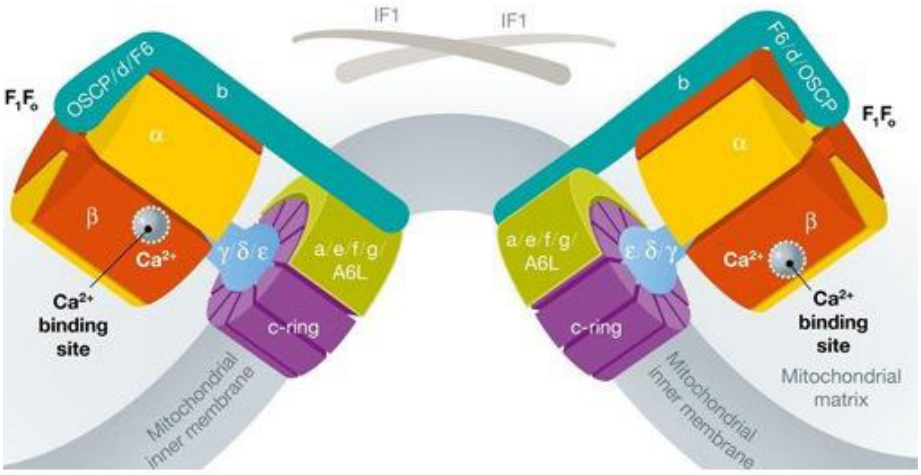

Figure 4: ATPase dimer stabilized by IF_1.

1.3 Ca^{2+} homeostasis and mPTP

It is clearly established that mitochondria play a key role in different pathophysiological contexts[9]. They are very efficient machines for decoding intracellular signals and in particular the calcium (Ca^{2+}) one.

Calcium is mainly stored in endoplasmatic reticulum and in Golgi apparatus, where it reaches a concentration of 300-600 µM and 200-500 µM. It is even present at lower concentration in the cytosol, which has normally Ca^{2+} of 100nM. Ca^{2+} can also be found into mitochondria in resting condition of 100nM concentration.

Ca^{2+} import across the outer mitochondrial membrane occurs through the voltage-dependent anion channels (VDAC). VDAC is as a large voltage-gated channel, fully opened with high-conductance and weak anion-selectivity at low transmembrane potentials (< 20–30 mV), but switching to cation selectivity and lower conductance at higher potentials. Ca^{2+} mitochondrial traffic across the inner mitochondrial membrane takes place essentially through two pathways: i) an electrophoretic "uniporter" that transports Ca^{2+} down the electrical gradient established by the respiratory chain, and ii) a Na^+/Ca^{2+} exchanger, mostly expressed in excitable cells (muscle and brain), and a

H^+/Ca^{2+} exchanger, that represents the prevailing route in most other tissues. These electroneutral antiporters prevent the attainment of an electrochemical equilibrium.

When the cytoplasmic Ca^{2+} increases above certain levels (>10 μM), a drastically rise of Ca^{2+} in the mitochondria and matrix is verified. Eventually, when the mitochondria is excessing of accumulation of Ca^{2+}, it causes the opening of a non-specific large-conductance channel in the inner mitochondrial membrane, commonly referred to as the permeability transition pore (PTP), that collapses the membrane potential, induces swelling of the inner membrane. This occurs because the increased permeability of the inner mitochondrial membrane to small molecules mediates equilibration of all low molecular weight osmolytes whilst retaining proteins within their respective compartments. Since the matrix protein concentration is higher than that in the cytosol and intermembrane space, it exerts a colloidal osmotic pressure leading to swelling of the matrix compartment. Swelling can occur without inner membrane rupture because the cristae unfold, but as the matrix expands, it exerts pressure on the outer membrane that eventually ruptures, making the release of the proteins from IMS into the cytoplasm.

As said before, the inner mitochondrial membrane no longer maintains a barrier to protons which leads to dissipation of the proton motive force. The resulting uncoupling of oxidative phosphorylation not only prevents mitochondria from making ATP, but the proton-translocating ATPase goes into reverse.

The precise mechanisms of PTP regulation are only partially understood, as the molecular structure of the pore remains an unsolved riddle. Assemblage of PTP components might be a rare event, to avoid unwanted mitochondrial depolarization and damage. A subset of proteins was proposed to constitute core components of the channel. These candidate components included: the outer mitochondrial membrane porin, also known as VDAC (voltage-dependent anion channel); the matrix chaperone CyP-D; the adenine nucleotide translocator (ANT) in the IMM; and more recently the mitochondrial phosphate carrier (PiC)[10].

Cyclophilin D is located in the matrix of mitochondria and it is thought to regulate the opening of the pore because cyclosporin A, which binds to CyP-D, inhibits the pore opening. ANT, mainly, exports ATP from the mitochondrial matrix and imports ADP into the matrix and it regulates the mPTP, as explained above. It can also cause aging-dependent degenerative cell death (DCD) in yeast, which is sequentially manifested by inner membrane stress, mtDNA loss, and progressive loss of cell viability[11]. The mitochondrial phosphate carrier SLC25A3 (PiC) transports inorganic phosphate into the mitochondrial matrix, essential for the aerobic synthesis of ATP. It may play a role in

mPTP formation[12]. Induction of the mPTP can lead to cell death, through apoptosis or necrosis.

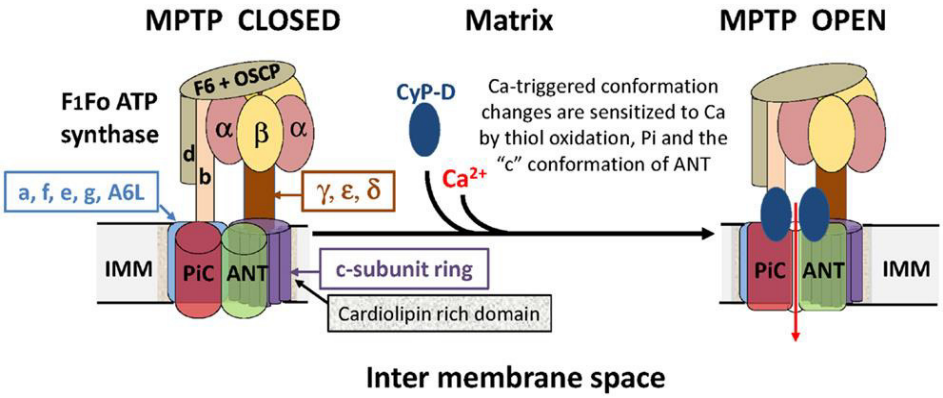

Figure 5: A hypothetical model of the mPTP that proposes an interaction among the ANT, PiC and F_1Fo ATP synthase in the ATP synthasome.

1.4 Mitochondria and apoptosis

Another main role of mitochondria is the regulation of the programmed cell death mechanism, also called apoptosis. During this process, a family of cysteine-aspartate proteases known as caspases accelerates cell death through restricted proteolysis of over 400 proteins. The two main pathways[13] through which this cell death process is initiated are the intrinsic and extrinsic cell death pathways, both converging on caspase activation.

In the extrinsic pathway, the cell ends its vital course because of extern signal by ligation of membrane receptors, called death receptors. The tumor necrosis factors (TNF) are proteins that indicate to the cell to start the apoptotic process. The death receptors are all different, but it seems that they all show a similar structure to FAS (CD95), a transmembrane trimer, that binds the ligand-FAS, starting the first step of the apoptosis.

The receptor is generally accompanied by a transmembrane domain and a DD domain (death domain). An adapter, that follows the DD domain, interfaces directly with the caspases.

The extrinsic pathway is mediated by FAS through the activation of caspase 8 that, making its dimerization, activates a caspase 3, that interacts with the complex CAD/ICAD[14]. Specifically, caspase 3 cleaves ICAD and thus causes CAD to become activated. So, CAD at this point can proceed to the DNA lysis action. Caspases are also called cysteine–aspartic proteases, because of their cysteine abilities to cleave a target protein only at the C-terminal of an aspartic acid amino acid. They are mainly distinguished into initiator caspases, able to activate the cascade, such as caspase 8 and 9, and effector caspases, such as 3, 6 and 7, responsible for the induction of apoptosis. Because of their important role in

cell death, they are normally in an inactive form, called procaspase, which can be turned into the active form.

In the intrinsic pathway, also named the mitochondria-mediated pathway, the signal, that starts apoptosis, comes from the intern of the cell. It is a result of uncompensated cell stress signaling. For example, exposition to oxygen, excessive accumulation of calcium, DNA damage. The main cause seems to be correlated with the mPTP, that modifies the permeability of the mitochondrial membrane, plus with the presence of ROS, that induce the lipid peroxidation and, consequently, the rupture of OMM, there is the releasing of pro-apoptotic molecules, including cytochrome C[15], that start the apoptotic cascade.

In physiological activity, cytochrome C leads to the transfer of one electron from ubiquinol to oxygen through complex III and IV and it is normally bind to cardiolipin, therefore, it cannot be extruded out of mitochondria. During ROS, which are generated as side product of ETC or during ischemia reperfusion injury, and Ca^{2+} induction, cardiolipin is oxidized and released cytochrome C out of OMM. Cytochrome C released binds itself to APAF-1, generating a multimolecular holoenzyme complex which is called apoptosome. Apoptosome is particularly important during apoptosis, because is able to activate procaspase 9 into caspase 9, thus inducing caspase cascade activity in an intrinsic way.

There are other important factors released from the OMM: AIF and Endo G, which are caspases-indipendent apoptosis effector, active in DNA degradation onto nucleus and in chromatine condensation; SMAC (second mitochondria-derived activator of caspases), called also DIABLO (direct IAP-binding protein with low PI) for the fact that inhibits cytosolic inhibitor (IAP) proteins thus freeing caspases to activate apoptosis[16].

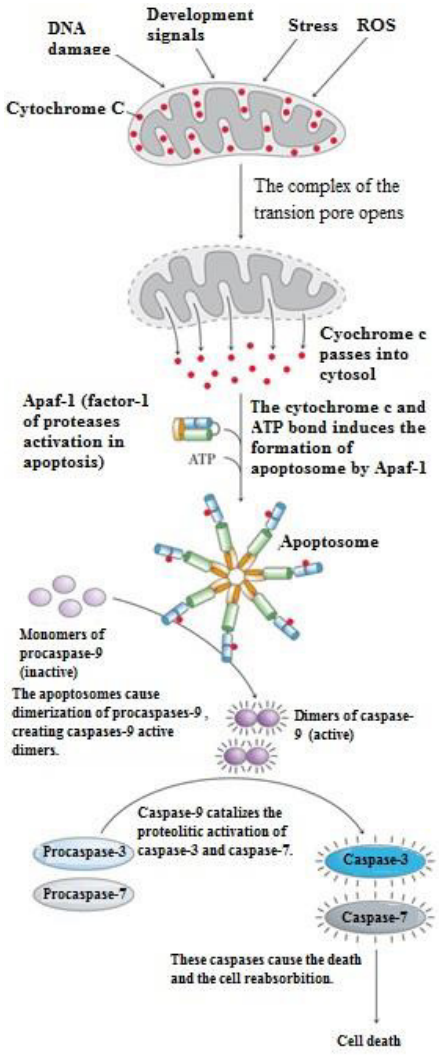

Figure 6: Apoptosis pathway.

1.5 p53 and mitochondria

The tumor suppressor gene TP53 and its protein product p53 were discovered in 1979, and have since been the topic of intense study in the cancer biology field.

It has a main role to maintain integrity of genetic heritage, stabilizing DNA and preventing mutations. p53 is now known to coordinate diverse cellular functions in response to a range of different stresses including oncogene activation, telomere shortening, hypoxia, metabolic stress, ribosomal stress, oxidative stress, viral infection, apoptosis and it rules as tumor suppressor.

p53 is a central protective node and its main function is to prevent the propagation of damaged cells that are potentially mutagenic by orchestrating defense pathways of apoptosis, cell cycle arrest, senescence and DNA repair. Upon activation by a diverse type of stress stimuli, p53 induces apoptosis via transcription-dependent and transcription-independent modes, two fundamentally different but synergistic mechanisms of action. In

the nucleus, p53 governs a complex transcriptional program that includes apoptotic target genes such as Puma, Noxa and Bax, but also genes with non-apoptotic, cell cycle arrest or as yet poorly defined functions. p53 works as tumor suppressor through some mechanisms: arresting temporary the cell cycle in G1-S to recognize the cell damage; activating the DNA repair through specific proteins; starting the apoptotic process, when the damage is irreparable.

There are two classes of transcriptional targets involved in the apoptotic process:

the components of the cell death extrinsic signals pathway (Death Receptor DR, TNF, receptors R); the main components of the intrinsic apoptotic pathway, mitochondria (APAF-1, key component of apoptosome, PUMA, NOXA).

The intensive study of these surprising pathways has identified mitochondria as a major site of transcriptional-independent apoptotic activity of p53. Indeed, numerous publications report that p53 itself relocates and induces apoptosis directly at mitochondria, via the interaction with members of the Bcl-2 family[17]. This interaction leads to the induction of MOMP (mitochondrial outer membrane permeabilization). The direct or indirect activation of Bak and Bax proapoptotic members plays a central role in this mechanism. Binding of p53 to Bak, an intrinsic outer mitochondrial membrane, was found to catalyze Bak activation and cytochrome c release. Characterization of the p53–Bak interaction revealed the crucial importance of the DNA binding domain of p53 for interacting and oligomerizing with Bak.

1.6 Interaction p53-MDM2 and cancerogenesis

P53 is regulated by a protein MDM2 (Murine Double Minute 2). It is an enzyme, ubiquitin-ligase E3: the third one involved in the ligation of ubiquitin (Ub) to the proteins. At first the ubiquitin is activated with a molecule of ATP, through a thioester bond between the carboxyl functional group of the ubiquitin terminal Gly and the residue of Cys of enzyme E1. Successively, Ub is transferred to the active site of enzyme E2, where it is another Cys residue. At this point the ubiquitin-protein-ligase (E3) interacts with the hetero-dimer E2-protein to degrade. Ub binds Lys portion of the protein to eliminate, which happens in the proteasome. The ubiquitination process of p53 in the nucleus starts with signals of transportation that mediate the migration of p53 to the cytosol, where depending on the sites and the numbers of Ub bounded, there are many different pathways. Generally, there is an equilibrium between MDM2 and p53 expression: when there are events that induce the raising of the p53 expression, it causes the enhancement of the MDM2 expression too, that inhibits p53. But this p53-MDM2 system doesn’t work when

there are tumor cells, because there is an increase MDM2 that causes the degradation of p53, inducing problems of maintaining the integrity of genome. Some studies show that *mdm2*, the gene coding for MDM2, is a proto-oncogene, meaning that it can become an oncogene if there is an increase of its expression[18, 19].

To prevent or to decrease the interaction between p53 and MDM2 would give as consequence an enhancement of the tumor suppressor p53 activity and this could be a promising new strategy to apply in cancer cure. About that, a possible approach for the therapy could be to avoid the interaction p53-MDM2 with molecules able to bind the two proteins and, then, leaving p53 free to express its function of tumor suppressor.

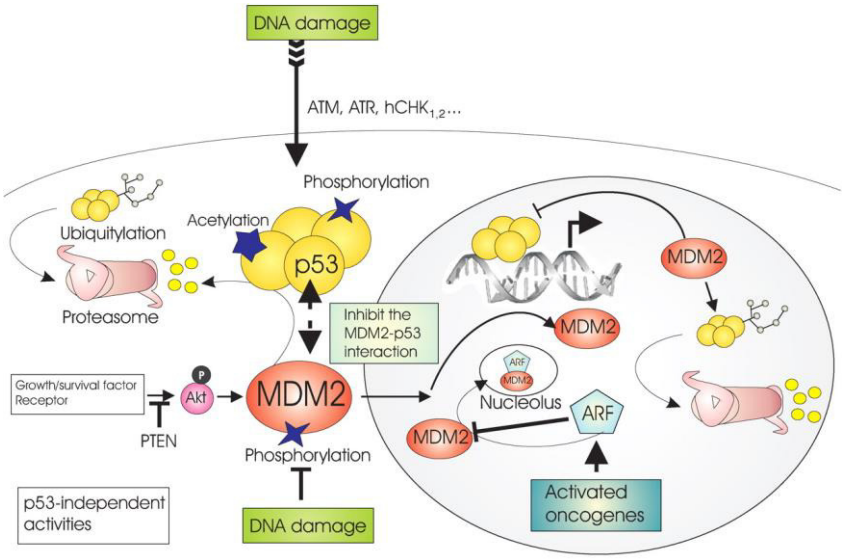

Figure 7: Regulation of p53 by MDM2. p53 and MDM2 form an autoregulatory feedback loop.

In the cancerogenesis framework it could be placed the MAGMAS (mitochondria-associated granulocyte macrophage CSF signaling molecule) protein.

Magmas is a mitochondrial protein, it is 13 kDa and it is expressed in the eukaryotic cells.

It is supposed that this protein is involved in transduction signals of factors stimulating colonies of macrophages-granulocytes (GM-CSF); it is formed by 125 aminoacids with a leader sequence that includes 21 aminoacids, among which many are hydrophobic, some basic and none acid.

It was possible to isolate the Magmas mitochondrial gene induced by GM-CSF and it was evaluated that its expression is variable in all tissues, but a big quantity of the protein is in the heart, in the skeletal muscle and in the pituitary gland. The induction of Magmas by GM-CSF could be a compensatory response to the energy required by cells, also it could be related to the cell differentiation or the reduced proliferation.

Magmas is located in the mitochondrial inner membrane and it is highly conserved, it is essential for mitochondrial activity and cell survival. This protein can also be called as Tim 16 or Pam 16. With the cooperation between Tim 14 (Pam 18) and Tim 16 and the formation of heterodimer, Magmas is able to regulate the carriage of protein precursors in the mitochondrion through transport proteins. It exists, also, a strong collaboration between protein complexes in IMM (as Tim 23) and the ones in the OMM (as TOM). The structure of the import protein is obtained through the crystals analysis of the complex Tim16/Tim14 in a solution of sodium citrate with pH 7 and published in 2006 [20].

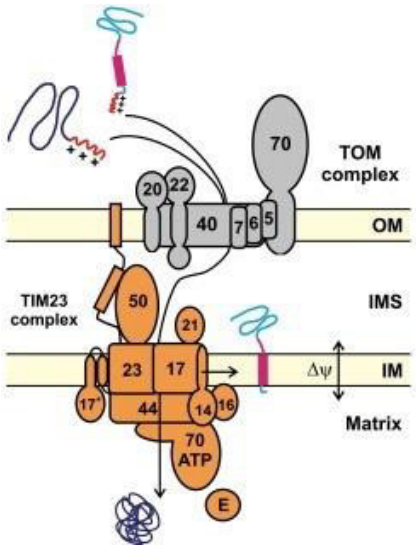

Figure 8: Import of protein precursors with a pre- sequence N-terminal (red) requires a cooperative action between TOM (grey) in the OMM and the TIM23 (orange) in IMM.

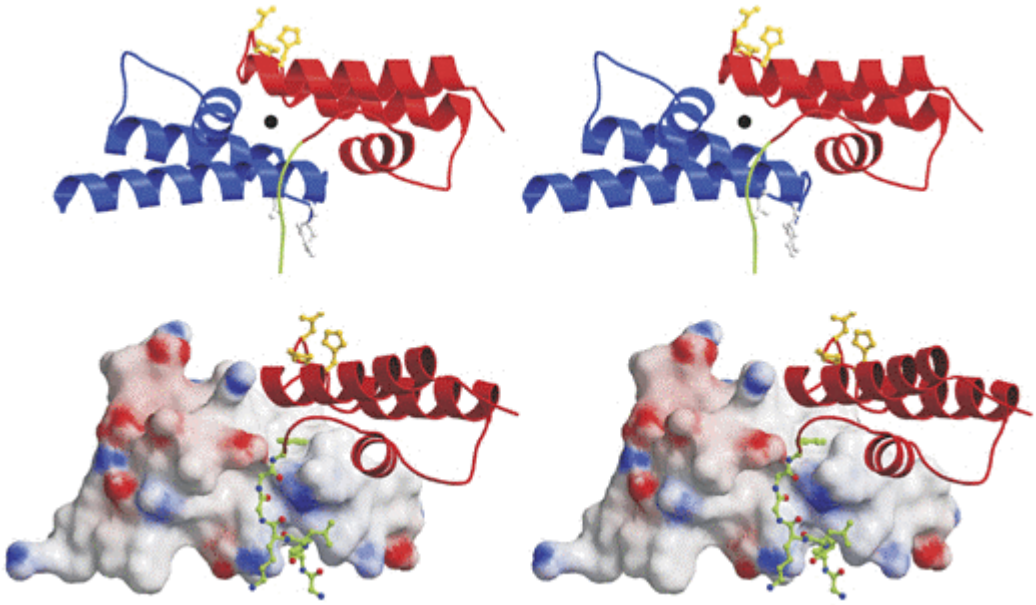

Figure 9: N-terminal arm of Tim14 embraces Tim16. (above) Ribbon model of Tim14–Tim16 heterodimer given in stereo representation. Tim14 is shown in red, Tim16 in blue. The N-terminal arm of Tim14 is highlighted in green. (below) Stereo representation of interacting parts of Tim14 and Tim16. Tim 14 is shown as ribbon model, Tim16 as surface model. The N-terminal arm of Tim14 that embraces helix III of Tim16 is represented as balls-and-sticks model, carbon atoms are colored in green, oxygen atoms in red and nitrogen atoms in blue.

Since Magmas is a gene that induces GM-CSF and it is involved in the transport of mitochondrial proteins, some studies have been accomplished to evaluate the effect of the gene expression in healthy and neoplastic tissues. It is been examined a prostatic tissue with carcinoma where it is expressed the receptor GM-CSF: comparing the healthy prostatic tissue with the malignant one, it is been showed that the first one has higher levels of magmas than the other in two cases of three.

These results don't get along with the immunohistochemical studies where the high gene expression is in the malignant cells. One possible interpretation of this is that the expression of the gene magmas could be regulated post-transcriptionally in the prostatic cancer[21]. But the rule of the gene in this cancer is not clear yet; other factors could be involved, as resistance to the apoptosis, sensibility of growth factors in cancer cells.

For this reason, there are many studies about Magmas and, specifically, if it can regulate the mitochondrial activity, if it is overexpressed or mutate in the malignant cells. The results could give a new approach to the cure of the prostatic cancer.

2. Ischemia and Reperfusion Injury (IRI) Inhibitors

2.1 Aim and objectives

Ischemia is a restriction in blood supply to tissues, causing a shortage of oxygen and glucose needed for cellular metabolism (to keep tissue alive). Ischemia is generally caused by problems with blood vessels, with resultant damage to or dysfunction of tissue. It also means local anemia in a given part of a body sometimes resulting from congestion (such as vasoconstriction, thrombosis or embolism). Ischemia comprises not only insufficiency of oxygen, but also reduced availability of nutrients and inadequate removal of metabolic wastes. Ischemia can be partial (poor perfusion) or total.

Thus, physicians and biomedical researchers have strived to better understand the underlying mechanisms of ischemia-induced tissue damage for almost two centuries, with the hope for developing therapies to limit the devastating health and economic burdens imposed by disorders characterized by reductions in organ-specific blood flow. Discoveries reported over the past 30 years have been particularly impressive, vastly increasing our understanding of the molecular, cellular, tissue-specific, as well as systemic events that occur during ischemia *per se*. Evidence supporting the concept that reperfusion could paradoxically induce and exacerbate tissue injury and necrosis was also discovered early in this period and provided a major impetus for research because this component of tissue injury is amenable to therapeutic intervention[22].

During ischemia, ATP synthesis is inhibited, and existing ATP is cleaved into ADP and phosphate. Since oxidative phosphorylation is interrupted, proton ions accumulate into mitochondrial matrix and pH quickly decreases. In order to raise the pH, Na^+-H^+ exchanger is activated and there is an influx of Na^+ into mitochondrial matrix. However, since Na^+-K^+ ATPase is also inactive during ischemia, the accumulation of Na^+ induces Na^+-Ca^{2+} antiporter with reverse activity. The final result is a Ca^{2+} accumulation into mitochondria and its inhibited reuptake by ER[23].

Reperfusion is needful to save the cells, however, it is also the cause of necrosis. That happens because when the capillary flow resumes, the catabolites that have accumulated are cleared and pH rises quickly. So, since ETC still inactive and ROS generated, these are inductors of mPTP opening and also they contribute to the decrease of IMM transmembrane potential, inducing the apoptosis intrinsic pathway.

Ischemia-reperfusion injury concerns microvascular dysfunction in most organs and this is very dangerous and problematic in medical/surgical procedures, such as thrombolytic therapy, organ transplant, cardiopulmonary bypass. Since the mPTP seems to have a key

role in the IRI, part of my project is the synthesis of some inhibitors, with the opening channel as target.

There are few agents known to be indirectly active as mPTP inhibitors, for example Bendavia, which interact with cardiolipin and is able to reduce ROS production and to maintain ETC activity during reperfusion, avoiding disproportion with gradient equilibrium. There are also some agents known to inhibit with alternative mechanism mPTP. One of them is Cyclosporin A (CsA), known since 1990 to bind mitochondrial cyclophilin D (mCypD), one of the most important member of mPTP, which is, hence, inhibited.

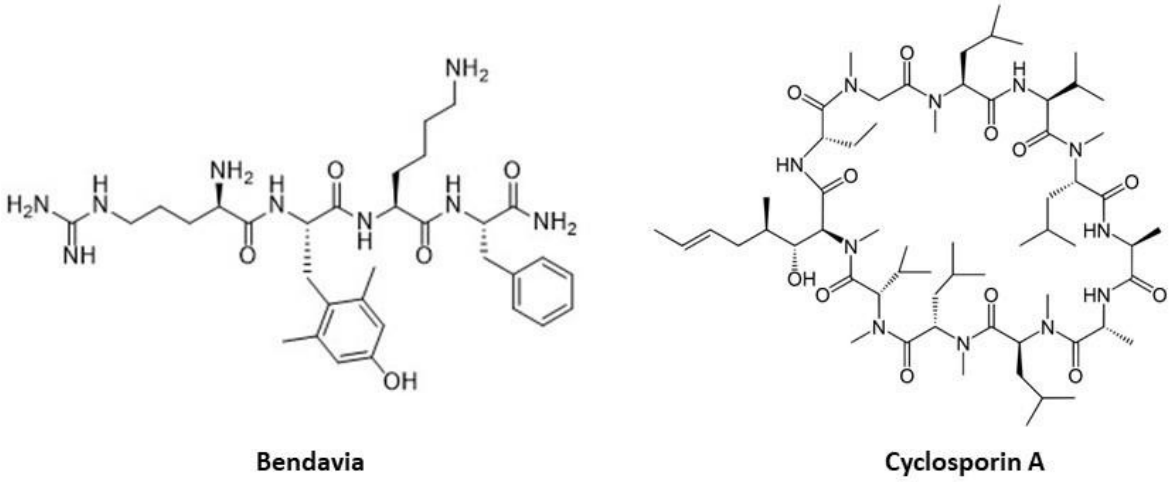

Figure 10: Bendavia and Cyclosporin A structures.

The most known inhibitor of mitochondrial ATP synthase is Oligomycin[24], that is a macrolide with a 26 membered lactone ring, isolated from *Streptomyces diastatochromogenes.* It binds at the interface of subunit a and c-ring, blocking the rotary proton translocation in Fo. If the enzyme is well-coupled, the activity of F_1 is also blocked. The mechanism provides that a subunit of mitochondrial F_1-portion that connects F_1 with Fo was named oligomycin-sensitivity conferring protein (OSCP). This is important to couple F_1 and Fo and so, making the first one sensitive to Fo inhibitor oligomycin.

The southern part (red in figure 11) of this macrolide binds to the surface of c_{10}-ring and the carboxyl side chain of Glu[59], which is essential for proton translocation, forms an H-bond with oligomycin via a bridging water molecule. The remaining contacts between oligomycin and subunit c are mainly hydrophobic[25] (figure 11).

Taking this molecule as reference compound for mPTP opening inhibitor, the 1,7-dioxaspiro[5.5]undecane portion of Oligomycin A could be an interesting starting point for the construction of new compounds libraries. Starting from evidences in a student's work thesis[26], where it was developed a synthetic approach that allowed us to obtain spiromolecules, having one spiro center as Oligomicyn A, we decided to advance the

research, synthetizing new molecules, having two spiro centers, to improve the activity. Specifically, I worked on synthesis of molecules having a dispiropyrrolidine structure, using Isatine and 5-Fluoroisatine as reagents and modifying many positions (Figure 12).

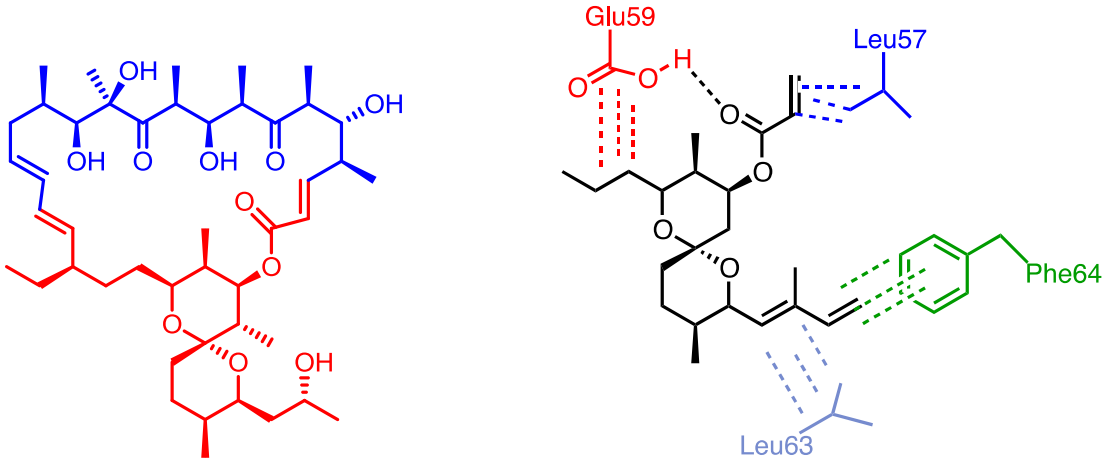

Figure 11: Structure of Oligomycin A and its connections with c-ring.

As shown in figure 12, several compounds have been obtained from Isatine and 5-Fluoroisatine, maintaining the same scaffold but with different modifications at key positions. Specifically we introduced diverse (poly)cyclic ketones without or with N-alkylation at the isatine nitrogen (a,b,c). In addition, we synthetized a small library of N-benzyl-piperidone derivatives with the general structure (d). We chose these last molecules because of the presence of two spiro centers that gives rigidity to the structure and also for their steric hindrance. They could be potentially interesting as inhibitors as well (Figure 12).

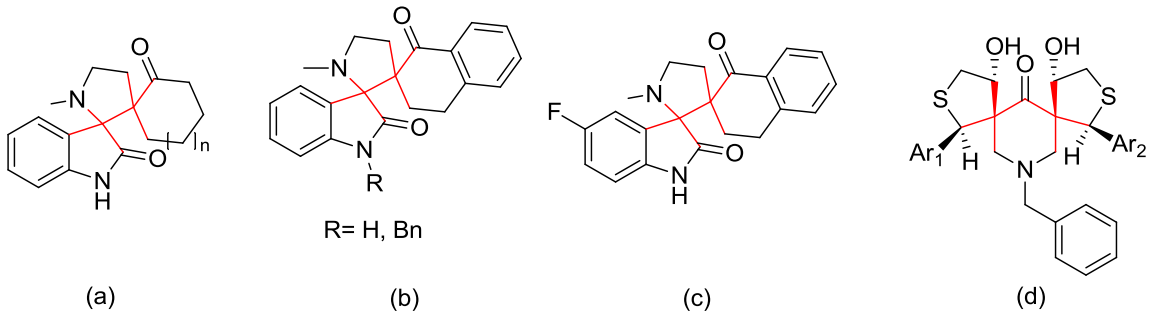

Figure 12: General structures of the compounds library.

2.2 Discussion

The target dispiropyrrolidine compounds have been synthetized through "one-pot reactions". These reactions are called, also, "tandem reactions" or "domino reactions". In this kind of processes, isolation of intermediates is not required, as each reaction composing the sequence occurs spontaneously. So, no new reagents are added after the initial step.

This category of multicomponent reactions can be included in "green chemistry", since the purification of intermediates is not required, meaning there is an economic reduction of time, costs and labor. These cascade reactions are very innovative, starting from a simple substrate, complex organic molecules will be obtained. They work with a mechanism that permits to have each atom of the reagents included in the final product.

Isatine has been used in biological field for being a precursor of many natural compounds.

5-Fluoro Isatine seems to have some interesting pharmacokinetic properties about the metabolism process.

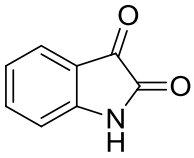

Figure 13: Isatine structure

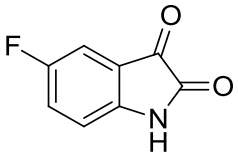

Figure 14: 5-Fluoroisatine structure

Another approach to synthesize di-spiromolecules led to a library of di-spiropiperidone-tetrahydrothiophene heterocycles via Micheal addition between the intermediate formed from N-benzyl piperidone reacted with different aromatic aldehydes, through a double aldolic reaction, and 1,4-dithiane-2,5-diol in presence of triethylamine. Tetrahydrothiophene is found in many natural and synthetic compounds that show biological activity: antibacterial, antioxidant, enzymatic activities[27,28].

Piperidone is interesting for many properties as anticancer, anticonvulsant, antimicrobial and anti-inflammatory[29].

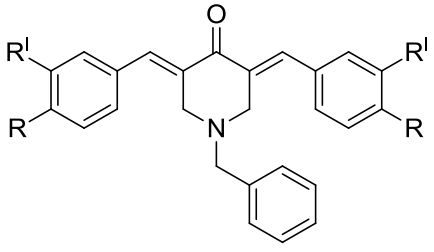

Figure 15: intermediate by double Aldolic reaction.

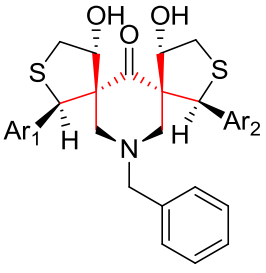

Figure 16: general structure of N-benzylpiperidone-tetrahydrothiophene derivatives.

2.2.1 Synthesis of dispiropyrrolidine derivatives using Isatine

Many compounds have been synthetized with Isatine as scaffold. It reacts with sarcosine and different cyclic ketones to give dispiropyrrolidine compounds with similar structures.

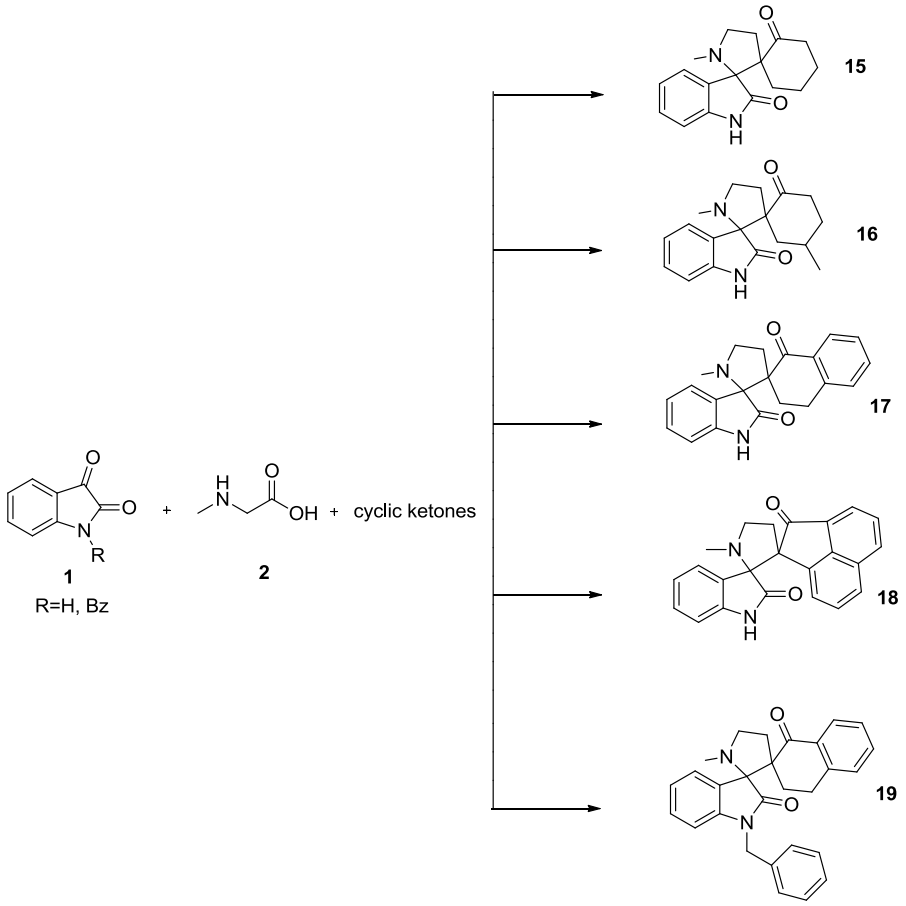

Scheme 1: Isatine derivatives library.

We firstly evaluated aliphatic cyclic ketones; then, we decided to use aromatic ones, as for example α-tetralone and acenaphthenone, inserting more aromatic elements, to increase the hydrophobic interactions with the enzyme.

Another strategy it was to alkylate the amide nitrogen with benzylbromide to increase the steric hindrance.

Moreover, I tried to use a different amino acid. So, instead of sarcosine, I utilized β-alanine, previously alkylated through a reductive amination by benzaldehyde.

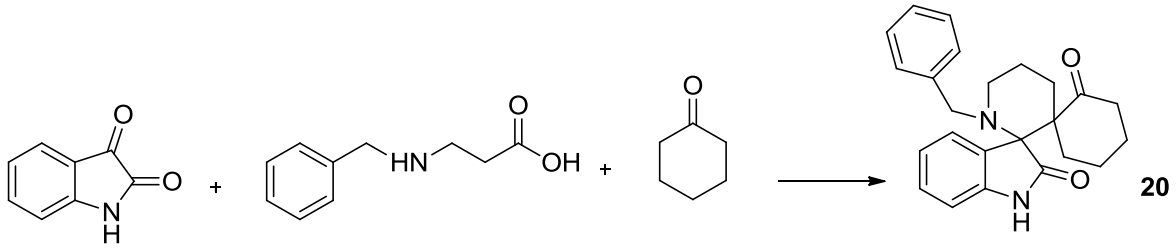

Scheme 2: Isatine derivative using benzyl-β-alanine.

In these conditions the reaction with isatine and cyclohexanone to give dispiropyrrolidine derivative didn't go well. The difficulty has been to purify the product, also obtained in low yield, because it comes as a diastereomeric mixture, confirmed from TLC and analytic HPLC, that shows two inseparable peaks, even by preparative HPLC. Also, our hypothesis is supported by NMR spectrum that shows unclear double peaks.

So, we left this strategy to go back to the one using sarcosine.

2.2.2 Synthesis of dispiropyrrolidine derivatives using 5-fluoro Isatine

A second small library was made from a synthesis using 5-fluoro Isatine, since from the pharmacodynamics profile, having a fluorine atom in *para* position compared to the most electronegative atom, seems to be interesting to avoid the metabolic degradation.

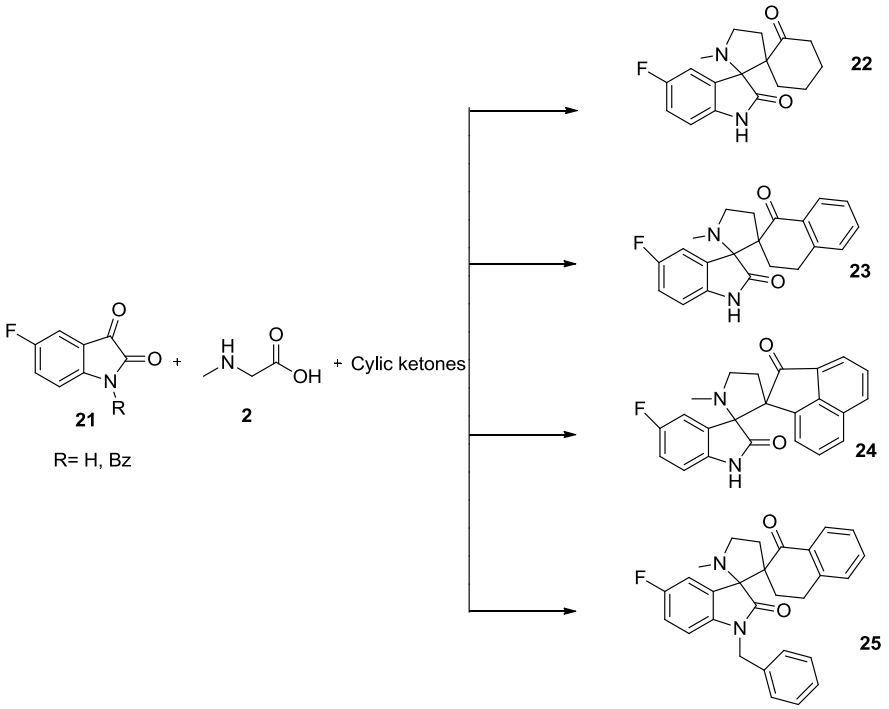

Scheme 3: 5-fluoro Isatine derivatives library.

2.2.3 Reaction mechanism for the synthesis of dispiropyrrolidines

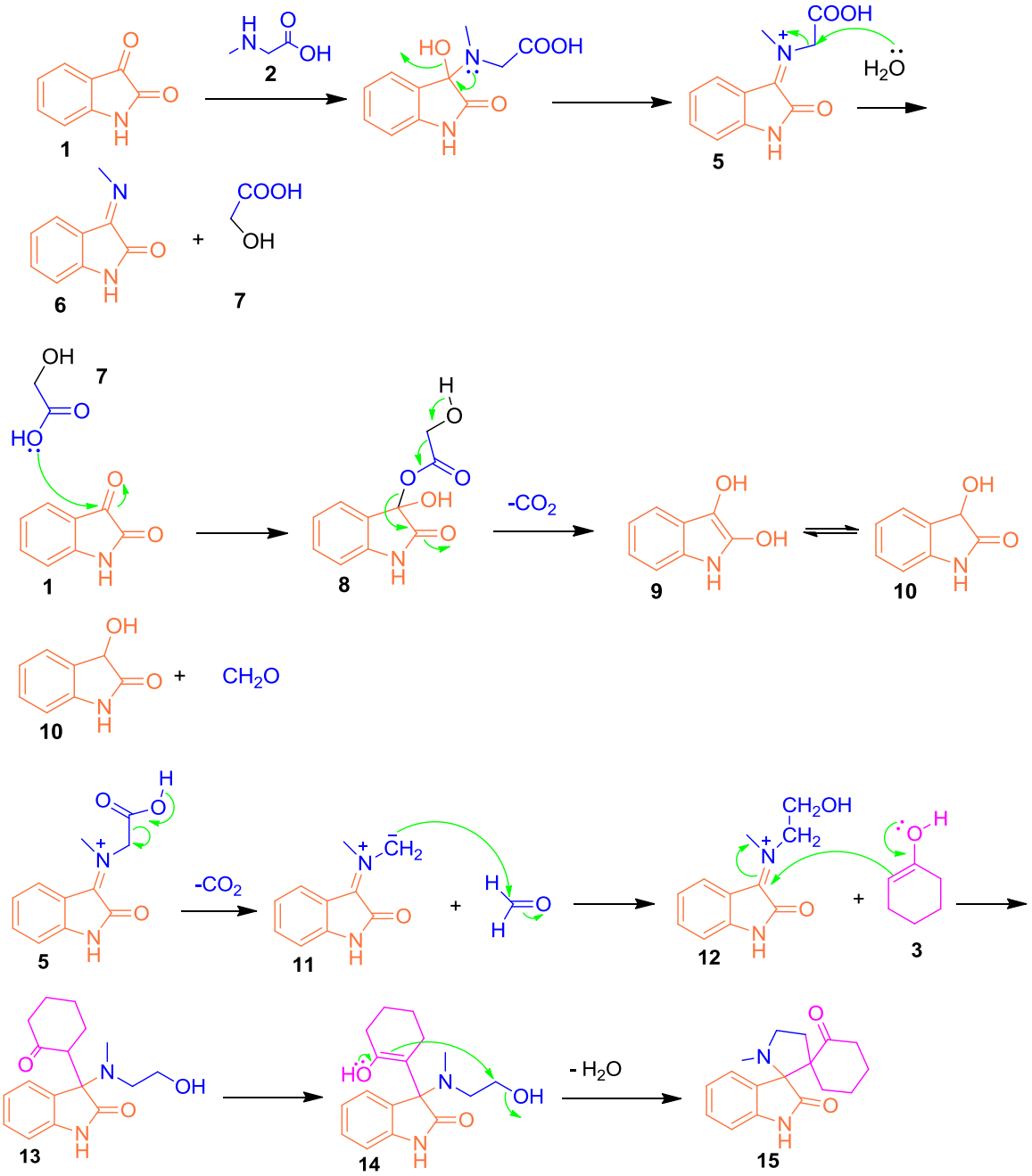

Scheme 4: mechanism of dispiropyrrolidines.

The reaction between isatine and sarcosine is known to give the azomethine ylide formation **11**. The imminium ion **5** undergoes two reactions hypothetically: a) decarboxylation to give **11** and b) nucleophilic substitution to give glycolic acid **7**, that undergoes the carboxylation after the reaction with isatine **1**, giving formaldehyde. Presumably, **11** reacts with formaldehyde to give imminium-alcohol **12**, that with the keto-

enol **3** to obtain **13**; it cyclizes and after the dehydration it is obtained the dispiropyrrolidine **4**.

The mechanism hypothesized by a work in literature[30] suggests that the reaction stoichiometry should be 2:2:1 (isatine:sarcosine:ketone); but it can actually be 1:1.5:1, since I obtained good yields, because of the isatine regeneration by dihydroisatine **10**[30].

2.2.4 Synthesis of dispiropiperidone-tetrahydrothiophene heterocycles

The other small chemical library synthetized was the dispiropiperidone-tetrahydrothiophene heterocycles. This synthesis is carried on in two steps:

1- From N-benzyl piperidone, after a double Aldolic reaction, it is alkylated in positions 3 and 5;

2- This product reacts with 1,4-dithiane-2,5-diol, in presence of triethylamine.

To obtain these compounds, at first, N-benzyl piperidone is made to react with different aromatic aldehydes. Through a double Aldolic reaction, followed by dehydration, the ketone is alkylated in positions 3 and 5.

Then, this product is used as an intermediate to start a second reaction with 1,4-dithiane-2,5-diol, obtaining a double cyclization through a tandem reaction, which is Michael reaction.

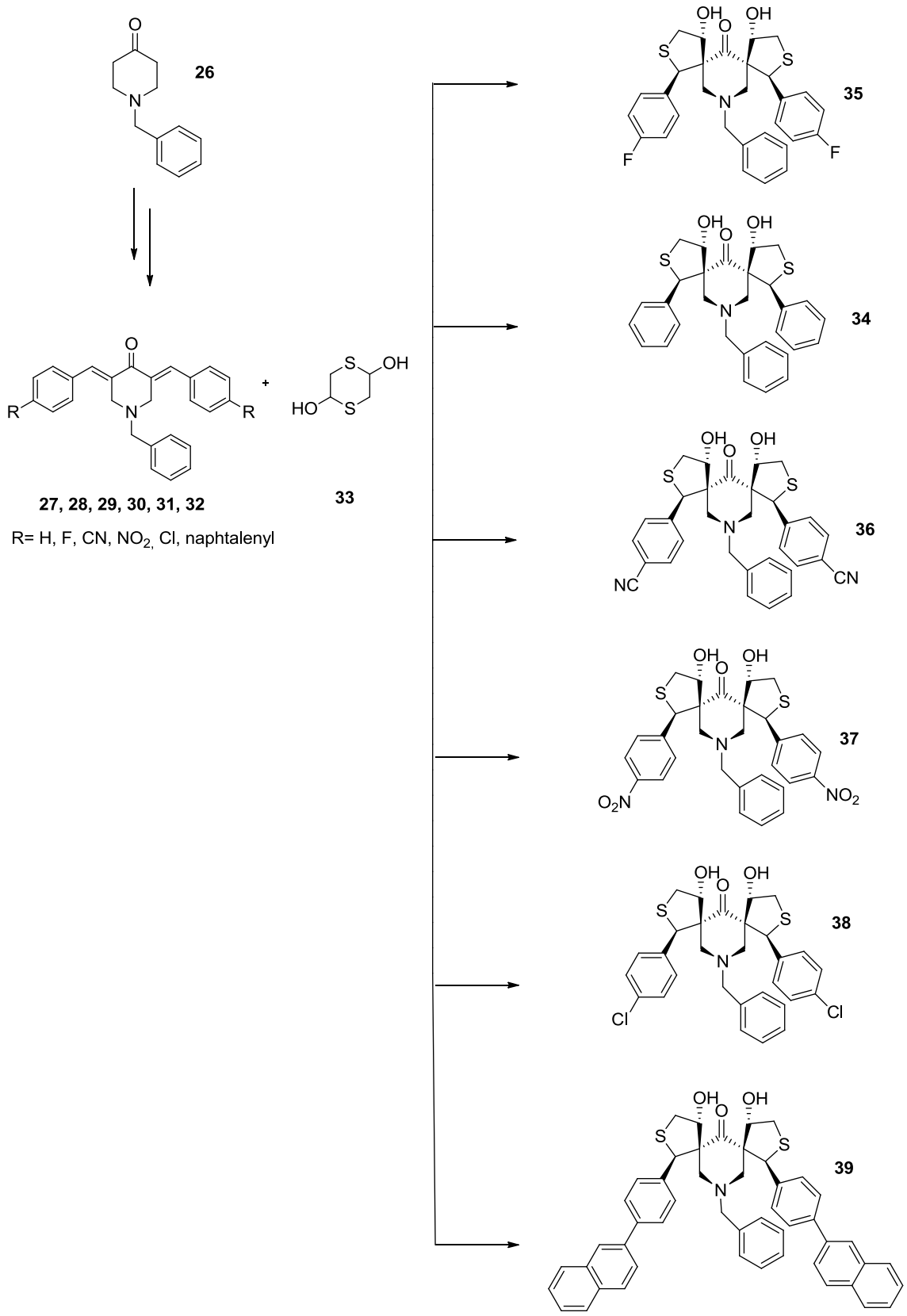

Scheme 5: N-benzyl piperidone-tetrahydrothiophene heterocycles library.

2.2.5 Reaction mechanism to synthetize dispiropiperidone-tetrahydrothiophene heterocycles

2.2.5.1 Aldolic Reaction

The first step is to alkylate N-benzyl piperidone in positions 3 and 5.

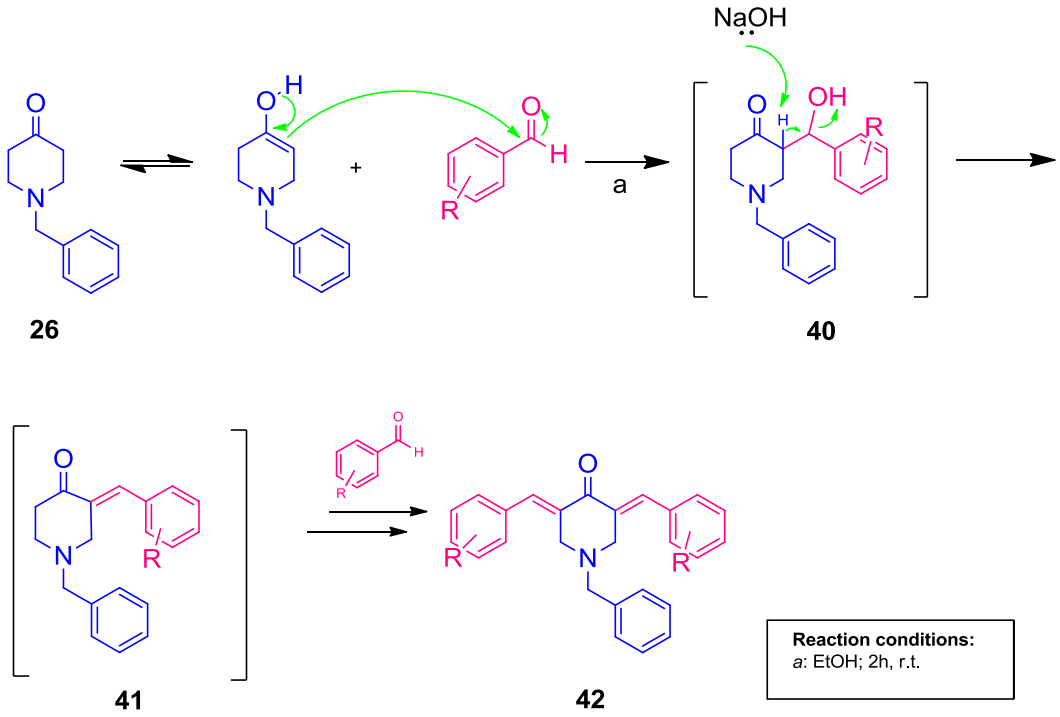

Scheme 6: Aldolic reaction mechanism.

N-benzyl piperidone **26**, in its enolic form, which works as nucleophile, attacks the aromatic aldehyde. It is obtained the intermediate **40**, which it can be seen as a β-hydroxyketone, that dehydrates thanks to the base (in this case NaOH); the monoalkylated **41** attacks for a second time another molecule of aldehyde and so, it is achieved the final product **42**, with the two positions 3 and 5 alkylated.

2.2.5.2 Tandem Micheal reaction

Once obtained the product **42,** the next reaction is a Micheal reaction and it is a tandem reaction, to give a final dispiro center compound.

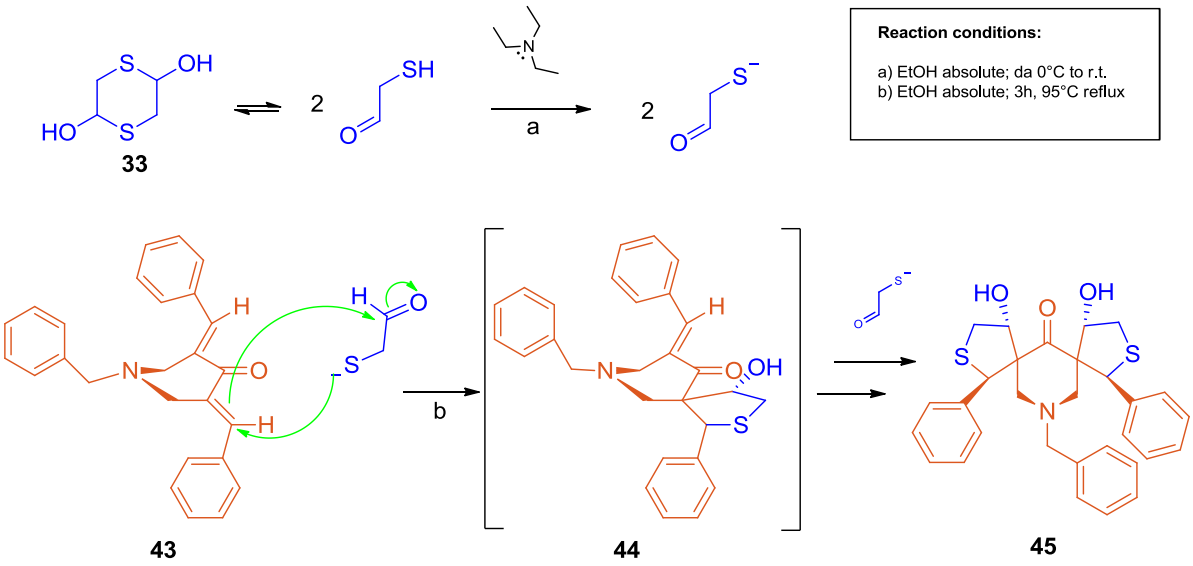

Scheme 7: Michael reaction mechanism.

The 2-mercaptoacetaldehyde molecules generated from the equilibrium with 1,4-dithiane-2,5-diol **33**, are deprotonated by the triethylamine (TEA) . The anion starts the Micheal addition over one of the conjugated double bonds of **43** in a stereoselective manner. Thanks to the aldolic reaction immediately after, it is obtained the monospiranic intermediate **44**. The next step is made by another mercapto acetaldehyde deprotonated in the same way, obtaining at the end the final product **45**.

It is interesting to know that the second annulation involving the reaction of another anion of 2-mercaptoacetaldehyde to the monospiro intermediate again occurs on the same side as the initial Micheal addition presumably in a bid to obviate its steric interaction with the initially generated benzylic carbon **44**[29].

Moreover, at the beginning I used a procedure that suggested to use DCM with catalytic quantities of TEA, but this didn't give me good results. So, following a second procedure, I changed the solvent in EtOH absolute and stoichiometric quantities of TEA, added at cold temperature[31]. This approach gave good results.

2.3 Conclusions and results

The aim of the thesis was to synthetize dispirocenter compounds as mPTP inhibitors.

Different synthetic strategies were used, to give three different chemical libreries. The synthesis of dispirocenter from isatine and 5-fluoro isatine with different cyclic ketones has been studied and the yields were high.

The other type of reactions was from the piperidine as scaffold.

These kind of reactions are different from the isatine derivatives and we are trying to optimize the conditions and to evaluate the optic purity. In some cases, it was not possible to obtain only dispiranic derivateves because for some the preference was to the monospiranic ones. This should be an advantage for synthetizing asymmetric molecules to be tested as mPTP inhibitors.

Finally, I can say that I reached the results I prefigured and this allowed us to evaluate the compounds with biological preliminary tests about their activity. In the future it will be possible to synthetize spiranic derivatives considering a variety of substitutions on the nucleous of the structure in a coherent way with the biological results.

A selection of these compounds were tested in order to determine their potency in inhibiting mPTP complex through the binding to the c-ring. To this aim, a Co^{2+}-calcein assay has been performed, as it directly and efficiently allows to misure mPTP opening. Specifically, the protocol was applied by the research group of professor P. Pinton at the Dept. of Morphology, Surgery and Experimental Medicine of the University of Ferrara.

This method is based on the decrease in calcein fluorescence, which is related to the mPTP opening.

Calcein AM, a non-fluorescent acetomethoxy derivate of calcein, is used in this protocol. Basically, calcein AM diffuses into cellular compartments, where it is then hydrolized by estereases. In this form, the calcein is no longer able to diffuse reamining trapped and acquiring green fluorescence properties, visible under fluorescency microscopy.

This protocol is applied to tumoral HeLa intact cells and there is a need to visualize selectively the mitochondrial calcein fluorescence. So, Co^{2+} is used, since it is a metal ion able to totally quench calcein emission and it is not connected to the mPTP opening pathway. When mPTP is closed, Co^{2+} is not able to influx into mitochondria. On the contrary, mPTP opening induce Co^{2+} entry into mitochondria, hence, a decrease in calcein fluorescence, which is used as mesaure for mPTP opening.

For this reason, the administration of a mPTP opening stimulus (as ionomycin-mediated Ca^{2+} influx) is used and the system monitored as vehicle and control.

When a mPTP opening inhibitor have been pre-administrated to the system, this result in a neat inhibition of calcein decrease. In a protocol[32] Cyclosporine A (CsA) was used for this purpose, as interact with Cyclophilin D (mCypD). As mentioned in the introduction section, mCypD is a component of the complex mPTP and its inhibitor CsA is tipically used to conduct mPTP opening studies.

From the preliminary tests on a variety of compounds, taking as reference **PP41** (figure 17), that was already tested and showed already a good potency of inhibition (about 40%), some compounds showed also potential good results as mPTP opening inhibitors.
As it is noticeable in figure 17, the compounds **22**, **24** and **35** inhibit the pore opening in a relevant way: from 60% to a number very close to 100%.
Other tests will study in deep their activity.

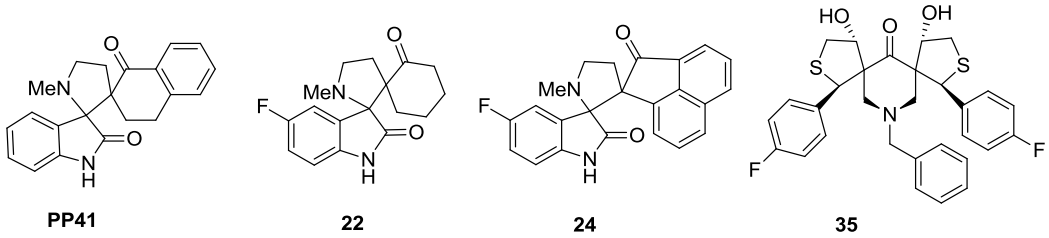

Figure 17: Best activity of IRI inhibitors.

In the follow graphic it is possible to see the results from the elaboration of these preliminary tests, where Ctrl is the ionomycin, as agonist of the mPTP opening. The concentration of the inhibitors are 5µM for these preliminary tests. Normally, the concentration is lower.

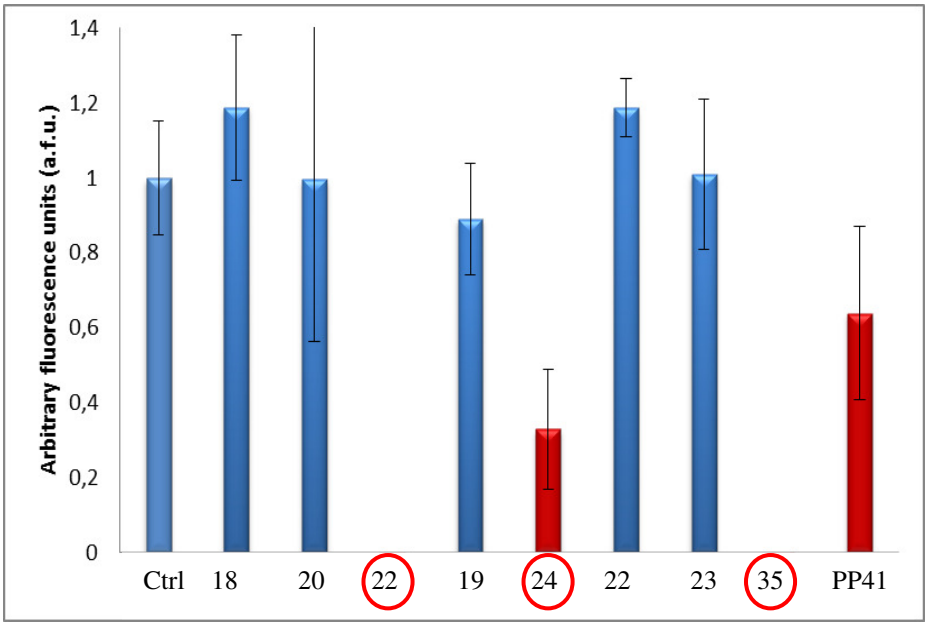

Graphic 1: preliminary tests Co^{2+}-calcein assay.

3 Nutlins as anti-cancer drugs

3.1 Aim and objectives

Among the different therapeutic strategies evaluated pharmacologically, the attention has been focused on the drug design able to modulate the p53-MDM2 interaction. The structure of this complex p53/MDM2 is known pretty well, as a matter of fact there is a tridimensional structure available with specific interaction sites of the MDM2 hydrophobic pocket[33]. The interface between the two proteins is very small and this makes possible to think about new molecules with low molecular weight and so, with a high oral bioavailability.

Among the various classes of compounds studied to inhibit the MDM2, only three showed an interesting pharmacological profile: *cis*-imidazolines, benzodiazepine-diones and spiro-oxindoles (figure 18).

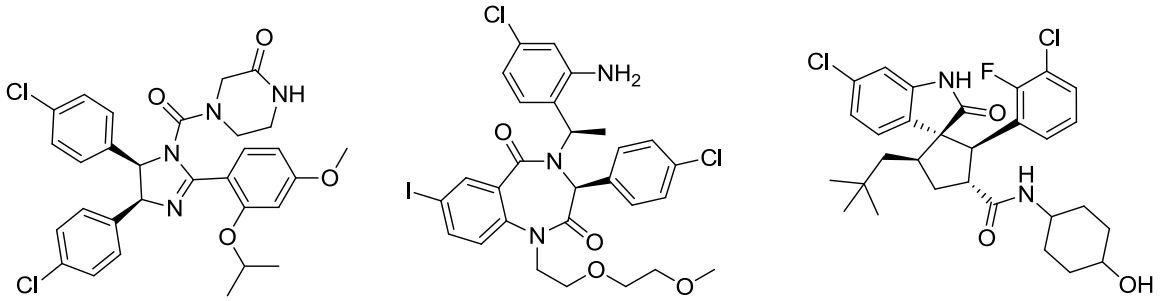

Figure 18: *cis*-imidazolines, benzodiazepine-diones and oxindoles structures.

The shared structure is a heterocyclic *scaffold* that supports three lipophilic groups mimicking the p53 α-helix conformation that exposes three lipophilic residues inside the pocket: Phe[19], Trp[23] and Leu[26] (Figure 19).

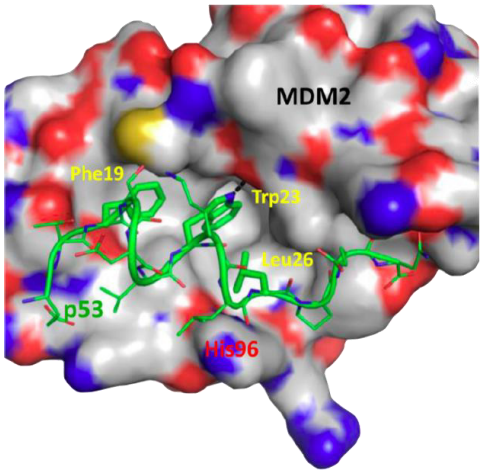

Figure 19: X-Rays structure of interaction between MDM2 and p53.

Some modifications have been made to these compounds. In particular, a polar group has been added to increase the solubility, in the same time one or more halogens as substituents in the aromatic functions allowed to improve the interaction intensity[34].

Nutlins, which is the first and more important class of small molecules, are *cis*-imidazoline analogs which inhibit the interaction between MDM2 and tumor suppressor p53. The most important is Nutlin-3, which is commonly used in anti-cancer studies.

This MDM2 inhibitor has been discovered since 2004 by Vassilev et al., Hoffmann-La Roche Company (HLR) research group, through a specific screening among compounds library in Nutley, New Jersey. It is known that the two enantiomers of Nutlin-3 are different in affinity to MDM2, in particular (-)-Nutlin-3 is a p53 inductor 150 fold more potent than its enantiomer (+)-Nutlin-3.

The aim of this project was to find a synthesis pathway to obtain only (-)-Nutlin-3 as product, instead of the racemic mixture of the two enantiomers, as mostly reported in literature.

3.2 Discussion

3.2.1 Synthesis of racemic Nutlin-3

Most of the synthesis in literature utilize the *meso*-diamine as *building block*, that is obtained through five steps starting from the 1,2-diphenylethan-1,2-dione (scheme 7), as described in Hoffmann-La Roche Company (HLR) synthesis[35].

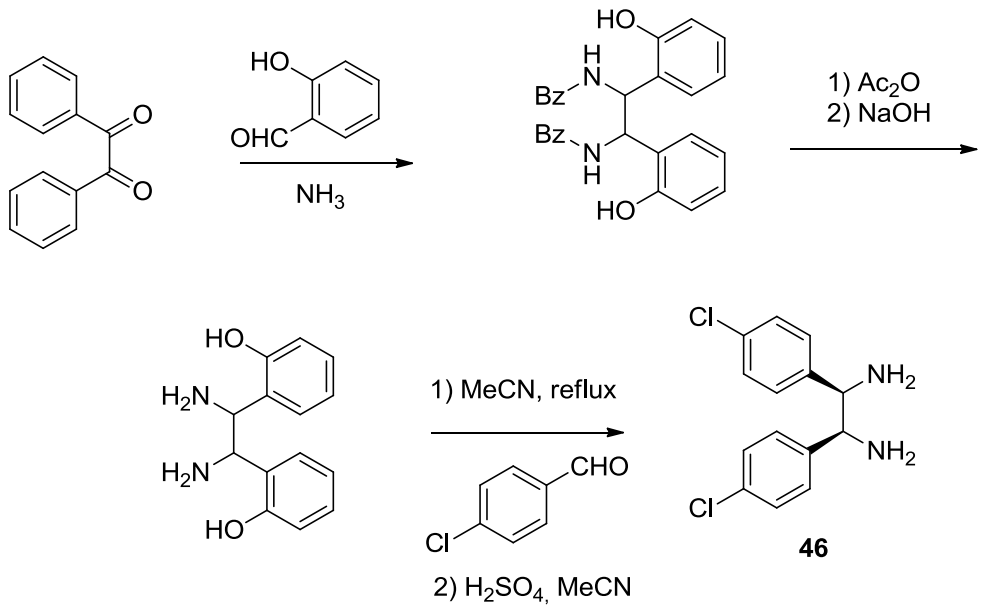

Scheme 8: Synthesis of *meso*-diamine.

The methods to synthetize *cis*-imidazoline scaffold, starting from *meso*-diamine **46**, can be classified in two categories: 1) through the formation of monoamide **47**, followed by cyclization, or 2) through condensation and cyclization in one step.

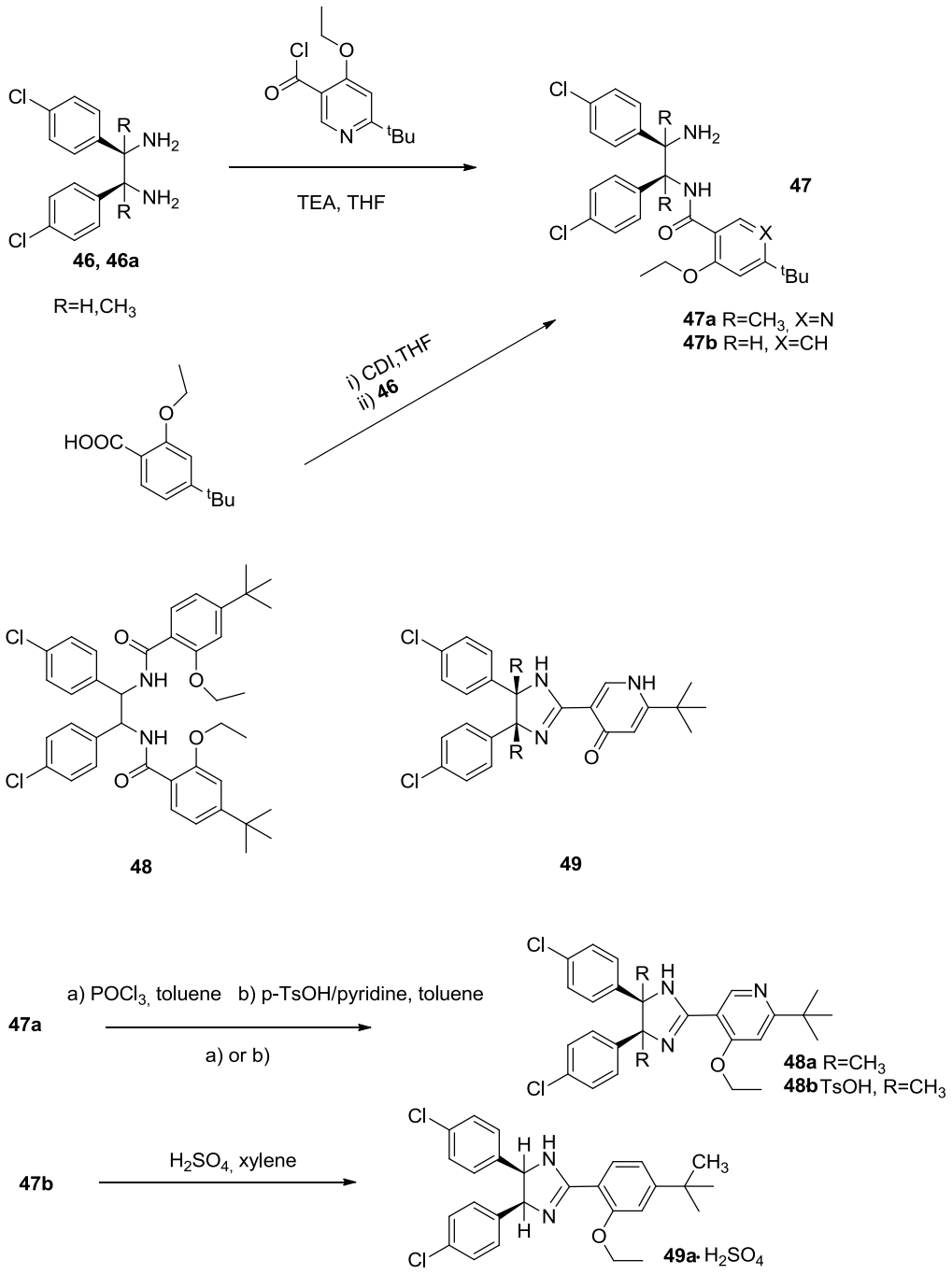

Scheme 9: First method to synthetize *cis*-imidazoline.

In the first case (Scheme 9) there is the problem of di-acylation and the low yield of cyclization reaction. Specifically, with the use of 1,1'-carboyldiimidazole (CDI), the mono-acylation is not favorable compared the di-amide **48**[36]. The cyclization with $POCl_3$ gives the formation of **49** in high quantity[37]. With *para*-toluenesulfonic acid the reaction with **47b** doesn't reach the completeness because of the formation of its anhydride, while **47a** gives high yield[38].

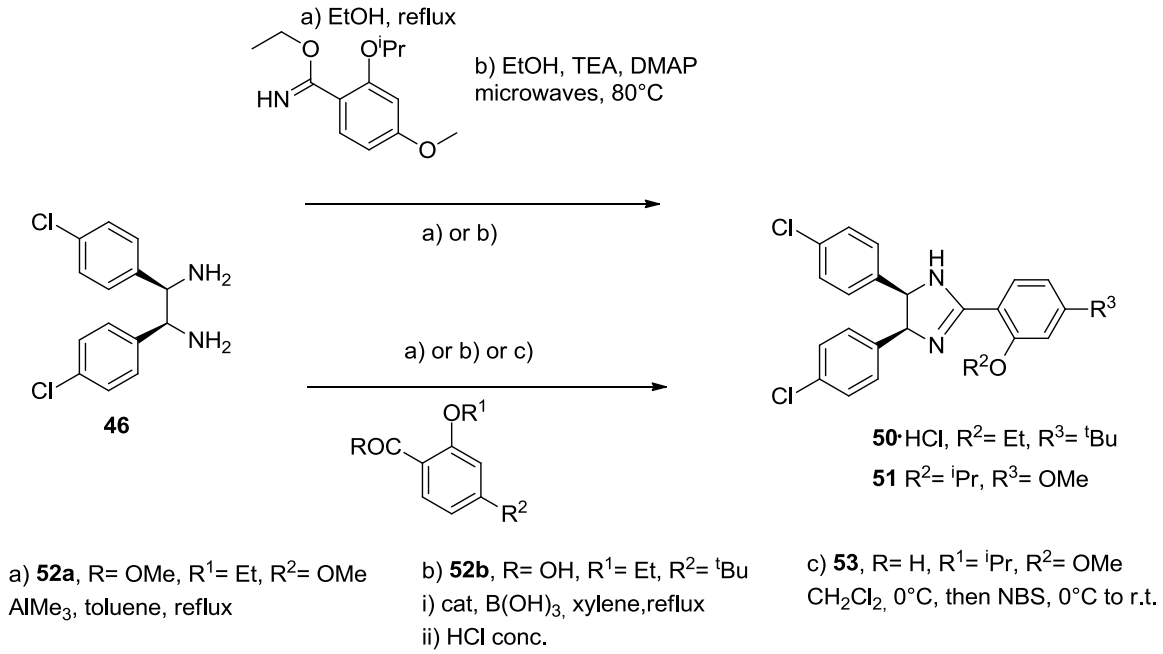

Scheme 10: Second method to synthetize *cis*-imidazoline.

In the second case (Scheme 10), the condensation-cyclization of *meso*-diamine with ester **52a** can work using with an alkyl-aluminum, that besides to be pyrophoric, it is not easy to work-up because of colloidal character.

The use of boric acid is another synthetic strategy to prepare **50-HCl** in large scale.

The imidazoline nitrogen is acylated by the use of phosgene, a gas very toxic, so it is preferable to use its synthetic equivalent, the triphosgene, less toxic and dangerous because also it is a solid.

As it is known, a prochiral compound as meso-diamine **46**, in absence of chiral agents, gives the racemic mixtures, because the possible transition states are enantiomeric and also isoenergetic. The enantiomers of Nutlin-3 have different activity, so the racemic mixture has to be treated to separate the pure enantiomer (-)-Nutlin-3. It can be used the supercritical chiral chromatography (FSC)[39] or a resolution with chiral derivatives[38].

The separation is difficult, not cheap and it doesn't follow the concept of atom economy, because the 50% of the product is lost.

In general, synthetic methodologies that allow to be enantioselective, especially in pharmaceutical field, it is an important challenge from organic synthesis point of view.

3.2.2 Asymmetric synthesis of (-)-Nutlin-3

In literature there are not many strategies to develop an enantioselective synthesis of (-)-Nutlin-3. Only studies by *Johnston et al.* found the first and efficient way to synthetize the active enantiomer of Nutlin-3, with a high enantiomeric excess[40,41,42].

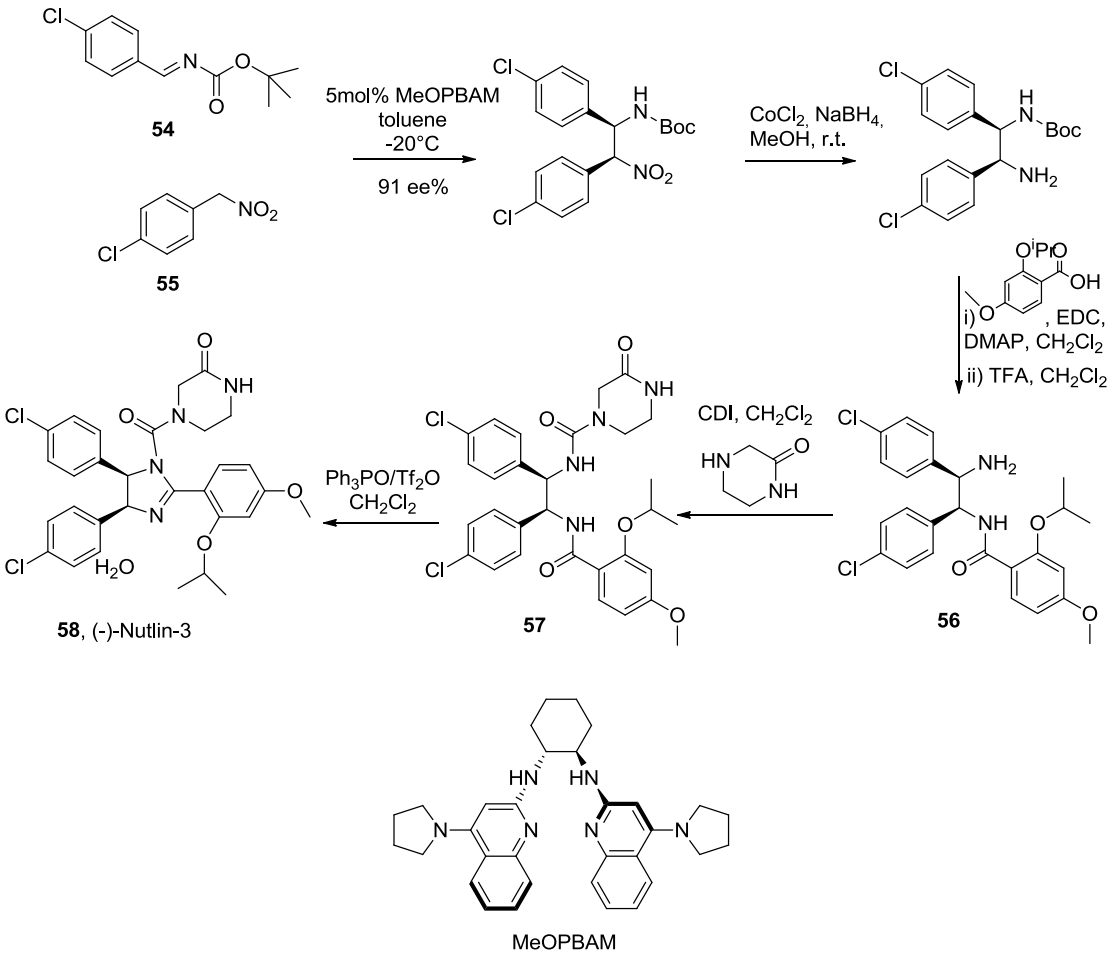

Scheme 11: asymmetric synthesis by Johnston *et al.*

A step very important of this synthesis (Scheme 11) is the addiction of aryl-nitromethane **55** to the N-Boc-immine **54**, through the aza-Henry (or nitro-Mannich) reaction diastero- and enantio-selective, organocatalyzed by MeOPBAM.

The next reduction of the nitro group with cobalt dichloride and $NaBH_4$ gives a mono-protected diamine, asymmetric (not *meso* anymore), that reacts with the 2-isopropoxy-4-methoxybenzoic acid to give the amide **56**. After deprotection, the primary amine is acylated with CDI, followed by 2-piperazinone. Finally, with phosphonium anhydride (Hendrickson reagent)[43], obtained *in situ* from triphenylphosphinoxide (PPO) and trifluoromethanesulfonic anhydride, it happens a chemoselective cyclization by dehydration of urea-amide **57**.

The disadvantages of this procedure are the high number of steps and purification through chromatography (considering also the preparation of the building blocks **54** and **55**); the high cost of the cobalt dichloride; the difficulties of the purification of the final product **58** because of the presence of PPO.

3.2.3 Synthesis of a precursor of (-)-Nutlin-3, enantiomerically enriched.

In 2011 Seidel *et al.* reported an interesting asymmetric reaction to prepare a mono-protected diamine.

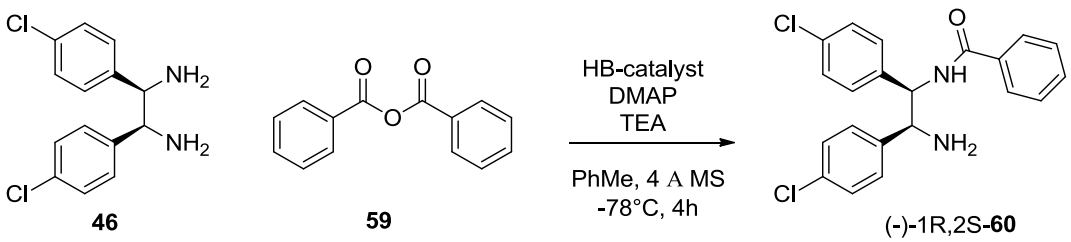

Scheme 12: Synthesis mono-protected diamine **60**.

It is a reaction of desymmetrization (scheme 12) of the compound **46**, using a new concept of nucleophile asymmetric catalysis, applied to the acylation with benzoic anhydride to the *cis*-1,2-diamine.

In general, to use nucleophile chiral catalysts[44] to acylate amines asymmetrically is very difficult because of the high nucleophilicity of primary amines. So, instead of this kind of catalysts, it is used an achiral catalyst, 4-dimethylamine pyridine (DMAP), in combination with a chiral anions receptor, called HB-*Catalyst (Hydrogen Bonding Catalyst)*, as a thiourea[45]. By a screening of different chiral receptors, the amide-thiourea **cat-1** is been identified and synthetized[46,47] to optimize the reaction conditions to be more efficient in giving high yields and enantiomeric excess (figure 20).

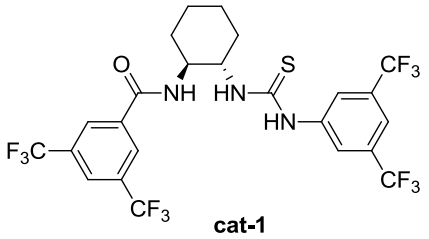

Figure 20: Structure of HB-catalyst (cat-1).

3.2.4 Co-catalysis DMAP-thiourea

It is known that amino derivatives of pyridine with a strong electron-donor (as $-NMe_2$ in DMAP), induce an acceleration of transfer speed of acyl, through a cationic intermediate N-acyl dimethylamino-pyridinium that, with the counter ion, makes an achiral ionic couple. There is an increase of reactivity because of the concentration of equilibrium of N-acyl dimethylamino-pyridinium[48] intermediate and its higher electrophilicity.

This pathway is commonly used in nucleophile asymmetric catalysis to transfer an acyl, introducing on the pyridine ring a chiral group[49].

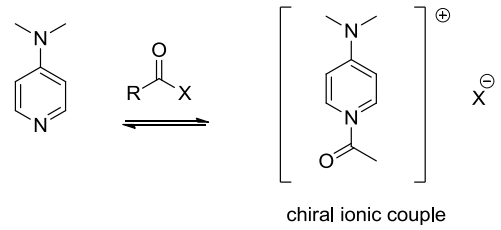

Scheme 13: Chiral ionic couple by the cation pyridinium.

Siedel *et al.* demonstrated that the effect that makes the cation pyridinium more reactive than the acylant agent, that generated it, can be improved if the counter ion is stabilized through a specific H-bonds donor: HB-catalyst. It is possible to have enantio-selection if the catalyst is enantio-pure. So, the ionic couple is made chiral *in situ* after a series of balances and the chirality is given by the anion (scheme 14).

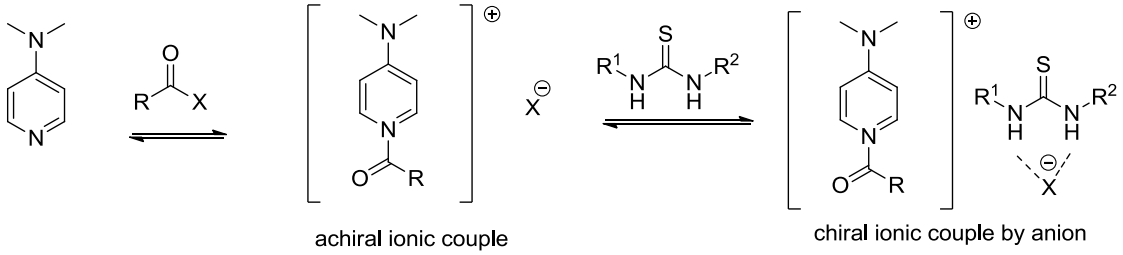

Scheme 14: chiral ionic couple made in situ.

The advantages of this new approach compared the use of chiral derivatives of DMAP are:

- The HB-catalyst gets the counter anion, leaving free the N-acyl pyridinium intermediate, increasing the electrophilicity;
- The right choice of the reaction conditions makes the chiral ionic couple more soluble than the achiral one, facilitating the enantio-selection;
- It is possible to use DMAP in stoichiometric quantities.

My work was to identify an easy, cheap and with not many steps procedure for an asymmetric synthesis of (-)-Nutlin-3, applying the concept of co-catalysis DMAP-thiourea chiral, developed by Seidel et al. to desymmetrize *meso*-diamine **46** with a symmetric anhydride (2-isopropoxy-4-methoxy benzoic anhydride).

Therefore, the retrosynthetic approach is this:

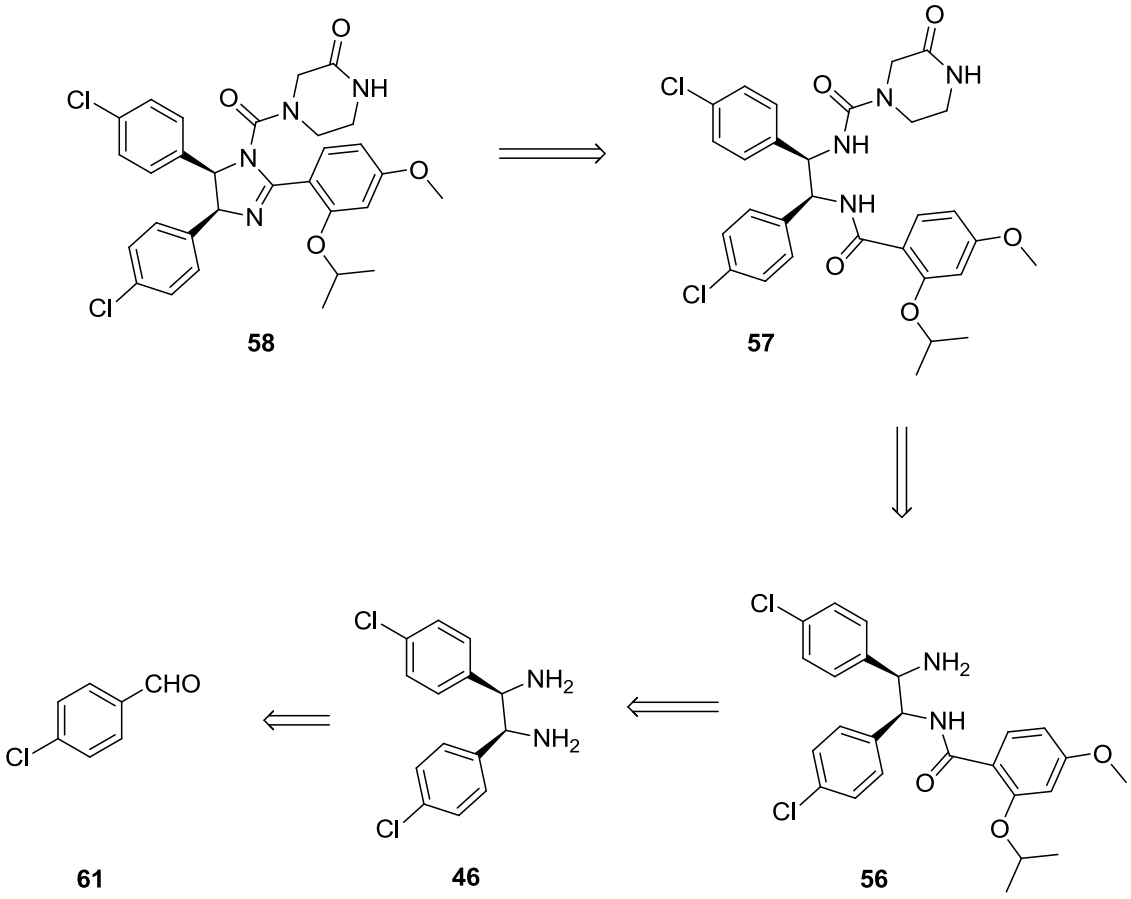

Scheme 15: Retrosynthesis of (-)-Nutlin-3.

3.2.5 Preparation of *meso*-diamine **46**

To prepare *meso*-diamine **46** the synthesis consists in two steps and it is efficient and stereospecific, without purifying through a chromatography; the yield is higher than the ones reported by HLR.

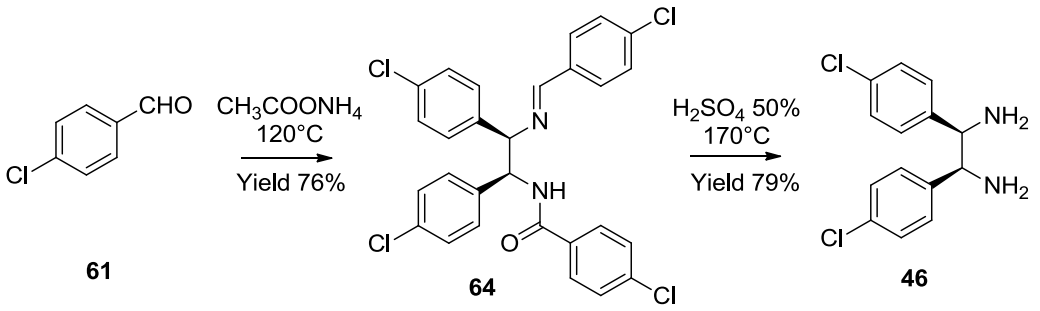

Scheme 16: Synthesis of **46**.

In the mechanism of the first step the ammonium gives the trichloro-hydrobenzamide **62**, that is deprotonated by a base and gives the ring formation to obtain the *cis*-trichloroamaridine **63**, analyzed by mass spectrometry. The intermediate **63** reacts with another molecule of *p*-chlorobenzaldehyde **61**, obtaining the benzyliden-amide **64** (Scheme 17).

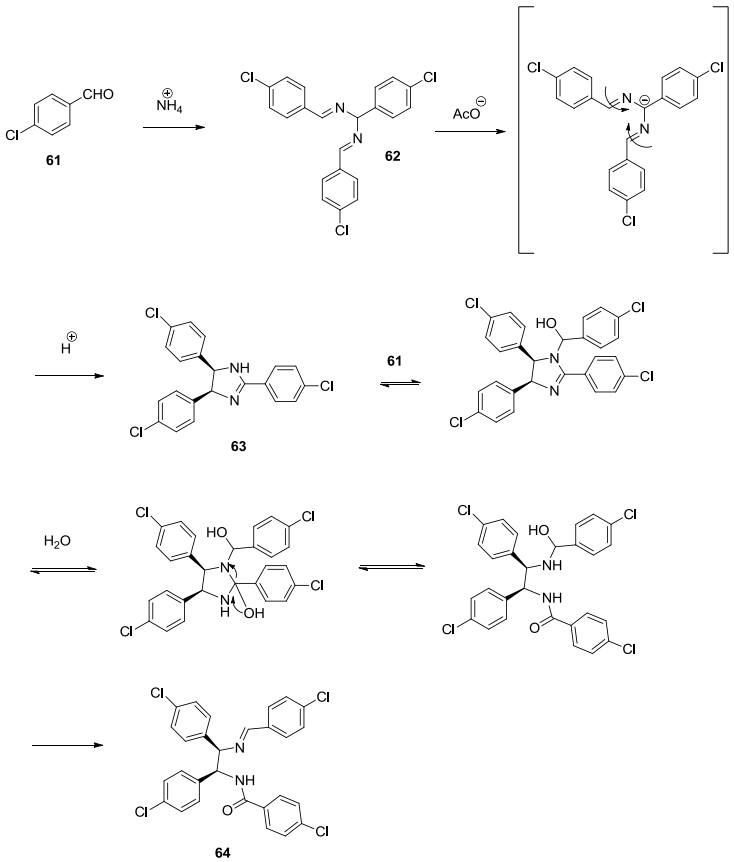

Scheme 17: Mechanism for the preparation of **64**.

A collateral reaction, probably for the oxygen in the air, is the formation of the **65**, not possible to hydrolyze in acid water. The opening of the cis-imidazoline ring with AlH_3 at 0°C in THF didn't give any results.

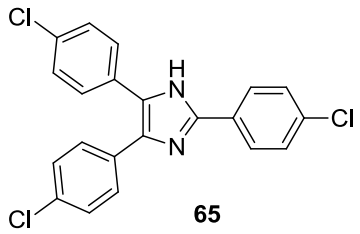

65

Figure 21: Aromatic trichloroamaridine structure.

To avoid or reduce the formation of **65**, the reaction is conducted in anaerobic atmosphere with presence of Argon.

3.2.6 Preparation of anhydride **69**

The commercial 4-methoxy salicylic acid **66** is been alkylated with 2-bromopropane in presence of 4 equivalents of K_2CO_3 in DMF reflux for 3.5 hours to give the derivative **67** with a 98% yield.

The next step in EtOH with a solution of NaOH 2N gives the product **68** with good yield (94%) without needing the purification. The anhydride **69** is obtained from the reaction of **68** with tosyl chloride. In this last step it is used a *solvent-free* method, giving a high yield (96%).

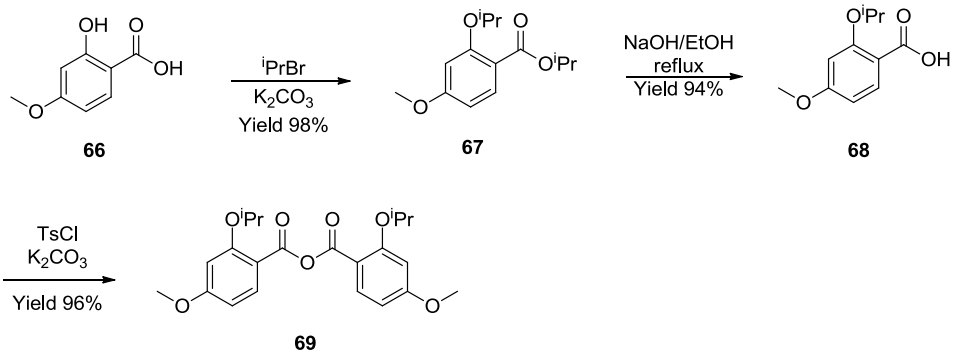

66 **67** **68**

69

Scheme 18: Preparation of anhydride **69**.

An alternative way to synthetize **69** was using the benzoic anhydride, in absence of solvents with acyl chloride and sodium 2-isopropoxy-4-methoxy benzoic salt in presence of DABCO (1,4-diazobicyclo[2.2.2]octane). But this procedure is been set aside because of low yields and the high numbers of steps.

3.2.7 Reaction of asymmetric acylation of *meso*-diamine **46** through DMAP-thiourea co-catalysis

The desymmetrization of *meso*-diamine **46**, through the co-catalysis between DMAP thiourea **cat-1** as HB catalyst, is an asymmetric acylation with 2-isopropoxy-4-methoxy benzoic anhydride **69**.

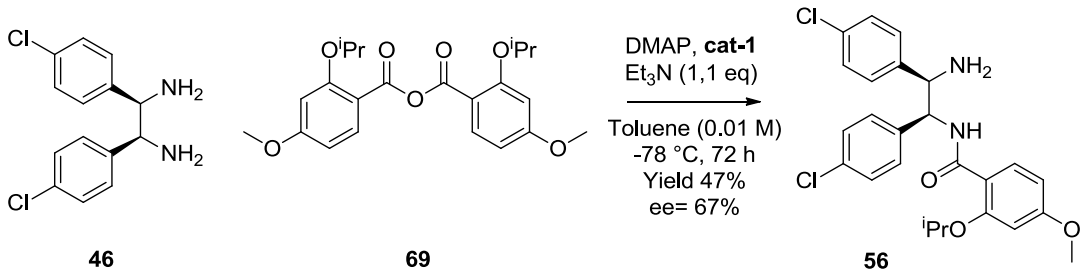

46 **69** **56**

Scheme 19: Asymmetric acylation of *meso*-diamine.

The hypothesis of the desymmetrization mechanism provides the equilibrium between the acylation of DMAP and the N-acyl pyridinium cation, that gives the achiral ionic couple **70**. After adding **cat-1** a second equilibrium is formed, that gives *in situ* the chiral ionic couple **71** with benzoate anion (scheme 20). The complex **71** has a steric hindrance that permits that the approach to the *meso*-diamine **46** comes preferably from only one side and the nucleophile attack to the carbonyl of N-acyl pyridinium happens from only one amine group of **46**. The fact that there is a discrimination of $-NH_2$ groups allows to obtain an enantiomeric enriched mixture of **56**.

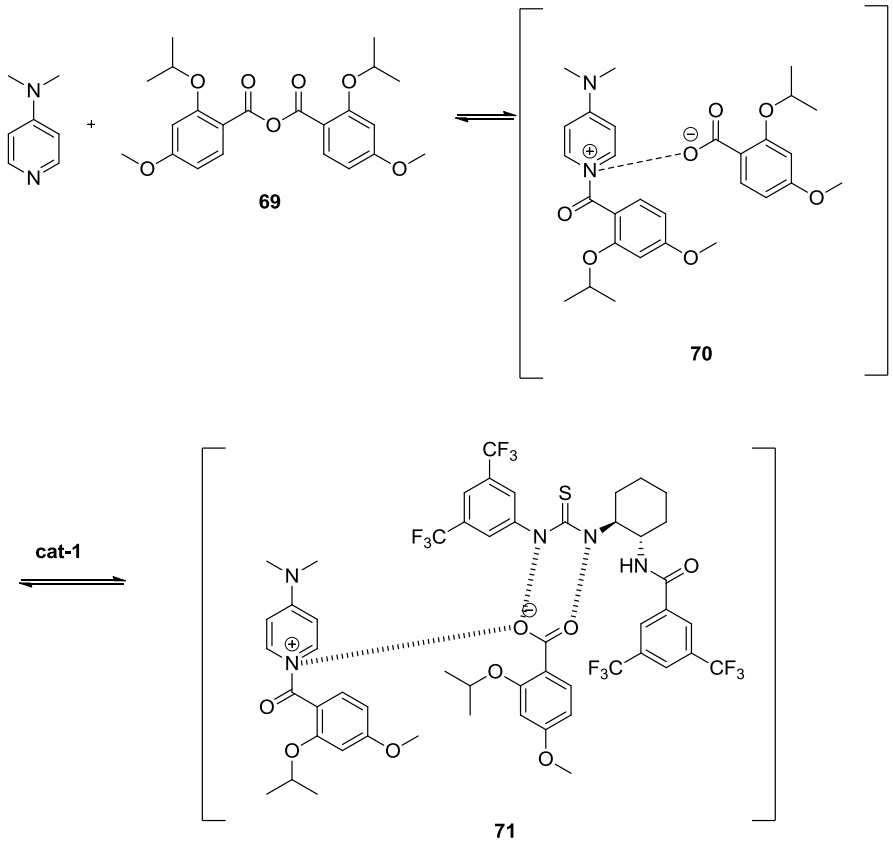

Scheme 20: Hypothesis of the mechanism.

The conditions used as first were the same of the Seidel and coworkers protocol[48] .

This one provides: 1) the anhydride **69** reacts with DMAP in toluene at -78°C with molecular sieves MS-4Å for 15 minutes; 2) adding amide-thiourea **cat-1** in catalytic quantities (10%) in toluene and after 15 minutes adding diamine **46**; 3) after 1h, to add TEA and to leave stirring at -78°C until the anhydride disappeared.

The yield of this procedure was very low and so it was necessary to optimize the reaction conditions, keeping in mind the mechanism that determines the selectivity. So, different parameters for the conditions are been studied, to improve the yield and the enantiomeric excess:

- Temperature;
- Time of reaction (when and how to add reagents);
- Quantity of DMAP and **cat-1**;
- The concentration.

Temperature

Working at room temperature the reaction, after adding all the reagents, the enantiomeric excess was 3% (entry 1, table 1). Increasing the catalytic quantity from 10% to 20% good

selectivity is been reached (entry 2, table 1). That probably means that the existence of a competition between the enantioselective way, having as intermediate **71**, and the non enantioselective way, at room temperature, the first one is in majority.
This hypothesis is confirmed by the background reaction between **69** and one equivalent of **46** in absence of DMAP and thiourea **cat-1** at rt. In these conditions the racemic product (± **56**) is obtained in 30 minutes with a yield of 46% (entry 3, table 1). The anhydride **69**, then, at room temperature shows a high reactivity to **46**.

Time of reaction

Using benzoic anhydride as substrate, the concentrations of the equilibrium between DMAP and N-acyl pyridinium salt are reached in 15 minutes at -78°C. But, verifying through mass spectrometry, the required time to obtain the intermediate **70**, with the anhydride **69**, is longer: the best results obtained were leaving stirring at rt **69** and DMAP for 18 hours, before to add thiourea and diamine (entry 7, table1).
From these data it can be explained that the speed of the equilibrium of DMAP acylated is highly influenced by the acylating agent, so the time for the formation of the ionic couple conditions the enantiomeric excess. Seen the high reactivity of anhydride **69**, if the *meso*-diamine **46** is added before the formation of the equilibrium reported in the scheme 20, the reaction proceeds through the non enantioselective pathway, that doesn't give the ee%.
Another important aspect about the enantioselectivity is how the *meso*-diamine **46** is added. If it is added in toluene to the reaction mixture, drop by drop, instead of a fast addition , the equilibrium to give **71** is favored, and so the enantioselectivity is improved.
For this reason the reaction time among anhydride **69**, DMAP and **cat-1** was increased to 5h at -78°C (entry 9, table 1). The overall reaction time necessary to obtain good selectivity and conversion of the anhydride **69** is more compared the one reported for the benzoic anhydride[48]: in the first case it was necessary to leave the reaction stirring for 3 days at -78°C, in the second one just 2 hours.

Catalytic quantity

To increase the ee of the amino-amide **56**, it was necessary to enhance the quantities of DMAP and thiourea from a catalytic quantity (entry 1 and 2, table 1) passing through sub-stoichiometric quantities (entry 4 and 5, table 1) to stoichiometric ones (entry 6 and 7, table 1). This is explained from the fact that on contrary of when it is used the benzoic anhydride, during the reaction with **69**, the DMAP-thiourea binomial, that permits the catalysis, doesn't happen and so there is no a catalytic cycle.

On the other hand, an excess of **cat-1** and DMAP doesn't improve the enantioselectivity either (entry 8 and 9, table 1).

Concentration

If the reaction mixture is diluted until a concentration 0,01 M, compared to the *meso*-diamine and anhydride, ee% values increase (entry 6 and 7, table 1).

ENTRY	DMAP and Cat. %	TIME	TEMPERATURE	YIELD	ee%
1	10%	15 min 21 h	-78°C -78°C – r.t.	35%	3%
2	20%	15 min 18 h	r.t. -78°C	18%	4%
3	None	/ 1 h	 r.t.	46%	0%
4	90%	3,5 h 18 h	r.t. -78°C	45%	38%
5	90%	3,5 h 72 h	r.t. -78°C – r.t.	45%	30%
6	100%[**]	4 h 72 h	r.t. -78°C	44%	58%
7	130%[§§]	18 h 72 h	r.t. -78°C	47%	67%
8	150%[ôô]	18 h 1 h 42,5 h	r.t. -78°C -78°C	47%	38%
9	200%[##]	27 h 5 h 27 h	r.t. -78°C -78°C	60%	44%

Table 1: Studies of different conditions to prepare compound **56**.

[**]Concentration *meso*-diamine and anhydride at 0,01M

[§§]Concentration *meso*-diamine and anhydride at 0,01M, 1.5 eq. DMAP and 1.3 eq. **cat-1**. Addition *meso*-diamine in 1h

[°°] Addition *meso*-diamine in 5 h

[##] Addition *meso*-diamine after 5h of reaction among anhydride, DMAP, **cat-1**. 2.2 eq. TEA.

3.2.8 *cis*-imidazoline ring formation

The final steps to synthetize (-)-Nutlin-3 include the condensation of 2-piperazinone and the closing *cis*-imidazoline ring.

The condensation reaction provides the intermediate **72** formation from a reaction with CDI, then the addition of 2-piperazinone pushes the reaction to completion, meaning having only the product **57** (yield 94%). This compound is a white solid and it doesn't need to be purify by chromatography.

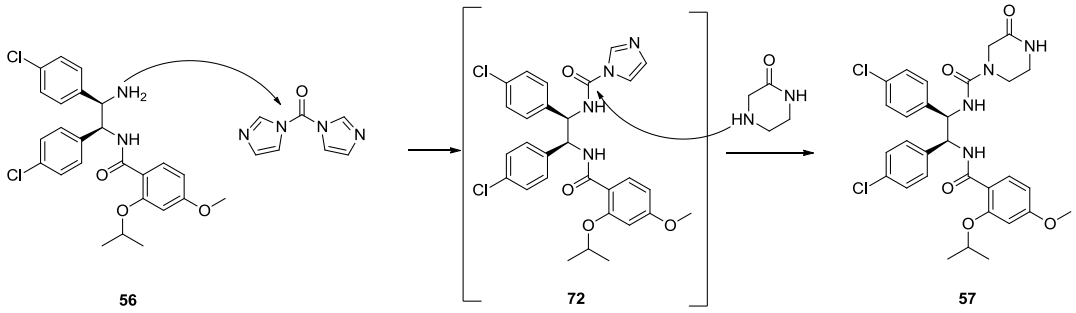

Scheme 21: Condensation mechanism.

The amide-urea **57** closing through dehydration was studied by Hendrickson and then by Johnston. The procedure requires the use of trifluoromethanesulfonic anhydride (Tf_2O) and 3 equivalents of triphenylphosphine oxide (PPO) to form *in situ* Hendrickson's reagent (figure 22), very efficient as dehydrating agent.

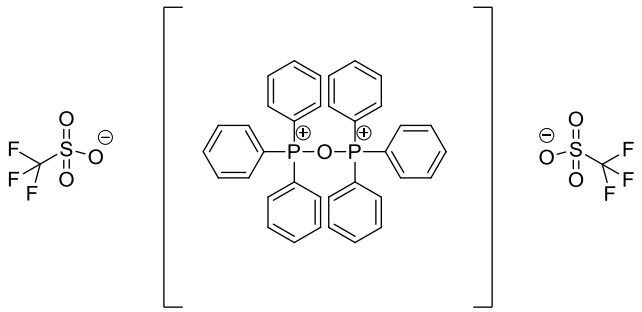

Figure 22: Hendrickson's reagent structure.

These conditions, as already said, are not advantageous because of the difficulty on eliminating the triphenylphosphine oxide. But anyway, with 4 equivalents of PPO and 4 equivalents of Tf_2O in CH_2Cl_2 at 0°C for 30 minutes, it is obtained the compound **57** with a 80% yield (Scheme 22).

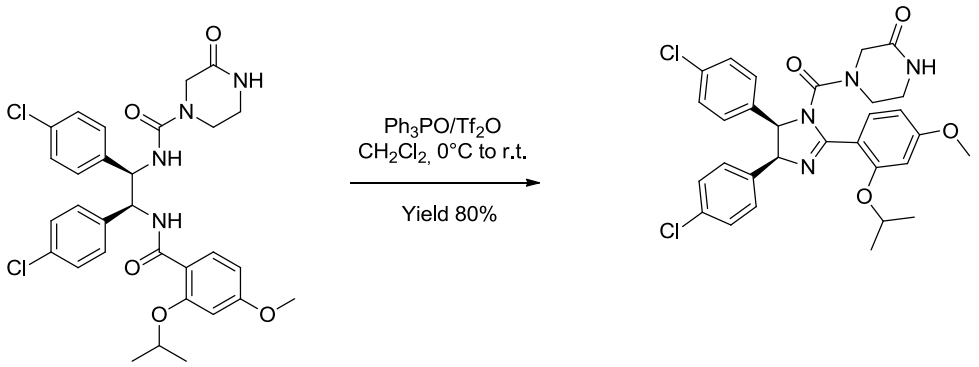

57 58

Scheme 22: Closing ring reaction.

Through HMBC analysis it was possible to establish that the isomer **73** wasn't obtained (Figure 23).

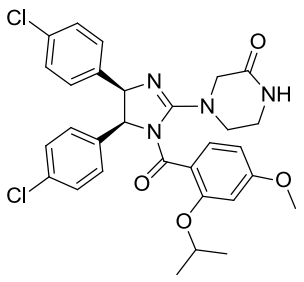

73

Figure 23: Not observed isomer of **58** structure**.**

The dehydration with Hendrickson's reagent was used also to the substrate **56** with a yield of 83%. The next acylation of imidazoline nitrogen of **51** with CDI, didn't bring the expected results. So it was necessary to use the triphosgene. Either way, the starting reagent was still present by mass spectrometry analysis.

Another way to cyclize the compound **56** was using *para*-toluene sulfonic acid and pyridine, as reported in literature[38].

Unfortunately, the yields, even increasing the number of the equivalents, were up to 17%.

So, we decided to abandon these procedures.

3.2.9 Synthesis of HB-catalyst, thiourea **cat-1**

The amide-thiourea **cat-1** was prepared in three steps without difficulties.

The commercial starting materials used are: 3,5-trifluoromethylbenzoic acid **74**, *trans*-cyclohexyl-diamine **75** and thiocyanate **76**.

As first step the anhydride-OSu **77** was prepared, starting from the acid **74** with an equivalent of N-hydroxy succinimide in dioxane, in presence of DCC (Dicyclohexylcarbodiimide)[47].

After purification through chromatography coloumn it was obtained a white solid with a yield of 91%. (scheme 23)

The reaction between the diamine **75** and thiocyanate **76** gave the aminothiourea **78** with 85% yield (scheme 23).

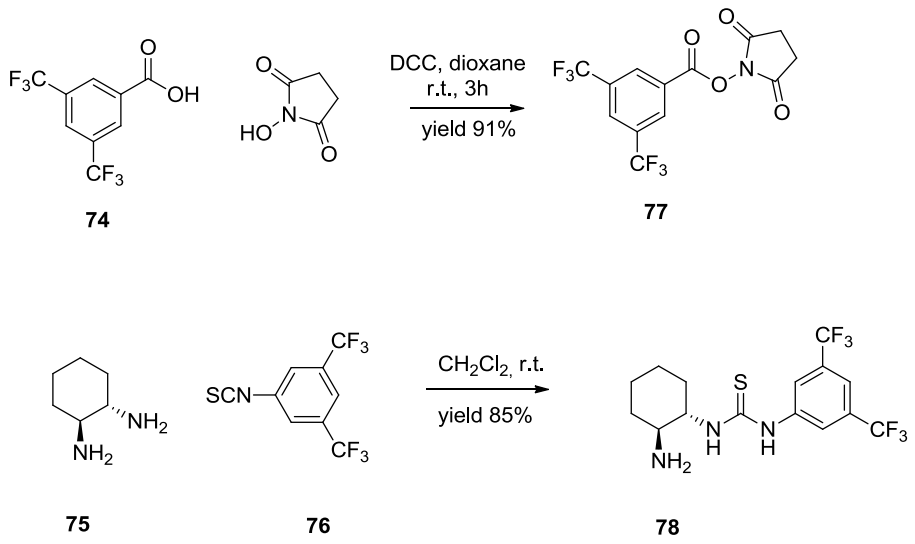

Scheme 23: Synthesis of HB-catalyst **cat-1**.

At the end, the conditions of the last step to synthetize **cat-1**, were the same reported by Siedel. The yield obtained is 72% (scheme 24).

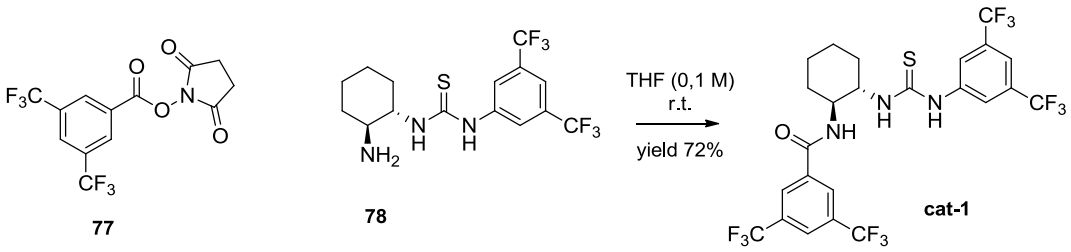

Scheme 24: Last step of **cat-1** synthesis.

3.3 Conclusions and results

The results described in this thesis permitted to develop an enantioselective synthesis with a cheap pathway and with just few number of steps and purifications of the inhibitor (-)-Nutlin-3.

The reaction of desymmetrization of the *meso*-diamine **46** showed to be very sensitive to the substrate used; the 2-isopropoxy-4-methoxy benzoic anhydride **69** synthesis was optimized to give enantiomeric excesses of 67% and yield 47%.

This type of approach can be used for analogs of (-)-Nutlin-3, after a similar study to optimize the conditions and the right substrates.

Our product was then biologically tested at the Dept. of Morphology, Surgery and Experimental Medicine at University of Ferrara.

In order to functionally validate scalemic-Nutlin, it was performed a combination of biological assays aimed at assessing its ability to activate p53 pathway[50]. For this purpose scalemic-Nutlin was comparatively tested on $p53^{wild\_type}$ (EHEB and JVM-2) as well as on $p53^{mutated/deleted}$ (BJAB and HL-60) leukemic cell lines used as control of specificity. In parallel, cell cultures were exposed to commercial Nutlin-3 used as positive control and for comparison. As shown in Figure 24, treatment with Nutlin-3 and scalemic-Nutlin, used in the range of 1–10 mM for up to 48 hours, exhibited a comparable dose-dependent cytotoxicity resulting in a significant reduction of cell viability (Figure 24A) coupled to apoptosis induction (Figure 24B) and cell cycle arrest (Figure 24C) specifically in $p53^{wild\_type}$ but not in $p53^{mutated/deleted}$ cell lines. Consistently with the observed biological effects, molecular analysis of p53 pathway by protein (Western Blot) and RNA (quantitative RT-PCR) documented accumulation of p53 and transcriptional induction of two p53 transcriptional canonical targets, involved in promoting cell cycle arrest (p21) and modulation of apoptosis (MDM2), in response to treatment with scalemic-Nutlin (Figure 24D). Moreover, as shown in Figure 23, the effects induced by scalemic-Nutlin was equally effective as commercial Nutlin-3.

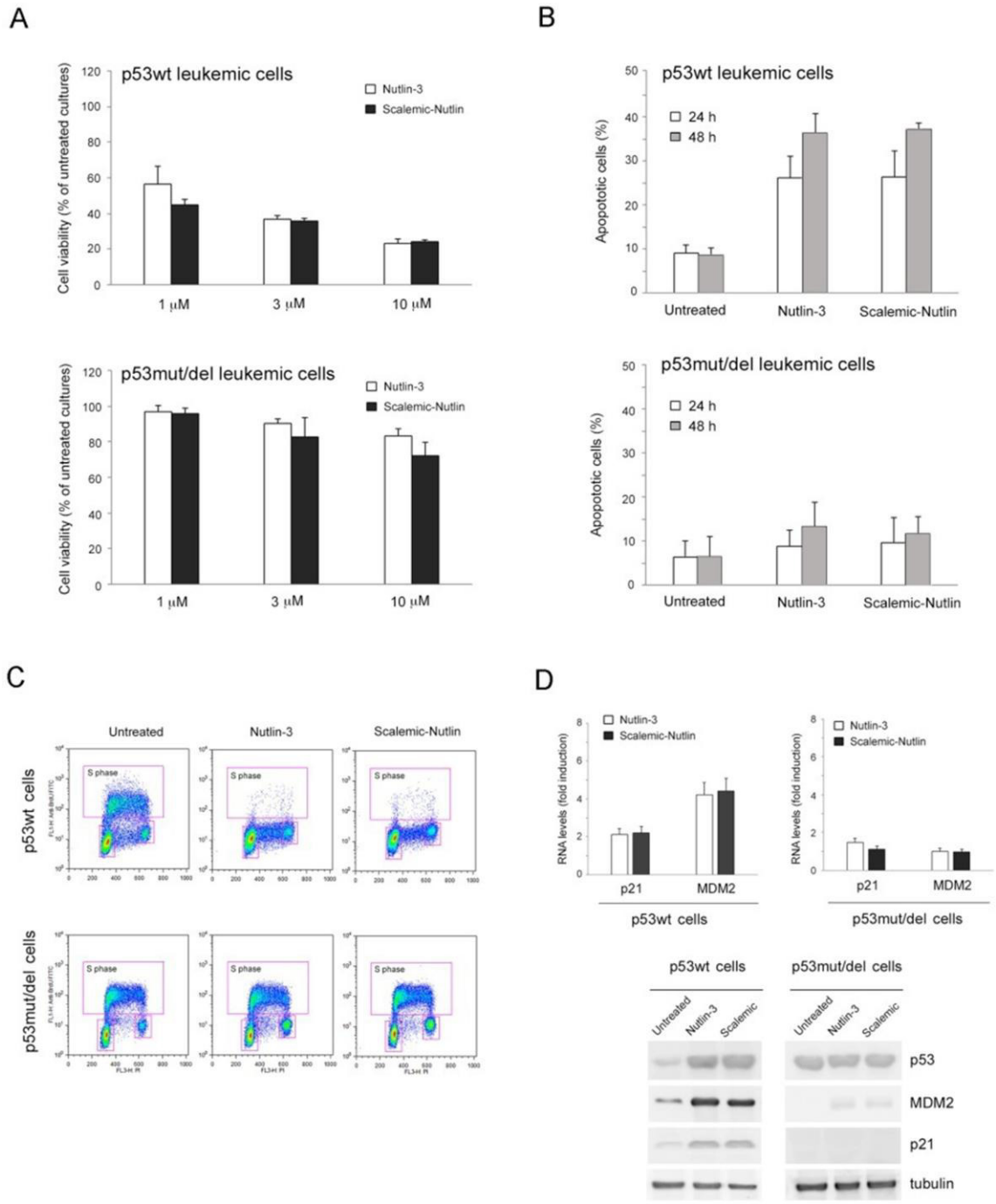

Figure 24: biological assays of scalemic Nutlin-3.

In conclusion, our biological tests established that (-)-Nutlin-3 we synthetized is as effective as the commercial eutomer in activating the p53 pathway[50].

4 MAGMAS Inhibitors

4.1 Aim and objectives

As reported in introduction section, Magmas complex, located in the mitochondrial inner membrane, is essential for the mitochondrial survival; its inhibition causes cell death.

Once the structure of the protein complex Tim14-Tim16 was confirmed by X-Ray, Prof. Jubinsky[51] and his team synthetized a small chemical library, including substituted oxazines, boronic acids, chromenes and guanidine as pharmacophores (figure 25).

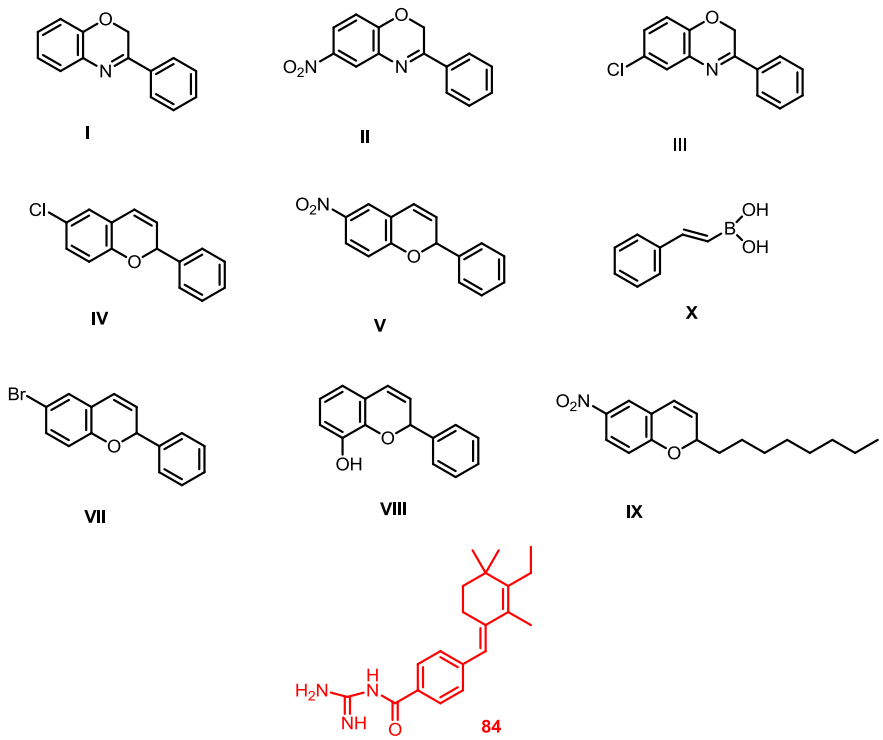

Figure 25: Small chemical library by Jubinsky group.

On the basis of published analysis by the American team, the compound **84** seems to be a good Magmas inhibitor, because the concentration of 10 μM is able to inhibit completely the cell proliferation.

Therefore, I synthetized the compound **84** following the Jubinsky procedure, developing a mechanistic study for the phosphonium salt formation, a synthetic intermediate, analyzing it using NMR techniques; a SAR study about the lead compound has also been carried out, to obtain analogs to be evaluated in biological tests.

4.2 Discussion

1.1.1 Synthesis of compound **84** (*(E)-N-carbamimidoyl-4-((3-ethyl-2,4,4-trimethylcyclohex-2-en-1-ylidene)methyl)benzamide)*

In *Bioorganic & Medicinal Chemistry letters* (2011) Paul T. Jubinsky[51] reported the synthesis of the compound **84**, potentially interesting in pharmaceutical field.

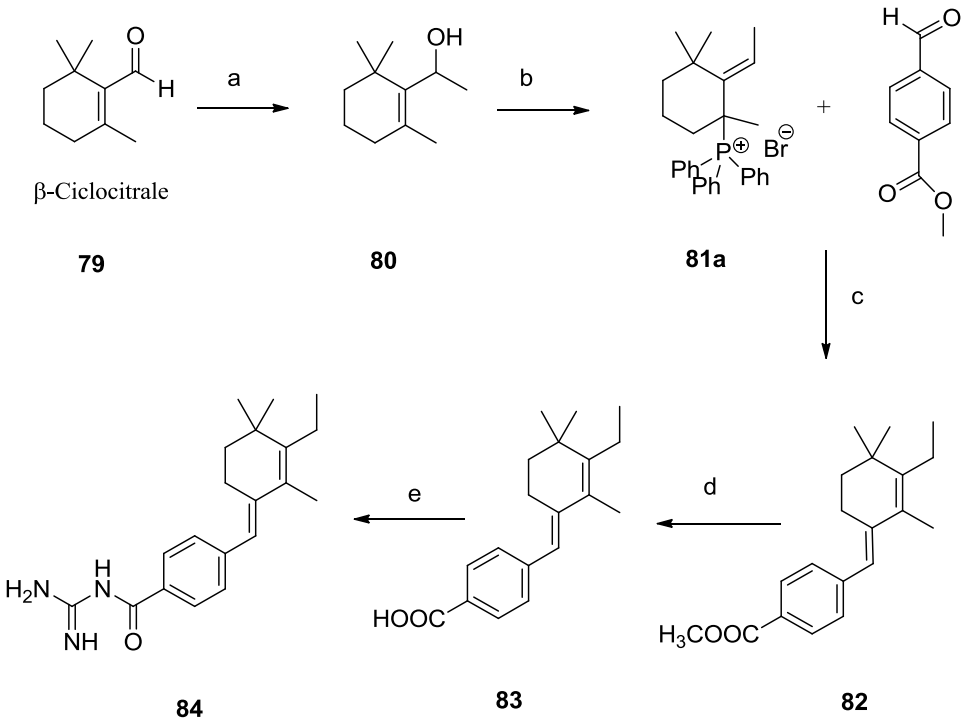

Scheme 25: Synthesis of compound **84**
Reaction conditions: a) CH_3MgBr, THF, 0°C, 72%; b) PPh_3*HBr, CH_3OH, 96%;
c) BuLi, Et_2O, Methyl 4-formylbenzoate, 27%; d) NaOH, EtOH, 80%; e) CDI, DMF, Guanidine 90%.

The first step is an alkylation of commercially available β-Cyclocitral **79**, to give the allylic alcohol **80**, using methylmagnesim bromide. The preparation of phosphonium salt **81** is made in MeOH at r.t. with an equivalent of PPh_3 hydrobromide.

The synthesis provides a Wittig reaction, starting from phosphonium salt **81**, in THF, with n-BuLi and Methyl-4-formylbenzoate. After the formation of phosphonium ylide **D** at r.t., the reaction is conducted at -78°C to add the aldehyde drop by drop. The reaction proceeds with the formation of olefin **82**, passing through the oxaphosphetane intermediate, with elimination of triphenylphosphine oxide. The Wittig product **82**, isolated and analyzed by NMR is obtained with a 29% yield (scheme 26).

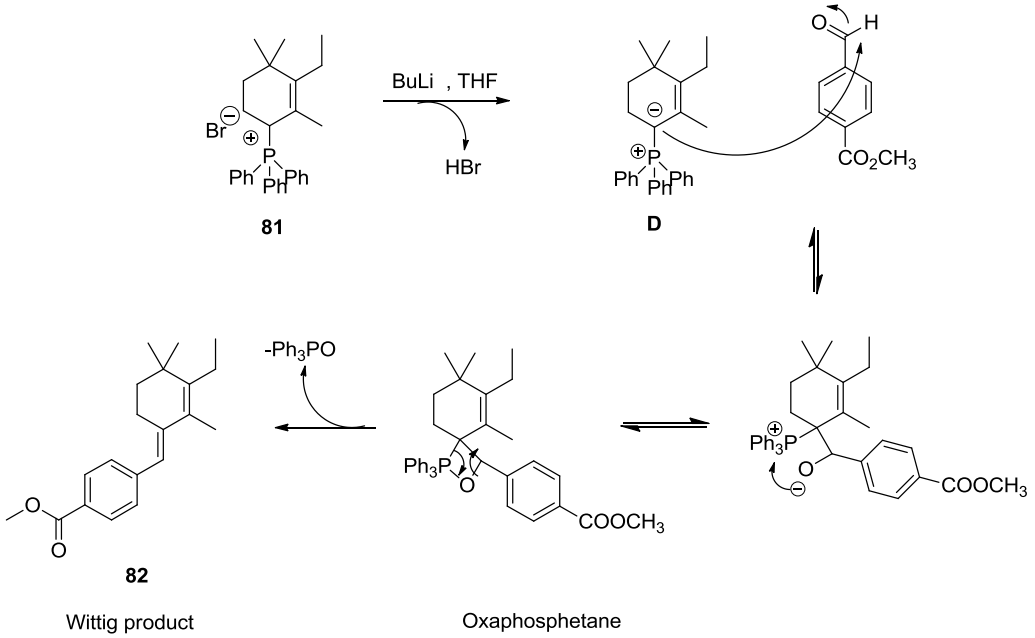

Scheme 26: Wittig reaction mechanism.

The next step is a reaction with the Wittig product in MeOH and NaOH added drop by drop. Then the acid treatment of the sodium salt formed and the crystallization with diethyl ether, it is obtained the intermediate **83** and it was possible to analyze it by X-Ray.

The final product **84** it was obtained with a condensation between the acid **83** and the guanidine hydrochloride, previously activation of the acid with CDI and deprotonation of the amine group using ^{t}BuOK. The product is characterized via NMR techniques.

4.2.2 Studies of the phosphonium salt

The synthetic scheme by Jubinsky and co-workers showed a formation of a strange phosphonium salt **81a**, that has a phosphonium atom bound to a quaternary carbon, so, it is devoid of an acid proton that allows the formation of phosphonium ylide. The reaction mechanism reported in literature[52] is this:

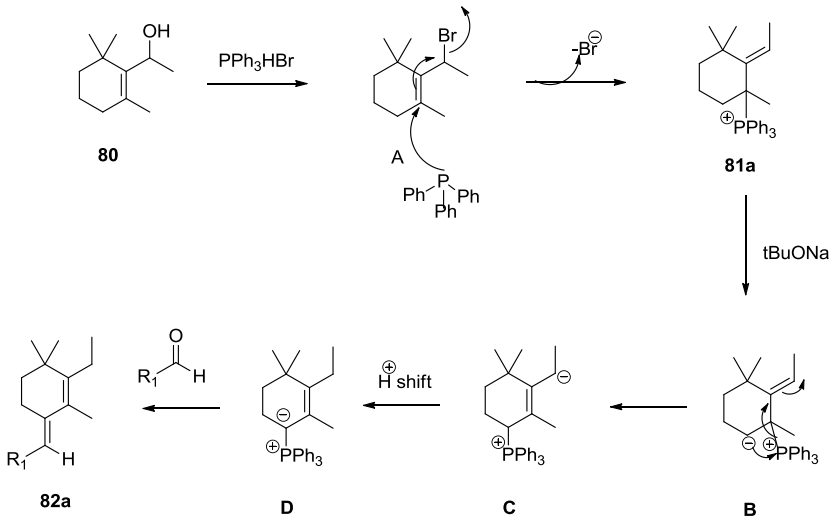

Scheme 27: Reaction mechanism by Bhaskar Das et al.

This postulated mechanism provides the obtaining of a strange phosphonium salt **81a**, that after treatment with *n*-BuLi converts to secondary ylide **C**. This intermediate, after intramolecular H^+ shift mechanism, gives the ylide **D**, which is active to react with the aldehyde to obtain Wittig product **82a**.

To support this mechanism, the authors show the NMR spectrum of the phosphonium salt **81a** (Figure 26).

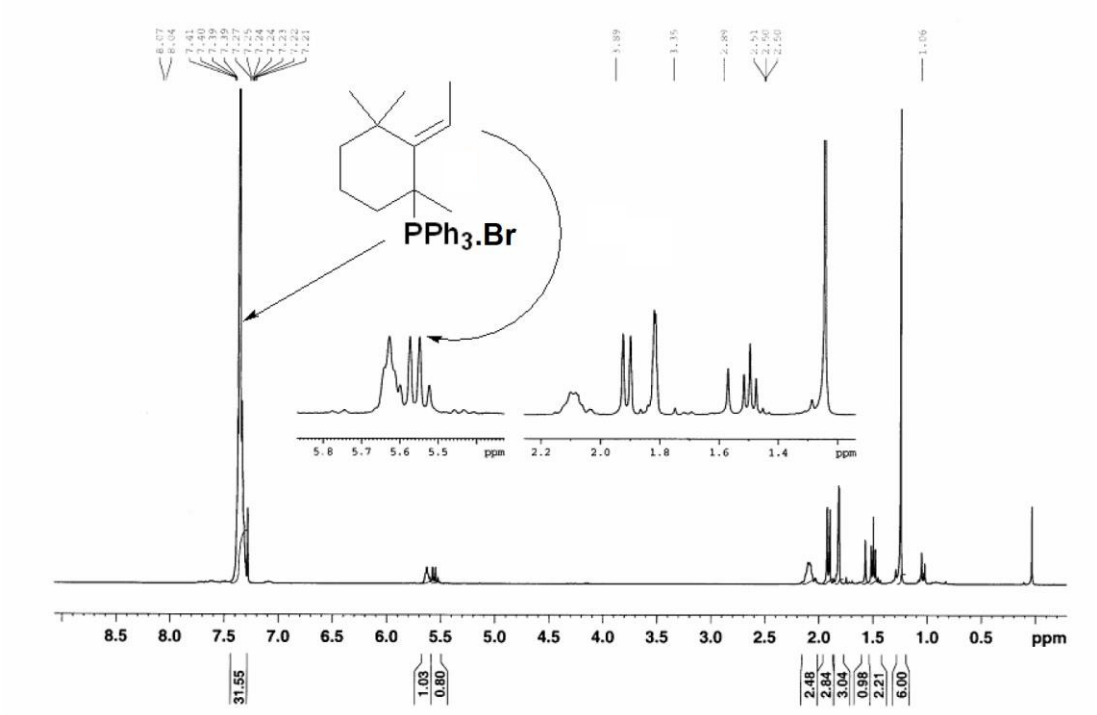

Figure 26: proton NMR of compound **81a**.

The ^{1}H spectrum shows many anomalies:

- The assignment of the chemical shift protons signals doesn't match with the signal peaks;
- The signals integration is not coherent: from the structure of **81a** should be aromatic 15H of the PPh_3 but in the spectrum there are 31H;
- The assignment of some protons is not correct: at 5.65-5.55 ppm there is a triplet that melts with a quartet; in **81a** spectrum in this area it should be the signal of one proton as a quartet. Also, in the aliphatic area between 2.5-1 ppm it is missing a signal of CH_2.

For all these incongruences, we decided to follow the procedure by them and to focus the work on the phosphonium salt formation.

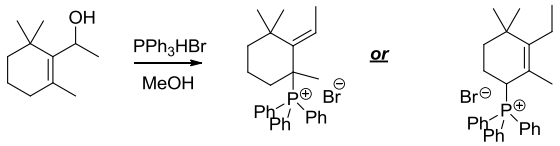

80 **81a** **81**

Scheme 28: Phosphonium salt formation.

The phosphonium salt **81** that we obtained was purified by chromatographyc coloumn and analyzed by NMR (^{1}H, ^{13}C, DEPT, g-COSY, HMQC, HMBC, NOE).

From this deep study the structure of the compound that we obtained is the **81** and not the **81a** (Figure 27).

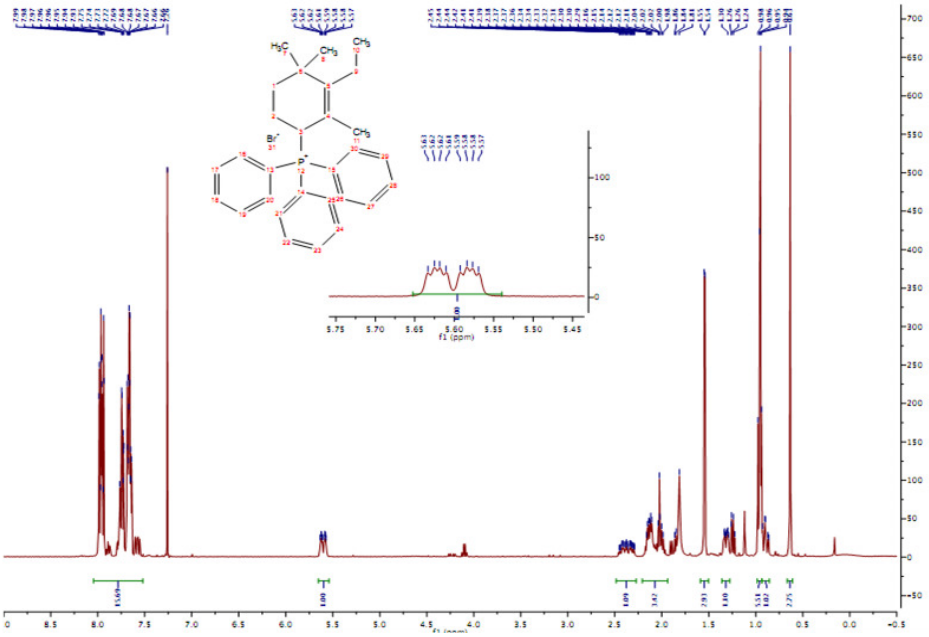

Figure 27: ^{1}H NMR of compound **81**.

To better understand the mechanism of this reaction we decided to study it step by step. The reaction needs the use of the PPh_3-HBr, for this reason we thought to reproduce an acid environment treating the allylic alcohol **80** with HBr, without phosphine (Scheme 29).

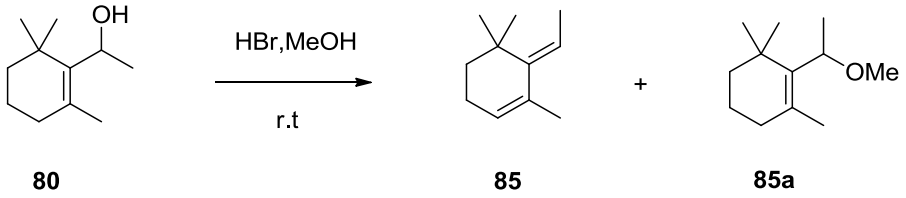

80 **85** **85a**

Scheme 29: Reaction with allylic alcohol **80**.

The secondary alcohol, in MeOH in acid conditions (HBr), protonates and loses a water molecule, generating an allylic secondary carbocation, that evolves in a diene intermediate **85**, because the reaction proceeds *via* elimination (E_1) and part of the product is from the nucleophile substitution (SN_1) **85a**. Using ^{t}BuOH as solvent (scheme 30), it was possible to complete the conversion of the product **80** to **85** only, through an elimination E_1 reaction.

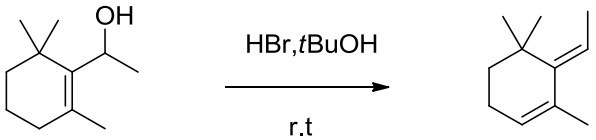

80 **85**

Scheme 30: Conversion to diene **85** using tBuOH.

Analyzing and comparing by NMR spectroscopy the compound **85** and the phosphonium salt **81a**, it can be seen that the two spectra are the same, besides the aromatic proton signals of PPh_3, probably present as impurity in the American compound.

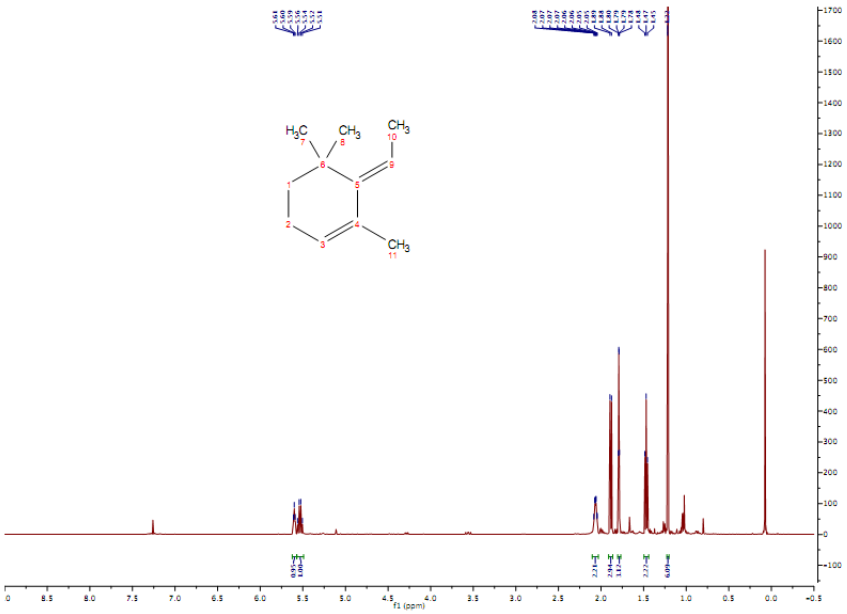

Figure 28: ^{1}H NMR of diene **85**.

The diene intermediate **85**, purified, reacts with PPh_3HBr in MeOH and it is obtained the phosphonium salt **81** (Scheme 31) that has a NMR spectrum as the product from the allylic alcohol **80** reaction with PPh_3HBr.

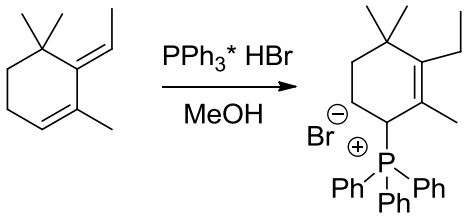

85 **81**

Scheme 31: Reaction between diene and PPh_3HBr.

On the basis of these evidences, the hypothetic mechanism is this:

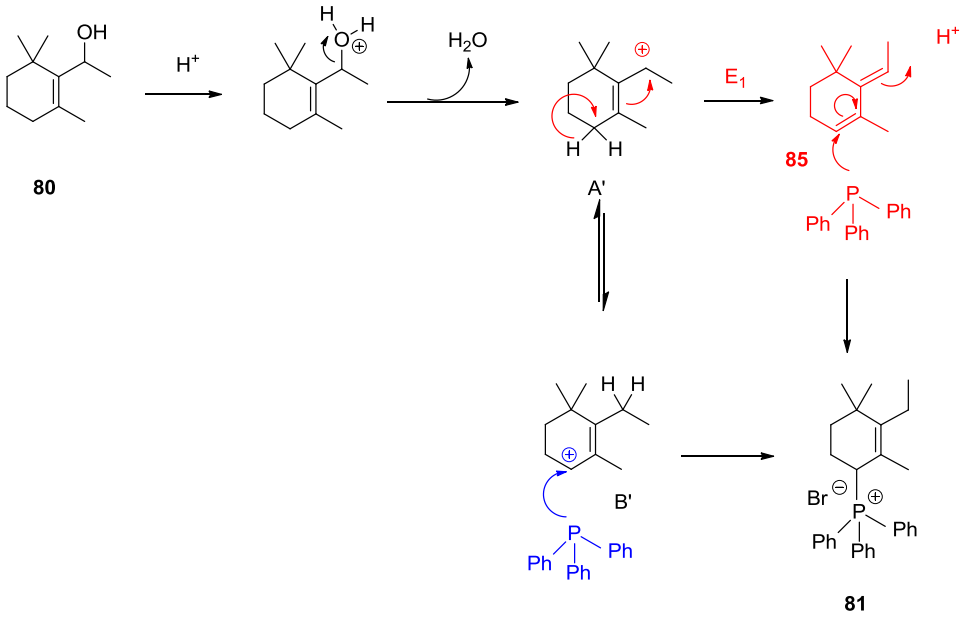

Scheme 32: Hypothetic mechanism of **81**.

In acid environment the allylic alcohol **80** is protonated with next loss of water molecule and formation of carbocation; so, three different species can exist: the exocyclic secondary carbocation **A'**, the endocyclic secondary carbocation **B'** and the diene **85**.

A' evolves to diene **85** through an elimination mechanism E_1 and in presence of triphenylphosphine there is an addition to the double bond to give the phosphonium salt **81**.

The endocyclic secondary carbocation **B',** in tautomeric equilibrium with **A'**, after the nucleophilic attack by the PPh_3, it gives the phosphonium salt **81**, via nucleophile substitution SN_1.

The phosphonium salt **81** is a classic phosphonium salt, in which the phosphorus atom is bound to the carbon that has an acid proton able to give the formation of ylide, after basic treatment.

4.2.3 SAR study about MAGMAS inhibitor

The structure published by Jubinsky could be divided in three main parts:

- Cyclohexene nucleus
- Benzoyl scaffold through a double bond
- A guanidine function

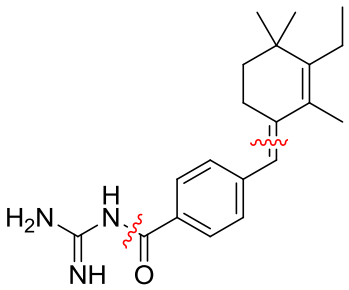

84

Figure 29: Main parts of the structure **84**.

The compound **84** seems to bind to the interface of dimers Tim14 and Tim16 through hydrophobic interactions both with Tim 14 (Leu^{100}, Lys^{111}, Leu^{114}, Gln^{115}, Thr^{120}) and with Tim16 (Phe^{95}) and interactions as H-bond only with the monomer Tim14 through residues Glu^{121} and Lys^{168}.

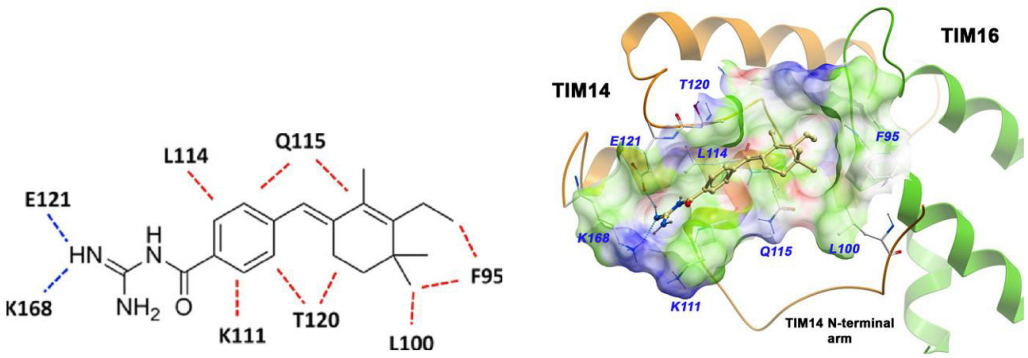

Figure 30: Compound 84 interactions with Tim14-Tim16.

This molecule with these interactions causes an inhibition to the cell growth.

For this reason we decided to synthetize different analogues of this compound to better understand the various functionalities.

From molecular modelling studies it seems necessary the presence of the guanidine to direct this compound to the interface. So, we thought to synthetize molecules that don't have the guanidine group, to see an expected different interaction.

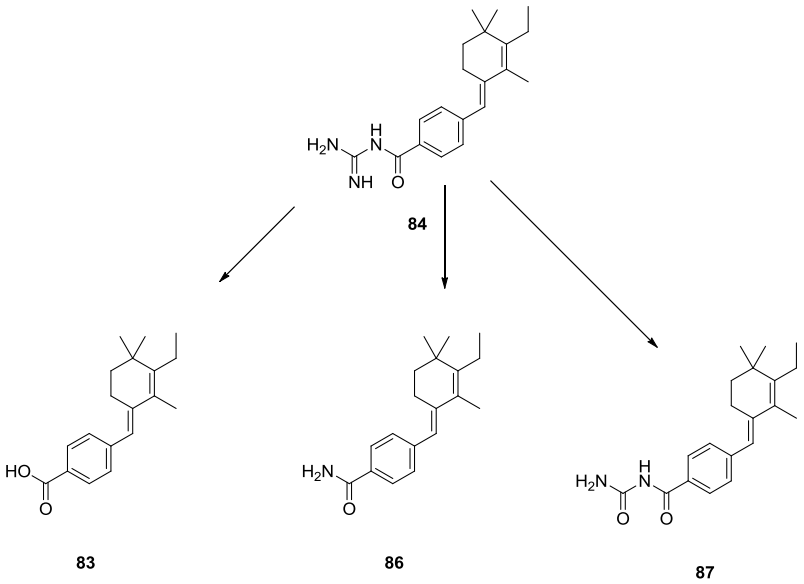

Scheme 33: Modification at the guanidine group.

1. The precursor **83** of the final molecule **84** was taken in consideration. It was characterized by spectroscopy and also, obtaining the crystals of this compound, it was possible to do a X-Rays analysis in collaboration with Prof. Bertolasi of the Department of Chemistry of the University of Ferrara.

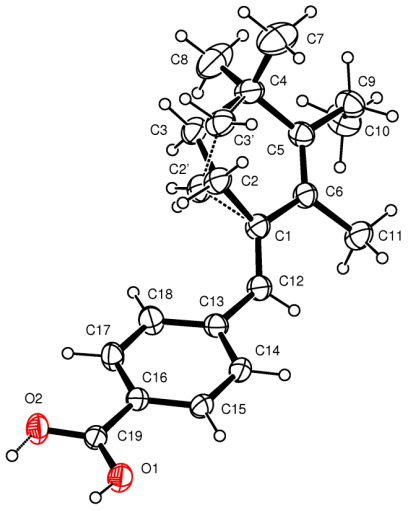

Figure 31: X-Rays of compound **83**.

The crystals data about this compound are collected at room temperature (T=295 K) using a diffractometer Nonius Kappa CCD with radiation Mo-Kα monocromatized through a grafite crystal and corrected for Lorentz effects and polarization.

The X-Rays structure permitted to confirm the result of NOE NMR analysis: the conformation of the esocyclic double bond is only *trans*.

2. It was synthetized also the compound **86** that it could be seen as the semplification of the guanidine derivative, obtained from the activation of the acid **83** with CDI and reacting with NH_4OH conc. (Scheme 34).

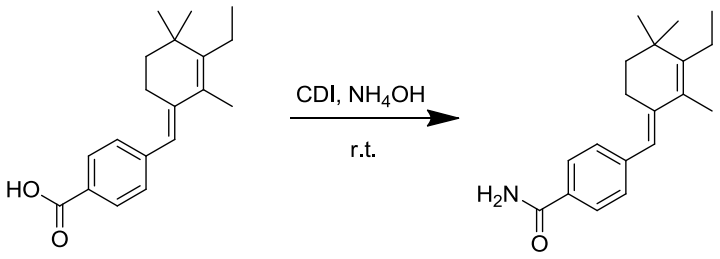

83 **86**

Scheme 34: synthesis of compound **86**.

3. We also thought that the compound **84** could have a metabolite as a ureic derivative as **87**. So the synthesis of this compound is from the acid **83** as starting material and the urea commercially available; the reaction was in toluene, using as catalyst the 3,4,5-trifluoromethylphenyl boronic acid, known as selective converter of acid function to urea derivatives[53] (scheme 35).

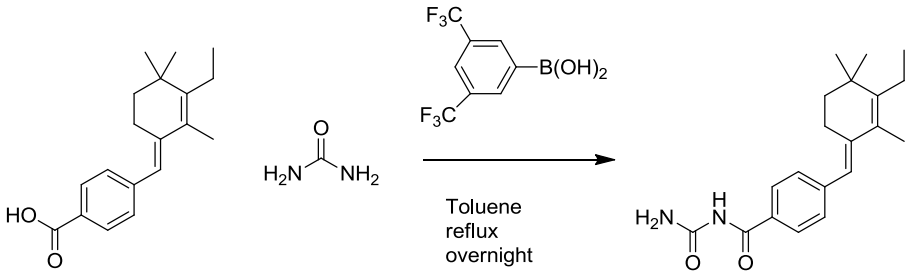

83 **87**

Scheme 35: Synthesis of compound **87**.

The high planarity of this structure (highlighted in red, figure 31), supported by X-Rays, seems to have an important rule to positionate the compound to the complex interface between Tim14 and Tim16.

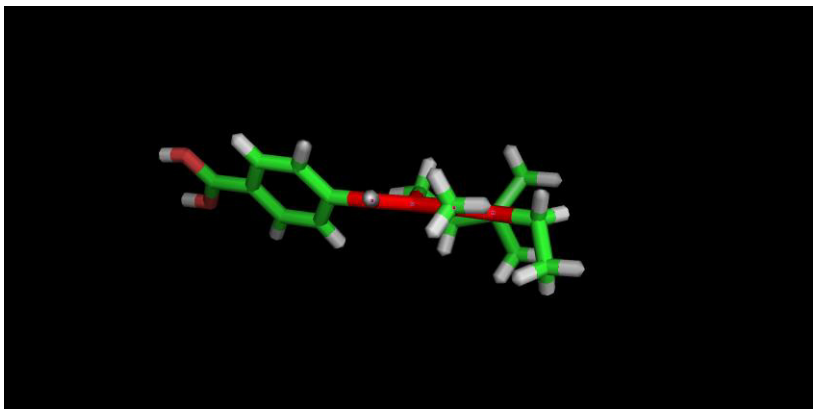

Figure 32: X-Rays structure of compound **87**.

Another study was to reduce selectively one double bond or both two double bonds, to increase the mobility of the conformation of the structure and evaluate the effects in biological activity.

The hydrogenation of double bonds was a catalytic process, using EtOH/AcOEt (50:50) with C/Pd 10% at atmospheric pressure and room temperature, gave a mixture of compounds **88** and **89**, separated then by preparative HPLC.

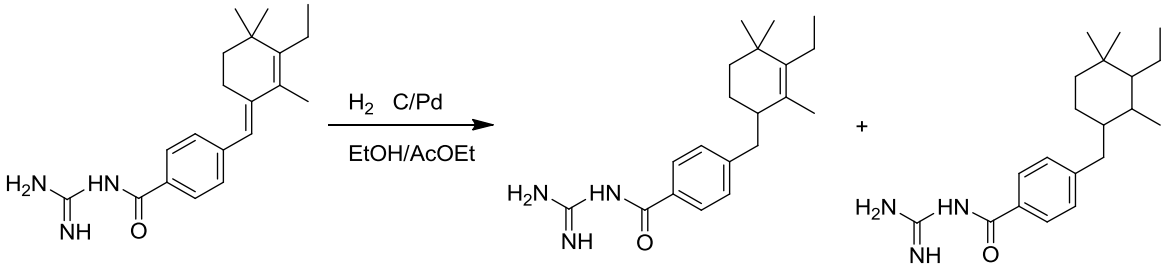

84 **88** **89**

Scheme 36: Reduction of double bonds.

Study abroad – USA project

4.2.4 2-amino-4(3H)-quinazolinone/2-aminoquinazoline derivatives as Magmas inhibitors analog

During my PhD I have been in United States, specifically in Kansas City (MO), working for some months in one part of the project Magmas, at Prof. Bhaskar Das laboratories in the VA hospital.

During these months I could focus myself in an interesting synthesis of aminoquinazoline derivatives as potential analogs of Magmas inhibitors. Starting from evidences in literature[54], quinazolines have many biological activities[55], as antibacterial, antifungal, antiinflammatory, cytotoxic, antihypertensive, anti-HIV, antioxidant, analgesic, anticonvulsivant, antimalarial and antitumoral, in particular in prostate cancer[56].

On this last one I focused my interest, because, as mentioned before, Magmas overexpression is verified in prostate cancer, so using the quinazoline biological properties mixed with the main important function of Magmas inhibitors as the guanidine in the structure seemed to be a good idea. Therefore, I decided to synthetize a small chemical library of amino-quinazolines and amino-quinazolinones, to then evaluate the biological activity as Magmas inhibitor.

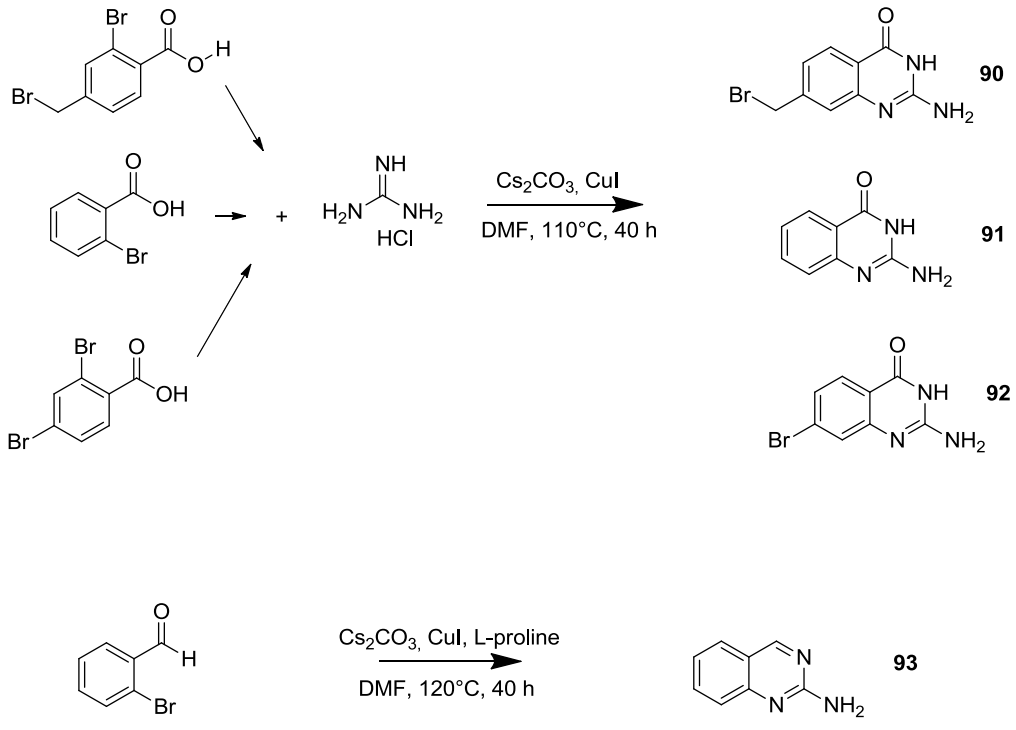

Scheme 37: Synthesis of 2-Amino-4(*3H*)-quinazolinone and 2-Aminoquinazoline Derivatives.

The common routes used are often troublesome and some starting materials are not readily available or are difficult to prepare, so it was highly desirable to develop a more convenient and efficient method.

Recently, great progress for copper-catalyzed N-arylations have been made and to synthetize these compounds I followed a procedure[55] based on copper-catalyst system. It is a simple, practical and efficient strategy for synthesis of aminoquinazolinone and aminoquinazoline derivatives.

The catalyst used was CuI and the solvent DMF in presence of the base Cs_2CO_3. It was observed that without the catalyst the reaction didn't give any target product. The yield were good, around 85% for the aminoquinazolinones and 78% for the aminoquinazolines.

The mechanism proposed for the reaction is the next:

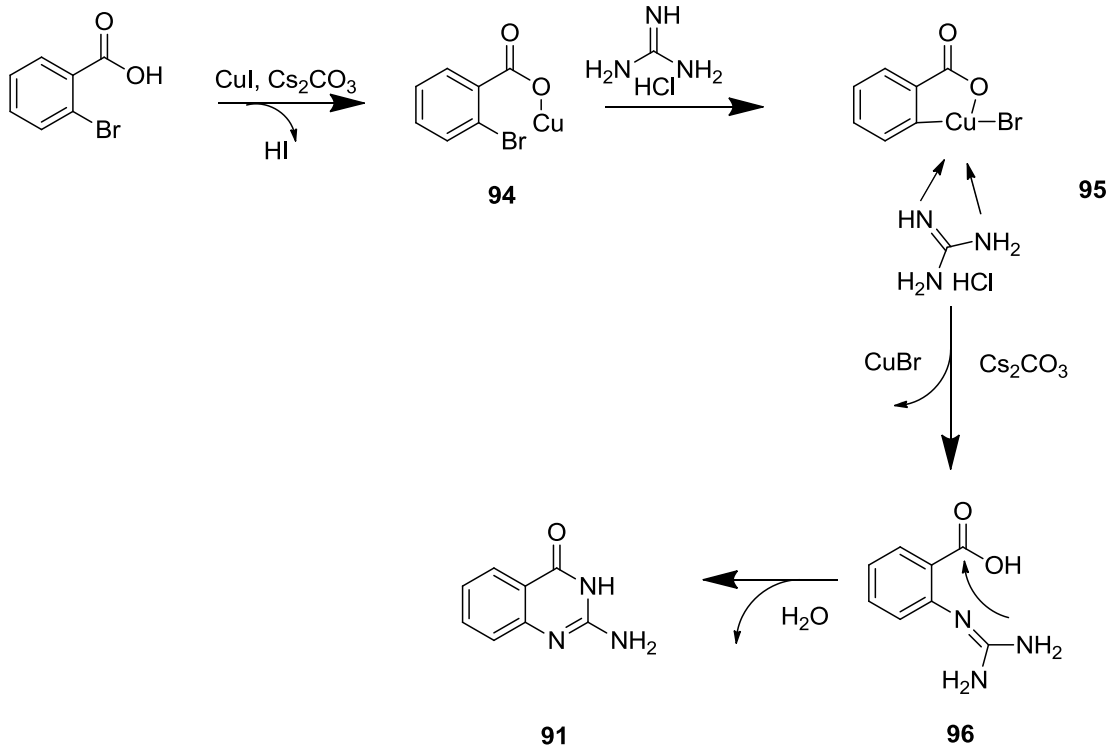

Scheme 38: Mechanism of the aminoquinazolinones, copper catalyzed.

Coordination of substituted 2-bromobenzoic acid with copper(I) iodide first forms **94** in the presence of base (Cs_2CO_3). Oxidative addition of this intermediate and a complex of copper with guanidine provides coordinate **95**, reductive elimination of **95** gives the N-arylation product **96** of guanidine, releasing copper catalyst, and coupling of the carboxyl and amino groups in **96** affords the target product **91** leaving water.

These compounds are still in biological evaluation.

4.3 Conclusions and results

The biological activity was evaluated at Prof Degli Uberti laboratories at Hospital of Cona. It was evaluated the compound **84** and at the beginning it was showed a high expression of mRNA codifying for the Magmas gene in TT cells (human cells lines of the tyroid carcinoma).

Then the expression was compared to the protein expression of Tim16.

The data showed a high expression of Tim16 in TT cells. So, TT cells represent a good cell model to study the biological effects of the Tim16 inhibitors, codifying for the Magmas gene.

The biological activity of **84** was evaluated through the cell vitality thanks to the ATPlite assay: a fluorescence assay that misures the quantity of ATP producted in the cells (graphic 2).

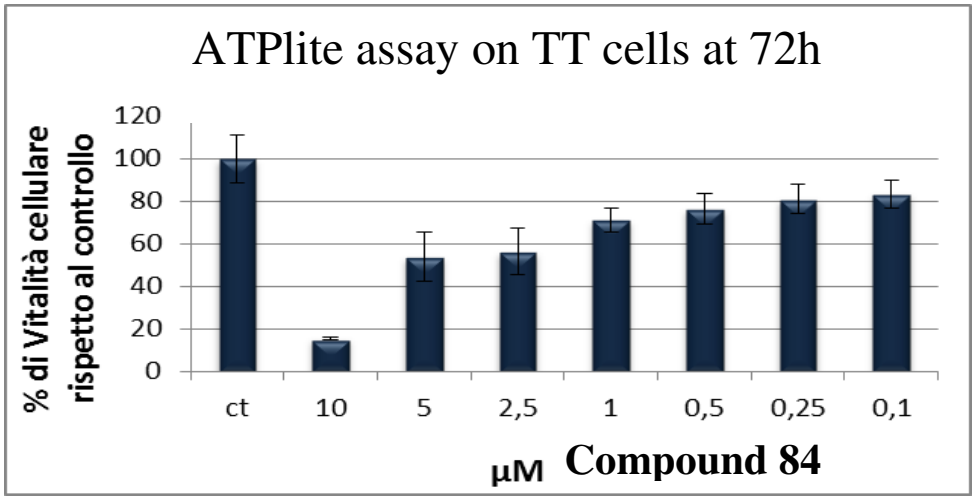

Graphic 2: ATPlite assay in TT cells.

The activation of the apoptosis has been evaluated by a Caspases 3/7 assay, also a fluorescence assay to evaluate the activation of caspases 3 and 7.

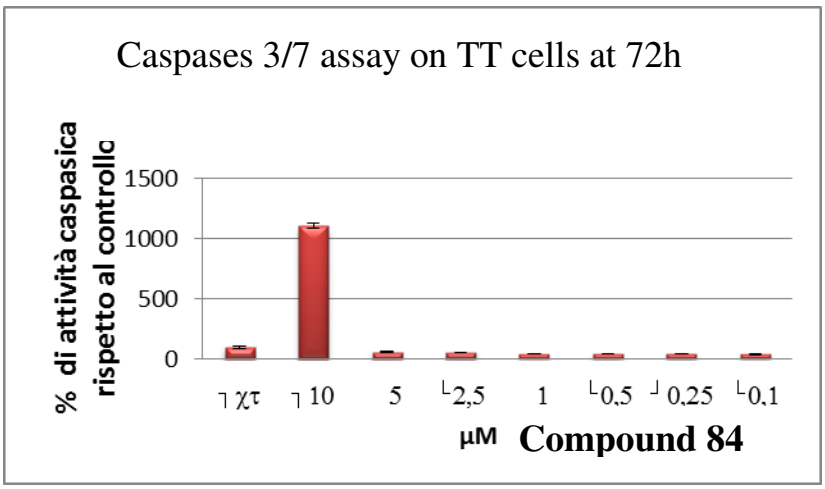

Graphic 3: Caspases 3/7 assay on TT cells.

The results show that the compound **84**, at concentration 10 μM after 72 hours of treatment, inhibits the cell vitality of 85%, this reduction is associated to the activation of caspases 3/7.

The compound **84** activates caspases 3/7 of the 900% more than the control. This result support the hypothesis that the compound **84** inhibits Tim 16 *in vivo*, in fact it was demonstrated that the Magmas overexpression protects the cells from apoptosis[57].

In conclusion, in this thesis it is proposed again the synthesis of the compound **84**, already published by Prof. Bhaskar Das and co-workers; it is a molecule with a good biological interest, because it is able to inhibit the cell growth after interaction with Magmas.

This biological effect is interesting in pharmacology field and more in oncology. In fact, it was shown that the Magmas expression is higher in tumor cells than healthy ones.

This research, in which Magmas complex is involved, opens the prospective to synthetize new analog molecules able to interact with the dimer Tim14-Tim16, arresting the cell growth in tumor cells.

Biological tests were also conducted on the compound **89** (the two double bonds are reduced).

The tests have been evaluated it and so, we can have more information about the characterization of the complex and interaction with Tim14-Tim16.

The compound was tested to see the chemioresistance getting lower, testing it with chemo drugs *in vitro* and *in vivo*. The compound should inhibit the overexpressed protein (Tim 16). Some tests were carried out: ATPlite assay, Caspases 3/7 assay, western blot, immunoprecipitation test *in vivo*.

Compound **89** has never been tested in this way and its effect on Tim16-Tim14 binding was unknown. To better understand the effects of it, the interaction of these proteins, including also mtHsp70, was investigated by co-immunoprecipitation (CoIP). This experiment was performed using the MCF7 cells, that display higher levels of Tim16, treated with the inhibitor at 5 μM concentration for 3 and 6 hours. Proteins were co-immunoprecipitated with the Tim16 antibody (Figure 33 A). Protein level quantification was performed by densitometry analysis and the results of each protein densitometry are represented in a graph (Figure 33 B), and expressed as a ratio of the protein of interest and Tim16 (p/Tim16).

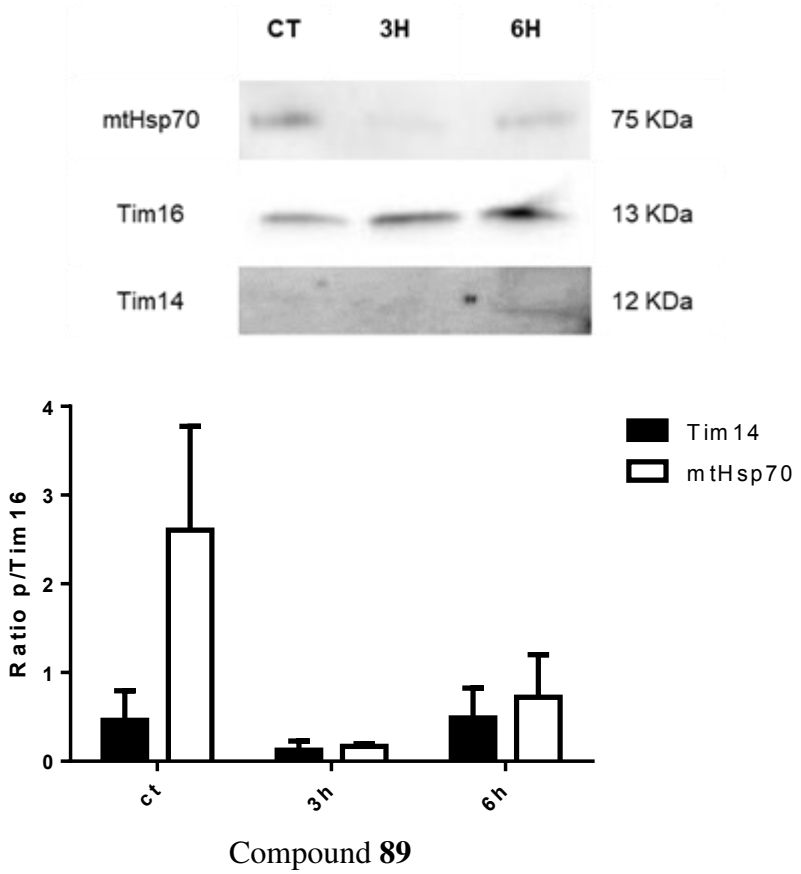

Compound **89**

Figure 33: Co-immunoprecipitation of Tim16, Tim14 and mtHsp70 after 3 or 6h of treatment with compound 89. A) MCF7 cells were collected, immunoprecipitated and analysed with immunoblotting. B) Protein expression in the untreated and the treated cells expressed as the ratio between total protein and Tim16.

In conclusion these tests suggest that compound **89** acts mainly at 3h, interfering in the binding between Tim16 and both Tim14 and mtHsp70. The compound seems to bind Tim16 in a reversible manner, since after 6 h the binding between Tim16 and both Tim14 and mtHsp70 is partially restored.

The LC-MS analysis showed that the compound **89** is able to interact with Magmas protein, since we see the compound inside the mitochondria (see figure 34 and 35).

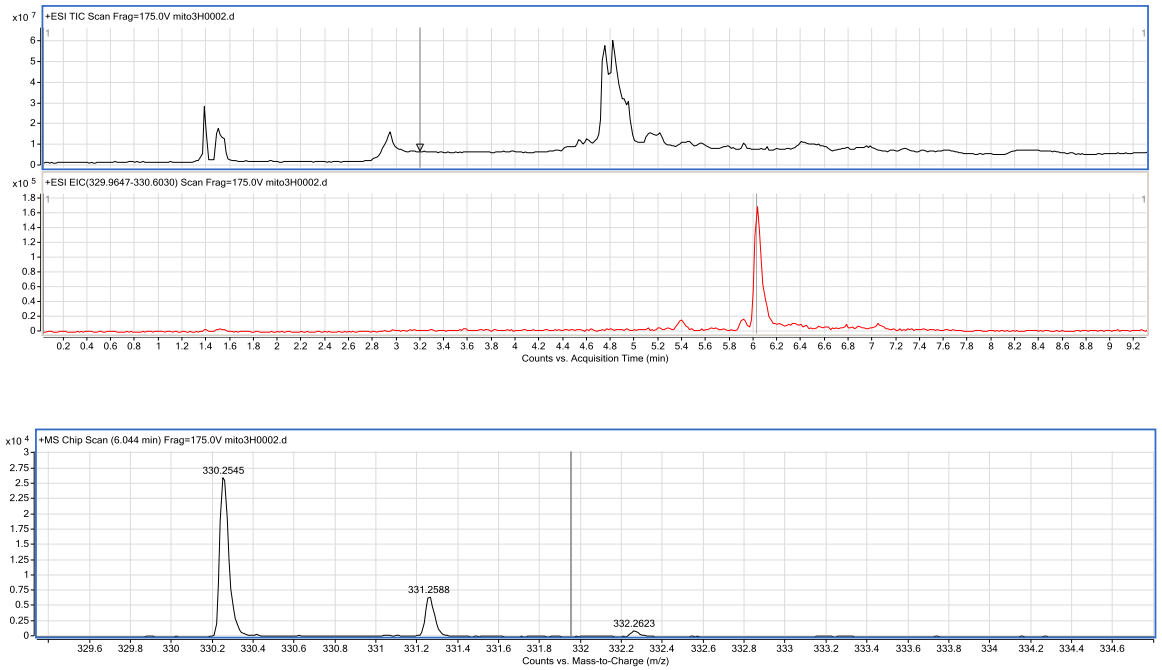

Figure 34: LC-MS spectrum of mitochondria collected at 3h, the compound **89** is inside it because we see the compound weight (330 as M+1).

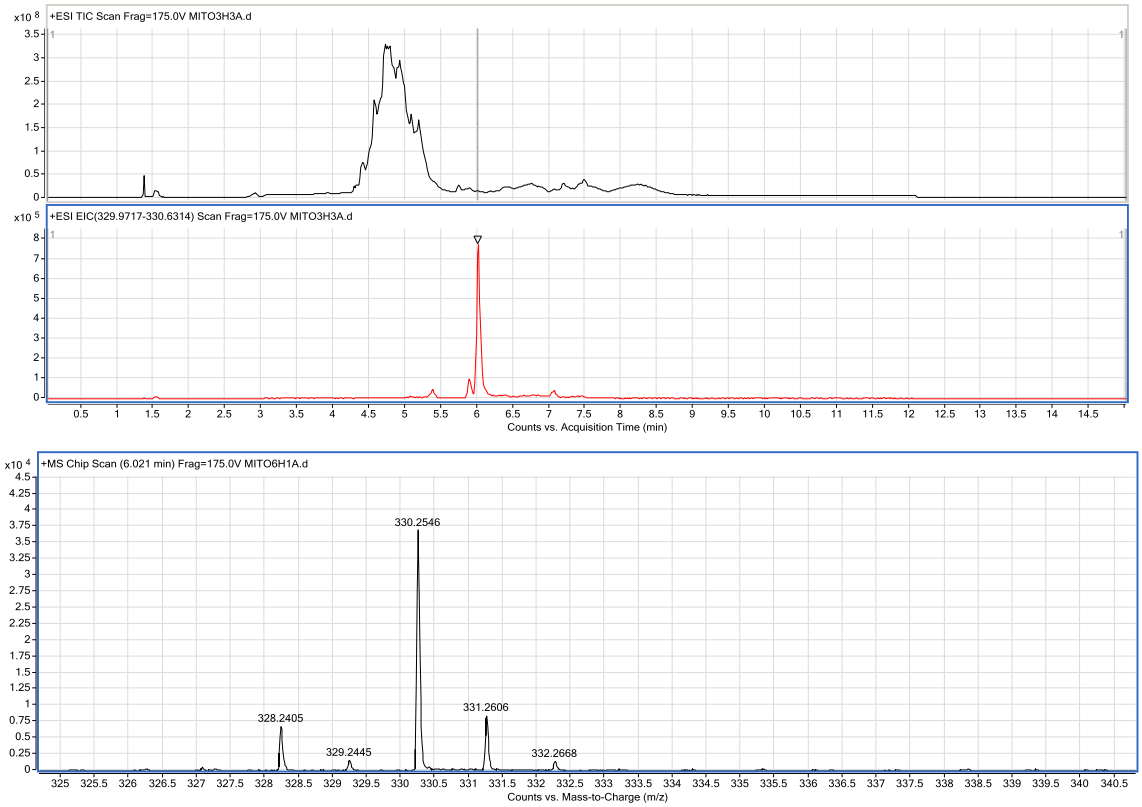

Figure 35: LC-MS spectrum of mitochondria collected at 6h, the compound **89** is inside it because we see the compound weight (330 as M+1).

The knowledge about the Magmas system and its inhibitors are still very limited nowadays. The inhibition of the cell growth, caused by the modulation of this system, has been evaluated only on tumor cells of prostate nature.

The obtaining of this biological effect on tumor thyroid cells and this new compound **89** test findings are a good result and permits to keep synthetizing new analogs, to increase the knowledge about Magmas complex interaction.

5 Experimental section

5.1 Chemicals and methods

Analytical thin-layer chromatography (TLC) was carried out using precoated silica gel plates Macherey-Nagel poligram SIL G/UV254 with thickness of the layer of 0,25 mm and further monitoring with 254/365 nm UV lamp. Column chromatography was performed using Isolera One (Biotage Sweden) or traditional column chromatography with silica gel 60 (40-63 um). Melting point was measured with a Reichert Termovar (Austria). 1H, 13C, DEPT, bidimensional (gCOSY) and heterocorrelated (gHMQC, gHMBC) NMR spectra were recorded on a VARIAN 400 MHz instrument. Chemical shifts (δ) are reported in parts per million (ppm), using 7.256 ppm peak of deuterated chloroform as an internal standard and coupling constants (J) are reported in Hertz. Following abbreviations have been used for multiplicity: s=singlet, d=doublet, t=triplet, q=quartet, m=multiplet, bs=broad signal, dd=doublet of doublets, dt=doublet of triplets, td=triplet of doublets. Mass spectral analysis were performed by ESI MICROMASS ZMD 2000 electrospray mass spectrometer, after dissolution of compounds in a solution composed by 40:60:0,1 of H_2O:CH_3CN:TFA. High resolution mass spectrometry data were achieved using a ESI-Q-TOF 6520 instrument coupled with a nano HPLC with Chip Cube® technology (Agilent Tecnologies, USA) For analytical controls Beckmann System Gold 168 HPLC have been used with LC column Kinetex 5µm EVO C18 100 A (250 X 4.6 mm) and a variable wavelength UV detector fixed to 220 nm. Analysis were conducted using two solution A and B containing, respectively, 100:0,1 H_2O:TFA and 40:60:0,1 of H_2O:CH_3CN:TFA with different gradients for the products. For purification Water Delta Prep 4000 HPLC have been used with column Jupiter 10 µm C18 AXIA (100x 30,00 mm). For the hydrogenation reactions we used a continuous flow reactor H-Cube® (Thales-Nano, Hungary).

5.2 IRI inhibitors synthesis

5.2.1 Synthesis of dispiropyrrolidines from Isatine

Synthesis of compounds **15**, **16**, **17**, **18**:

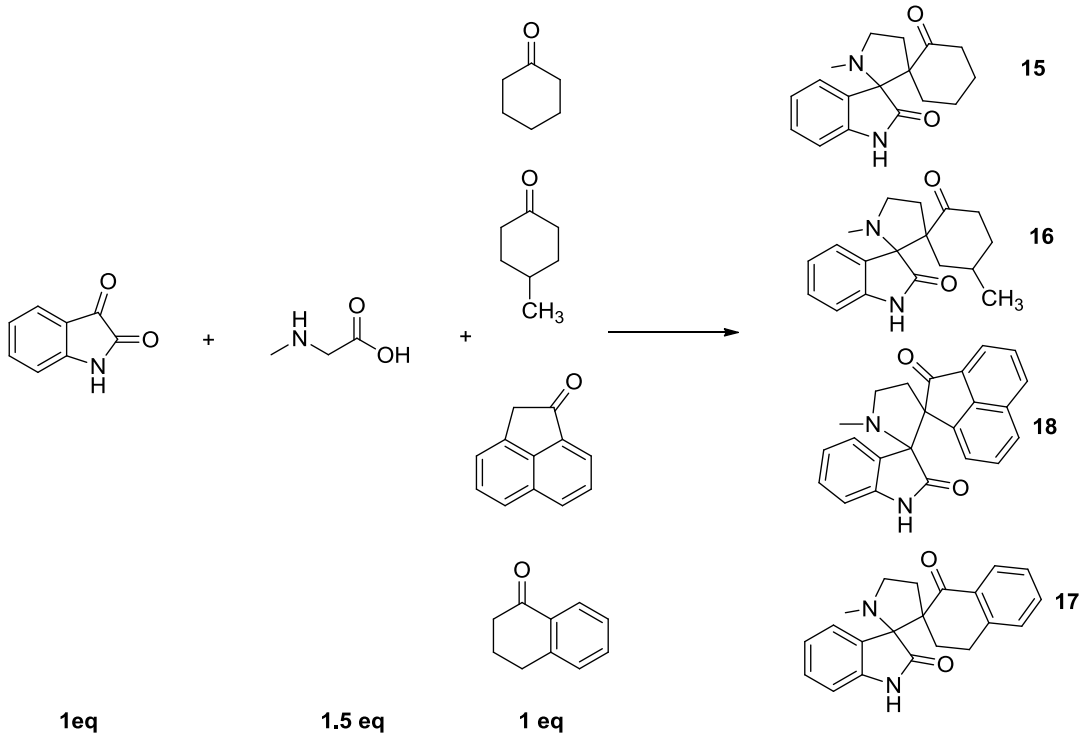

To a solution of isatine in MeOH, it is added sarcosine (1.5 eq) and the cyclic ketone (1 eq). The reaction was stirred at 90°C for 12 hours. It was monitored by TLC (A1P1) and mass spectrometry (ESI). When the reaction was complete, it was quenched with $NaHCO_3$ sat. and H_2O. The MeOH was evaporated and then, the reaction was extracted with EtOAc. After anhydrification with anhydrous sodium sulfate, the solution was evaporated under reduced pressure to give a crude product. It was purified by coloumn chromatography (Petroleum ether/ EtOAc 1:1).

After crystallization (ethyl ether/petroleum ether 3:7) I obtained the final product.

These compounds are solid and with a variable color from pale pink to yellowish.

Compound **15**:

Yield 51%

MS (ESI): [M+H]+ = 285,16

^{1}H NMR (400 MHz, Chloroform-*d*) δ 8.86 (s, 1H), 7.32 – 7.09 (m, 1H), 7.09 – 6.93 (m, 2H), 6.90 (d, *J* = 7.8 Hz, 1H), 3.26 (h, *J* = 3.9, 3.4 Hz, 2H), 2.68 (ddd, *J* = 12.7, 7.5, 5.3 Hz, 1H), 2.44 (dt, *J* = 13.5, 3.9 Hz, 1H), 2.22 (dd, *J* = 14.6, 4.4 Hz, 1H), 2.08 (s, 3H), 2.03 – 1.91 (m, 1H), 1.77 (ddd, *J* = 14.9, 11.5, 7.0 Hz, 1H), 1.67 (ddd, *J* = 14.7, 10.9, 3.7 Hz, 2H), 1.59 – 1.45 (m, 2H), 1.43 – 1.32 (m, 1H).

^{13}C NMR (101 MHz, CDCl3) δ 212.01, 179.02, 141.71, 135.09, 129.55, 128.33, 127.09, 123.44, 122.75, 115.29, 110.23, 62.83, 52.14, 41.30, 35.85, 35.64, 34.10, 27.70, 25.44, 21.69.

^{1}H-NMR compound 15

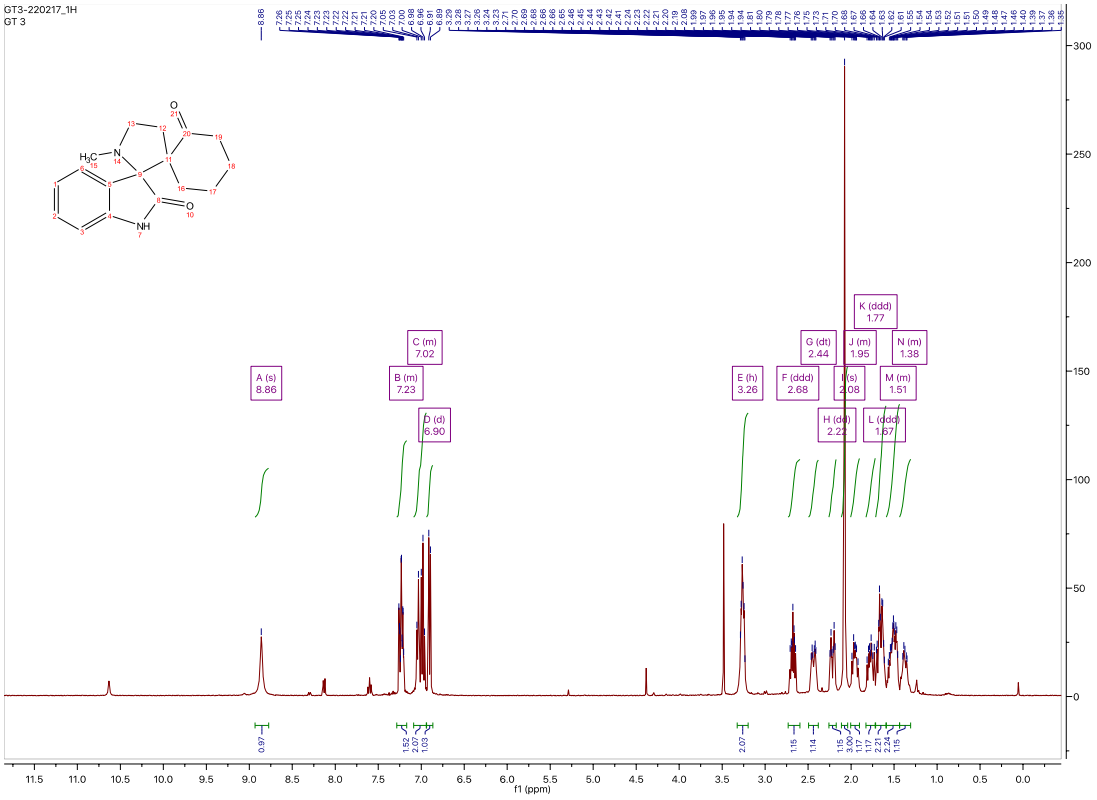

^{13}C-NMR compound 15

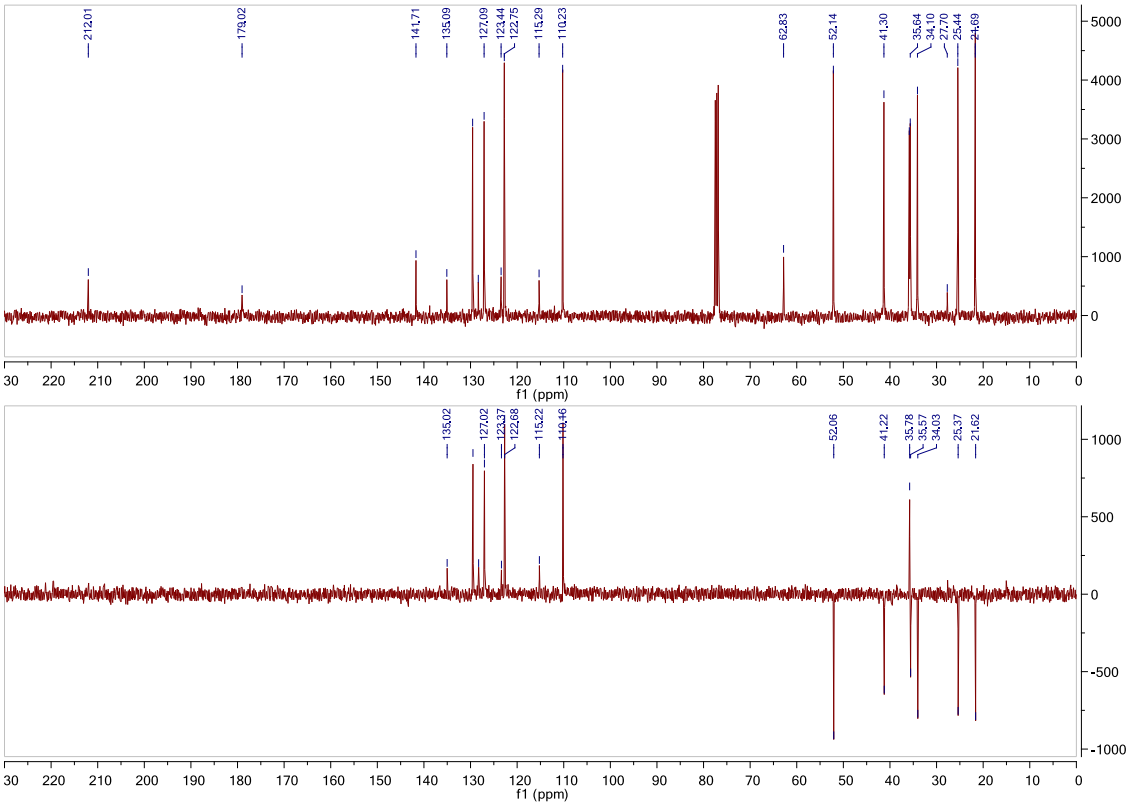

Compound **16**:

Yield 51%

MS (ESI): [M+H]+ = 299,17

^{1}H NMR (400 MHz, Chloroform-*d*) δ 9.01 (s, 1H), 7.29 – 7.09 (m, 1H), 7.05 – 6.75 (m, 3H), 3.29 – 3.13 (m, 2H), 2.83 – 2.69 (m, 1H), 2.60 (dt, *J* = 14.6, 3.1 Hz, 1H), 2.26 – 2.11 (m, 1H), 2.03 (s, 3H), 1.90 – 1.62 (m, 2H), 1.40 – 1.06 (m, 3H), 0.79 (d, *J* = 6.4 Hz, 3H).

^{13}C NMR (101 MHz, $CDCl_3$) δ 211.40, 179.40, 141.51, 129.51, 127.51, 126.93, 122.64, 110.30, 76.34, 62.84, 52.07, 45.37, 41.70, 35.71, 34.66, 34.54, 28.66, 21.86.

^{1}H-NMR compound 16

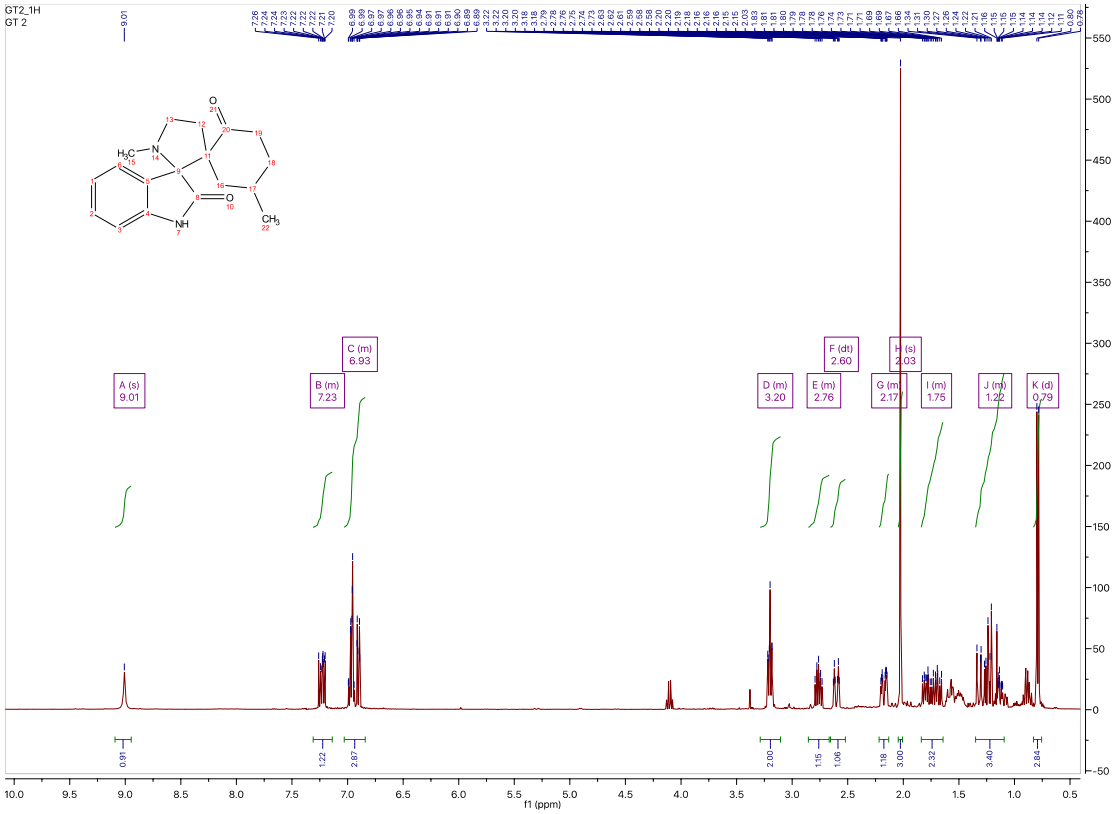

^{13}C-NMR compound 16

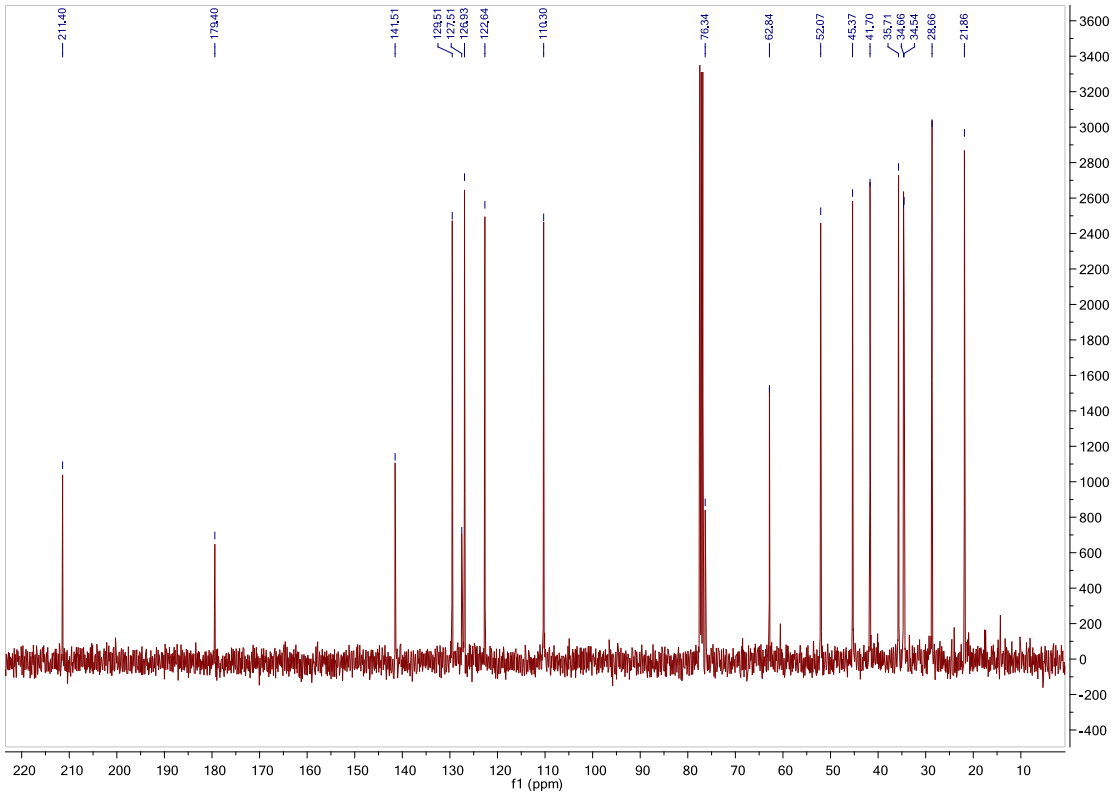

Compound **17**:

Yield 52%

MS (ESI): $[M+H]^+$ = 332,40

^{1}H NMR (400 MHz, Chloroform-*d*) δ 10.20 (s, 1H), 8.35 – 8.01 (m, 4H), 7.62 (ddd, *J* = 8.6, 7.3, 1.5 Hz, 1H), 7.41 – 6.43 (m, 20H), 4.39 (s, 3H), 3.49 (s, 4H), 2.79 – 2.02 (m, 18H).

^{13}C NMR (101 MHz, $CDCl_3$) δ 210.13, 162.80, 152.08, 143.47, 138.59, 135.13, 133.27, 131.81, 128.45, 127.94, 126.87, 125.20, 123.52, 118.73, 115.15, 114.57, 109.84, 57.72, 51.38, 27.74, 26.04.

^{1}H-NMR compound 17

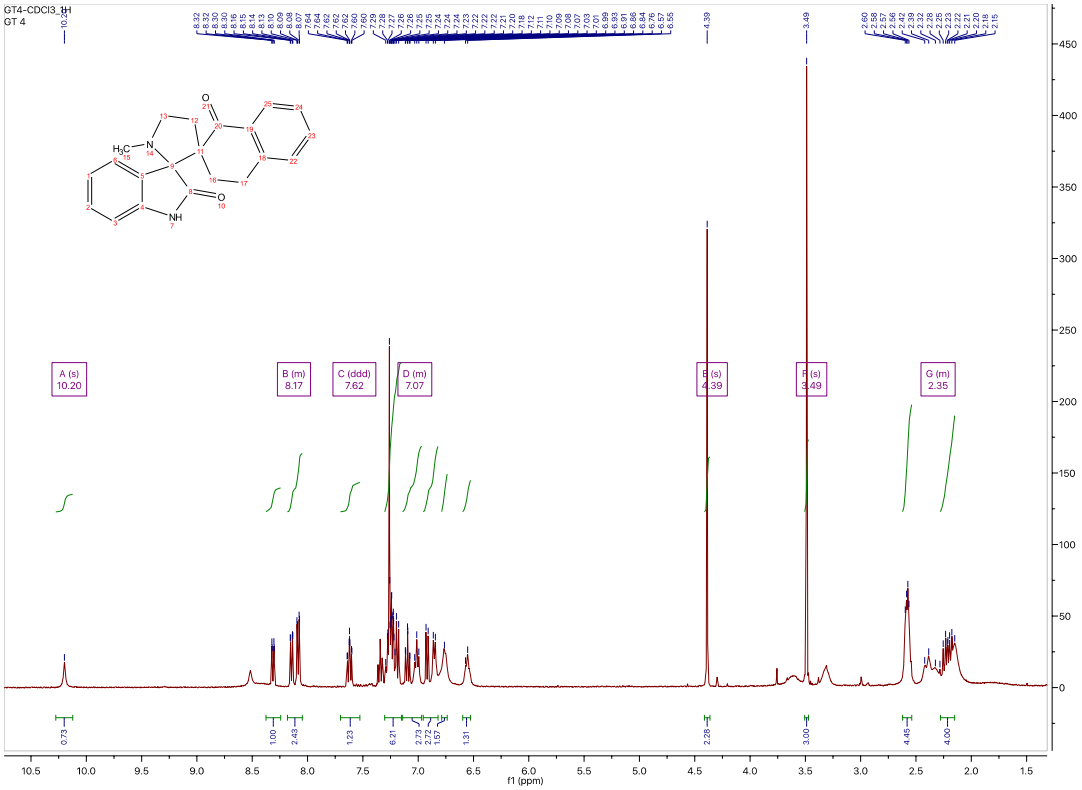

^{13}C-NMR and DEPT compound 17

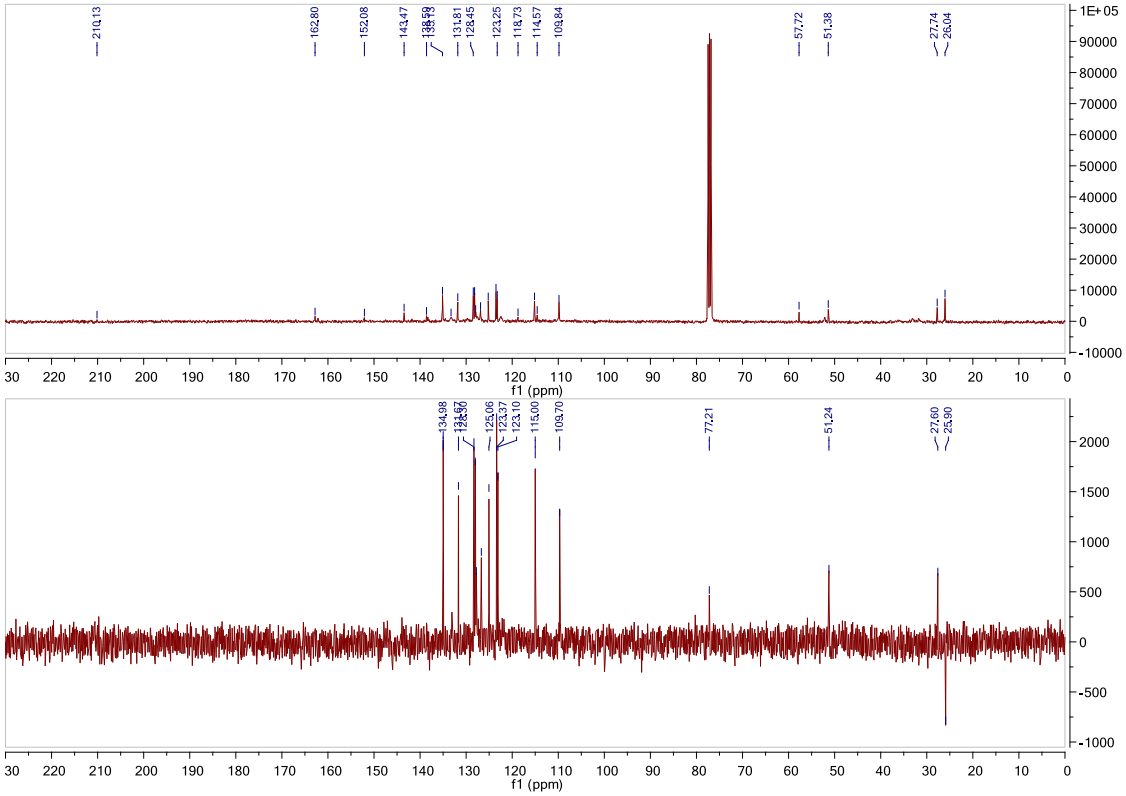

Compound **18**:

Yield 90%

MS (ESI): $[M+H]^+$ = 354,40

^{1}H NMR (400 MHz, Chloroform-*d*) δ 7.90 (d, *J* = 8.1 Hz, 1H), 7.85 (d, *J* = 7.0 Hz, 1H), 7.70 (dd, *J* = 7.7, 5.8 Hz, 2H), 7.56 (dd, *J* = 8.1, 7.0 Hz, 1H), 7.47 (dd, *J* = 8.4, 7.0 Hz, 1H), 6.91 (td, *J* = 7.7, 1.3 Hz, 1H), 6.76 (td, *J* = 7.6, 1.1 Hz, 1H), 6.46 (d, *J* = 7.7 Hz, 1H), 3.84 (s, 1H), 3.64 (td, *J* = 9.5, 8.6, 4.1 Hz, 1H), 3.06 (td, *J* = 11.9, 5.1 Hz, 1H), 2.46 (ddd, *J* = 12.8, 8.5, 4.2 Hz, 1H), 2.30 (s, 4H).

^{13}C NMR (101 MHz, Chloroform-*d*) δ 204.87 , 177.95 , 142.05 , 141.52 , 132.66 , 132.53 , 131.68 , 131.28 , 130.34 , 129.92 , 129.44 , 128.94 , 128.68 , 128.22 , 128.12 , 126.65 , 124.89 , 122.66 , 122.53 , 121.70 , 121.58 , 109.67 , 109.60 , 79.00 , 63.48 , 52.45 , 35.98 , 31.73 .

^{1}H-NMR compound 18

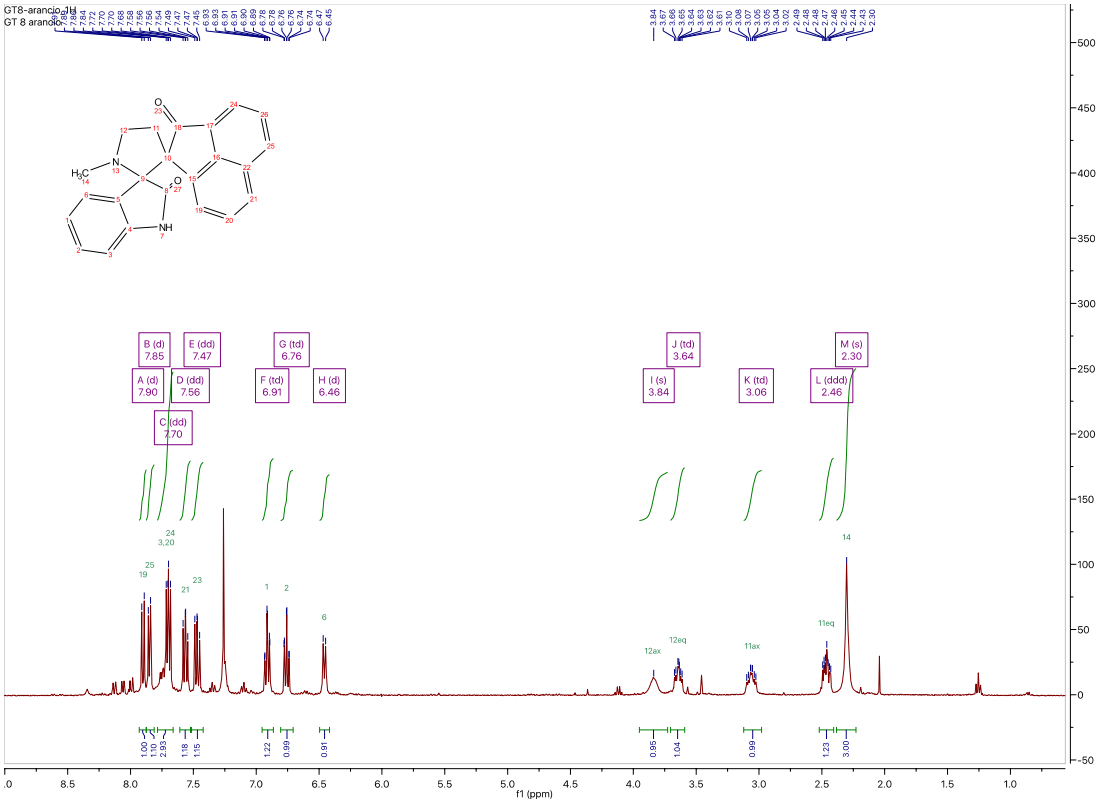

^{13}C-NMR and DEPT compound 18

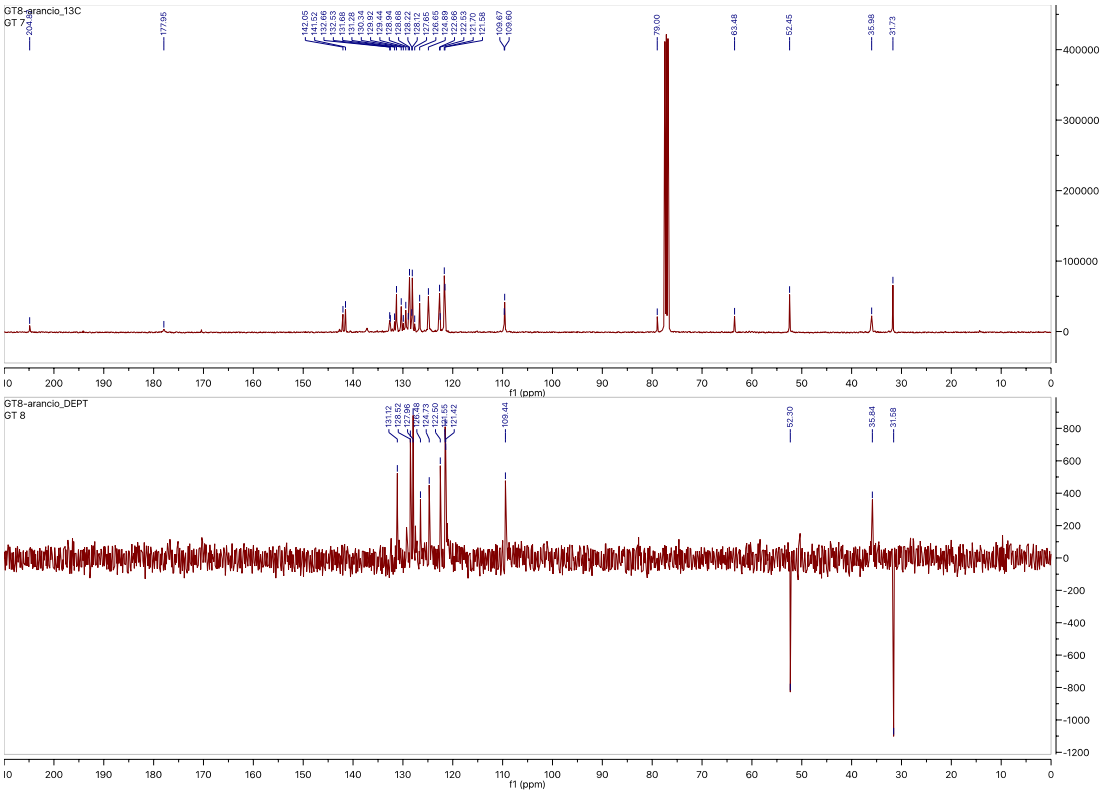

Synthesis of compound **20**:

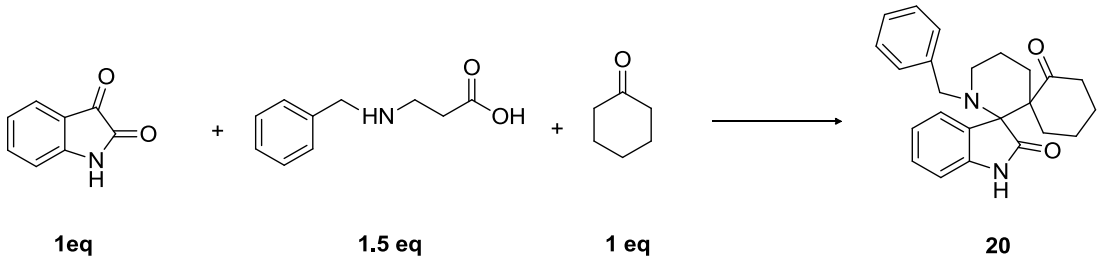

1eq **1.5 eq** **1 eq** **20**

To a solution of isatine in MeOH, it is added N-benzyl-β-alanine (1.5 eq) and the cyclohexane (1 eq). The reaction was stirred at 90°C for 12 hours. It was monitored by TLC (A3P1) and mass spectrometry (ESI). When the reaction was complete, it was quenched with $NaHCO_3$ sat. and H_2O. The MeOH was evaporated and then, the reaction was extracted with EtOAc.

After anhydrification with anhydrous sodium sulfate, the solution was evaporated under reduced pressure to give a crude product. It was purified by coloumn chromatography (Petroleum ether/ EtOAc 1:3).

After crystallization with ethanol, I obtained the final product white-yellowish.

Yield 32%

MS (ESI): $[M+H]^+ = 374,14$

Since this is diastereomeric racemic mixture, the NMR below show many and a little confusing peaks.

^{1}H-NMR compound 20

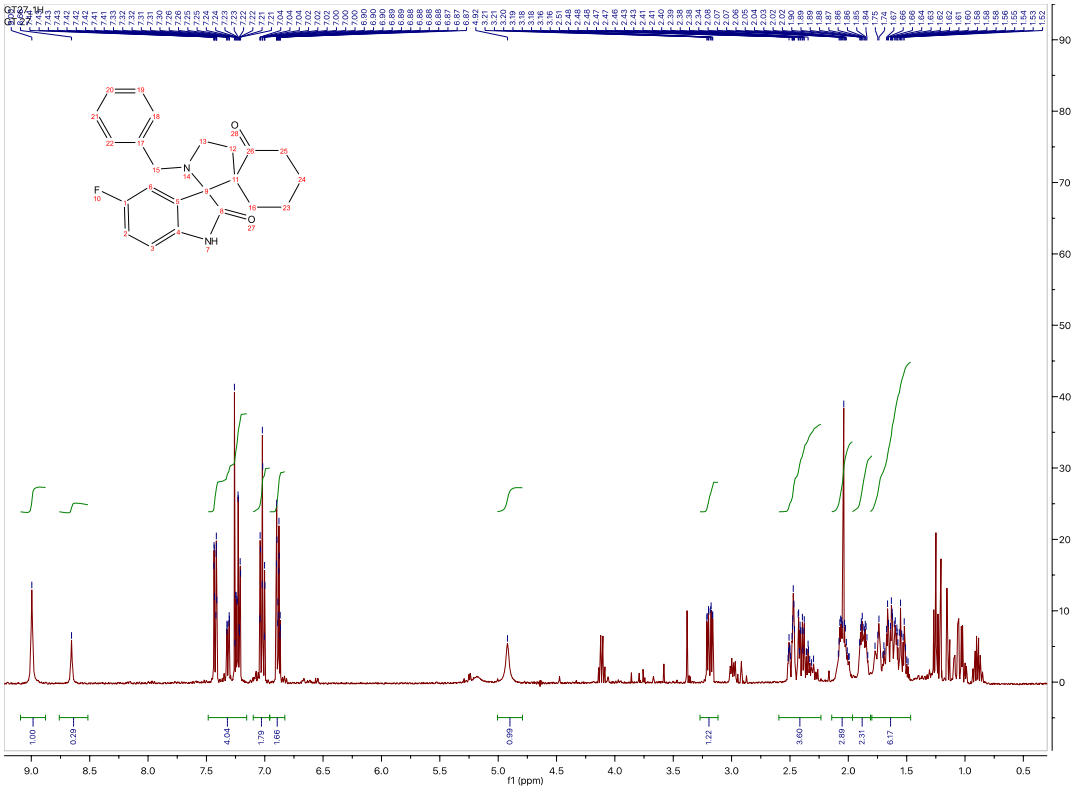

^{13}C-NMR and DEPT compound 20

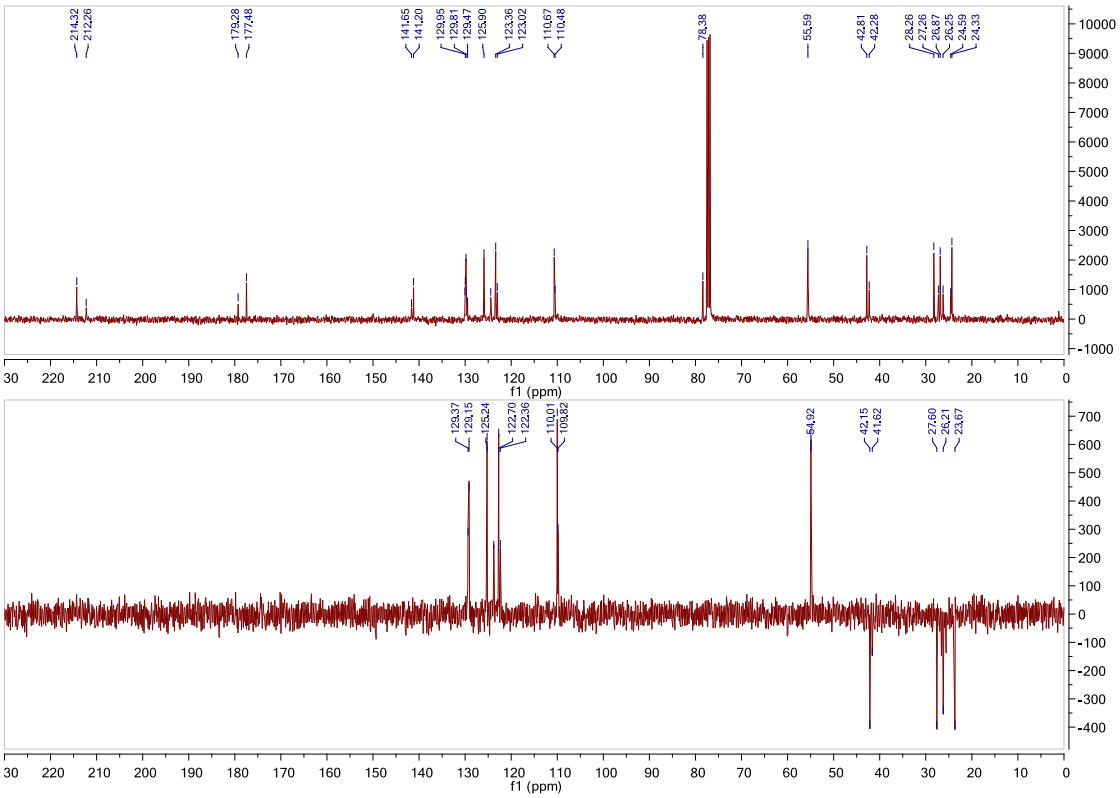

Synthesis of compound **19**:

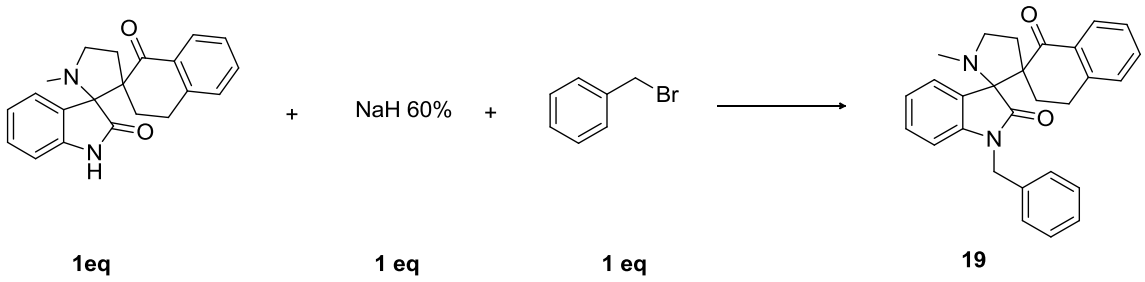

1eq **1 eq** **1 eq** **19**

In a two-neck round bottom flask, previously treated to be humidity-free ambient, the dispiropyrrolidine is dissolved in DMF and NaH is added. Then, benzyl-bromide is added too.

There is a chromatic change from yellow to green. The reaction goes in a short time: after 30 minutes, monitored by TLC (A1P1), the organic solvent was evaporated. With diethyl ether the NaH salts rush. So, the solution is filtered off with a Gooch filter and the solvent is evaporated. Through a column chromatography (A1P1) we obtain the compound as a yellow solid.

Yield 65%

MS (ESI): $[M+H]^+ = 422,16$

^{1}H NMR (400 MHz, Chloroform-*d*) δ 8.07 (dd, *J* = 7.3, 2.1 Hz, 1H), 7.43 – 7.13 (m, 8H), 6.95 (t, *J* = 7.6 Hz, 1H), 6.86 – 6.72 (m, 2H), 6.62 (d, *J* = 7.8 Hz, 1H), 6.51 (t, *J* = 7.6 Hz, 1H), 4.99 (d, *J* = 15.3 Hz, 1H), 4.84 (d, *J* = 15.3 Hz, 1H), 3.58 (s, 1H), 3.40 – 3.20 (m, 1H), 2.57 (ddd, *J* = 12.6, 8.6, 4.2 Hz, 1H), 2.49 – 2.12 (m, 5H), 2.08 (s, 3H).

^{13}C NMR (101 MHz, $cdcl_3$) δ 198.48, 142.95, 142.73, 135.37, 132.57, 132.20, 128.53, 128.28, 127.41, 127.30, 127.16, 127.07, 126.21, 126.02, 121.47, 107.98, 57.18, 51.30, 43.13, 35.01, 32.83, 31.37, 25.34.

^{1}H-NMR compound 19

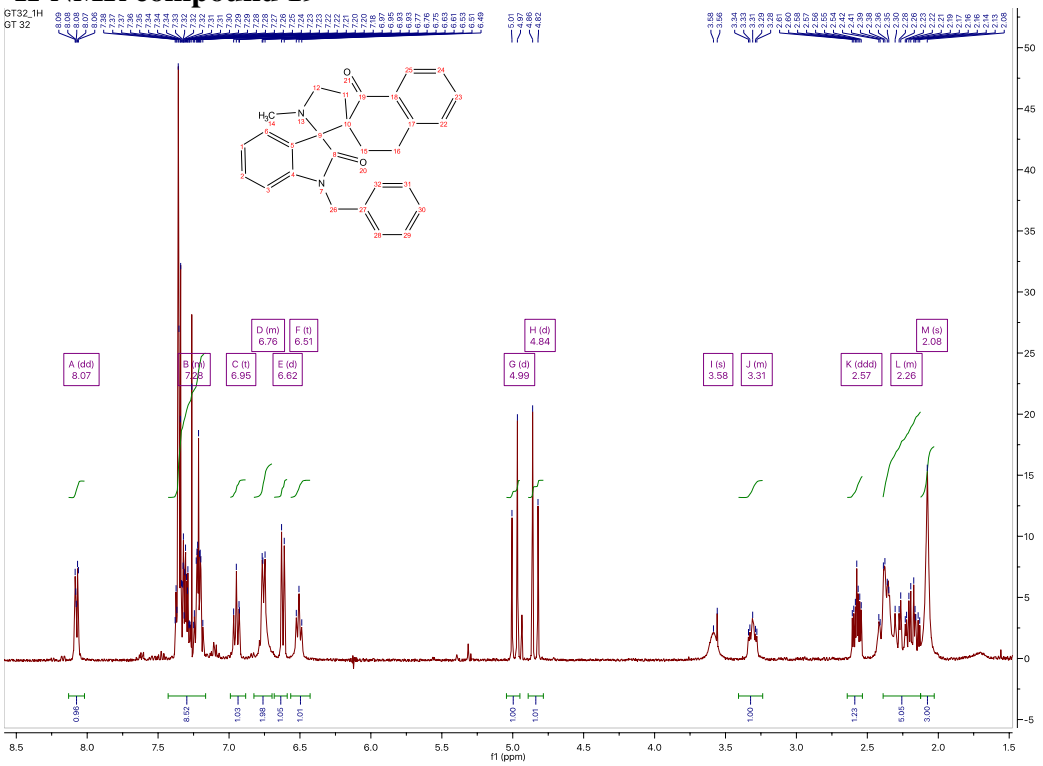

^{13}C-NMR and DEPT compound 19

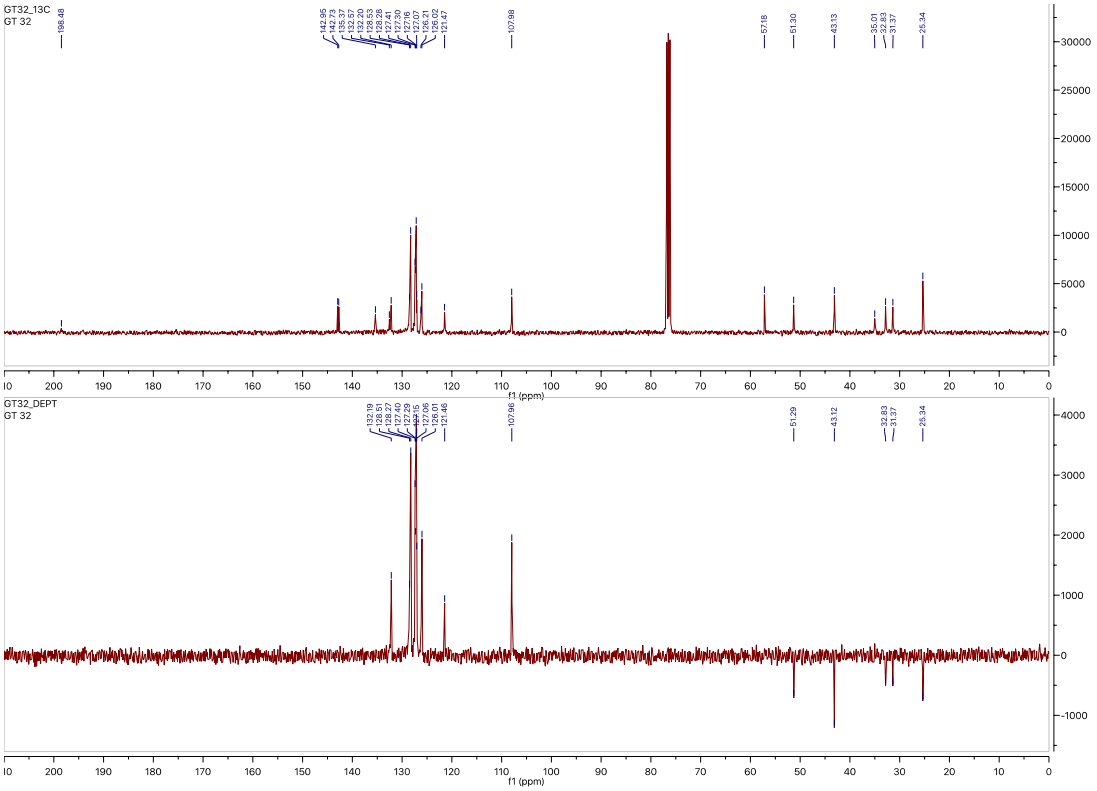

5.2.2 Synthesis of dispiropyrrolidines from 5-fluoro isatine

Synthesis of compounds **22**, **23**, **24**:

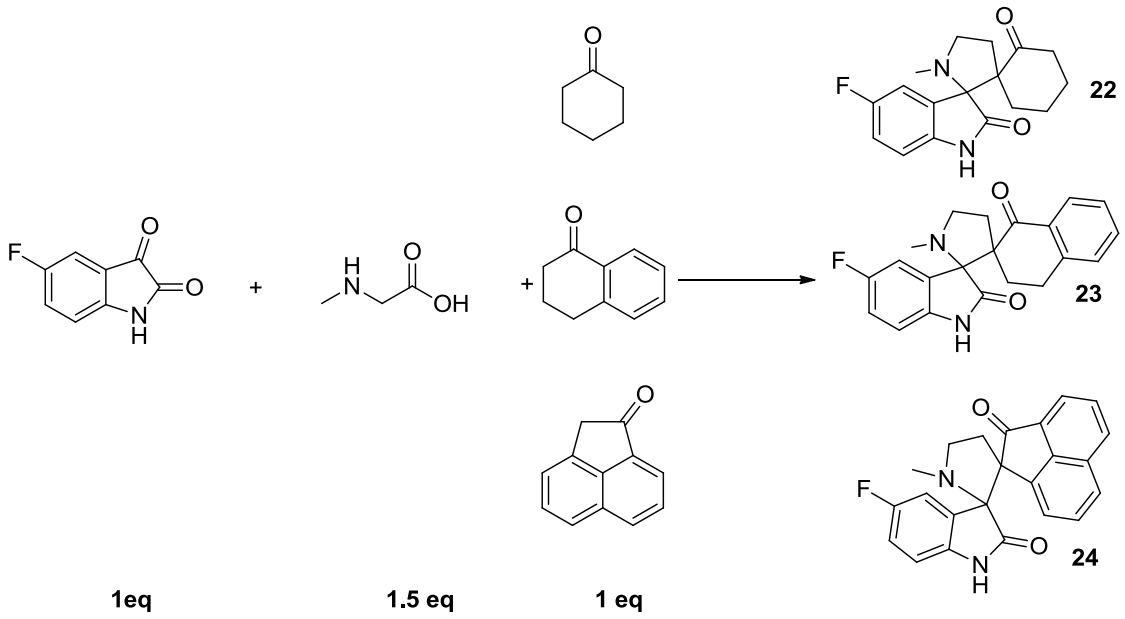

To a solution of 5-fluoro isatine in MeOH, it is added sarcosine (1.5 eq) and the cyclic ketone (1 eq). The reaction was stirred at 90°C for 12 hours. It was monitored by TLC (A1P1) and mass spectrometry (ESI). When the reaction was complete, it was quenched with $NaHCO_3$ sat. and H_2O. The MeOH was evaporated and then, the reaction was extracted with EtOAc.

After anhydrification with anhydrous sodium sulfate, the solution was evaporated under reduced pressure to give a crude product. It was purified by coloumn chromatography (Petroleum ether/ EtOAc 1:1).

After crystallization (ethyl ether/petroleum ether 3:7) I obtained the final product.

Compound **22**:

It is a white solid.

Yield 72%

MS (ESI): $[M+H]^+ = 302,14$

^{1}H NMR (400 MHz, Chloroform-*d*) δ 8.56 (s, 1H), 6.95 (td, *J* = 8.7, 2.6 Hz, 1H), 6.89 – 6.76 (m, 2H), 3.33 – 3.12 (m, 2H), 2.62 (ddd, *J* = 12.8, 7.4, 5.7 Hz, 1H), 2.43 – 2.22 (m,

2H), 2.07 (s, 3H), 1.99 (ddd, *J* = 12.6, 8.4, 6.8 Hz, 1H), 1.83 (ddd, *J* = 15.0, 11.1, 7.0 Hz, 1H), 1.75 – 1.55 (m, 2H), 1.45 – 1.37 (m, 1H).

^{13}C NMR (101 MHz, cdcl$_3$) δ 211.58, 179.03, 160.25, 157.86, 137.59, 116.13, 115.89, 115.21, 114.96, 110.65, 110.57, 62.95, 52.02, 41.19, 35.79, 35.36, 34.03, 25.34, 21.67.

^{19}F NMR (376 MHz, cdcl$_3$) δ -119.58, -119.59, -119.61, -119.62, -119.63, -119.64.

^{1}H-NMR compound 22

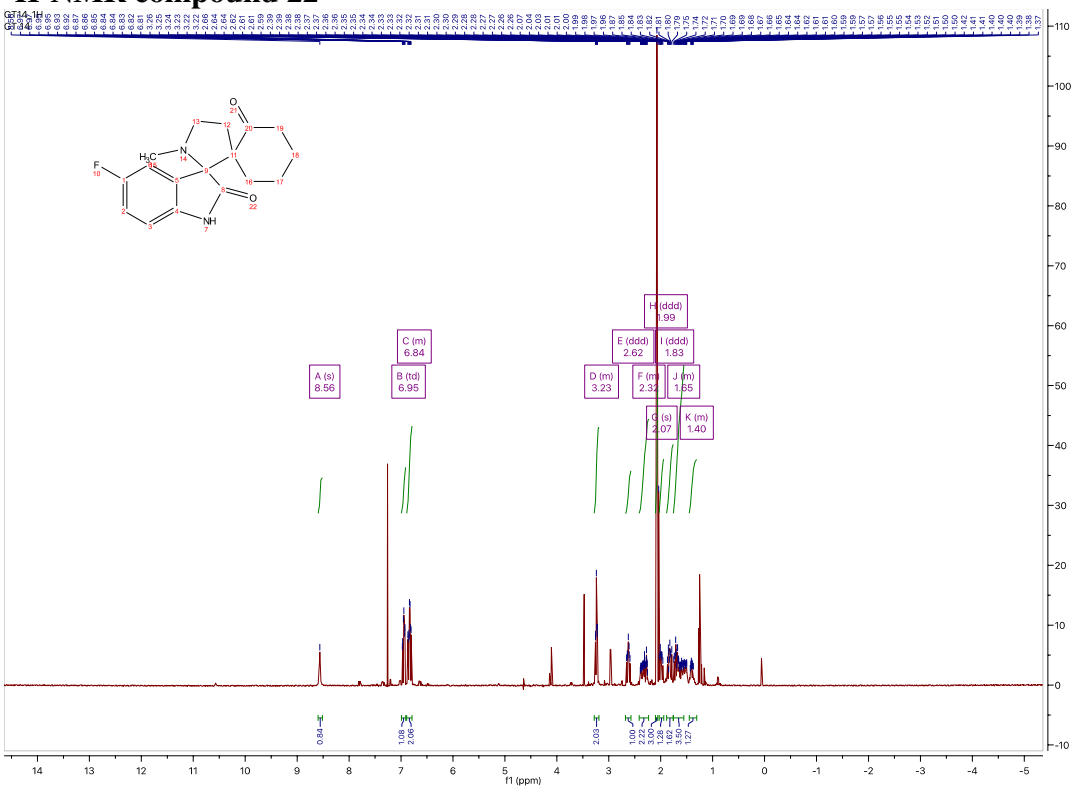

^{13}C-NMR, DEPT e ^{19}F-NMR compound 22

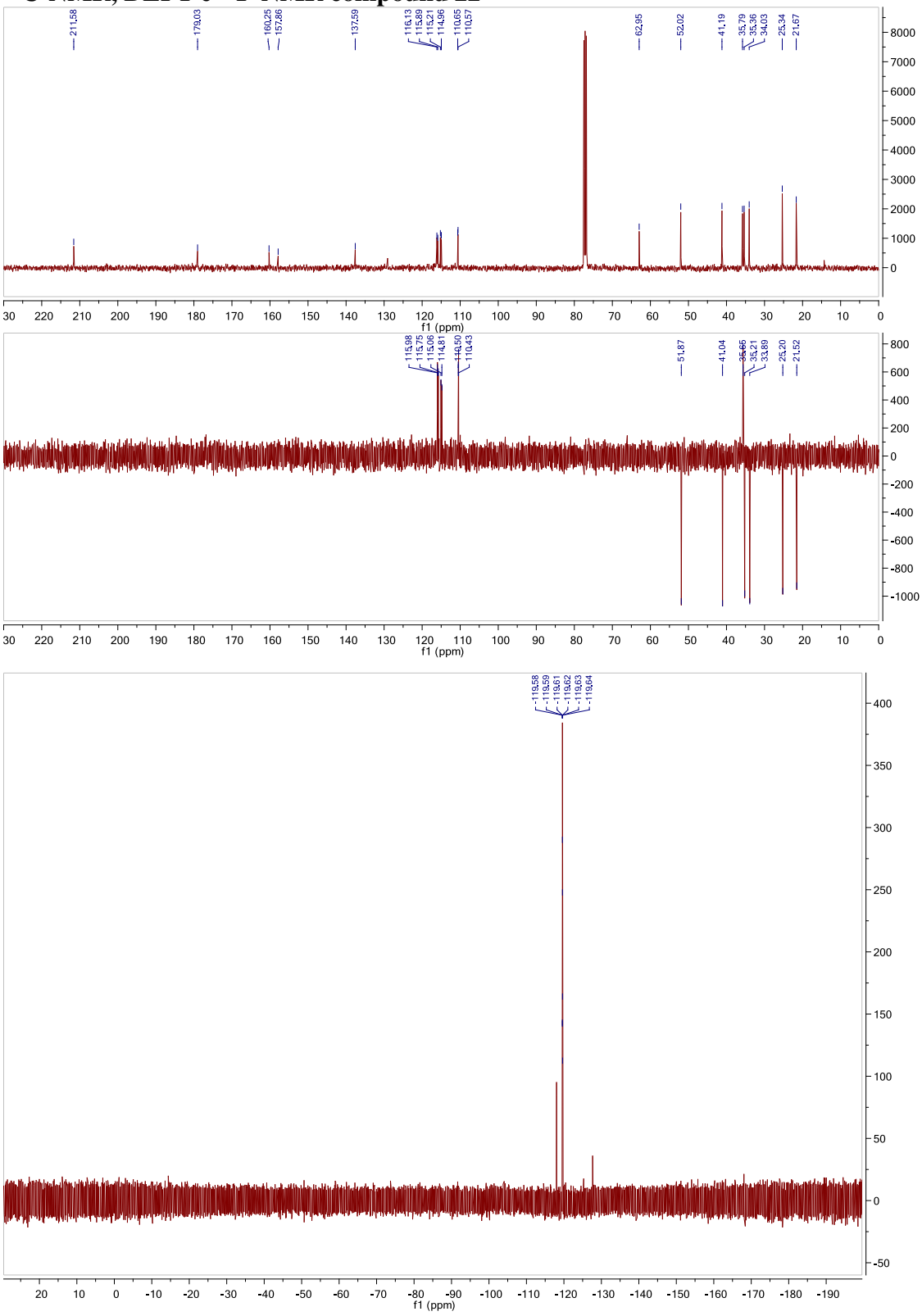

Compound **23**:

It is an orange solid.

Yield 38%

MS (ESI): $[M+H]^+$ = 350,16

^{1}H NMR (400 MHz, Chloroform-*d*) δ 8.29 (s, 1H), 8.09 (dd, *J* = 7.7, 1.7 Hz, 1H), 7.37 – 7.16 (m, 3H), 6.94 – 6.81 (m, 1H), 6.76 – 6.62 (m, 2H), 6.62 – 6.44 (m, 1H), 3.53 (q, *J* = 8.4 Hz, 1H), 3.25 (ddd, *J* = 10.6, 8.8, 4.3 Hz, 1H), 2.58 (ddd, *J* = 12.7, 9.1, 4.2 Hz, 3H), 2.42 (dt, *J* = 14.5, 4.1 Hz, 1H), 2.34 – 2.19 (m, 2H), 2.10 (s, 3H).

^{13}C NMR (101 MHz, cdcl$_3$) δ 198.74, 159.86, 157.46, 143.25, 137.47, 137.45, 133.26, 133.03, 128.14, 127.85, 126.97, 115.82, 115.58, 110.06, 109.98, 57.97, 51.89, 35.57, 33.37, 31.96, 26.07.

^{19}F NMR (376 MHz, cdcl$_3$) δ -120.56.

^{1}H-NMR compound 23

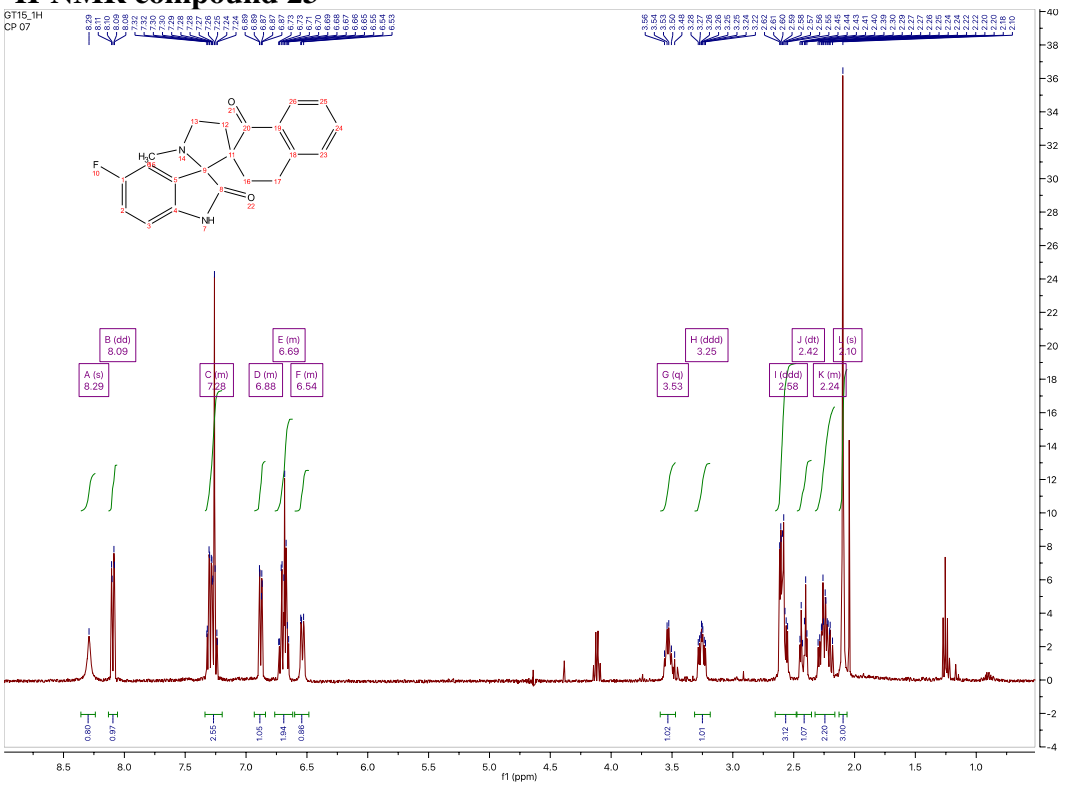

^{13}C-NMR, DEPT e ^{19}F-NMR compound 23

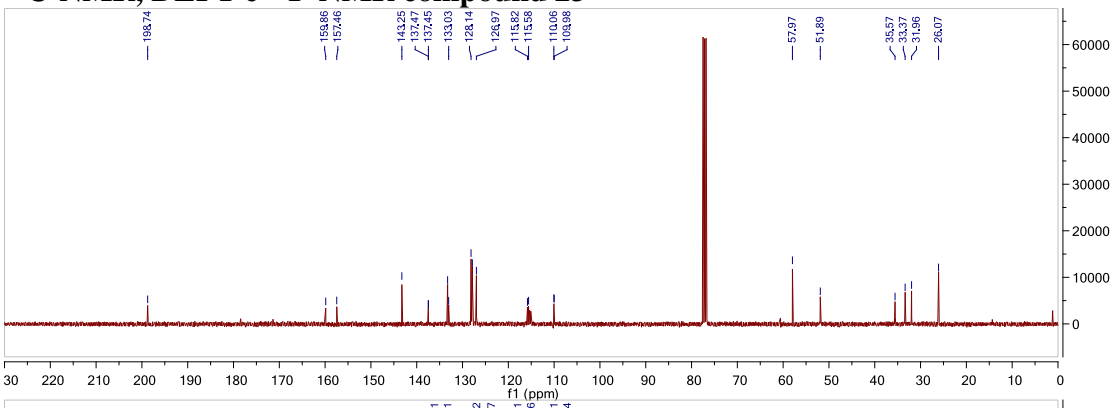

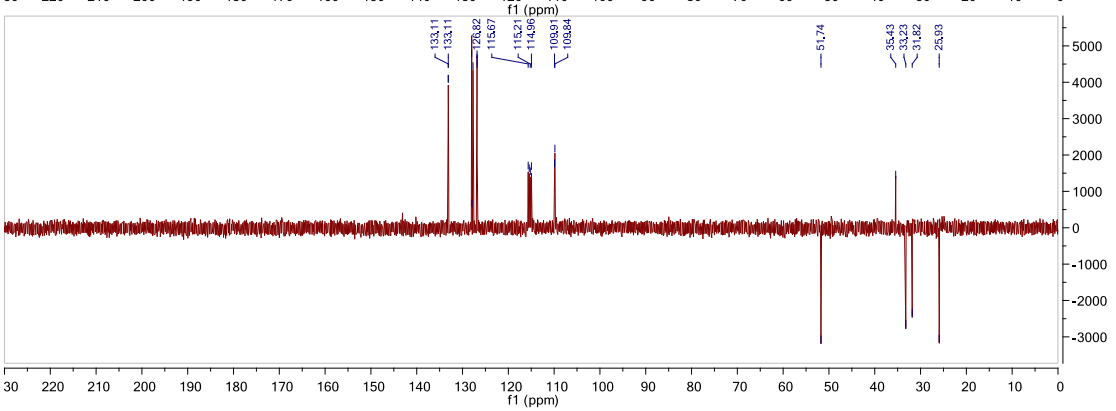

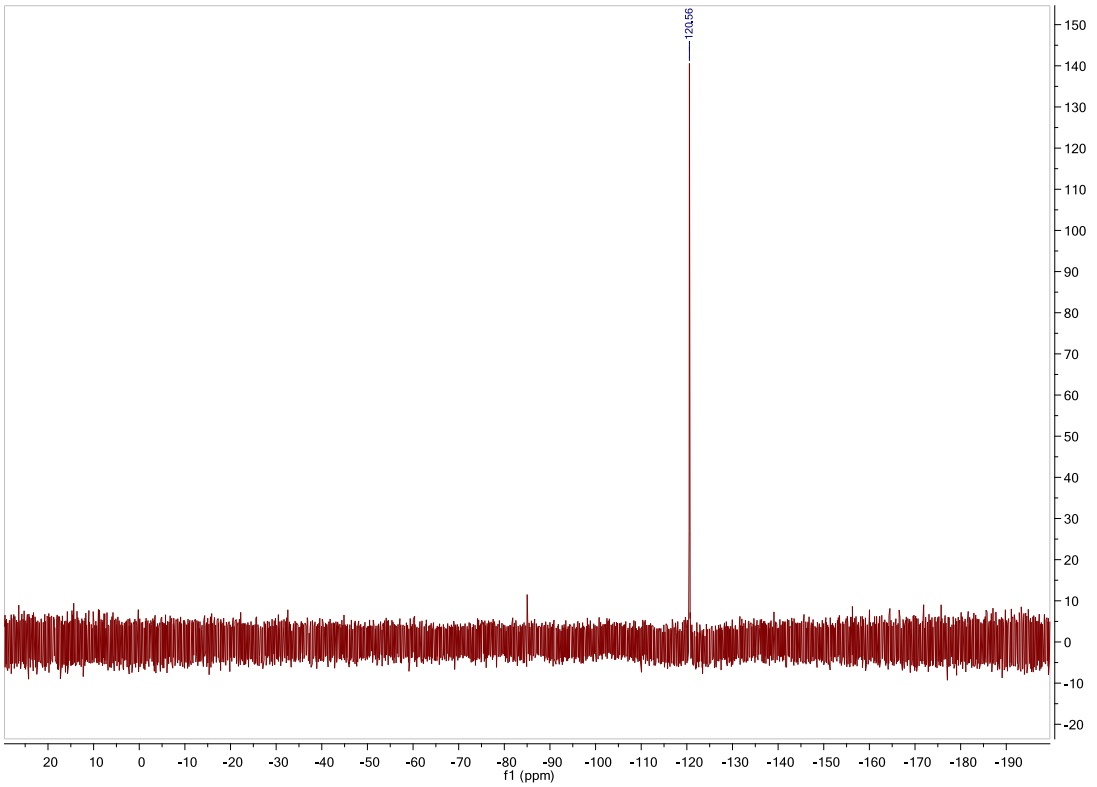

Compound **24**:

It is an orange solid.

Yield 40%

^{1}H NMR (400 MHz, Chloroform-*d*) δ 7.98 – 7.87 (m, 1H), 7.77 – 7.66 (m, 1H), 7.60 (ddd, *J* = 8.1, 7.1, 5.5 Hz, 1H), 7.50 (dd, *J* = 8.3, 7.1 Hz, 1H), 7.02 (dd, *J* = 8.6, 2.6 Hz, 1H), 6.66 – 6.57 (m, 1H), 6.39 (dd, *J* = 8.4, 4.2 Hz, 1H), 3.87 – 3.78 (m, 3H), 3.61 (ddd, *J* = 10.7, 8.8, 4.1 Hz, 1H), 3.05 (ddd, *J* = 13.0, 10.7, 5.4 Hz, 1H).

^{13}C NMR (101 MHz, Chloroform-*d*) δ 204.60 , 160.14 , 157.74 , 142.01 , 132.47 , 132.00 , 131.43 , 130.35 , 128.70 , 128.28 , 128.06 , 125.01 , 122.59 , 121.83 , 121.77 , 116.04 , 115.81 , 114.67 , 114.41 , 110.15 , 110.07 , 63.59 , 52.43 , 35.89 , 31.78 .

^{19}F NMR (376 MHz, Chloroform-*d*) δ -120.60 (d, *J* = 488.2 Hz).

^{1}H-NMR compound 24

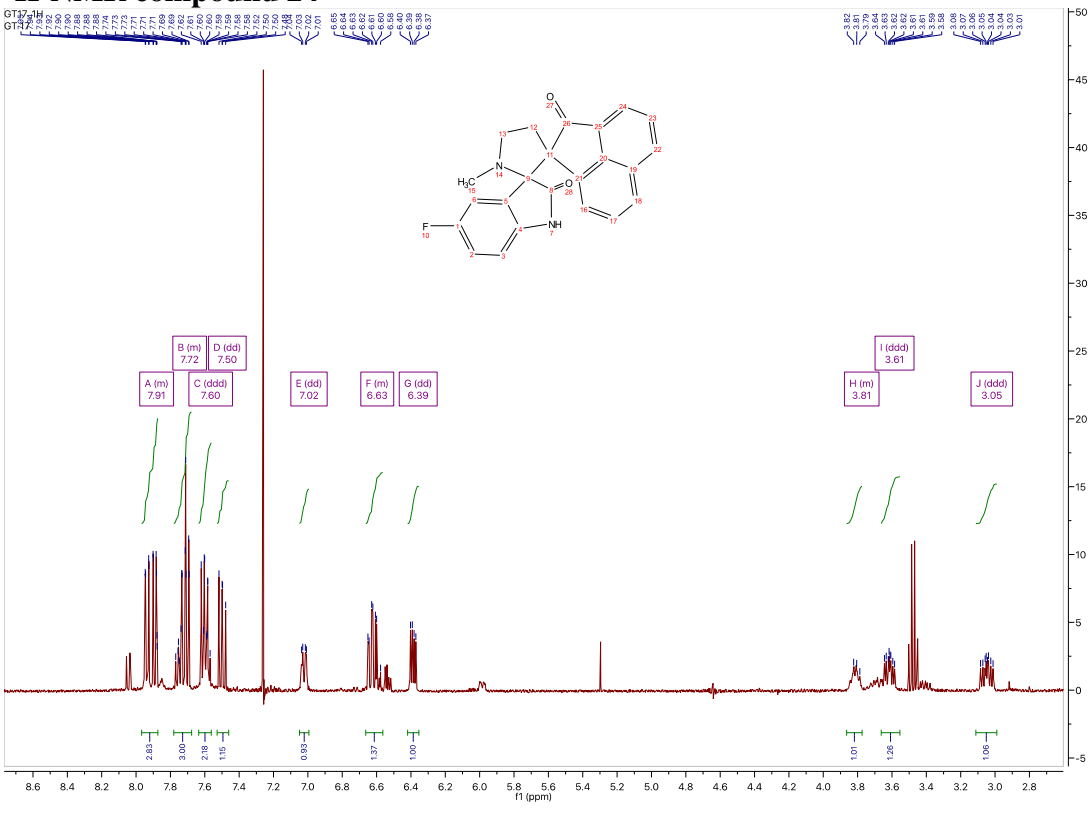

^{13}C-NMR, DEPT e ^{19}F-NMR compound 24

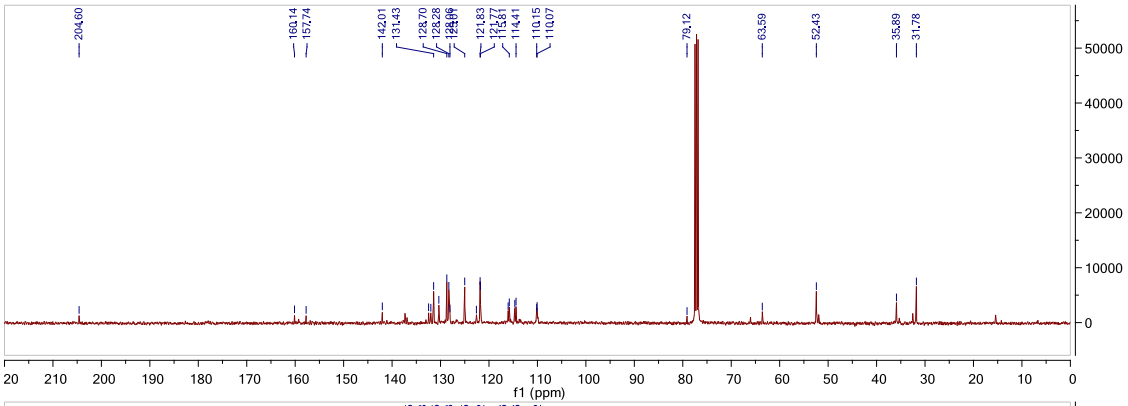

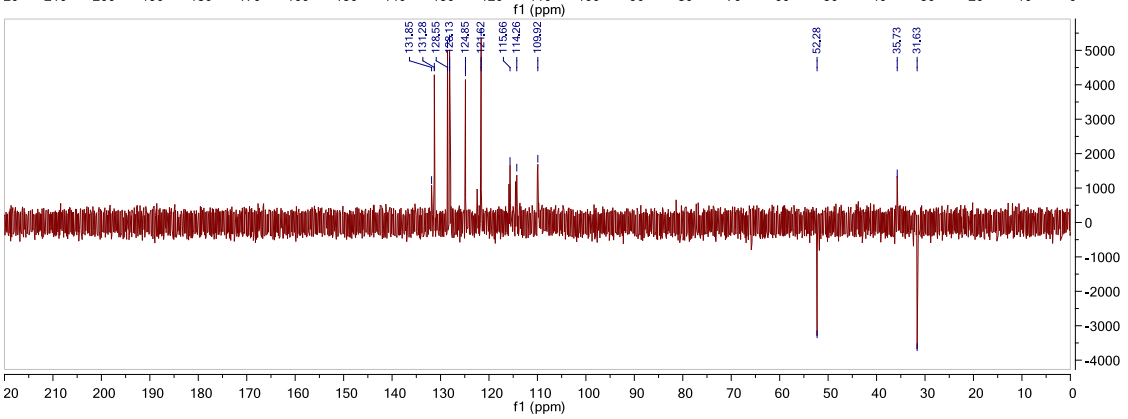

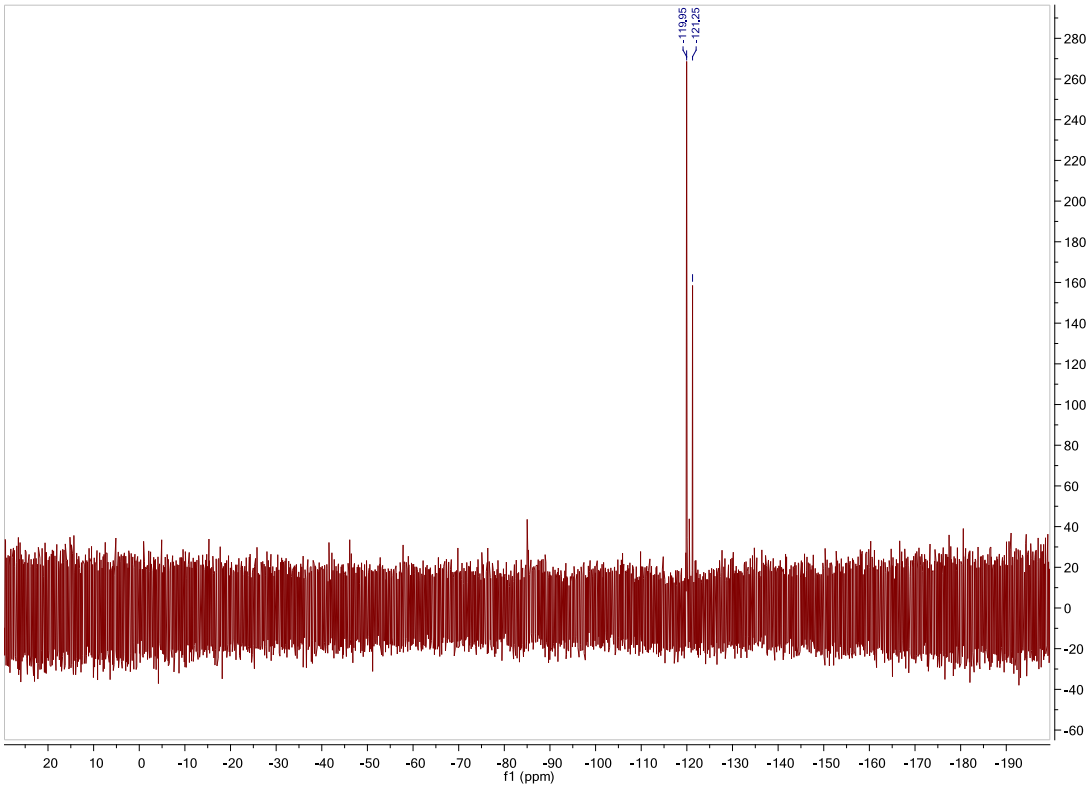

Synthesis of compound **25:**

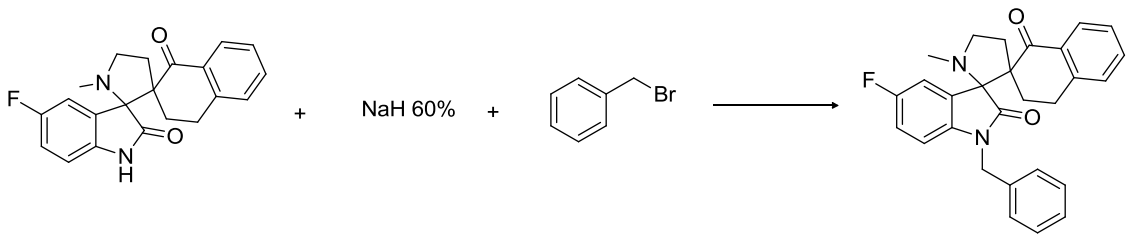

1eq **1 eq** **1 eq** **25**

In a two-neck round bottom flask, previously treated to be humidity-free ambient, the dispiropyrrolidine is dissolved in DMF and NaH is added. Then, benzyl-bromide is added too.

There is a chromatic change from yellow to green. The reaction goes in a short time: after 30 minutes, monitored by TLC (A1P1), the organic solvent was evaporated. With diethyl ether the NaH salts rush. So, the solution is filtered with a Gooch filter and the solvent is evaporated. Through a coloumn chromatography (A1P1) we obtain the compound as a yellow solid.

Yield 99%

MS (ESI): $[M+H]^+ = 441,16$

^{1}H NMR (400 MHz, Chloroform-*d*) δ 8.09 (dd, *J* = 7.5, 1.9 Hz, 1H), 7.42 – 7.18 (m, 7H), 6.89 – 6.76 (m, 1H), 6.65 (dd, *J* = 8.6, 2.6 Hz, 1H), 6.51 (dd, *J* = 8.5, 4.2 Hz, 1H), 5.01 – 4.76 (m, 2H), 3.56 (s, 1H), 3.31 (td, *J* = 9.7, 8.6, 4.2 Hz, 1H), 2.58 (ddd, *J* = 12.7, 8.6, 4.2 Hz, 1H), 2.52 – 2.15 (m, 4H), 2.08 (s, 3H).

^{13}C NMR (101 MHz, $cdcl_3$) δ 198.75, 159.99, 157.58, 143.11, 139.51, 135.70, 133.15, 129.02, 128.10, 127.84, 127.78, 126.96, 115.56, 115.32, 114.97, 109.16, 58.15, 52.00, 43.94, 35.67, 33.47, 31.91, 26.02.

^{19}F NMR (376 MHz, acetone) δ -125.90.

^{1}H-NMR compound 25

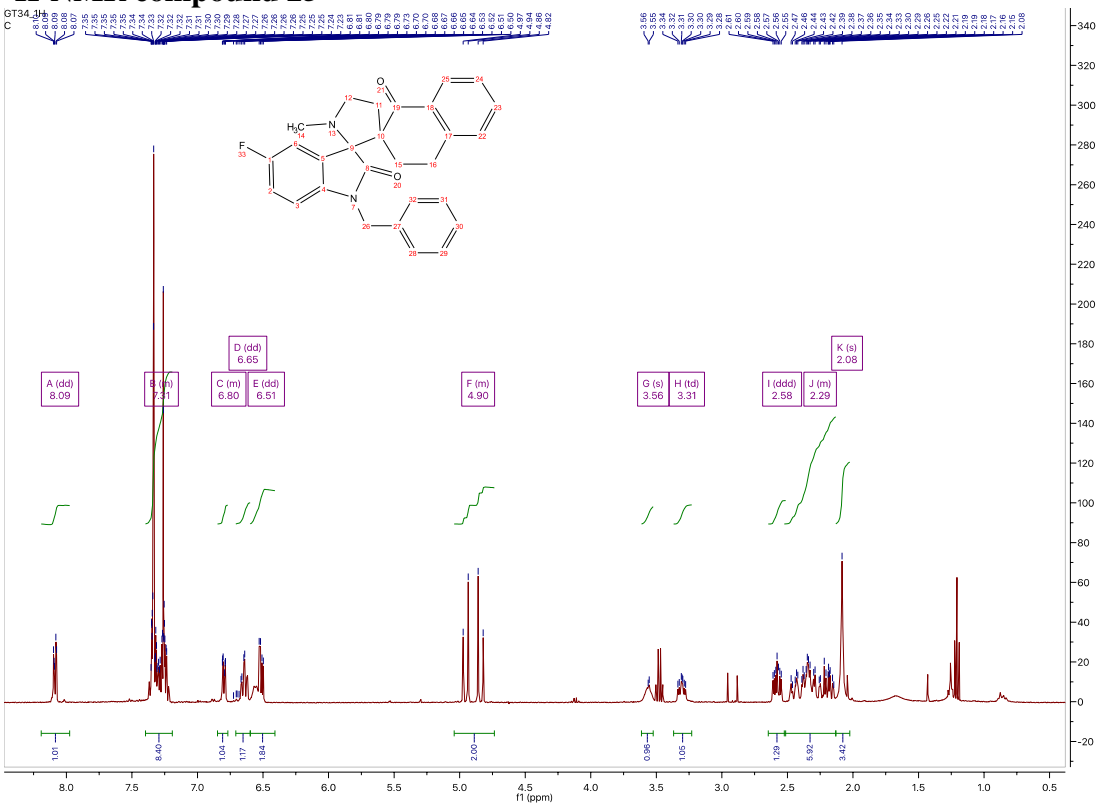

^{13}C-NMR, DEPT e ^{19}F-NMR compound 25

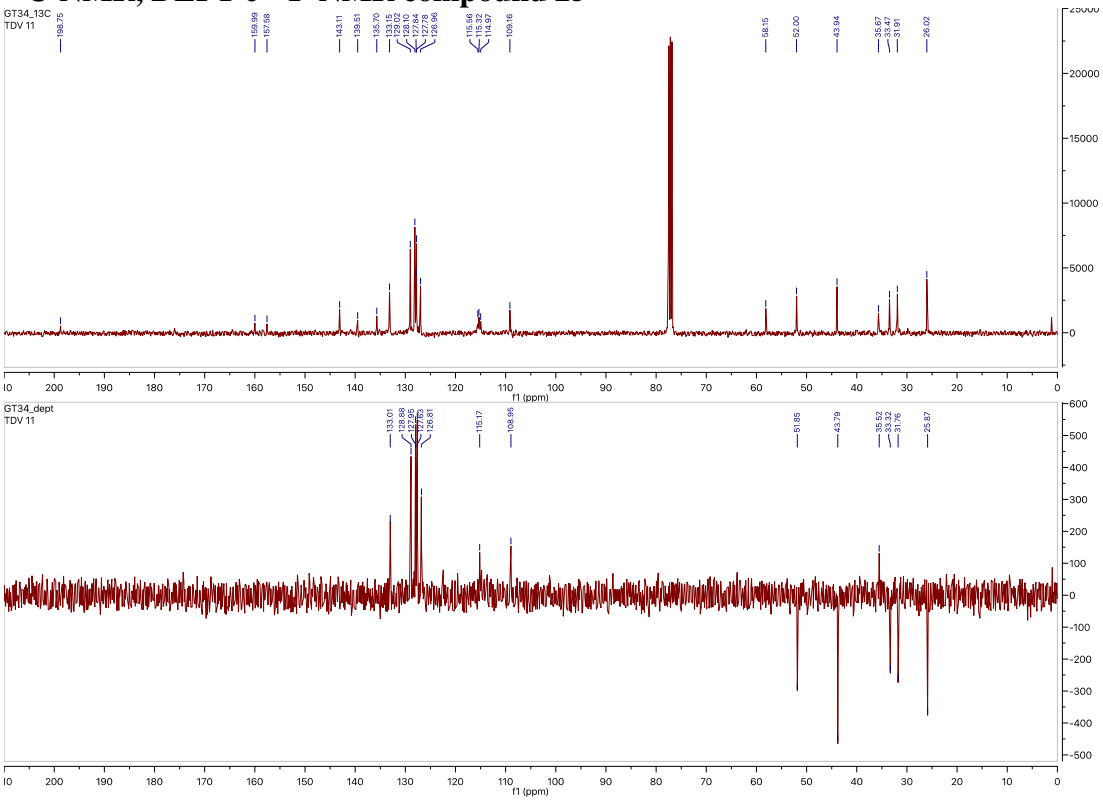

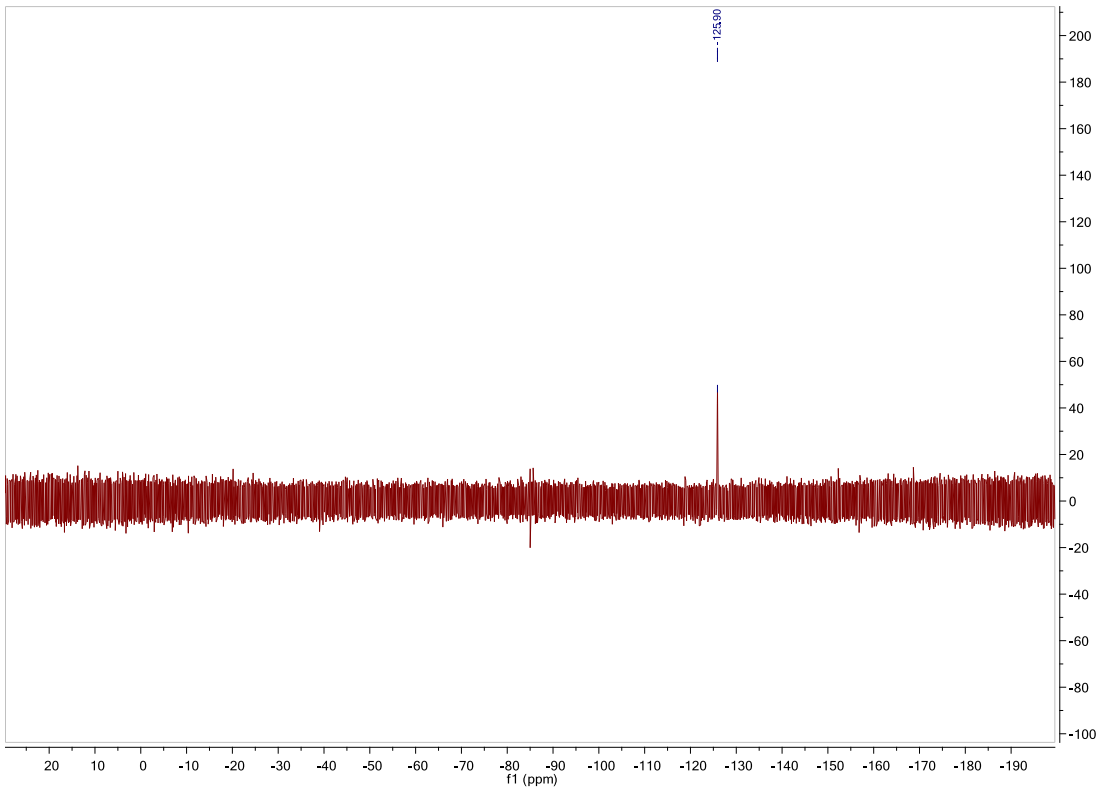
-125.90
200
180
160
140
120
100
80
60
40
20
0
-20
-40
-60
-80
-100
20 10 0 -10 -20 -30 -40 -50 -60 -70 -80 -90 -100 -110 -120 -130 -140 -150 -160 -170 -180 -190
f1 (ppm)

5.2.3 Synthesis of intermediates through a double aldolic reaction

Synthesis of compounds **27**, **28**, **29**, **30**, **31**:

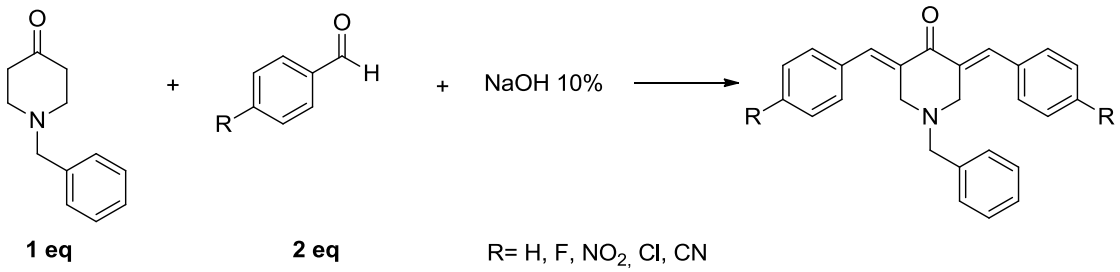

1 eq **2 eq** R= H, F, NO_2, Cl, CN

To a solution of aldehyde in EtOH, it was added N-benzyl piperidone. Then, it was added NaOH and the reaction was stirred at r.t. for 2 hours.

It was noticed a chromatic change from yellow to red, until to become brown.

After 2 hours there is a rush and it was necessary to filter on Gooch, separating a yellow solid.

Compound **27** (R=H):

Yield 60%

MS (ESI): $[M+H]^+$ = 365,34

^{1}H NMR (400 MHz, Chloroform-*d*) δ 7.84 (s, 1H), 7.45 – 7.32 (m, 6H), 7.32 – 7.16 (m, 3H), 3.89 (s, 2H), 3.73 (s, 1H).

^{13}C NMR (101 MHz, $cdcl_3$) δ 136.77, 135.32, 130.48, 130.44, 129.14, 129.10, 128.79, 128.66, 128.54, 128.47, 127.52, 61.47, 54.47.

^{1}H-NMR compound 27

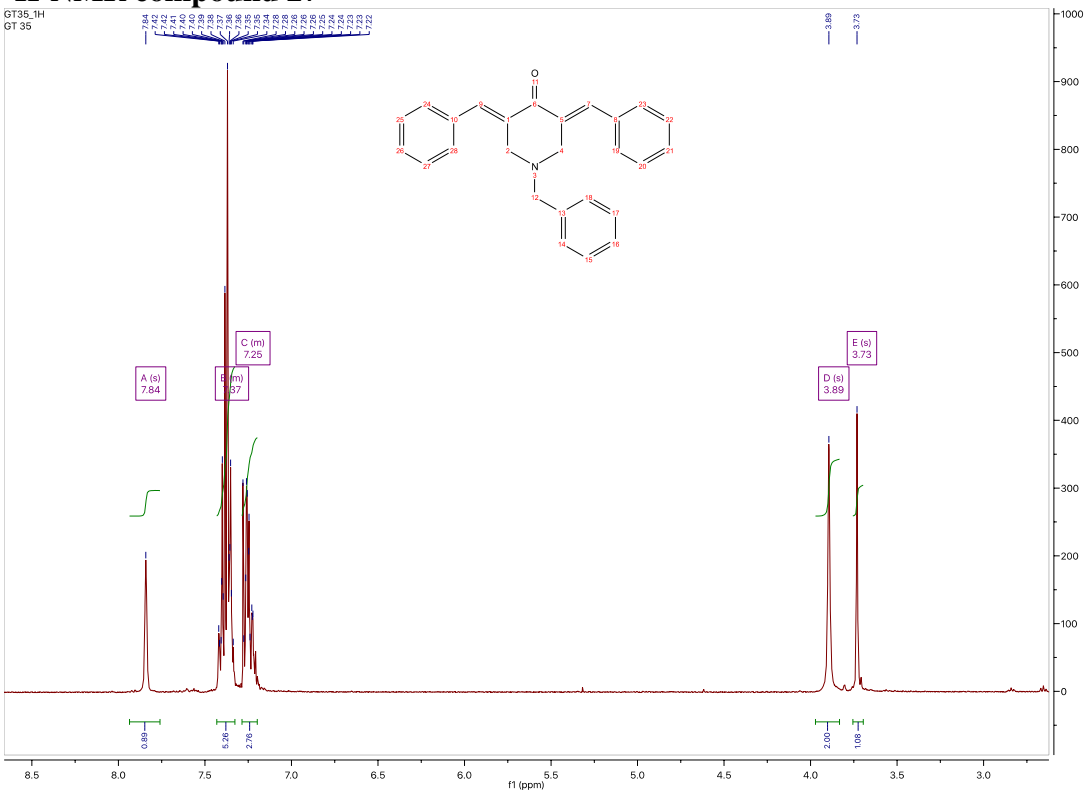

^{13}C-NMR, DEPT compound 27

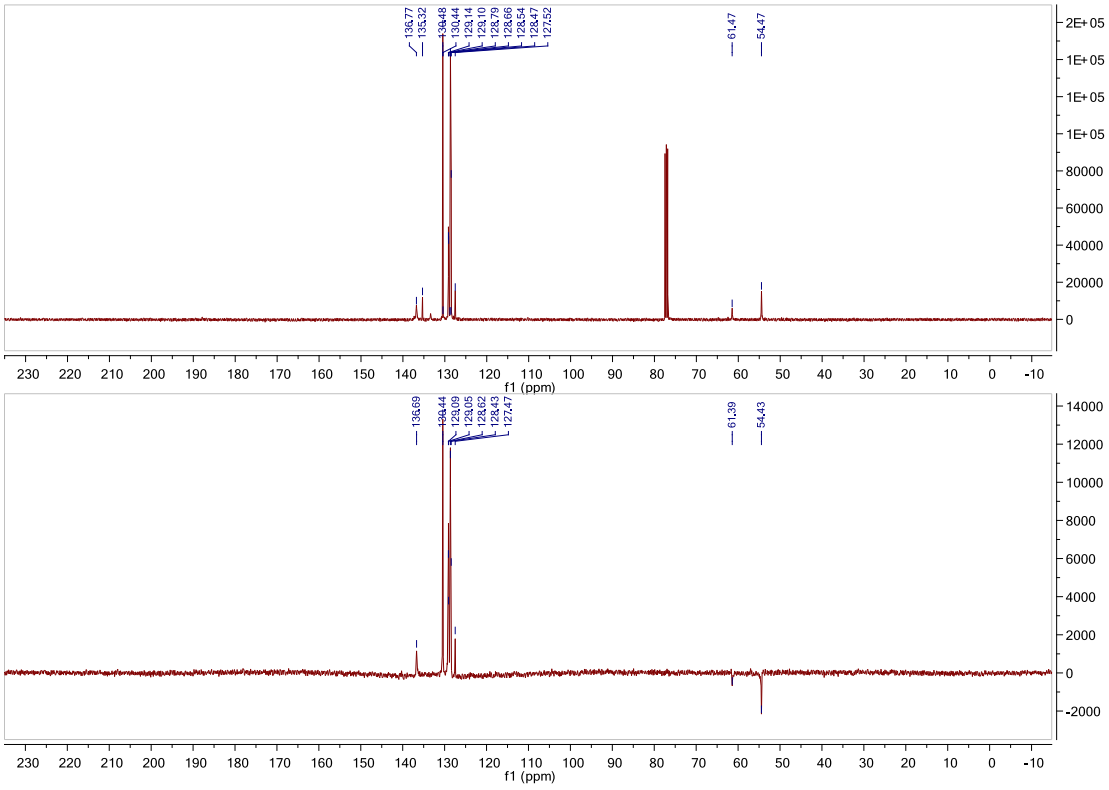

Compound **28** (R=F):

Yield 62%

MS (ESI): $[M+H]^+$ = 401,18

^{1}H NMR (400 MHz, Chloroform-*d*) δ 7.79 (s, 1H), 7.39 – 7.22 (m, 5H), 7.18 – 7.02 (m, 2H), 3.85 (d, *J* = 1.9 Hz, 2H), 3.73 (s, 1H).

^{13}C NMR (101 MHz, cdcl$_3$) δ 187.55, 164.26, 161.76, 137.22, 135.66, 132.95, 132.44, 132.35, 131.43, 129.11, 128.53, 127.63, 115.97, 115.75, 61.50, 54.32.

^{19}F NMR (376 MHz, cdcl$_3$) δ -110.89.

^{1}H-NMR compound 28

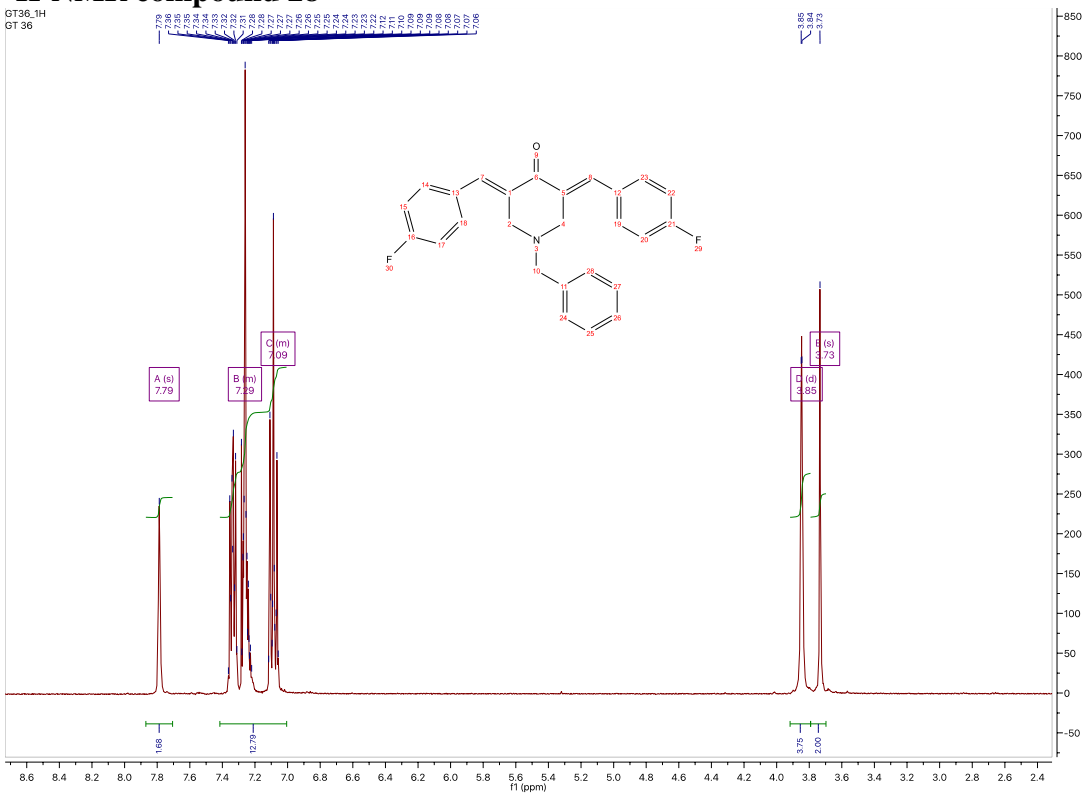

^{13}C-NMR, DEPT e ^{19}F-NMR compound 28

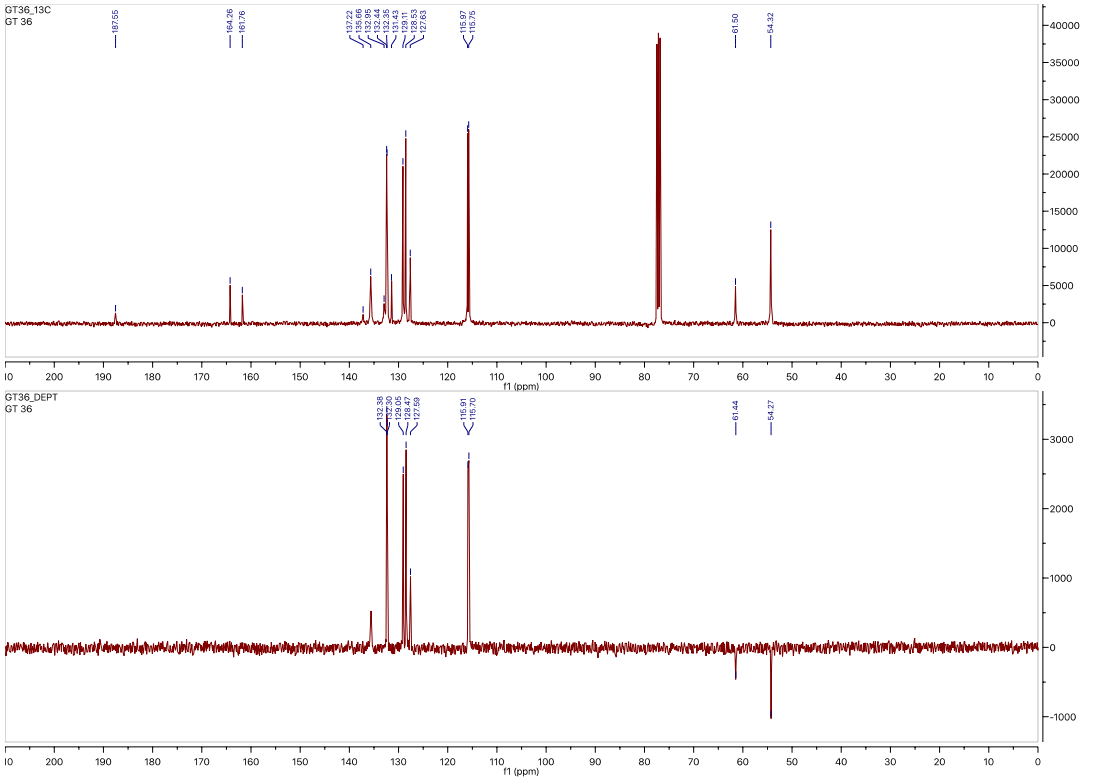

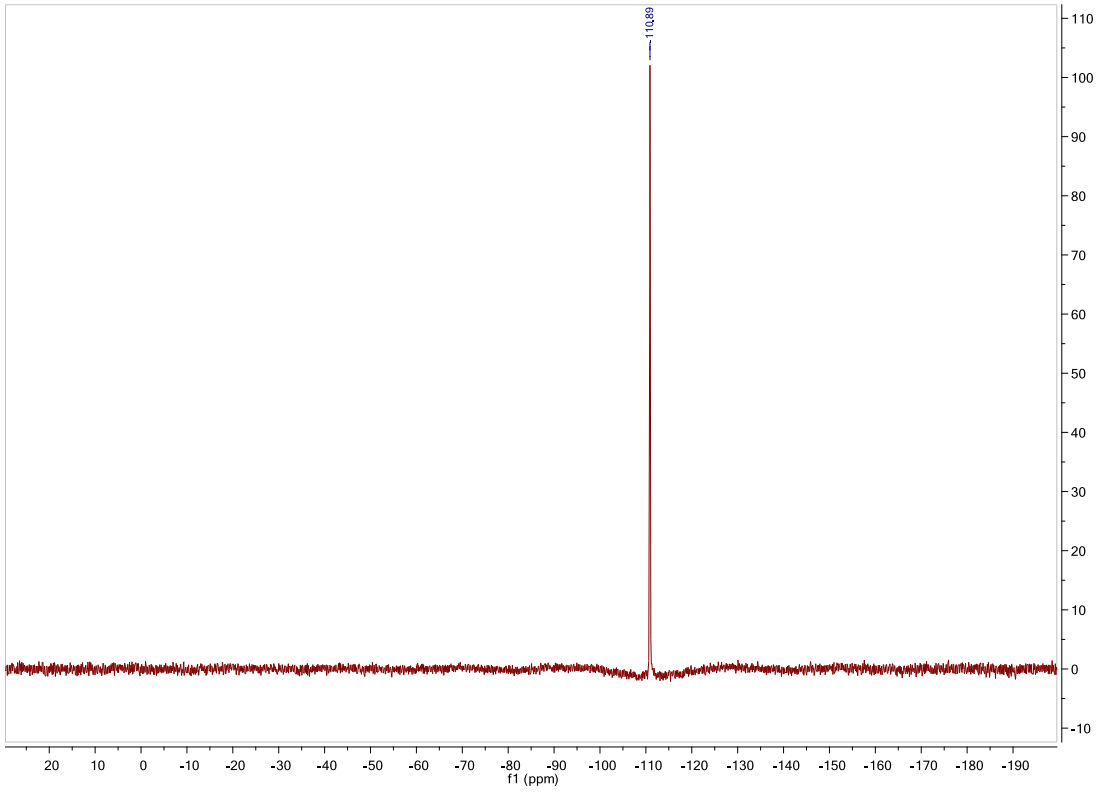

Compound **30** (R=NO_2):

Yield 73%

MS (ESI): $[M+H]^+$ = 455,18

^{1}H NMR (400 MHz, Chloroform-*d*) δ 8.35 – 8.14 (m, 1H), 7.82 (d, *J* = 1.8 Hz, 4H), 7.54 – 7.40 (m, 4H), 7.33 – 7.06 (m, 5H), 3.85 (d, *J* = 1.8 Hz, 4H), 3.74 (s, 2H).

^{13}C NMR (101 MHz, cdcl$_3$) δ 186.93, 147.64, 141.42, 136.76, 136.06, 134.36, 130.85, 129.00, 128.66, 127.89, 123.91, 61.57, 54.20.

^{1}H-NMR compound 30

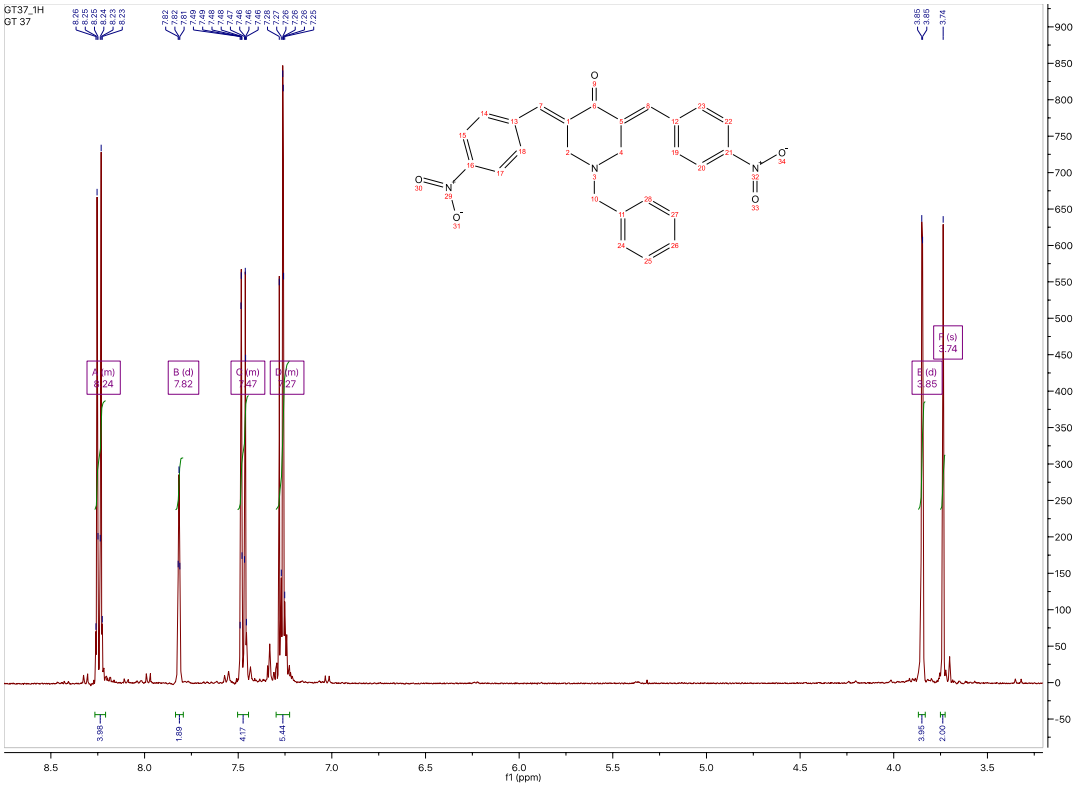

^{13}C-NMR, DEPT compound 30

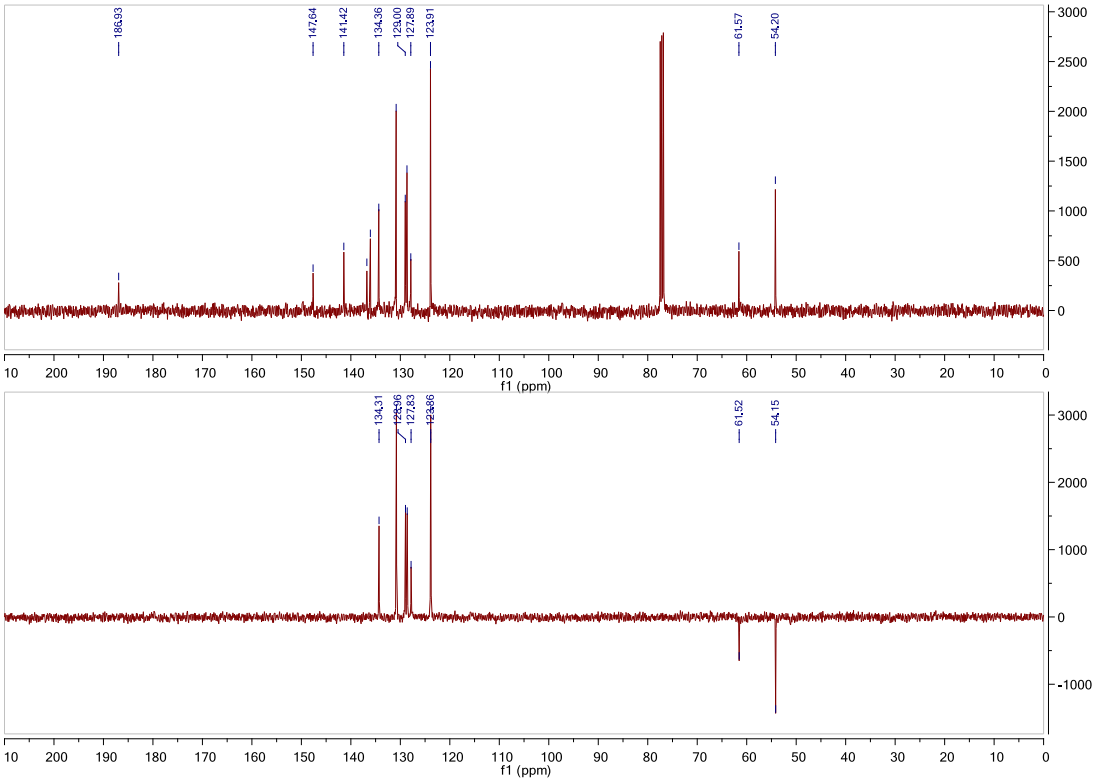

Compound **31** (R=Cl):

Yield 55%

MS (ESI): $[M+H]^+$ = 433,18

^{1}H NMR (400 MHz, Chloroform-*d*) δ 7.76 (s, 4H), 7.40 – 7.32 (m, 4H), 7.28 (d, *J* = 0.5 Hz, 4H), 3.87 – 3.80 (m, 4H), 3.73 (s, 2H).

^{13}C NMR (101 MHz, $cdcl_3$) δ 135.50, 135.20, 133.66, 131.65, 129.09, 128.98, 128.57, 127.69, 61.53, 54.34.

^{1}H-NMR compound 31

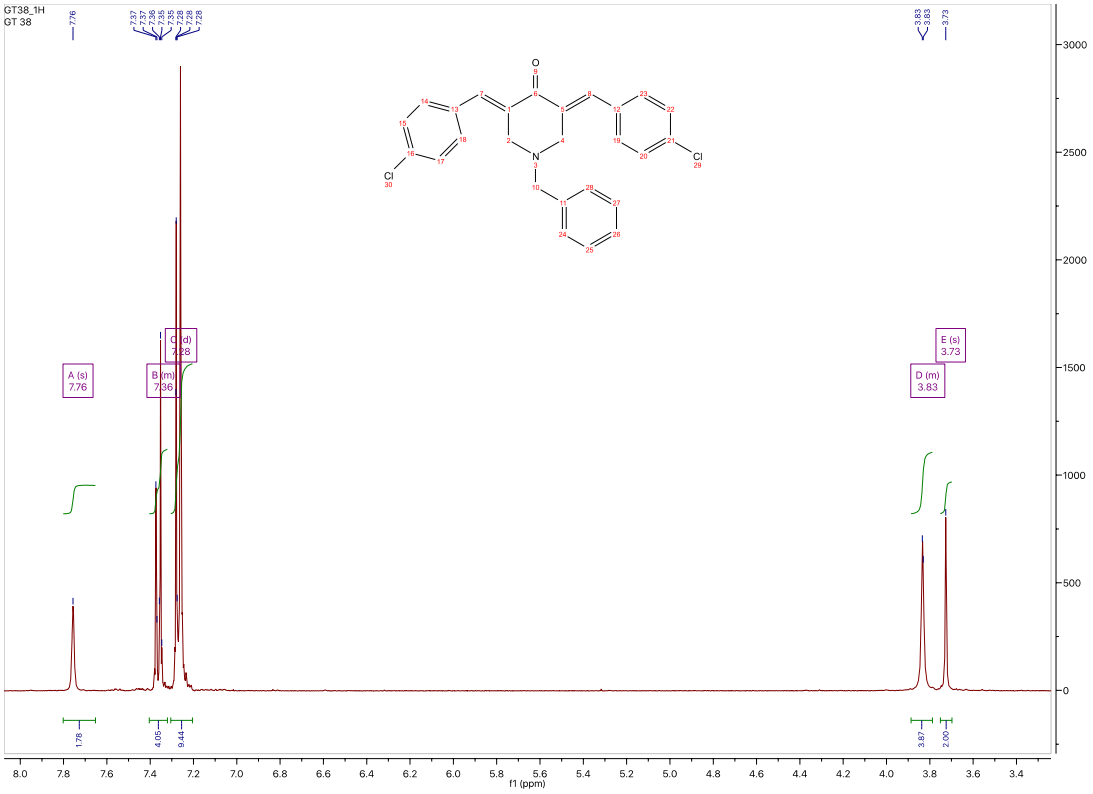

^{13}C-NMR, DEPT compound 31

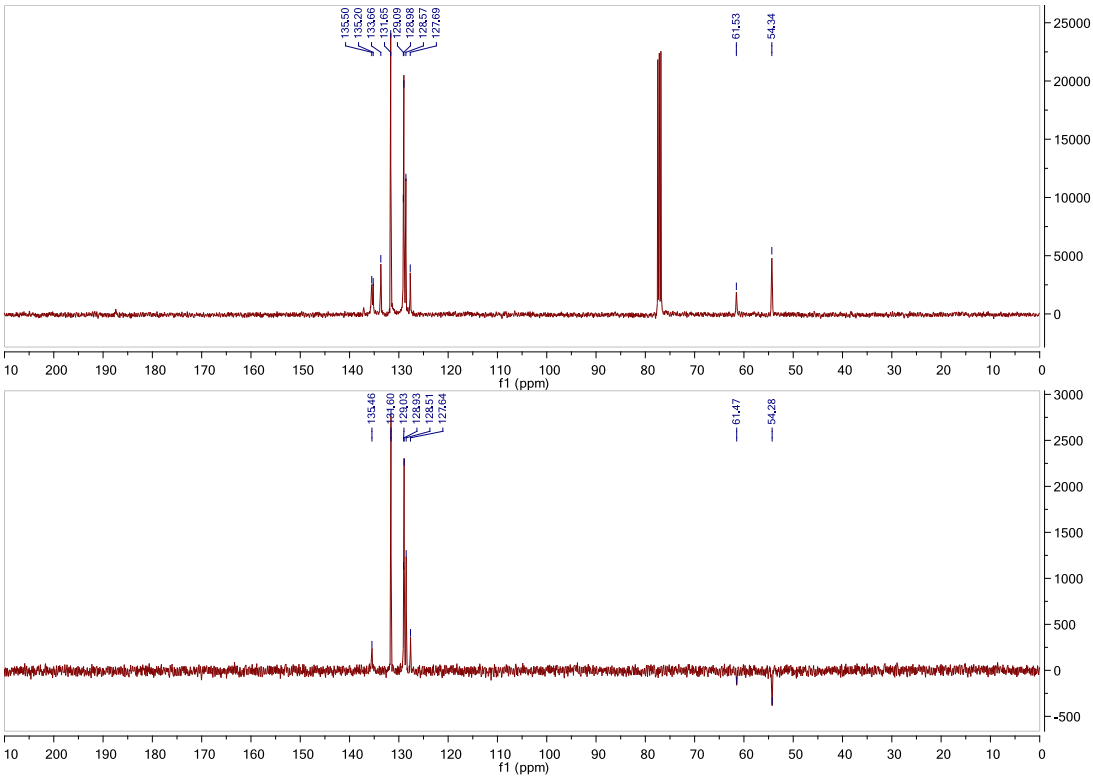

Compound **29** (R=CN):

Yield 32%

MS (ESI): $[M+H]^+$ = 415,26

^{1}H NMR (400 MHz, Chloroform-*d*) δ 7.77 (s, 1H), 7.70 – 7.64 (m, 4H), 7.46 – 7.37 (m, 4H), 7.33 – 7.20 (m, 5H), 3.82 (d, *J* = 1.8 Hz, 4H), 3.72 (s, 2H).

^{13}C NMR (101 MHz, cdcl$_3$) δ 187.00, 139.52, 136.82, 135.61, 134.77, 132.38, 130.60, 129.01, 128.78, 128.62, 127.84, 118.53, 112.46, 61.50, 54.16.

^{1}H-NMR compound 29

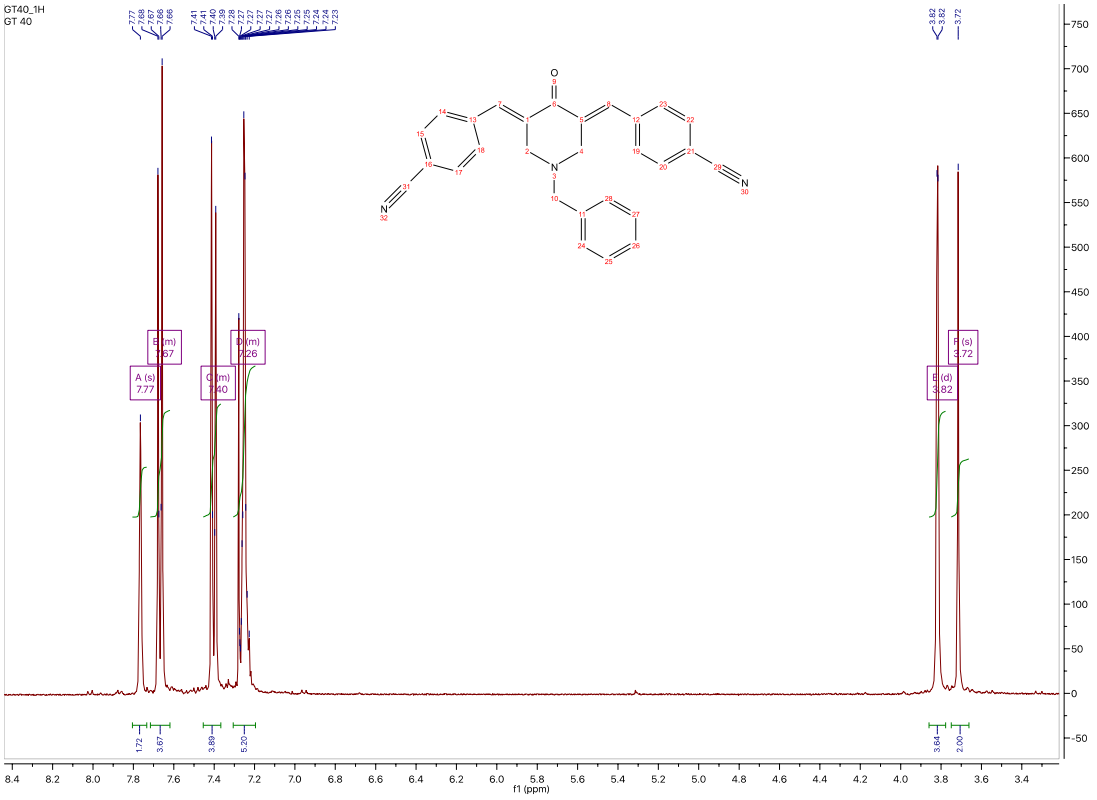

^{13}C-NMR, DEPT compound 29

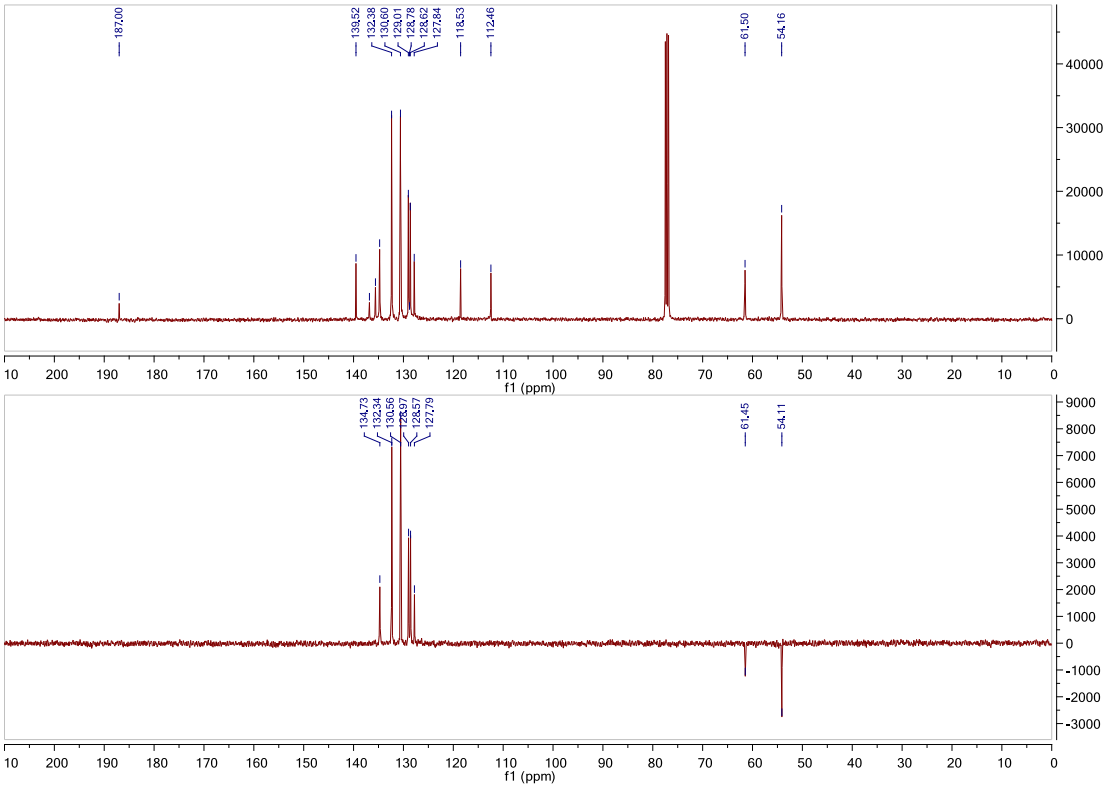

Synthesis of compound **32**:

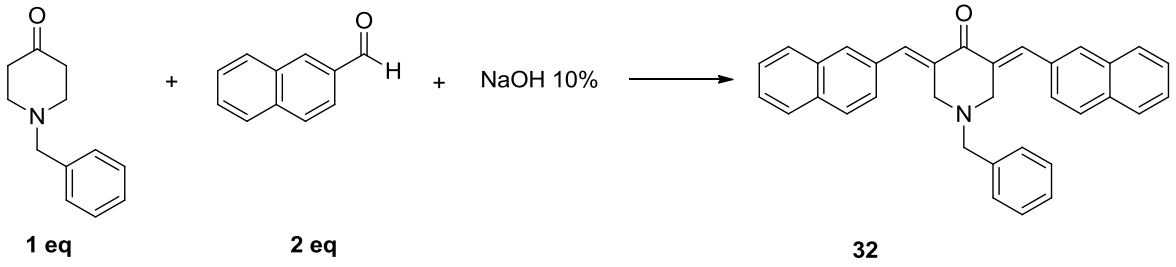

1 eq **2 eq** **32**

To a solution of aldehyde in EtOH, it was added N-benzyl piperidone. Then, it was added NaOH and the reaction was stirred at r.t. for 2 hours.

It was noticed a chromatic change from yellow to red, until to become brown.

After 2 hours there is a rush and it was necessary to filter on Gooch, separating a yellow solid.

Yield 60%

MS (ESI): $[M+H]^+ = 465{,}26$

^{1}H NMR (400 MHz, Chloroform-*d*) δ 8.00 (t, *J* = 1.6 Hz, 1H), 7.91 – 7.80 (m, 4H), 7.61 – 7.42 (m, 3H), 7.35 – 7.11 (m, 3H), 4.01 (d, *J* = 1.8 Hz, 2H), 3.75 (s, 1H).

^{13}C NMR (101 MHz, $cdcl_3$) δ 187.80, 137.34, 136.89, 133.68, 133.31, 133.19, 132.94, 130.62, 129.17, 128.63, 128.49, 128.28, 127.79, 127.55, 127.21, 126.67, 61.60, 54.66.

^{1}H-NMR compound 32

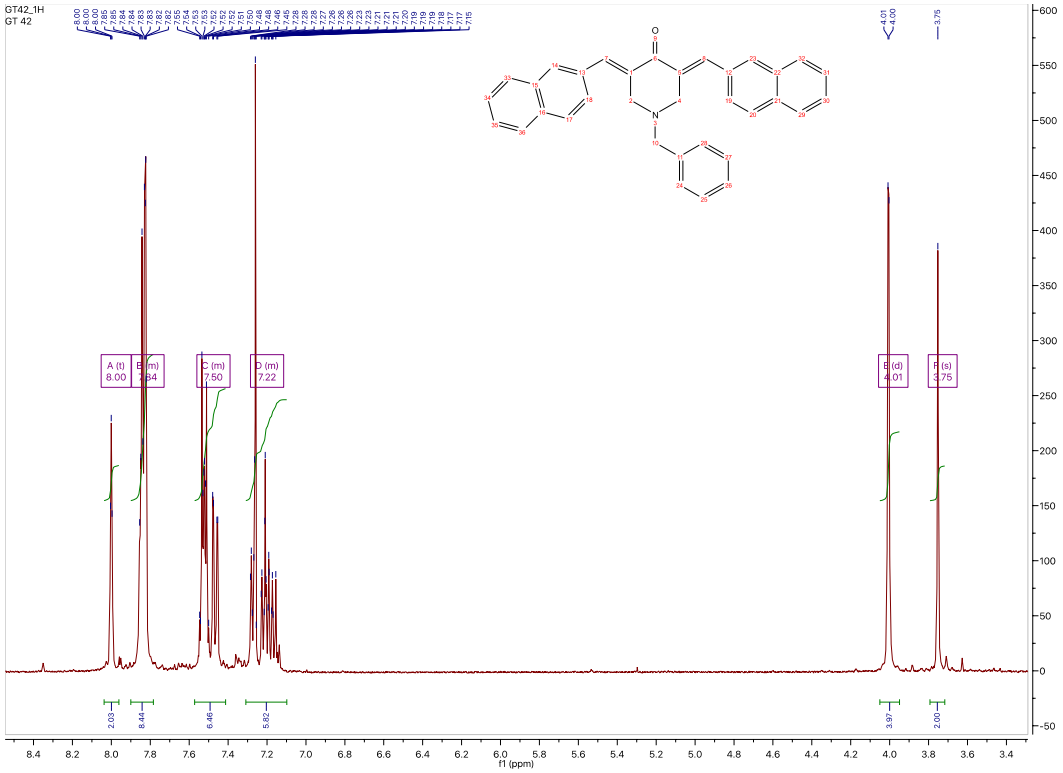

^{13}C-NMR, DEPT compound 32

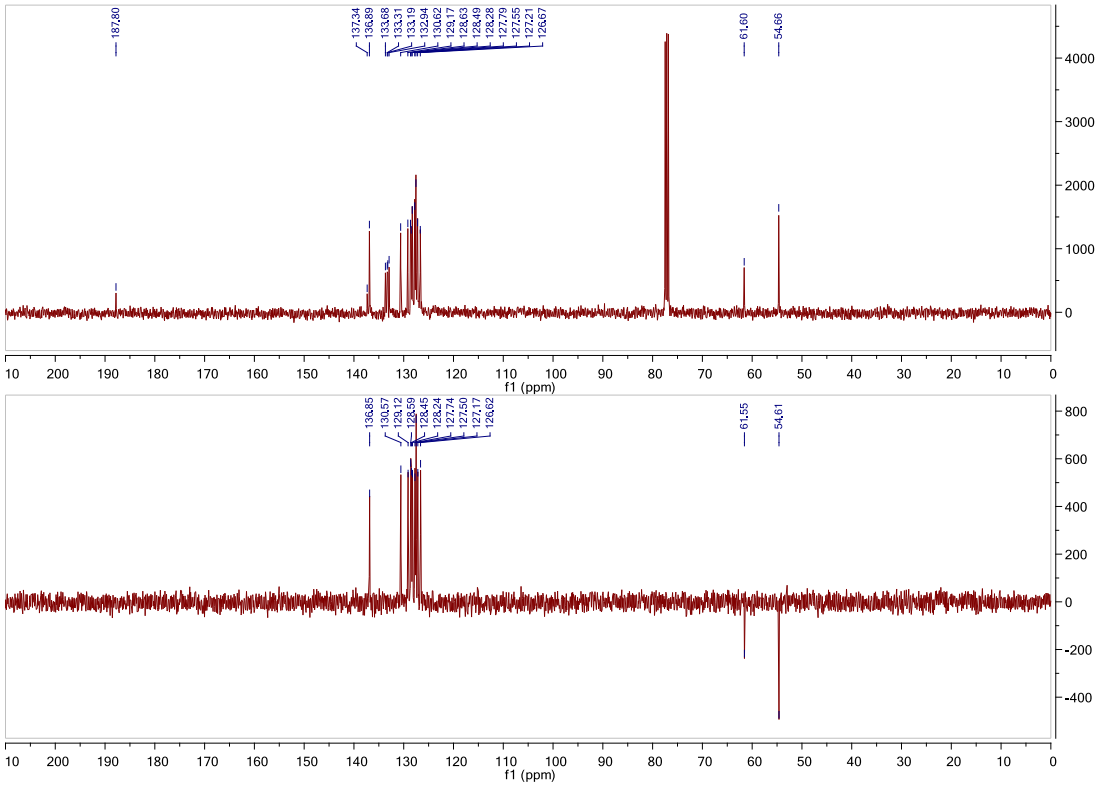

5.2.4 Synthesis of dispiropiperidone-tetrahydrothiophene derivatives

Synthesis of compounds **34**, **35**, **36**, **37**, **38**:

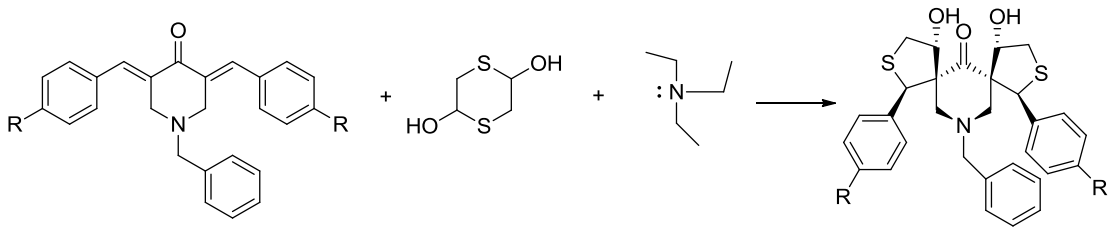

1 eq **2 eq** **2 eq**

R= H, F, NO_2, Cl, CN

To a solution of the intermediate from the aldolic reaction in EtOH absolute (5ml), it was added the 1,4-dithiane-2,5-diol. The round-bottom flask was stirred at 0°C, once cold, it was added to the reaction triethylamine. The reaction was stirred from 0°C to r.t. for 3 hours.

After monitoring the formation of the product by TLC (A1P4), the solvent is evaporated and it was purified by coloumn cromatography.

The NMR spectra are analyzed in DMSO.

Compound **34** (R=H):

White solid.

Yield 92%

MS (ESI): $[M+H]^+$ = 517,17

^{1}H NMR (400 MHz, DMSO-d_6) δ 7.75 – 7.59 (m, 8H), 7.47 – 7.39 (m, 4H), 7.40 – 7.26 (m, 2H), 7.26 – 7.14 (m, 4H), 5.57 (s, 2H), 5.22 (t, *J* = 4.4 Hz, 2H), 5.16 (d, *J* = 4.1 Hz, 1H), 3.40 (s, 1H), 3.34 (s, 1H), 3.18 (dd, *J* = 12.1, 4.5 Hz, 1H), 2.79 (d, *J* = 12.1 Hz, 1H), 2.70 (d, *J* = 12.1 Hz, 1H), 1.56 (d, *J* = 12.2 Hz, 1H).

^{13}C NMR (101 MHz, dmso) δ 203.34, 141.97, 131.69, 130.66, 128.76, 128.29, 118.51, 110.10, 79.25, 68.59, 60.73, 54.60, 51.32, 36.66.

^{1}H-NMR compound 34

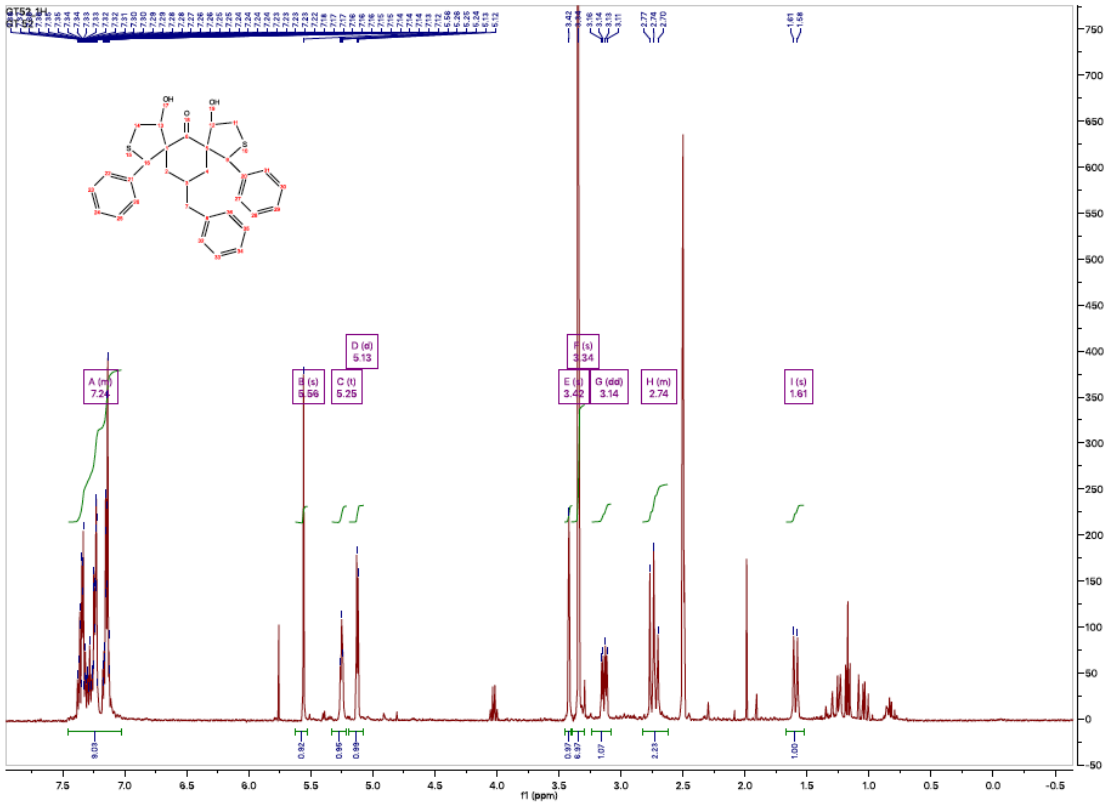

^{13}C-NMR and DEPT compound 34

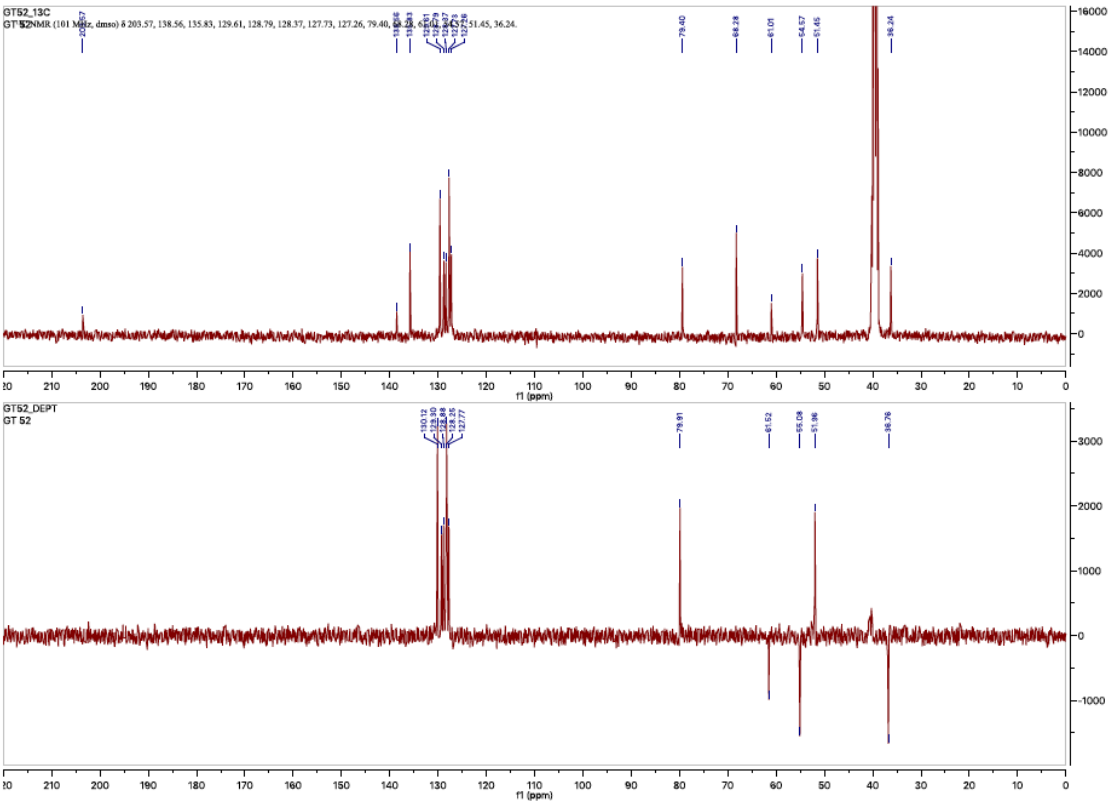

Compound **35** (R=F):

White solid.

Yield 30%

MS (ESI): $[M+H]^+$ = 553,16

^{1}H NMR (400 MHz, DMSO-d_6) δ 7.49 – 7.21 (m, 8H), 7.15 – 6.99 (m, 4H), 5.53 (s, 2H), 5.22 (d, J = 4.6 Hz, 2H), 3.44 (s, 4H), 3.14 (dd, J = 12.2, 4.8 Hz, 2H), 2.73 (dd, J = 14.8, 12.0 Hz, 2H), 1.56 (d, J = 12.1 Hz, 2H).

^{13}C NMR (101 MHz, dmso) δ 203.59, 162.45, 160.02, 138.45, 131.82, 131.56, 131.48, 128.80, 128.35, 127.33, 114.61, 114.40, 79.14, 68.18, 60.95, 54.53, 50.70, 36.28.

^{1}H-NMR compound 35

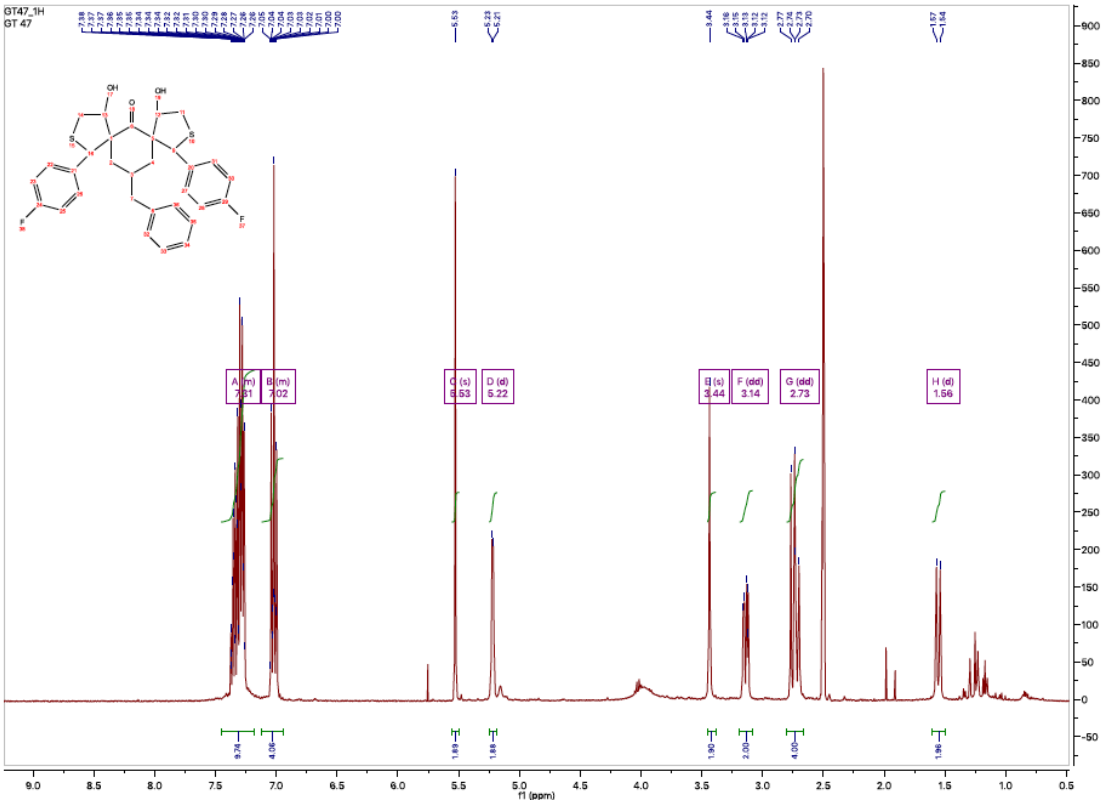

^{13}C, ^{19}F-NMR and DEPT compound 35

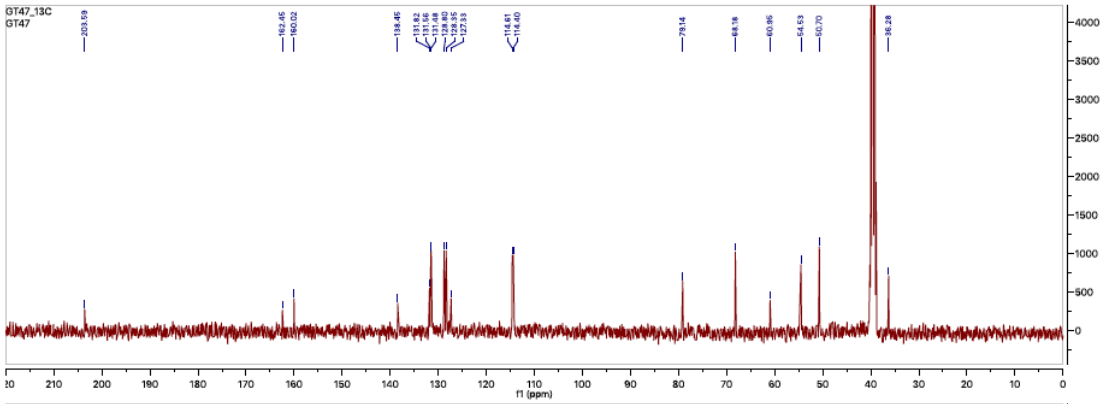

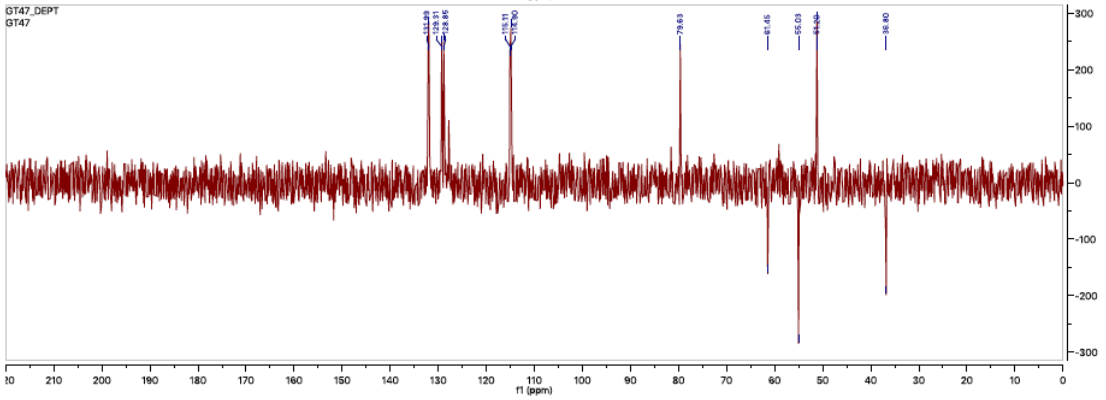

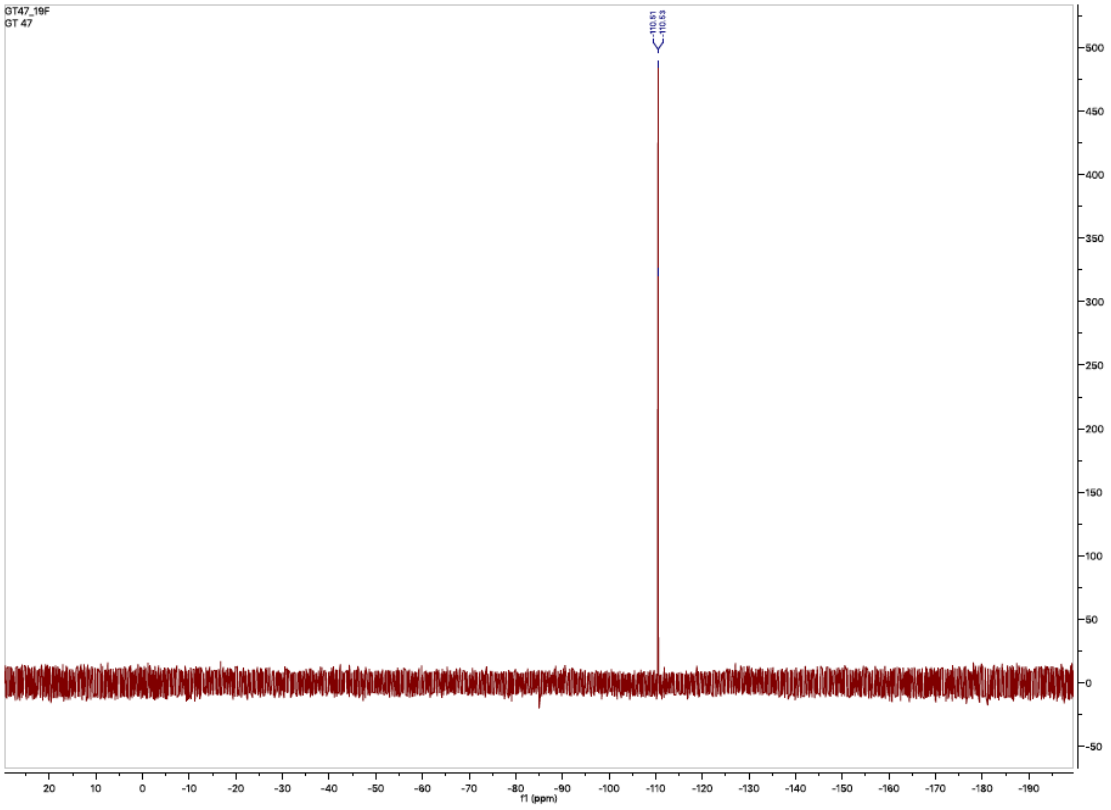

Compound **37** (R=NO_2):

White solid.

Yield 87%

MS (ESI): $[M+H]^+$ = 607,18

Compound **38** (R=Cl):

White solid.

Yield 90%

MS (ESI): $[M+H]^+$ = 586,98

^{1}H NMR (400 MHz, DMSO-d_6) δ 7.49 – 7.21 (m, 8H), 7.15 – 6.99 (m, 4H), 5.53 (s, 2H), 5.22 (d, *J* = 4.6 Hz, 2H), 3.44 (s, 4H), 3.14 (dd, *J* = 12.2, 4.8 Hz, 2H), 2.73 (dd, *J* = 14.8, 12.0 Hz, 2H), 1.56 (d, *J* = 12.1 Hz, 2H).

^{13}C NMR (101 MHz, dmso) δ 203.59, 162.45, 160.02, 138.45, 131.82, 131.56, 131.48, 128.80, 128.35, 127.33, 114.61, 114.40, 79.14, 68.18, 60.95, 54.53, 50.70, 36.28.

^{1}H-NMR compound 38

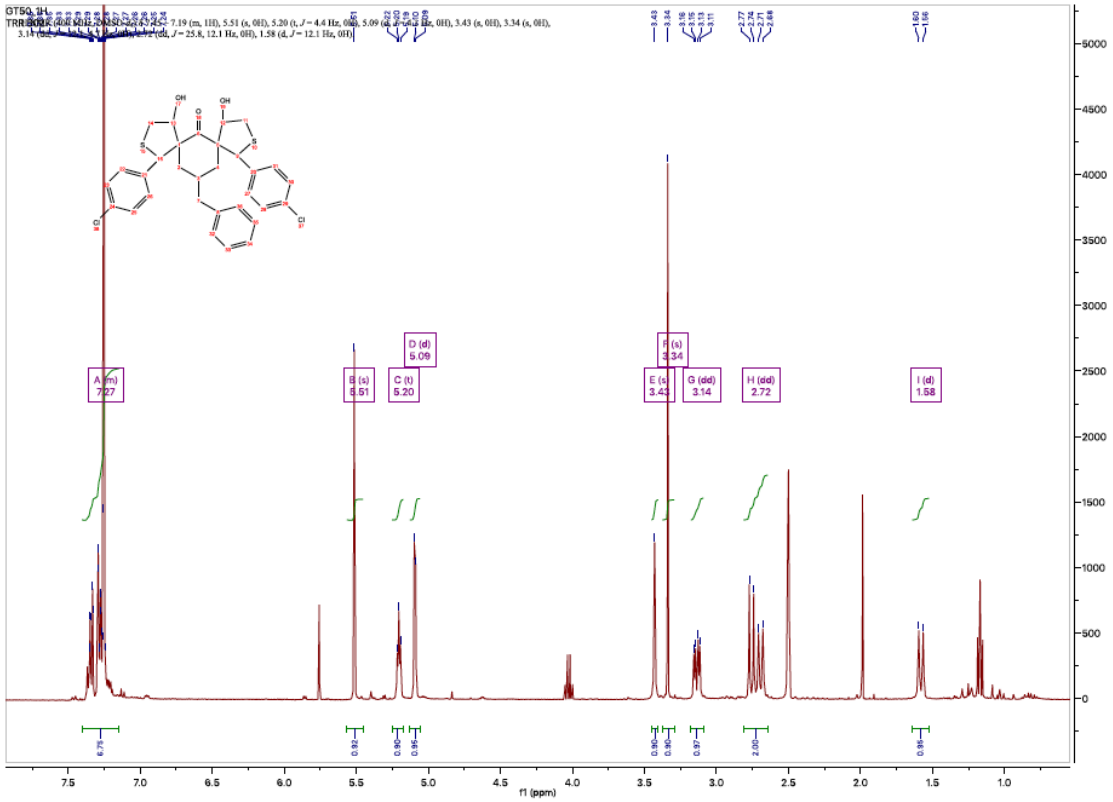

^{13}C-NMR and DEPT compound 38

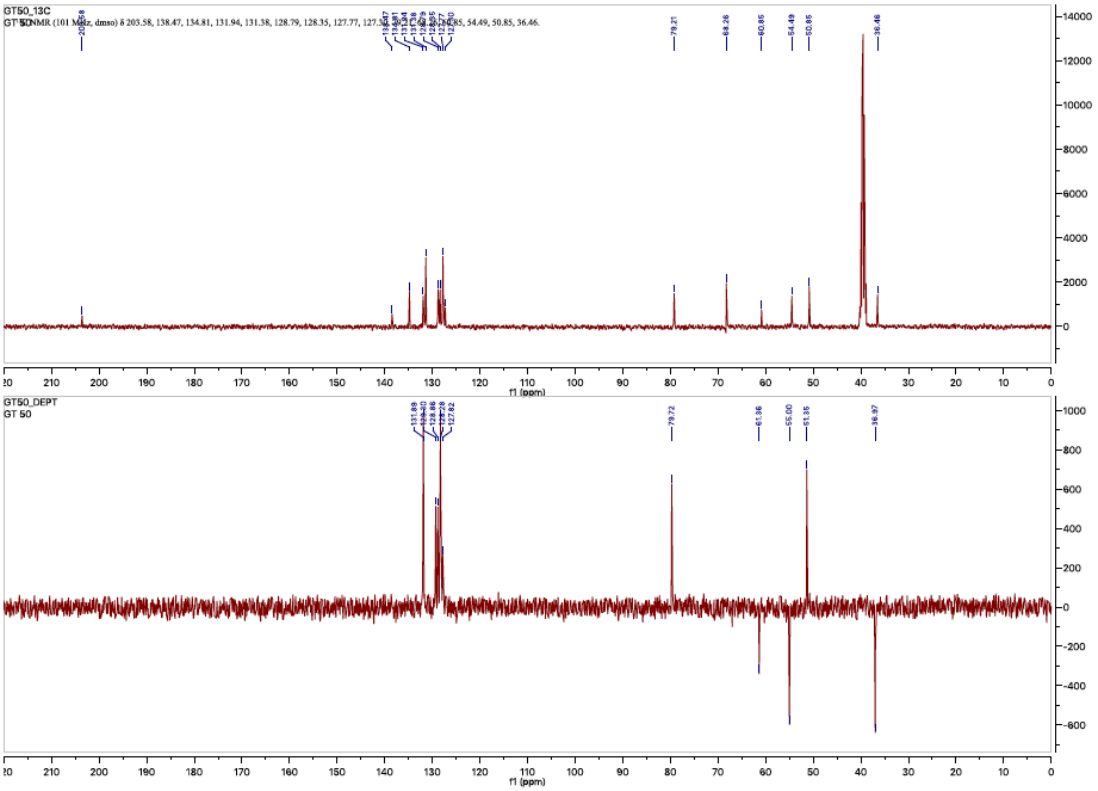

Compound **36** (R=CN):

White solid.

Yield 79%

MS (ESI): $[M+H]^+$ = 567,25

^{1}H NMR (400 MHz, DMSO-d_6) δ 7.45 – 7.19 (m, 8H), 5.51 (s, 4H), 5.20 (t, J = 4.4 Hz, 2H), 5.09 (d, J = 4.1 Hz, 2H), 3.43 (s, 4H), 3.34 (s, 2H), 3.14 (dd, J = 12.1, 4.7 Hz, 2H), 2.72 (dd, J = 25.8, 12.1 Hz, 2H), 1.58 (d, J = 12.1 Hz, 2H).

^{13}C NMR (101 MHz, dmso) δ 203.58, 138.47, 134.81, 131.94, 131.38, 128.79, 128.35, 127.77, 127.30, 79.21, 68.26, 60.85, 54.49, 50.85, 36.46.

^{1}H-NMR compound 36

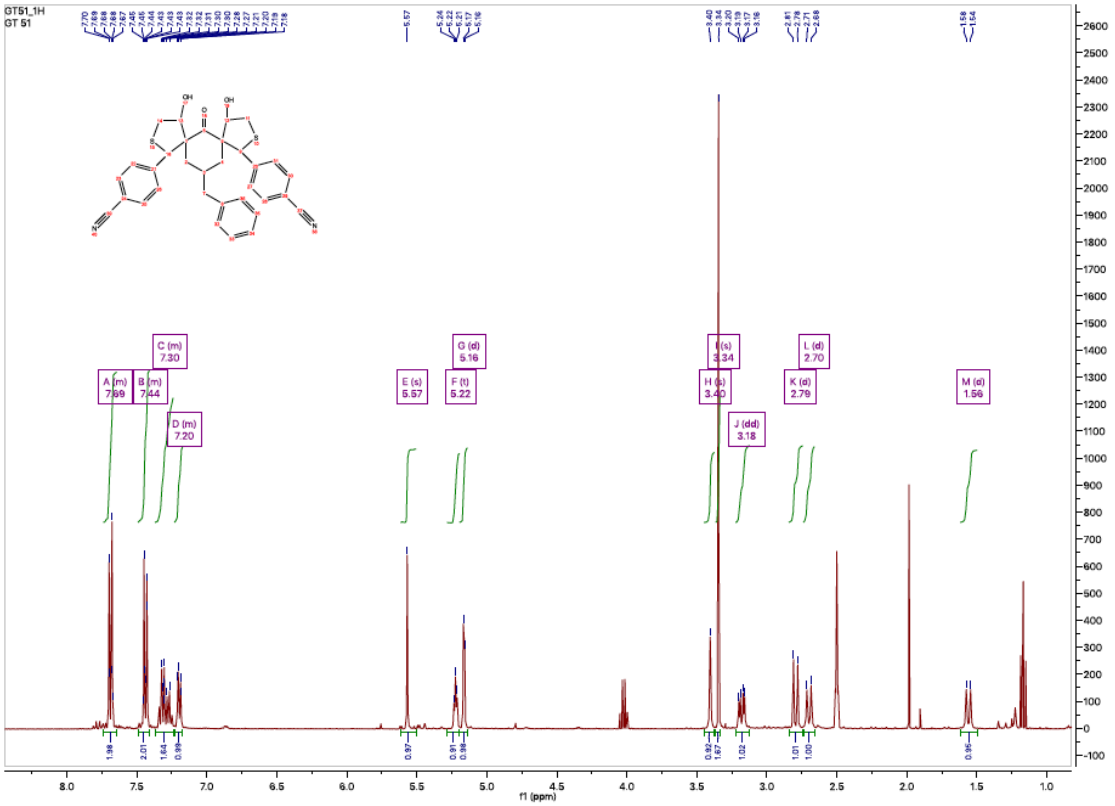

^{13}C-NMR and DEPT compound 36

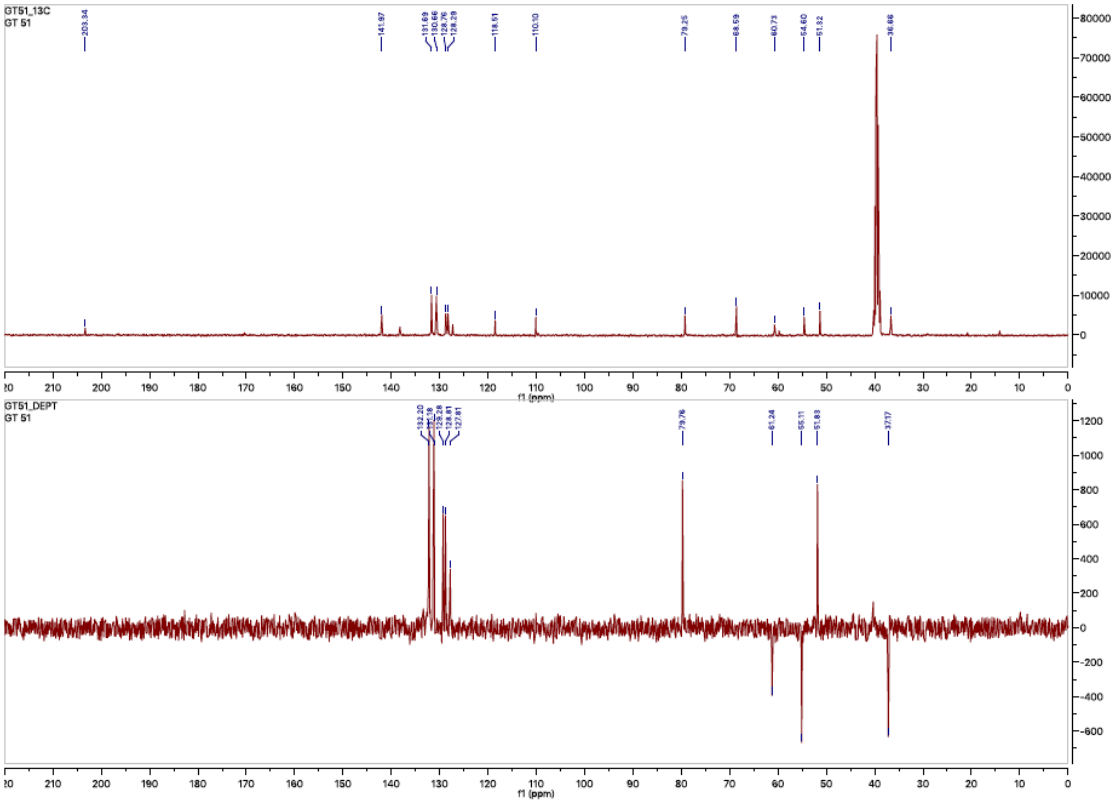

Synthesis of compound **39**:

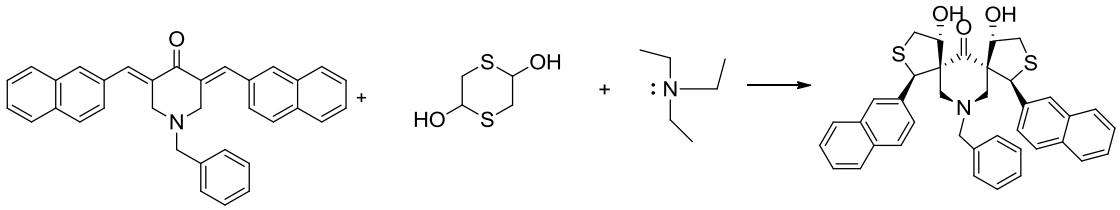

To a solution of the intermediate from the aldolic reaction in EtOH absolute (5ml), it was added the 1,4-dithiane-2,5-diol. The round-bottom flask was stirred at 0°C, once cold, it was added to the reaction TEA. The reaction was stirred from 0°C to r.t. for 3 hours.

After monitoring the formation of the product by TLC (A1P4), the solvent is evaporated and it was purified by coloumn cromatography.

The NMR spectra are analyzed in DMSO.

White solid.

Yield 80%

MS (ESI): $[M+H]^+ = 617,21$

^{1}H NMR (400 MHz, DMSO-d_6) δ 7.47 – 6.99 (m, 8H), 5.56 (s, 4H), 5.25 (t, J = 4.4 Hz, 2H), 5.13 (d, J = 4.0 Hz, 2H), 3.42 (s, 4H), 3.34 (s, 2H), 3.14 (dd, J = 12.1, 4.7 Hz, 2H), 2.83 – 2.67 (m, 2H), 1.61 (s, 2H).

^{13}C NMR (101 MHz, dmso) δ 203.57, 138.56, 135.83, 129.61, 128.79, 128.37, 127.73, 127.26, 79.40, 68.28, 61.01, 54.57, 51.45, 36.24.

^{1}H-NMR compound 39

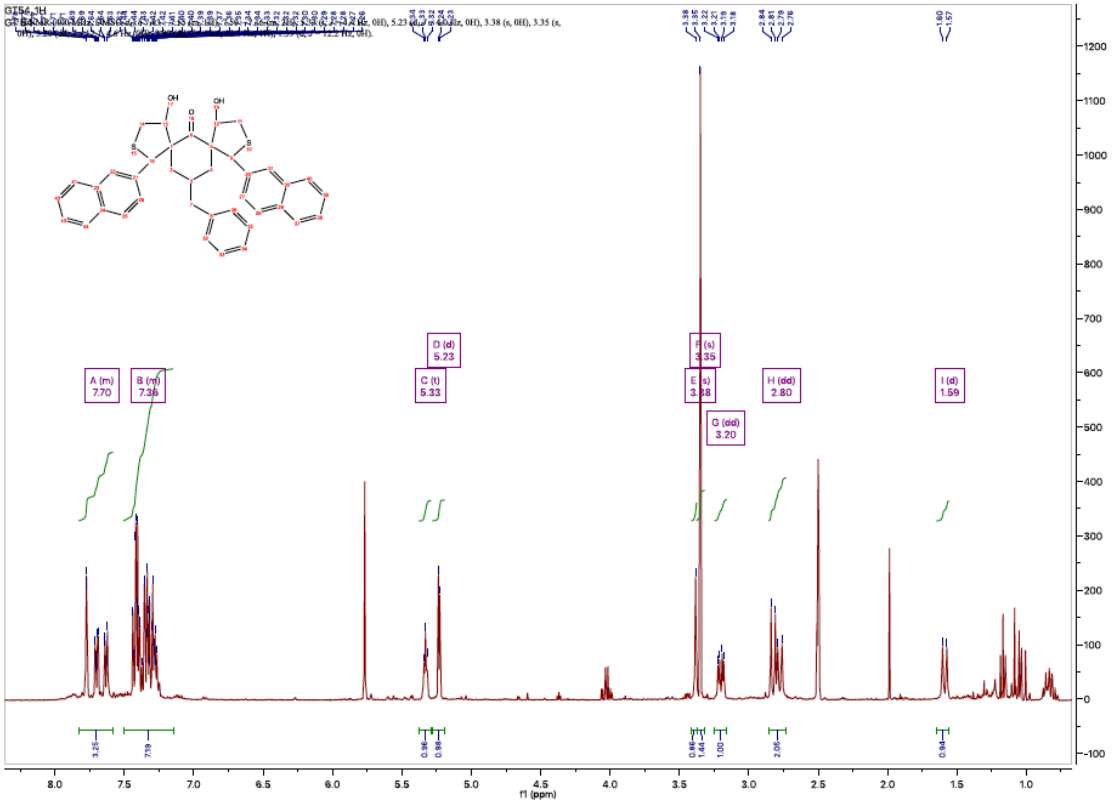

^{13}C-NMR and DEPT compound 39

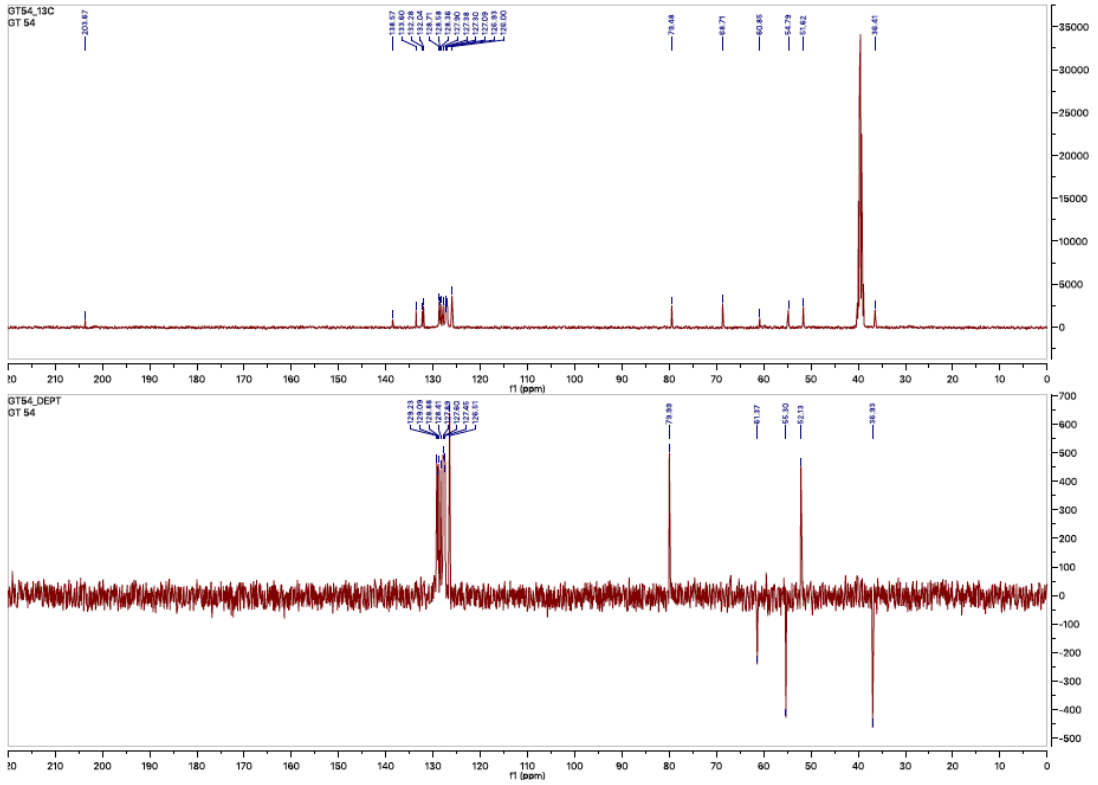

5.3 (-)-Nutlin-3

Synthesis of 4-chloro-N-((1S,2R)-2-((E)-(4-chlorobenzylidene)amino)-1,2-bis(4-chlorophenyl)ethyl)benzamide **64**:

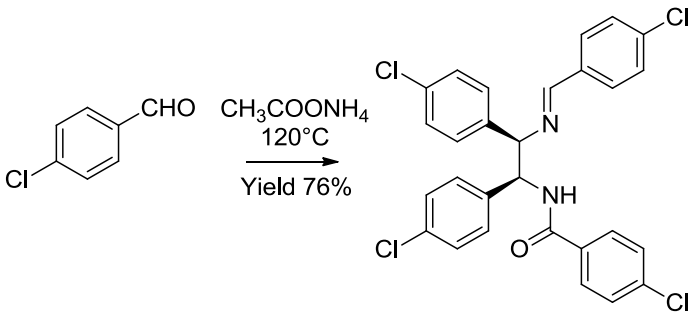

In a round-bottom flask it is added *p*-chlorobenzaldehyde (75.4 mmol) and ammonium acetate (3.5 eq.) in four aliquots every 5 minutes and the reaction was stirred at 120°C. After 18 h the residue was left to cool at r.t. and washed with petroleum ether. The crude product was then washed with NaOH 2N (pH>9) and filtered on gooch. The yellow compound was washed with Et_2O and filtered again. Finally, it was obtained 7.8 g. of benzylidene-amide **64** (yield 76%) as a white solid.

M.P. : 208-212°C.
MS (ESI): $[M+H]^+ = 419.04$

^{1}H NMR (400 MHz, Chloroform-*d*) δ 8.24 (s, 1H), 7.71 (d, *J* = 8.1 Hz, 2H), 7.59 (d, *J* = 8.4 Hz, 2H), 7.48 – 7.35 (m, 4H), 7.23 (dd, *J* = 8.4, 2.9 Hz, 3H), 7.14 (t, *J* = 7.7 Hz, 4H), 6.58 (s, 1H), 5.47 (dd, *J* = 7.7, 4.9 Hz, 1H), 4.94 (d, *J* = 4.9 Hz, 1H).

^{13}C NMR (101 MHz, $CDCl_3$) δ 162.03, 129.92, 129.73, 129.31, 129.13, 128.71, 128.49, 128.37, 76.06, 59.49.

^{1}H-NMR of compound 64

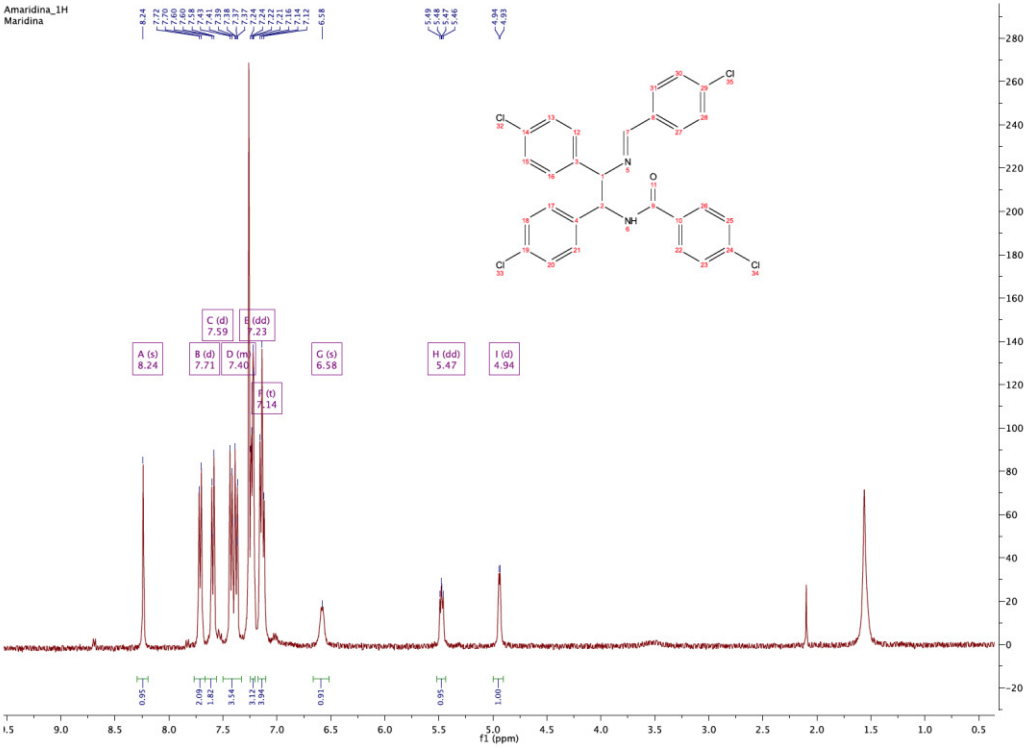

^{13}C-NMR and DEPT of compound 64

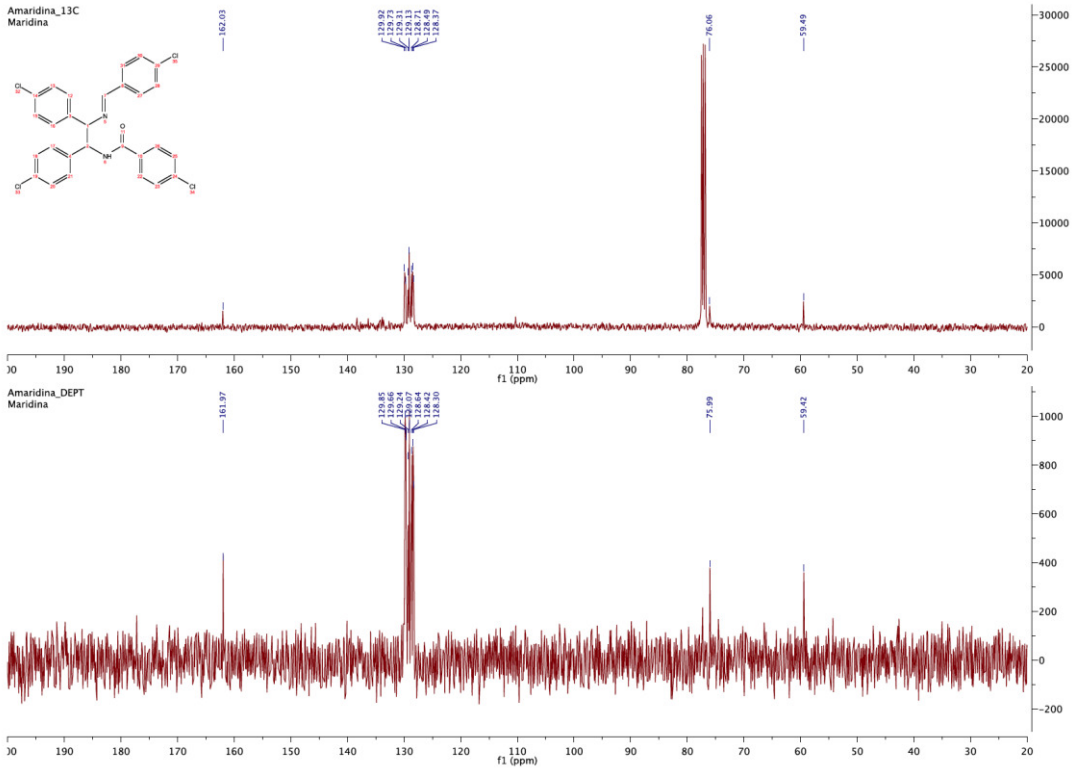

Synthesis of (1R,2S)-1,2-bis(4-chlorophenyl)ethane-1,2-diamine **46:**

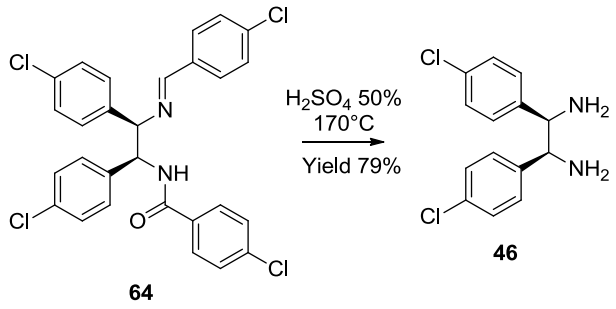

To a solution of benzylidene-amide **64** in H_2SO_4 (50% v/v) at 170°C for 24h, it was added water (30ml), after leaving the reaction to cool at r.t. and it was washed twice with Et_2O. The aqueous phase was treated with NaOH 2N to pH 9 at 0°C and extracted with Et_2O. The organic phase was dried on Na_2SO_4, filtered and the solvent evaporated.

The final product **46** is a yellow solid.

Yield 79%

M.P. 128-130°C

MS (ESI): $[M+H]^+ = 281.06$

^{1}H NMR (400 MHz, Chloroform-*d*) δ 7.37 - 7.18 (m, 8H), 3.99 (s, 2H), 1.52 (s, 4H).

^{13}C NMR (101 MHz, $CDCl_3$) δ 141.07, 133.53, 129.05, 128.72, 128.40, 62.1.

^{1}H-NMR of compound 46

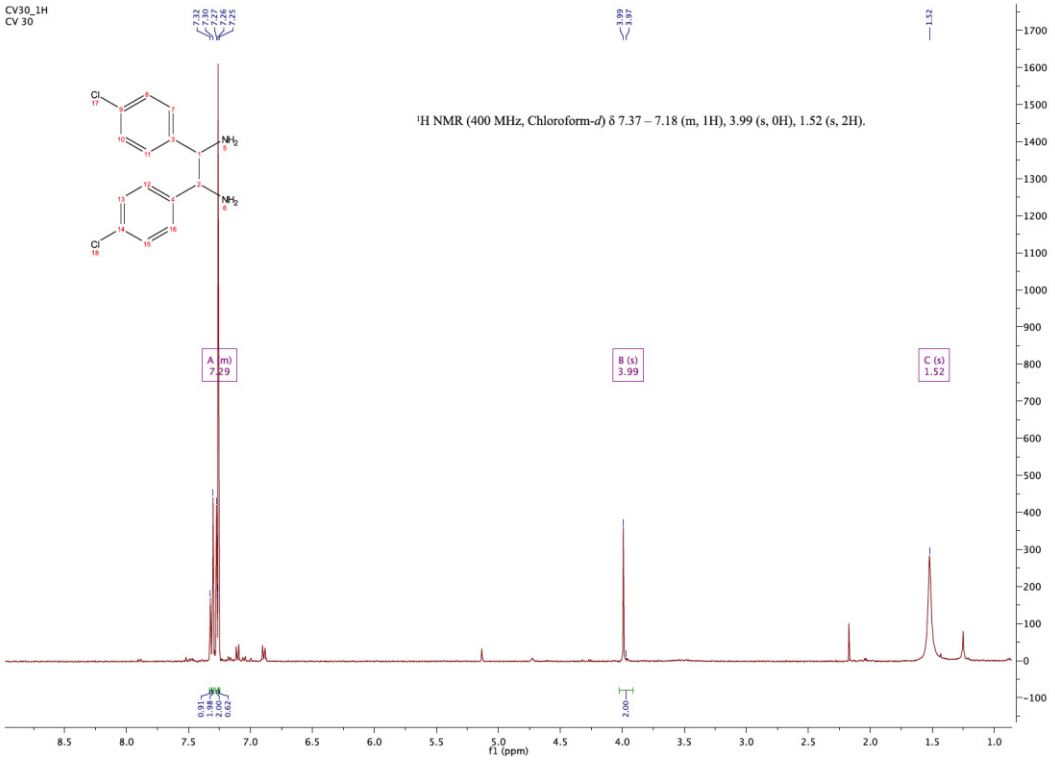

^{13}C-NMR and DEPT of compound 46

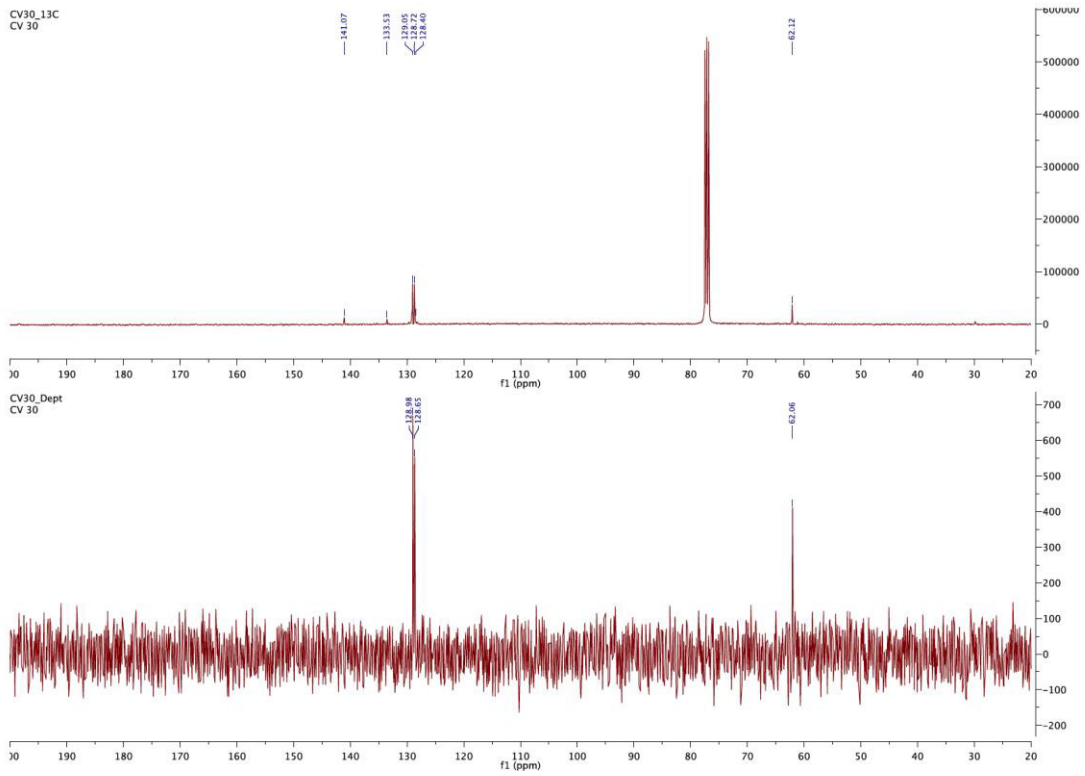

Synthesis of isopropyl 2-isopropoxy-4-methoxybenzoate **67**:

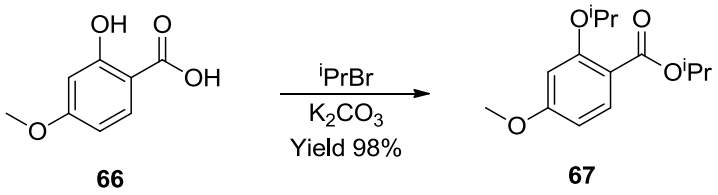

To a solution of 2-hydroxy-4-methoxybenzoic acid **66** (23.8 mmol) in DMF, it was added K_2CO_3 (4 eq.). After 15 minutes it was added 2-bromopropane (4 eq.). The mixture was stirred at 120°C for 3.5 h, then cooled at r.t. and the solvent evaporated. The residue was dissolved in EtOAc, then filtered on Gooch through diatomaceous earth and the solvent was washed with sodium bicarbonate. The organic phase was dried over Na_2SO_4 and evaporated to give the ester **67** as a yellow oil.

Yield 98%.

MS (ESI): $[M+H]^+ = 253.14$

^{1}H NMR (200 MHz, Chloroform-*d*) δ: 7.75-7.70 (m, 1H), 6.45-6.39 (m, 2H), 5.16 (p, J= 7.4 Hz, 1H), 4.50 (p, J= 6.2 Hz, 1H), 3.75 (s, 3H), 1.30 (m, 12H).

Synthesis of 2-isopropoxy-4-methoxybenzoic acid **68**:

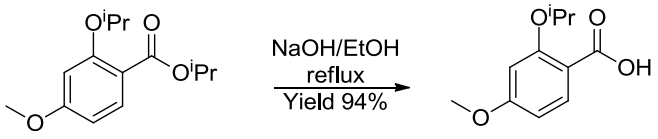

67 **68**

To a solution of ester **67** (16.5 mmol) in EtOH (30 ml), it was added NaOH 2N (33ml). The mixture was stirred at 80°C for 2.5 h, then evaporated the solvent, it was dissolved in H_2O and it was added HCl 2N until pH 3. The solution was extracted with EtOAc and the organic phase was dried over Na_2SO_4 and evaporated, to give an oil.

Yield 94%.

MS (ESI): $[M+H]^+$= 211,09

^{1}H NMR (200 MHz, Chloroform-*d*) δ: 10.83 (bs, 1H), 8.14 (d, J= 9 Hz, 1H), 6.64 (dd, J= 8.8, 2.4 Hz, 1H), 6.52 (d, J= 2.4 Hz, 1H), 4.80 (p, J= 6 Hz, 1H), 3.85 (s, 3H), 1.48 (d, J= 6.2 Hz, 6H).

IR: 3262.83, 2979.76, 1726.91, 1564.43 cm $^{-1}$

Synthesis of benzoic 2-isopropoxy-4-methoxybenzoic anhydride **69**:

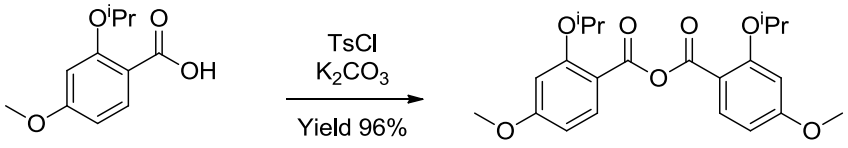

68 **69**

Method A:

In a round-bottom flask it was added the acid **68** and K_2CO_3 (4.34 eq.), then added drop to drop the tosyl chloride (0.6 eq.) in EtOAc (4 ml). The mixture was stirred for 20 min adding some drops of EtOAc to keep it homogeneous. Then, CH_2Cl_2 (15ml) was added and the solution was filtered on Gooch and the solvent evaporated, to obtain the anhydride **44** as a white solid.

Yield 96%.

IR: 2980.15, 2843.06, 1737.45, 1715.92, 1603.27, 1566,35 cm^{-1}

^1H NMR (200 MHz, Chloroform-*d*) δ: 8.02 (d, J= 9 Hz, 2H), 6.47 (m, 4H), 4.58 (p, J= 6 Hz, 2H), 3.85 (s, 6H), 1.33-1.20 (m, 12H).

Method B:

2-isopropoxy-4-methoxybenzoyl chloride (2.42 mmol) was mixed with DABCO (1 eq.). Then sodium 2-isopropoxy-4-methoxybenzoate (1 eq.) was added and the crude was pestle for 20 minutes. The mixture was added to a solution of Et_2O and water (30 ml and 25 ml) and extracted. The organic phase was dried over Na_2SO_4, filtered and the solvent evaporated to give the anhydride **69**.

Yield 18%.

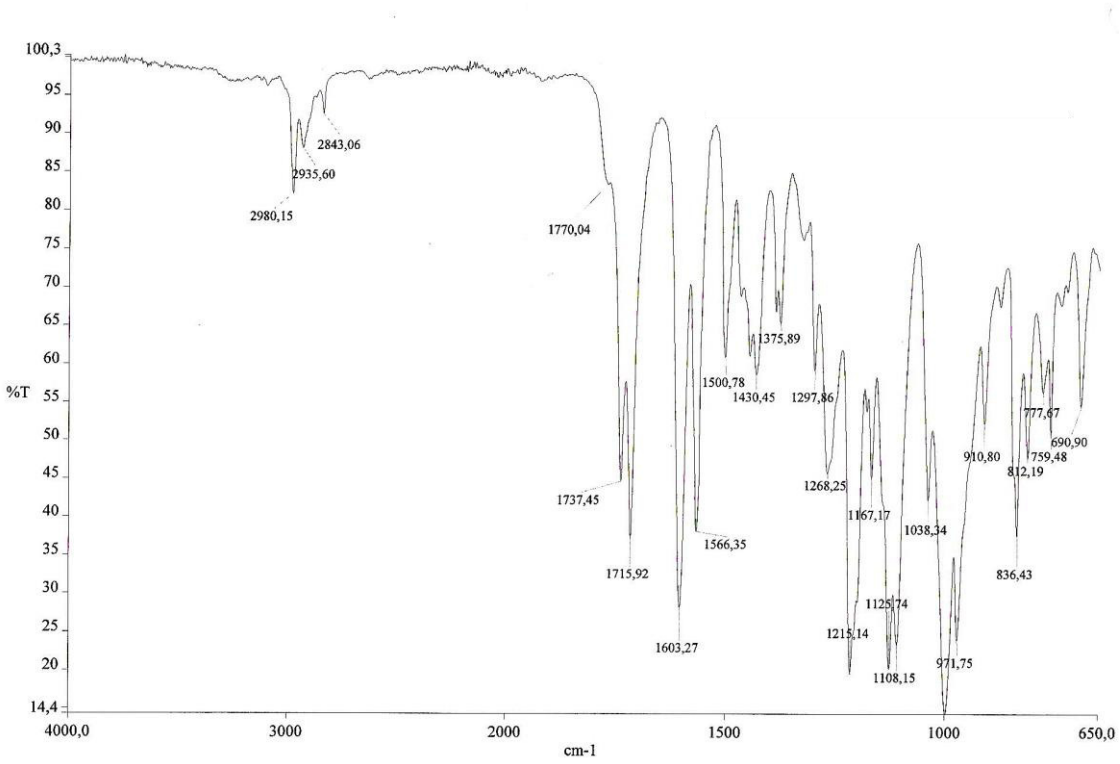
100,3
95
90
85
80
75
70
65
60
55
50
45
40
35
30
25
20
14,4
%T
4000,0
3000
2000
1500
1000
650,0
cm-1
2980,15
2935,60
2843,06
1770,04
1737,45
1715,92
1603,27
1566,35
1500,78
1430,45
1375,89
1297,86
1268,25
1215,14
1167,17
1125,74
1108,15
1038,34
971,75
910,80
836,43
812,19
777,67
759,48
690,90

Synthesis of N-((1S,2R)-2-amino-1,2-bis(4-chlorophenyl)ethyl)-2-isopropoxy-4-methoxybenzamide **56**:

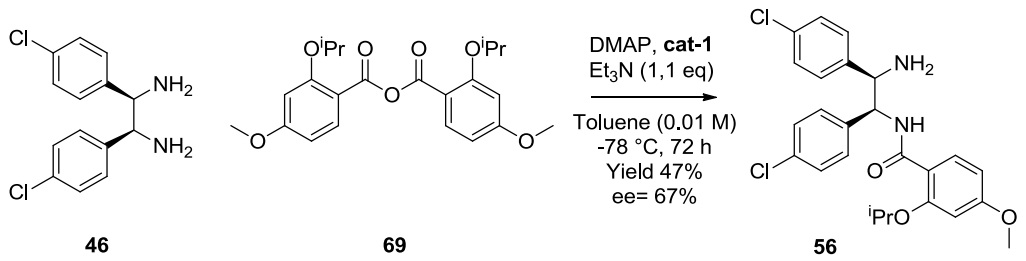

46 **69** **56**

To a solution of anhydride **69** (0.74 mmol) in toluene (10ml), it was added DMAP (1.5 eq.) dissolved in dry toluene. The reaction was stirred at r.t. for 18 h and then brought to -78°C. In a flask the (1R,2R)-**cat-1** was dissolved in toluene and EtOAc and this solution was added to the reaction through syringe. The reaction was stirred for 30 minutes, then a solution of meso-diamine **46** in toluene was added dropwise for 1 h. After 1 h, TEA (114 μL) is added to the reaction. After 18 h the reaction is quenched with a solution of ammonia in methanol and washed with a solution of water and brine (1:1). The organic phase is extracted and evaporated. The crude is a rubbery yellow solid. It was purified by coloumn chromatography (petroleum ether/EtOAc 1.5:10), to obtain the final product **56** as a white solid.

Yield 47%

ee 67%

M. P.= 181-185°C

MS (ESI): $[M+H]^+$ = 473,13

^{1}H NMR (400 MHz, Chloroform-*d*) δ 8.84 (d, *J* = 7.8 Hz, 1H), 8.11 (d, *J* = 8.8 Hz, 1H), 7.29 – 7.16 (m, 5H), 7.01 (dd, *J* = 8.5, 3.0 Hz, 4H), 6.55 (dd, *J* = 8.8, 2.3 Hz, 1H), 6.48 (d, *J* = 2.3 Hz, 1H), 5.47 (dd, *J* = 7.9, 4.6 Hz, 1H), 4.74 (p, *J* = 6.1 Hz, 1H), 4.43 (d, *J* = 4.6 Hz, 1H), 3.83 (d, *J* = 0.7 Hz, 3H), 1.41 (t, *J* = 5.8 Hz, 6H).

^{13}C NMR (101 MHz, $CDCl_3$) δ 165.08, 163.51, 157.37, 140.00, 136.84, 134.31, 133.42, 129.26, 128.56, 128.41, 114.95, 105.30, 100.51, 71.67, 59.25, 58.63, 55.66, 22.33, 22.18.

^{1}H-NMR compound 56

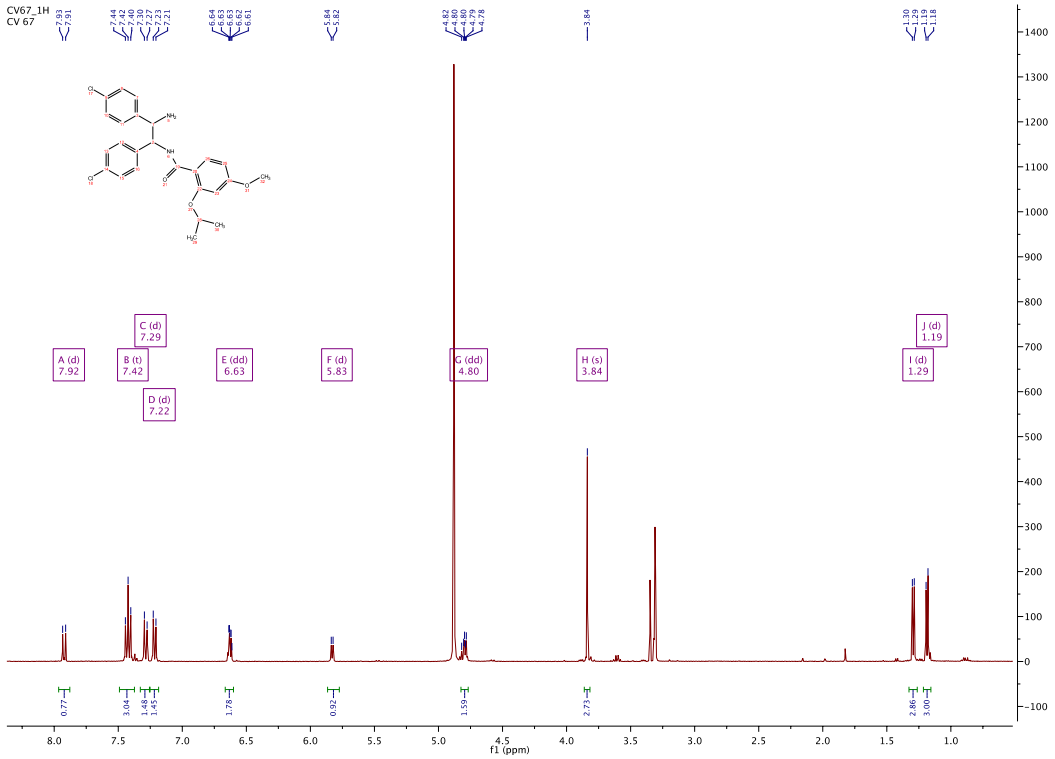

^{13}C-NMR and DEPT compound 56

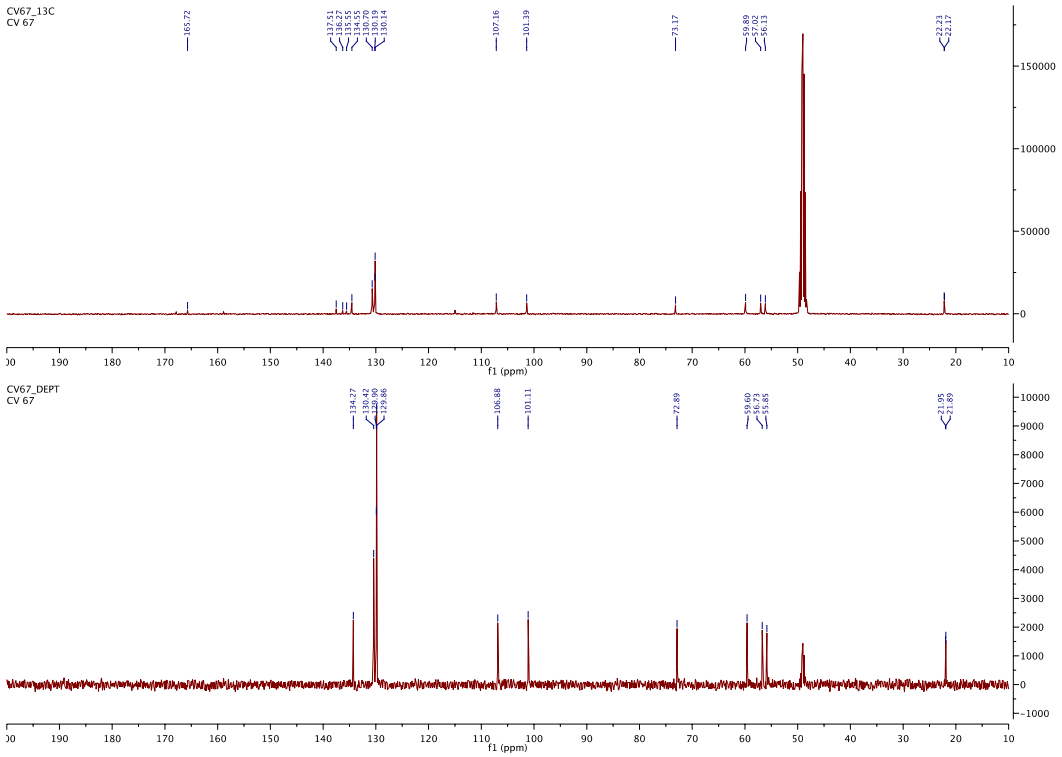

g-COSY, HMQC and HMBC compound 56

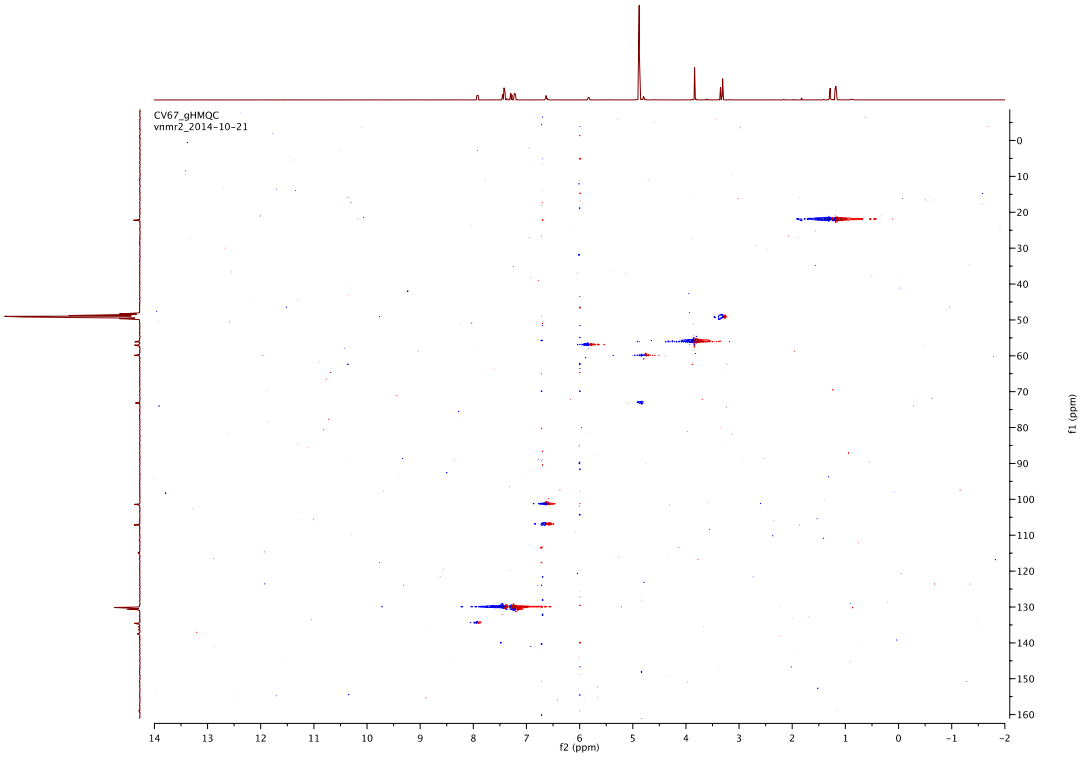

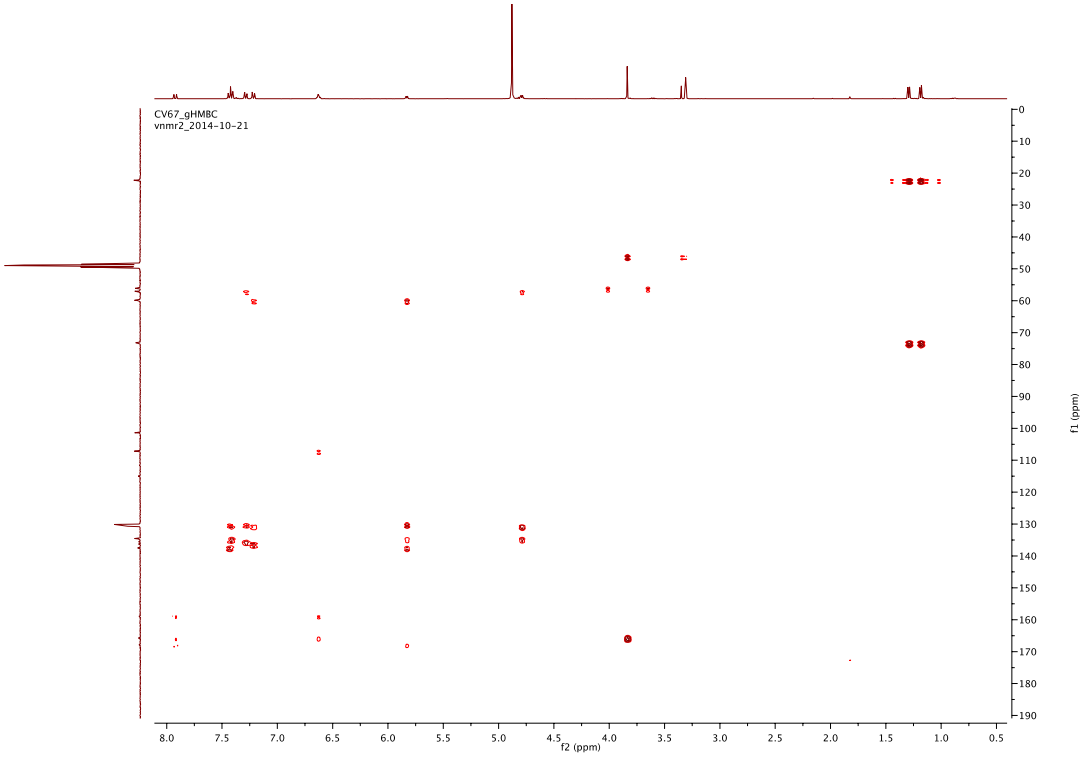
CV67_gHMBC
vnmr2_2014-10-21
f2 (ppm)
f1 (ppm)

Synthesis of N-((1R,2S)-2-amino-1,2-bis(4-chlorophenyl)ethyl)benzamide **60**:

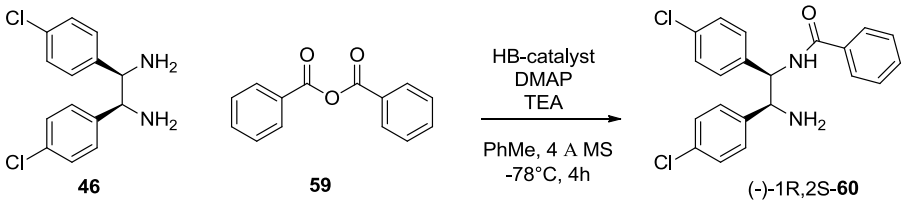

To a solution of benzoic anhydride **59** (0.35 mmol) in toluene, it was added DMAP (0.1 eq.) dissolved in toluene. The mixture was cooled at -78°C and stirred for 20 minutes.

To the mixture it was added amide-thiourea (1R,2R)-**cat-1** (0.1 eq), 5ml of toluene and 2ml of ethyl acetate. It was stirred for 15 minutes, and then meso-diamine **46** (1 eq.) was added. After 1h TEA (1.1 eq.) was added. The reaction was quenched after 2 h with a solution of ammonia in methanol and washed with brine and water (1:1). The organic phase is extracted and evaporated. The crude is a rubbery yellow solid. It was purified by coloumn chromatography (petroleum ether/EtOAc 2.5:10) to give the amide **60** as a white solid.

Yield 79%

ee 43%

M.P. = 168-172°C

$[\alpha]_d$ = - 2,05 (0,146 *c*, MeOH)

MS (ESI): $[M+H]^+$ = 385.21

^{1}H NMR (400 MHz, Methanol-*d*4) δ 7.57-7.25 (m, 13H), 5.29 (d, *J* = 9.2 Hz, 1H), 4.31 (d, *J* = 9.2 Hz, 1H).

^{13}C NMR (101 MHz, CD_3OD) δ 169.52, 142.01, 139.78, 135.67, 134.79, 134.51, 132.63, 130.79, 130.26, 129.84, 129.54, 129.45, 128.18, 60.47, 60.04.

^{1}H-NMR compound 60

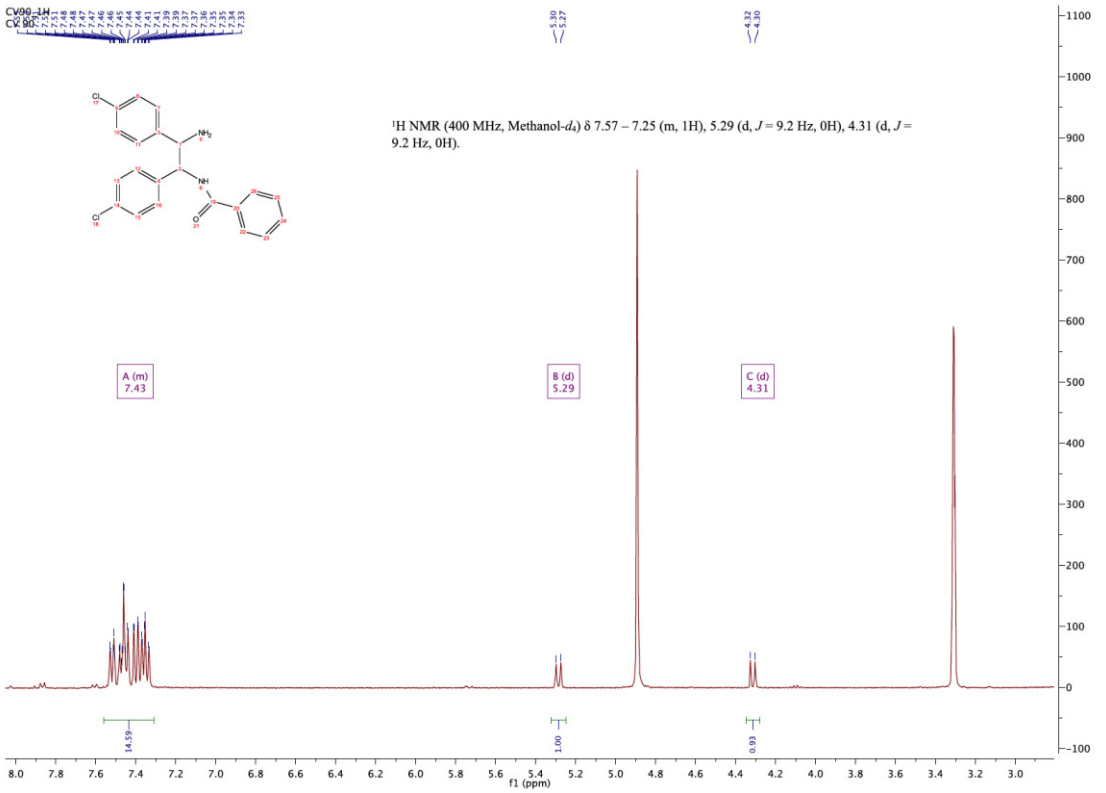

^{1}H NMR (400 MHz, Methanol-d_4) δ 7.57 – 7.25 (m, 1H), 5.29 (d, J = 9.2 Hz, 0H), 4.31 (d, J = 9.2 Hz, 0H).

^{13}C-NMR and DEPT compound 60

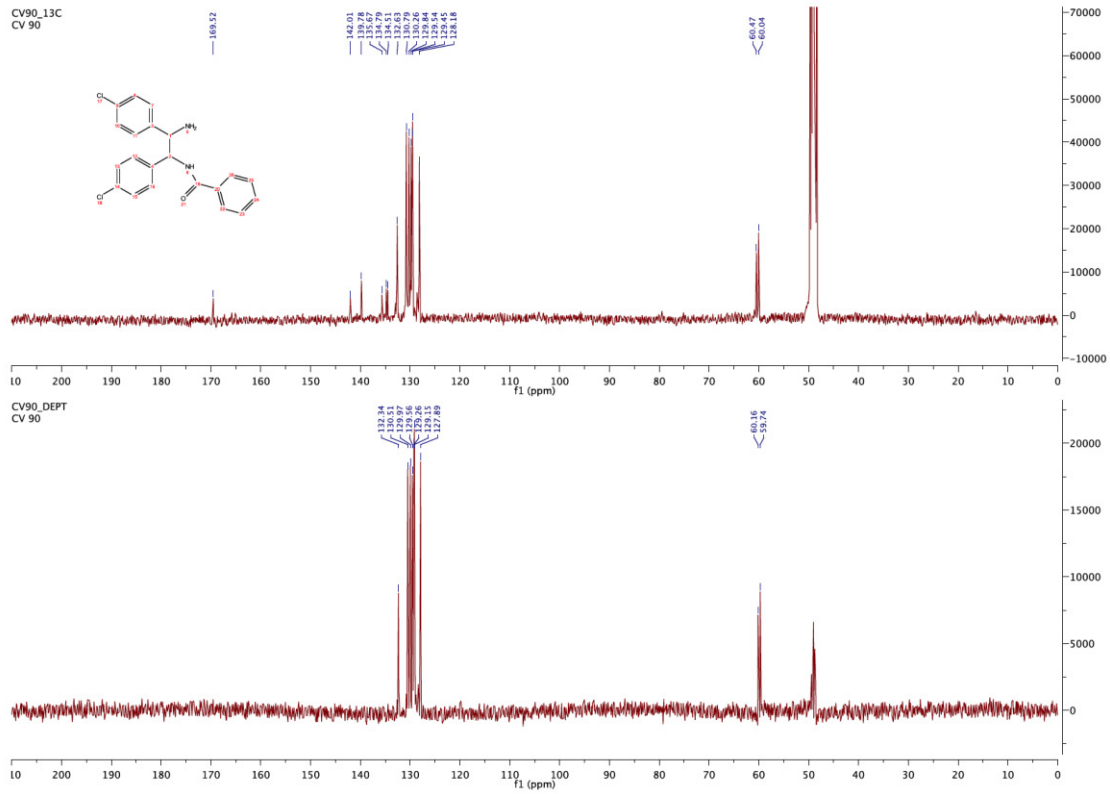

Synthesis of N-((1R,2S)-1,2-bis(4-chlorophenyl)-2-(2-isopropoxy-4-methoxybenzamido)ethyl)-3-oxopiperazine-1-carboxamide **57**:

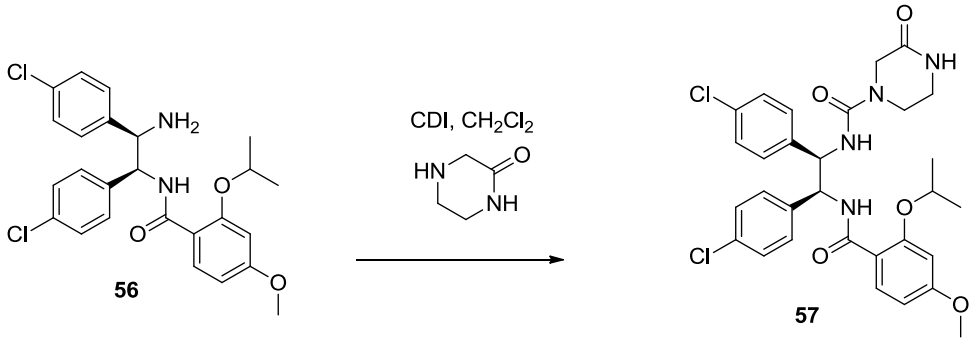

To a solution of amine **56** (0.62 mmol) in dry CH_2Cl_2, it was added the CDI (1.2 eq.). The reaction was stirred at r.t. for 5 h and then, 2-piperazinone (1.6 eq.) was added. After 18 h, the solution was diluted with 30 ml of dry CH_2Cl_2 , extracted and washed with water three times and once with NaCl. The organic phase was dried over Na_2SO_4, evaporated the solvent, to give the urea **57**, a white solid.

Yield 94%

M.P. = 210-213 °C

$[\alpha]_d$ = + 29,67 (0,1 *c*, $CHCl_3$)

MS (ESI): $[M+H]^+$ = 599.18

^{1}H NMR (400 MHz, Chloroform-*d*) δ 8.38 (d, *J* = 7.7 Hz, 1H), 8.26 (d, *J* = 8.8 Hz, 1H), 8.02 (s, 1H), 7.82 (s, 1H), 7.28 (d, *J* = 8.2 Hz, 2H), 7.17 (d, *J* = 8.2 Hz, 2H), 6.95 (d, *J* = 8.2 Hz, 2H), 6.89 (d, *J* = 8.1 Hz, 2H), 6.62 (dd, *J* = 8.9, 2.2 Hz, 1H), 6.45 (d, *J* = 2.1 Hz, 1H), 5.77 (d, *J* = 7.6 Hz, 1H), 5.09 (s, 1H), 4.65 (p, *J* = 6.1 Hz, 1H), 4.15 (s, 2H), 3.85 (s, 3H), 3.72 (d, *J* = 13.0 Hz, 1H), 3.60 (d, *J* = 12.6 Hz, 1H), 3.41 (s, 2H), 1.20 (d, *J* = 6.0 Hz, 3H), 1.14 (d, *J* = 6.0 Hz, 3H).

^{13}C NMR (101 MHz, $CDCl_3$) δ 167.48, 164.17, 157.44, 156.09, 136.56, 134.64, 134.08, 133.51, 129.60, 128.83, 128.58, 128.22, 113.56, 105.55, 100.50, 71.64, 62.11, 57.94, 55.77, 47.61, 41.40, 40.12, 22.12, 21.73.

^{1}H-NMR compound 57

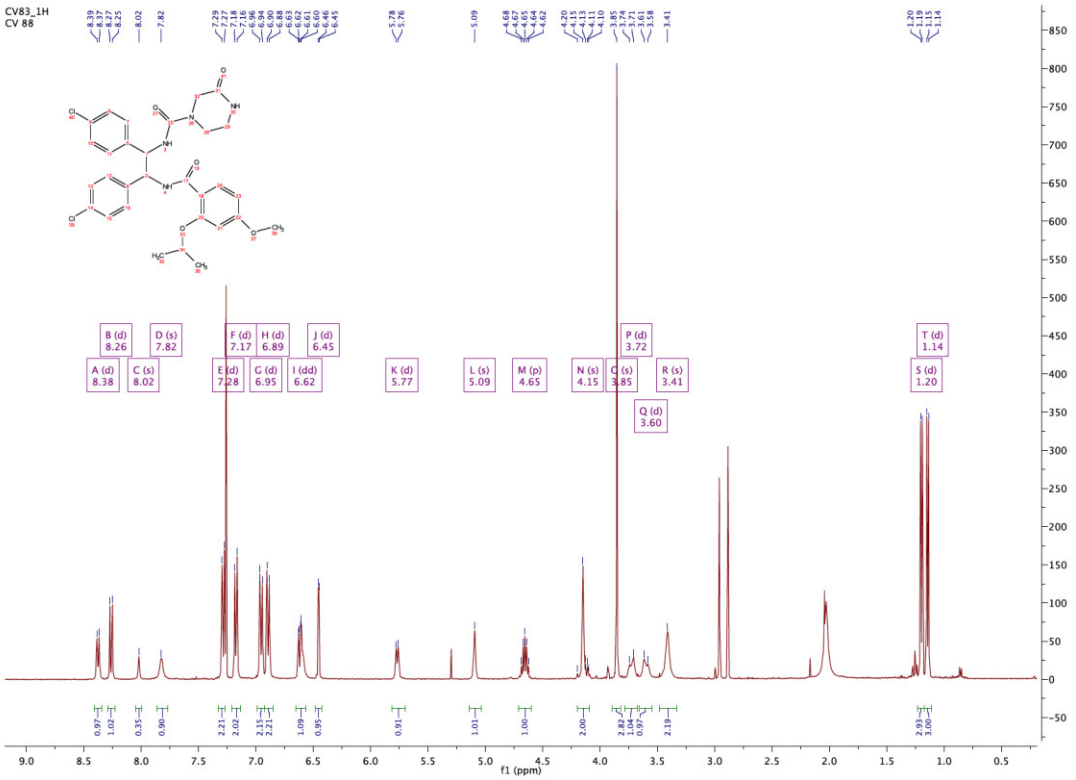

^{13}C-NMR and DEPT compound 57

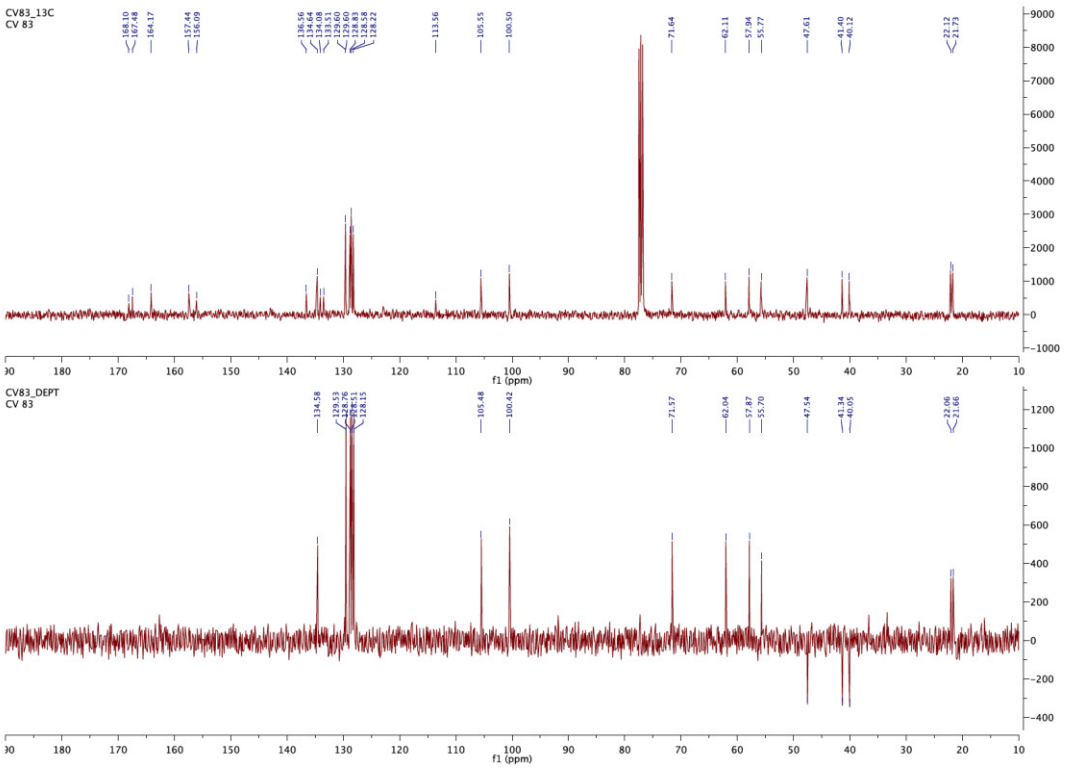

•

g-COSY, HMQC, HMBC compound 57

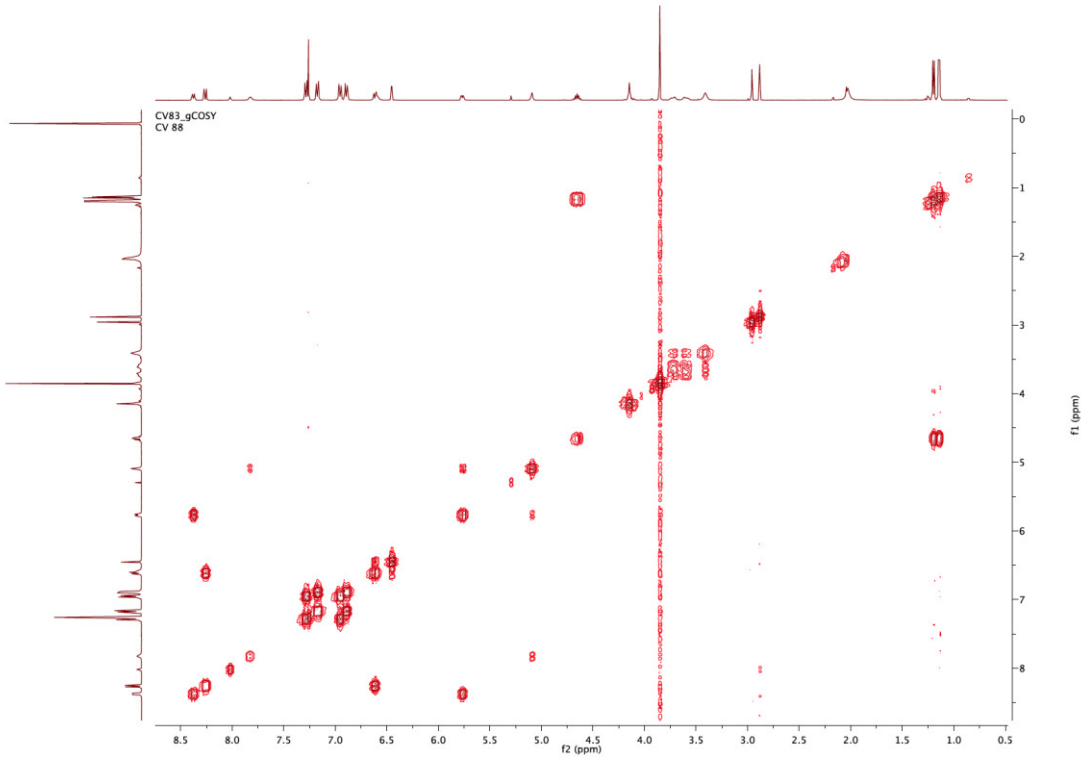

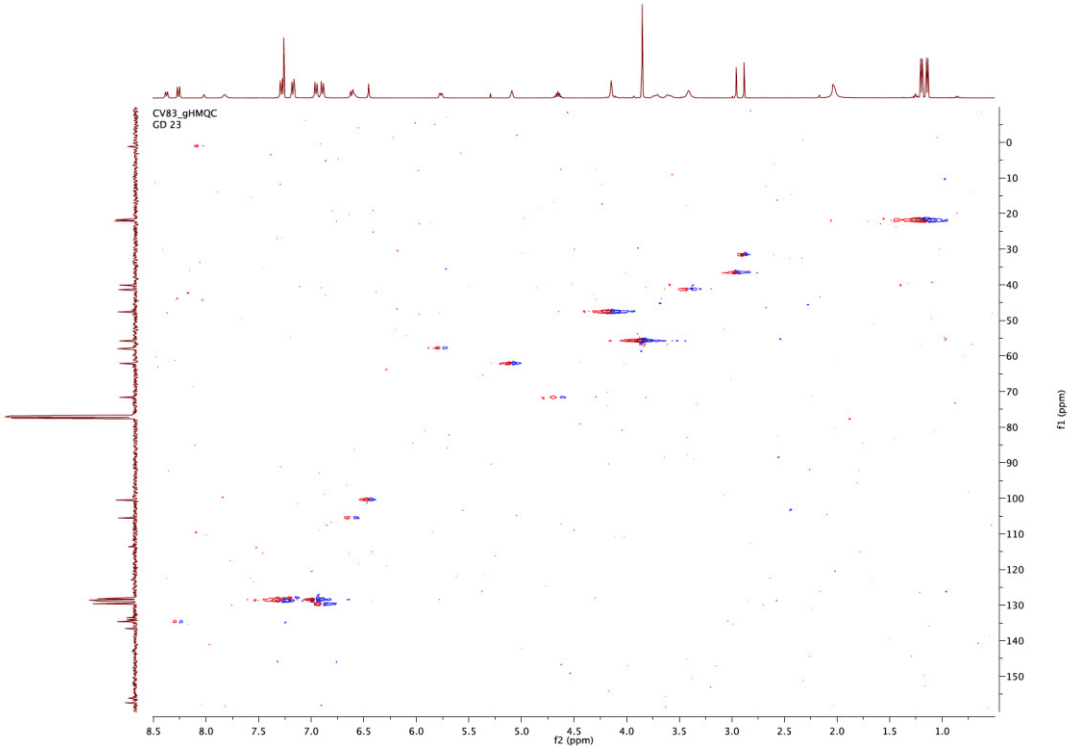

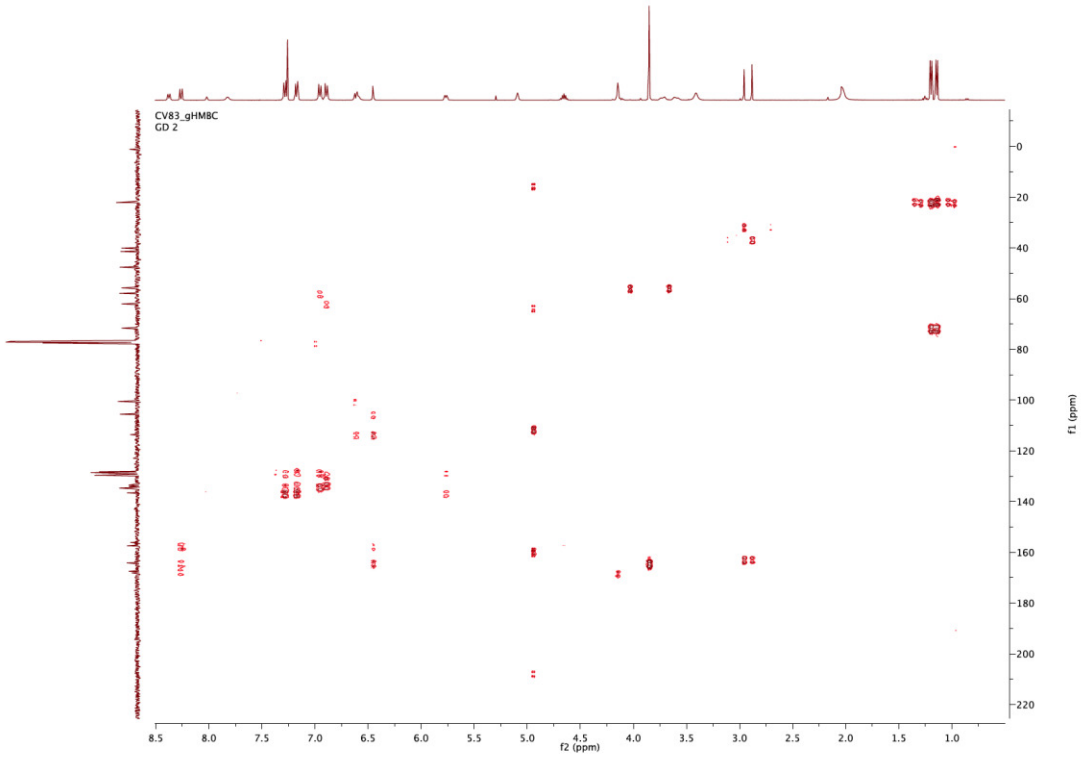
CV83_gHMBC
GD 2
f1 (ppm)
f2 (ppm)

Synthesis of 4-((4S,5R)-4,5-bis(4-chlorophenyl)-2-(2-isopropoxy-4-methoxyphenyl)-4,5-dihydro-1H-imidazole-1-carbonyl)piperazin-2-one hydrate **58**:

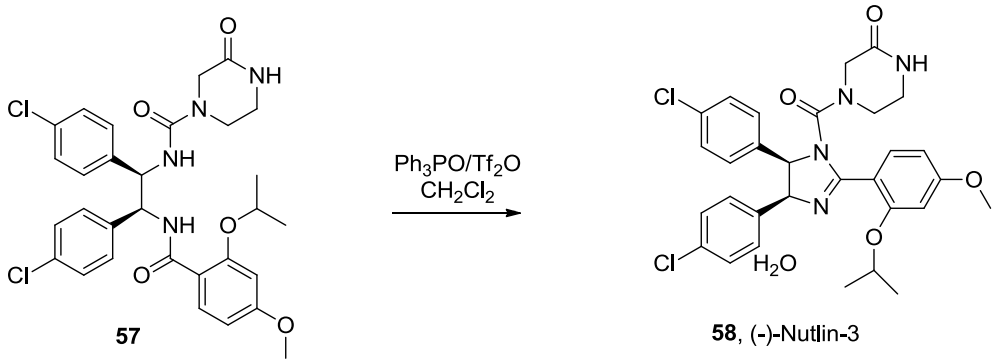

Method A:

To a solution of triphenyl phosphine oxide (1.17 mmol) in 25 ml of dry CH_2Cl_2 at 0°C, after 10 minutes triflic anhydride (4 eq.) was added and the reaction was stirred for 30 minutes, then the amide-urea **57** (0.25 eq.) was added at 0°C. The solution was stirred for 18 h at 0°C to r.t. and monitored by TLC. Once the starting material disappeared, the reaction was quenched with a solution of $NaHCO_3$ saturated. The organic phase was extracted and dried over Na_2SO_4. The crude was purified by column chromatography ($MeOH/CH_2Cl_2$ 0.5:9.5) to obtain (-)-**58** as white solid.

Yield 80%

M.P.= 143-147°C

$[\alpha]_d$ = - 53,67 (0,1 *c*, $CHCl_3$)

MS (ESI): $[M+H]^+$ = 581.17

Method B:

To a solution of **51** (0.043 mmol) in THF, Et_3N (5.3 eq.) and triphosgene (8 eq.) at 0°C.

The ixture was stirred for 2.5 h and the solvent evaporated. The residue was dissolved in CH_2Cl_2 and at 0°C a solution of 2-piperazinone in CH_2Cl_2 was added dropwise. The reaction was stirred for 1h at 0°C, then it was quenched with a satured solution of $NaHCO_3$ and it was extracted and washed with NaCl aq.; the organic phase was dried over Na_2SO_4, the solvent evaporated.

^{1}H NMR (400 MHz, Chloroform-*d*) δ 7.70 – 7.56 (m, 2H), 7.08 (d, *J* = 8.2 Hz, 2H), 7.03 (d, *J* = 8.5 Hz, 2H), 6.93 (d, *J* = 8.4 Hz, 2H), 6.87 (d, *J* = 8.1 Hz, 2H), 6.62 (s, 1H), 6.55

(dd, *J* = 8.6, 2.1 Hz, 1H), 6.47 (d, *J* = 2.1 Hz, 1H), 5.66 – 5.56 (bs, 1H), 4.61 (p, *J* = 6.0 Hz, 1H), 3.84 (s, 3H), 3.77 (d, *J* = 18.2 Hz, 1H), 3.63 (d, *J* = 18.3 Hz, 1H), 3.40 – 3.37 (m, 1H), 3.27 – 3.15 (m, 1H), 3.00 (s, 2H), 1.38 (d, *J* = 6.0 Hz, 3H), 1.33 (d, *J* = 6.0 Hz, 3H).

^{13}C NMR (101 MHz, $CDCl_3$) δ 166.76, 163.63, 161.07, 157.30, 154.33, 135.46, 134.58, 133.55, 133.24, 132.63, 129.31, 128.63, 128.29, 128.18, 104.92, 100.30, 71.29, 69.41, 55.74, 49.51, 42.09, 40.53, 22.19.

^{1}H-NMR compound 58

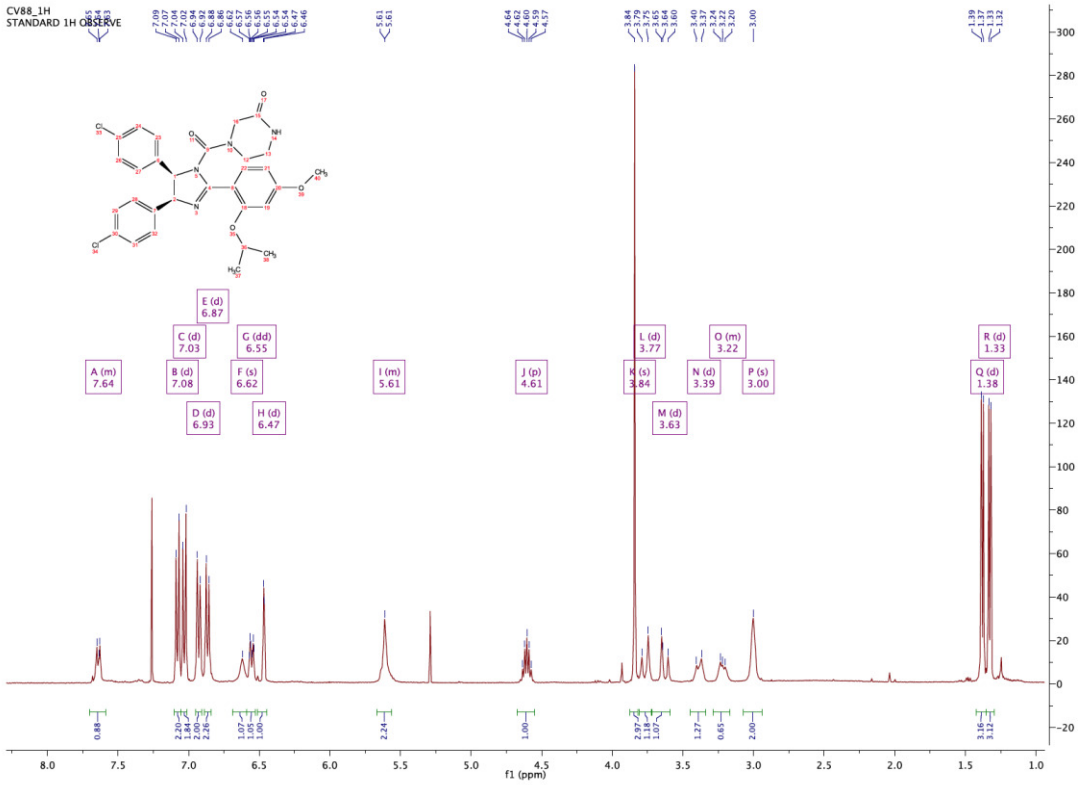

^{13}C-NMR and DEPT compound 58

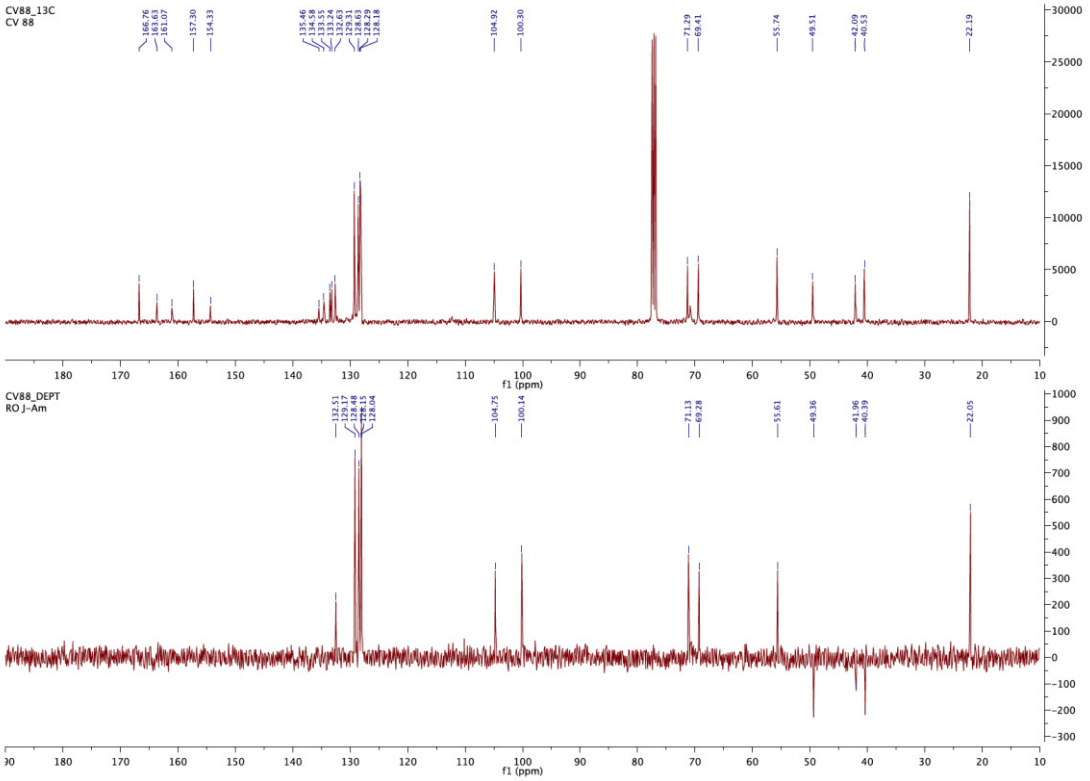

g-COSY, HMQC, HMBC compound 58

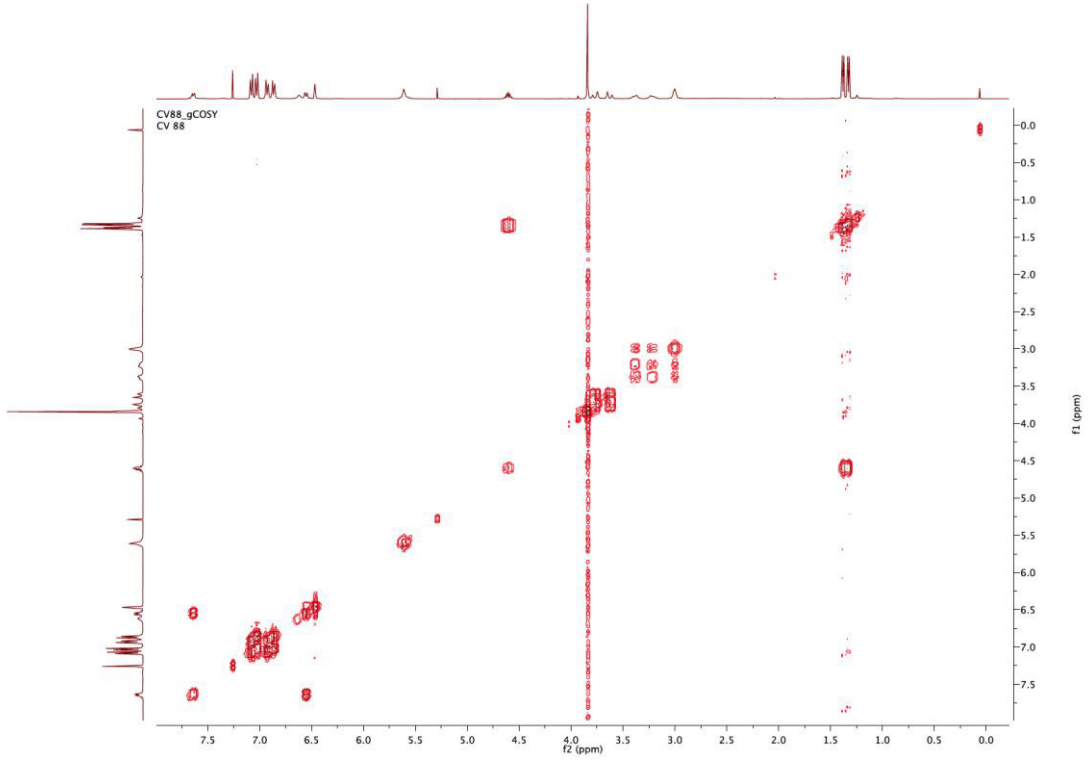

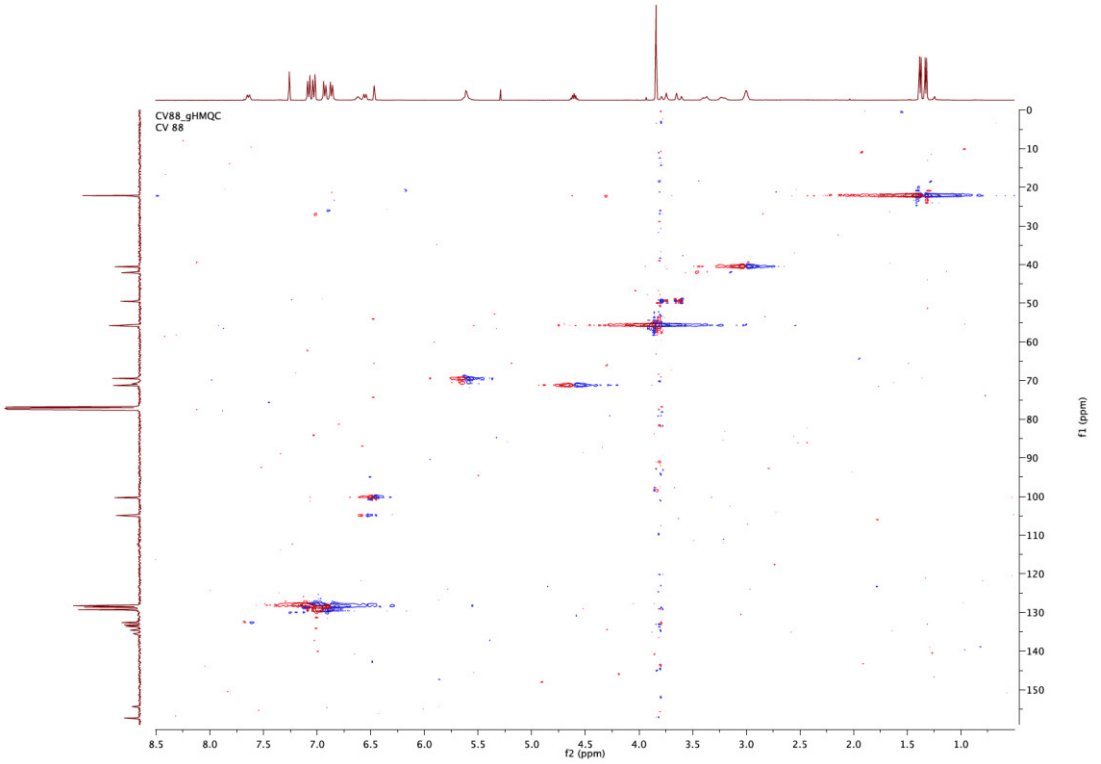
CV88_gHMQC
CV 88
f2 (ppm)
f1 (ppm)

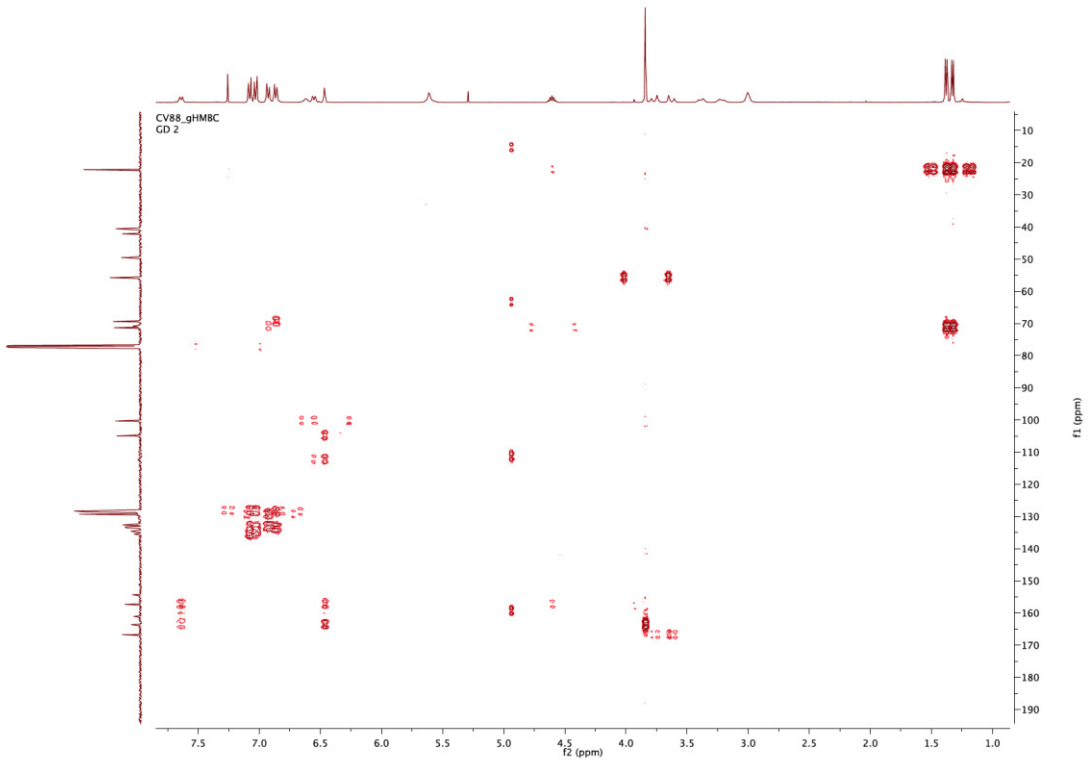
CV88_gHMBC
GD 2
f2 (ppm)
f1 (ppm)

Synthesis of the catalyst **cat-1**:

Synthesis of 2,5-dioxopyrrolidin-1-yl 3,5-bis(trifluoromethyl)benzoate **77**:

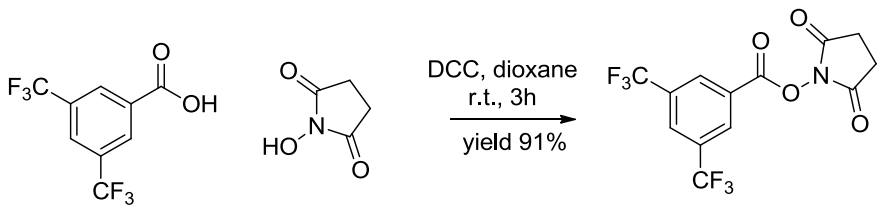

74 **77**

To a solution of N-hydroxysuccinimide (1 eq.) and 3,5-trifluormethyl benzoic acid **74** (10.0 mmol) in dry 1,4-dioxane, DCC (1.05 eq.) was added. After 3 h the precipitate was filtered on Gooch and the solvent evaporated. The crude was purified by column chromatography (EtOAc/Petroleum ether) to give the anhydride-Osu **77**, as a white solid.
Yield 91%

^{1}H NMR (400 MHz, Chloroform-*d*) δ 8.58 (d, *J* = 1.7 Hz, 2H), 8.19 (td, *J* = 1.6, 0.8 Hz, 1H), 2.95 (m, 4H).

^{13}C NMR (101 MHz, $CDCl_3$) δ: 168.73, 159.79, 132.82, 130.73, 128.42, 128.38, 127.61, 123.96, 121.24, 25.79.

^{1}H-NMR compound 77

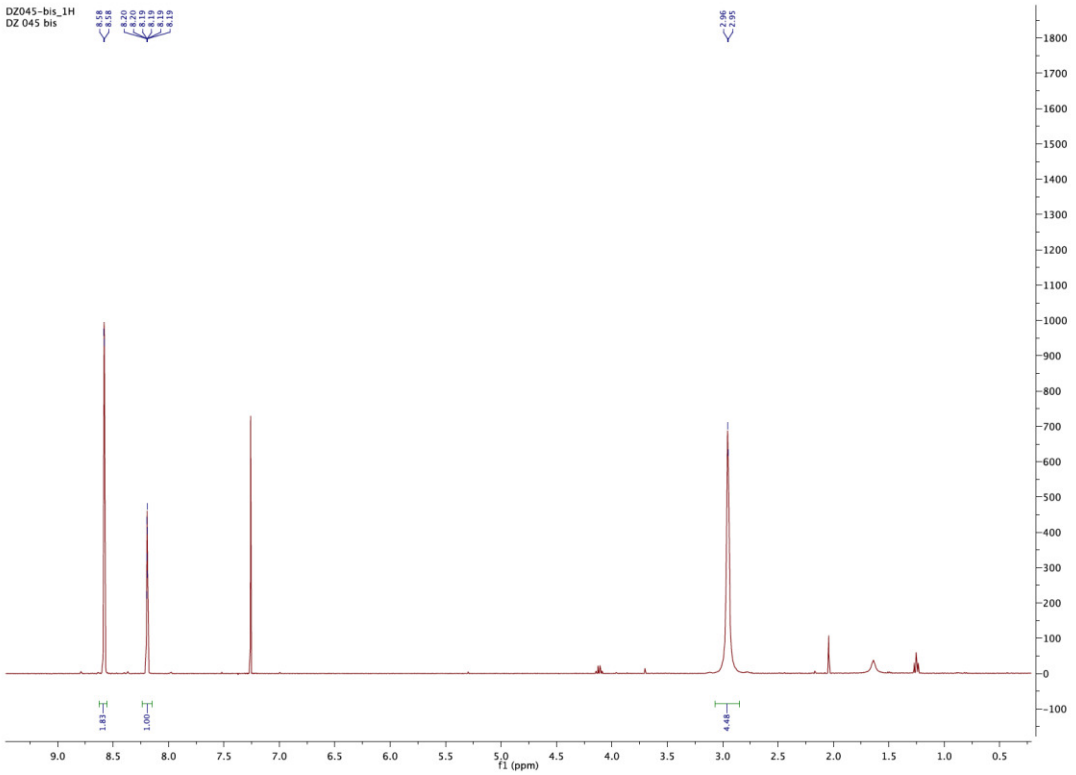

^{13}C-NMR and DEPT compound 77

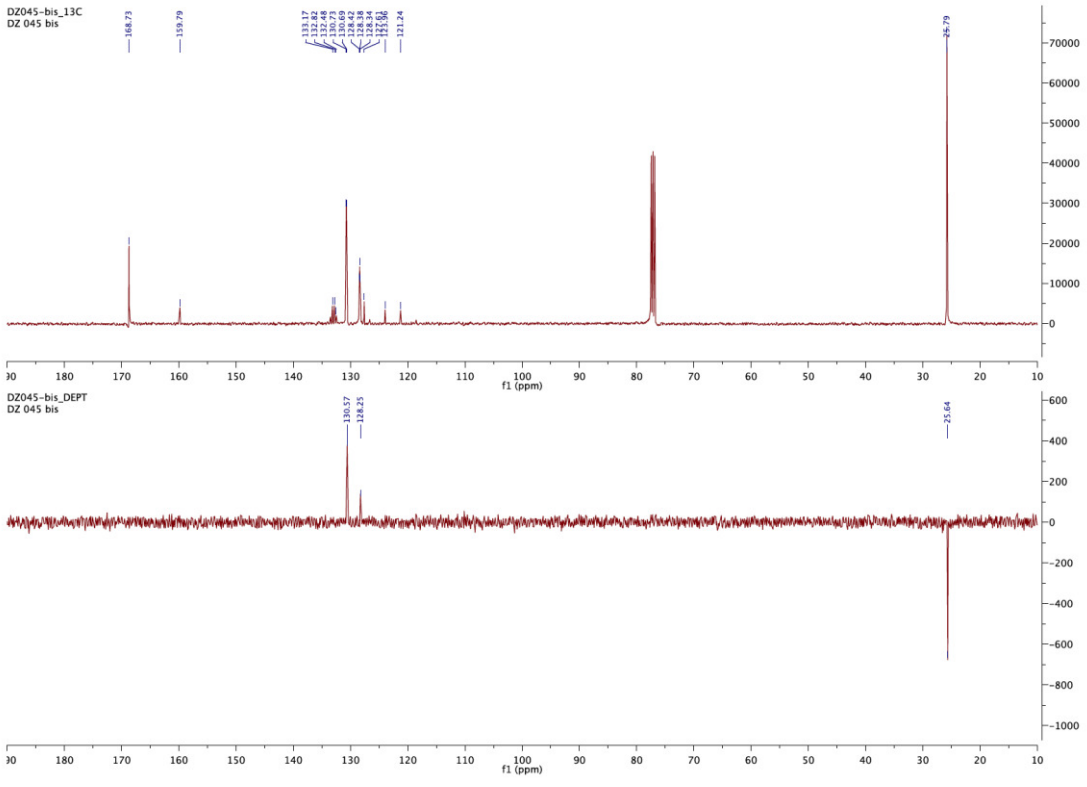

Synthesis of 1-((1S,2S)-2-aminocyclohexyl)-3-(3,5-bis(trifluoromethyl)phenyl)thiourea **78**:

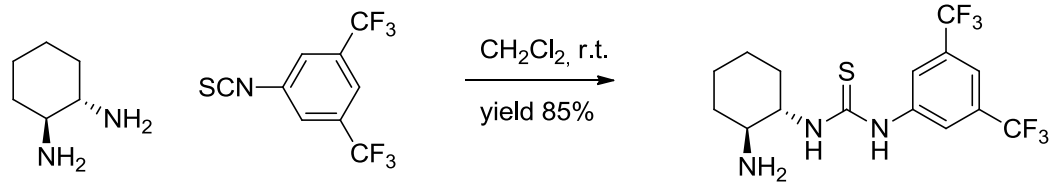

75 **76** **78**

To a solution of cyclohexyl diamine **75** (1.2 eq.) in CH_2Cl_2, isocyanate **76** (7.30 mmol) was added. The reaction was stirred at r.t. for 10 h. The solvent then was evaporated and the crude was purified by column chromatography (MeOH/EtOAc) to give the product **78.**

Yield 85%

$[\alpha]_d$ = -58,6 (0,5 *c*, $CHCl_3$)

^{1}H NMR (400 MHz, Chloroform-*d*) δ: 8.03 (bs, 2H), 7.57 (s, 3H), 6.40 (bs, 1H), 3.38 (bs, 1H), 2.72 (bs, 2H), 1.95 (m, 2H), 1.75 (m, 2H), 1.26 (m, 4H).

^{13}C NMR (101 MHz, $CDCl_3$) δ: 183.12, 171.26, 131.52, 122.73, 117.56, 63.07, 56.58, 34.71, 32.10, 24.49.

Synthesis of N-((1S,2S)-2-(3-(3,5-bis(trifluoromethyl)phenyl)thioureido)cyclohexyl)-3,5-bis(trifluoromethyl)benzamide **cat-1:**

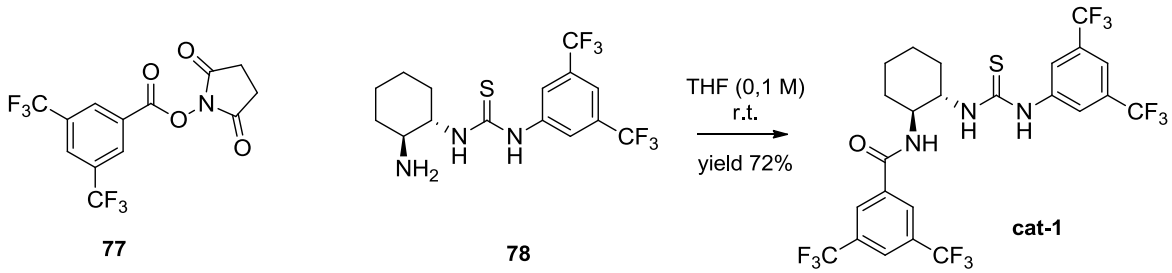

To a solution of amino-thiourea **78** (1.61 mmol) in THF (33ml), the anhydride-Osu **77** (1 eq.) was added. The mixture was stirred for 24 h at r.t., then 2 ml of NH_4OH were added and then the solvent was evaporated. The crude was purified by column chromatography (EtOAc/Petroleu ether 3:7) to give the amide-thiourea **cat-1** as a white solid.

M.P.= 161-165 °C

$[\alpha]_d$ = +30 (0,5 *c*, $CHCl_3$)

MS (ESI): $[M+H]^+$ = 626.11

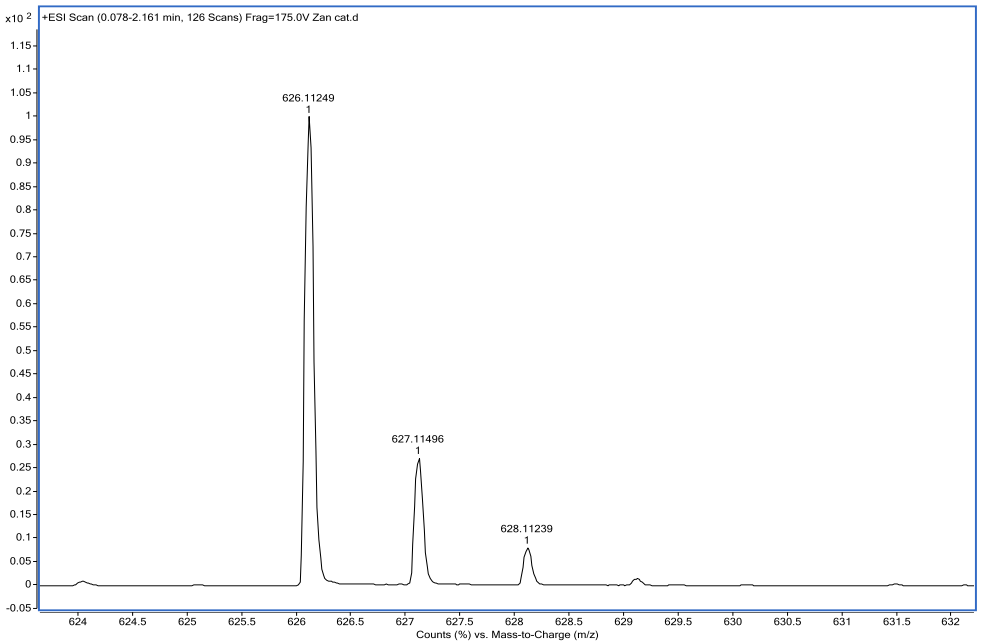

^{1}H NMR (400 MHz, Chloroform-d) δ 8.84 (s, 1H), 8.30 - 8.18 (m, 2H), 7.94 (s, 1H), 7.79 (d, *J* = 7.9 Hz, 1H), 7.71 (s, 2H), 7.60 (s, 1H), 4.68 (s, 1H), 4.00 - 3.90 (m, 1H), 2.28 - 2.16 (m, 2H), 1.94 - 1.82 (m, 3H), 1.59 - 1.32 (m, 5H).

^{13}C NMR (101 MHz, $CDCl_3$) δ 181.68, 165.78, 139.40, 135.87, 132.61, 132.31, 127.58, 127.58, 125.50, 124.15, 123.75, 119.18, 60.68, 57.13, 56.95, 32.24, 24.75, 21.24, 14.29.

^{1}H-NMR compound cat-1

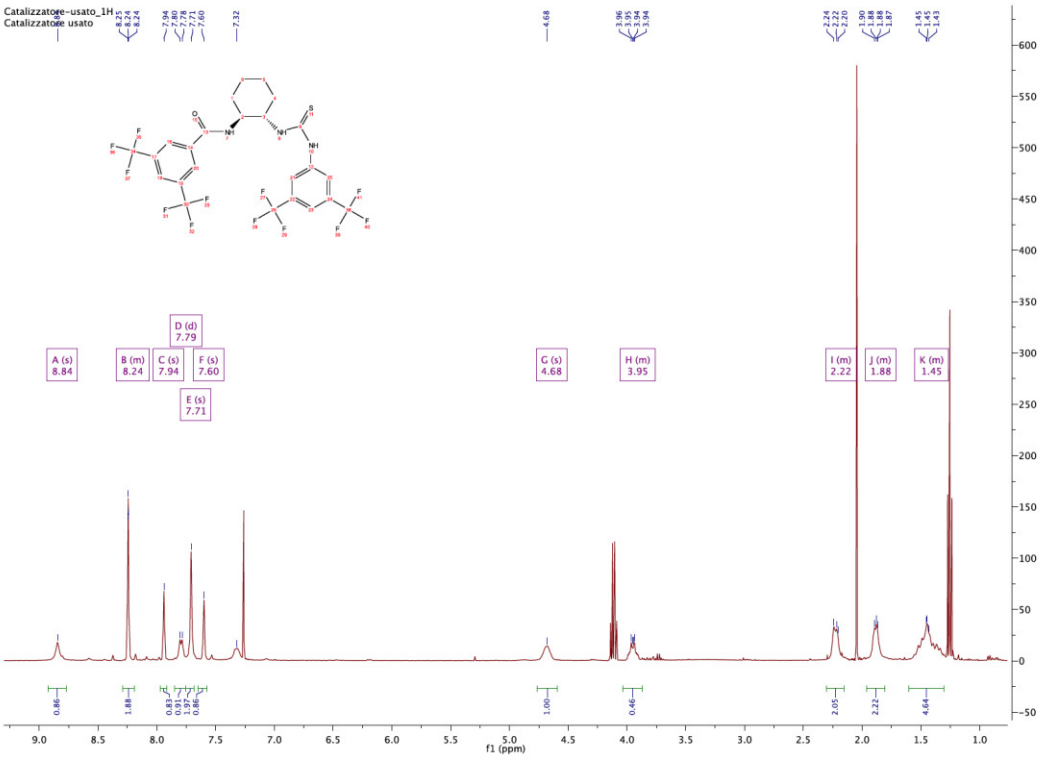

^{13}C-NMR and DEPT compound cat-1

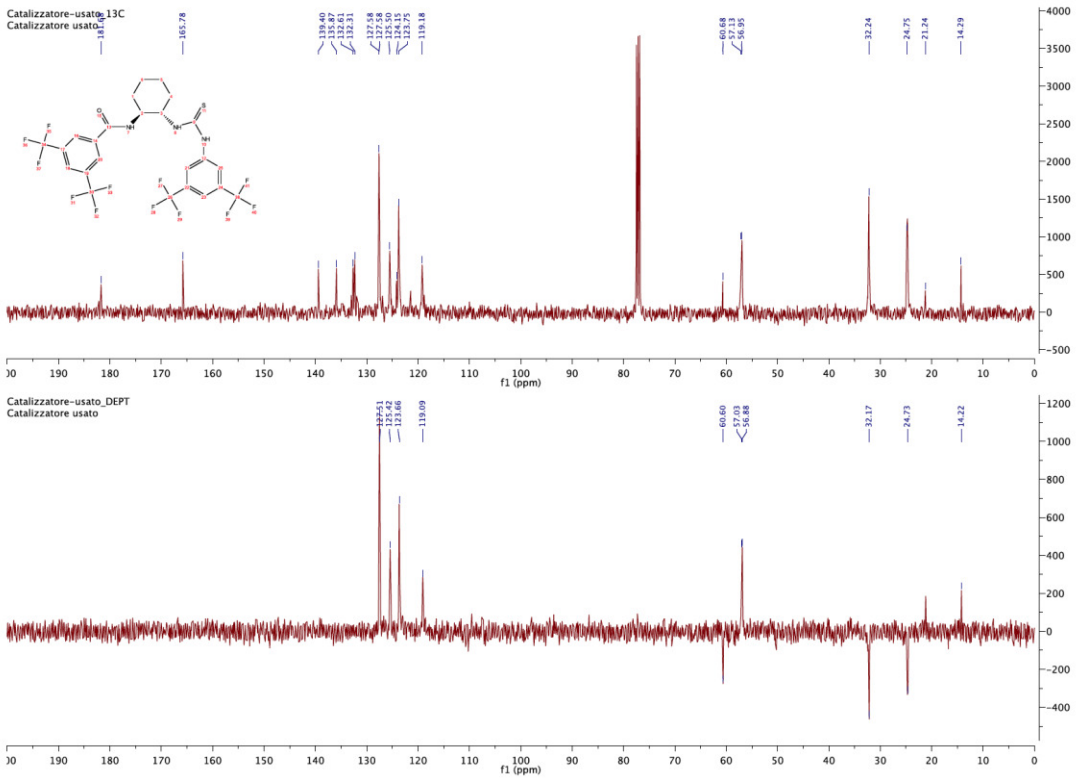

5.4 Magmas Inhibitors

Synthesis of 1-(2,6,6-trimethylcyclohex-1-en-1-yl)ethanol **80**:

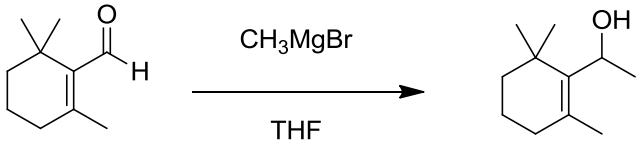

79 **80**

To a solution of β-cyclocitral **79** (6.56 mmol) in THF, CH_3MgBr (1.1 eq.) was added at 0°C. The reaction was stirred overnight. The formation of the alcohol was monitored by TLC (EtOAc/Petroleum ether 1:6) and by mass spectrometry. The reaction was then quenched with NH_4Cl sat. THF was then evaporated and the crude extracted with ethyl acetate. The organic phase was dried over Na_2SO_4 and after evaporated the solvent the compound was purified by column chromatography (EtOAc/Petroleum ether 1:9). The product **80** obtained was a white solid.

Yield 82%

MS (ESI): $[M-H]^+$= 168.38

IR: cm^{-1}3378.96 OH-stretching, 2906.78 C-H stretching, 1652.40 C=C stretching, 1064.62 C-O stretching.

^{1}H NMR (400 MHz,$CDCl_3$) δ 4.50 (q, 1H, *J* =6.7 Hz, CH_3-C<u>H</u>-OH), 1.92 (dd, 2H, *J* =13.9, 6.5 Hz, CH_2-CH_2-C<u>H_2</u>), 1.85 (s, 3H, C<u>H_3</u>-C=C), 1.57-1.37 (m, 2H, CH_2-C<u>H_2</u>-CH_2), 1.41 (d, 3H, *J* =6.7 Hz, C<u>H_3</u>-CH-OH), 1.40-1.37 (m, 2H, C<u>H_2</u>-CH_2-CH_2), 1.09 (s, 3H, CH_3-Cq-C<u>H_3</u>), 0.95 (s, 3H, C<u>H_3</u>-Cq-CH_3).

^{13}C NMR (400 MHz, $CDCl_3$) δ 141.25, 130.92, 67.12, 39.95, 34.70, 34.06, 28.64, 28.01, 23.06, 21.03, 19.37

^{1}H-NMR compound 80

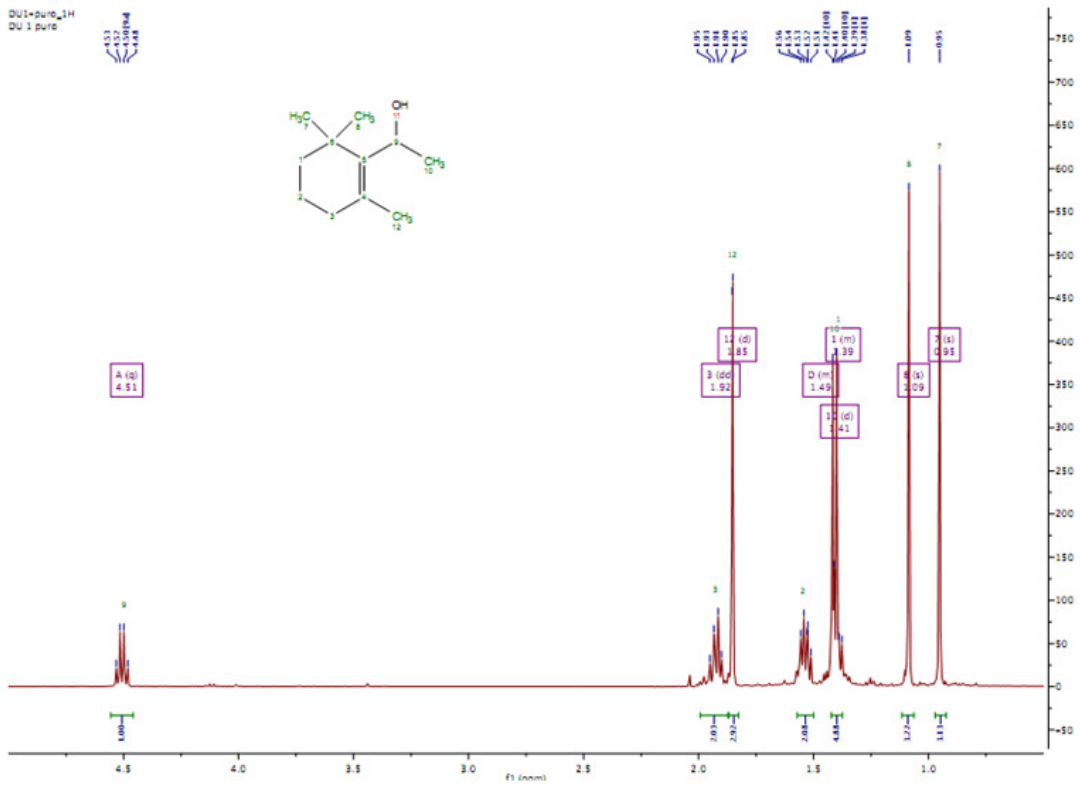

^{13}C-NMR and DEPT compound 80

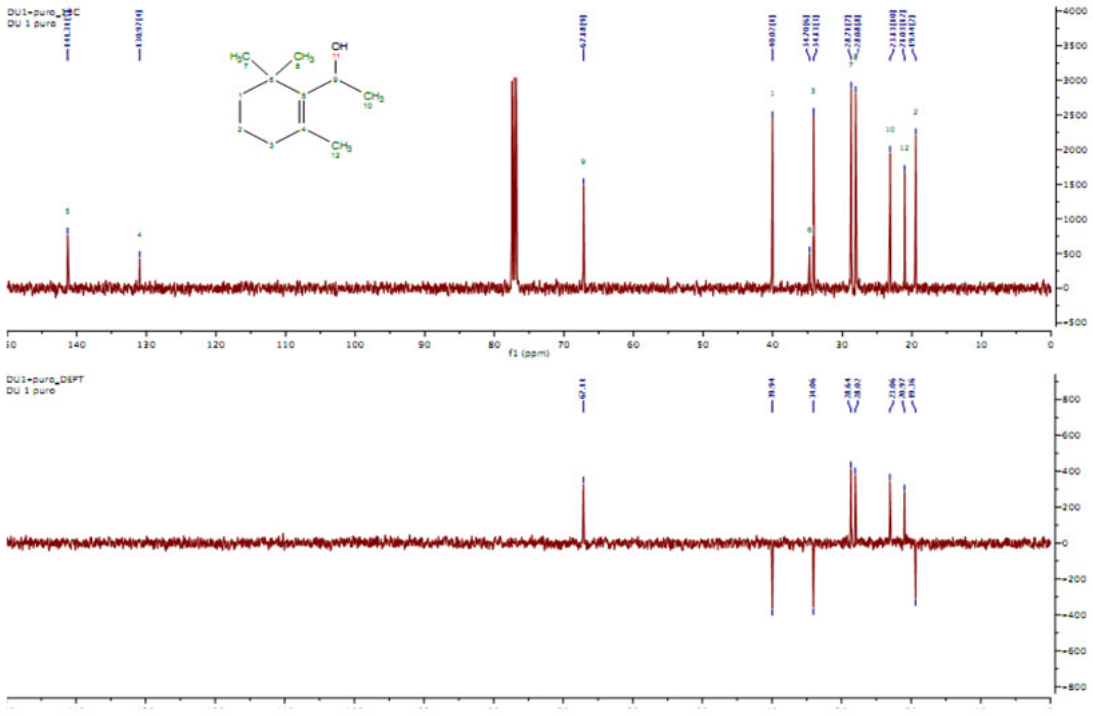

Synthesis of 1-(3-ethyl-2,4,4-trimethyl-2 cyclohexane)-triphenyl phosphoranyliden bromide **81:**

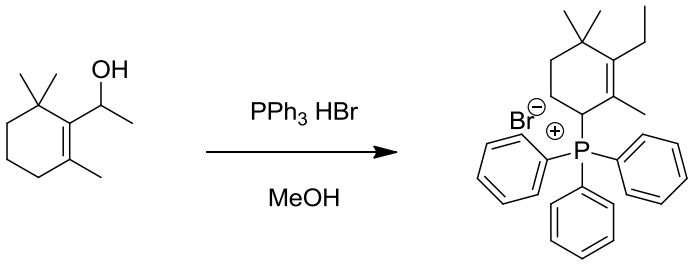

80 **81**

To a solution of allylic alcohol **80** in MeOH, PPh_3-HBr was added. The reaction was stirred at r.t. overnight. It was monitored by TLC (EtOAc/Petroleum ether 0.2:9.8) and by mass spectrometry. MeOH was evaporated and the compound is a sticky yellow solid. The isolation of the salt is made through a filtration on silica with EtOAc. After the evaporation of the solvent, the product **81** obtained is a white solid.

Yield 96%

M.P.= over 220°C

MS (ESI): $[M-H]^+ = 493,17$

^{1}H NMR (400 MHz,$CDCl_3$) δ 8.01-7.55 (m, 15H, $\underline{Ph_3}$-P), 5.60 (ddd, 1H, J = 16.6 Hz, 5 Hz, 3.2 Hz, H_3), 2.49-2.40 (m, 1H, H_2 or $H_{2'}$), 2.20-2.10 (m, 3H, H_2 or $H_{2'}$, H_1 e $H_{1'}$), 1.54 (d, 3H, J =3 Hz, H_{11}), 1.32 (ddd, 1H, J = 13.3, 5.5, 2.8, H_9 or $H_{9'}$), 0.96 (s, 3H, H_7 or H_8), 0.95 (t, 3H, J = 7.5 Hz, H_{10}), 0.94 (m, 1H, H_9 or $H_{9'}$), 0.63 (s, 3H, H_7 o H_8).

^{13}C NMR (400 MHz, $CDCl_3$) δ 149.63, 134.57, 130.80, 130.17, 119.97, 119.18, 40.17, 35.53, 27.82, 27.51, 22.64, 21.81, 21.53, 13.78.

^{1}H-NMR compound 81

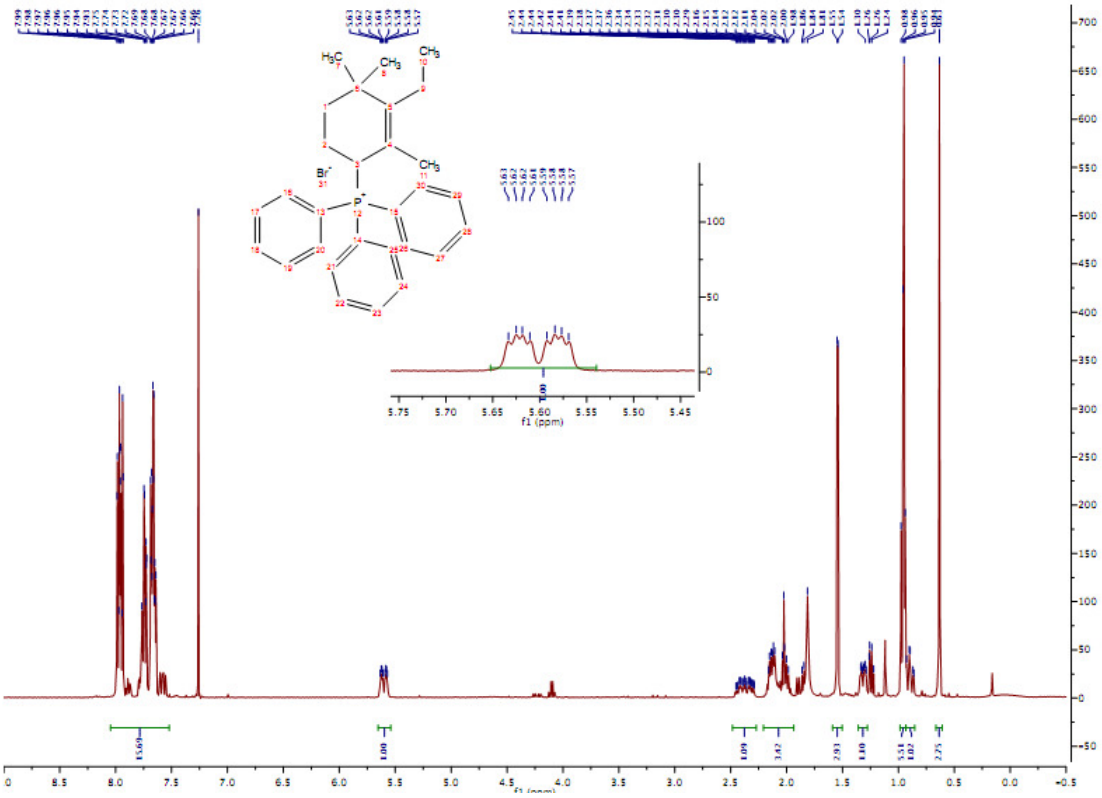

^{13}C-NMR and DEPT compound 81

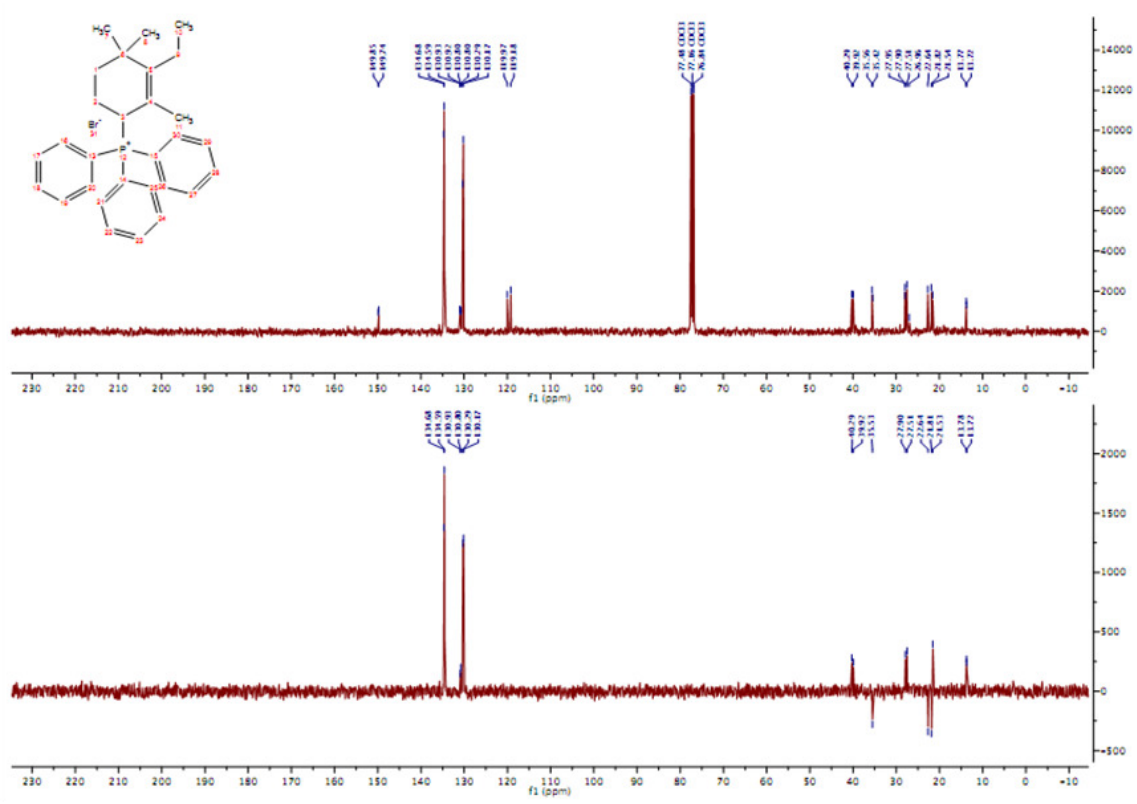

^{31}P-NMR compound 81

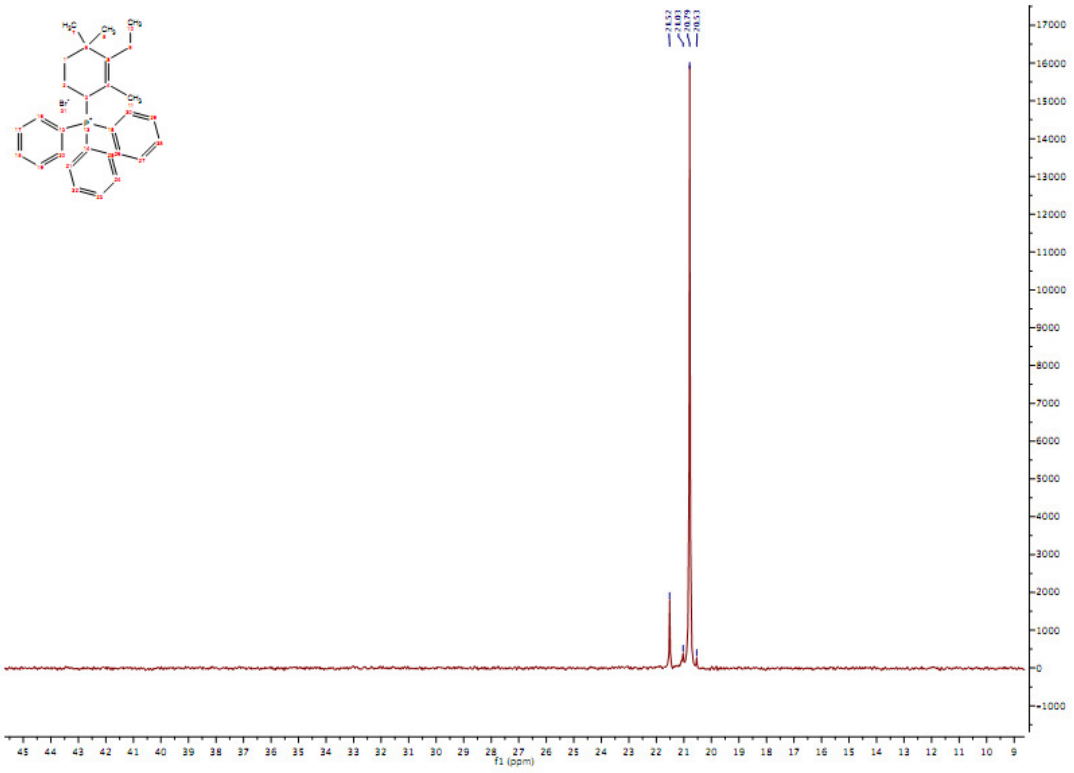

Synthesis of (E)-methyl 4-((3-ethyl-2,4,4-trimethylcyclohex-2-en-1-ylidene)methyl)benzoate **82**:

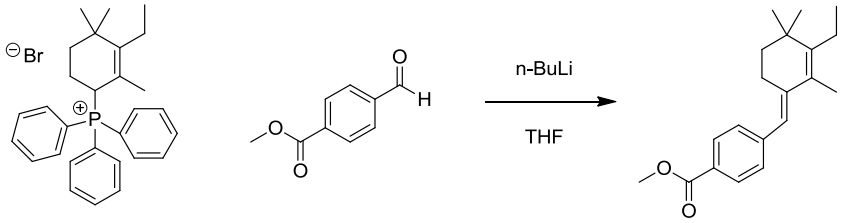

81 **82**

To a solution of salt **81** (2.13 mmol) in THF, BuLi was added (1 eq.) at r.t. and the reaction was stirred for 30 minutes, then the temperature was cooled to -78°C to add methyl 4-formyl benzoate (1.1 eq.). The Wittig reaction was stirred overnight and monitored by TLC and mass spectrometry. Once the product was formed, the reaction was quenched with NH_4Cl sat., THF evaporated and then extracted with ethyl acetate. The organic phase was dried over Na_2SO_4 and the solvent evaporated. The crude was purified by column chromatography and the product **82** was obtained as a brownish oil.

Yield 29%

MS (ESI): $[M-H]^+$= 299.42

IR: cm^{-1} 2952 C-H stretching, 1717 C=O stretching, 1602 C =C stretching, 1102 C-O-C stretching; 961-610 C-H aromatic bending.

^{1}H NMR (400 MHz,$CDCl_3$) δ 7.95 (d, 2H, *J* = 8.4 Hz, $H_{ar.}$), 7.32 (d, 2H, *J* = 8.2 Hz, $H_{ar.}$), 6.40 (s, 1H, Cq-C<u>H</u>=Cq), 3.95 (s, 3H, OCH_3), 2.6 (ddd, 2H, *J* = 8.2, 4.7, 1.7 Hz,CH_2-C<u>H$_2$</u>-Cq=), 2.20 (q, 2H, *J* = 7.2 Hz, C<u>H$_2$</u>-CH_3), 1.95 (s, 3H, Cq-C<u>H$_3$</u>), 1.50 (m, 2H, C<u>H$_2$</u>-CH_2-Cq=), 1.15 (t, 3H, *J* = 7.2 Hz, CH_2-C<u>H$_3$</u>), 1.15 (s, 6H, C<u>H$_3$</u>-Cq-C<u>H$_3$</u>).

^{13}C NMR (400 MHz,$CDCl_3$) δ 167.20, 148.91, 144.00, 142.29, 136.07, 129.95, 129.30, 127.12, 126.17, 120.57, 52.06, 38.84, 35.95, 27.69, 24.36, 22.99, 15.28, 14.80.

^{1}H-NMR compound 82

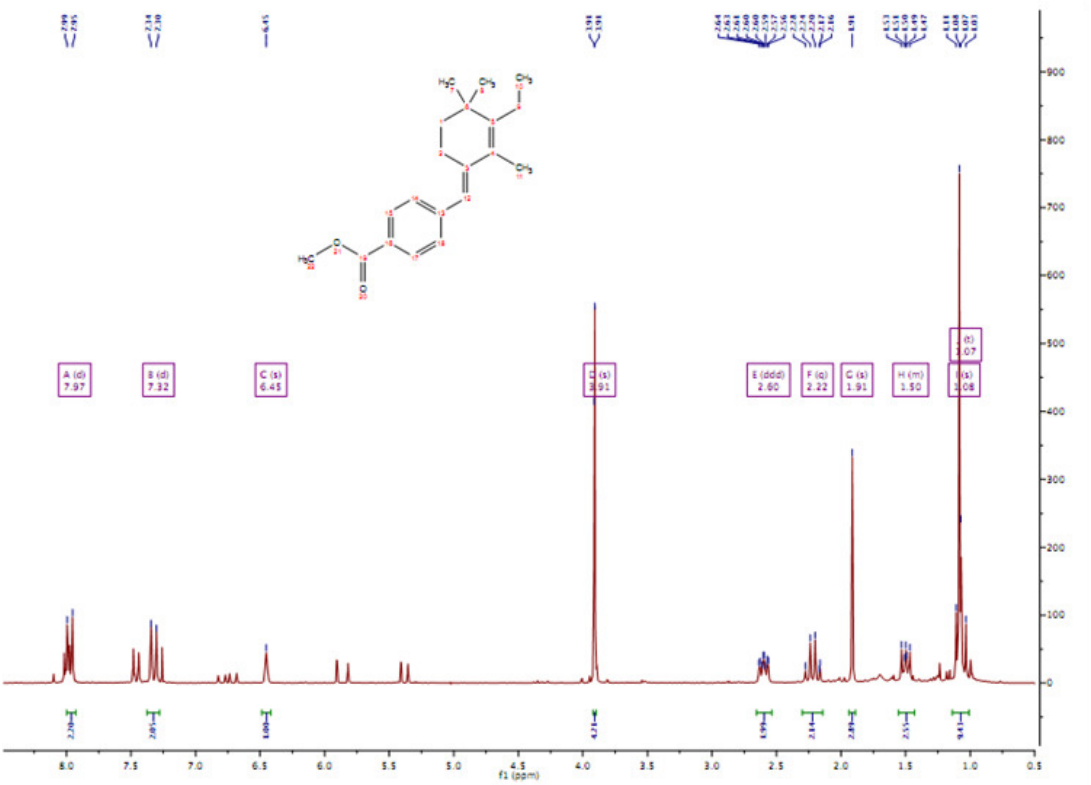

^{13}C-NMR and DEPT compound 82

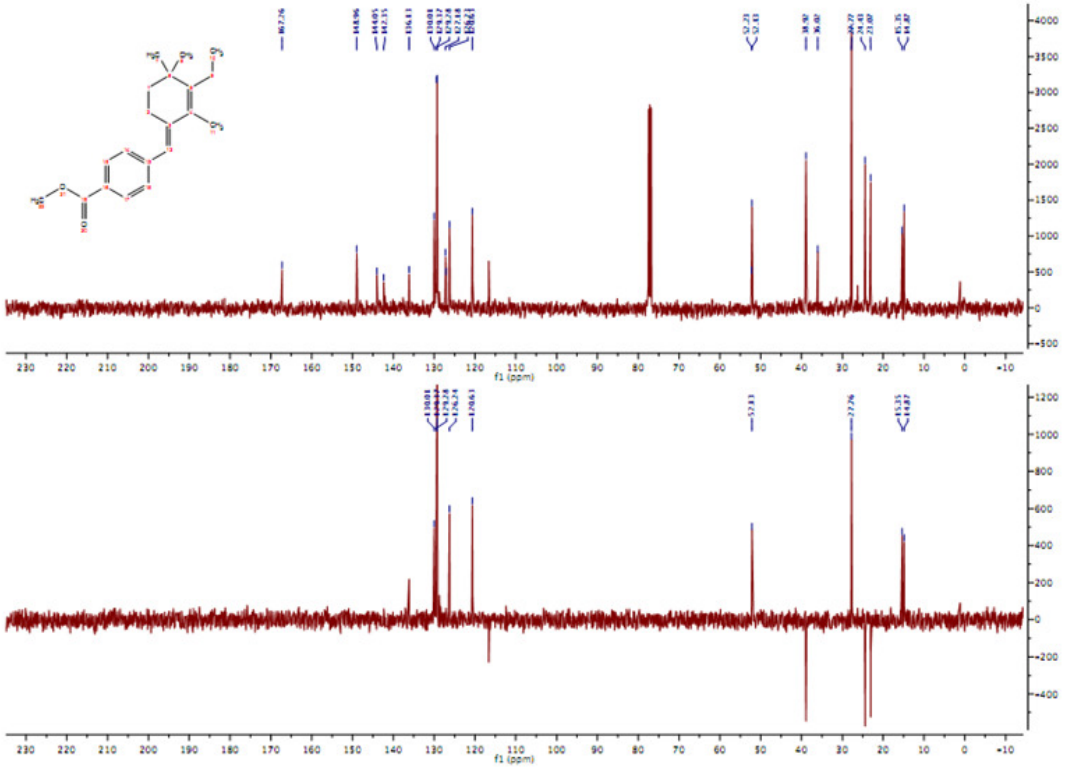

Synthesis of (E)-4-((3-ethyl-2,4,4-trimethylcyclohex-2-en-1-ylidene)methyl)benzoic acid **83**:

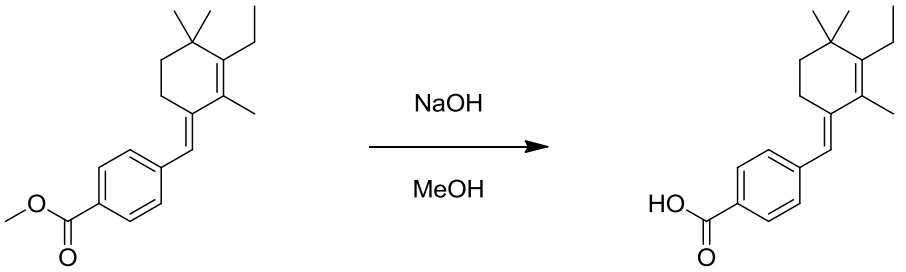

82 **83**

To a solution of the Wittig product **82** (0.38 mmol) in MeOH, NaOH 2N (3 eq.) was added drop to drop. The reaction was stirred at r.t. and monitored by TLC (EtOAc/Petroleum ether 0.2:9.8) and by mass spectrometry. After 16 h the MeOH was evaporated, the reaction was treated with HCl (1N) until acid pH and the compound was extracted with ethyl acetate. The organic phase was dried and evaporated. Then the product was crystallized in diethyl ether and centrifuged. The product **83** was a white solid.

Yield 74%

M.P.=150-155° C

MS (ESI): $[M-H]^+$= 285.39

^{1}H NMR (400 MHz, MeOD) δ 7.95 (d, 2H, *J* =8.4Hz, C$\underline{H}_{ar}$), 7.39(d, 2H, *J* =8.4 Hz, C$\underline{H}_{ar}$), 6.50 (s ,1H, C$\underline{H}$=Cq), 2.60 (m , 2H, CH_2-C$\underline{H_2}$-Cq=), 2.30 (q, 2H, *J* = 7.6 Hz, C$\underline{H_2}$-CH_3), 1.91 (s, 3H, C$\underline{H_3}$-C=), 1.50 (m, 2H, C$\underline{H_2}$-CH_2-Cq=), 1.15 (t, 3H, *J* = 7.6 Hz, CH_2-C$\underline{H_3}$), 1.15 (s, 6H, C$\underline{H_3}$-C-C$\underline{H_3}$).

^{13}C NMR (400 MHz, MeOD) δ 149.59,142.91, 142.12, 134.92, 130.12, 129.75, 128.41, 127.17, 40.10, 36.80, 28.14, 25.31, 23.73, 15.48, 15.21.

^{1}H-NMR compound 83

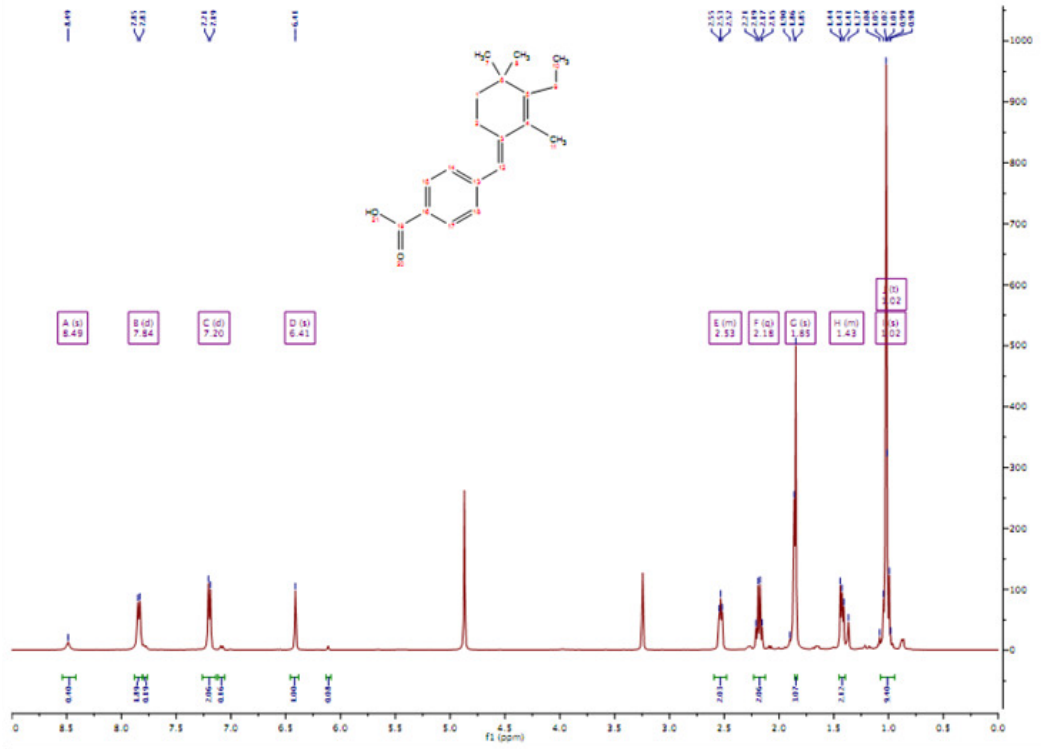

^{13}C-NMR and DEPT compound 83

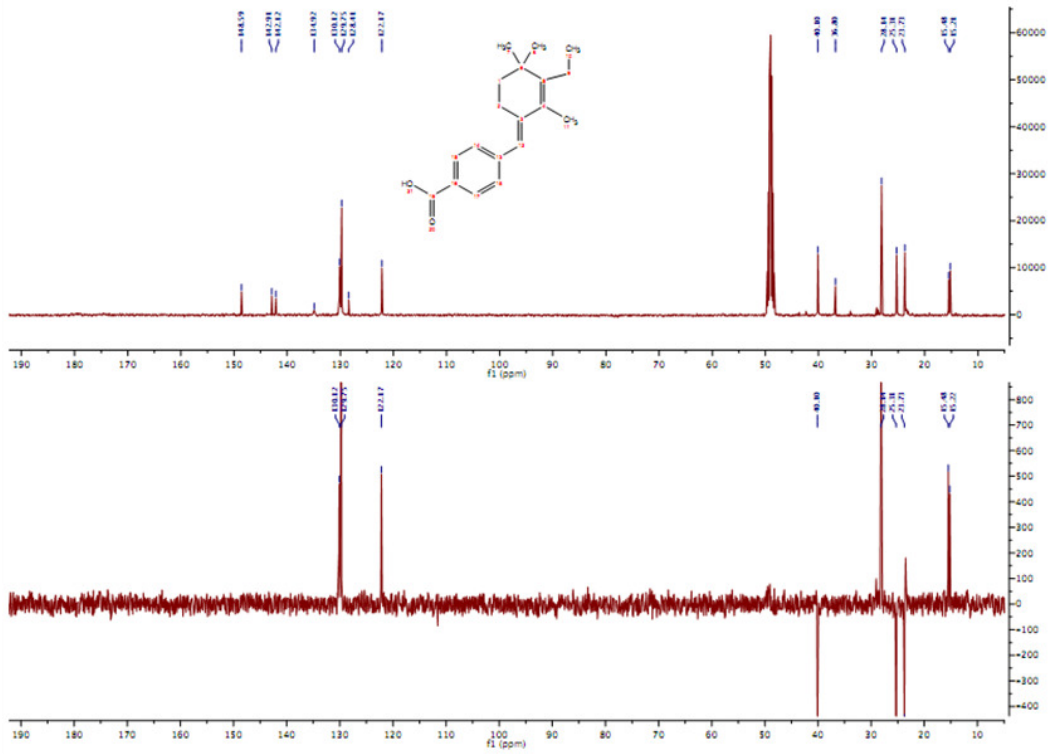

Synthesis of (E)-N-carbamimidoyl-4-((3-ethyl-2,4,4-trimethylcyclohex-2-en-1-ylidene)methyl)benzamide **84**:

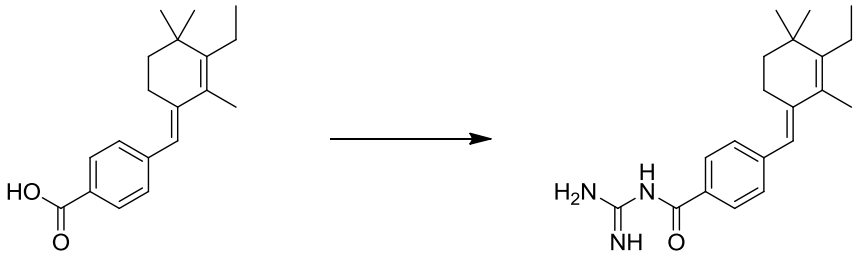

83 **84**

The first step is the activation of the acid function **83** (1.33 mmol) with CDI (1 eq.) in DMF, the reaction was stirred at r.t. for 1 h. In another round-bottom flask a solution of guanidine chloride (2 eq.) in DMF and Dioxane (1:1.8) was added, and then the ^{t}BuOK (2 eq.) was added too at 55°C for 30 minutes. There was the formation of KCl, that was removed by filtration. The guanidine solution then was added to the acid reaction. It was monitored by mass spectrometry and was stirred for 15 minutes. DMF and Dioxane then were removed by evaporation and the product was crystallized in water at 0°C and MeOH to give a white solid **84**.

Yield 77%

M.P.= 125-130 ° C

MS (ESI): $[M-H]^{+}$= 326.45

^{1}H NMR (400 MHz, Acetone-d_6) δ 8.15 (s, NH), 8.00 (d, 2H, *J* = 8 Hz, CH_{ar}), 7.25 (d, 2H, *J* = 8 Hz, CH_{ar}), 6.50 (s, 1H, C<u>H</u>=Cq), 3.40 (s, NH), 2.60 (m, 2H, CH_2-C<u>H_2</u>-Cq=), 2.25 (q, 2H, *J* = 7.6 Hz, C<u>H_2</u>-CH_3), 1.95 (s, 3H, C<u>H_3</u>-C=), 2.50 (m, 2H, C<u>H_2</u>-CH_2-Cq=), 1.15 (s, 6H), 1.15 (t, 3H).

^{13}C NMR (400 MHz, Acetone-d_6) δ 173.13, 160.62, 147.94, 141.41, 141.14, 136.56, 130.05, 129.60, 129.32, 128.10, 122.30, 39.68, 36.46, 30.46, 30.27, 30.08, 29.88, 29.69, 29.50, 29.31, 28.02, 24.98, 23.40, 15.48, 15.17.

^{1}H-NMR compound 84

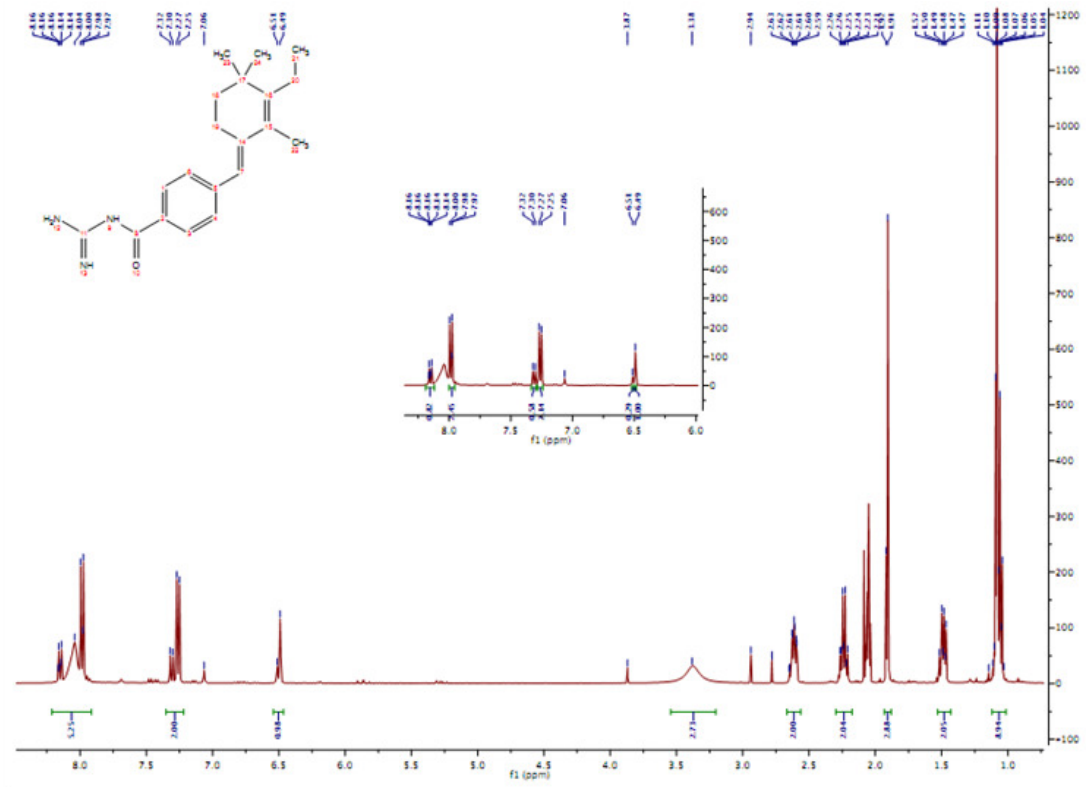

^{13}C-NMR and DEPT compound 84

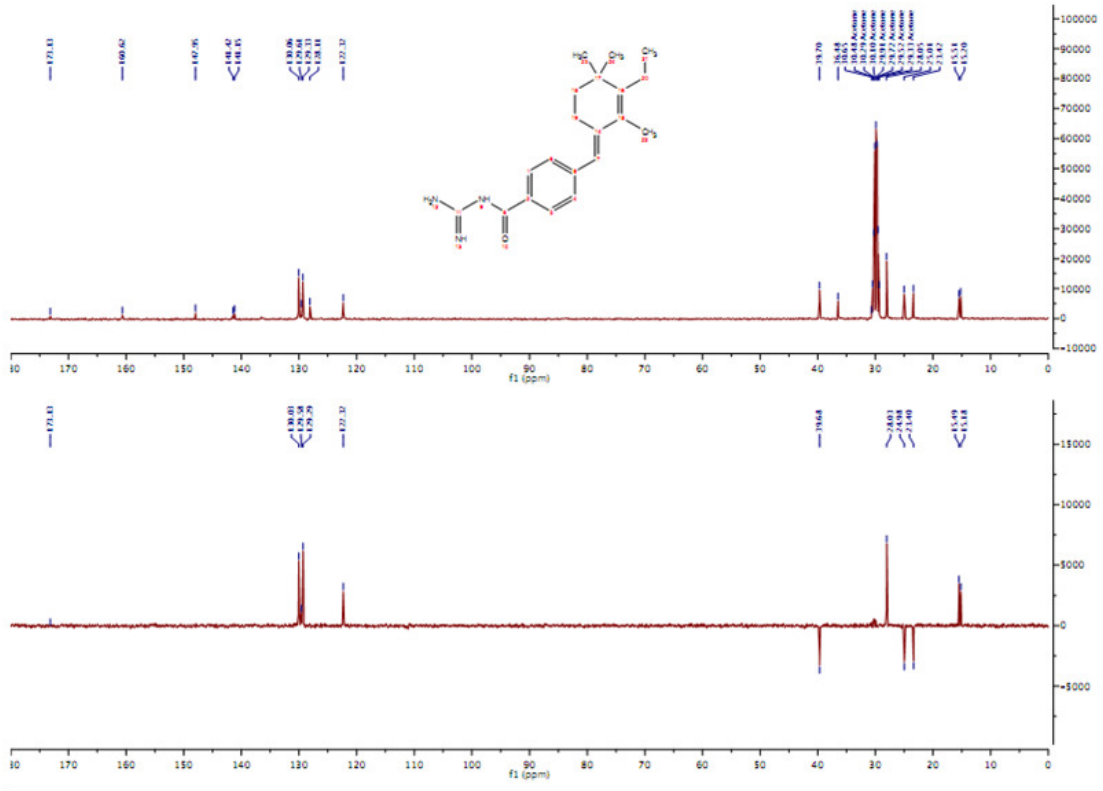

HMBC compound 84

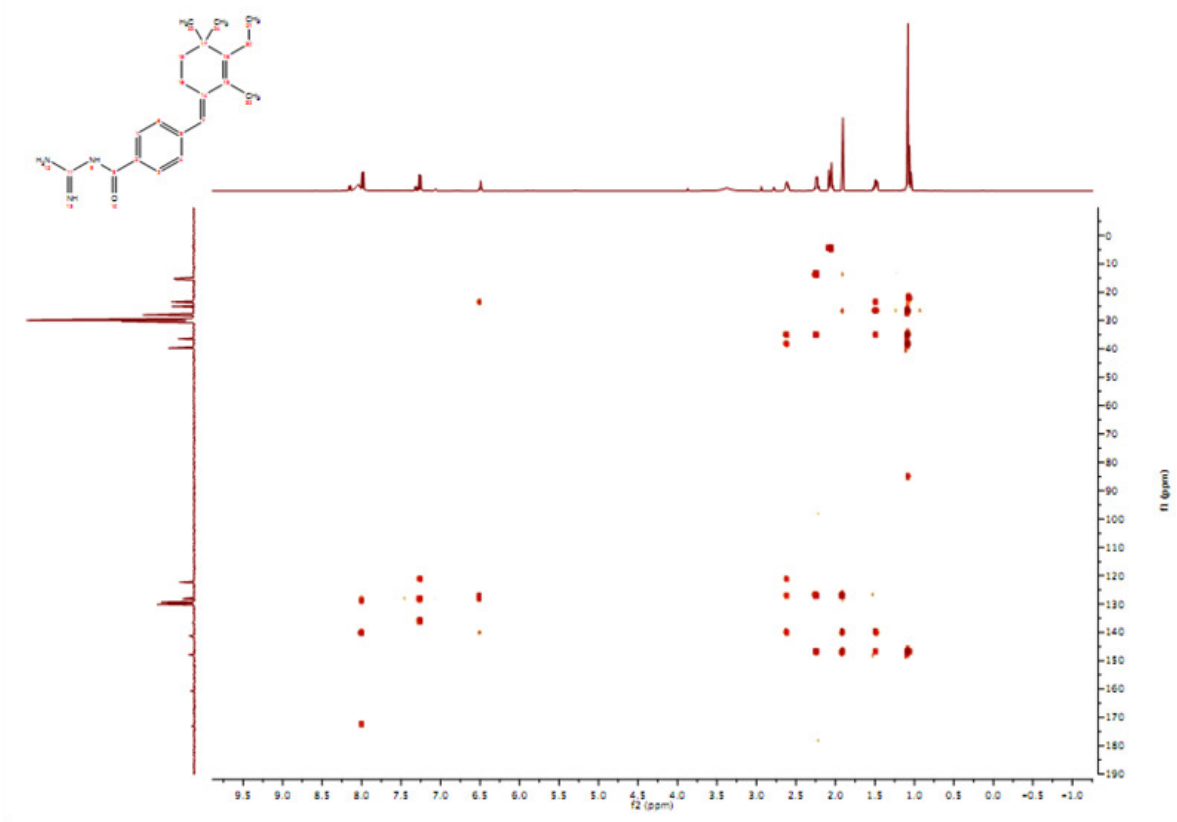

Synthesis of (E)-6-ethylidene-1,5,5-trimethylcyclohex-1-ene **85**:

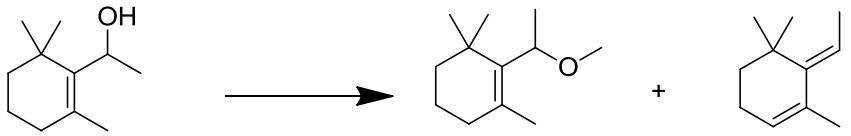

80 **85a** **85**

To a solution of the allylic alcohol **80** (1.19 mmol) in MeOH, HBr was added. The reaction was stirred for 30 minutes, when the starting material disappeared, monitoring by TLC (EtOAc/Petroleum ether 1:6), there was the formation of diene **85** and methyl ether **85a**. The solvent was evaporated and NaOH 2N was added to remove the excess of HBr. Then the solution was extracted with ethyl acetate and the organic phase, dried and evaporated. The crude was purified by column chromatography and it was obtained the product as an oil.

^{1}H NMR (400 MHz, $CDCl_3$) δ 3.95 (q, 1H, *J* = 6.8 Hz, CH_3O-C<u>H</u>-CH_3), 3.20 (s, 3H, OCH_3), 1.90 (t, 2H, *J* = 4.8 Hz,CH_2-CH_2-C<u>H</u>$_2$-), 1.75 (s, 3H, C<u>H</u>$_3$-Cq), 1.45 (m, 2H, CH_2-C<u>H</u>$_2$-CH_2-), 1.35 (d, 3H, *J* =6.8 Hz,C<u>H</u>$_3$-CH), 1.30 (m, 2H, C<u>H</u>$_2$-CH_2-CH_2-), 1.15 (s, 3H, C<u>H</u>$_3$-Cq-CH_3), 0.95 (s, 3H, CH_3-Cq-C<u>H</u>$_3$).

^{13}C NMR (400 MHz,$CDCl_3$) 136.89, 130.76, 75.65, 55.63, 40.27, 34.04, 29.78, 29.03, 27.91, 26.99, 21.49, 19.46.

Synthesis of (E)-6-ethylidene-1,5,5-trimethylcyclohex-1-ene **85**:

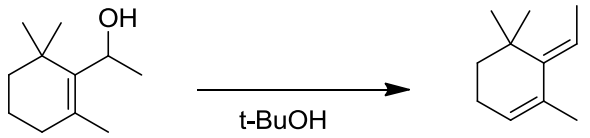

61 **63**

To a solution of allylic alcohol **80** (0.59 mmol) in t-BuOH, HBr was added to have the formation of the diene **85**. The reaction was stirred and monitored by TLC and after 30 minutes the reagent disappeared and the product formed. The t-BuOH was evaporated and NaOH 2 N was added at 0°C to basic pH to remove HBr in excess. After extraction with ethyl acetate, the organic phase was dried and evaporated. The crude was purified by column chromatography obtaining the diene **85** as a colorless oil.
Yield 32%

^{1}H NMR (400 MHz,$CDCl_3$) δ 5.60 (m, 1H, CH=Cq-CH_3), 5.53 (q, 1H, *J* = 7.5 Hz, C<u>H</u>-CH_3), 2.15 (m, 2H, CH_2-C<u>H_2</u>-CH), 1.95 (d, 3H, *J* = 7.2 Hz, CH-C<u>H_3</u>), 1.79 (s, 3H, C<u>H_3</u>-C=), 2.45 (t, 2H, *J* = 12.2 Hz, CH_2-C<u>H_2</u>-CH), 1.20 (s, 6H, C<u>H_3</u>-Cq-C<u>H_3</u>).

^{13}C NMR (400 MHz, $CDCl_3$) δ 144.34, 133.67, 125.20, 119.47, 40.48, 34.79, 27.88, 22.95, 21.88, 16.14.

^{1}H-NMR compound 85

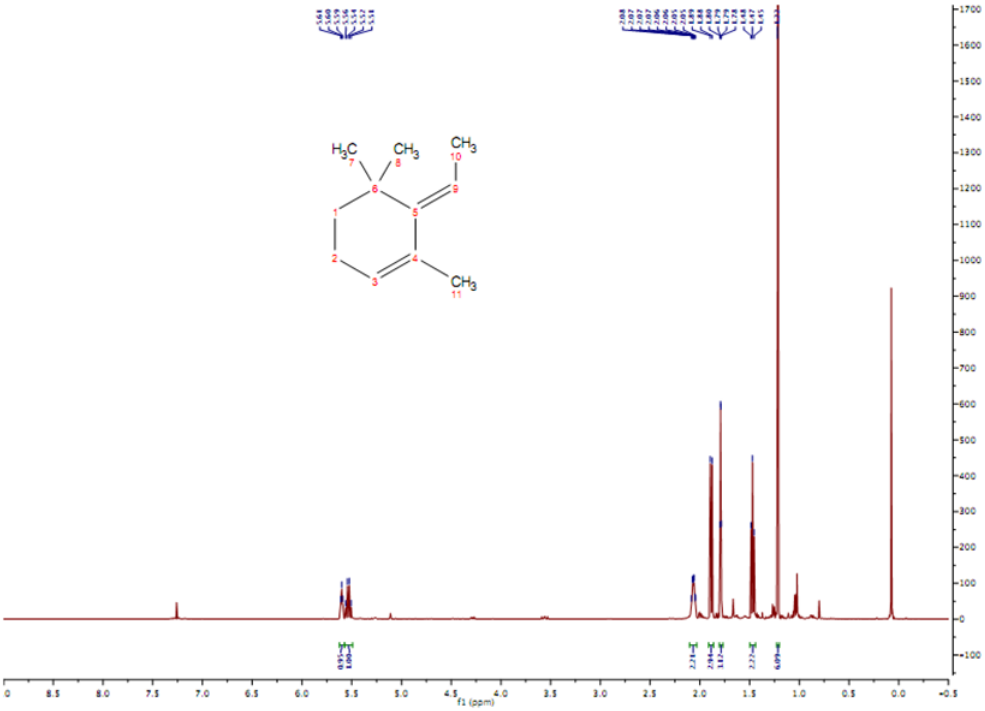

^{13}C-NMR and DEPT compound 85

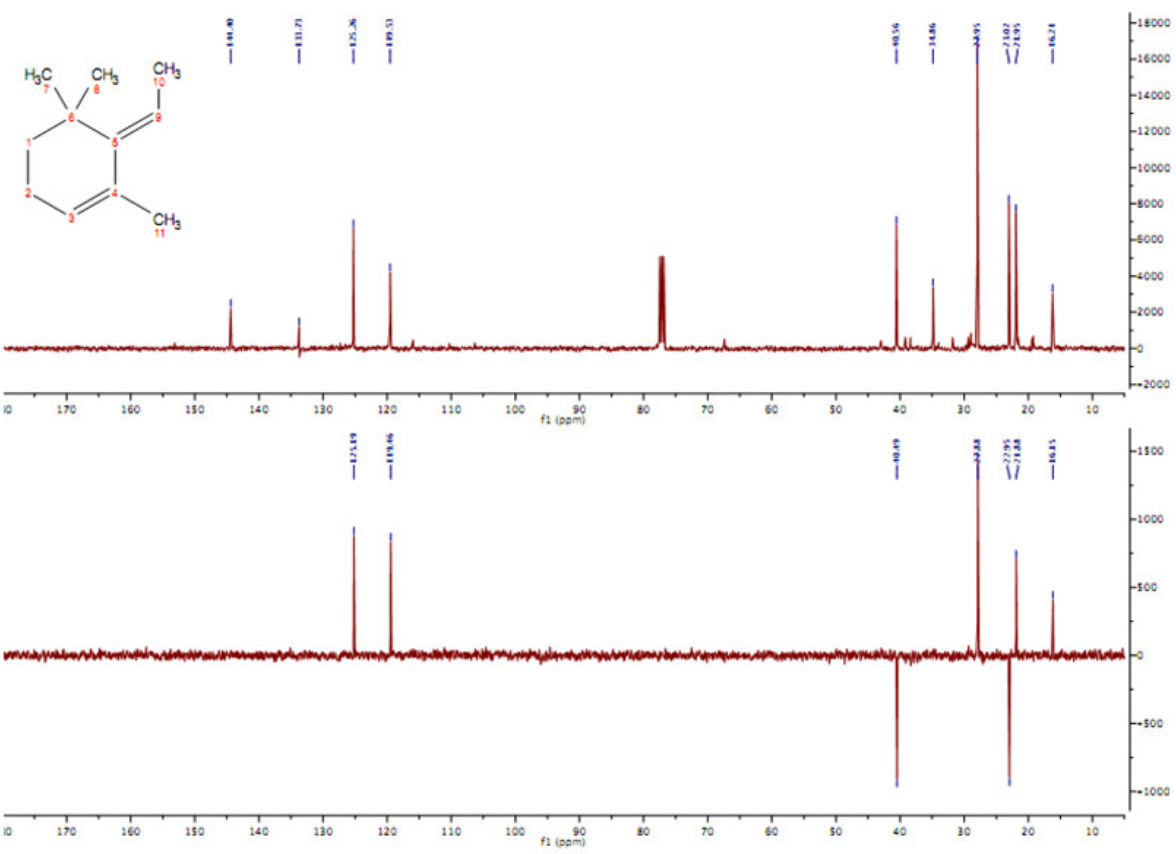

Synthesis of (E)-4-((3-ethyl-2,4,4-trimethylcyclohex-2-en-1-ylidene)methyl)benzamide **86**:

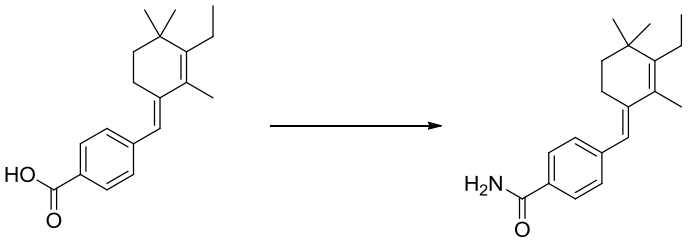

83 **86**

To a solution of the acid **83** (0.21 mmol) in DMF, CDI was added (1 eq.) and the NH_4OH conc. (1.2 eq.) was too. The solvent was evaporated and the compound **86** was crystallized with Et_2O and centrifuged.

Yield 20%

M.P.= over 220°C

MS (ESI): $[M-H]^+$= 284.41

IR : 2966.39 C-H stretching benzene,1583.04,1543.12 N-H bending.

^{1}H NMR (200 MHz,$CDCl_3$) δ 8.00 (d, 2H, *J* = 8.3 Hz, NH_2) 7.77 (d, 2H, *J* = 8.2 Hz, C$\underline{H}_{ar}$), 7.35 (d, 1H, *J* = 8.1 Hz, C$\underline{H}_{ar}$), 6.50 (s, 1H, C$\underline{H}$=C), 2.60 (m, 2H, CH_2-C$\underline{H}_2$-C=), 2.20 (q, 2H, *J* = 2 Hz, C$\underline{H}_2$-CH_3), 1.95 (s, 3H, C$\underline{H}_3$-C=), 1.55 (m, 2H, C$\underline{H}_2$-CH_2-C=), 1.15 (s, 6H, C$\underline{H}_3$-Cq-C$\underline{H}_3$), 1.15 (t, 2H, *J* = 2 Hz, CH_2-C$\underline{H}_3$).

Synthesis of (E)-N-carbamoyl-4-((3-ethyl-2,4,4-trimethylcyclohex-2-en-1-ylidene)methyl)benzamide **87**:

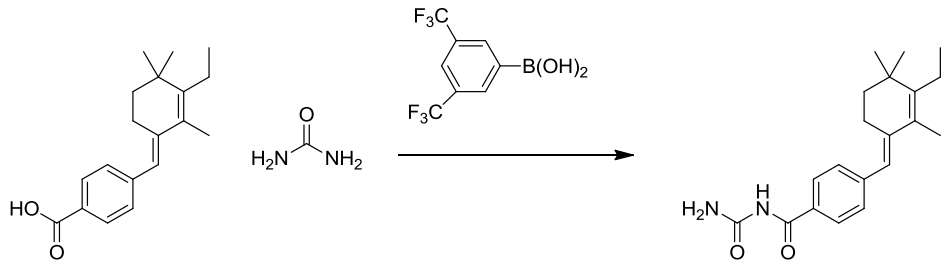

83 **87**

To a solution of the acid **83** (0.28 mmol) and urea in toluene, the catalyst 3,4,5-trifluoromethyl-phenyl boronic acid (1.1 eq.) was added and the reaction was stirred at 90°C overnight. The reaction was monitored by TLC and mass spectrometry. The solvent was evaporated and the compound washed with basic aqueous solution and extracted with ethyl acetate. The organic phase was dried and evaporated. The product **87** was purified by preparative HPLC.

MS (ESI): $[M-H]^+$= 327.46

Synthesis of N-carbamimidoyl-4-((3-ethyl-2,4,4-trimethylcyclohexyl)methyl)benzamide **89**:

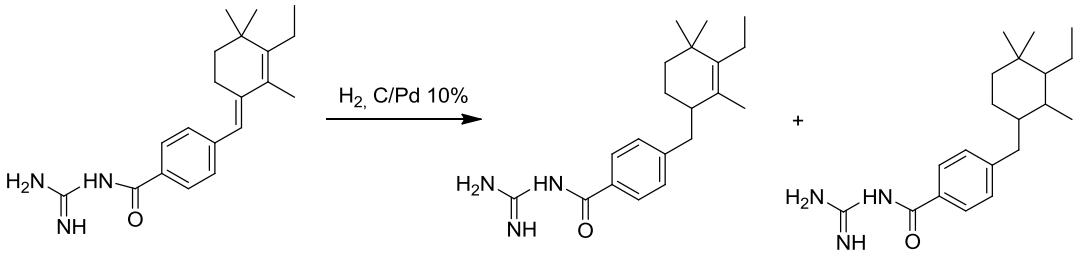

84 **88** **89**

The compound **84** was dissolved in EtOH and EtOAc, C/Pd was added and it was used a balloon of H_2. The reaction was stirred overnight and the day after was observed a green color. The product was filtered on Gooch through diatomeus earth to remove C/Pd.
The liquid phase contained the products **88** and **89**. The solvent was evaporated and through HPLC was possible to separate the two compounds because of their different retention time. The preparative HPLC was on column C18 using a gradient as A H_2O+0.1% TFA and as B CH_3CN 60%, H_2O 40% + 0.1% TFA.

Another method was to use the ThalesNano nanotechnology H-Cube machine to hydrogenate the compound **84** dissolved in EtOH (2M) and using C/Pd 10% as catalyst.
At 60°C and 60 bar.
The yield of product **89** of the reaction is almost 100%.

MS (ESI): $[M-H]^+$= 328.46 for **88** and 330.25 for **89**

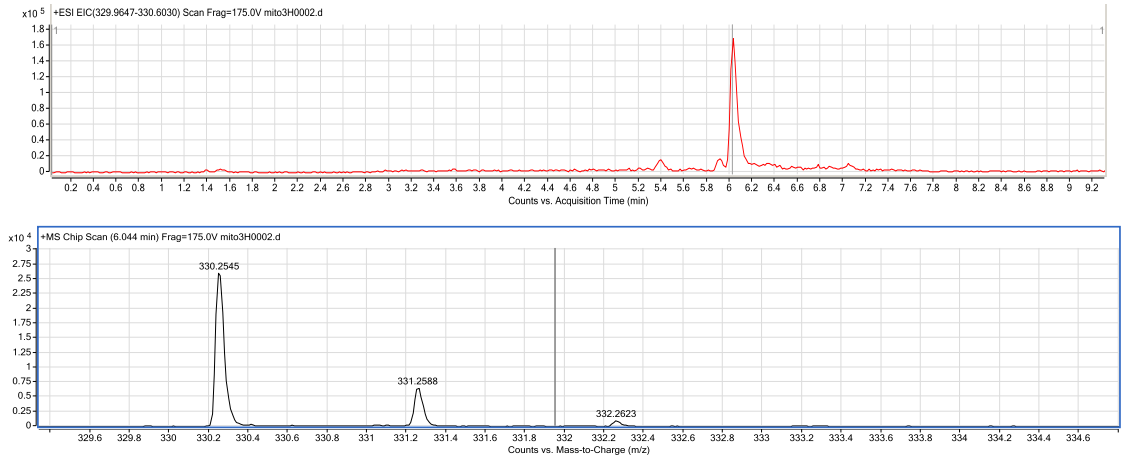

Synthesis of 2-amino-4(3H)-quinazolinone derivatives **90, 91, 92**:

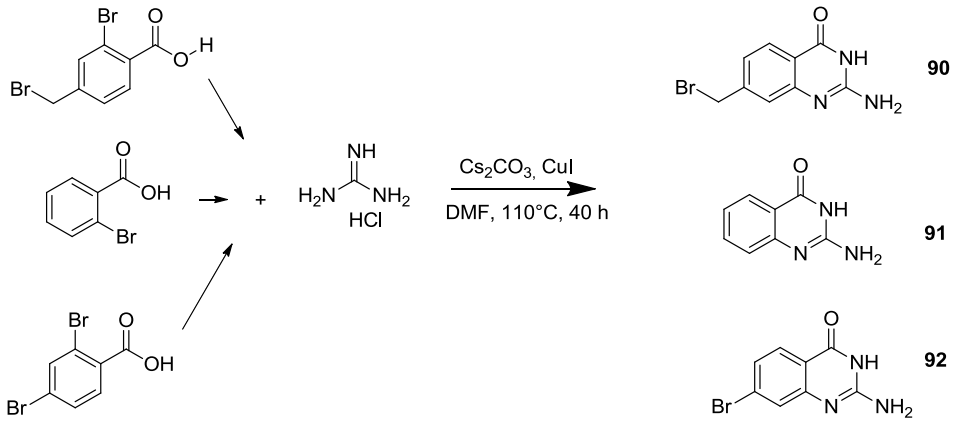

A two-neck round bottom flask was charged with a magnetic stirrer, evacuated and backfilled with N_2. Substituted 2-bromobenzoic acid
(0.5 mmol), guanidine hydrochloride (1 mmol), Cs_2CO_3 (2 mmol, 652 mg) and DMF (3 mL) were added. After stirring for 20 min under N_2, CuI (0.1 mmol) was added to the flask. The reaction temperature was raised to 110 °C. After 40 h the resulting solution was cooled to r.t. and filtered, and the solid was washed with DMF (3 mL). The combined filtrate was concentrated with a rotary evaporator, and the residue was purified by column chromatography on silica gel to provide the final products as a white solid.
Yield 64-85%
MS (ESI): $[M-H]^+$= 255.08 compound **90**, 162.20 compound **91**, 241.10 compound **92**

NMR spectra compound 91

^{1}H NMR (DMSO-*d*6, 300 MHz): d = 11.18 (br s, 1 H), 7.87 (dd, *J* = 7.9, 1.4 Hz, 1 H), 7.55 (dt, *J* = 7.4, 1.7 Hz, 1 H), 7.19 (d, *J* = 8.3 Hz, 1 H), 7.09 (t, *J* = 7.6 Hz, 1 H), 6.50 (br s, 2 H).

^{13}C NMR (DMSO-*d*6, 75 MHz): d = 163.5, 152.7, 134.6, 126.5, 123.7, 122.1, 117.6.

Synthesis of quinazolin-2-amine **93**:

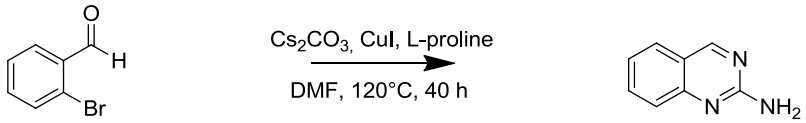

93

A two-neck round bottom flask was charged with a magnetic stirrer, evacuated and backfilled with N2. 2-Bromobenzaldehyde and guanidine hydrochloride (1 mmol), L-proline (0.2 mmol), Cs_2CO_3 (2 mmol, 652 mg) and DMF (5 mL) were added (200 mg of 4 Å MS was added for 2-bromobenzaldehyde). After stirring for 20 min under N_2, CuI (0.1 mmol) was added to the flask, and then the reaction temperature was raised to 120 °C. After 40 h, the resulting solution was cooled to r.t. and filtered, and the solid was washed with DMF (3 mL). The combined filtrate was concentrated with the aid of a rotary evaporator, and the residue was purified by column chromatography on silica gel to provide the product **93** as yellow solid.

Yield 48%

MS (ESI): [M + H]+ = 229.2.

^{1}H NMR ($CDCl_3$, 300 MHz): d = 8.99 (s, 1 H), 7.65 (m, 2 H), 7.56 (d, *J* = 8.4 Hz, 1 H), 7.21 (t, *J* = 6.9 Hz, 1 H), 4.03 (m, 4 H), 2.57 (m, 4 H), 2.39 (s, 3 H).

^{13}C NMR ($CDCl_3$, 75 MHz): d = 161.5, 159.2, 152.3, 134.2, 127.5, 125.7, 122.6, 119.7, 55.1, 46.2, 43.9.

5.4.1 Biological experimental section

Qproteome Mitochondria Isolation kit protocol

These tests are based on MCF7 cell lines (they are breast cancer cell lines isolated in 1970 from 69 years old Caucasian woman, before these cells it was no possible to obtain breast cancer cell lines that were able to live longer than few months).

The cells are seeded in a Petri dish, 1 million/mL each Petri, for 5 million total, (5 mL of DMEM-High Glucose added with 10% of FBS, 10 U/mL of antibiotic P/S, 0.025 µg/mL of antifungal fungizone).

The day after the cells are treated with the compound **89** and collected after 3 hours and 6 hours following the protocol Qproteome Mitochondria Isolation kit to extract the mitochondria.

This protocol[58] provides some steps:

Transfer a cell suspension containing approximately 5 x 106 to 2 x 107 cells into a 15 ml conical tube and centrifuge at 500 x g for 10 min at 4°C. Carefully remove and discard the supernatant.

Wash the cells using 1 ml 0.9% sodium chloride solution.

Resuspend the cell pellet in 1 mL or 2 mL ice-cold Lysis Buffer by pipetting up and down using a 1 mL pipette tip. Incubate for 10 min at 4°C on an end-over-end shaker.

Ensure that Protease Inhibitor Solution has been added to Lysis Buffer.

Centrifuge the lysate at 1000 x g for 10 min at 4°C.

Carefully remove the supernatant. This fraction primarily contains cytosolic proteins.

Resuspend the cell pellet in 1.5 mL ice-cold Disruption Buffer by pipetting up and down using a 1 ml pipette tip. Complete cell disruption by using a blunt-ended needle and a syringe. Draw the lysate slowly into the syringe and eject with one stroke. Repeat 10 times.

Ensure that Disruption Buffer has been supplemented with Protease Inhibitor Solution.

Centrifuge the lysate at 1000 x g for 10 min at 4°C and carefully transfer the supernatant to a clean 15 ml tube. The pellet contains nuclei, cell debris, and unbroken cells. If desired, proteins can be re-extracted from the cell pellet by repeating steps 6 and 7 using 500 µl ice-cold Disruption Buffer. The supernatants from each extraction should be combined before the next step.

Carefully transfer the supernatant(s) into a fresh microcentrifuge tube and centrifuge at 6000 x g for 10 min at 4°C.

Carefully remove the supernatant. The pellet contains mitochondria. The supernatant constitutes the microsomal fraction.

Wash the mitochondrial pellet from step 10 with 1 ml Mitochondria Storage Buffer by carefully pipetting up and down using a 1 ml pipette tip. Centrifuge at 6000 x g for 20 min at 4°C.

Resuspend the mitochondrial pellet in Mitochondria Storage Buffer or a buffer of choice for further analysis.

LC/MS analysis procedure

The mitochondria pellets collected at 3 and 6 hours were treated with 1 mL of a mixture of CH_3CN and H_2O (6:4) with CF_3COOH (0.1 %). Cell membrane disruption was induced by ultrasonication for 10 min. After filtration (0.2 µm), the obtained solutions were analysed through LC-HRMS analysis performed by a ESI-Q-TOF Nano HPLC-CHIP Cube® Agilent 6520 instrument (Agilent Technologies USA) using a linear gradient (0.4µL/min) from 100% solvent A (97% water/3% acetonitrile/0.1% formic acid) to 90% solvent B (97% acetonitrile/3% water/0.1% formic acid) in 5 minutes and from 90% solvent B to 0% solvent B in 5 minutes, using a Zorbax C18 Coloumn (43mmX75µm, 5µm) equipped with enrichment coloumn (4mm 40nL).

References

1. Gray W., Burger G., Lang B. F., *Science*, **1999**, 283(5407), 1476-81.
2. Friedman J. R. and Nunnari J., *Nature*, **2014**, 505(7483), 335-343.
3. Anderson S., Bankier A. T., Barrell B. G., de Bruijn M. H. L., Coulson A. R. et al., *Nature,* **1981**, 290, 457 – 465.
4. Yang K. C., Kyle J. W., Makielski J. C., Dudley S. C. Jr, *Circulation* Research, **2015**, 1937-1955.
5. Jonckheere A. I., Smeitink J. A. M., and Rodenburg R. J. T., *J Inherit Metab Dis.*, **2012**, 35(2), 211-225.
6. Nakamoto R. K., Baylis Scanlon J. A., and Al-Shawi M. K., *Arch Biochem Biophys*., **2008**, 476(1), 43-50.
7. García J., Morales-Ríos E., Cortés-Hernández P., and Rodríguez-Zavala J., *Biochemistry*, **2006,** *45* (42), 12695–12703.
8. Nelson D. L., Cox M. M., I principi di biochimica di Lehninger, ed. fifth.
9. Duchen M.R.*, Mol. Aspects Med*. **2004**, 25, 365–451.
10. Rasola A., Sciacovelli M., Pantic B., and Bernardi P., *FEBS Lett*., **2010**, 584(10), 1989-1996.
11. Liu Y. and Chen X. J., *Oxid Med Cell Longev*, **2013**, 146860.
12. Leung A. W., Varanyuwatana P. and Halestrap A. P., *J Biol Chem*, **2008**, 283(39),26312-23.
13. Elmore S., *Toxicol Pathol*., **2007**, 35(4), 495-516.
14. Samejima K., Ogawa H., Ageichik A. V., Peterson K. L., Kaufmann S. H. *et al*, *JBC*, **2014**, 289, 31617-31623.
15. Wang C. and Youle R. J., *Annu. Rev. Genet.,* **2009**, 43, 95-118.
16. Vucic D, Deshayes K, Ackerly H *et al.*, *J. Biol. Chem.* , **2002**; 277, 12275–12279.
17. Marchenko N. D.,Wolff S., and Moll U. M., *EMBO J*, **2007**, 26(4), 923-934.
18. Bond **.**, Hu W., E. Bond, Robinson H., Lutzker G. *et al*., *Cell*, **2004**, 119, 591-602.
19. Zhao Y.,Aguilar A., Bernard D., Wang S., *J. Med. Chem*., **2014**, 1038-1052.
20. Mokranjac D., Bourenkov G., Hell K., Neupert W., Groll M., *EMBO J.*, **2006**, 25(19), 4675-4685.
21. Jubinsky P. T., *J. Mol. Hist*., **2005**, 69-75.
22. Kalogeris T., Baines C. P., Krenz M., Korthuis R. J., *Int. Rev. Cell. Mol. Biol.,***2012**, 298, 229-317.
23. Imahashi K, Pott C, Goldhaber JI *et al.*, *Circ. Res.* **2005**; 97, 916–921.
24. Pagliarani, A.; Nesci, S.; Ventrella, **2016**,16, 815-824(10).

25. Symersky J, Osowski D, Walters DE *et al., Proc. Natl. Acad. Sci. U. S. A,* **2012**, 109, 13961–13965.

26. Boz I., Synthesis of modulators of mitochondrial c-ring protein with spiro/ureidic motif, **2016**.

27. Benetti S.; De Risi C.; Pollini G. P.; Zanirato V., *Chem. Rev.,* **2012**, *112*, 2129–2163.

28. Chauhan P., Mahajan S., Enders D., *Chem. Rev* **, 2014**, *114*, 8807–8864.

29. Bharkavi C., Sundaravel V., Kumar R. S., Subbu P, *Synlett ,* **2015**, 26, 1665–1670.

30. Kumar R., S.; Perumal S., *Tetrahedron Letters* , **2007**, 48, 7164–7168.

31. Romagnoli R., Baraldi P.G., Carrion M.D., Lopez Cara C., Cruz-Lopez O., Iaconinoto M.A., Preti D., Shryock J.C., Moorman.R., Vincenzi F., Varani K., Borea P.A., *J. Med. Chem.,* **2008,** 51, 5875–5879.

32. Bonora M., Morganti C., Morciano G., Giorgi C., Wieckowski M. R., Pinton P., *Nature Protocols*, **2016**, 11, 1067-1080.

33. Anil B., Riedinger C., Endicott JA, Noble ME *, Acta Crystallogr. D Biol. Crystallogr.* , **2013**, 69, 1358-1366.

34. Millard M., Pathania D., Grande F., Xu S., Neamati N., *Current Pharmaceutical Design,* **2011**, 17, 000.

35. Vassilev L., Vu T., Graves B., Carvajal D., Podlaski F. *et al*., *Science,* **2004,** 303, 844-848.

36. Shu L., Wang P., Liu W., Gu C., *Org. Process Res. Dev.,***2012**, 16,1866-1869.

37. Bartkovitz J., Cai J., Chu J., Lovey H., Vu B., Zhao C., *Chem. Abstr. PCT. Int. Appl.,***2009**, 150, 447932.

38. Shu L., Gu C., Dong Y., Brinkman R., *Org. Process Res. Dev.*, **2012**, 16, 1940.

39. Wang Z., Jonca M., Lambros T., *J. Biomed. Anal.*, **2007**, 45, 720-729.

40. Davis T. A., Vilgelm A. E., Richmond A., Johnston J. N., *J. Org. Chem.*, **2013**, 78(21), 10605-10616.

41. Davis T. A., Johnston J. N., *Chem. Sci.*, **2011**, 2,1076-1079.

42. Vara B. A., Mayasundari A., Tellis J. C., Danneman M. W., Arrendondo V., Davis T. A., Min J., Finch K., Guy R. K., Johnston J. N., *J. Org. Chem.*, **2014**, 6913-6938.

43. Hendrickson J. B., Hussoin M. S., *J. Org. Chem.*, **1989**, 54, 1144.

44. Denmark S., Beutner G., *Angew. Chem. Int. Ed.*, **2008**, 47, 1560-1638.

45. Zhang Z., Schreiner P., *Chem. Soc. Rev.*, **2009**, 38, 1187-1198.

46. Klauber E. G., De C. K., Shan T. K., Seidel D., *J. Am. Chem. Soc.*, **2010**, 132, 13624.

47. Rubin H., Cockrell J., Morgan J. B., *J. Org. Chem.*, **2013**, 78, 8865-8871.

48. Kanta De C., Seidel D., *J. Am. Chem. Soc.*, **2011**, 133, 14538-14541.

49. Muller C., Schreiner P., *Angew. Chem. Int. Ed.*, **2011**, 50, 6012-6042.

50. Fantinati A., Bianco S., Cristofori V., Cavazzini A., Catani M. *et al.*, *Chemistry Select*, **2017**, 2, 8504-8508.

51. Jubinsky P. T., Short M. K., Ghanem M., Das B. C., *Bioorganic & Medicinal Chemistry letters*, **2011,** 21, 3479-3482.

52. Das B. *et al*, *Chem. Comm.*, **2009**, 2133-2135.

53. Maki T.*et al.*, *Synlett* , **2004**, 8, 1355-1358.

54. Srivastava S., Srivastava S., *International Journal of Pharma Sciences and Research* , **2015**, 6, 1206-1213.

55. Huang X., Yang H., Fu H., Qiao R., Zhao Y., *SYNTHESIS*, **2009**, 16, 2679–2688.

56. Garrison J. B., Shaw Y. J., Chen C. S., and Kyprianou N.*, Cancer Res.* ,**2007** , 67(23), 11344–11352.

57. Tagliati F, Gentilin E, Buratto M, Molè D, degli Uberti EC, Zatelli MC., *Endocrinology*. **2010**, 151(10), 4635-42.

58. Qproteome™ Mitochondria Isolation Handbook, QIAGEN, April **2006**.

Abbreviations

ADP Adenosin Diphosphate, ATP Adenosin Triphosphate, CDI Carbonyldiimidazole, CsA Cyclosporin A, CH2Cl2 Dichloromethane, CH3CN Acetonitrile, DIPEA Diisopropyl-ethyl-amine, DMSO-d6 Dimethyl-sulfoxide, ETC Electron transport chain, EtOH Ethanol; Et2O Diethylether, EtOAc Ethyl Acetate, FAD Flavinic transporter, h hours, HCl hydrochloric acid H2O water, IMS Inter-membrane space, IRI Ischemia - reperfusion injury, K2CO3 Potassium carbonate, KRB Krebs-Ringer Buffer, mp Melting point, MeOH methanol; mCypD Mitochondrial Cyclophilin D; MPT Mitochondrial Permeability Transition; mPTP Mitochondrial Permeability Transition Pore; NAD Nicotinammidic transporters, NaOH Sodium Hydroxide, NH4OH Ammonium Hydroxide, Pi inorganic phosphate, RT Room Temperature, SAR Structure - Activity Relationship, THF Tetrahydrofuran, TCA tricarboxylic acid, $CDCl_3$ deuterium chloroform, IMM: Inner Mitochondrial Membrane, ANT: Adenine Nucleotide Translocator, Glu59: Glutammate 59, Leu63: Leucine 63, Phe64: Phenylalanine 64, TEA: Triethylamine, OMM outer mitochondrial membrane, OXPHOS oxidative phosphorylation, mtDNA mitochondrial DNA , SMAC second mitochondria-derived activator of caspases, DMAP 4-Dimethylaminopyridine, DMF dimethylformamide.

ChemPubSoc Europe

DOI: 10.1002/slct.201701059

Chemistry SELECT Full Papers

Medicinal Chemistry & Drug Discovery

Expeditious Synthesis and Biological Characterization of Enantio-Enriched (-)-Nutlin-3

Anna Fantinati,[a] Sara Bianco,[a] Virginia Cristofori,[a] Alberto Cavazzini,[a] Martina Catani,[a] Vinicio Zanirato,[a] Salvatore Pacifico,[a] Erika Rimondi,[b] Daniela Milani,[b] Rebecca Voltan,[b] Paola Secchiero,[b] and Claudio Trapella*[a]

A concise and operationally simple synthesis of enantio-enriched Nutlin-3 featuring the desymmetrization of 1,2-bis(4-chlorophenyl)ethane-1,2-diamine as the key step is described. The easy-to-make *N*-((1*R*,2*R*)-2-(3-(3,5-bis(trifluoromethyl) phenyl)thioureido)cyclohexyl)-3,5-bis(trifluoromethyl)benzamide (and *N*-((1*S*,2*S*)-2-(3-(3,5-bis(trifluoromethyl)phenyl)thioureido)cyclohexyl)-3,5-bis(trifluoromethyl)benzamide)) involved as anion binding in the key desymmetrization step is the completely recoverable chiral auxiliary. An array of biological tests performed with the 84:16 (-)-Nutlin-3 scalemic mixture showed activities comparable to those of the commercial eutomer.

Introduction

In 2004, scientists from Hoffmann-La Roche discovered the first class of highly potent, specific, and orally active MDM2 inhibitors featuring a tetrasubstituted imidazoline scaffold, known as Nutlins.[1,2] Modifications and optimizations resulted in a host of derivatives, the most potent in this series being (-)-Nutlin-3 (Figure 1) which revealed a promising *in vitro* and *in vivo* antitumor activity.[3]

Both experimental and computational studies have shown that Phe^{19}, Trp^{23}, and Leu^{26} residues in p53 α-helix are the crucial residues for the interaction with the binding cleft of MDM2, while Nutlin-3 bound to MDM2 shows that both 4-chlorophenyl groups perfectly fill the Leu^{26} and Trp^{23} pockets and the isopropoxy group reaches deep into the Phe^{19} pocket.[4] Notably, Hoffmann-La Roche entered one of the member of this family into phase I clinical trials against advanced solid and soft-tissue tumors and hematological malignancies.[5,6] The intriguing overcrowded structure of nutlins stimulated intensive chemical research aimed at developing efficient and flexible synthetic strategies for their preparation.

Thus, Nutlin-3 in racemic form could be obtained following the Hoffmann-La Roche synthesis reported both in patents[7] as well as in two papers[8] in late 2012 but the obtainment of the more potent enantiomer required the need for supercritical fluid chromatography.[9]

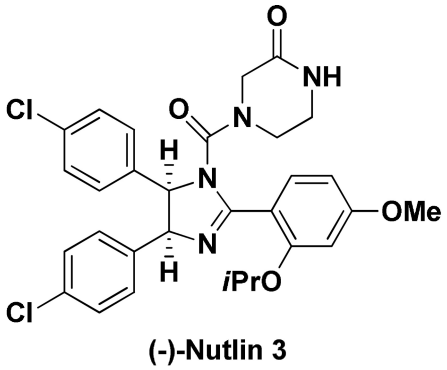

(-)-Nutlin 3

Figure 1. Structure of (-)-Nutlin-3.

A series of paper by Johnston and co-workers[10–12] described the first catalytic enantioselective synthesis of (−)-Nutlin-3 featuring a crucial carbon-carbon bond-forming addition of aryl nitromethanes to imines, producing aza-Henry adducts at noncryogenic temperature (−20 °C) in high levels of stereocontrol thanks to the identification of an electron rich chiral Bis(Amidine) catalyst (BAM) and later to the discovery of novel mono(amidine) organocatalysts (MAM). Thus, the aza-Henry adduct **3** obtained by BAM-catalyzed reaction of the *N*-Boc imine **1** and the aryl nitroalkane **2** underwent nitro group reduction with $CoCl_2$/$NaBH_4$ to produce the free amine **4**. The latter compound was first acylated with 2-isopropoxy-4-methoxybenzoic acid **5** using EDC coupling conditions, later submitted to standard TFA-promoted Boc removal. Thus, the monoamide **6**, obtained as a white solid, could be taken to (-)-Nutlin-3 by further two steps including carbamoylation

[a] Dr. A. Fantinati, Dr. S. Bianco, Dr. V. Cristofori, Prof. A. Cavazzini, Dr. M. Catani, Prof. V. Zanirato, Dr. S. Pacifico, Prof. C. Trapella
Department of Chemical and Pharmaceutical Sciences and LTTA center
University of Ferrara
Via Fossato di Mortara,17 I-44121 Ferrara, Italy
E-mail: trap@unife.it

[b] Dr. E. Rimondi, Dr. D. Milani, Dr. R. Voltan, Prof. P. Secchiero
Department of Morphology, Surgery, Experimental Medicine and LTTA center
University of Ferrara
I-44121, Ferrara, Italy

Supporting information for this article is available on the WWW under https://doi.org/10.1002/slct.201701059

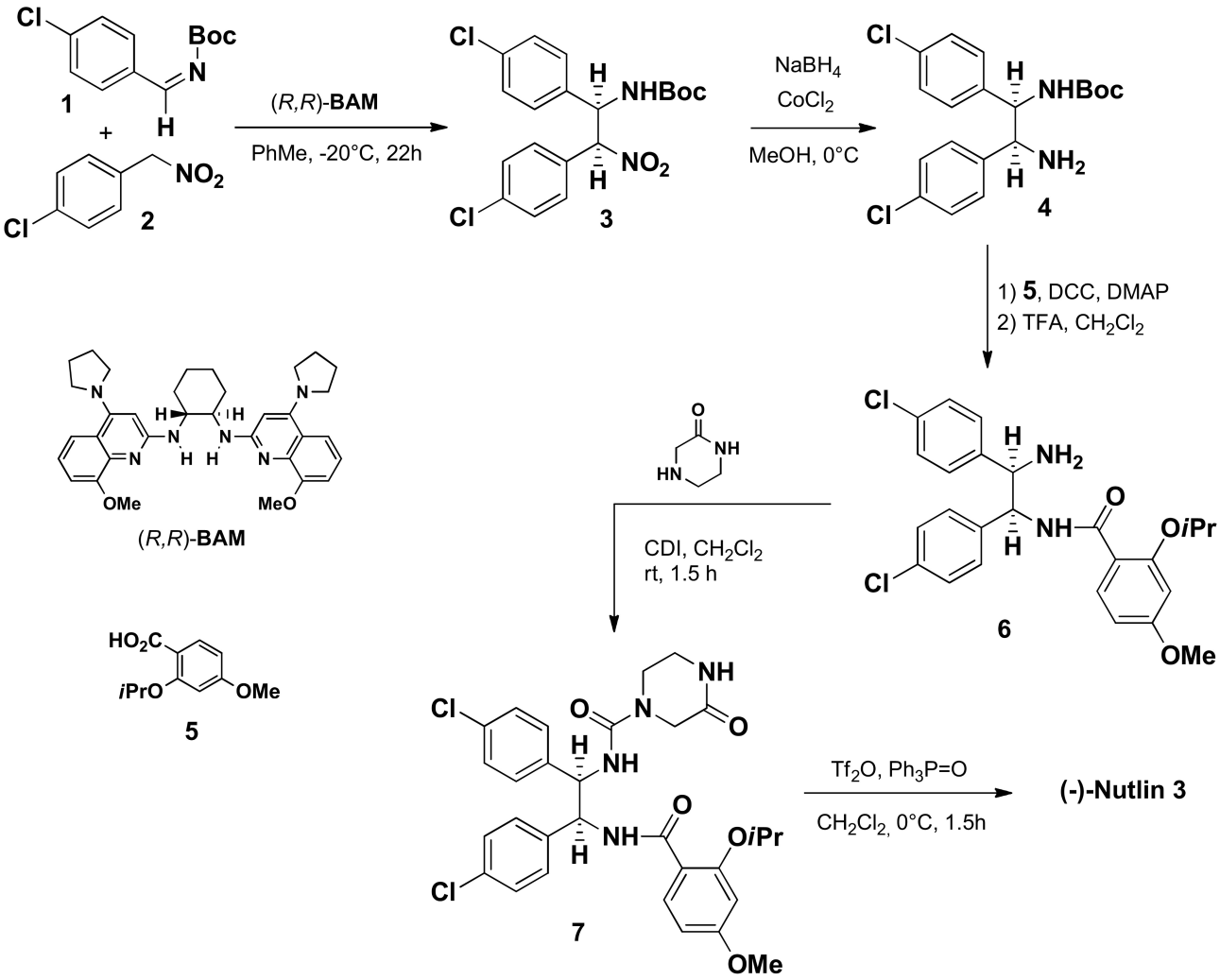

Scheme 1. Johnston and co-workers route to (-)-Nutlin 3.

reaction with 2-oxopiperazine to give **7** and final Hendrickson's dehydrative cyclization.[13] Notably, the procedure has been used to prepare 17 g of (−)-Nutlin-3 in a single batch, with column chromatography necessary after only three of the steps.[12] This very nice synthetic approach is depicted in the Scheme 1.

However, the relevant number of steps, the starting materials themselves not being easily to make compounds, our own interest in the field[14] coupled with the significant financial hurdle represented by the price of (−)-Nutlin-3 from commercial sources prompted us to examine the possibility to open a shorter synthetic route shown in Scheme 2.

Results and Discussion

We were attracted to apply the Seidel's desymmetrization approach[15] of *meso*-1,2-diaryl-1,2-diaminoethanes in the presence of benzoic anhydride, DMAP as a nucleophilic catalyst, and the thiourea-amide **9** as a benzoate-receptor co-catalyst.

The ternary organocatalyst complex resulting from the ion pairing of the achiral benzoyl pyridinium cation and the chiral thiourea-amide benzoate allowed for the preferential benzoylation of the (*S*) configured benzylamino group in a small library of *meso*-1,2-diaryl-1,2-diaminoethanes including **8**. The latter being readily available by reaction of *p*-Cl-benzaldehyde with ammonium acetate following reported directions.[16]

We were interested to apply this protocol using 2-isopropoxy-4-methoxybenzoic acid anhydride **11**, instead of benzoic anhydride, as acylating agent of the *meso*-diamine **8** thus shortening the approach to the monoamide **6** already described by Johnston and co-workers[12] avoiding the required tedious protection-deprotection steps.

To this end, the chiral hydrogen-bonding anion receptor 9 required for the selective acylation of the (*S*)-configured amino group of 8 according to Seidel's findings[17] was prepared starting from 1(*R*),2(*R*)-cyclohexanediamine while the *meso*-diamine 8 was conveniently obtained by reaction of *p*-Cl-benzaldehyde with ammonium acetate entailing on a stereospecific disrotatory ring closure.[16] The requisite anhydride 11

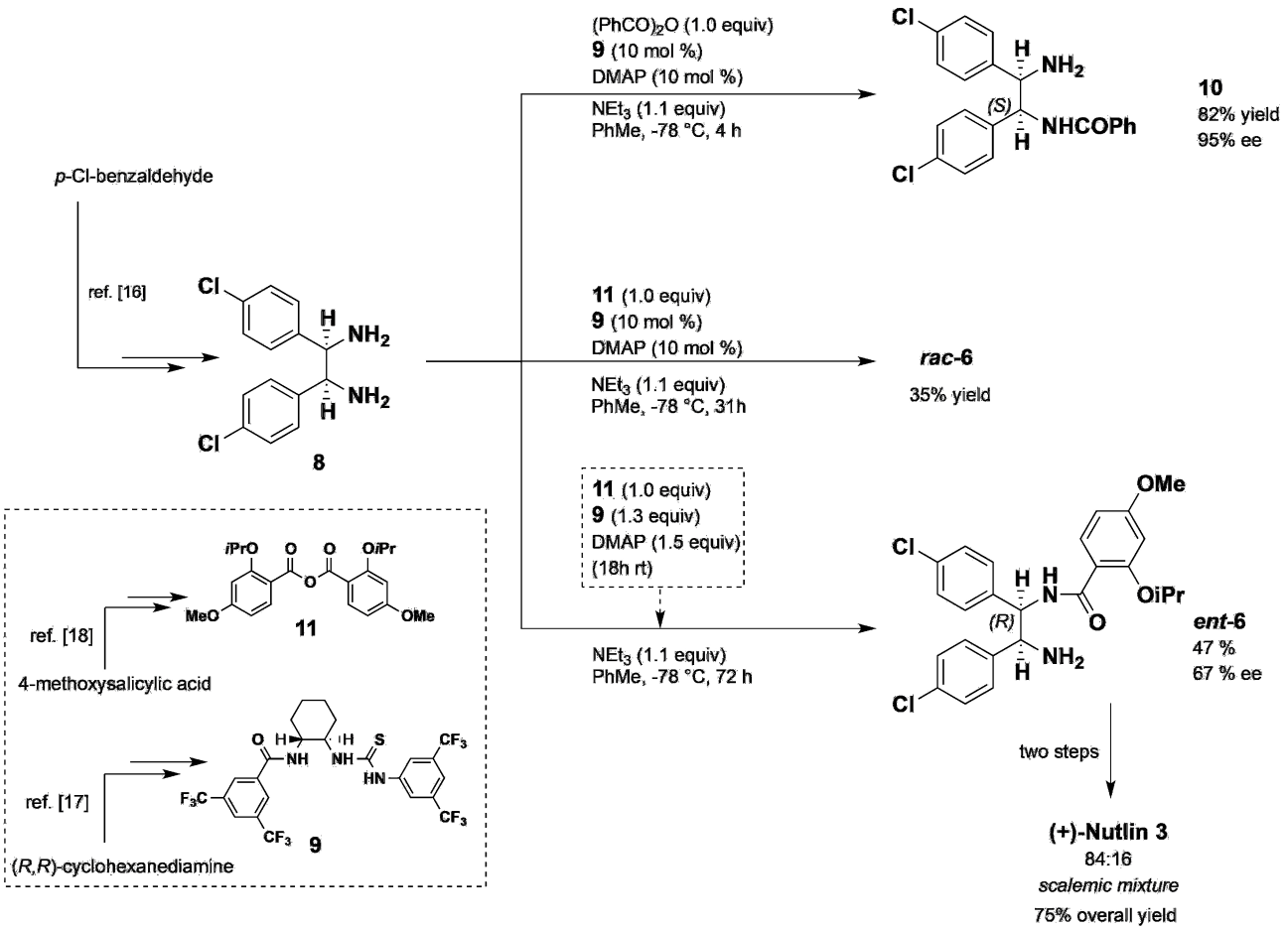

Scheme 2. Route to Enantio-Enriched (-)-Nutlin-3.

was synthesized from commercially available 4-methoxysalicylic acid through dialkylation with isopropyl bromide in the presence of potassium carbonate followed by saponification of the dialkylated compound.[18] Eventually, the free acid underwent smoothly $TsCl/K_2CO_3$-promoted intermolecular dehydration to the corresponding anhydride **11**.

Having in hands the required reagents, we accomplished the monobenzoylation of **8** following the directions established by De and Seidel. Actually, the monoamide **10** could be obtained in yield and optical purity overlapping data in the literature.[15]

Instead, and not completely unexpectedly, the related reaction with anhydride **11** gave rise to the anticipated monoamide essentially as a racemate. We presume that, due to steric reason, the assembly of the ternary organocatalyst complex is prevented thus ***rac*-6** was produced under non catalytic conditions. In fact, recent studies by Seidel and co-workers[19] on kinetic resolution of racemic benzylic amines *via* organo-catalyzed amidation showed that substituted benzoic anhydrides, without exception, provided poorer results without showing a discernible trend with regard to electronics.

Therefore, we were forced to evaluate different reaction parameters to improve the pivotal mono-amidation reaction with gradual increasing of the thiourea catalyst loading and/or reaction time (Table S1 Supporting Information). We were aware that the monoacylation of a diamine is challenging since the resulting monoamide is usually more reactive than the diamine.[20] Actually, the a posteriori stereo-defined amino amide *ent*-6 was recovered in 47% yield and 68% ee submitting a cooled (-78 °C) toluene solution of *meso*-diamine **8** for 72 h to the action of pre-formed chiral acyl-transfer reagent. The latter, was in turn prepared mixing the anhydride 11(1.0 equiv.), DMAP (1.5 equiv.), and the amide-thiourea **9** (1.3 equiv.) for 18 h at rt.

Much to our surprise, the positive optical power measured for the Nutlin-3 produced following Johnston directions[12] revealed that the undesired antipode was the predominant enantiomer in the scalemic mixture.

For reasons that are not yet clear, in our hands the desymmetrization reaction of **8** took place with reversal of the enantioselectivity as compared to the closely related Seidel's organo-catalyzed mono benzoylation.[15] We cannot exclude a different nature of the aroyl-transfer reagent involved in the acylation step in comparison to the one advanced by Seidel and co-workers. Thus, in order to produce the (-)-Nutlin-3 eutomer, we were forced to prepare ***ent*-9** starting from

1(*S*),2(*S*)-cyclohexanediamine. As expected, we were able to obtain levorotatory Nutlin-3 as 84:16 scalemic mixture. Noteworthy, the chiral auxiliary thiourea ***ent*-9** could be recovered almost-quantitatively from the reaction mixture by column chromatography.

Biological results

In order to functionally validate scalemic-Nutlin, we have performed a combination of biological assays aimed at assessing its ability to activate p53 pathway. For this purpose scalemic-Nutlin was comparatively tested on $p53^{wild-type}$ (EHEB and JVM-2) as well as on $p53^{mutated/deleted}$ (BJAB and HL-60) leukemic cell lines used as control of specificity. In parallel, cell cultures were exposed to commercial Nutlin-3 used as positive control and for comparison. As shown in Figure 2, treatment with Nutlin-3 and scalemic-Nutlin, used in the range of 1–10 μM for up to 48 hours, exhibited a comparable dose-dependent cytotoxicity resulting in a significant reduction of cell viability (Figure 2A) coupled to apoptosis induction (Figure 2B) and cell cycle arrest (Figure 2C) specifically in $p53^{wild-type}$ but not in $p53^{mutated/deleted}$ cell lines. Consistently with the observed biological effects, molecular analysis of p53 pathway by protein (Western Blot) and RNA (quantitative RT-PCR) documented accumulation of p53 and transcriptional induction of two p53 transcriptional canonical targets, involved in promoting cell cycle arrest (p21) and modulation of apoptosis (MDM2), in response to treatment with scalemic-Nutlin (Figure 2D).

Moreover, as shown in Figure 2, the effects induced by scalemic-Nutlin was equally effective as commercial Nutlin-3.

Conclusions

An expeditious synthetic approach to enantio-enriched (-)-Nutlin-3 has been developed by exploiting an unprecedented chiral thiourea-promoted enantioselective *N*-acylation of *meso*-1,2-diaryl-1,2-diaminoethane **8**. Noteworthy, the enantioselectivity we observed in the key desymmetrization step was opposite to the one found by Seidel *et al.* in their innovative related catalytic approach. Our protocol is advantageous in terms of time-saving, atom-economy and costs. The need of stoichiometric amounts of the chiral thiourea ***ent*-9** was partially compensated by its easy recover through chromatographic purification. Our biological tests clearly established that the scalemic (-)-Nutlin-3 we reached was as effective as the commercial eutomer in activating the p53 pathway.

Supporting Information Summary

The detailed experimental section, one-dimension and two-dimension NMR spectra, chiral HPLC and HRMS spectra of all products are provided in the supporting information.

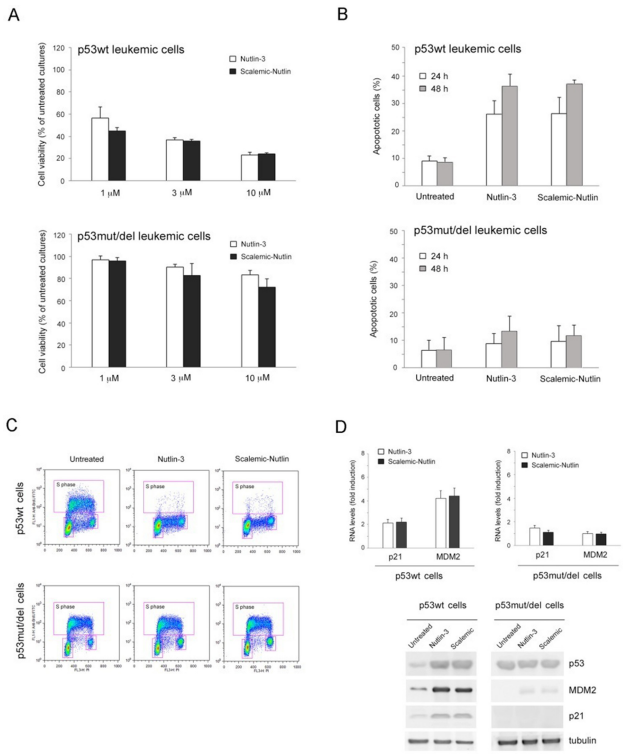

Figure 2. Effects of Nutlin-3 and scalemic-Nutlin on leukemic cell lines. $p53^{wild-type}$ as well as $p53^{mutated/deleted}$ B leukemic cell lines were exposed to Nutlin-3 or scalemic-Nutlin (range 1–10 μM) for the times indicated in each set of experiments. In A, cell viability in response to serial doses of both Nutlin-3 and scalemic-Nutlin (range 1–10 μM), was calculated at 48 hours of treatment as percentage with respect to the control vehicle cultures (set to 100%). In B, the percentage of apoptotic cells in response to Nutlin-3 or scalemic-Nutlin (each used at 10 μM) was determined by flow-cytometry after annexin-V/PI staining. In A and B, data are reported as the mean ± SD of results from four independent experiments. The asterisk indicates $p < 0.05$ with respect to the untreated cultures of each cell line. In C, cell distribution in the different phases of the cell cycle was analyzed by flow cytometry after BrdU/PI staining. Representative cell cycle profiles of cultures, either left untreated or treated with Nutlin-3 or scalemic-Nutlin, analyzed by flow cytometry are shown. For each cytofluorimetric analysis, the rectangles represent the cells in G0/G1, S, G2/M phases of the cell cycle. In D, the expression levels of p53 target genes, p21 and MDM2, were assessed by quantitative RT-PCR and results were indicated as folds of modulation with respect to the control untreated cultures set at 1. Data are reported as mean ± SD of results from independent experiments. The asterisk indicates $p < 0.05$ with respect to untreated cultures. At the bottom, representative Western Blot results documenting modulation of MDM2, p53 and p21 proteins by Nutlin-3 or scalemic-Nutlin are show.

Acknowledgements

This study was supported by grants from MIUR-FIRB (grant RBFR109SBM_001 to C.T.). The authors are grateful to Prof. G.P. Pollini for the helpful discussion and Dr. A. Casolari and Dr. E Marzola for NMR and Mass spectra analysis.

Conflict of Interest

The authors declare no conflict of interest.

Keywords: Anticancer agents · *Meso*-diamine desymmetrization · (-)-Nutlin-3 · p53/MDM2 · Thiourea catalyst

[1] L. T. Vassilev, B. T. Vu, B. Graves, D. Carvajal, F. Podlaski, Z. Filipovic, N. Kong, U. Kammlott, C. Lukacs, C. Klein, N. Fotouhi, E. A. Liu, *Science* **2004**, *303*, 844–848.
[2] K. Hoe, C. Verna, P. Lane, *Nat. Rev. Drug. Discovery* **2014**, *13*, 217–236.
[3] L. J. Valente, B. J. Aubrey, M. J. Herold, G. L. Kelly, L. Happo, C. L. Scott, A. Newbold, R. W. Johnstone, D. C. S. Huang, L. T. Vassilev, A. Strasser *Cell Reports* **2016**, *14*, 1858–1866.
[4] P. Kussie, S. Gorina, V. Marechal, B. Elenbaas, J, Moreu, N. Lev Pavletich, *Science* **1996**, *274*, 948–953.
[5] B. Vu, P. Wovokulich, G. Pizzolato, A. Lovey, Q. Ding, J. Liu, C. Zhao, K. Glenn, Y. Wen, C. Tovar, K. Packman, L. Vassilev, B. Graves, *ACS Med. Chem. Lett.* **2013**, *4*, 466–469.
[6] For recent reviews, see: a) N. Estrada-Ortiz, C. G. Neochoritis, A. Dömling, *ChemMedChem* **2016**, *11*, 757–772; b) A. Lemos, M. Leão, J. Soares, A. Palmeira, M. Pinto, L. Saraiva, M. E. Sousa, *Med Res Rev.* **2016**, *36*, 789–844.
[7] a) N. Kong, E. A. Liu, B. T. Vu, (F. Hoffmann-La Roche AG). Cis-Imidazolines as MDM2 Inhibitors. Int. PCT Pub. No. WO/2003/ 051360, **2003**; b) D. J. Bartkovitz, J. Cai, X.-J. Chu, H. Li, A. J. Lovey, B. T. Vu, C. Zhao, (F. Hoffmann-La Roche AG). Chiral Cis-Imidazolines. Int. PCT Pub. WO/2009/ 047161, **2009**.
[8] a) L. Shu, P. Wang, W. Liu, C. Gu, *Org. Process Res. Dev.* **2012**, *16*, 1866–1869; b) L. Shu, C. Gu, Y. Dong, R. Brinkman, *Org. Process Res. Dev.* **2012**, *16*, 1940–1946.
[9] Z. Wang, M. Jonca, T. Lambros, S. Ferguson, R. Goodnow, *J. Pharm. Biomed. Anal.* **2007**, *45*, 720–729.
[10] T. A. Davis, J. N. Johnston, *Chem. Sci.* **2011**, *2*, 1076–1079.
[11] T. A. Davis, A. E. Vilgelm, A. Richmond, J. N. Johnston, *J. Org. Chem.* **2013**, *78*, 10605 – 10616.
[12] B. A. Vara, A. Mayasundari, J. C. Tellis, M. W. Danneman, V. Arredondo, T. A. Davis, J. Min, K. Finch, R. K. Guy, J. N. Jonhston, *J. Org. Chem.* **2014**, *79*, 6913–6938.
[13] J. B. Hendrickson, M. S. Hussoin, *J. Org. Chem.* **1989**, *54*, 1144.
[14] P. Secchiero, R. Bosco, C. Celeghini, G. Zauli, *Curr Pharm Des.* **2011**, *17*(6), 569–577.
[15] a) C. K. De, D. Seidel . *J. Am. Chem. Soc.* **2011**, *133*, 14538–14541; b) C. Min, N. Mittal, C. K. De, D. Seidel, *Chem. Commun.* **2012**, *48*, 10853–10855.
[16] M. V. Proskurnina, N. A. Lozinskaya, S. E. Tkachenko, N. S. Zefirov, *Russ. J. Org. Chem.* **2002**, *38*, 1149–1153.
[17] E. G. Klauber, C. K. De, T. K. Shah, D. Seidel, *J. Am. Chem. Soc.* **2010**, *132*, 13624–13626.
[18] T. Hattori, Y. Shimazumi, H. Goto, O. Yamabe, N. Morohashi, W. Kawai, S. Miyano, *J. Org. Chem.* **2003**, *68*, 2099–2108.
[19] N. Mittal, K. M. Lippert, C. K. De, E. G. Klauber, T. J. Emge, P. R. Schreiner, D. Seidel, *J. Am. Chem. Soc.* **2015**, *137*, 5748 – 5758.
[20] J. A. Bender, N. A. Meanwell, T. Wang, *Tetrahedron* **2002**, *58*, 3111–3128.

Submitted: May 16, 2017
Revised: September 6, 2017
Accepted: September 6, 2017

SCIENTIFIC REPORTS

OPEN

A diastereoselective synthesis of Cebranopadol, a novel analgesic showing NOP/mu mixed agonism

Received: 7 December 2016
Accepted: 12 April 2017
Published online: 25 May 2017

Anna Fantinati[1], Sara Bianco[1], Remo Guerrini[1], Severo Salvadori[1], Salvatore Pacifico[1], Maria Camilla Cerlesi[2], Girolamo Calo[2] & Claudio Trapella[1]

A diastereoselective synthesis of the title compound as a single *E* diastereomer has been efficiently accomplished by assembling the featured pyrano-indole scaffold of the spiro[cyclohexane-dihydropyrano[3,4-b]-indole]-amine framework through an oxa-Pictet-Spengler reaction, promoted by a cheap and green Zeolite catalyst. Basic pharmacological experiments demonstrate that Cebranopadol acts as a mixed nociception/orphanin FQ (NOP) and mu (MOP) opioid receptor agonist useful for treatment of chronic pain.

Nociceptin/orphanin FQ (N/OFQ), the endogenous agonist of the N/OFQ peptide receptor (NOP) regulates various biological functions[1] including pain transmission[2]. Grünenthal researchers have recently reported the results of structure activity studies[3,4] that led to the identification of Cebranopadol (trans-6′-fluoro-4′-9′-dihydro-N,N-dimethyl-4-phenyl-spiro[ciclohexane-1,1′(3′H)-pyrano[3,4-b]indol]-4-amine) as a potent NOP and mu receptor (MOP) agonist (Fig. 1).

This compound binds with high affinity to the NOP and the MOP receptors and behaves as full agonist. Rodent studies demonstrated that Cebranopadol elicits potent and efficacious antinociceptive action in several models of nociceptive and neuropathic pain. Importantly, compared to morphine, Cebranopadol displayed a favorable side effect profile and reduced tolerance liability[5]. Cebranopadol is under clinical development and several clinical trials are assessing its analgesic therapeutic potential in different pain conditions[6].

Results and Discussion

Grünenthal researchers synthetized Cebranopadol as retrosynthetically depicted in Fig. 2 based on a oxa-PictetSpengler reaction between the fluoro-silyl-indole **6**, in turn prepared by Larock indole synthesis[7] of the commercially available 2-iodo-4-fluoroaniline **8** and 1-silyl-1-butynol **9**, and the aminoketone **7** bearing the structurally important 4-N,Ndimethylamino-4-phenyl-cyclohexane head by a two step approach involving a Strecker synthesis[8] of monoketal protected 1,4-cyclohexanedione **1** by treatment with $HNMe_2$. HCl/KCN (67–99%) and a Bruylants reaction[9] of the resulting aminonitrile with PhMgCl in THF at 0 °C to room temperature (low overall yield). It deals with a classical approach that at the end of the synthesis requires a diastereomer separation by HPLC.

Our interest in this area led us to be contemporaneously involved in the synthesis of Cebranopadol with two important guidelines in our project developed along the same pathway: a) avoid the use of highly toxic potassium cyanide; b) identifying suitable experimental conditions to make the oxa-PictetSpengler reaction diastereoselective. (Fig. 3).

The approach proposed a start from the cheap and commercially available ketone **1** that undergoes a Grignard reaction with phenyl magnesium bromide in THF for 12 h yielding the corresponding alcohol **3** at 70% yield. A nucleophilic substitution of the tertiary and benzylic alcohol using the classical sodium azide/TFA in chloroform approach failed. Different methods have been tried to overcome the very low yield (5%) because of the competitive elimination reaction to an alkene. In our hands the best way to obtain the azide **5** was the reaction with trimethylsilylazide catalysed by indium tribromide[10] that allowed us to obtain compound **5** in a clean and fast step with good yield (50%). Lithium aluminium hydride reduction to the primary amine **10** followed by reductive amination with formaldehyde allowed us to obtain the tertiary amine **4** in good overall yield. Deprotection of

[1]Department of Chemical and Pharmaceutical Sciences and LTTA, University of Ferrara, 44121, Ferrara, Italy. [2]Department of Medical Sciences, Section of Pharmacology and National Institute of Neuroscience, University of Ferrara, 44121, Ferrara, Italy. Correspondence and requests for materials should be addressed to C.T. (email: trap@unife.it)

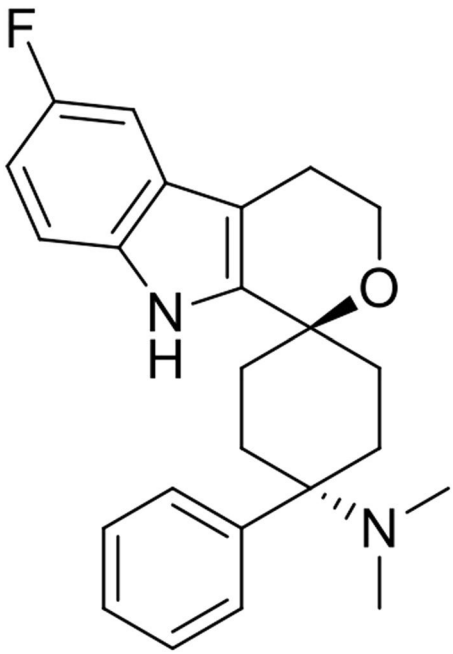

Figure 1. Cebranopadol.

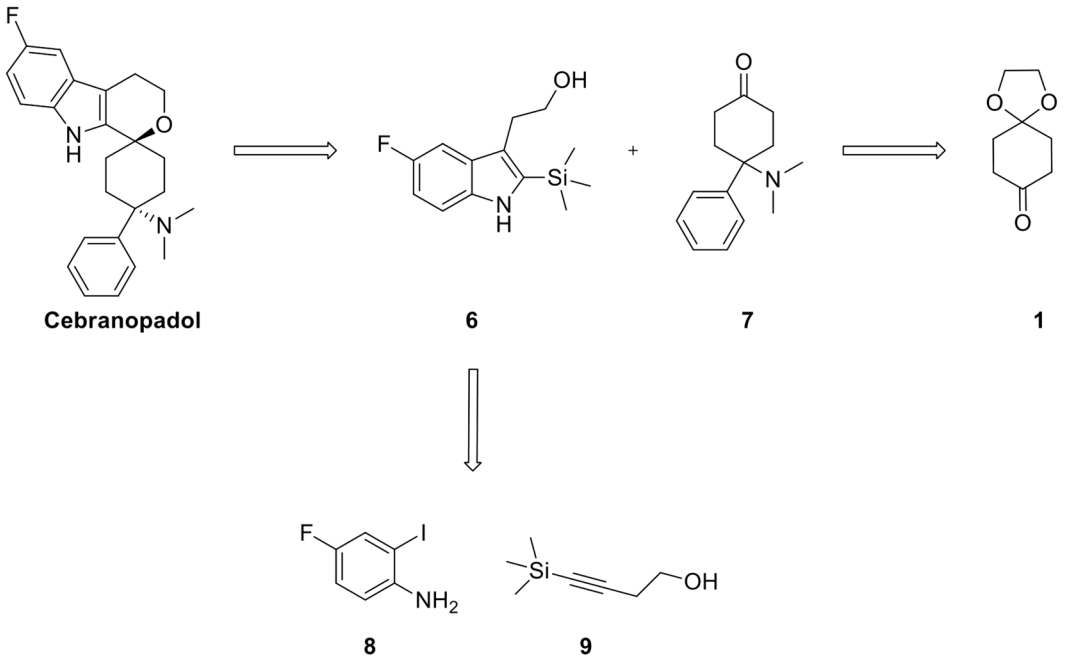

Figure 2. Retrosynthesis of Cebranopadol.

the ketone using hydrochloric acid in acetone produced the intermediate **7** (Fig. 4). The stage was set for the crucial oxa-Pictet-Spengler reaction which has been performed in different conditions such as bismuth triflate[11,12], hydrochloric acid, Zeolite beta-25 and 4 Å molecular sieves giving rise to a mixture of diastereomers in low yield. The cyclization reaction has been tried also using a TMSOTf at room temperature producing Cebranopadol in 90% yield but lacking stereoselectivity[4].

Much to our delight, the last synthetic steps involving an oxaPictet-Spengler reaction to install the dihydropyrano[3,4-b]indole moiety have been performed in a diastereoselective manner using an unusual and green Zeolite catalyst[11] and catalytic *p*-toluenesulphonic acid in refluxing toluene that allowed us to obtain the E diastereomer exclusively as depicted in Fig. 5.

The setting up of an oxa-Pictet-Spengler reaction, allowed us to also obtain different pyrano indole scaffolds starting from commercially and non commercially available ketones. ROESY NMR experiments (see Supporting

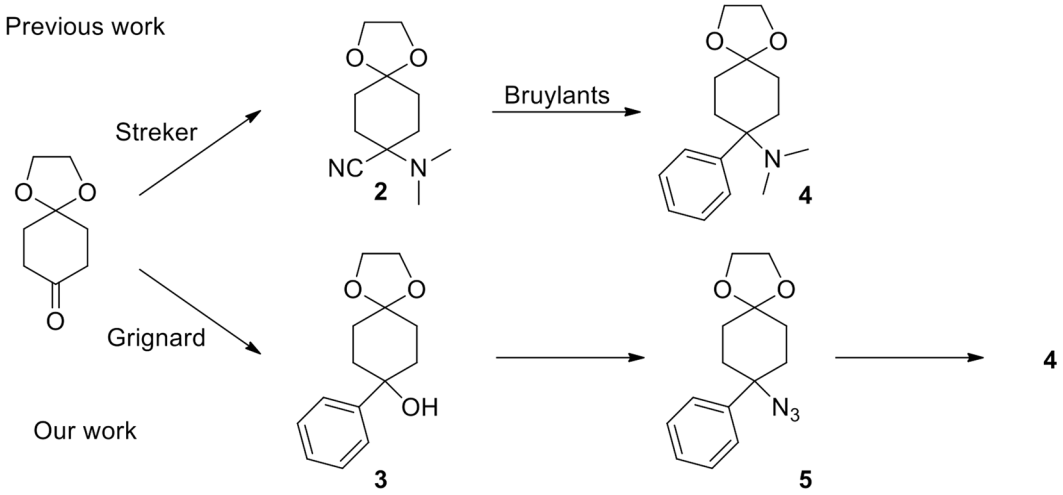

Figure 3. Different approaches to the synthesis of Cebranopadol.

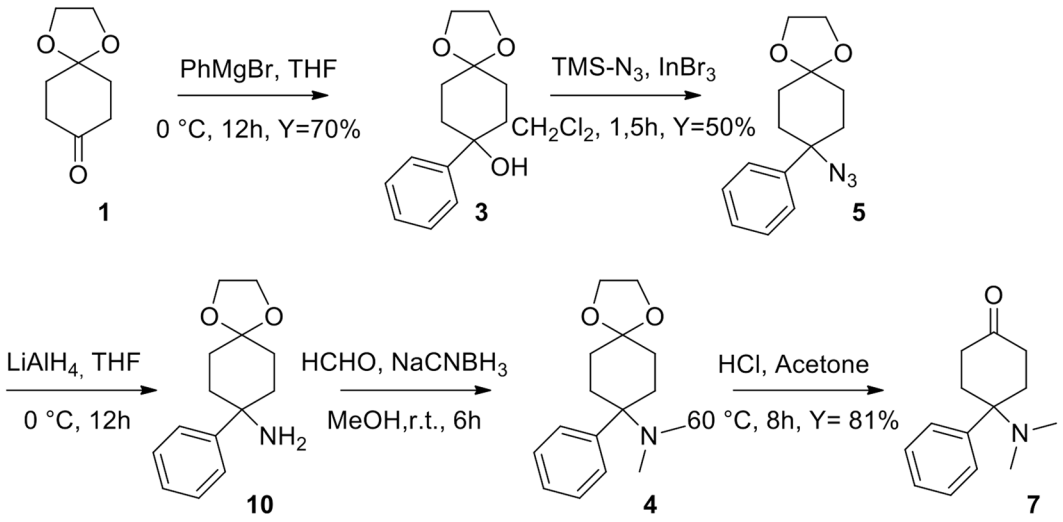

Figure 4. Synthesis of intermediate 7.

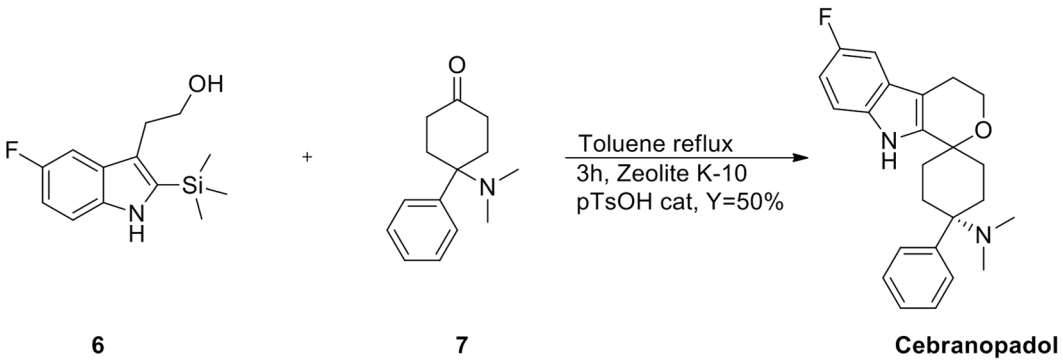

Figure 5. Unusual diastereoselective oxa-Pictet-Spengler reaction.

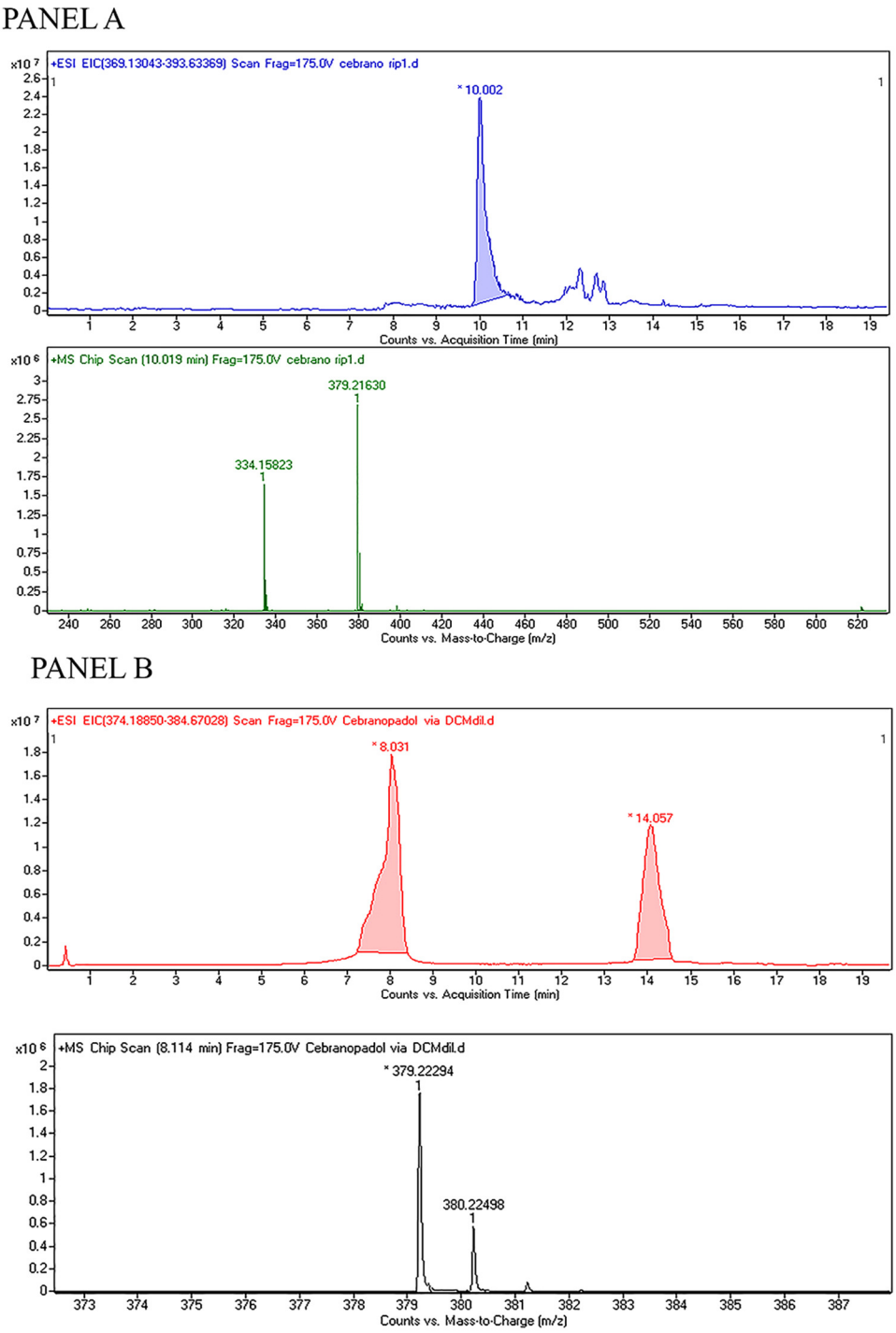

Figure 6. The HR-LC-MS spectra of Cebranopadol.

Information page S20)of the final compound confirms that the zeolite K-10 catalyst produced a single E diastereomer during the oxa-Pictet-Spengler reaction. On the contrary, the trimethylsilyl triflate approach allowed us to obtain a mixture of E and Z diastereomer with a good overall yield but without regioselectivity. The zeolite catalyst is easily recovered and its catalytic properties did not change up to 5 times reusing-cycle.

HR-LC-MS spectra of Cebranopadol obtained using Zeolite catalyst (panel A) and TMSOTf (panel B) are depicted in Fig. 6.

The basic pharmacological profile of Cebranopadol has been investigated by measuring calcium mobilization in cells coexpressing NOP or classical opioid receptors and chimeric G proteins as described in detail in Camarda *et al.*[13,14].

The results of these experiments, summarized in Table 1, indicated that Cebranopadol behaved as full agonist showing very similar potency at NOP and MOP receptors. Cebranopadol was also able to activate kappa (KOP)

	NOP		MOP		KOP		DOP	
	pEC_{50}	α	pEC_{50}	α	pEC_{50}	α	pEC_{50}	α
N/OFQ	9.59	1.00	inactive		inactive		inactive	
Fentanyl	inactive		8.13	1.00	inactive		inactive	
Dyn A	inactive		6.67	0.82	8.54	1.00	7.73	0.99
DPDPE	inactive		inactive		inactive		8.15	1.00
Cebra	7.28	0.89	7.20	0.99	5.98	0.55	6.31	0.81

Table 1. Pharmacological profile of Cebranopadol (Cebra) in cells coexpressing human recombinant NOP or classical opioid receptors and chimeric G protein.

and delta (DOP) opioid receptors but with lower potency and, in the case of the KOP receptor, lower efficacy. These findings are in line with those reported by Grünenthal researchers in receptor binding and stimulated [^{35}S] GTPgS binding experiments[5].

Conclusions

In conclusion, we have developed a robust and easy method for the synthesis of Cebranopadol (in 15% overall yield) as a single E diastereomer using a green Zeolite catalyst in the key oxaPictet-Spengler reaction. The azide approach will allow us to easily insert different substituents onto the basic amine to better understand the crucial role of tertiary amines in the interaction with Asp^{130} and Asp^{147} of the NOP and MOP receptor binding pockets. Basic pharmacological experiments demonstrate that Cebranopadol acts as a mixed NOP/MOP agonist.

Methods

Chemical Materials and Methods. All NMR spectra were analysed using Mestre Nova 6.0.2 software and FID data are available on request. Analytical thin layer chromatography (TLC) was performed on silica gel Macherey-Nagel poligram SIL/UV 254 of 0.25 mm, visualization was achieved using UV light (254) and Potassium Permanganate ($KMnO_4$) 2% in water. Flash column chromatography was undertaken using Isolera one (Biotage Sweden). Products were dried using sodium sulfate anhydrous Carlo Erba. Proton nuclear magnetic resonance (^{1}H NMR) and carbon nuclear magnetic resonance (^{13}C NMR) were recorded using VARIAN 400 MHz. All spectra were recorded using $CDCl_3$ as a solvent otherwise the solvent was specified. Chemical shifts (δ) were quoted in ppm relative to residual solvent and coupling constants (J) were quoted in Hertz (Hz). Multiplicity was reported with the following abbreviations: s = singlet; d = doublet; t = triplet; q = quartet; m = multiplet; dd = doublet of doublet; dt = doublet of triplet, dq = doublet of quartet; Infrared (IR) spectra were recorded on a Perkin-Elmer FT-IR Spectrum 100 using zirconium-selenium diamond as a cell. Melting points were recorded using a Buchi-Tottoli and were reported uncorrected. Molecular weights were measured with a mass spectrometer electrospray ESI MICROMASS ZMD 2000 and high resolution spectra with an Agilent ESI-Q-TOF LC/MS 6520 System. Solvents and chemicals used for TLC, chromatographic purification, crystallization and reactions were reported with the following abbreviations: Et_2O for diethyl ether, THF for tetrahydrofuran, AcOEt for ethyl acetate, DCM for methylene chloride, $LiAlH_4$ for lithium aluminium hydride.

Synthesis of 8-phenyl-1,4-dioxaspiro[4.5]decan-8-ol (3). In a two neck round bottom flask, under an argon atmosphere, 1,4-cyclohexanedione monoethylene acetale (**1**) (1.5 g, 9.6 mmol) was dissolved in THF (50 mL). At 0 °C, phenyl magnesium bromide (20 ml, 19.22 mmol) was added and the reaction was stirred overnight at room temperature. The reaction mixture was checked by TLC (AcOEt/Petroleum ether 1:6), quenched with NH_4Cl saturated solution and washed with AcOEt. The organic layers were dried with Na_2SO_4, filtered and the solvent was removed under vacuum. The crude product was purified by flash chromatography (AcOEt/ Petroleum ether 1:1) with an yield of 70% to give the title compound (**3**) as a white solid. MS (ESI): $[M\text{-}OH]^+$. = 217.27, m. p.: 98–100 °C

^{1}H-NMR (400 MHz, Chloroform-d), δ: 7.58–7.46 (m, 1 H, Ar), 7.41–7.31 (m, 2 H, Ar), 7.30–7.22 (m, 2 H, Ar), 4.03–3.91 (m, 4 H, O-CH_2-CH_2-O-), 2.24–2.05 (m, 4 H, CH_2 cyclohexane), 1.86–1.77 (m, 2 H CH_2 cyclohexane), 1.74–1.64 (m, 3 H CH_2 cyclohexane and -OH). ^{13}C-NMR (100 MHz, Chloroform-d), δ: 148.59 (Cq-Ar), 128.74, 128.42, 127.06, 124.64, (CH-Ar), 108,55 (-O-Cq-O), 72.57 (Ar-Cq-OH), 64.49 (-O-CH_2-CH_2-O), 64.38 (-O-CH_2-CH_2-O), 36.73 (CH_2 cyclohexane), 30.89 (CH_2 cyclohexane).

Synthesis of 8-azido-8-phenyl-1,4-dioxaspiro[4.5]decane (5). In a round bottom flask, compound (**3**) (1 g, 4.27 mmol) was disolved in DCM (30 mL) and then trimehylsilyl azide (1.13 ml, 6.41 mmol) and indium tribromide (151.38 mg, 0.427 mmol) were added. The reaction mixture was stirred for 1 hour and then worked up with $NaHCO_3$ until basic in pH. The reaction mixture was extracted twice with 30 mL of DCM each time, the organic layers were dried, filtered and concentrated. The crude product was purified by flash chromatography on silica gel in AcOEt/petroleum ether 1:3 to give the title compound (**5**) with a yield of 50% as a pale yellow oil. MS (ESI): $[M\text{-}N_3]^+$ = 217.25; 1H-NMR (400 MHz, Chloroform-d), δ: 7.57–7.11 (m, 5 H, Ar), 4.02–3.93 (m, 4 H, O-CH_2-CH_2-O), 2.28–1.82 (m, 6 H, CH_2 cyclohexane), 1.88–1.49 (m, 2 H, CH_2 cyclohexane). ^{13}C-NMR (100 MHz, Chloroform-d), δ: 143.36 (Cq-Ar), 128.81, 128.81, 127.63, 125.54 (CH-Ar), 107.89 (-O-Cq-O-), 65.90 (Cq-N_3), 64.59 (-O-CH_2-CH_2-O), 64.41 (-O-CH_2-CH_2-O), 33.74 (CH_2 cyclohexane), 31.19 (CH_2 cyclohexane).

Synthesis of 8-phenyl-1,4-dioxaspiro[4.5]decan-8-amine (10). To a solution of $LiAlH_4$ (437 mg, 11.53 mmol) in 15 mL of THF, was added the azide (**5**) (1 g, 3.83 mmol) disolved in the same solvent at 0 °C. The

reaction mixture was stirred overnight and was monitored by ESI-mass and TLC (AcOEt/Petroleum ether 1:3), worked up with NaOH 5%(10 mL) and filtered over celite pad in Et_2O. The solvent was removed under vacuum to give the compound (**10**) in quantitative yield pure enough to be used without purification in the next step. MS (ESI): $[M+H]^+ = 234.36$, $[M\text{-}NH_2]^+. = 217.39$.

Synthesis of N,N-dimethyl-8-phenyl-1,4-dioxaspiro[4.5]decan-8-amine (4). To a solution of compound (**10**) (1 g, 3.71 mmol) in 50 mL of MeOH, formaldehyde (1.04 ml, 37.17 mmol), sodium triacetoxyborohydride (1.57 g, 7.43 mmol) and a catalytic amount of AcOH were added at room temperature. The reaction mixture was stirred overnight at room temperature until the formation of the title compound. The solvent was concentrated to dryness, diluted in AcOEt and the organic layers were washed with NaOH 5% solution (2×20 mL) in order to obtain the tertiary amine (**4**) as a colourless sticky solid with a quantitative yield. The tertiary amine was purified by flash chromatography (eluent AcOEt/EtPt 3:1). MS (ESI): $[M+H]^+ = 262.35$; HRMS (ESI): $[M+H]^+$ Calc. = 262.180155; $[M+H]^+$ Found = 262.18122. ^{1}H NMR (400 MHz, Chloroform-d), δ: 7.34 (m, 5 H, Ar), 3.95 (ddd, 2 H, J = 6.1, 5.6, 1.4, -O-CH_2-CH_2-O), 3.89 (m, 2 H, -O-CH_2-CH_2-O), 2.31 (m, 2 H, CH_2 Cyclohexyl), 2.16 (m, 2 H, CH_2 Cyclohexyl), 2.09 (s, 6 H, $N(CH_3)_2$), 1.80 (m, 2 H, CH_2 Cyclohexyl), 1.49, (ddd, 2 H, J = 13.9, 10.9, 3.7, CH_2 Cyclohexyl). ^{13}C-NMR (100 MHz, Chloroform-d), δ:128.30, 128.00, 127.88, 127.63, 125.33 (C-Ar), 108.75 (O-Cq-O) 64.62 (O-CH_2-CH_2-O), 64.38 (O-CH_2-CH_2-O), 48.82 (Cq-$N(CH_3)_2$), 38.44 ($N(CH_3)_2$), 31.37 (CH_2 Cyclohexyl), 30.38 (CH_2 Cyclohexyl).

Synthesis of 4-(dimethylamino)-4-phenylcyclohexan-1-one (7). To a stirred solution of tertiary amine (**4**) (1 g, 3.81 mmol) in 70 mL of acetone, hydrochloric acid 10% was added to achieve an acid pH, the reaction mixture was stirred overnight at 65 °C. The reaction mixture was monitored by ESI-mass spectrometry (peak 218) and TLC (AcOEt/Petroleum ether /NH3 3:1: 0.3). The solvent was removed under vacuum and the residue diluted in 50 mL of AcOEt. The organic layers were washed with NaOH 10% (2×20 mL), dried, filtered and concentrated to give a crude product purified by flash chromatography on silica gel using as solvents AcOEt/Petroleum ether/NH3 3:1:0.3 to give the title compound (**7**) as a white solid with a yield of 81%. HRMS (ESI): $[M+H]^+$ Calc. = 218.153941; $[M+H]^+$ Found = 218.15313. ^{1}H NMR (400 MHz, Chloroform-d), δ: 7.43 (m, 5 H, CH-Ar), 2.65–2.57 (m, 4 H, CH_2 Cyclohexyl), 2.37–2.24 (m, 4 H, CH_2 Cyclohexyl), 2.19 (s, 6 H, $N(CH_3)_2$). ^{13}C NMR (100 MHz, Chloroform-d), δ: 210.92 (C=O), 128.40, 127.74, 127.57, 125.33 (C-Ar), 62.92 (Cq-$N(CH_3)_2$), 38.43 ($N(CH_3)_2$), 37.34 (CH_2 Cyclohexyl), 32.54 (CH_2 Cyclohexyl).

Synthesis of 2-(5-fluoro-2-(trimethylsilyl)-1H-indol-3-yl)ethan-1-ol (6). In a two neck round bottom flask, under an argon atmosphere, the 4-fluoro-2-iodoaniline (**8**) (2 g, 8.43 mmol) was disolved in 15 mL of DMF. 4-(trimethylsilyl)but-3-yn-1-ol (**9**) (1.55 ml, 9.27 mmol), potassium carbonate (1.165 g, 8.43 mmol), lithium chloride (357 mg, 8.43 mmol), triphenylphosphine (144 mg, 0.42 mmol), palladium acetate (94 mg, 0.42 mmol) were added and the reaction was stirred overnight under reflux. The reaction was monitored by TLC (AcOEt/Petroleum ether 1:4) and the solvent was removed under vacuum. The residue was dissolved in 30 mL of AcOEt and washed twice with brine (10 mL each), the organic layers were dried, filtered and concentrated in vacuo. The crude product was purified by flash chromatography with AcOEt/Petroleum ether 1:4 with a yield of 40% to give the title compound (**6**) as a yellow liquid. MS (ESI): $[M+H]^+ = 252.22$; ^{1}H-NMR (400 MHz, Chloroform-d), δ: 8.21–8.14 (bs, 1 H, NH), 7.28–7.22 (m, 1 H, CH-Ar), 7.09–7.05 (m, 1 H, CH-Ar), 6.99–6.91 (m, 1 H, CH-Ar), 3.92–3.84 (m, 2 H, Indol-CH_2-CH_2-OH), 2.98 (m, 2 H, Indol-CH_2-CH_2-OH), 0.12 (s, 9 H, Si-$C(CH_3)_3$). ^{13}C-NMR (100 MHz, Chloroform-d), δ: 158.88, 156.55, 132.92, 128.04, 124.36, 113.42, 111.94, 111.75, 103.97, 63.16, 28.86, 2.06, 0.38.

Synthesis of (1 s,4 s)-6′-fluoro-N,N-dimethyl-4-phenyl-4′,9′-dihydro-3′H-spiro[cyclohexane-1,1′-pyrano[3,4-b]indol]-4-amine. (Cebranopadol). *Method A.* The ketone (**7**) (125 mg, 0.66 mmol), was solved in 15 mL of toluene with a catalytic amount of p-toluensulfonic acid; to the solution were added compound (**6**) (149 mg, 0.6 mmol)) and Zeolite K-10 (300 mg). The solution was heated under reflux with a Dean-Stark apparatus for 4 hours. The solvent was removed under vacuum and NaOH 2 N (20 mL) was added to the reaction mixture. The residue was filtered over a celite pad and disolved in AcOEt (20 mL). The organic layers were dried, filtered and concentrated to give a crude product that was purified by flash chromatography (AcOEt/Petroleum ether 2:1) with a yield of 50% as a yellow solid that crystallized in MeOH.

Method B. In a two neck round bottom flask, under an argon atmosphere, compound (**6**) (84 mg, 0.336 mmol) was disolved in DCM (10 mL). Compound (**7**) (61 mg, 0.28 mmol), and trimethylsyliltriflate (65 mL, 0.28 mmol) were added whilst stirring at minus 78 °C for 20 hours. The reaction mixture was treated with NaOH 1 N whilst stirring for 30 minutes and was then washed with water (2 X 20 mL). The organic layers were dried, filtered and concentrated under vacuum to obtain a yellow solid that was crystallized in methanol to yield Cebranopadol as a diastereomeric mixture with 90% yield. MS (ESI): $[M+H]^+ = 379.21$; HRMS (ESI): $[M+H]^+$ Calc. = 379.218018; $[M+H]^+$ Found = 379.21809. $[M\text{-}N(CH_3)_2]^+. = 334.16032$; m.p. = 220 °C with decomposition. ^{1}H-NMR (400 MHz, Chloroform-d),δ: 8.54 (s, 1 H, NH), 7.37 (m, 5 H, CH-Ar), 7.28 (m, 1 H, CH15), 7.13 (dd, J = 9.6, 2.5 Hz, 1 H, CH18), 6.89 (ddd, J = 9.4, 8.8, 2.5 Hz, 1 H, CH16), 3.96 (t, J = 5.4 Hz, 2 H, -CH_2 10), 2.75 (t, J = 5.4 Hz, 2 H, -CH_2 9), 2.53 (d, J = 13.7 Hz, 2 H, CH_2, C6e, C4e), 2.21 (d, J = 12.8 Hz, 2 H, CH_2, C1a, C3a), 2.10 (s, 6 H, $N(CH_3)_2$), 2.07 (m, 2 H, -CH_2, CH4a, CH6a), 1.93 (m, 2 H, -CH_2, CH1e, CH3e). 13C-NMR(100 MHz, Chloroform-d), δ: 159.09 (C-17-Ar), 156.76 (Cq-13), 141.34 (Cq-N-7), 139.06 (Cq, 21), 132.24 (Cq-N-13), 127.57, 127.05, 126.82 (CH-Ar), 125.57 (Cq-indol, 14), 111,57 (CH, 15), 109.74 (CH, 16), 107.31 (Cq, 8), 103.44 (CH, 18), 72.20 (Cq Spiro, 2), 59.81 (CH_2, 10), 58.79 (Cq, 5), 38.34 (N-CH_3, 22, 23), 30.93 (CH_2, 1, 3), 28.35 (CH_2, 4,6), 22.67 (-CH_2, 9). ^{19}F-NMR: δ: -125.60.

References

1. Lambert, D. G. The nociception/orphanin FQ receptor: a target with broad therapeutic potential. *Nat. Rev. Drug Discov.* **7**, 694–710, doi:10.1038/nrd2572 (2008).
2. Schroder, W., Lambert, D. G., Ko, M. C. & Koch, T. Functional plasticity of the N/OFQ-NOP receptor system determines analgesic properties of NOP receptor agonists. *Br. J. Pharmacol.* **171**, 3777–3800, doi:10.1111/bph.2014.171.issue-16 (2014).
3. Schunk, S. *et al*. Discovery of Spiro[cyclohexane-Dihydropyrano [3,4- B]indole]-Amines as Potent NOP and Opioid Receptor Agonists. *ACS Med. Chem. Lett.* **5**, 851–856, doi:10.1021/ml500116x (2014).
4. Schunk, S. *et al*. Discovery of a Potent Analgesic NOP and Opioid Receptor Agonist: Cebranopadol. *ACS Med. Chem. Lett.* **5**, 857–862, doi:10.1021/ml500117c (2014).
5. Linz, K. *et al*. Cebranopadol: A Novel Potent Analgesic Nociceptin/Orphanin FQ Peptide and Opioid Receptor Agonist. *J. Pharmacol. Exp. Ther.* **349**, 535–548, doi:10.1124/jpet.114.213694 (2014).
6. Lambert, D. G., Bird, M. F. & Rowbotham, D. J. Cebranopadol: a first in-class example of a nociceptin/orphanin FQ receptor and opioid receptor agonist. *Br. J. Anaesth.* **114**, 364–366, doi:10.1093/bja/aeu332 (2015).
7. Larock, R. C. & Yum, E. K. Synthesis of indoles via palladium-catalyzed heteroannulation of internal alkynes. *JACS* **113**, 6689–6690, doi:10.1021/ja00017a059 (1991).
8. Dyker, G. Amino Acid Derivatives by Multicomponent Reactions. *Angew. Chem. Int. Ed. Engl.* **36**, 1700–1702, doi:10.1002/(ISSN)1521-3773 (1997).
9. Kudzma, L. V., Spencer, H. K. & Severnak, S. A. A variant of the bruylants reaction. *Synthesis of 4-heteroaryl-4-anilinopiperidines. Tetrahedron Letters* **29**, 6827–6830 (1988).
10. Kumar, A., Sharma, R. K., Singh, T. V. & Venugopalan, P. Indium(III) bromide catalyzed direct azidation of α-hydroxyketones using $TMSN_3$. *Tetrahedron* **69**, 10724–10732, doi:10.1016/j.tet.2013.10.055 (2013).
11. Lherbet, C. *et al*. Bismuth triflate-catalyzed oxa- and thia-Pictet–Spengler reactions: access to iso- and isothio-chroman compounds. *Tetrahedron Letters* **49**, 5449–5451, doi:10.1016/j.tetlet.2008.07.007 (2008).
12. Hegedus, A. & Hell, Z. Zeolite-catalyzed simple synthesis of isochromans via the oxa-Pictet–Spengler reaction. *Org. Biomol. Chem.* **4**, 1220–1222, doi:10.1039/b601314g (2006).
13. Camarda, V. *et al*. Pharmacological profile of NOP receptors coupled with calcium signaling via the chimeric protein $G_{\alpha qi5}$. *Naunyn Schmiedebergs Arch. Pharmacol.* **379**, 599–607, doi:10.1007/s00210-009-0396-x (2009).
14. Camarda, V. & Calò, G. Chimeric G proteins in fluorimetric calcium assays: experience with opioid receptors. *Methods Mol. Biol.* **937**, 293–306, doi:10.1007/978-1-62703-086-1 (2013).

Acknowledgements

This work was supported by funds from the Italian Ministry of University and Research (Grant FIRB RBFR109SBM to C.T.) The authors also greatly acknowledge Dr. Alberto Casolari and Dr. Elisa Durini for the one-dimension and two-dimensional NMR experiments and Dr. Erika Marzola for HR-LC-MS determinations.

Author Contributions

A.F., S.B. and C.T., designed research; A.F., S.B., R.G. S.P., and C.T. synthesized and purified the compounds; M.C.C. and G.C. performed pharmacological studies; G.C., R.G., S.S. and C.T. analyzed data; S.P., A.F., S.B., G.C. and C.T. wrote the paper.

Additional Information

Supplementary information accompanies this paper at doi:10.1038/s41598-017-02502-9

Competing Interests: The authors declare that they have no competing interests.

Publisher's note: Springer Nature remains neutral with regard to jurisdictional claims in published maps and institutional affiliations.

Taylor & Francis
Taylor & Francis Group

Journal of Enzyme Inhibition and Medicinal Chemistry

ISSN: 1475-6366 (Print) 1475-6374 (Online) Journal homepage: http://www.tandfonline.com/loi/ienz20

Naphthoquinone amino acid derivatives, synthesis and biological activity as proteasome inhibitors

Mauro Marastoni, Claudio Trapella, Alessandra Scotti, Anna Fantinati, Valeria Ferretti, Erika Marzola, Gallerani Eleonora, Riccardo Gavioli & Delia Preti

To cite this article: Mauro Marastoni, Claudio Trapella, Alessandra Scotti, Anna Fantinati, Valeria Ferretti, Erika Marzola, Gallerani Eleonora, Riccardo Gavioli & Delia Preti (2017) Naphthoquinone amino acid derivatives, synthesis and biological activity as proteasome inhibitors, Journal of Enzyme Inhibition and Medicinal Chemistry, 32:1, 865-877, DOI: 10.1080/14756366.2017.1334649

To link to this article: https://doi.org/10.1080/14756366.2017.1334649

JOURNAL OF ENZYME INHIBITION AND MEDICINAL CHEMISTRY, 2017
VOL. 32, NO. 1, 865–877
https://doi.org/10.1080/14756366.2017.1334649

Taylor & Francis
Taylor & Francis Group

ORIGINAL ARTICLE

OPEN ACCESS Check for updates

Naphthoquinone amino acid derivatives, synthesis and biological activity as proteasome inhibitors

Mauro Marastoni[a], Claudio Trapella[a], Alessandra Scotti[a], Anna Fantinati[a], Valeria Ferretti[a], Erika Marzola[a], Gallerani Eleonora[b], Riccardo Gavioli[b] and Delia Preti[a]

[a]Department of Chemical and Pharmaceutical Sciences, University of Ferrara, Ferrara, Italy; [b]Department of Life Sciences and Biotechnology, University of Ferrara, Ferrara, Italy

ABSTRACT

The ubiquitin-proteasome system has been largely investigated for its key role in protein degradation mechanisms that regulate both apoptosis and cell division. Because of their antitumour activity, different classes of proteasome inhibitors have been identified to date. Some of these compounds are currently employed in the clinical treatment of several types of cancer among which multiple myeloma. Here, we describe the design, chemistry, biological activity and modelling studies of a large series of amino acid derivatives linked to a naphthoquinone pharmacophoric group through variable spacers. Some analogues showed interesting inhibitory potency for the β1 and β5 subunits of the proteasome with IC_{50} values in the sub-μm range.

ARTICLE HISTORY
Received 3 April 2017
Revised 12 May 2017
Accepted 15 May 2017

KEYWORDS
Proteasome; naphthoquinone; amino acid derivatives; post-acidic inhibition

Introduction

The proteasome enzymatic complex is widely involved in the cytosolic and nuclear catabolism of most proteins behaving as a protease with multiple catalytic sites[1]. The proteolytic action of proteasome allows the elimination of impaired proteins and results in the production of short-chain peptides that can be exposed by the MHC complexes[2]. The ubiquitin-proteasome system has been largely investigated for its key role in protein degradation mechanisms that regulate both apoptosis and cell division[3,4]. According to this system, the degradation of proteins is the result of their conjugation with multiple ubiquitin units that allow the recognition by the 26 S proteasome. The 26 S proteasome is composed of multiple subunits and is characterised by a central 20 S core and two distal regions (19 S) displaying regulatory activity. In the 20 S core, two external heptameric rings of α-subunits enclose two central heptameric rings of β-subunits. The 20 S core exerts three typical catalytic activities that are specifically located in the β1 (the peptidyl glutamyl peptide hydrolysing activity, PGPH), β2 (the trypsin-like activity, T-L) and β5 (the chymotrypsin-like, ChT-L) subunits[5]. The three catalytic β subunits have a slightly different substrate specificity with a common mechanism of proteolysis through an N-terminal threonine-dependent nucleophilic attack. Most of the cellular proteins undergo degradation through this pathway that affects several processes such as cell division, apoptosis or repair of DNA damages. As a consequence, any alteration of this system may result in important pathologies, including cancer.

Proteasome regulation by exogenous molecules able to manipulate cellular activities has been receiving increasing attention[6]. Inhibitors of this multicatalytic complex are potential drugs suitable in various therapeutic applications, therefore, natural and synthetic molecules have been studied as 20 S catalytic subunits inhibitors[7–16]. The first-generation proteasome inhibitor (PI) bortezomib is currently employed as an anti-cancer drug, although its effectiveness seems to be restricted to a limited number of cancers[17,18]. The FDA-approved carfilzomib[19] and ixazomib[20] along with oprozomib[21], currently in advanced clinical trials, are examples of second-generation irreversible PIs with a peptide structure.

In the last years, we developed several classes of peptide-based PIs having different pharmacophoric units such as electrophilic groups potentially able to interact with the catalytic threonine[22–24]. We have recently investigated a new series of dipeptide-based derivatives bearing at the C-terminal a 2-chloronaphthoquinone pharmacophoric group (structure **b** in Figure 1)[25]. Some compounds of this series have been shown to inhibit the post-acidic-like and the ChT-L active sites of the proteasome in the μm range. The compound named PI-083(NSC-45382), bearing the 2-cloronaphthoquinonic unit, and other non-peptide analogues (general structure **a** in Figure 1), are known to express a good inhibition against chymotryptic activity of the proteasome and the capacity to selectively inhibit tumour cell proliferation[26–28].

Herein, we describe the synthesis, the *in vitro* biological evaluation of proteasome inhibition and modelling studies of a new series of amino acid derivatives linked through the α-carboxylic function to the 2-chloronaphthoquinone pharmacophoric group (general structure **c** in Figure 1). The 2-chloronaphthoquinone (ClNafQ), a potential electrophilic substrate for the catalytic threonine, is linked to the selected residues by a diamine alkyl spacers. Studies regarding the non-peptide PI-083 and its analogues, in addition to our docking analysis with the previous dipeptidic derivatives, suggest the potential interaction of the γ-hydroxyl

CONTACT Delia Preti prtdle@unife.it Department of Chemical and Pharmaceutical Sciences, University of Ferrara, Via Luigi Borsari 46, Ferrara 44121, Italy
Supplemental data for this article can be accessed here.

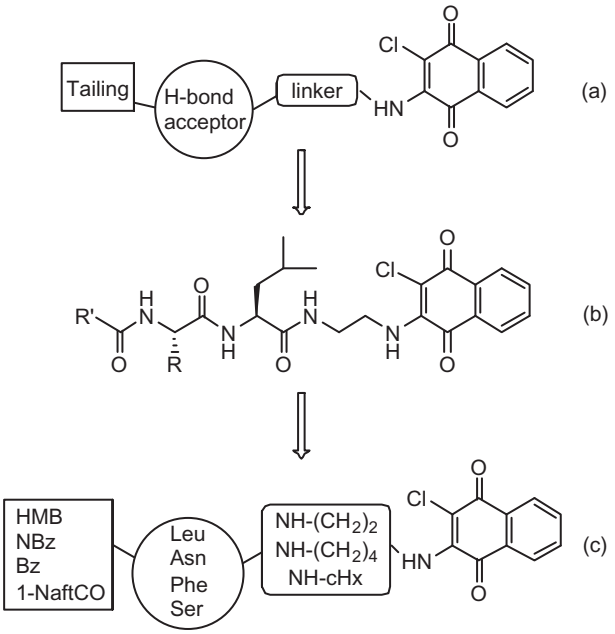

Figure 1. (a) Schematic structure of non-peptide inhibitors bearing the 2-cloronaphthoquinonic unit. (b) The general structure of dipeptide derivatives with a 2-chloronaphthoquinone group. (c) The generic structure of the new amino acid derivatives linked to the 2-chloronaphthoquinone group.

group of catalytic threonine with the 2-chloronaphthoquinone unit. The L-amino acids (Leu, Asn, Phe, Ser) were selected for their different physicochemical features. The chloronaphthoquinone pharmacophore is linked to the carboxylic group of the central residue by ethylenediamine (compounds **1**–**16**), butylenediamine (**17**–**32**) and cyclohexyldiamine (**33**–**48**) spacers having different length and flexibility (see Table 1 for the detailed structures). Finally, the α-amino group is functionalised with 2-methyl-3-hydroxybenzoyl (HMB), p-nitrobenzoyl (NBz), benzoyl (Bz) or 1-naphthoyl (1-NaftCO) aromatic groups having variable electronic and steric peculiarity.

Methods and materials

Chemistry-general

Amino acids, amino acid derivatives and chemicals were purchased from Bachem, Novabiochem, and Fluka (Switzerland). Crude products were purified by preparative reversed-phase HPLC using a Waters Delta Prep 3000 system with a Jupiter column C_{18} (250 × 30 mm, 300 Å, 15 μ spherical particle size). The column was perfused at a flow rate of 20 ml/min, with a mobile phase-containing solvent A (10%, v/v, acetonitrile in 0.1% TFA), and a linear gradient from 0% to 100% of solvent B (60%, v/v, acetonitrile in 0.1% TFA); 30 min was the time adopted for elution of the compounds. HPLC analysis was performed using a Beckman System Gold with a Luna C_{18} column (4.6 × 100 mm, 3 μ particle size). Analytical determination and retention time (T_r) of the peptides were assayed via HPLC conditions in the above solvent system (solvents A and B), programmed at flow rates of 0.5 ml/min, using the following linear gradients: (a) from 0% to 90% B for 25 min and (b) from 30% to 100% B for 25 min. No naphthoquinone derivative showed more than 1% impurity when monitored at 220 and 254 nm. The molecular weights of the compounds were determined by electrospray ionisation (ESI) (MICROMASS ZMD 2000), and the values are expressed as $[M + H]^+$. TLC was performed on pre-coated plates of silica gel F254 (Merck, Darmstadt, Germany), exploiting the following solvent systems: (c) AcOEt/*n*-hexane (1:1, v/v), (d) CH_2Cl_2/methanol (9.5:0.5, v/v), (e) CH_2CL_2/methanol (9:1, v/v) and (f) CH_2CL_2/methanol/toluene (17:2:1, v/v/v). Ninhydrin (1%) or chlorine iodine spray reagents were employed to detect the peptides. Melting points were determined by a Kofler apparatus and are uncorrected. Optical rotations were determined by a Perkin–Elmer 141 polarimeter with a 10-cm water-jacketed cell. ^{1}H NMR spectroscopy was obtained using a Varian 400 MHz spectrometer. All the assayed compounds described in this manuscript were at least 95% pure as judged by HPLC and NMR.

Synthesis

The synthesis applied for the preparation of compounds **1**–**48** is reported in Scheme 1. This synthetic strategy allowed us to obtain the compounds with the least possible number of steps. The entire synthesis was performed in solution wherein the L-amino acids were suitably protected at the Nα and linked to the selected diamine spacers at the carboxylic group. The alkyldiamine linkers were protected at one of the amine functionality with the Boc group. Subsequently, the Fmoc-protected amino acids were condensed at the mono-protected diaminic spacers using 1-ethyl-3-(3-dimethylaminopropyl)-carbodiimmide (WSC) and N-hydroxybenzotriazole (HOBt) as acylating agents. After treatment with piperidine to remove the fluorenylmethoxycarbonyl (Fmoc), the Nα functionalisation was carried out by acylation with 3-hydroxy-2-methylbenzoic acid, 4-nitrobenzoic acid, benzoic acid or alpha-naphthoic acid using 2-(1H-9-azabenzotriazole-1-yl)-1,1,3,3-tetramethyl-aminium hexafluorophosphate (HATU) as a coupling agent. After the Boc removal via TFA treatment, we proceeded to the final reaction with 2,3-dichloro-naphthoquinone that takes place in a solution of 95% EtOH, in presence of *N*-methyl-morpholine. All products, after purification by RP-HPLC, were analysed by mass spectrometry and NMR. The analytical data of the compounds are reported in the supporting material.

General synthetic procedures

a. *Condensation with Fmoc-amino acids.* The carboxylic component (1 mmol) was dissolved DMF (10 ml) and, after cooling at 0 °C, WSC (1.1 mmol), HOBt (1.1 mmol) and the amine component (1.1 mmol) were added. The reaction mixture was stirred for 1 h at 0 °C then overnight at room temperature. The solvent was evaporated to give a residue that was suspended with EtOAc and washed successively with 10% citric acid (10 ml), 5% $NaHCO_3$ (10 ml) and again with brine (10 ml). The organic phase was dried with Na_2SO_4, filtered and evaporated to furnish the desired products that were used without further purification.

b. *Condensation with 2-methyl-3-hydroxybenzoic acid, p-nitrobenzoic acid, benzoic acid or α-naphthoic acid.* The carboxylic component (1 mmol) was dissolved DMF (6 ml) and HATU (1mmol) and DIPEA (1 mmol) were added. Then a solution of the appropriate amine (1 mmol) and TEA (1 mmol) in DMF (6 ml) was added. The mixture was stirred overnight at room temperature. The solvent was evaporated to obtain a residue that was suspended with EtOAc. The organic phase was washed successively with 10% citric acid (2 × 5 ml), 5% $NaHCO_3$ (2 × 5 ml) and again with brine (2 × 5 ml). The organic phase was dried with Na_2SO_4, filtered and evaporated to give a solid residue that was crystallised (Et_2O) and collected after centrifugation.

Table 1. Inhibition of the proteasome subunits by the synthesised compounds.

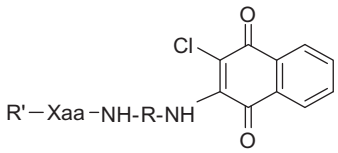

Compd	R'	Xaa	R	IC_{50} (μm)[a] T-L	IC_{50} (μm)[a] ChT-L	IC_{50} (μm)[a] PGPH
1	HMB	Leu	$-(CH_2)_2-$	77.44 ± 6.51	>100	1.21 ± 0.08
2	NBz	Leu	$-(CH_2)_2-$	65.32 ± 5.91	>100	2.35 ± 0.21
3	Bz	Leu	$-(CH_2)_2-$	58.43 ± 5.13	>100	2.61 ± 0.23
4	1-NaftCO	Leu	$-(CH_2)_2-$	21.08 ± 1.85	0.82 ± 0.08	0.91 ± 0.07
5	HMB	Asn	$-(CH_2)_2-$	68.35 ± 5.14	8.47 ± 0.75	6.18 ± 0.55
6	NBz	Asn	$-(CH_2)_2-$	17.23 ± 1.09	0.92 ± 0.09	1.19 ± 0.13
7	Bz	Asn	$-(CH_2)_2-$	49.66 ± 3.87	7.99 ± 0.67	11.23 ± 0.98
8	1-NaftCO	Asn	$-(CH_2)_2-$	35.23 ± 2.77	76.25 ± 6.82	10.01 ± 1.27
9	HMB	Phe	$-(CH_2)_2-$	>100	0.85 ± 0.07	0.88 ± 0.08
10	NBz	Phe	$-(CH_2)_2-$	35.40 ± 2.91	0.77 ± 0.06	0.24 ± 0.3
11	Bz	Phe	$-(CH_2)_2-$	53.18 ± 6.70	6.22 ± 0.48	1.05 ± 0.09
12	1-NaftCO	Phe	$-(CH_2)_2-$	49.75 ± 3.97	9.14 ± 1.02	35.76 ± 4.03
13	HMB	Ser	$-(CH_2)_2-$	>100	>100	91.52 ± 7.69
14	NBz	Ser	$-(CH_2)_2-$	63.36 ± 7.01	83.47 ± 8.03	78.66 ± 8.14
15	Bz	Ser	$-(CH_2)_2-$	53.82 ± 4.88	24.11 ± 1.98	5.78 ± 4.35
16	1-NaftCO	Ser	$-(CH_2)_2-$	>100	>100	>100
17	HMB	Leu	$-(CH_2)_4-$	>100	11.50 ± 1.02	7.82 ± 0.71
18	NBz	Leu	$-(CH_2)_4-$	>100	8.40 ± 0.72	10.54 ± 0.82
19	Bz	Leu	$-(CH_2)_4-$	>100	10.12 ± 0.70	2.41 ± 0.14
20	1-NaftCO	Leu	$-(CH_2)_4-$	>100	49.30 ± 5.02	45.35 ± 4.03
21	HMB	Asn	$-(CH_2)_4-$	>100	65.38 ± 6.50	9.52 ± 1.09
22	NBz	Asn	$-(CH_2)_4-$	>100	28.52 ± 3.05	>100
23	Bz	Asn	$-(CH_2)_4-$	>100	24.19 ± 2.05	>100
24	1-NaftCO	Asn	$-(CH_2)_4-$	>100	78.34 ± 6.95	>100
25	HMB	Phe	$-(CH_2)_4-$	>100	17.50 ± 1.07	8.82 ± 0.71
26	NBz	Phe	$-(CH_2)_4-$	>100	9.10 ± 0.6	10.54 ± 0.82
27	Bz	Phe	$-(CH_2)_4-$	>100	10.12 ± 0.70	5.43 ± 0.44
28	1-NaftCO	Phe	$-(CH_2)_4-$	79.71 ± 6.97	9.30 ± 1.02	25.65 ± 3.03
29	HMB	Ser	$-(CH_2)_4-$	80.24 ± 6.91	45.68 ± 2.59	61.52 ± 4.99
30	NBz	Ser	$-(CH_2)_4-$	83.26 ± 7.21	88.74 ± 8.03	83.66 ± 8.16
31	Bz	Ser	$-(CH_2)_4-$	>100	84.11 ± 6.08	3.55 ± 1.65
32	1-NaftCO	Ser	$-(CH_2)_4-$	60.75 ± 4.88	>100	83.62 ± 5.48
33	HMB	Leu	–cHx–	>100	>100	>100
34	NBz	Leu	–cHx–	>100	42.10 ± 5.02	>100
35	Bz	Leu	–cHx–	>100	23.12 ± 1.70	>100
36	1-NaftCO	Leu	–cHx–	>100	59.30 ± 6.42	73.67 ± 1.45
37	HMB	Asn	–cHx–	>100	>100	>100
38	NBz	Asn	–cHx–	>100	>100	>100
39	Bz	Asn	–cHx–	>100	>100	>100
40	1-NaftCO	Asn	–cHx–	>100	>100	>100
41	HMB	Phe	–cHx–	>100	>100	>100
42	NBz	Phe	–cHx–	>100	82.10 ± 6.52	>100
43	Bz	Phe	–cHx–	>100	73.31 ± 3.90	>100
44	1-NaftCO	Phe	–cHx–	>100	>100	83.37 ± 4.58
45	HMB	Ser	–cHx–	>100	>100	>100
46	NBz	Ser	–cHx–	>100	>100	5.78 ± 0.62
47	Bz	Ser	–cHx–	>100	>100	3.42 ± 0.51
48	1-NaftCO	Ser	–cHx–	>100	>100	11.71 ± 1.25
MG132				1.04 ± 0.092	0.0018 ± 0.00022	>10

[a]The values reported are the mean ± SEM of three independent determinations.

c. *Fmoc Removal*. The Fmoc protection was removed by treatment at room temperature with a 20% piperidine solution in DMF for 1 h. The solvent was evaporated and the desired products were precipitated with ethyl ether, then separated by centrifugation and collected.

d. *Boc Removal*. The Boc protection was removed by treatment with 90% aqueous TFA (1 ml for 1 mmol of the Boc-protected compound) for 1 h. After evaporation of the solvent, the residue was triturated with ethyl ether and separated by centrifugation.

e. *Condensation with 2,3-dichloro-1,4-naphthoquinone*. The amine component (0.3 mmol) was dissolved in 95% EtOH (15 ml) then N-methyl-morpholine (0.3 mmol) and 2,3-dichloro-1,4-naphthoquinone (0.6 mmol) were added. The mixture was heated at 115 °C for 3 d under stirring. After evaporation of the solvent, the residue was triturated with ethyl ether and separated by centrifugation.

Preparation of Boc-ethylene/butylene/trans-cyclohexyldiamine

The diamine (10 mmol) was dissolved in a mixture of t-ButOH/H_2O (2:1, 20 ml) then $(Boc)_2O$ (7 mmol) was added and the reaction was stirred for 2 h at room temperature. Water (20 ml) was added and the aqueous phase was extracted with n-pentane (2 × 10 ml).

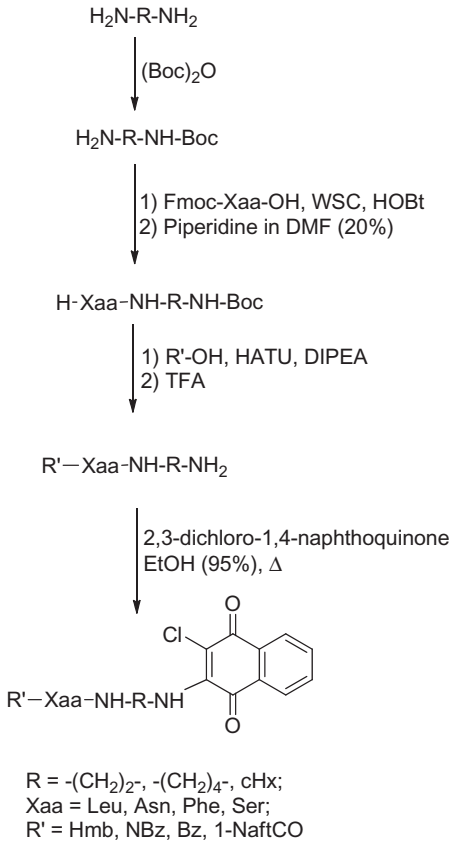

Scheme 1. Synthesis of naphthoquinone amino acid derivatives.

After separation, the aqueous phase was further extracted with EtOAc (2×50 ml) and the latter organic phase was dried with anhydrous Na_2SO_4 and evaporated to yield the desired compounds that were employed without further purification.

Boc-ethylenediamine. Colourless oil, yield 85%.^{1}H NMR ($CDCl_3$) δ5.98 (bs, 1H), 3.08 (m, 2H), 2.69 (m, 2H), 1.75 (bs, 2H), 1.39 (s, 9H); MS ($M+H^+$) 161.20; HPLC (T_r) 6.54 min. Spectroscopic data are consistent with those previously reported[25].

Boc-butylenediamine. Colourless oil, yield 75%. ^{1}H NMR ($CDCl_3$) δ 4.70 (bs, 1H), 3.14 (m, 2H), 2.68 (t, 2H, J = 6.7), 1.68 (bs, 2H), 1.50–1.45 (m, 4H), 1.48 (s, 9H). MS ($M+H^+$) 189.22; HPLC (T_r) 7.24 min. Spectroscopic data are consistent with those previously reported[29].

Boc-trans-cyclohexyldiamine. White solid, yield 96%. ^{1}H NMR ($CDCl_3$): δ 4.91–5.12 (bs, 1H), 3.31–3.41 (bs, 1H), 2.57–2.68 (m, 1H), 1.90–2.03 (bs, 2H), 1.87–1.97 (m, 4H), 1.44 (s, 9H), 1.10–1.24 (m, 4H). MS ($M+H^+$) 214.26; HPLC (Tr) 7.56 min. Spectroscopic data are consistent with those previously reported[30].

Preparation of H-Xaa-NH-R-NH-boc

The intermediates with general structure Fmoc-Xaa-NH-R-NH-Boc were first prepared by acylation of the appropriate Boc-protected diamine with Fmoc-Xaa-OH following the general procedure (a). Fmoc-protected derivatives were then treated according to the general procedure for Fmoc removal (c) to give the desired H-Xaa-NH-R-NH-Boc intermediates.

H-Leu-NH-$(CH_2)_2$-NH-Boc. White solid, yield 77%; ^{1}H NMR, ($CDCl_3$) δ: 3.49–3.41 (m, 2H), 3.18–3.14 (m, 1H), 3.05–3.00 (m, 1H), 2.90–2.88 (m, 1H), 1.78–1.76 (m, 1H), 1.39 (s, 9H), 1.36–1.32 (m, 2H), 0.94 (d, 3H, $J = 7.4$ Hz), 0.89 (d, 3H, $J = 7.4$ Hz); MS ($M+H^+$) 274.31.

H-Asn-NH-$(CH_2)_2$-NH-Boc. White solid, yield 67%; ^{1}H NMR, ($CDCl_3$) δ: 7.82 (bs, 1H), 5.11 (s, 2H), 3.79–3.76 (m, 1H), 3.58–3.54 (m, 2H), 3.47–3.42 (m, 2H), 3.12–2.90 (m, 1H), 2.85–2.72 (m, 1H), 1.45 (s, 9H);MS ($M+H^+$) 275.32.

H-Phe-NH-$(CH_2)_2$-NH-Boc. White solid, yield 88%; ^{1}H NMR, ($CDCl_3$) δ: 7.76 (bs, 1H), 7.44–7.42 (m, 2H), 7.32–7.29 (m, 3H), 5.13 (s, 2H), 3.91–3.88 (m, 1H), 3.56–3.52 (m, 2H), 3.46–3.45 (m, 2H), 3.44–3.42 (m, 1H), 3.20–3.18 (m, 1H), 1.44 (s, 9H);MS ($M+H^+$) 308.30.

H-Ser-NH-$(CH_2)_2$-NH-Boc. White solid, yield 67%; ^{1}H NMR, ($CDCl_3$) δ: 7.74 (bs, 1H), 5.13 (bs, 2H), 4.18–4.16 (m, 1H), 3.92–3.90 (m, 1H), 3.66–3.64 (m, 1H), 3.53–3.50 (m, 2H), 3.48–3.46 (m, 2H), 1.38 (s, 9H);MS ($M+H^+$) 248.28.

H-Leu-NH-$(CH_2)_4$-NH-Boc. White solid, yield 77%; ^{1}H NMR, ($CDCl_3$) δ: 8.00 (bs, 1H), 5.40 (bs, 2H), 3.49–3.41 (m, 5H), 1.78–1.76 (m, 1H), 1.55–1.54 (m, 2H), 1.51–1.49 (m, 2H), 1.43 (s, 9H), 1.34–1.33 (m, 2H), 0.93 (d, 3H, $J = 7.4$ Hz), 0.90 (d, 3H, $J = 7.4$ Hz);MS ($M+H^+$) 302.24.

H-Asn-NH-$(CH_2)_4$-NH-Boc. White solid, yield 87%; ^{1}H NMR, ($CDCl_3$) δ: 7.79 (bs, 1H), 5.33 (bs, 2H), 3.79–3.77 (m, 1H), 3.55–3.53 (m, 2H), 3.44–3.42 (m, 2H), 2.91–2.89 (m, 1H), 2.87–2.86 (m, 1H), 1.54–1.53 (m, 2H), 1.50–1.49 (m, 2H), 1.43 (s, 9H);MS ($M+H^+$) 303.27.

H-Phe-NH-$(CH_2)_4$-NH-Boc. White solid, yield 64%;^{1}H NMR, ($CDCl_3$) δ: 7.99 (bs, 1H), 7.44–7.42 (m, 2H), 7.31–7.29 (m, 3H), 5.22 (bs, 2H), 3.89–3.87 (m, 1H), 3.56–3.53 (m, 1H), 3.22–3.18 (m, 5H), 1.52–1.50 (m, 2H), 1.49–1.47 (m, 2H), 1.42 (s, 9H);MS ($M+H^+$) 336.18.

H-Ser-NH-$(CH_2)_4$-NH-Boc. White solid, yield 77%; ^{1}H NMR, ($CDCl_3$) δ: 8.03 (bs, 1H), 5.20 (bs, 2H), 4.17–4.15 (m, 1H), 3.90–3.89 (m, 1H), 3.64–3.62 (m, 1H), 3.50–3.49 (m, 2H), 3.48–3.47 (m, 2H), 1.54–1.53 (m, 2H), 1.51–1.49 (m, 2H), 1.43 (s, 9H);MS ($M+H^+$) 276.29.

H-Leu-NH-cHx-NH-Boc. White solid, yield 77%; ^{1}H NMR, ($CDCl_3$) δ: 7.64 (bs, 1H), 5.44 (bs, 2H), 3.55–3.54 (m, 1H), 3.52–3.51 (m, 1H), 3.35–3.33 (m, 1H), 1.77–1.75 (m, 1H), 1.70–1.69 (m, 4H), 1.54–1.53 (m, 4H), 1.39 (s, 9H), 1.34–1.32 (m, 2H), 0.94 (d, 3H, $J = 7.4$ Hz), 0.89 (d, 3H, $J = 7.4$ Hz); MS ($M+H^+$) 328.22.

H-Asn-NH-cHx-NH-Boc. White solid, yield 87%; ^{1}H NMR, ($CDCl_3$) δ: 8.26 (bs, 1H), 7.24 (bs, 2H), 5.54 (bs, 2H), 3.78–3.76 (m, 1H), 3.55–3.53 (m, 2H), 2.90–2.88 (m, 1H), 2.85–2.83 (m, 1H), 1.77–1.73 (m, 4H), 1.50–1.47 (m, 4H), 1.38 (s, 9H);MS ($M+H^+$) 329.32.

H-Phe-NH-cHx-NH-Boc. White solid, yield 56%; ^{1}H NMR, ($CDCl_3$) δ: 8.44 (bs, 1H), 7.42–7.40 (m, 2H), 7.31–7.29 (m, 3H), 5.44 (bs, 2H), 3.89–3.87 (m, 1H), 3.58–3.56 (m, 1H), 3.54–3.53 (m, 2H), 3.19–3.18 (m, 1H), 1.78–1.73 (m, 4H), 1.49–1.44 (m, 4H), 1.38 (s, 9H);MS ($M+H^+$) 362.15.

H-Ser-NH-cHx-NH-Boc. White solid, yield 57%; ^{1}H NMR, ($CDCl_3$) δ: 8.15 (bs, 1H), 5.44 (bs, 2H), 4.16–4.13 (m, 1H), 3.97–3.96 (m, 1H), 3.64–3.62 (m, 1H), 3.58–3.56 (m, 1H), 3.54–3.52 (m, 1H), 1.77–1.73 (m, 4H), 1.54–1.51 (m, 4H), 1.38 (s, 9H);MS ($M+H^+$) 302.28.

Preparation of R'-Xaa-NH-R-NH$_2$

The compounds with general structure R'-Xaa-NH-R-NH_2 were prepared through a first HATU-mediated coupling of intermediates H-Xaa-NH-R-NH-Boc with 2-methyl-3-hydroxybenzoic acid, p-nitrobenzoic acid, benzoic acid or α-naphthoic acid following the general procedure (b). The resulting Boc-protected derivatives were then treated according to the general method for Boc removal (d) to give the target compounds as trifluoroacetate salts. Analytical data and ^{1}H-NMR spectra of representative compounds are listed below. NMR spectra of the whole series can be found in the Supplementary Material.

HMB-Leu-NH-$(CH_2)_2$-NH_2. White solid, yield 54%; ^{1}H NMR (400 MHz, $CDCl_3$) δ 7.30 (dd, $J = 7.5$, 1.4 Hz, 1H), 7.21–7.04 (m, 1H),

6.90 (dd, $J = 7.5$, 1.4 Hz, 1H), 6.55 (s, 1H), 5.19 (s, 3H), 5.02 (s, 1H), 4.41 (t, $J = 7.6$ Hz, 1H), 3.95 (t, $J = 7.6$ Hz, 2H), 3.55 (s, 1H), 3.03 (t, $J = 7.6$ Hz, 2H), 2.31 (s, 3H), 1.98–1.66 (m, 2H), 1.58 (t, $J = 7.5$ Hz, 1H), 1.23–0.86 (m, 6H);MS ($M + H^+$) 308.21.

HMB-Asn-NH-$(CH_2)_2$-NH_2. Pale yellow solid, yield 79%; ^{1}H NMR (400 MHz, $CDCl_3$) δ 7.30 (dd, $J = 7.5$, 1.5 Hz, 1H), 7.22–7.06 (m, 1H), 6.91 (dd, $J = 7.5$, 1.4 Hz, 1H), 6.55 (s, 1H), 5.58 (s, 3H), 5.19 (s, 1H), 5.07 (s, 2H), 4.83–3.91 (m, 2H), 3.61 (s, 1H), 3.14–2.96 (m, 3H), 2.87–2.83 (m, 1H), 2.19 (s, 3H);MS($M + H^+$) 309.17.

HMB-Phe-NH-$(CH_2)_2$-NH_2. White solid, yield 81%; ^{1}H NMR (400 MHz, $CDCl_3$) δ 7.36–7.33 (m, 1H), 7.30–7.03 (m, 6H), 6.91 (dd, $J = 7.5$, 1.4 Hz, 1H), 6.80 (s, 1H), 5.07 (s, 3H), 4.69–4.67 (m, 1H), 4.30 (s, 1H), 3.97–3.90 (m, 2H), 3.56 (s, 1H), 3.30–3.28 (m, 1H), 3.03–2.78 (m, 3H), 2.31 (s, 3H); MS($M + H^+$) 342.18.

HMB-Ser-NH-$(CH_2)_2$-NH_2. White solid, yield 77%; ^{1}H NMR (400 MHz, $CDCl_3$)δ 7.18–7.01 (m, 2H), 6.97–6.87 (m, 1H), 5.50 (bs, 1H), 5.21 (s, 3H), 4.99 (s, 1H), 4.75–4.73 (m, 1H), 4.29–4.28 (m, 1H), 4.02–3.75 (m, 3H), 3.54 (s, 1H), 3.05–3.02 (m, 2H), 2.29 (s, 3H); MS ($M + H^+$) 282.27.

HMB-Leu-NH-$(CH_2)_4$-NH_2. Pale yellow solid, yield 57%; ^{1}H NMR (400 MHz, $CDCl_3$)δ 7.30–7.26 (m, 1H), 7.14–7.11 (m, 1H), 6.91–6.89 (m, 1H), 6.03 (s, 3H), 5.26 (s, 1H), 5.23–5.11 (m, 2H), 3.74 (s, 1H), 3.50–3.48 (m, 1H), 3.19–3.17 (m, 1H), 2.82–2.75 (m, 2H), 2.24 (s, 3H), 2.02–1.89 (m, 2H), 1.83–1.58 (m, 4H), 1.54–1.52 (m, 1H), 1.04–0.93 (m, 6H); MS ($M + H^+$) 336.31.

HMB-Asn-NH-$(CH_2)_4$-NH_2. White solid, yield 73%; ^{1}H NMR (400 MHz, $CDCl_3$)δ 7.70 (s, 1H), 7.61 (s, 1H), 7.32–7.28 (m, 1H), 7.15 (t, $J = 7.5$ Hz, 1H), 6.91–6.94 (m, 1H), 5.26 (s, 2H), 4.94 (s, 3H), 4.63–4.58 (m, 1H), 3.31–3.17 (m, 2H), 3.05–3.02 (m, 1H), 2.82–2.65 (m, 3H), 2.32 (s, 3H), 1.86–1.79 (m, 2H), 1.55–1.50 (m, 2H); MS ($M + H^+$) 337.32.

HMB-Phe-NH-$(CH_2)_4$-NH_2. White solid, yield 77%; ^{1}H NMR (400 MHz, $CDCl_3$)δ 7.40–7.36 (m, 1H), 7.34–7.08 (m, 7H), 6.95–6.91 (m, 1H), 5.16 (s, 3H), 4.73–4.70 (m, 1H), 4.39 (s, 1H), 3.41 (s, 1H), 3.28–3.17 (m, 3H), 2.92–2.89 (m, 1H), 2.78–2.75 (m, 2H), 2.31 (s, 3H), 2.02–1.77 (m, 2H), 1.65–1.55 (m, 2H); MS ($M + H^+$) 370.22.

HMB-Ser-NH-$(CH_2)_4$-NH_2. Pale yellow solid, yield 44%; ^{1}H NMR (400 MHz, $CDCl_3$)δ 7.18–7.13 (m, 1H), 7.10–7.05 (m, 1H), 6.88–6.97 (m, 1H), 5.32 (s, 2H), 4.96 (s, 3H), 4.67–4.58 (m, 1H), 4.14–4.10 (m, 1H), 3.90–3.85 (m, 1H), 3.56 (s, 1H), 3.32–3.18 (m, 2H), 2.76–7.68 (m, 2H), 2.32 (s, 3H), 1.99–1.85 (m, 2H), 1.76–1.62 (m, 2H); MS ($M + H^+$) 310.17.

HMB-Leu-NH-cHx-NH_2. Pale yellow solid, yield 81%; ^{1}H NMR (400 MHz, $CDCl_3$)δ 7.40 (s, 1H), 7.30 (dd, $J = 7.5$, 1.5 Hz, 1H), 7.14 (t, $J = 7.5$ Hz, 1H), 6.91 (dd, $J = 7.5$, 1.4 Hz, 1H), 5.70 (s, 3H), 4.96 (s, 1H), 4.72–4.70 (m, 1H), 3.67–3.63 (m, 1H), 3.59–3.45 (m, 1H), 2.36–2.29 (m, 3H), 2.17–2.05 (m, 2H), 1.84–1.55 (m, 7H), 1.07–0.96 (m, 6H); MS ($M + H^+$) 362.14.

HMB-Asn-NH-cHx-NH_2. Pale yellow solid, yield 72%; ^{1}H NMR (400 MHz, $CDCl_3$)δ 7.50 (s, 1H), 7.36 (dd, $J = 7.5$, 1.4 Hz, 1H), 7.17 (t, $J = 7.5$ Hz, 1H), 6.91 (dd, $J = 7.5$, 1.4 Hz, 1H), 5.27 (s, 2H), 5.16 (s, 3H), 4.49–4.45 (m, 1H), 4.32–4.28 (m, 1H), 3.56 (s, 1H), 3.36–3.31 (m, 1H), 3.07–3.03 (m, 1H), 2.68–2.64 (m, 1H), 2.55–2.49 (m, 2H), 2.35–2.22 (m, 5H), 2.03–1.96 (m, 2H), 1.74–1.68 (m, 2H); MS ($M + H^+$) 363.32.

HMB-Phe-NH-cHx-NH_2. White solid, yield 68%; ^{1}H NMR (400 MHz, $CDCl_3$)δ 7.41 (dd, $J = 7.5$, 1.5 Hz, 1H), 7.34–7.24 (m, 4H), 7.24–7.08 (m, 2H), 7.02–6.85 (m, 2H), 5.27 (s, 1H), 5.18 (s, 3H), 4.90 (t, $J = 3.6$ Hz, 1H), 4.19–4.15 (m, 1H), 3.56–3.34 (m, 2H), 3.00–2.97 (m, 1H), 2.40–2.22 (m, 5H), 2.10–2.05 (m, 2H), 1.81–1.76 (m, 2H), 1.48–1.36 (m, 2H); MS ($M + H^+$) 396.33.

HMB-Ser-NH-cHx-NH_2. Pale yellow, yield 69%; ^{1}H NMR (400 MHz, $CDCl_3$)δ 7.32 (dd, $J = 7.5$, 1.4 Hz, 1H), 7.18 (t, $J = 7.5$ Hz, 1H), 6.91 (dd, $J = 7.5$, 1.4 Hz, 1H), 5.04 (s, 1H), 4.75 (s, 1H), 4.68 (s, 3H), 4.31–4.06 (m, 2H), 4.03–3.88 (m, 1H), 3.87–3.66 (m, 1H), 3.61–3.32 (m, 2H), 2.29 (s, 3H), 2.23–2.10 (m, 2H), 2.05–1.79 (m, 4H), 1.67–1.45 (m, 2H); MS ($M + H^+$) 336.52.

Preparation of R'-Xaa-NH-R-NH-ClNafQ

The final compounds **1**–**48** were obtained by the reaction of intermediates R'-Xaa-NH-R-NH_2 with 2,3-dichloro-1,4-naphthoquinone following the general procedure (e). All the compounds were purified by RP-HPLC. Analytical data and ^{1}H-NMR spectra of representative compounds (**1–16**) are listed below. NMR spectra of the whole series can be found in the Supplementary Material.

HMB-Leu-NH-$(CH_2)_2$-NH-ClNafQ (**1**). White solid; yield 58%;mp =111–114 °C; $[\alpha]_D^{20}$–30.2 (c = 1, MeOH). ^{1}H NMR (400 MHz, $CDCl_3$)δ 8.29–8.07 (m, 2H), 8.05 (bs, 1H), 7.78–7.66 (m, 2H), 7.23–6.98 (m, 2H), 6.95–6.78 (m, 1H), 5.79 (bs, 1H), 5.71 (bs, 1H), 4.72–4.66 (m, 1H), 3.56–3.45 (m, 4H), 2.29 (s, 3H), 1.85–1.69 (m, 2H), 1.56 (t, $J = 6.6$ Hz, 1H), 0.97–0.87 (m,6H); MS (ESI): $[MH]^+ = 498.12$.HPLC (T_r) 16.76 min.

NBz-Leu-NH-$(CH_2)_2$-NH-ClNafQ (**2**). White solid; yield 66%;mp =134–137 °C; $[\alpha]_D^{20}$–26.4 (c = 1, MeOH); ^{1}H NMR (400 MHz, $CDCl_3$)δ 8.22–8.13 (m, 4H), 8.08 (d, $J = 7.4$ Hz, 2H), 7.80–7.69 (m, 2H), 7.41 (bs, 1H), 6.80 (bs, 1H), 5.65 (bs, 1H), 3.93–3.86 (m, 1H), 3.89–3.41 (m, 4H), 1.86–1.57 (m, 2H), 1.45–1.43 (m, 1H), 0.97–0.87 (m, 6H); MS (ESI): $[MH]^+ = 513.11$; HPLC (T_r) 18.40 min.

Bz-Leu-NH-$(CH_2)_2$-NH-ClNafQ (**3**). White solid; yield 89%;mp =128–130 °C; $[\alpha]_D^{20}$ –22.4 (c = 1, MeOH); ^{1}H NMR (400 MHz, $CDCl_3$)δ 8.25–8.10 (m, 2H), 7.89–7.83 (m, 2H), 7.79–7.68 (m, 2H), 7.53–7.358 (m, 3H), 6.54 (s, 1H), 5.45 (s, 1H), 5.31 (s, 1H), 4.23–4.18 (m, 1H), 3.58–3.44 (m, 3H), 3.40–3.36 (m, 1H), 1.68–1.42 (m, 3H), 1.06 (d, $J = 6.1$ Hz, 6H); MS (ESI): $[MH]^+ = 468.03$; HPLC (T_r) 17.71 min.

1-NaftCO-Leu-NH-$(CH_2)_2$-NH-ClNafQ (**4**). White solid; yield 74%;mp =145–148 °C; $[\alpha]_D^{20}$–33.2 (c = 1, MeOH); ^{1}H NMR (400 MHz, $CDCl_3$)δ 8.52–8.47 (m, 1H), 8.18–8.02 (m, 2H), 7.99–7.93 (m, 2H), 7.82–7.78 (m, 1H), 7.74–7.64 (m, 2H), 7.58–7.46 (m, 3H), 7.21 (s, 1H), 7.05 (s, 1H), 5.75 (s, 1H), 4.52–4.47 (m, 1H), 3.64–3.39 (m, 4H), 1.99–1.86 (m, 1H), 1.73–1.34 (m, 2H), 1.12–0.93 (m, 6H); MS (ESI): $[MH]^+ = 518.15$; HPLC (T_r) 19.11 min.

HMB-Asn-NH-$(CH_2)_2$-NH-ClNafQ (**5**). White solid; yield 66%;mp =128–130 °C; $[\alpha]_D^{20}$–42.1 (c = 1, MeOH); ^{1}H NMR (400 MHz, $CDCl_3$)δ 8.57 (s, 1H), 8.34–8.23 (m, 1H), 7.95–7.86 (m, 1H), 7.67–7.58 (m, 2H), 7.32–7.29 (m, 1H), 7.14–7.10 (m, 1H), 6.89–6.81 (m, 1H), 5.50 (s, 1H), 5.35 (s, 1H), 5.23–5.18 (m, 1H), 4.73 (s, 2H), 3.62–3.54 (m, 3H), 3.46–3.40 (m, 1H), 3.03–2.98 (m, 1H), 2.51–2.46 (m, 1H), 2.33 (s, 3H); MS(ESI): $[MH]^+ = 499.24$; HPLC (T_r) 13.21 min.

NBz-Asn-NH-$(CH_2)_2$-NH-ClNafQ (**6**). White solid; yield 52%;mp =168–170 °C; $[\alpha]_D^{20}$–38.8 (c = 1, MeOH); ^{1}H NMR (400 MHz, $CDCl_3$)δ 8.74 (s, 1H), 8.20–8.05 (m, 6H), 7.79–7.68 (m, 2H), 5.69–5.66 (m, 3H), 5.30 (s, 1H), 4.72–4.66 (m, 1H), 3.70–3.56 (m, 1H), 3.55–3.32 (m, 3H), 2.96–2.91 (m, 1H), 2.50–2.45 (m, 1H); MS (ESI): $[MH]^+ = 514.08$; HPLC (T_r) 13.66 min.

Bz-Asn-NH-$(CH_2)_2$-NH-ClNafQ (**7**). White solid; yield 48%;mp =165–167 °C; $[\alpha]_D^{20}$ –26.6 (c = 1, MeOH); ^{1}H NMR (400 MHz, $CDCl_3$)δ 8.27–8.08 (m, 2H), 7.87 (dd, $J = 7.4$, 1.3 Hz, 2H), 7.74–7.65 (m, 2H), 7.41–7.21 (m, 3H), 7.24 (s, 1H), 6.47 (s, 1H), 6.00 (s, 1H), 5.02 (s, 2H), 4.87–4.82 (m, 1H), 3.60–3.37 (m, 4H), 3.13–3.08 (m, 1H), 2.86–7.82 (m, 1H);MS (ESI): $[MH]^+ = 469.12$; HPLC (T_r) 14.30 min.

1-NaftCO-Asn-NH-$(CH_2)_2$-NH-ClNafQ (**8**). White solid; yield 87%;mp =178–180 °C; $[\alpha]_D^{20}$–42.8 (c = 1, MeOH); ^{1}H NMR (400 MHz, $CDCl_3$) δ 8.57–8.41 (m, 2H), 8.20–8.04 (m, 2H), 8.00–7.87 (m, 2H), 7.84–7.80 (m, 1H), 7.76–7.60 (m, 2H), 7.61–7.44 (m, 3H), 5.66 (s, 1H), 5.38 (s, 2H), 4.59–4.45 (m, 1H), 4.17 (s, 1H), 3.60–3.51

(m, 1H), 3.45–3.34 (m, 4H), 2.91–2.89 (m, 1H);MS (ESI): $[MH]^+ = 519.14$; HPLC (T_r) 15.43 min.

HMB-Phe-NH-$(CH_2)_2$-NH-ClNafQ (**9**). White solid; yield 72%;mp =121–124 °C; $[\alpha]_D^{20}$–31.4 (c = 1, MeOH); ^{1}H NMR (400 MHz, $CDCl_3$) δ 8.17–8.02 (m, 2H), 7.72–7.66 (m, 2H), 7.35–7.04 (m, 8H), 6.90 (dd, J = 7.5, 1.4 Hz, 1H), 6.20 (s, 1H), 5.05 (s, 1H), 4.77–4.68 (m, 1H), 3.64–3.40 (m, 4H), 3.42–3.22 (m, 2H), 2.95–2.92 (m, 1H), 2.28 (s, 3H); MS (ESI): $[MH]^+ = 532.02$; HPLC (T_r) 16.91 min.

NBz-Phe-NH-$(CH_2)_2$-NH-ClNafQ (**10**). White solid; yield 59%;mp =141–144 °C; $[\alpha]_D^{20}$–28.9 (c = 1, MeOH); ^{1}H NMR (400 MHz, $CDCl_3$)δ 8.83 (s, 1H), 8.25–8.15 (m, 3H), 8.09 (dd, J = 7.5, 1.6 Hz, 1H), 8.03 (d, J = 7.5 Hz, 2H), 7.84–7.80 (m, 1H), 7.70–7.66 (m, 1H), 7.23–7.20 (m, 2H), 7.16–7.04 (m, 3H), 6.23 (s, 1H), 4.69 (s, 1H), 4.03–3.98 (m, 1H), 3.68–3.50 (m, 2H), 3.50–3.42 (m, 1H), 3.45–3.32 (m, 1H), 3.25–3.15 (m, 1H), 2.98–2.96 (m, 1H); MS (ESI): $[MH]^+ = 547.30$; HPLC (T_r) 18.73 min.

Bz-Phe-NH-$(CH_2)_2$-NH-ClNafQ (**11**). White solid; yield 86%;mp =122–124 °C; $[\alpha]_D^{20}$–23.4 (c = 1, MeOH); ^{1}H NMR (400 MHz, $CDCl_3$)δ 8.23–8.13 (m, 1H), 8.05–7.83 (m, 3H), 7.77–7.65 (m, 3H), 7.52–7.48 (m, 3H), 7.31–7.19 (m, 2H), 7.19–7.11 (m, 3H), 4.87 (s, 1H), 4.55 (s, 1H), 4.10–4.02 (m, 1H), 3.57–3.41 (m, 4H), 3.30–3.27 (m, 1H), 2.98–2.96 (m, 1H);MS (ESI): $[MH]^+ = 502.15$; HPLC (T_r) 18.05 min.

1-NaftCO-Phe-NH-$(CH_2)_2$-NH-ClNafQ (**12**). White solid; yield 66%;mp =130–134 °C; $[\alpha]_D^{20}$–33.2 (c = 1, MeOH); ^{1}H NMR (400 MHz, $CDCl_3$)δ 8.51 (dd, J = 7.4, 1.5 Hz, 1H), 8.39 (s, 1H), 8.23–8.03 (m, 2H), 7.95–7.94 (m, 1H), 7.84–7.81 (m, 1H), 7.74–7.60 (m, 2H), 7.58–7.56 (m, 2H), 7.49–7.48 (m, 1H), 7.28–7.18 (m, 3H), 7.10–7.01 (m, 3H), 6.67 (s, 1H), 5.56 (s, 1H), 4.81–4.76 (m, 1H), 3.59–3.51 (m, 1H), 3.51–3.39 (m, 3H), 3.33–3.30 (m, 1H), 3.03–3.00 (m, 1H); MS (ESI): $[MH]^+ = 552.16$; HPLC (T_r) 19.65 min.

HMB-Ser-NH-$(CH_2)_2$-NH-ClNafQ (**13**). White solid; yield 76%;mp =117–120 °C; $[\alpha]_D^{20}$–45.1 (c = 1, MeOH); ^{1}H NMR (400 MHz, $CDCl_3$)δ 8.11–7.99 (m, 2H), 7.70–7.64 (m, 2H), 7.36–7.32 (m, 1H), 7.10–7.07 (m, 2H), 6.91–6.89 (m, 1H), 6.08 (s, 1H), 5.06 (s, 1H), 4.28–4.17 (m, 1H), 4.19–4.17 (m, 1H), 3.78–3.76 (m, 1H), 3.56–3.40 (m, 4H), 2.32 (s, 3H); MS (ESI): $[MH]^+ = 472.08$; HPLC (T_r) 12.84 min.

NBz-Ser-NH-$(CH_2)_2$-NH-ClNafQ (**14**). White solid; yield 56%;mp =142–146 °C; $[\alpha]_D^{20}$–39.8 (c = 1, MeOH); ^{1}H NMR (400 MHz, $CDCl_3$)δ 8.21–8.10 (m, 3H), 8.08–8.00 (m, 3H), 7.91 (s, 1H), 7.79–7.62 (m, 2H), 5.56 (s, 1H), 5.21 (s, 1H), 4.26–4.08 (m, 2H), 3.99–3.96 (m, 1H), 3.68–3.50 (m, 2H), 3.50–3.41 (m, 1H), 3.41–3.27 (m, 1H);MS (ESI): $[MH]^+ = 487.09$; HPLC (T_r) 13.22 min.

Bz-Ser-NH-$(CH_2)_2$-NH-ClNafQ (**15**). White solid; yield 69%;mp =155–157 °C; $[\alpha]_D^{20}$ –30.6 (c = 1, MeOH); ^{1}H NMR (400 MHz, $CDCl_3$)δ 8.25–8.19 (m, 1H), 8.10–8.05 (m, 1H), 7.74–7.70 (m, 4H), 7.66–7.64 (m, 1H), 7.48–7.41 (m, 1H), 7.36 (t, J = 7.4 Hz, 2H), 5.71 (s, 1H), 5.54 (s, 1H), 4.74–4.65 (m, 1H), 4.24–4.20 (m, 1H), 3.84–3.80 (m, 1H), 3.62–3.32 (m, 4H); MS (ESI): $[MH]^+ = 442.11$; HPLC (T_r) 13.97 min.

1-NaftCO-Ser-NH-$(CH_2)_2$-NH-ClNafQ (**16**). White solid; yield 65%;mp =163–166 °C; $[\alpha]_D^{20}$–41.5 (c = 1, MeOH);^{1}H NMR (400 MHz, $CDCl_3$) δ 8.78 (dd, J = 7.4, 1.5 Hz, 1H), 8.15–7.99 (m, 2H), 7.95–7.94 (m, 1H), 7.79–7.77 (m, 1H), 7.72–7.62 (m, 4H), 7.56–7.41 (m, 3H), 5.68 (s, 1H), 5.08–5.05 (m, 2H), 4.20–4.17 (m, 1H), 3.96–3.94 (m, 1H), 3.67–3.61 (m, 1H), 3.49–3.47 (m, 3H); MS (ESI): $[MH]^+ = 492.12$; HPLC (T_r) 14.86 min.

Biological assay

Proteasome purification and subunit inhibition

Proteasomes were isolated and purified from lymphoblastoid cell lines (LCL) as previously described[31]. Suc-LLVY-AMC, Boc-LRR-AMC and Z-LLE-AMC (Sigma-Aldrich, Milano, Italy) were used to determine chymotrypsin-like, trypsin-like and post-acidic proteasome activities, respectively. Substrates were incubated at 37 °C for 30 min with proteasomes, untreated or pretreated with 0.1–100 μm of test compounds **1**–**48** and reference inhibitor MG132, in activity buffer. Fluorescence was determined by a fluorimeter (Spectrafluor plus, Tecan, Salzburg, Austria), using an excitation of 360 nm and emission of 465 nm. Activity was evaluated in fluorescence units and the inhibitory capacity of the compounds is expressed as IC_{50}.

Growth inhibition assays

Cell growth inhibition assays were carried out using the breast cancer cell line MDA and ovarian cancer cell line A2780. Cells were obtained from ATCC (Manassas, VA) and maintained in DMEM and RPMI respectively, supplemented with 10% foetal bovine serum, penicillin (100 U ml^{-1}), streptomycin (100 U ml^{-1}) and glutamine (2 mm); incubation was performed at 37 °C in a 5% CO_2 atmosphere. Cells were routinely passaged every 3 d at 70% confluence; 0.05% trypsin-EDTA was used. The antiproliferative activity of new molecules was tested with the 3-(4,5-dimethylthiazol-2-yl)-2,5-diphenyltetrazolium bromide (MTT) assay. Cells were seeded in triplicate in 96-well plates at a density of 15×10^3 in 50 μl of complete medium. Stock solutions (10 mm) of selected analogues were made in DMSO and diluted in complete medium to give final concentrations of 10 and 100 μm. MG-132 was employed as a control. Untreated cells were placed in every plate as a negative control. The cells were exposed to the compounds, in 100 μl total volume, for 72 h, and then 25 μl of a 12 mm solution of MTT was added. After 2 h of incubation, 100 μl of lysing buffer (50% DMF +20% SDS, pH 4.7) was added to convert the MTT solution into a violet-coloured formazan. After an additional 18 h the solution absorbance, proportional to the number of live cells, was measured by spectrophotometer at 570 nm and converted into % of growth inhibition.

Docking

The equilibrium geometry of selected molecules was obtained using semi-empirical PM3 calculations; the molecules were subsequently docked to both β1 and β5 binding sites of 20 S proteasome. The simulation was performed utilising the crystal structures of PDB codes **1G65**[32] and **3E47**[33] for β1 and β5 binding sites, respectively. All molecules were placed in β1 and β5 binding sites using a pharmacophore query derived from the bound inhibitors epoxomicin (structure 1G65) and homobelactosin C (structure 3E47), respectively, as a filter for docking placement. Epoxomicin and homobelactosin C inhibitors have been chosen because they share size/shape similarities with the present molecules. Before the simulation, hydrogen atoms were added to the inner part of the enzyme and the energy of the structure was minimised keeping fixed the atoms of the main frame and using the MMFF94 molecular mechanics force field[34]. Out of 50 unique poses obtained, the 10 having the highest score on the base of the value assumed by the enthalpic contribution to the free energy of binding were retained. These poses were in turn rescored considering the estimation of the free energy of binding of the ligand, i.e. the sum of the electrostatic and dispersive interaction energy between the ligand and the target as well as the intramolecular energy of the ligand due to changes in its conformation. All the calculations were performed using MOE-Dock integrated into the MOE system of programs [MOE, Chemical Computing Group, release 2016.08].

Results and discussion

The synthesised compounds were evaluated for their potency in inhibiting the β1, β2 and β5 catalytic activities of the 20 S proteasome isolated from LCLs[31]. Specific fluorogenic substrates for each active site were employed: Suc-LLVY-AMC (for the ChT-L), Boc-LRR-AMC (for the T-L) and Z-LLE-AMC (for the PGPH). The proteasome was pretreated with increasing concentrations (0.1–100 μm) of the new naphthoquinone amino acid derivatives and MG132 as a reference inhibitor in an activity buffer. Substrates were then incubated with the proteasome at 37 °C for 30–180 min. Substrate degradation was evaluated in fluorescence units. The inhibitory activity of all compounds is expressed here as IC_{50}. From the data reported in Table 1, after 30 min of incubation, it can be observed that some of the naphthoquinone analogues present a significant biological response. The inhibition of the PGPH and ChT-L activities is remarkable for some of the derivatives. In particular, the inhibition of the β1 and β5 subunits is interesting for compounds **4**, **6**, **9** and **10** with IC_{50} values lower than 1 μm. Generally, the molecules bearing the ethylenediamine linker (**1–16**) displayed a quite good activity against post-acidic and chymotryptic sites of the proteasome and retain a detectable ($IC_{50} < 100$ μm) inhibition of the tryptic-like activity in the β2 subunit. The most effective β1 inhibitors of the subseries with the ethylenediamine spacer present leucine or phenylalanine, while for the β5 inhibition are favourable asparagine and phenylalanine.

Regarding the Nα substituents, the NBz group is slightly preferred as indicated by the analogue **10** which is the most potent inhibitor of the whole series. A similar structure-activity relationship profile is evident within the naphthoquinone amino acid derivatives bearing the butylendiaminic linker (**17–32**). Also in this subset, the inhibition is mainly directed to the catalytic cavity β1 and β5, while the answer against the tryptic activity is irrelevant. Generally, it can be speculated that the increase of the distance between the pharmacophoric unit and the aminoacidic residue at the P1 position is negative for the interaction with the catalytic pocket of the enzyme complex. Finally, analogues **33**–**48** are the least active of the whole series with only a mild inhibition of the β5 subsite for derivatives with leucine (i.e. **34**–**36**) and of the post-acidic activity (β1) for products having serine as the central residue (i.e. **46**–**48**). Clearly, the length and molecular rigidity of the cyclohexyldiamine bridge are not favourable for the interaction with the catalytic proteasome pockets.

Considering the fundamental role of the proteasome for cell viability and proliferation, we investigated the antiproliferative activities of five selected compounds (**4**, **6** and **9**–**11**) on MDA and A2780 tumour cells compared to the reference aldehydic inhibitor MG132[35]. The choice of analogues has been carried out in view of their ability to inhibit the chymotryptic subunit of the proteasome, directly related to the anti-cancer activity. The cells were treated with 10 or 100 μm concentrations of the selected naphthoquinone derivatives and MG132. After 3 d, cell proliferation was evaluated and, as shown in Figure 2(a and b), compounds **4**, **6** and **9** were shown to inhibit cell proliferation at levels slightly lower than the reference pseudotripeptide MG132 in both tumoural cell lines at

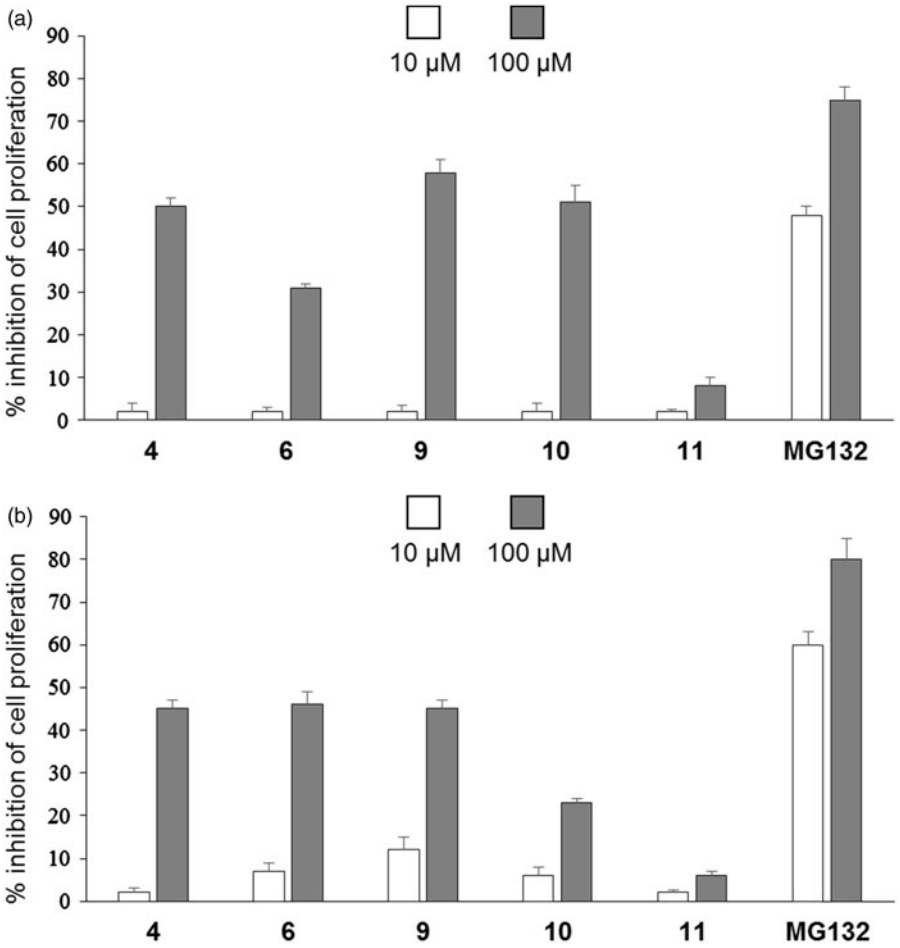

Figure 2. Effect of compounds **4**, **6**, **9**–**11** on cell proliferation. (a) MDA and (b) A2780 tumour cells cultured for 3 d in the presence or absence of the indicated concentrations of compounds. The means of three independent experiments performed in duplicate are shown.

100 μm. No significant antiproliferative activity was observed at 10 μm.

A general analysis of the structure-activity relationship of this new series of amino acidic derivatives suggests that the naphthoquinone pharmacophoric unit can function as potential electrophilic substrate for the proteasome N-terminal catalytic threonine. The strength of the interaction with the enzyme subsites depends on the molecular components that bind the naphthoquinonic group. The ethylenediamine binder between the amino acid residue and the pharmacophore was shown to be the most effective since increasing the alkyl chain with the insertion of the butylenediamine and making it more rigid with the cyclohexyldiamine, a progressive reduction of activity was observed. The biological response is more evident for phenylalanyl and asparagyl derivatives that display a significant preference for the chymotryptic and post-acidic proteasome subunits. In addition, the different Nα-aryl groups, with variable physicochemical characteristics, poorly influence the capacity of inhibition of the new compounds. It can reasonably be assumed that the inhibition is reversible by analysing the data obtained with the docking experiments that exclude a covalent bond between the inhibitor and the enzyme (see below). In addition, the enzymatic inhibition assays of catalytic subsites of the isolated enzyme confirm that the IC_{50} values for the naphthoquinone amino acid derivatives, progressively decrease during the time of incubation.

A computational docking study was performed for selected compounds (**10**, **16**, **26** and **42**) on the basis of their different molecular characteristics and biological profile. The results of the docking study of the most active molecule **10** to both β1 and β5 binding sites of 20 S proteasome seem to support the previous considerations. In the docking simulation to the β1 site, five poses (out of 10) having the highest docking scores are characterised by the presence of the naphthoquinonic moiety located ca. 3.5 Å away from the nucleophilic threonine residue. In view of the fact

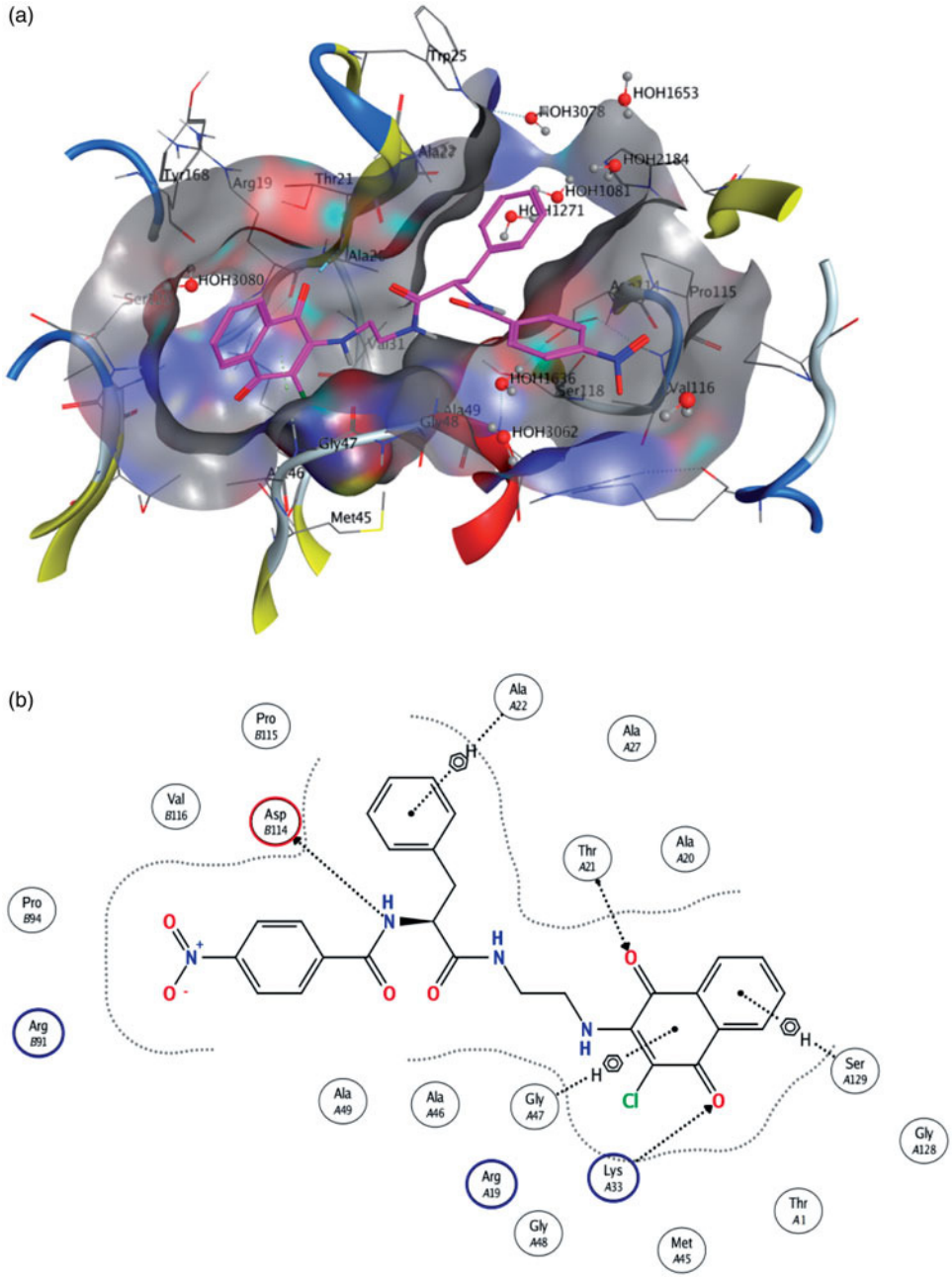

Figure 3. (a) Molecule **10** in the β1 active site (best pose). (b) Schematic view of the interactions between the receptor and the docked molecule.

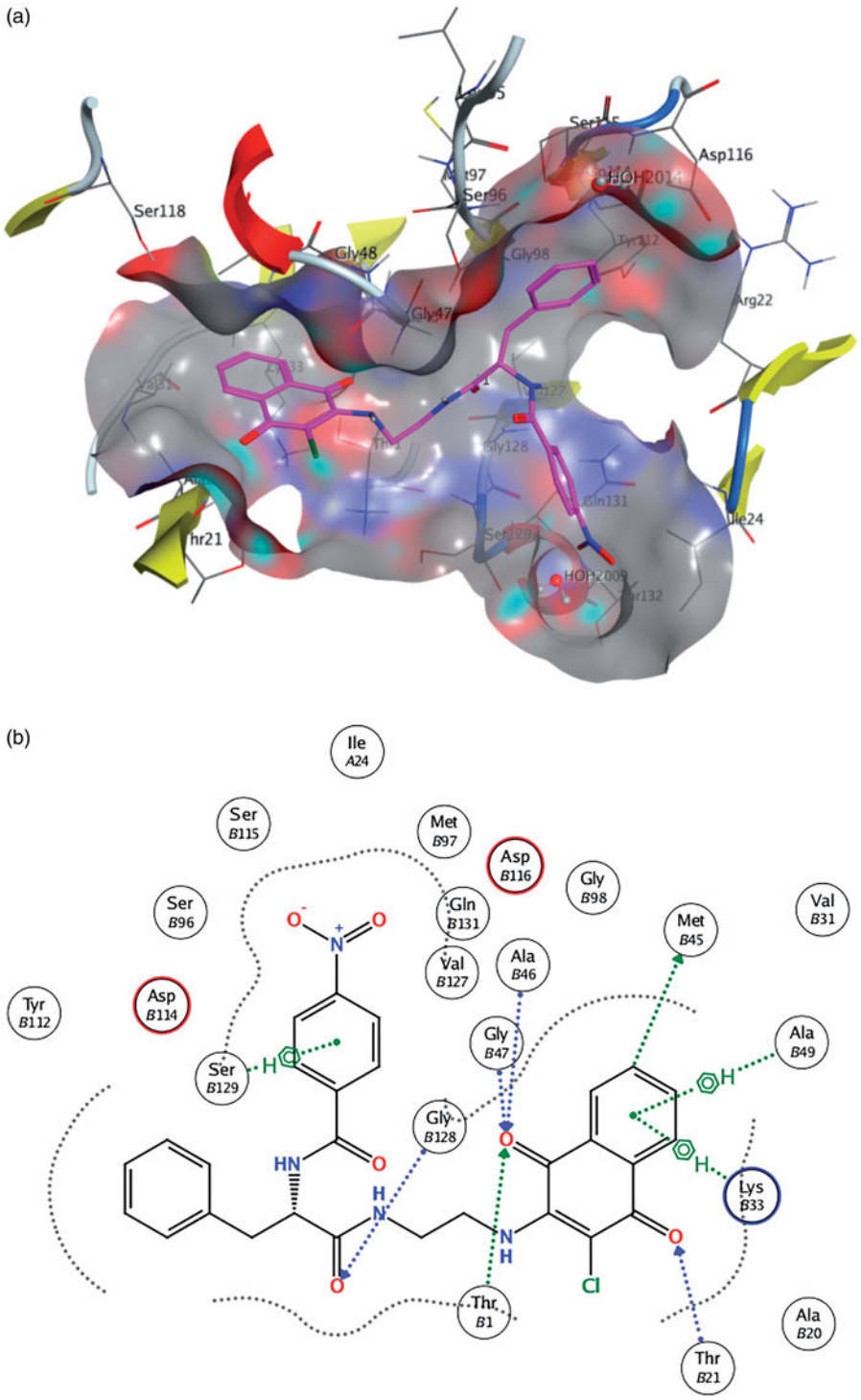

Figure 4. (a) Molecule **10** in the β5 active site. (b) Schematic view of the interactions between the receptor and the docked molecule.

that the protein frame is kept rigid during the simulation, such a distance is compatible with an H-bonding interaction. Molecule **10** docked to the enzyme and a scheme of the ligand-enzyme interactions are depicted in Figure 3(a and b), respectively. The ligand **10**-binding pocket presents a Y shape, that is appropriate to well fit the molecule conformation. Moreover, it is formed by a number of amino acid residues, i.e. Thr21, Ala20, Gli47, Lys33, Asp114, which are found to be involved in epoxomicin-enzyme interactions as well. Additionally, the aromatic rings seem to play an important role in "anchoring" the molecule inside the binding pocket through C-H … π short contacts (Figure 3(a)).

The same considerations can be drawn from the molecule **10** docked to the $\beta 5$ site. Indeed, the interactions with the binding-site residues (Figure 4) are even more significant: in this case, for instance, a direct tight interaction with the active threonine has been found, with a ligand-residue distance of some 2.8 Å. A number of additional short contacts can be observed between the functional groups of the ligand and the amino acids constituting the homobelactosin receptor, e.g. Ser129, Gly47, Lys33 and, just like the $\beta 1$ case, C-H … π interactions involving the ligand aromatic parts are established (Figure 4(b)).

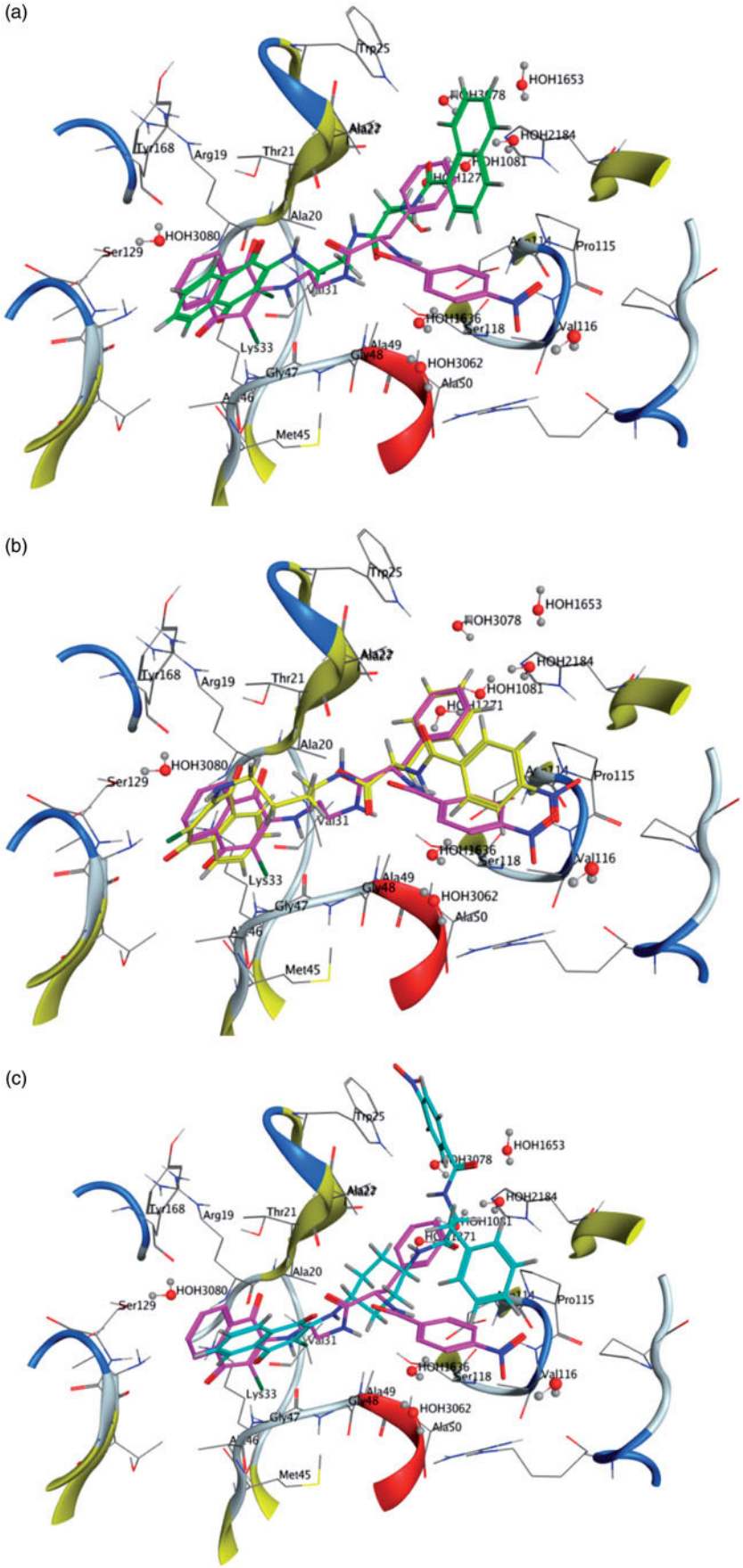

Figure 5. Molecule **16** (a), **26** (b) and **42** (c) docked into the β1 binding site. Molecule **10** docked in the same binding site is reported for comparison.

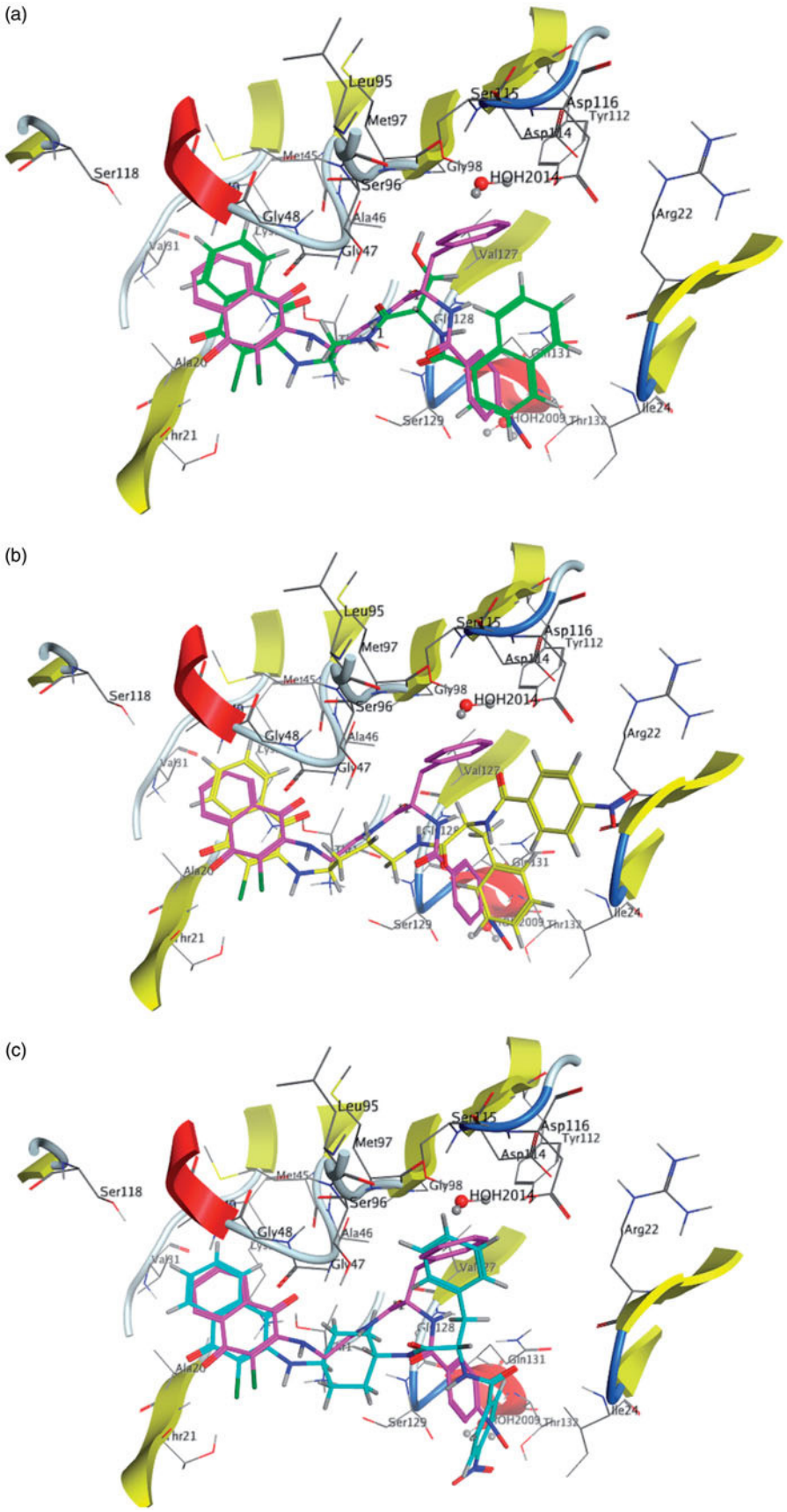

Figure 6. Molecule **16** (a), **26** (b) and **42** (c) docked into the β5 binding site. Molecule **10** docked in the same binding site is reported for comparison.

The different biological behaviour of molecules **16**, **26** and **42** can be rationalised by directly comparing their best-docked poses with **10** (Figures 5 and 6). The inactive molecule **16** does not fit in both the β1 and the β5 sites, the terminal naphthyl group being located in an area outside the binding pocket (Figures 5(a) and 6(a)). As for molecules **26** and **42**, they share with **10** the terminal parts (ClNafQ and NBz-Phe) but with linkers different in length (molecule **26**) or in flexibility (molecule **42**). As a consequence, **26** can achieve a not very strained conformation to accommodate itself into the receptor in a position close to **10,** due to the flexibility of the alkyl chain (Figures 5(b) and 6(b)); conversely, in **42** the presence of a rigid cyclohexane linker restricts the conformational adjustments adoptable by the molecule.

Conclusion

In summary, this work reports the design, synthesis and molecular modelling study of 48 amino acid derivatives assayed as inhibitors of three major catalytic activities of the proteasome. These compounds have at the Cα position of the aminoacidic residues a 2-chloronaftoquinone group pharmacophoric unit primary responsible for the interaction with the active subunits of the enzymatic complex. The same scaffold is present in non-peptidic molecules and pseudodipeptide derivatives previously reported as inhibitors of the 20 S proteasome. Data on the biological response of some analogues of this new series showed an interesting inhibition of the proteasome. Derivatives **4**, **6**, **9** and **10** were the most active against the β1 and β5 subunits, with a biological profile that makes them potentially capable of operating such as antineoplastic agents. The molecular structure of the new inhibitors allows further studies on the structure-activity relationships.

Disclosure statement

The authors declare no competing financial interest.

ORCID

Delia Preti http://orcid.org/0000-0002-1075-3781

References

1. Ciechanover A. Proteolysis: from the lysosome to ubiquitin and the proteasome. Nat Rev Mol Cell Biol 2005;6:79–87.
2. Inobe T, Matouschek A. Paradigms of protein degradation by the proteasome. Curr Opin Struct Biol 2014;24:156–64.
3. Finley D. Recognition and processing of ubiquitin-protein conjugates by the proteasome. Annu Rev Biochem 2009;78:477–513.
4. Ciechanover A. The ubiquitin-proteasome pathway: on protein death and cell life. EMBO J 1998;17:7151–60.
5. Groll M, Heinemeyer W, Jäger S, et al. The catalytic sites of 20S proteasomes and their role in subunit maturation: a mutational and crystallographic study. Proc Natl Acad Sci USA 1999;96:10976–83.
6. Borissenko L, Groll M. 20S proteasome and its inhibitors: crystallographic knowledge for drug development. Chem Rev 2007;107:687–717.
7. Kisselev AF, Goldberg AL. Proteasome inhibitors: from research tools to drug candidates. Chem Biol 2001;8:739–58.
8. Nazif T, Bogyo M. Global analysis of proteasomal substrate specificity using positional-scanning libraries of covalent inhibitors. Proc Natl Acad Sci USA 2001;98:2967–72.
9. Kisselev AF, van der Linden WA, Overkleeft HS. Proteasome inhibitors: an expanding army attacking a unique target. Chem Biol 2012;19:99–115.
10. Groll M, Huber R, Moroder L. The persisting challenge of selective and specific proteasome inhibition. J Pept Sci 2009;15:58–66.
11. Genin E, Reboud-Ravaux M, Vidal J. Proteasome inhibitors: recent advances and new perspectives in medicinal chemistry. Curr Top Med Chem 2010;10:232–56.
12. Micale N, Scarbaci K, Troiano V, et al. Peptide-based proteasome inhibitors in anticancer drug design. Med Res Rev 2014;34:1001–69.
13. Dorsey BD, Iqbal M, Chatterjee S, et al. Discovery of a potent, selective, and orally active proteasome inhibitor for the treatment of cancer. J Med Chem 2008;51:1068–72.
14. Mroczkiewicz M, Winkler K, Nowis D, et al. Studies of the synthesis of all stereoisomers of MG-132 proteasome inhibitors in the tumor targeting approach. J Med Chem 2010;53:1509–18.
15. Bazzaro M, Anchoori RK, Mudiam MK, et al. α,β-unsaturated carbonyl system of chalcone-based derivatives is responsible for broad inhibition of proteasomal activity and preferential killing of human papilloma virus (HPV) positive cervical cancer cells. J Med Chem 2011;54:449–56.
16. Desvergne A, Genin E, Maréchal X, et al. Dimerized linear mimics of a natural cyclopeptide (TMC-95A) are potent noncovalent inhibitors of the eukaryotic 20S proteasome. J Med Chem 2013;56:3367–78.
17. Moreau P, Richardson PG, Cavo M, et al. Proteasome inhibitors in multiple myeloma: 10 years later. Blood 2012;120:947–59.
18. Adams J. The development of proteasome inhibitors as anticancer drugs. Cancer Cell 2004;5:417–21.
19. Demo SD, Kirk CJ, Aujay MA, et al. Antitumor activity of PR-171, a novel irreversible inhibitor of the proteasome. Cancer Res 2007;67:6383–91.
20. Richardson PG, Baz R, Wang M, et al. Phase 1 study of twice-weekly ixazomib, an oral proteasome inhibitor, in relapsed/refractory multiple myeloma patients. Blood 2014;124:1038–46.
21. Zhou HJ, Aujay MA, Bennett MK, et al. Design and synthesis of an orally bioavailable and selective peptide epoxyketone proteasome inhibitor (PR-047). J Med Chem 2009;52:3028–38.
22. Marastoni M, Baldisserotto A, Canella A, et al. Arecoline tripeptide inhibitors of proteasome. J Med Chem 2004;47:1587–90.
23. Baldisserotto A, Ferretti V, Destro F, et al. Alpha, beta-unsaturated N-acylpyrrole peptidyl derivatives: new proteasome inhibitors. J Med Chem 2010;53:6511–15.
24. Franceschini C, Trapella C, Calia R, et al. C-terminal trans, trans-muconic acid ethyl ester partial retro-inverso pseudopeptides as proteasome inhibitors. J Enzyme Inhib Med Chem 2013;28:1034–9.
25. Scotti A, Trapella C, Ferretti V, et al. Studies of C-terminal naphthoquinone dipeptides as 20S proteasome inhibitors. J Enzyme Inhib Med Chem 2016;3:456–63.
26. Lawrence HR, Kazi A, Luo Y, et al. Synthesis and biological evaluation of naphthoquinone analogs as a novel class of proteasome inhibitors. Bioorg Med Chem 2010;18:5576–92.

27. Xu K, Xiao Z, Tang YB, et al. Design and synthesis of naphthoquinone derivatives as antiproliferative agents and 20S proteasome inhibitors. Bioorg Med Chem Lett 2012;22:2772–4.
28. Ge Y, Kazi A, Marsilio F, et al. Discovery and synthesis of hydronaphthoquinones as novel proteasome inhibitors. J Med Chem 2012;55:1978–98.
29. Chadwick J, Jones M, Mercer AE, et al. Design, synthesis and antimalarial/anticancer evaluation of spermidine linked artemisinin conjugates designed to exploit polyamine transporters in *Plasmodium falciparum* and HL-60 cancer cell lines. Bioorg Med Chem 2010;18:2586–97.
30. Yang H, Xiang J, Wang N, et al. Converse conformational control of smoothened activity by structurally related small molecules. J Biol Chem 2009;284:20876–84.
31. Gavioli R, Vertuani S, Masucci MG. Proteasome inhibitors reconstitute the presentation of cytotoxic T-cell epitopes in Epstein-Barr virus-associated tumors. Int J Cancer 2002;101:532–8.
32. Groll M, Kim KB, Kairies N, et al. Crystal structure of epoxomicin: 20S proteasome reveals a molecular basis for selectivity of α, β-epoxyketone proteasome inhibitor. J Am Chem Soc 2000;122:1237–8.
33. Groll M, Larionov OV, Huber R, de Meijere A. Inhibitor-binding mode of homobelactosin C to proteasomes: new insights into class I MHC ligand generation. Proc Natl Acad Sci USA 2006;103:4576–9.
34. Halgren TA. Merck molecular force field. I. Basis, form, scope, parameterization, and performance of MMFF94. J Comput Chem 1996;17:490–519.
35. Hansen MB, Nielsen SE, Berg K. Re-examination and further development of a precise and rapid dye method for measuring cell growth/cell kill. J Immunol Methods 1989;119:203–10.

DOI: 10.1002/hup.2560

WILEY

SPECIAL ISSUE ON NOVEL PSYCHOACTIVE SUBSTANCES

1-cyclohexyl-x-methoxybenzene derivatives, novel psychoactive substances seized on the internet market. Synthesis and in vivo pharmacological studies in mice

Anna Fantinati[3]* | Andrea Ossato[4]* | Sara Bianco[3] | Isabella Canazza[1,4] | Fabio De Giorgio[4] | Claudio Trapella[3] | Matteo Marti[1,2]

[1] Department of Life Sciences and Biotechnology (SVeB), University of Ferrara, Ferrara, Italy

[2] Center for Neuroscience and Istituto Nazionale di Neuroscienze, Ferrara, Italy

[3] Department of Chemistry and Pharmaceutical Sciences, University of Ferrara, Ferrara, Italy

[4] Institute of Public Health, Section of Legal Medicine, Catholic University of Rome, Rome, Italy

Correspondence
Marti Matteo, Department of Life Sciences and Biotechnology (SVeB), University of Ferrara, via Fossato di Mortara 17-19, 44121 Ferrara, Italy.
Email: m.marti@unife.it

Funding information
University of Ferrara, Presidency of the Council of Ministers, Drug Policies Department, Grant/Award Number: RBFR12LDOW.

Abstract

Introduction Among novel psychoactive substances notified to EMCDDA and Europol were 1-cyclohexyl-x-methoxybenzene stereoisomers (*ortho*, *meta*, and *para*). These substances share some structural characteristics with phencyclidine and tramadol. Nowadays, no information on the pharmacological and toxicological effects evoked by 1-cyclohexyl-x-methoxybenzene are reported. The aim of this study was to investigate the effect evoked by each one stereoisomer on visual stimulation, body temperature, acute thermal pain, and motor activity in mice.

Methods Mice were evaluated in behavioral tests carried out in a consecutive manner according to the following time scheme: observation of visual placing response, measures of core body temperature, determination of acute thermal pain, and stimulated motor activity.

Results All three stereoisomers dose-dependent inhibit visual placing response (rank order: *meta* > *ortho* > *para*), induce hyperthermia at lower and hypothermia at higher doses (*meta* > *ortho* > *para*) and cause analgesia to thermal stimuli (*para* > *meta* = *ortho*), while they do not alter motor activity.

Conclusions For the first time, this study demonstrates that systemic administration of 1-cyclohexyl-x-methoxybenzene compounds markedly inhibit visual response, promote analgesia, and induce core temperature alterations in mice. This data, although obtained in animal model, suggest their possible hazard for human health (i.e., hyperthermia and sensorimotor alterations). In particular, these novel psychoactive substances may have a negative impact in many daily activities, greatly increasing the risk factors for workplace accidents and traffic injuries.

KEYWORDS

1-cyclohexyl-x-methoxybenzene, behavior, body temperature, mice, Novel Psychoactive Substances, tail withdrawal

1 | INTRODUCTION

Over the past 5 years, there has been an unprecedented increase in the number, type, and availability of novel psychoactive substances (NPS) in Europe that are sold openly as "legal" replacements for illicit drugs. Continuing this trend, during 2015, a total of 100 new substances (i.e., cathinones, cannabinoids, phenethylamines, opioids, tryptamines, benzodiazepines, arylalkylamines, and other groups) were reported for the first time to the EU Early Warning System, bringing the total number of new substances monitored to more than 560, with more than 380 (70%) of these detected in the last 5 years alone and with two new substances detected every week (EMCDDA, 2016). With increased availability, harms have increased, such as acute, sometimes fatal, poisonings (Chiappini et al., 2015; Loi et al., 2015; Dines et al., 2015; Zawilska & Andrzejczak, 2015; Bersani et al., 2014;

*Equally contributed to the experimental work.

Abbreviations: ortho, 1-cyclohexyl-2-methoxybenzene; meta, 1-cyclohexyl-3-methoxybenzene; para, 1-cyclohexyl-4-methoxybenzene; NPS, Novel Psychoactive Substances; PCP, Phencyclidine

Schifano et al., 2005), harms associated with injecting drugs (Hope et al., 2016), and the possibility to develop psychiatric symptoms (Martinotti et al., 2014; Martinotti et al., 2015; Bersani et al., 2014). Beside acute toxicological effects, many NPS seem to have addictive properties (Miliano et al., 2016). In addition to the "classical" NPS, which are classified into known classes of compounds (i.e., cathinones, cannabinoids, phenethylamines, opioids, tryptamines, benzodiazepines, and dissociative anesthetics), law enforcements carry out seizures of compounds that are not classified into these groups of molecules and which are labeled as "other substances" (EMCDDA, 2016). In view of this grows the urgency to understand the pharmaco-toxicological effects of these "other substances" and getting to know their use among consumers. Among these NPS notified to the EMCDDA and Europol, for the first time in 2012 was 1-cyclohexyl-x-methoxybenzene, a molecule that shares some structural characteristics with phencyclidine (PCP) and tramadol although, lacking the amine functionality (Figure 1; EMCDDA, 2012). There has been growing clinical, public, and media awareness and concern about the availability and potential harmfulness of tramadol and PCP. The first one, tramadol, is an atypical, centrally acting synthetic analgesic used to treat moderate to severe pain, with antinociceptive effects that are mediated by a combination of mu opioid agonist effects and norepinephrine (NE) and serotonin reuptake inhibition (Lanier et al., 2010). On the other hand, PCP is a potent hallucinogenic drug, representing a synthetic arylcyclohexylamine originally developed as an anesthetic that acts as a glutamatergic N-methyl-D-aspartate antagonist and also showing cholinergic and monoaminergic activity (Kyzar et al., 2012). Both these drugs are abused (Simonsen et al., 2015; Baumeister, Tojo, and Tracy 2015; Awadalla & Salah-Eldin, 2016) and produced severe adverse effects, characterized by sensory changes, with dissociative, out-of-body feelings and distorted visual and auditory perceptions; cognitive changes, such as memory impairments, altered perception of time, and slowness; affective changes, although quite labile, varying between euphoric, anxious, apathetic, and irritable; unpredictable behavioural changes, potentially including aggression; and changes in consciousness. Moreover, there are considerable risks associated with use, including pulmonary oedema, cerebrovascular accidents, and cardiac arrest (Baumeister et al., 2015; Ryan & Isbister, 2015).

It is important to underline that the "street name" of 1-cyclohexyl-x-methoxybenzene has yet to be discovered. This is highly significant to the understanding of the potential impact of this substance on the market. In fact, there are numerous brand names that identified the NPS (Corazza et al., 2014).

1-cyclohexyl-x-methoxybenzene, seized in Austria by law enforcement as white powder form, has not been stereochemically analyzed, and therefore, it was not possible to know if the seized substance was a single isomer or a mixture of two or all three isomers (*ortho*, *meta* and *para*). This aspect is very important because the different replacements of methoxy group on the benzyl ring (i.e., *ortho*, *meta*, and *para*) may confer different pharmacological and toxicological properties to the molecule. In fact, as reported for other NPS (synthetic cannabinoids), the substitution of a hydroxyl group in ortho, meta, or para position on the benzene ring of the naphthoylindole structure determines a change in the pharmacodynamic properties and biological activity of compounds (Brents et al., 2012; Wiley, Marusich, and Huffman 2014). Nowadays, there is no information on the pharmaco-toxicological effects evoked by 1-cyclohexyl-x-methoxybenzene neither in animal studies and human reports from emergency rooms. Moreover, these NPS are not under legislative control in the world.

Therefore, in this study, the first step was to have synthesized pure and isolated 1-cyclohexyl-x-methoxybenzene derivatives (*ortho*, *meta*, and *para* isomers). Second, because there is an existence of three different isomers of 1-cyclohexyl-x-methoxybenzene, all three of these derivatives were studied to better understand the behavioral effects evoked by each one and their possible comparison. For this purpose, we used a selected battery of behavioral tests widely used in studies of "safety-pharmacology" for the preclinical characterization of new molecules in rodents (Irwin 1968; Mattsson, Spencer, and Albee 1996; Porsolt et al., 2002; Redfern et al., 2005; Hamdam et al., 2013; ICHS7A, 2001). From this behavioral test, we evaluated the acute effects of 1-cyclohexyl-x-methoxybenzene isomers (*ortho*, *meta*, and *para*) on sensorimotor responses to visual stimulation, body temperature, acute thermal analgesia, and motor activity in CD-1 male mice.

2 | MATERIAL AND METHODS

2.1 | Animals

Outbred albino male (CD-1®) mice, 25–30 g (Harlan Italy; S. Pietro al Natisone, Italy), were group-housed (8 to 10 mice per cage; floor area per animal was 80 cm^2; minimum enclosure height was 12 cm) on a 12:12-h light–dark cycle (light period from 6:30 AM to 6:30 PM), temperature of 20–22°C, humidity of 45–55% and were provided with ad libitum access to food (Diet 4RF25 GLP; Mucedola, Settimo Milanese, Milan, Italy) and water. The experimental protocols performed in thi study were in accordance with the U.K. Animals (Scientific Procedures) Act, 1986, and associated guidelines and the new European Communities Council Directive of September 2010 (2010/63/EU) a revision of the Directive 86/609/EEC. Moreover, experimental protocols were approved by Italian Ministry of Health and by the Ethical Committee of the University of Ferrara. Adequate measures were taken to minimize the number of animals used, their pain, and discomfort.

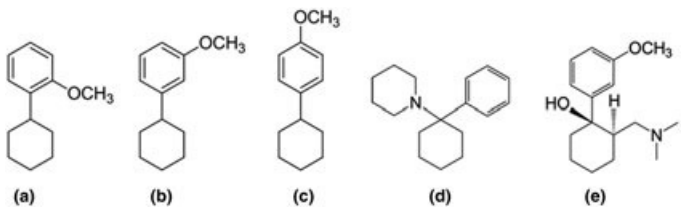

FIGURE 1 Chemical structures of (a) 1-cyclohexyl-2-methoxybenzene (*ortho*), (b) 1-cyclohexyl-3-methoxybenzene (*meta*), (c) 1-cyclohexyl-4-methoxybenzene (*para*), (d) phencyclidine and (e) tramadol

2.2 | Drug preparation and dose selection

1-cyclohexyl-x-methoxybenzene derivatives were synthesized (see Supplementary Materials) and purified (in the laboratory of Dott. Claudio Trapella) with a medium pressure system ISOLERA ONE (Biotage Sweden) and subsequently characterized by Agilent 6520 nano HPLC ESI-Q-TOF (Agilent Technologies) and a Varian 400 MHz NMR. Drugs were initially dissolved in absolute ethanol (final concentration was 2%) and Tween 80 (2%) and brought to the final volume with saline (0.9% NaCl). The solution made with ethanol, Tween 80, and saline was also used as the vehicle. Drugs were administered by intraperitoneal injection at a volume of 4 uL/g. The wide range of doses of 1-cyclohexyl-x-methoxybenzene derivatives tested (0.1–100 mg/kg i.p.) were chosen based on previous safety pharmacology studies on NPS (Vigolo et al., 2015; Ossato et al., 2015, 2016).

2.3 | Behavioral studies

The effect of 1-cyclohexyl-x-methoxybenzene derivatives were investigated using behavioral tests widely used in studies of "safety-pharmacology" for the preclinical characterization of new molecules in rodents (Irwin 1968; Mattsson et al., 1996; Porsolt et al., 2002; Redfern et al., 2005; Hamdam et al., 2013; ICH S7A, 2001). These tests have also been validated to describe effects of cannabinoids on the "tetrad" and sensorimotor changes in mice (Compton et al., 1992; Vigolo et al., 2015; Ossato et al., 2015, 2016).

Behavioral tests were conducted in a thermostated (temperature 20–22°C, humidity about 45–55%) and light controlled (about 150 lux) room in which there was a background noise of about 40 ± 4 dB. The mice were evaluated in functional observational behavioral tests carried out in a consecutive manner according to the following time scheme: observation of visual placing response, measures of core (rectal measurement) body temperature, determination of thermal (tail withdrawal) acute pain, and stimulated motor activity (accelerod test). All experiments were performed from 8:30 AM to 2:00 PM. Experiments were conducted blindly by trained observers working together in pairs (Redfern et al., 2005). The behavior of the mice (sensorimotor responses) were videotaped and analyzed off-line by a different trained operator that would give the test scores.

2.3.1 | Sensorimotor study. *Evaluation of the visual response*

The mice's visual responses were verified by *visual object response* test, which evaluated the ability of the animal to capture visual information even when the animals were stationary. This test was used to evaluate the ability of the mice to see an object approaching from the front (frontal view) or the side (lateral view), then inducing the animals to shift or turn the head, bring the forelimbs into the position of "defence" or retreat from it. For the frontal visual response, a white horizontal bar was moved frontally to the mouse heads and the manoeuvre was repeated three times. For the lateral visual response, a small dentist's mirror was moved into the mice's field of view in a horizontal arc, until the stimulus was between the mice's eyes. The procedure was conducted bilaterally (Ossato et al., 2015, 2016) and was repeated three times. The score assigned was a value of 1 if there was a reflection in the mouse movement, or 0 if not. The total value was calculated by adding the scores obtained in the frontal with that obtained in the lateral visual object responses (overall score 9). Evaluation of the visual object responces were measured at 0, 10, 30, 60, 120, 180, 240, and 300 min post injection. Each mouse was housed in an experimental chamber (350 × 350 × 350 [hr] mm), which was made with black methacrylate walls and a transparent front door. At the top and/or side of the box was placed a camera (B/W USB Camera day & night with varifocal lens; Ugo Basile, Italy). Before the experimental sessions, each mouse was placed in the box and was handled and trained for every other day (once a day) for a week (three days of training in total) in order to get used to the environment and to the experimenter (Ossato et al., 2016). To avoid mice olfactory cues, cages were carefully cleaned with a dilute (5%) ethanol solution and washed with water.

2.3.2 | Evaluation of core body temperature

To better assess the effects of the ligands on thermoregulation, we measured changes in the core (rectal) temperature. Rectal body temperature was used as an index of total body heat at various times during the experiment. The core temperature was evaluated by a probe (1 mm diameter) that was gently inserted, after lubrication with liquid vaseline, into the rectum of the mouse (to about 2 cm) and left in position until the stabilization of the temperature (about 10 s; Vigolo et al., 2015). The probe was connected to a Cole Parmer digital thermometer, model 8402. Stress was equalized to a normal routine clinical procedure. Core (rectal) mouse body temperatures were measured at 0, 30, 50, 85, 140, 200, 260, and 320 min post injection.

2.3.3 | Evaluation of pain induced by a thermal stimulus

Acute thermal nociception was evaluated using the tail withdrawal test (Vigolo et al., 2015). Mice were restrained in a dark plastic cylinder (3 cm long and 6.3 cm diameter) closed at the sides with plastic mesh, which allowed the mice to breathe normally. Then half of the tail was dipped in water of 48°C, and the latency (in seconds), or time, that the tail was left in water was recorded. A cut off (15 s) was set to avoid tissue damage. No signs of damage, burn or variation in mice's tail sensitivity were observed after the repetition of three consecutive tests at 48°C. Acute thermal nociception was measured at 35, 55, 90, 145, 205, 265, and 325 min post injection.

2.3.4 | Motor activity assessment

Alterations of motor activity induced by 1-cyclohexyl-x-methoxybenzene derivatives were evaluated using a behavioral test validated to specifically assess motor behavior (Marti et al., 2004, 2005; Vigolo et al., 2015; Ossato et al., 2016) in dynamic conditions (accelerod test).

The accelerod test measures different motor parameters such as motor coordination, locomotive ability (akinesia/bradykinesia), balance ability, muscular tone, and motivation to run. The animals were placed on a rotating cylinder that increases velocity automatically in a constant manner (0–60 rotations/min in 5 min). The time spent on the

cylinder was also measured. The accelerod test was performed at 0, 40, 60, 95, 150, 210, 270, and 330 min post injection.

2.4 | Data and statistical analysis

The data is expressed in arbitrary units (visual objects response), Δ°C (core temperature, as the difference between control temperature (before injection) and temperature following drug administration), Emax % (tail withdrawal test, calculated as percent of maximal possible effect {EMax% = [(test − control latency)/(cut off time − control)] × 100}) and percentage of basal (accelerod test). All of the numerical data is given as mean ± SEM. The data was analyzed by utilizing repeated measures ANOVA. Results from treatments showing significant overall changes were subjected to *post hoc* Tukey tests with significance for $p < 0.05$.

The statistical analysis of the effects of the individual substances in different concentrations over time was performed by two-way ANOVA followed by Bonferroni's test for multiple comparisons. The analysis of the total average effect induced by treatments (expressed in the panels d) was performed with one-way ANOVA followed by Tukey's test for multiple comparisons. The statistical analysis was performed with the program Prism software (GraphPad Prism, USA).

3 | RESULTS

3.1 | Behavioral studies

3.1.1 | Sensorimotor studies. *Evaluation of the visual object response*

Visual object response tended to be reduced in vehicle-treated mice over the 5 hr of observation (~20% of reduction at 300 min; Figure 2a–c), and the effect of which was similar to that observed in naïve untreated animals (data not shown). Systemic administration of 1-cyclohexyl-x-methoxybenzene derivatives (0.1–100 mg/kg i.p.) reduced in a dose dependent manner the visual object response in mice and the effect persisted up to 5 hr at higher doses (Figure 2a: significant effect of treatment [$F_{4,280} = 27.59$, $p < 0.0001$], time [$F_{7,280} = 15.53$, $p < 0.0001$], and time x treatment interaction [$F_{28,280} = 138.6$, $p < 0.0001$]. Figure 2b: significant effect of treatment ($F_{4,280} = 602.8$,

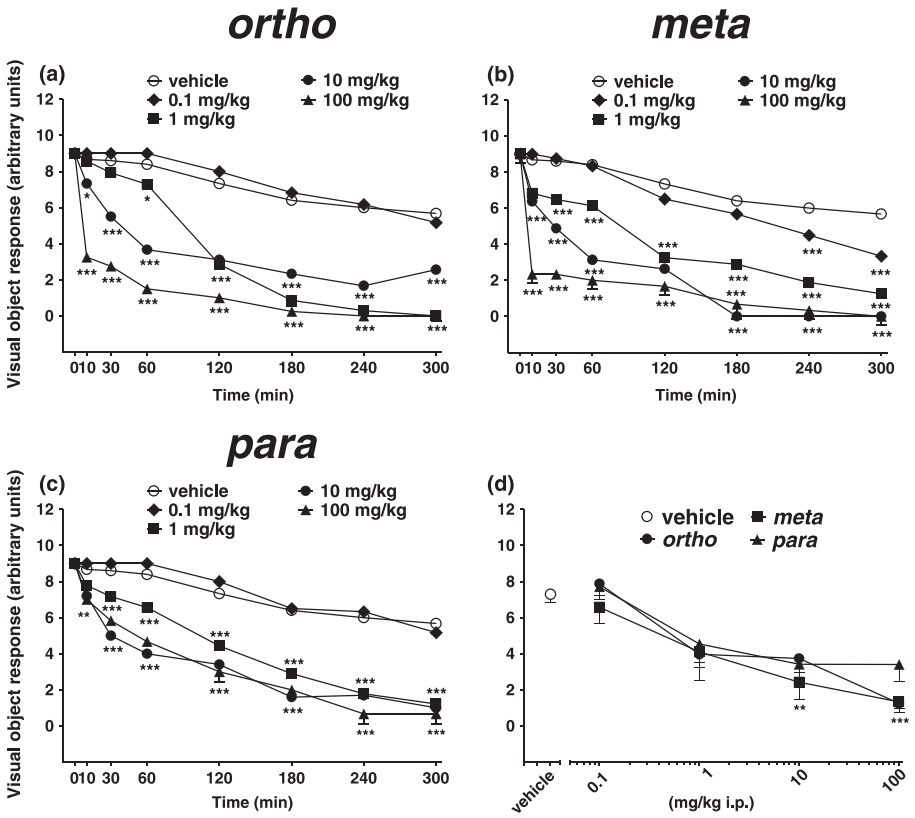

FIGURE 2 Effect of the systemic administration (0.1–100 mg/kg i.p.) of 1-cyclohexyl-2-methoxybenzene (*ortho*; a), 1-cyclohexyl-3-methoxybenzene (*meta*; b), and 1-cyclohexyl-4-methoxybenzene (*para*; c) on the visual object test in mice. Comparison of the total average effect observed in 5 hr (d). Data are expressed (see 2) as arbitrary units and represent the mean ± SEM of eitht determinations for each treatment. Statistical analysis was performed by two-way ANOVA followed by the Bonferroni's test for multiple comparisons for both the dose response curve of each compounds at different times (a–c), and the statistical analysis of the comparison of the total average effect of the compounds (d) was performed with one-way ANOVA followed by Tukey's test for multiple comparisons. (a) Significant effect of treatment ($F_{4,280} = 27.59$, $p < 0.0001$), time ($F_{7,280} = 15.53$, $p < 0.0001$), and time x treatment interaction ($F_{28,280} = 138.6$, $p < 0.0001$). (b) Significant effect of treatment ($F_{4,280} = 602.8$, $p < 0.0001$), time ($F_{7,280} = 416.4$, $p < 0.0001$) and time x treatment interaction ($F_{28,280} = 20.66$, $p < 0.0001$). (c) Significant effect of treatment ($F_{4,280} = 768.00$, $p < 0.0001$), time ($F_{7,280} = 734.2$, $p < 0.0001$), and time x treatment interaction ($F_{28,280} = 30.20$, $p < 0.0001$). (d) 1-cyclohexyl-x-methoxybenzene derivatives ($F_{12,103} = 7.221$, $p < 0.0001$). $^{*}p < 0.05$, $^{**}p < 0.01$, $^{***}p < 0.001$ versus vehicle

$p < 0.0001$), time [$F_{7,280} = 416.4$, $p < 0.0001$], and time x treatment interaction [$F_{28,280} = 20.66$, $p < 0.0001$]. Figure 2c: significant effect of treatment [$F_{4,280} = 768.00$, $p < 0.0001$], time [$F_{7,280} = 734.2$, $p < 0.0001$], and time x treatment interaction [$F_{28,280} = 30.20$, $p < 0.0001$]). Moreover, the effect induced by *ortho* and *meta* derivatives at 100 mg/kg seems to be earlier than that induced by 1-cyclohexyl-*para*-methoxybenzene at the same dose. The inhibitory effect caused by 1-cyclohexyl-*meta*-methoxybenzene appeared to be more potent than that induced by the other derivatives (Figure 2 d; [$F_{12,103} = 7.221$, $p < 0.0001$]).

3.1.2 | Evaluation of the core body temperature

The core temperature of mice tends to be reduced in vehicle-treated over the 5 hr of observation (~1°C of reduction at 300 min; Figure 3a–c), and the effect was similar to that observed in naïve untreated animals (data not shown). Systemic administration of 1-cyclohexyl-x-methoxybenzene derivatives (0.1–100 mg/kg i.p.) transiently alter the core temperature in mice.

Moreover, although para stereoisomer evoked only a transient moderate reduction in core temperature at 100 mg/kg (approximately −3°C at 30 min time point; Figure 3c; significant effect of treatment [$F_{4,245} = 38.94$, $p < 0.0001$], time [$F_{6,245} = 1.701$, $p = 0.1212$], and time x treatment interaction [$F_{24,245} = 1.374$, $p = 0.1195$]), ortho and meta derivatives induced a biphasic effect (Figure 3a: significant effect of treatment [$F_{4,245} = 21.258$, $p < 0.0001$], time [$F_{6,245} = 1.441$, $p = 0.1995$], and time x treatment interaction [$F_{24,245} = 1.205$, $p = 0.2375$]; and Figure 3b: significant effect of treatment [$F_{4,245} = 28.19$, $p < 0.0001$], time [$F_{6,245} = 0.8032$, $p = 0.5683$], and time x treatment interaction [$F_{24,245} = 0.5357$, $p = 0.9647$]).

In particular, injection of *ortho* and *meta* derivatives at low dose (0.1 mg/kg) induced a transient mild hyperthermia (~1°C at 30 min time point for both drugs; Figure 3a,b). Nevertheless, at the highest dose tested (100 mg/kg), 1-cyclohexyl-*ortho*-methoxybenzene evoked a mild hypothermia during the first 30 min after administration (approximately −1°C Figure 3a), and 1-cyclohexyl-*meta*-methoxybenzene induced a moderate hypothermia in the same time point (approximately −3°C at 30 min time point; Figure 3b).

3.1.3 | Evaluation of pain induced by a thermal stimulus

Systemic administration of 1-cyclohexyl-x-methoxybenzene derivatives (0.1–100 mg/kg i.p.) increased the threshold to acute thermal pain stimulus in mice in the tail withdrawal test ([Figure 4a: significant

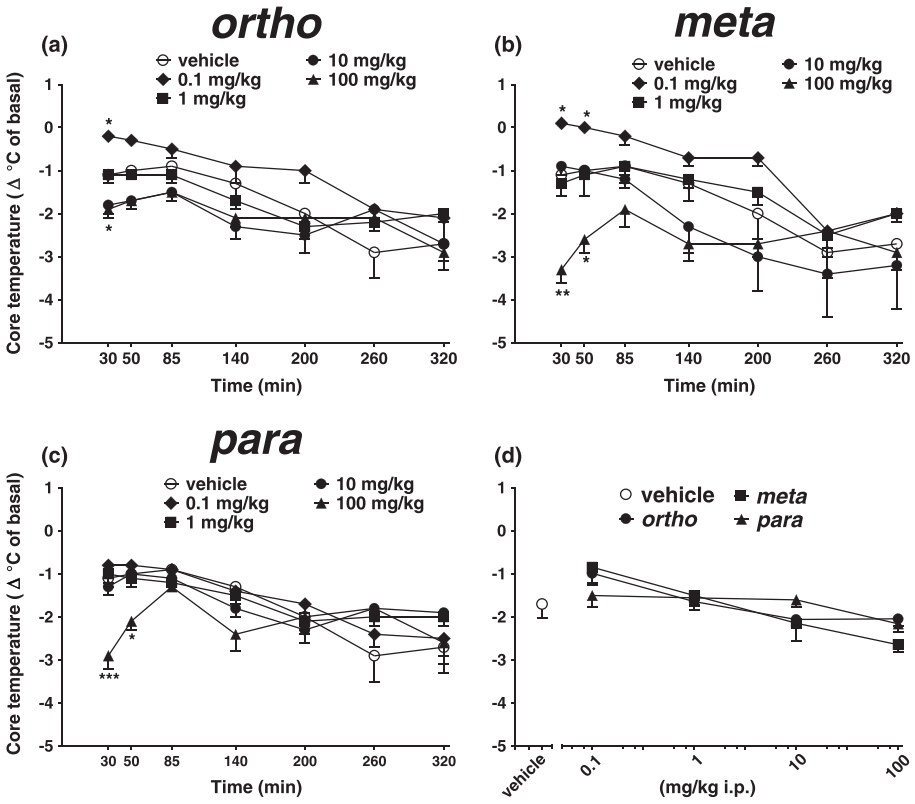

FIGURE 3 Effect of the systemic administration (0.1–100 mg/kg i.p.) of 1-cyclohexyl-2-methoxybenzene (*ortho*; a), 1-cyclohexyl-3-methoxybenzene (*meta*; b), and 1-cyclohexyl-4-methoxybenzene (*para*; c) on mouse core temperature. Comparison of the total average effect observed in 5 hr (d). Data are expressed as the difference between control temperature (before injection) and temperature following drug administration (Δ°C; see 2) and represent the mean ± SEM of eight determinations for each treatment. Statistical analysis was performed by two-way ANOVA followed by the Bonferroni's test for multiple comparisons for both the dose response curve of each compounds at different times (a–c), and the statistical analysis of the comparison of the total average effect of the compounds (d) was performed with one-way ANOVA followed by Tukey's test for multiple comparisons. (a) Significant effect of treatment ($F_{4,245} = 13.33$, $p < 0.0001$), time ($F_{6,245} = 15.25$, $p < 0.0001$), and time x treatment interaction ($F_{24,245} = 1.1$, $p = 0.3440$). (b) Significant effect of treatment ($F_{4,245} = 16.27$, $p < 0.0001$), time ($F_{6,245} = 11.67$, $p < 0.0001$), and time x treatment interaction ($F_{24,245} = 1.343$, $p = 0.1368$). (c) Significant effect of treatment ($F_{4,245} = 5.062$, $p = 0.0006$), time ($F_{6,245} = 12.56$, $p < 0.0001$), and time x treatment interaction ($F_{24,245} = 1.940$, $p = 0.0067$). (d) 1-cyclohexyl-x-methoxybenzene derivatives ($F_{12,103} = 3.723$, $p = 0.0001$). $^{**}p < 0.01$, $^{***}p < 0.001$ versus vehicle

effect of treatment [$F_{4,245}$ = 21.258, p < 0.0001], time [$F_{6,245}$ = 1.441, p = 0.1995], and time x treatment interaction [$F_{24,245}$ = 1.205, p = 0.2375]. Figure 4b: significant effect of treatment [$F_{4,245}$ = 28.19, p < 0.0001], time [$F_{6,245}$ = 0.8032, p = 0.5683], and time x treatment interaction [$F_{24,245}$ = 0.5357, p = 0.9647]. Figure 4c: significant effect of treatment [$F_{4,245}$ = 38.94, p < 0.0001], time [$F_{6,245}$ = 1.701, p = 0.1212], and time x treatment interaction [$F_{24,245}$ = 1.374, p = 0.1195]). In particular, administration of *ortho*, *meta*, and *para* derivatives at a dose of 10 mg/kg induced a long lasting analgesic effect up to the end of the experimental observation.

Furthermore, only *para* derivative at the higher dose (100 mg/kg) increased the threshold to acute thermal pain stimulus (Figure 4c: significant effect of treatment [$F_{4,245}$ = 38.94, p < 0.0001], time [$F_{6,245}$ = 1.701, p = 0.1212], and time x treatment interaction [$F_{24,245}$ = 1.374, p = 0.1195]), and the *ortho* and *meta* derivatives lose their analgesic activity (Figure 4d: 1-cyclohexyl-x-methoxybenzene derivatives [$F_{12,103}$ = 21.97, p < 0.0001]).

3.1.4 | Accelerod test

Systemic administration of 1-cyclohexyl-x-methoxybenzene derivatives (0.1–100 mg/kg i.p.) did not change the motor activity in the accelerod test in mice (Figure 5a: significant effect of treatment [$F_{4,280}$ = 6.781, p < 0.0001], time [$F_{7,280}$ = 0.1394, p = 0.9951], and time x treatment interaction [$F_{28,280}$ = 0.1639, p = 1.00]. Figure 5b: significant effect of treatment [$F_{4,280}$ = 6.075, p = 0.0001], time [$F_{7,280}$ = 0.1622, p = 0.9922], and time x treatment interaction [$F_{28,280}$ = 0.3637, p = 0.9989]. Figure 5c: significant effect of treatment [$F_{4,280}$ = 2.392, p = 0.0509], time [$F_{7,280}$ = 0.2697, p = 0.9653], and time x treatment interaction [$F_{28,280}$ = 0.4221, p = 0.9961]. Figure 5d: significant effect of 1-cyclohexyl-x-methoxybenzene derivatives [$F_{12,103}$ = 17.12, p < 0.0001]).

4 | DISCUSSION

For the first time, this study demonstrates that systemic administration of 1-cyclohexyl-x-methoxybenzene derivatives (*ortho*, *meta*, and *para*) impairs the visual sensorimotor response, the thermal analgesia and modulates core temperature without affecting motor performance on the accelerod test in CD-1 male mice. All three molecules are pharmacologically active with a similar profile of action that slightly differs on core temperature (Figure 3) and thermal pain (tail withdrawal test;

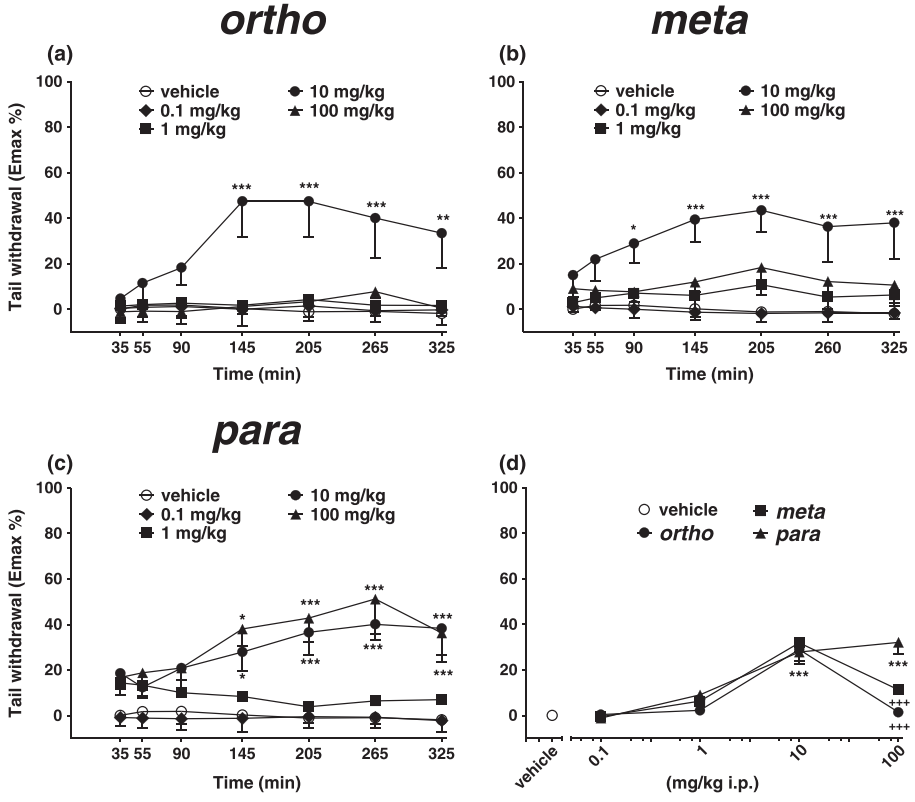

FIGURE 4 Effect of the systemic administration (0.1–100 mg/kg i.p.) of 1-cyclohexyl-2-methoxybenzene (*ortho*; a), 1-cyclohexyl-3-methoxybenzene (*meta*; b), and 1-cyclohexyl-4-methoxybenzene (*para*; c) on the tail withdrawal test of the mouse. Comparison of the total average effect observed in 5 hr (d). Data are expressed as percentage of maximum effect (see 2) and represent the mean ± SEM of eight determinations for each treatment. Statistical analysis was performed by two-way ANOVA followed by the Bonferroni's test for multiple comparisons for both the dose response curve of each compounds at different times (a–c), and the statistical analysis of the comparison of the total average effect of the compounds (d) was performed with one-way ANOVA followed by Tukey's test for multiple comparisons. (a) Significant effect of treatment ($F_{4,245}$ = 21.258, p < 0.0001), time ($F_{6,245}$ = 1.441, p = 0.1995), and time x treatment interaction ($F_{24,245}$ = 1.205, p = 0.2375). (b) Significant effect of treatment ($F_{4,245}$ = 28.19, p < 0.0001), time ($F_{6,245}$ = 0.8032, p = 0.5683), and time x treatment interaction ($F_{24,245}$ = 0.5357, p = 0.9647). (c) Significant effect of treatment ($F_{4,245}$ = 38.94, p < 0.0001), time ($F_{6,245}$ = 1.701, p = 0.1212), and time x treatment interaction ($F_{24,245}$ = 1.374, p = 0.1195). (d) 1-cyclohexyl-x-methoxybenzene derivatives ($F_{12,103}$ = 21.97, p < 0.0001). *p < 0.05, **p < 0.01, ***p < 0.001 versus vehicle; ++ +p < 0.001 versus 1-cyclohexyl-4-methoxybenzene

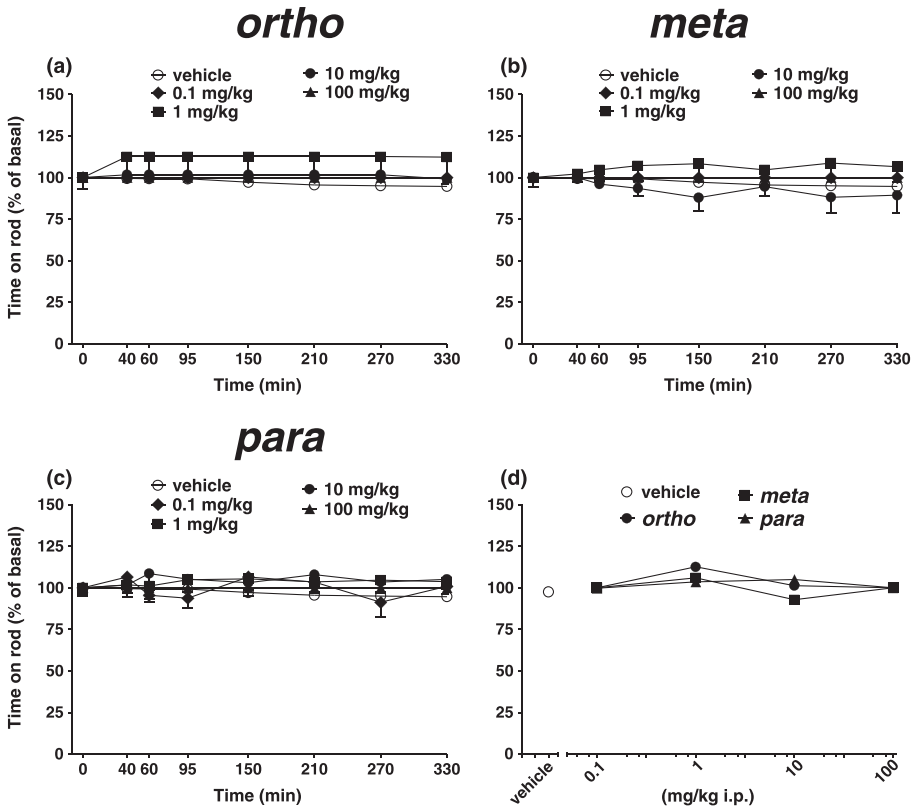

FIGURE 5 Effect of the systemic administration (0.1–100 mg/kg i.p.) of 1-cyclohexyl-2-methoxybenzene (*ortho*; a), 1-cyclohexyl-3-methoxybenzene (*meta*; b), and 1-cyclohexyl-4-methoxybenzene (*para*; c) on the accelerod test of the mouse. Comparison of the total average effect observed in 5 hr (d). Data are expressed (see 2) as percentage of baseline and represent the mean ± SEM of eight determinations for each treatment. Statistical analysis was performed by two-way ANOVA followed by the Bonferroni's test for multiple comparisons for both the dose response curve of each compounds at different times (a–c), and the statistical analysis of the comparison of the total average effect of the compounds (d) was performed with one-way ANOVA followed by Tukey's test for multiple comparisons. (a) Significant effect of treatment ($F_{4,280} = 6.781$, $p < 0.0001$), time ($F_{7,280} = 0.1394$, $p = 0.9951$), and time x treatment interaction ($F_{28,280} = 0.1639$, $p = 1.00$). (b) Significant effect of treatment ($F_{4,280} = 6.075$, $p = 0.0001$), time ($F_{7,280} = 0.1622$, $p = 0.9922$), and time x treatment interaction ($F_{28,280} = 0.3637$, $p = 0.9989$). (c) Significant effect of treatment ($F_{4,280} = 2.392$, $p = 0.0509$), time ($F_{7,280} = 0.2697$, $p = 0.9653$), and time x treatment interaction ($F_{28,280} = 0.4221$, $p = 0.9961$). (d) significant effect of 1-cyclohexyl-x-methoxybenzene derivatives ($F_{12,103} = 17.12$, $p < 0.0001$). ***$p < 0.001$ versus vehicle; °°°$p < 0.001$ versus 1-cyclohexyl-3-methoxybenzene; +++$p < 0.001$ versus 1-cyclohexyl-4-methoxybenzene

Figure 4) modulation probably due to their different substitution on the benzyl ring of the methoxylic group. In particular, systemic administration of 1-cyclohexyl-*ortho*-methoxybenzene and 1-cyclohexyl-*meta*-methoxybenzene evokes a mild core hyperthermia at the lower dose (0.1 mg/kg) and a transient hypothermia at the higher dose (100 mg/kg), and the *meta* derivate seems to be more effective than the *ortho* compound. Otherwise, the 1-cyclohexyl-*para*-methoxybenzene only induces transient hypothermia at the higher dose (100 mg/kg). In the tail withdrawal test, the *para* derivate sustained thermal analgesia up to 100 mg/kg dose, and the *ortho* and *meta* derivates were active at 10 mg/kg, but lose their activity at the higher dose (100 mg/kg).

These NPS were notified for the first time in 2012, and they share some structural characteristics with the "dissociative" anesthetic PCP and the analgesic drug tramadol (EMCDDA, 2012).

In particular, the dual modulation caused by *ortho* and *meta* derivatives on mice's body temperature, with low doses producing hyperthermia and higher doses resulting in hypothermia, resembles that induced by both systemic administration of PCP (Hiramatsu, Nabeshima, and Kameyama 1986) and opioid receptor agonists (Chen et al. 2005) in rodents. In fact, high doses of PCP (40 mg/kg) induced hypothermia, and low doses (5 and 10 mg/kg) evoked hyperthermia or had no effect on body temperature (Itoh et al., 1986; Hiramatsu et al., 1986; Bejanian, Pechnick, and George 1990) through a naloxone-dependent mechanism (Hiramatsu et al., 1986). Similarly, the administration of morphine to rats at doses of 4 to 15 mg/kg produces robust hyperthermia, but progressively higher doses induce hypothermia (Geller et al., 1983). Experiments using selective opioid receptor agonists and antagonists reveal that mu opioid receptor activation is responsible for the hyperthermic response to morphine whereas kappa and delta opioid receptor activation mediates the hypothermic effect of morphine (Rawls & Benamar, 2011). However, other mechanisms controlling the thermoregulation in rodents should be considered since the 1-cyclohexyl-x-methoxybenzene compounds resemble the molecular structures of tramadol (EMCDDA, 2012). This analgesic drug induces in humans a slightly hypothermic status by decreasing the precision of thermoregulatory control in addition to reducing the setpoint (De Witte et al., 1998). This effect is possibly due to its complex mechanism of action characterized by inhibition of the neuronal reuptake of

NE and 5-hydroxytryptamine (5-HT), facilitation of 5-HT release, and stimulation of mu opioid receptors (Raffa, 2006). Each of these mechanisms are likely to influence thermoregulatory control even if little experimental evidence is reported for tramadol. In particular, it has been reported that thermal homeostasis involves a balance between heat production and heat dissipation, and NPS affects both aspects of this homeostatic equation. In fact, administration of psychostimulants like MDMA increase cellular metabolic heat output and stress heat dissipation mechanisms with the onset of sweating delayed. This altered thermal regulation inducing acute hyperthermia can include rare fatalities in human (Parrott et al., 2012; Schifano et al., 2003).

Overall this evidence suggests that *ortho*, *meta*, and *para* derivatives could affect thermal homeostasis in mice possibly through opioid/NE/5-HT receptor mechanisms. Further studies using selective receptor antagonists will be undertaken to better investigate this hypothesis.

Moreover, systemic administration of 1-cyclohexyl-x-methoxybenzene derivatives significantly increases the threshold to acute thermal pain stimulus in mice at the 10 mg/kg dose (Emax ~40%). However, the *ortho* and *meta* isomers lose their analgesic activity at higher dose (100 mg/kg), and the *para* isomer was effective up to 100 mg/kg (Figure 4a–d). The analgesic profile induced by the 1-cyclohexyl-x-methoxybenzene derivates in mice (Figure 4) was similar to that evoked by tramadol in rats and mice (Raffa, 2006; Ozdogan, Lahdesmaki, and Scheinin 2006; Zhang et al., 2011; Aydin, Ek, and Temocin 2012). Because the analgesic actions of tramadol arise from agonist activity of the drug at the μ-opioid receptor and the blockade of serotonin and NE uptake (Raffa, 2006; Andurkar, Gendler, and Gulati 2012), we can hypothesize that these NPS had a similar mechanism of action with tramadol, but with different pharmacokinetic. However, PCP-like mechanisms should be considered also in the analgesic effect of 1-cyclohexyl-x-methoxybenzene derivatives. In fact, although the PCP does not possess an analgesic action to the thermal stimulus, it was reported that methyl substitution on *para* position of the phenyl ring of PCP structure generates a strong analgesic effect (Ahmadi et al., 2011).

It is interesting to note that 1-cyclohexyl-x-methoxybenzene derivatives did not impair Rotarod test performance (Figure 5) as well as tramadol (Ozdogan et al., 2006) but differently by PCP. In fact, PCP caused dose-dependent increases in locomotor activity, assessed in rodents as well as increases in horizontal locomotion, vertical movements such as rearing, and/or stereotypies (Benneyworth, Basu, and Coyle 2011).

Interestingly, these NPS (1-cyclohexyl-x-methoxybenzene derivatives) induced a deep dose-dependent impairment of visual sensorimotor responses in mice during a wide range of doses (0.1–100/kg) that did not cause catalepsy (data not shown), or reduced stimulated motor activity (accelerod test Figure 5). Therefore, these findings point out that effects induced by 1-cyclohexyl-x-methoxybenzene derivatives on visual responses do not result from a disruption of motor function as previously demonstrated also for synthetic cannabinoids (Ossato et al., 2015, 2016). These effects were observed at lower doses that did not affect others behavioral and physiological parameters, suggesting that these compounds primarily induce visual sensorimotor alterations, as caused by the hallucinogenic drug PCP (Morris & Wallach, 2014).

In fact, differently from tramadol, recent evidence show that administration of PCP impairs visual attention in rodents (Varvel et al., 2001; Stefani & Moghaddam, 2002; Terry et al., 2002; Jentsch & Anzivino, 2004), and decreases accuracy in a task designed to evaluate visual perceptual ability at lower doses, but not at the higher ones (Talpos et al., 2015).

5 | CONCLUSION

For the first time, this study reports the chemoselective synthesis of 1-cyclohexyl-x-methoxybenzene derivatives and their in vivo pharmacological effects in CD-1 male mice. This data reveals that these NPS markedly inhibit visual response, promote analgesia and cause core temperature alterations in mice showing a pharmaco-toxicological profile similar to that of PCP and tramadol and suggests their possible dangerousness potential for human health (i.e., hyperthermia and sensorimotor alterations). Although obtained in animal model, this data reinforces the hypothesis that these NPS may have a negative impact in many daily activities, greatly increasing the risk factors for workplace accidents and traffic injuries.

ACKNOWLEDGMENTS

This research has been funded by the Drug Policies Department, Presidency of the Council of Ministers, Italy (project NS-Drugs to M. Marti), by local funds from the University of Ferrara (FAR 2016 to M. Marti) and by FIRB 2012 from the Italian Ministry of the University (Grant no. RBFR12LDOW to F. De Giorgio). All applicable international, national, and/or institutional guidelines for the care and use of animals were followed. All procedures performed in the studies involving animals were in accordance with the ethical standards of the institution or practice at which the studies were conducted. We thank Dr. Justin Ellison for the proofreading.

CONFLICT OF INTEREST

The authors have no conflict of interest to declare.

REFERENCES

Ahmadi, A., Solati, J., Hajikhani, R., Pakzad, S. (2011). Synthesis and analgesic effects of new pyrrole derivatives of phencyclidine in mice. *Arzneimittel-Forschung*, *61*, 296–300.

Andurkar, S. V., Gendler, L., & Gulati, A. (2012). Tramadol antinociception is potentiated by clonidine through alpha(2)-adrenergic and I(2)-imidazoline but not by endothelin ET(A) receptors in mice. *European Journal of Pharmacology*, *683*, 109–115.

Awadalla, E. A., & Salah-Eldin, A. E. (2016). Molecular and histological changes in cerebral cortex and lung tissues under the effect of tramadol treatment. *Biomedicine & pharmacotherapy = Biomedecine & pharmacotherapie*, *82*, 269–280.

Aydin, O. N., Ek, R. O., Temocin, S., Ugur, B., Alacam, B., Sen, S. (2012). The antinociceptive effects of systemic administration of tramadol, gabapentin and their combination on mice model of acute pain. *Agri: Agri (Algoloji) Dernegi'nin Yayin organidir = The journal of the Turkish society of algology*, *24*, 49–55.

Baumeister, D., Tojo, L. M., & Tracy, D. K. (2015). Legal highs: Staying on top of the flood of novel psychoactive substances. *Therapeutic advances in psychopharmacology*, *5*, 97–132.

Bejanian, M., Pechnick, R. N., & George, R. (1990). Effects of acute and chronic administration of (+)-SKF 10,047 on body temperature in the rat: Cross-sensitization with phencyclidine. *The Journal of Pharmacology and Experimental Therapeutics*, *253*, 1253–1258.

Benneyworth, M. A., Basu, A. C., & Coyle, J. T. (2011). Discordant behavioral effects of psychotomimetic drugs in mice with altered NMDA receptor function. *Psychopharmacology*, *213*, 143–153.

Bersani, F. S., Corazza, O., Albano, G., Valeriani, G., Santacroce, R., Bolzan, Mariotti, Posocco, F. (2014). 25C-NBOMe: preliminary data on pharmacology, psychoactive effects, and toxicity of a new potent and dangerous hallucinogenic drug. *BioMed Research International*, *2014*, 734749.

Brents, L. K., Gallus-Zawada, A., Radominska-Pandya, A., Vasiljevik, T., Prisinzano, T. E., Fantegross, W. E., … Prather, P. L. (2012). Monohydroxylated metabolites of the K2 synthetic cannabinoid JWH-073 retain intermediate to high cannabinoid 1 receptor (CB1R) affinity and exhibit neutral antagonist to partial agonist activity. *Biochemical Pharmacology*, *83*, 952–961.

Chen, X., McClatchy, D. B., Geller, E. B., Tallarida, R. J., Adler, M. W. (2005). The dynamic relationship between mu and kappa opioid receptors in body temperature regulation. *Life Sciences*, *78*, 329–333.

Chiappini, S., Claridge, H., Corkery, J. M., Goodair, C., Loi, B., Schifano, F. (2015). Methoxetamine-related deaths in the UK: An overview. *Human Psychopharmacology*, *30*, 244–248.

Compton, D. R., Johnson, M. R., Melvin, L. S., Martin, B. R. (1992). Pharmacological profile of a series of bicyclic cannabinoid analogs: Classification as cannabimimetic agents. *The Journal of Pharmacology and Experimental Therapeutics*, *260*, 201–209.

Corazza, O., Valeriani, G., Bersani, F. S., Corkery, J., Martinotti, G., Bersani, G., Schifano, F. (2014). "Spice," "kryptonite," "black mamba": an overview of brand names and marketing strategies of novel psychoactive substances on the web. *Journal of Psychoactive Drugs*, *46*, 287–294.

De Witte, J. L., Kim, J. S., Sessler, D. I., Bastanmehr, H., Bjorksten, A. R. (1998). Tramadol reduces the sweating, vasoconstriction, and shivering thresholds. *Anesthesia and Analgesia*, *87*, 173–179.

Dines, A. M., Wood, D. M., Yates, C., Heyerdahl, F., Hovda, K. E., Giraudon, I. (2015). Acute recreational drug and new psychoactive substance toxicity in Europe: 12 months data collection from the European Drug Emergencies Network (Euro-DEN). *Clinical Toxicology (Philadelphia, Pa.)*, *53*, 893–900.

EMCDDA. 2012. New drugs in Europe, EMCDDA–Europol, annual report on the implementation of council decision 2005/387/JHA. 2012; http://www.emcdda.europa.eu/attachements.cfm/ att_212366_EN_ EMCDDA-Europol%202012%20Annual%20Report_final.pdf.

EMCDDA. 2016. EU drug markets report: In-depth analysis. EMCDDA–Europol joint publications, publications office of the European Union, Luxembourg. http://emcdda.europa.eu/system/files/publications/2373/TD0216072ENN.pdf.

Geller, E. B., Hawk, C., Keinath, S. H., Tallarida, R. J., Adler, M. W. (1983). Subclasses of opioids based on body temperature change in rats: acute subcutaneous administration. *The Journal of Pharmacology and Experimental Therapeutics*, *225*, 391–398.

Hamdam, J., Sethu, S., Smith, T., Alfirevic, A., Alhaidari, M., Atkinson, J., … Goldring, C. (2013). Safety pharmacology — Current and emerging concepts. *Toxicology and Applied Pharmacology*, *273*, 229–241.

Hiramatsu, M., Nabeshima, T., & Kameyama, T. (1986). Involvement of opioid receptors in hypo- and hyperthermic effects induced by phencyclidine in mice. *Journal of Pharmacobio-Dynamics*, *9*, 466–472.

Hope, V. D., Parry, J. V., Ncube, F., Hickman, M. (2016). Not in the vein: 'missed hits', subcutaneous and intramuscular injections and associated harms among people who inject psychoactive drugs in Bristol, United Kingdom. *The International Journal on Drug Policy*, *28*, 83–90.

ICH S7A. 2001. US Food and Drug Administration Guidance for industry: Safety pharmacology studies for human pharmaceuticals (S7 A). http://www.fda.gov/downloads/drugs/guidancecomplianceregulatoryinformation/guidances/ucm074959.pdf.

Irwin, S. (1968). Comprehensive observational assessment: Ia. A systematic, quantitative procedure for assessing the behavioral and physiologic state of the mouse. *Psychopharmacologia*, *13*, 222–257.

Itoh, Y., Oishi, R., Nishibori, M., Saeki, K. (1986). Comparison of effects of phencyclidine and methamphetamine on body temperature in mice: A possible role for histamine neurons in thermoregulation. *Naunyn-Schmiedeberg's Archives of Pharmacology*, *332*, 293–296.

Jentsch, J. D., & Anzivino, L. A. (2004). A low dose of the alpha2 agonist clonidine ameliorates the visual attention and spatial working memory deficits produced by phencyclidine administration to rats. *Psychopharmacology*, *175*, 76–83.

Kyzar, E. J., Collins, C., Gaikwad, S., Green, J., Roth, A., Monnig, L., … Kalueff, A. V. (2012). Effects of hallucinogenic agents mescaline and phencyclidine on zebrafish behavior and physiology. *Progress in Neuro-Psychopharmacology & Biological Psychiatry*, *37*, 194–202.

Lanier, R. K., Lofwall, M. R., Mintzer, M. Z., Bigelow, G. E., Strain, E. C. (2010). Physical dependence potential of daily tramadol dosing in humans. *Psychopharmacology*, *211*, 457–466.

Loi, B., Corkery, J. M., Claridge, H., Goodair, C., Chiappini, S., Gimeno Clemente, C., Schifano, F. (2015). Deaths of individuals aged 16–24 years in the UK after using mephedrone. *Human Psychopharmacology*, *30*, 225–232.

Marti, M., Mela, F., Fantin, M., Zucchini, S., Brown, J. M., Witta, J., … Morari, M. (2005). Blockade of nociceptin/orphanin FQ transmission attenuates symptoms and neurodegeneration associated with Parkinson's disease. *The Journal of Neuroscience*, *25*, 9591–9601.

Marti, M., Mela, F., Veronesi, C., Guerrini, R., Salvadori, S., Federici, M., … Morari, M. (2004). Blockade of nociceptin/orphanin FQ receptor signaling in rat substantia nigra pars reticulata stimulates nigrostriatal dopaminergic transmission and motor behavior. *The Journal of neuroscience: The official journal of the society for neuroscience*, *24*, 6659–6666.

Martinotti, G., Lupi, M., Acciavatti, T., Cinosi, E., Santacroce, R., Signorelli, M. S., … Di Giannantonio, M. (2014). Novel psychoactive substances in young adults with and without psychiatric comorbidities. *BioMed Research International*, *2014*, 815424.

Martinotti, G., Lupi, M., Carlucci, L., Cinosi, E., Santacroce, R., Acciavatti, T., … Di Giannantonio, M. (2015). Novel psychoactive substances: use and knowledge among adolescents and young adults in urban and rural areas. *Human Psychopharmacology*, *30*, 295–301.

Mattsson, J. L., Spencer, P. J., & Albee, R. R. (1996). A performance standard for clinical and functional observational battery examinations of rats. *International Journal of Toxicology*, *15*, 239–254.

Miliano, C., Serpelloni, G., Rimondo, C., Mereu, M., Marti, M., De Luca, M. A. (2016). Neuropharmacology of new psychoactive substances (NPS): Focus on the rewarding and reinforcing properties of cannabimimetics and amphetamine-like stimulants. *Frontiers in Neuroscience*, *10*, 153.

Morris, H., & Wallach, J. (2014). From PCP to MXE: A comprehensive review of the non-medical use of dissociative drugs. *Drug Testing and Analysis*, *6*, 614–632.

Ossato, A., Canazza, I., Trapella, C., Vincenzi, C., De Luca, M. A., Rimondo, C., … Marti, M. (2016). Effect of JWH-250, JWH-073 and their interaction on "tetrad", sensorimotor, neurological and neurochemical responses in mice. *Progress in Neuro-Psychopharmacology & Biological Psychiatry*, *67*, 31–50.

Ossato, A., Vigolo, A., Trapella, C., Seri, C., Rimondo, C., Serpelloni, G., Marti, M. (2015). JWH-018 impairs sensorimotor functions in mice. *Neuroscience*, *300*, 174–188.

Ozdogan, U. K., Lahdesmaki, J., & Scheinin, M. (2006). The analgesic efficacy of partial opioid agonists is increased in mice with targeted inactivation of the alpha2A-adrenoceptor gene. *European Journal of Pharmacology*, *529*, 105–113.

Parrott, A. C. (2012). MDMA and temperature: A review of the thermal effects of 'Ecstasy' in humans. *Drug and Alcohol Dependence*, *121*, 1–9.

Porsolt, R. D., Lemaire, M., Dürmüller, N., Roux, S. (2002). New perspectives in CNS safety pharmacology. *Fundamental & Clinical Pharmacology*, *16*, 197–207.

Raffa, R. (2006). Pharmacological aspects of successful long-term analgesia. *Clinical Rheumatology*, *25*(Suppl 1), 9–15.

Rawls, S. M., & Benamar, K. (2011). Effects of opioids, cannabinoids, and vanilloids on body temperature. *Frontiers in Bioscience (Scholar Edition)*, *3*, 822–845.

Redfern, W. S., Strang, I., Storey, S., Heys, C., Barnard, C., Lawton, K., … Valentin, J-P. (2005). Spectrum of effects detected in the rat functional observational battery following oral administration of non-CNS targeted compounds. *Journal of Pharmacological and Toxicological Methods*, *52*, 77–82.

Ryan, N. M., & Isbister, G. K. (2015). Tramadol overdose causes seizures and respiratory depression but serotonin toxicity appears unlikely. *Clinical Toxicology (Philadelphia, Pa.)*, *53*, 545–550.

Schifano, F., Deluca, P., Agosti, L., Martinotti, G., Corkery, J. M., Alex, B. (2005). New trends in the cyber and street market of recreational drugs? The case of 2C-T-7 ('Blue Mystic'). *Journal of psychopharmacology (Oxford, England)*, *19*, 675–679.

Schifano, F., Oyefeso, A., Corkery, J., Cobain, K., Jambert-Gray, R., Martinotti, G., Ghodse, A. H. (2003). Death rates from ecstasy (MDMA, MDA) and polydrug use in England and Wales 1996-2002. *Human Psychopharmacology*, *18*, 519–524.

Simonsen, K. W., Christoffersen, D. J., Banner, J., Linnet, K., Andersen, L. V. (2015). Fatal poisoning among patients with drug addiction. *Danish Medical Journal*, *62*, A5147.

Stefani, M. R., & Moghaddam, B. (2002). Effects of repeated treatment with amphetamine or phencyclidine on working memory in the rat. *Behavioural Brain Research*, *134*, 267–274.

Talpos, J. C., Riordan, J., Olley, J., Waddell, J., Steckler, T. (2015). Opposing effects of glutamatergic and GABAergic pharmacological manipulations on a visual perception task with relevance to schizophrenia. *Psychopharmacology*, *232*, 3967–3976.

Terry, A. V. Jr., Risbrough, V. B., Buccafusco, J. J., Menzaghi, F. (2002). Effects of (+/−)-4-[[2-(1-methyl-2-pyrrolidinyl)ethyl]thio]phenol hydrochloride (SIB-1553 A), a selective ligand for nicotinic acetylcholine receptors, in tests of visual attention and distractibility in rats and monkeys. *The Journal of Pharmacology and Experimental Therapeutics*, *301*, 284–292.

Varvel, S. A., Hamm, R. J., Martin, B. R., Lichtman, A. H. (2001). Differential effects of delta 9-THC on spatial reference and working memory in mice. *Psychopharmacology*, *157*, 142–150.

Vigolo, A., Ossato, A., Trapella, C., Vincenzi, F., Rimondo, C., Seri, C., … Marti, M. (2015). Novel halogenated derivates of JWH-018: Behavioral and binding studies in mice. *Neuropharmacology*, *95*, 68–82.

Wiley, J. L., Marusich, J. A., & Huffman, J. W. (2014). Moving around the molecule: relationship between chemical structure and in vivo activity of synthetic cannabinoids. *Life Sciences*, *97*, 55–63.

Zawilska, J. B., & Andrzejczak, D. (2015). Next generation of novel psychoactive substances on the horizon - A complex problem to face. *Drug and Alcohol Dependence*, *157*, 1–17.

Zhang, Y., Du, L., Pan, H., Li, L., Su, X. (2011). Enhanced analgesic effects of propacetamol and tramadol combination in rats and mice. *Biological & Pharmaceutical Bulletin*, *34*, 349–353.

SUPPORTING INFORMATION

Additional Supporting Information may be found online in the supporting information tab for this article.

How to cite this article: Fantinati A, Ossato A, Bianco S, et al. 1-cyclohexyl-x-methoxybenzene derivatives, novel psychoactive substances seized on the internet market. Synthesis and in vivo pharmacological studies in mice. *Hum Psychopharmacol Clin Exp*. 2017;32:e2560. https://doi.org/10.1002/hup.2560

Journal of Medicinal Chemistry

Article

pubs.acs.org/jmc

Design, Synthesis, and Biological Characterization of Novel Mitochondria Targeted Dichloroacetate-Loaded Compounds with Antileukemic Activity

Claudio Trapella,[*,†,⊥] Rebecca Voltan,[‡,⊥] Elisabetta Melloni,[‡] Veronica Tisato,[‡] Claudio Celeghini,[§] Sara Bianco,[†] Anna Fantinati,[†] Severo Salvadori,[†] Remo Guerrini,[†] Paola Secchiero,[‡] and Giorgio Zauli[*,∥]

[†]Department of Chemical and Pharmaceutical Sciences and LTTA Centre, University of Ferrara, Via Fossato di Mortara 17, 44121 Ferrara, Italy

[‡]Department of Morphology, Surgery, Experimental Medicine and LTTA Centre, University of Ferrara, 44121 Ferrara, Italy

[§]Department of Life Sciences, University of Trieste, 34128 Trieste, Italy

[∥]Institute for Maternal and Child Health, IRCCS "Burlo Garofolo", Via dell'Istria 65/1, 34137 Trieste, Italy

Supporting Information

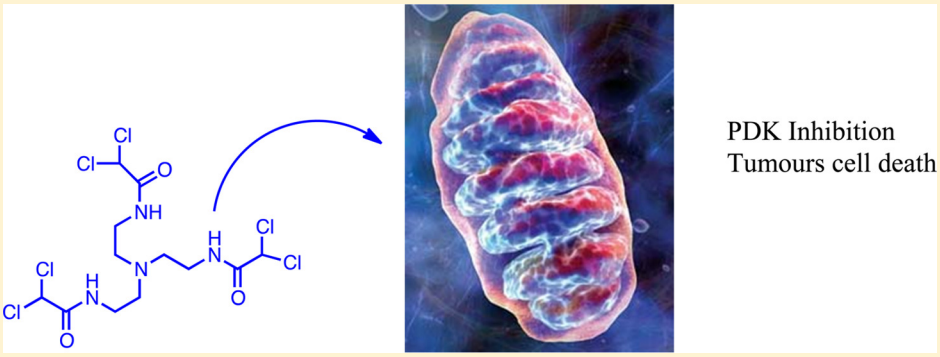

ABSTRACT: The mitochondrial kinase inhibitor dichloroacetate (DCA) has recently received attention in oncology due to its ability to target glycolysis. However, DCA molecule exhibits poor bioavailability and cellular uptake with limited ability to reach its target mitochondria. To overcome these biases, we have synthesized novel DCA-loaded compounds. The selection of the most promising therapeutic molecule was evaluated by combining in vitro assays, to test the antitumoral potential on leukemic cells, and a preliminary characterization of the molecule stability in vivo, in mice. Among the newly synthesized compounds, we have selected the multiple DCA-loaded compound **10**, characterized by a tertiary amine scaffold, because it exhibited enhanced (>30-fold) in vitro antitumor activity with respect to DCA and increased in vivo stability. On the basis of these results, we believe that compound **10** should be considered for further preclinical evaluations for the treatment of cancers and/or other diseases characterized by altered metabolic origin.

INTRODUCTION

Dichloroacetic acid and in particular dichloroacetate (DCA) is an inhibitor of mitochondrial pyruvate dehydrogenase kinase (PDK) that down-regulates the activity of pyruvate dehydrogenase (PDH), controlling the switch between oxidative phosphorylation and glycolysis. Besides the use for the chronic treatment of lactic acidosis,[1] in more recent years DCA has gained increased attention for the treatment of cancers for its ability to target altered metabolism that makes cancer cells resistant to death by normal apoptotic processes.[2−5] In this field, several works have demonstrated DCA activity against tumor cells of different origin in preclinical settings, using monotreatments or combinational treatments.[6,7] The data reported in literature addressed the activity of DCA against solid tumors, in particular human breast and colorectal carcinoma and neuroblastoma,[8−10] and against hematological neoplasia,[11−13] suggesting DCA as a promising molecule to halt tumor development and/or, when used in combination, to overcome resistance to conventional chemo- or radiotherapy.[14,15]

Nevertheless, there are major issues associated with clinical use of DCA for cancer treatment which are principally related to its low stability in the biological environment and to the low permeability of the cellular membrane to DCA molecule, which translates into high dosages required to reach therapeutic efficacy and clinical results.[6,7,15,16] As a matter of fact, DCA is unable to cross the cell membrane through passive diffusion due to its anionic charge. Moreover, the classical mitochondrial pyruvate carrier (MPC)[17] does not work for dissociated acid

Received: July 24, 2015
Published: December 11, 2015

DOI: 10.1021/acs.jmedchem.5b01165
J. Med. Chem. 2016, 59, 147−156

Scheme 1[a]

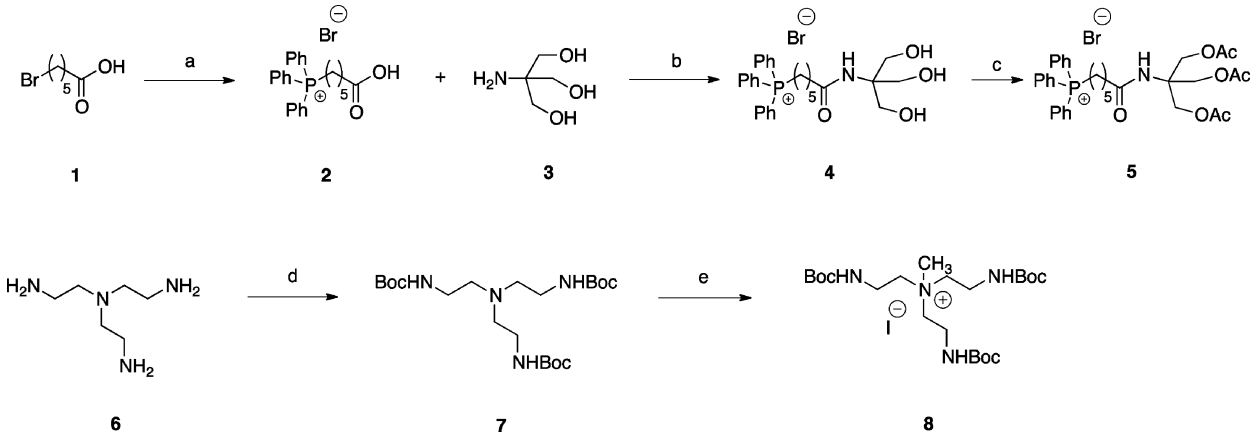

[a]Conditions: (a) CH_3CN, TPP, reflux, 24 h, Y = quant; (b) EtOH, EEDQ, 50 °C, 12 h, Y = 60%; (c) DCM, AcCl, rt, 4 h, Y = quant; d) water/dioxane 1/2, NaOH, BOC_2O, rt, 12 h, Y = 96%; (e) CH_3CN, CH_3I, 60 °C, 12 h, Y = quant.

but only for the carboxylic form, and in addition, the plasma protein SLC5A8, which can mediate DCA entry into cells, is down-regulated in several cancer types.[18] On the basis of these reasons, there is increasing interest for the develop of new strategies aimed to engineer DCA analogues able to cross the cellular membranes, thus facilitating the cellular uptake and entry of DCA into mitochondria of cancer cells, characterized by a $\Delta\psi_m$ higher than normal cells.

To overcome the drawbacks (e.g., problems of solubility, cellular uptake, biological availability, and stability) of DCA and/or the DCA analogues recently described,[19] which hamper the translation of this molecule to clinic, in this work we envisioned the design and synthesis of novel compounds backboned with ammonium salts and/or tertiary amine scaffolds. The ability of these scaffolds to carry DCA into mitochondrial matrix, and thus to access to the PDK protein, has been assessed in vitro on leukemic cell models as well as in in vivo settings, with the final intent to select a new molecule with enhanced antitumoral efficacy and improved potential clinical applications with respect to primitive DCA.

RESULTS

Design and Synthesis of the Mitochondria Backbone Carriers. Different strategies have been previously applied for the design and synthesis of mitochondria targeting molecules, such as phosphonium salt,[20] guanidine moiety,[21,22] or poly-amine structures.[23] In this work, besides the phosphonium salt,[19] we adopted a classical ammonium salt and tertiary amine with the aim to generate soluble, noncytotoxic, and stable carriers specifically designed for the targeted delivery of DCA to the mitochondria. As depicted in Scheme 1, commercially available 6-bromohexanoic acid **1** was reacted with triphenyl-phosphine in acetonitrile at reflux to obtain the corresponding phosphonium salt, compound **2**. The latter was reacted with 2-amino-2-(hydroxymethyl)propane-1,3-diol **3** in the presence of EEDQ in ethanol at 50 °C to yield amide compound **4** in 60% yield. Compound **4** was acetylated using acetyl chloride (AcCl) in DCM to obtain the first targeting mitochondria compound **5** in quantitative yield. The second targeting mitochondria carrier was obtained by protection of primary amine functions of tris(2-aminoethyl)amine compound **6** with di-*tert*-butyl carbonate in a mixture of water, dioxane, and sodium hydroxide to obtain the fully protected derivative compound **7** in quantitative yield. Compound **7** was methylated in acetonitrile using methyl iodide as an acylating agent to obtain the third targeting compound **8** in quantitative yield.

As first comparative analysis, we tested the cytotoxicity of the backbone carriers, compounds **5**, **7**, and **8**, by using a panel of leukemic cell line cultures (JVM-2, MAVER, MEC-1, MEC-2, and HL-60) exposed to the different compounds, used in a range of concentrations from 3 to 300 μM. As shown in Figure 1, after 48 h of treatment, while a significant reduction in cell viability was observed with the carrier **5** starting at the concentration of 30 μM, no significant toxicity was observed for both carriers **7** and **8** at any of the concentrations assessed. Similar results were observed in all the leukemic cell lines employed.

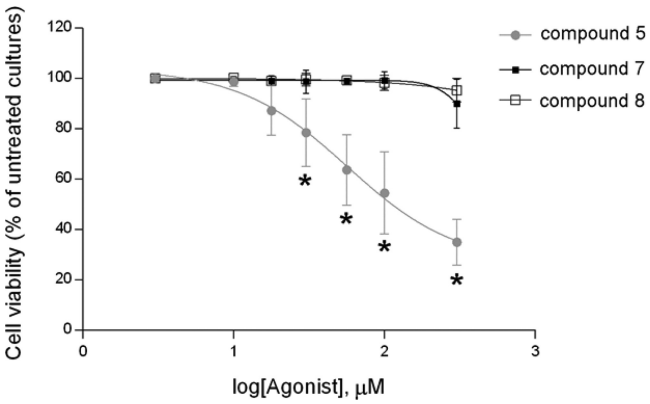

Figure 1. Assessment of the potential cytotoxicity of backbone carriers. Different leukemic cell lines (n = 5) were exposed at growing concentrations (range: 3–300 μM) for 48 h to the indicated scaffold molecules before analysis of cell viability. Cell viability was calculated as percentage with respect to untreated cultures set to 100%. Data are reported as the mean ± SD of results from three independent experiments performed in all cell lines. The asterisk indicates $p < 0.05$ with respect to the untreated cultures.

Conjugation of Carriers with Dichloroacetate Molecules. After the chemical strategy to obtain the carriers moieties was validated, the backbone compounds were conjugated with DCA to obtain the corresponding DCA analogues. For this purpose, as represented in Scheme 2,

DOI: 10.1021/acs.jmedchem.5b01165
J. Med. Chem. 2016, 59, 147–156

Scheme 2[a]

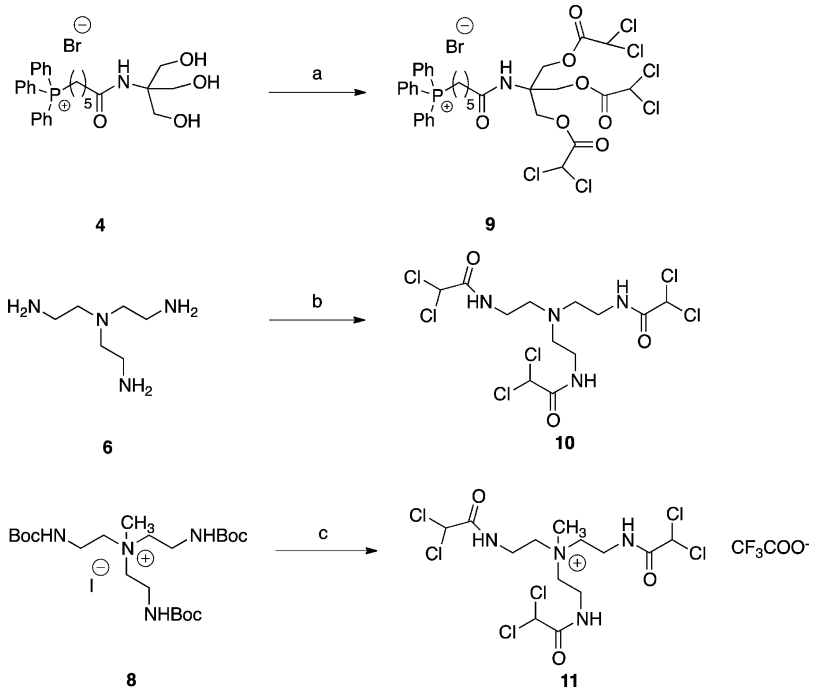

[a]Conditions: (a) DCM, $Cl_2CHC{=}OCl$, rt, 2 h, Y = 92%; (b) DCM/NaOH 2 N, $Cl_2CHC{=}OCl$, rt, 2 h, Y = 20%; (c) (1) DCM, TFA, rt, 12 h; (2) DCM/NaOH 2 N, $Cl_2CHC{=}OCl$, rt, overnight, Y = 50%.

dichloroacetyl chloride was reacted with compound **4** in DCM at room temperature to obtain the corresponding acylated product **9** in high yield (92%) and purity (>95%) in a single step, corresponding to the Mito-DCA molecule.[19] In parallel, compound **10** was obtained by reacting compound **6** with dichloroacetyl chloride in heterogeneous phase in a mixture of DCM and NaOH 2 N solution to obtain the conjugated compound **10** (20% yield). The same procedure was adopted for the synthesis of the corresponding tertiary amine derivative compound starting from compound **8** after its deprotection with TFA in DCM, leading to the conjugated compound **11** in 56% of yield. Of note, the relative easy synthesis of conjugated molecules allowed multigram scale preparation for the in vitro and in vivo experiments.

For the next biological characterization of the DCA-loaded compounds **9**, **10**, and **11**, we have used as controls the corresponding backbone carriers **5**, **7**, and **8**, respectively. The choice for the backbone molecules was made taking into account not only the possible metabolic products coming from the DCA compounds but also considering the physicochemical properties of the carriers (id, cell permeability).

Biological Validation of the DCA-Loaded Compounds. Because the aim of our study was to develop new DCA analogues for antitumor applications, we next assessed the activity of the novel mitochondria targeted DCA-loaded compounds, in comparison with DCA, in in vitro cell models. On the bases of recent evidence of the antileukemic activity of DCA,[12,13] we analyzed the biologic activity of the new compounds using a panel of leukemic cell lines as well as primary cell cultures derived from B-CLL patients. For this purpose, the different cell cultures were exposed to compounds **9**, **10**, and **11** used in the range of concentrations of 10−300 μM, and cell viability was assessed at 24 and 48 h of treatment. The analysis of cell viability in response to DCA-loaded compounds was assessed with respect to the corresponding carriers (**5**, **7**, and **8**). We found of potential interest the compounds **10** and **11** because of the lack of cell toxicity of their backbones (compounds **7** and **8**, respectively; Figure 1), which allows us to discriminate the specific action of the DCA-loaded molecules (Supporting Information Figure 1). Anyhow, while no significant effects on cell viability were observed when the cell cultures were treated with the compound **11** (Supporting Information Figure 1), we observed a dose-dependent cytotoxicity when cell cultures were treated with the compound **10** (Figure 2A). In particular, the IC_{50} values for compound **10** are reported in Table 1 and document an antileukemic activity on all cell lines, irrespective of the p53 status, which was validated also on B-CLL patients' cell cultures. On the other hand, PBMCs obtained from healthy blood donors were less susceptible to compound **10**, with IC_{50} mean values approximately 3-fold higher (1.26 ± 0.19 mM), suggesting that normal PBMCs were substantially resistant to this molecule in the range of concentrations effective against leukemic cells. Of particular relevance, the comparative analysis of the antileukemic activity revealed that the compound **10** was able to exhibit the antileukemic effect of DCA at significantly lower concentrations (>1 log; Figure 2A), as indicated also by the IC_{50} values (Table 1 and Supporting Information Figure 2), both acting through the same mechanisms. Indeed, in depth analysis of the cytotoxicity induced by compound **10** confirmed that its effect on cell viability was the cumulative result of induction of cell cycle arrest (Figure 2B) and induction of apoptosis (Figure 2C,D), coupled to induction of the p21 molecular mediator (Figure 2E), exhibiting results comparable to those induced by treatment with DCA used at 30- to 100-fold higher concentrations than compound **10**.

In parallel, the new synthesized compounds were assessed for their ability to deliver DCA to the mitochondria by using the

DOI: 10.1021/acs.jmedchem.5b01165
J. Med. Chem. 2016, 59, 147−156

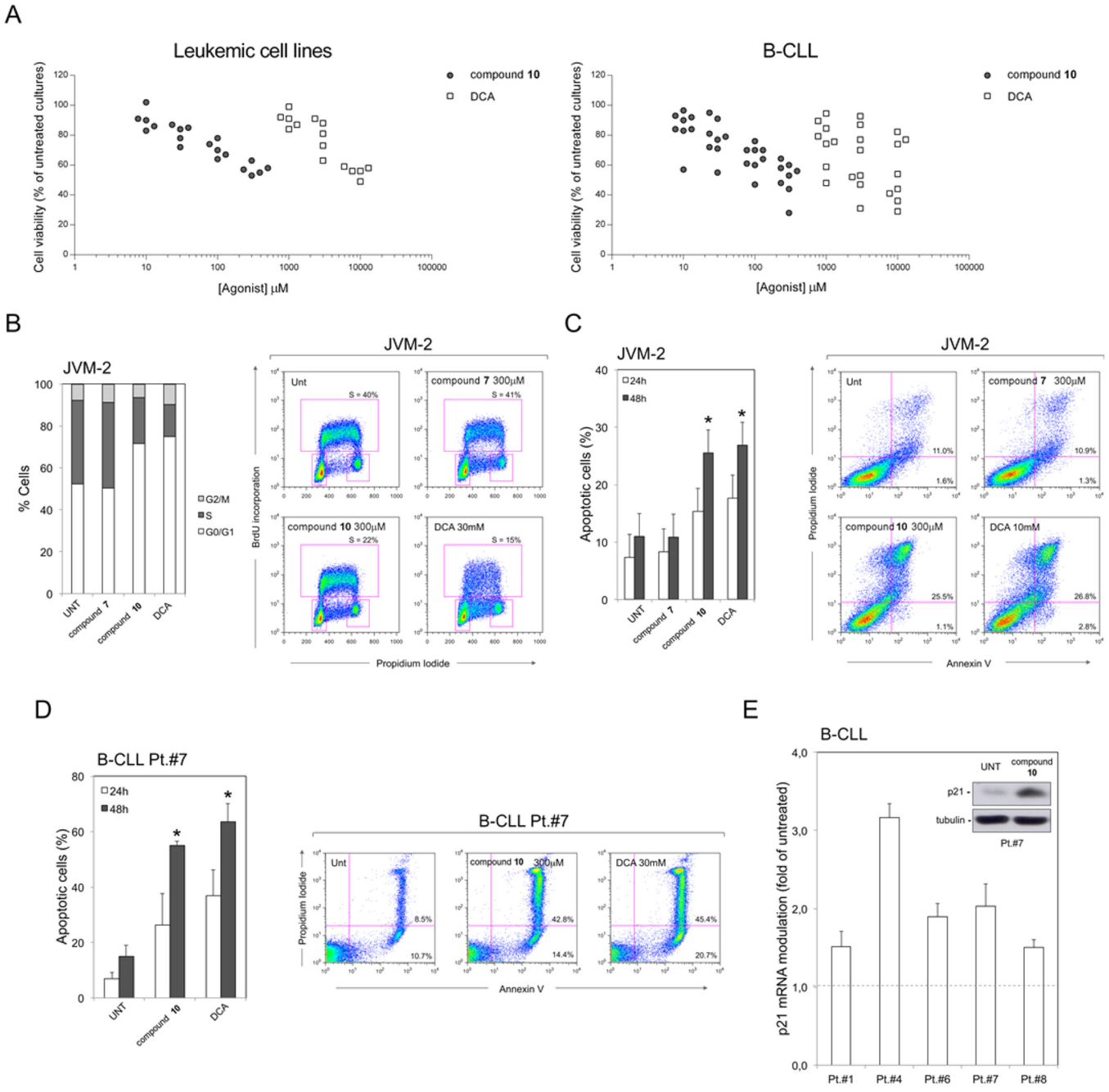

Figure 2. Characterization of the antileukemic effect of the DCA-loaded compound 10. In part A, a panel of leukemic cell lines and of B-CLL patient cell samples (as reported in Table 1) were exposed to serial doses of compound **10** (10−300 μM) or DCA (1−10 mM). Cell viability was analyzed after 48 h of treatment and calculated as percentage with respect to untreated cultures set to 100%. Data are graphed as scatter plots of at least six independent experiments for leukemic cell lines and B-CLL samples, respectively. In parts B−E, leukemic cells were treated for 24 or 48 h with 300 μM of either compound **10** or control scaffold compound **7**. In most experiments, scaffold-treated cultures are not shown, since they were highly comparable to the untreated cultures. For comparison, in some experiments, results obtained by treating the same cultures with a 100-fold higher dose of DCA (30 mM) are also shown. In part B, cell distribution in the different phases of cell cycle was calculated from the flow-cytometry dot plots after BrdU/PI staining and expressed as percentage of the total population. In the right panel, representative cell cycle profiles of cultures, either left untreated or treated with the indicated compounds, analyzed by flow cytometry are shown. For each cytofluorimetric analysis, the rectangles represent the cells in G0/G1, S, G2/M phases of the cell cycle. In part C, the percentage of leukemic apoptotic cells was determined by flow cytometry after annexin V/PI staining. In the right panel, a representative flow-cytometry analysis of apoptosis is shown. In part D, induction of apoptosis was calculated as percentage of annexin V/PI cells in leukemic cells from a primary B-CLL sample. In the right panel, a representative flow-cytometry analysis of apoptosis is shown. In part E, levels of p21 mRNA were analyzed in primary B-CLL samples by quantitative RT-PCR and data are expressed as fold of modulation with respect to the control untreated cultures set at 1. A representative Western blot result documenting the induction of p21 protein in a B-CLL patient sample is shown in the inset. Data are reported as the mean ± SD of results from at least three independent experiments. In parts C and D, the asterisk indicates $p < 0.05$ with respect to the untreated or to compound 7 treated cultures.

DOI: 10.1021/acs.jmedchem.5b01165
J. Med. Chem. 2016, 59, 147−156

Table 1. IC_{50} Values for DCA and Compound 10 in Leukemic Cell Lines and in Primary B-CLL Patient Derived Cells[a]

cell	IC_{50} (mM)	
	DCA	compd **10**
leukemic cell line		
JVM-2	11.47 ± 1.07	0.41 ± 0.03
MAVER	11.83 ± 0.96	0.55 ± 0.06
MEC-1	8.29 ± 0.70	0.40 ± 0.02
MEC-2	12.19 ± 1.11	0.37 ± 0.03
HL-60	13.87 ± 1.29	0.34 ± 0.02
primary B-CLL cells		
B-CLL Pt.#1	29.28 ± 2.75	0.40 ± 0.04
B-CLL Pt.#2	25.65 ± 1.98	0.27 ± 0.02
B-CLL Pt.#3	4.92 ± 0.35	0.14 ± 0.01
B-CLL Pt.#4	1.54 ± 0.09	0.12 ± 0.01
B-CLL Pt.#5	13.34 ± 0.99	0.53 ± 0.03
B-CLL Pt.#6	3.02 ± 0.26	0.34 ± 0.02
B-CLL Pt.#7	3.77 ± 0.29	0.61 ± 0.04
B-CLL Pt.#8	47.70 ± 3.63	0.56 ± 0.06

[a]Values are the mean ± standard deviation calculated after 48 h of culture treatment of experiments carried out at least in triplicate for each cell culture.

most advanced assay, based on the XF technology, which is able to measure the oxygen consumption rate (OCR) as an indicator of mitochondrial respiratory capacity (Figure 3 and Supporting Information Figure 3). Results showed that a pretreatment with the mitochondria targeted DCA-loaded compound **10** (Figure 3), but not **11** (Supporting Information Figure 3), significantly reduced the basal respiration (OCR values before oligomycin addition) as well as the maximal respiration (OCR values after FCCP) of the leukemic cells, while the coupling efficiency was less affected (not reaching statistical significance) as well as the spare respiratory capacity, indicating a decrease of oxidative phosphorylation levels with a preservation of a residual mitochondrial activity. These results are in line with recent observations indicating that CLL cells are characterized by high oxidative phosphorylation (due to intrinsic oxidative stress) and that targeting the mitochondrial respiratory chain in these cells brakes the redox balance and thereby induces cell death.[24]

Finally, it is important to underline that in all the in vitro assays (Figure 2 and Figure 3) the cell cultures treated with the compound **7** were substantially indistinguishable from the untreated cultures, confirming that the backbone carrier **7** did not account for any of the biological−molecular effects observed upon treatment with the DCA-loaded compound **10**.

In Vivo Analysis of Compound 10 Stability. Having observed that compound **10** exhibits antileukemic activity in

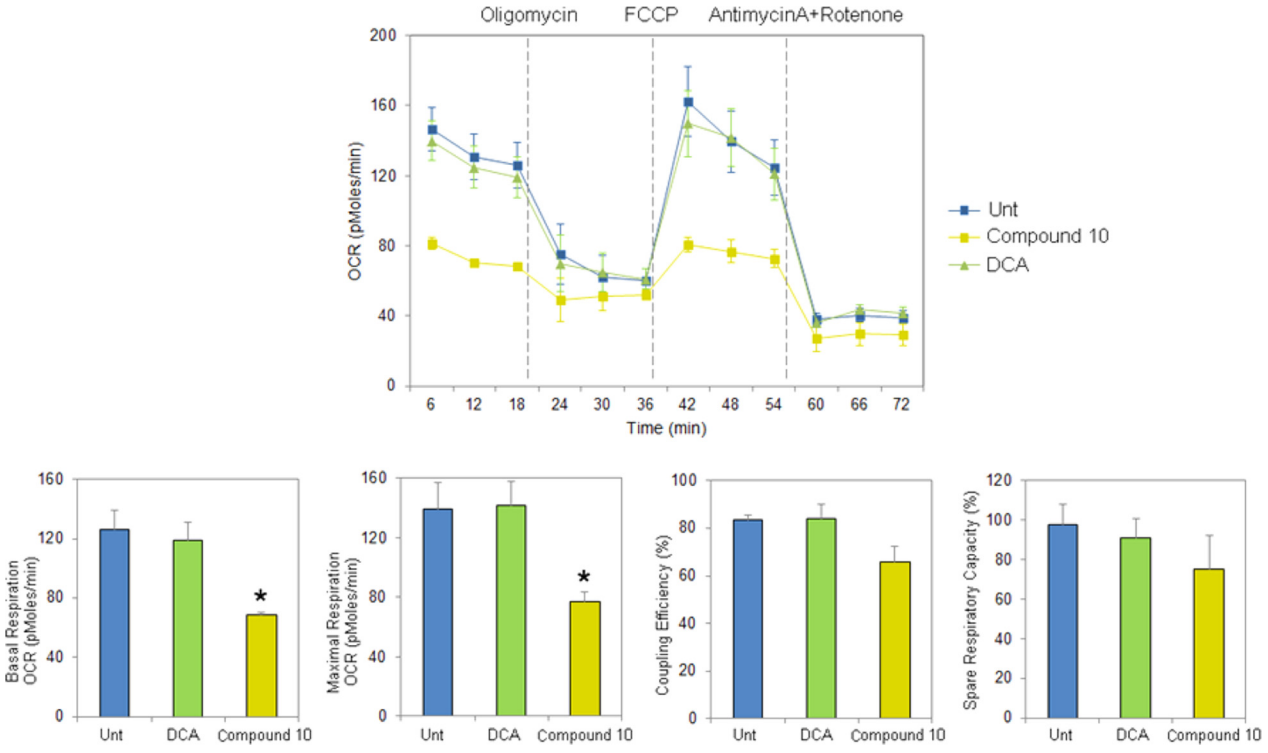

Figure 3. Characterization of the effects of the DCA-loaded compound **10** on cellular bioenergetics functions. Leukemic cells were left untreated or treated for 3 h with 300 μM compound **10** or compound **7** (control carrier) or with DCA and run on the Seahorse analyzer. Oxygen consumption rate (OCR) measurements were recorded after the sequential addition of oligomycin, FCCP (carbonyl cyanide *p*-(trifluoromethoxy)-phenylhydrazone), and the combination of antimycin A and rotenone. OCR traces are expressed as picomoles of O_2 per minute and normalized to cell number. Each data point represents means ± SD of six independent experiments. The graphs reports the different parameters of cellular respiration analyzed. The basal respiration corresponds to the OCR measurement before oligomycin injection. The maximal respiration corresponds to the OCR measurement after FCCP addition. The coupling efficiency and the spare respiratory capacity were calculated by subtracting the minimum Mito inhibitor (i.e., antimycin A + rotenone) responses that account for nonmitochondrial respiration from the values registered before and after FCCP addition respectively, and results are referred above the basal respiration. Scaffold (compound **7**) treated cultures are not shown, since they were highly comparable to the untreated cultures. The asterisk indicates $p < 0.05$ with respect to the untreated cultures.

DOI: 10.1021/acs.jmedchem.5b01165
J. Med. Chem. 2016, 59, 147−156

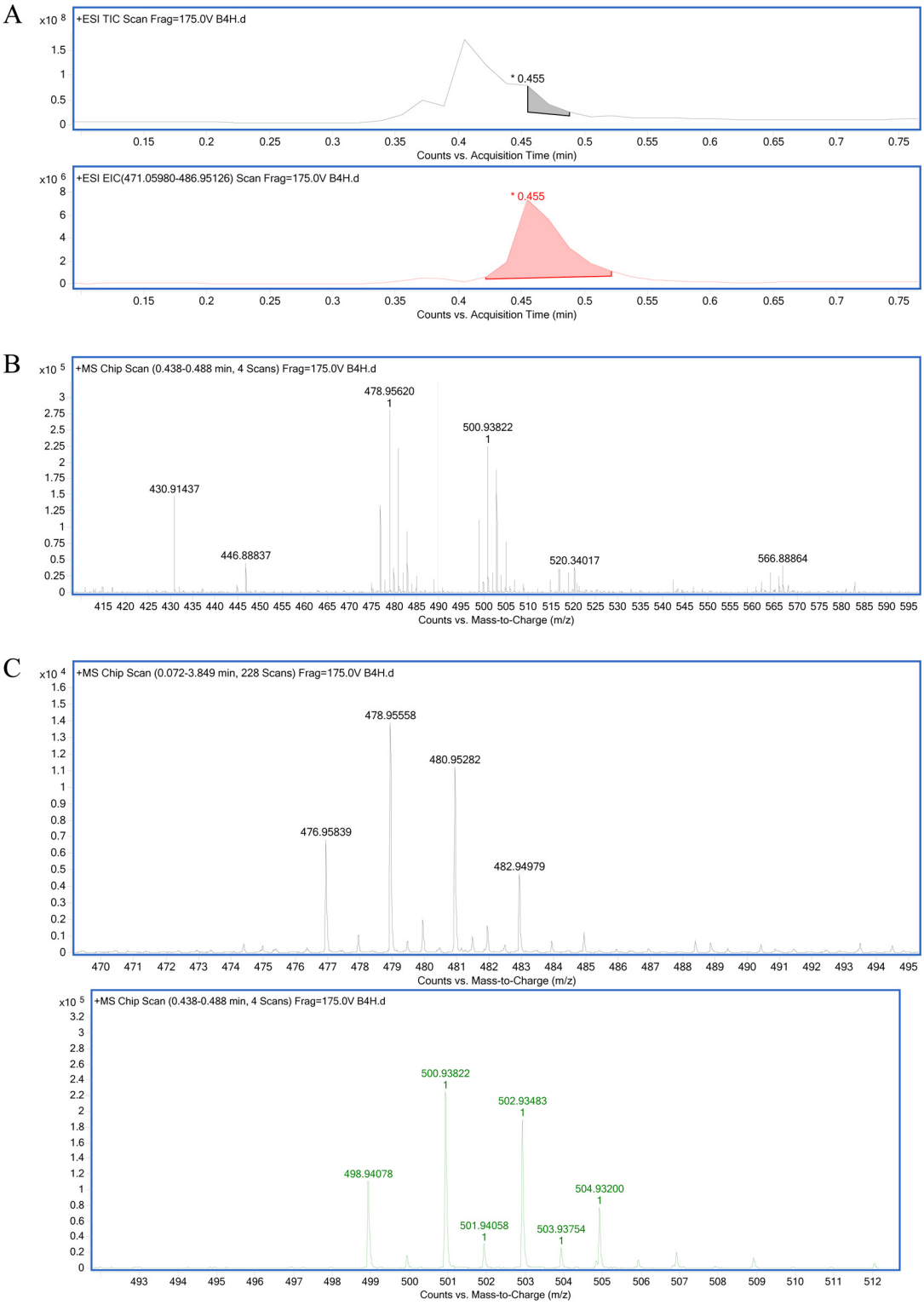

Figure 4. In vivo analysis of compound **10** stability by HPLC−MS analysis of mice plasma. A representative HPLC−MS analysis of a plasma sample collected from mice 4 h after a subcutaneous (sc) injection of a single dose (57 mg/kg) of compound **10** is reported. In part A, the total ion current chromatogram (TIC) and the peak corresponding to compound **10** (t_R = 0.455 min) are shown. In part B, the total MS spectra for the selected TIC indicate the 478.95558u $[M + H]^+$ peak ascribed to the presence of compound **10** and the peak at 500.93822u $[M + Na]^+$. In part C is shown the enlargement of MS region of interest showing the presence of $[M + H]^+$ peak at 476.95839u corresponding to compound **10**.

vitro at significant lower concentrations with respect to DCA, we next preliminarily evaluated its potential bioavailability and stability in vivo in mice. For this purpose, a single dose of compound **10** (57 mg/kg) was given by subcutaneous inoculation (sc) and blood was collected at different time-points after injection. Plasma samples were then analyzed for the presence of the compound **10** with Agilent 6520 LC−MS instrument equipped with nano-HPLC Chip cube separative

DOI: 10.1021/acs.jmedchem.5b01165
J. Med. Chem. 2016, 59, 147−156

system. The unambiguously identification of compound **10** was possible by a comparison between the calculated exact mass (that is absolutely typical due to the presence of six chlorine atoms) and the found value, leading to the classification of a specific molecule profile (Figure 4). Results showed that compound **10** was present in the mice blood circulation for more than 5 h after injection (Figure 4; Supporting Information S27–S29) and at the same time no metabolites were found, proving that the amide bond between the carrier and the dichloroacetic moiety was stable.

DISCUSSION AND CONCLUSION

Different carrier moieties, such as phosphonium salts and polyamine and guanidine derivatives, have been proposed for targeting different molecules, such as ROS inhibitors or anticancer agents, into the mitochondria.[20,25] In the present study, in order to enhance the potential of DCA for clinical applications, such as to target the tumor metabolic alterations,[6,7,15,16] we explored the ability of a tertiary amine scaffold and the corresponding quaternary ammonium salt to carry DCA. As a first step, the results of assays performed in vitro on different cell models revealed that these scaffolds had significant lower cell toxicity compared with the corresponding phosphonium salts, as well as a good solubility in physiological medium. On this base, the amine scaffolds were used for the synthesis of compounds **10** and **11**, delivering multiple DCA molecules, with the aim to reach relevant therapeutic concentrations of the drug into tumor cells. In fact, in analogy with other molecules bringing positively charged atoms, such as guanidine and polyamine,[10−25] compounds **10** and **11** were expected to pass more efficiently than the DCA molecule the inner mitochondrial membrane (IMM), because of the great negative membrane potential ($\Delta\psi_m$) that exists across the IMM, and thus to reach the PDK target in the mitochondrial matrix.

The biological validation of the new synthesized DCA-loaded compounds **10** and **11** was performed assessing their antitumor efficiency that revealed a completely different behavior between the two DCA-compounds. Of interest, the multiple DCA-loaded compound **10** exhibited in vitro antitumor activity at significantly lower (>30 fold) concentrations compared to DCA, when tested both on a panel of leukemic cell lines and on B-CLL patient derived cell cultures. Of interest, similar results were obtained also on cell models of human solid tumors of epithelial origin (Supporting Information Table 1). On the opposite, the quaternary salt compound **11** was completely inactive in affecting cell viability in all cell lines employed. Although this result was quite unexpected, due to the strong mitochondrial affinity for positively charged molecules, one possible explanation could be related to the high hydrophilic behavior of compound **11** that limits the cell membrane crossing.

The in vitro characterization of the antileukemic activity of compound **10**, supported by its low toxicity on human healthy primary cells, was integrated by a preliminary assessment of its in vivo stability in mouse models. The data obtained from mice injected subcutaneously with a relative low dose (single injection of 57 mg/kg) of drug indicated that compound **10** entered the blood circulation from the subcutaneous compartment without being degraded. In fact, HPLC−MS analysis of murine plasma suggests that the molecule was quite stable in the blood for a relatively long period of time (5.5 h), if compared with the rapid metabolism of DCA described in literature.[26,27] Moreover the lack of detection of metabolites in plasma samples at each time point assessed suggested that the dichloroacetyl moiety carried by a neutral tertiary amine scaffold was more stable and long lasting when exposed to the biological environment in in vivo experiments, compared to dichloroacetyl anion.[26,27]

Considering the increased interest for DCA as a potential metabolic targeting therapy for cancer,[3−7] we believe that our strategy design for DCA-carrying molecules deserves further preclinical characterization since it could provide future advancements for the treatment of cancer, as well as for other diseases (such as proliferative vascular diseases)[28] characterized by an altered metabolic origin.

EXPERIMENTAL SECTION

Chemistry: General Information. All the NMR spectra were elaborated using Mestre Nova 6.0.2 software, and FID data are available on request. Analytical thin layer chromatography (TLC) was performed on silica gel Macherey-Nagel Polygram SIL/UV 254 of 0.25 mm, and visualization was achieved using UV light (254) and potassium permanganate ($KMnO_4$) 2% in water. Flash column chromatography was undertaken on silica gel Merck 60−200 mesh using Isolera Biotage (Sweden). Products were dried using sodium sulfate anhydrous (Carlo Erba). Proton nuclear magnetic resonance (^{1}H NMR) and carbon nuclear magnetic resonance (^{13}C NMR) were recorded using VARIAN 400 MHz. All spectra were recorded using as solvent $CDCl_3$; otherwise the solvent was specified. Chemical shifts (δ) were quoted in ppm relative to residual solvent, and coupling constants (J) were quoted in hertz (Hz). Multiplicity was reported with the following abbreviations: s = singlet; d = doublet; t = triplet; q = quartet; m = multiplet, bs = broad signal. Molecular weights were measured with a mass spectrometer ESI MICROMASS ZMD 2000 (Waters, U.K.) and high resolution spectra with an Agilent ESI-Q-TOF LC/MS 6520 system (Agilent Technologies, USA). Solvents and chemicals used for TLC, chromatographic purification, crystallizations, and reactions were reported with the following abbreviations: Et_2O for diethyl ether, THF for tetrahydrofuran, AcOEt for ethyl acetate, DCM for methylene chloride, CH_3CN for acetonitrile, TFA for trifluoroacetic acid.

Synthesis of (5-Carboxypentyl)triphenylphosphonium Bromide (2). In a round-bottom flask, 6-bromohexanoic acid (4000 mg, 20.50 mmol) and triphenylphosphine (5600 mg, 21.49 mmol) were dissolved in 80 mL of acetonitrile and heated at reflux for 24 h. The title compound was obtained in quantitative yield as white sticky oil. MS (ESI) of compound **1**: $[M + H]^+$ = 377.32.

Synthesis of (6-((1,3-Dihydroxy-2-(hydroxymethyl)propan-2-yl)amino)-6-oxohexyl)triphenylphosphonium Bromide (4). Compound **2** (1000 mg, 2.18 mmol), 2-amino-2-(hydroxymethyl)-propane-1,3-diol (292 mg, 2.40 mmol), and *N*-ethoxycarbonyl-2-ethoxy-1,2-dihydroquinoline (650 mg, 2.62 mmol) were dissolved in 50 mL of EtOH and heated at 50 °C for 12 h. The reaction mixture was concentrated in vacuo, dissolved in 30 mL of AcOEt, and washed twice with 20 mL of brine. The organic phase was dried to yield compound **4** as sticky yellow oil. MS (ESI) of compound **4**: $[M + H]^+$ = 480.45. ^{1}H NMR (400 MHz, chloroform-*d*), δ 8.92, (bs, 1H, N*H*), 7.82−7.38 (15 H, *CHar*), 3.72−3.65 (m, 9H,-CH_2-*OH*), 3.51−3.44 (m, 2H, CH_2-CONH), 2.37 (t, 2H, J = 7.2 Hz, CH_2−CH_2-CH_2-C=O), 1.65−1.79, (m, 6H, -CH_2-CH_2-CH_2). ^{13}C NMR (101 MHz, CDCl3) δ 175.75, 150.52, 136.22, 135.37, 133.70, 133.60, 130.79, 130.67, 129.59, 127.92, 126.67, 121.20, 117.68, 64.13, 62.46, 36.42, 29.46, 25.05, 23.10, 22.60, 21.89, 18.55.

Synthesis of (6-((1,3-Diacetoxy-2-(acetoxymethyl)propan-2-yl)amino)-6-oxohexyl)triphenylphosphonium Bromide (5). To a stirred solution of compound **4** (460 mg, 0.82 mmol) dissolved in 50 mL of DCM, 0.192 mL of acetyl chloride (212 mg, 2.71 mmol) was added, and the reaction mixture was allowed to stay at room temperature for 4 h. After this time the reaction was completed (checked by ESI mass spectrometry), and the DCM was evaporated in

DOI: 10.1021/acs.jmedchem.5b01165
J. Med. Chem. 2016, 59, 147−156

vacuum to yield compound **5** in quantitative yield. ^{1}H NMR (400 MHz, chloroform-*d*), δ 8.92, (bs, 1H, N*H*), 8.20−8.12 (m, 2H, *CHar*), 7.85−7.41 (m, 13H, *CHar*), 4.44 (s, 6H, CH_2-OAc), 2.34 (m, 2H, CH_2-CH_2-CH_2-C═O), 2.05 (s, 9H, O-C═O-CH_3) 1.69, (m, 6H, -CH_2-CH_2-CH_2). ^{13}C NMR (101 MHz, $CDCl_3$) δ 174.32, 170.79, 150.25, 136.59, 135.19, 130.69, 130.64, 129.81, 129.28, 127.95, 126.83, 121.22, 118.84, 117.99, 66.18, 62.66, 57.71, 36.49, 29.72, 29.56, 24.69, 22.93, 22.43, 21.89.

Synthesis of (6-((1,3-Bis(2,2-dichloroacetoxy)-2-((2,dichloroacetoxy)methyl)propan-2-yl)amino)-6-oxohexyl)-triphenylphosphonium (9). A stirred solution of compound **4** and 2,2-dichloroacetyl chloride (627 mg, 4.25 mmol, 410 μL) in DCM (30 mL) was reacted at room temperature for 2 h. The reaction mixture was checked by ESI mass spectrometry, and when the product was observed, the solvent was removed under vacuum. The title compound was obtained as off white oil with 92% yield. HRMS (ESI) of compound **9**: $[M + H]^+$ = 812.028640. ^{1}H NMR (400 MHz, chloroform-*d*), δ 7.72−7.80 (m, 15 H, *CHar*), 5.90 (s, 3H, C*H*-Cl_2), 4.45 (m, 2H, CH_2-PPh_3), 3.86 (m, 4H, -CH_2-CH_2-CH_2), 3.44 (bs, 2H, CH_2-CONH), 2.43 (m, 2H, -$C\underline{H}_2$-*CO*), 1.64(6H, -CH_2-CH_2-CH_2). ^{13}C NMR (400 MHz, chloroform-*d*), δ: 177.7, 174.0, 166.0, 146.4, 141.1, 138.1, 135.0, 133.6, 130.7, 129.8, 128.7, 121.5, 118.4, 117.9, 66.4, 64.3, 62.1, 61.5, 59.7, 50.3, 34.1, 29.5, 23.9, 22.7, 22.2.

Synthesis of Tri-*tert*-butyl (Nitrilotris(ethane-2,1-diyl))-tricarbamate (7). In a round-bottom flask the amine (1 g, 6.83 mmol, 1.02 mL) was solved in a mixture of water and dioxane (10 mL/20 mL). NaOH (2.5 g, 61.47 mmol) and $(Boc)_2O$ were added at 0 °C, and the solution was stirred overnight at room temperature. The reaction mixture was extracted with 40 mL of AcOEt, dried over sodium sulfate anhydrous, filtered, and the solvent was removed under vacuum. The title compound **7** was obtained as a white solid in quantitative yield. MS (ESI) of compound **7**: $[M + H]^+$ = 447.36.

Synthesis of 2-((*tert*-Butoxycarbonyl)amino)-*N*,*N*-bis((2-((*tert*-butoxycarbonyl)amino)ethyl)-*N*-methylthanaminium Iodide (8). To a stirred solution of compound **7** (1.8 g, 4.21 mmol) dissolved in 50 mL of CH_3CN, methyl iodide (33.69 mmol, 2.1 mL) was added, and the reaction mixture was heated at 60 °C for 24 h. After 1 day, the reaction mixture was concentrated in vacuo, dissolved in 50 mL of AcOEt, and washed twice with water (20 mL). The organic layers were dried to achieve a yellow solid salt in a quantitative yield. Mp = 140−145 °C. MS (ESI) of compound **8**: $[M + H]^+$ = 461.63. ^{1}H NMR (400 MHz, chloroform-*d*), δ: 3.56 (s, 12H, CH_2-CH_2), 3.27 (s, 3H, N-CH_3), 1.44 (m, 27H, $C(CH_3)_3$). ^{13}C NMR (400 MHz, chloroform-*d*), δ: 160.56, 83.51, 64.75, 52.95, 38.79, 37.91, 31.39.

Synthesis of *N*,*N*′,*N*″-(Nitrilotris(ethane-2,1-diyl))tris(2,2-dichloroacetamide) (10). Schotten−Baumann reaction involves the amine (500 mg, 3.42 mmol, 512.29 μL) dissolved in DCM (10 mL) and NaOH 2 N solution (5.13 mL) to have a heterogeneous system by adding 2,2-dichloroacetyl chloride (1515 mg, 10.26 mmol, 990 μL) at room temperature overnight. The reaction mixture was washed with water (10 mL), and the organic layers were dried, filtered, and concentrated under vacuum. The crude was purified by flash chromatography (AcOEt/petroleum ether 5:1) to give the title compound **10** with 20% yield and used for the tests as hydrochloric salt. Mp = 134−137 °C. HRMS (ESI) of compound **10**: $[M + H]^+$ = 476.958 39. ^{1}H NMR (400 MHz, methanol-*d*), δ: 6.34 (s, 3H, C*H*-Cl_2) 3.31 (t, 6H, *J* = 6.2 Hz, N-CH_2-CH_2), 2.67 (t, 6H, *J* = 6.2 Hz, N-CH_2-CH_2). ^{13}C NMR (400 MHz, methanol-*d*), δ: 39.50, 54.39, 67.72, 166.97.

Synthesis of 2-(2,2-Dichloroacetamido)-*N*,*N*-bis(2-(2,2-dichloroacetamido)ethyl)-*N*-methylethanaminium Iodide (11). Compound **8** (1,8 g, 6.5 mmol), earlier treated with 10 mL of TFA in 50 mL of DCM to remove Boc protecting group, was dissolved in DCM (40 mL), and NaOH 2 N solution (20 mL) and 2,2-dichloroacetyl chloride (39 mmol, 3 mL) were added. The reaction mixture worked overnight at room temperature. After this time, the reaction mixture was extracted in AcOEt (50 mL) and the product was purified by flash chromatography (AcOEt) to give a white solid in 50% yield. HRMS (ESI) of compound **11**: $[M + H]^+$ = 490.974 115. ^{1}H NMR (400 MHz, methanol-*d*), δ: 6.34 (s, 3H, CHCl_2), 3.81−3.78 (t, 6H, *J* = 6.2 Hz, -N-CH_2-CH_2), 3.61−3.59 (t, 6H, *J* = 6.2 Hz, -N-CH_2-CH_2), 3.28 (s, 3H, N-CH_3). ^{13}C NMR (400 MHz, methanol-*d*), δ: 167.45, 60.85, 34.75.

Further details on compound characterization (spectra analysis and purity grade ≥95% for each compound) are present in Supporting Information S8−S26.

Cell Cultures and Treatments. Primary peripheral blood samples were collected in heparin-coated tubes from B-CLL patients (n = 8) and healthy blood donors (n = 4) after informed consent provided for research purposes, in accordance with the Declaration of Helsinki and in agreement with institutional guidelines (University-Hospital of Ferrara). All patients had been without prior therapy at least 3 weeks before blood collection. Peripheral blood mononuclear cells (PBMC) were isolated as previously described.[29] The $p53^{wild\text{-}type}$ JVM-2, the $p53^{mutated}$ MAVER, MEC-1, MEC-2, and the $p53^{null}$ HL-60 leukemic cell lines were purchased from DSMZ (Deutsche Sammlung von Mikroorganismen and Zellkulturen GmbH, Braunschweig, Germany). Primary cells were cultured in RPMI-1640 medium containing 10% FBS, L-glutamine and penicillin/streptomycin (all from Gibco, Grand Island, NY). The leukemic JVM-2, MAVER and HL-60 cell lines were routinely cultured in RPMI-1640, whereas MEC-1 and MEC-2 cell lines were maintained in IMDM, all supplemented with 10% FBS, L-glutamine, and penicillin/streptomycin (all from Gibco).

For the in vitro assays, leukemic cells and normal PBMC were seeded at a density of 1×10^6 cells/mL and treated with DCA (Sigma-Aldrich, St. Louis, MO; used in the range of 1−30 mM) and DCA-loaded compounds and carriers (used in the range of 3−300 μM).

Assessment of Cell Viability, Apoptosis, and Cell Cycle Profile. At different time points after treatments, cell viability was evaluated by both Trypan blue dye exclusion and MTT (3-(4,5-dimethylthiazol-2-yl)-2,5-diphenyltetrazolium bromide) colorimetric assay (Roche Diagnostics Corporation, Indianapolis, IN), as previously reported.[30] In order to investigate the concentration required to induce death in 50% of cells relative to control, IC_{50} values were calculated after 48 h of culture for DCA (range of 0.1−30 mM) and compound **10** (range of 3−1000 μM). The cell cycle profile was analyzed by flow cytometry after 5-bromodeoxyuridine (BrdU) incorporation as previously described.[31] Levels of apoptosis were quantified by annexin V-FITC/PI staining (Immunotech, Marseille, France) and analyzed by using a FACS Calibur flow cytometer (Becton-Dickinson, San Jose, CA).[32]

Analysis of p21 Expression. Total RNA was extracted from cells using the QIAGEN RNeasy Plus mini kit (Qiagen, Hilden, Germany) according to the supplier's instructions and as previously described.[33] Total RNA was transcribed into cDNA and amplified using the Express One-Step Superscript qRT-PCR kit (Invitrogen, Carlsbad, CA). Analysis of *CDKN1A* (p21) gene expression was carried out with validated TaqMan gene expression assays specific PCR primers sets (Invitrogen). Expression values were normalized to the housekeeping gene *POLR2A* amplified in the same sample.[12] For p21 protein analysis, cells were lysed and processed for Western blot, as previously described,[34] by using the anti-p21 (C-19) antibody, purchased from Santa Cruz Biotechnology (Santa Cruz, CA).

Bioenergetics Assays. Bioenergetics assays were performed by using the XF^{e}96 extracellular flux analyzer (Seahorse Bioscience, North Billerica, MA) and the Seahorse XF96 cell Mito stress test kit (Seahorse Bioscience). After treatments, leukemic cells were seeded in specific tissue culture plates, previously coated with poly-L-lysine solution (Sigma-Aldrich), in the optimized concentration of 3×10^5 cells per well. One hour before measurement, cells were incubated at 37 °C in a CO_2-free atmosphere. Different parameters of respiration, i.e., basal respiration, coupling efficiency, and spare respiratory capacity, were analyzed by using a XF96 Mito stress assay kit. For this purpose, after establishment of a baseline, basal oxygen consumption rate (OCR), a measure of mitochondrial respiration, was first detected before sequentially injecting the following mitochondrial inhibitors: the ATP synthase inhibitor oligomycin (1.0 μM), the uncoupling agent FCCP (carbonyl cyanide *p*-(trifluoromethoxy)phenylhydrazone) (1.0 μM), and the combination of complex III inhibitor antimycin A (1.0 μM) and the complex I

DOI: 10.1021/acs.jmedchem.5b01165
J. Med. Chem. 2016, 59, 147−156

inhibitor rotenone (1.0 μM). OCR values were automatically calculated by the Seahorse XF96 software. All experiments were performed at least in hexaplicate.

Experiments in Mice and HPLC−MS Analysis of Plasma. Female BALB/c mice (8 weeks old) were purchased from Charles River Laboratories (Hollister, CA). All the experimental procedures were approved by the Institutional Animal Ethical Care Committee (CEASA) of the University of Ferrara and by the Italian Ministry of Health. Upon arrival, mice were acclimated for 1 week before starting the study. Mice were housed under pathogen-free conditions in vented cabinet, exposed to a regular light−dark cycle of 12 h each, and food and water were available ad libitum, in compliance with the guidelines for the care and use of laboratory animals. Mice (n = 12) were administered via subcutaneous (sc) injection with a single dose of compound **10** solution (57 mg/kg in 200 μL of PBS/25% DMSO). Blood samples were collected from the tail vein into microvials containing 2 μL of heparinized saline (Epsoclar 25.000 UI/5 mL, Hospira), at different time points (1, 2.5, 4, 5.5, 7, 16, and 24 h) after sc injection.[35] Plasma samples were obtained after centrifugation of blood samples at 10.000 rpm for 10 min at room temperature and stored immediately at −80 °C.

Analysis of plasma samples was performed using Agilent 6520 LC−MS instrument equipped with nano-HPLC Chip cube separative system. For each sample, an amount of 100 μL of plasma was diluted with 300 μL of acetonitrile/water/TFA (60%/40%/0.1%) solution and then passed onto a 0.22 μm regenerated cellulose filter before the LC−MS injection. The HPLC−MS analysis was performed in a linear gradient from 100% of solvent A (97% water, 3% acetonitrile, and 0.1% formic acid) to 100% of solvent B (97% acetonitrile, 3% water, and 0.1% formic acid) in 15 min using a Zorbax 300SB C-18 (43 mm × 75 μm) separation column.

Statistical Analysis. Descriptive statistics were calculated. For each set of experiments, values were reported as the mean ± standard deviation (SD). The results were evaluated by using analysis of variance with subsequent comparisons by Student's t test and with the Mann−Whitney rank-sum test. Statistical significance was defined as $p < 0.05$. All statistical analyses were performed with SPSS Statistic 20 software (SPSS Inc., Chicago, IL).

■ ASSOCIATED CONTENT

Supporting Information

The Supporting Information is available free of charge on the ACS Publications website at DOI: 10.1021/acs.jmedchem.5b01165.

Cytoxic effects, IC_{50} data, effects on bioenergetics, spectra of compounds, and HPLC−MS analysis results of mouse plasma (PDF)

Molecular formula strings (CSV)

■ AUTHOR INFORMATION

Corresponding Authors

*C.T.: phone, +39-0532-455924; fax, +39-0532-455953; e-mail, trap@unife.it.

*G.Z.: phone, +39-0532-455572; fax, +39-0532-207351; e-mail, giorgio.zauli@unife.it.

Author Contributions

⊥C.T. and R.V. contributed equally.

The manuscript was written through contributions of all authors. All authors have given approval to the final version of the manuscript.

Notes

The authors declare no competing financial interest.

■ ACKNOWLEDGMENTS

This study was supported by grants from MIUR-FIRB (Grant RBFR109SBM_001 to C.T.) and from the Italian Association for Cancer Research (Grant AIRC IG 11465 to G.Z.).

■ ABBREVIATIONS USED

B-CLL, B-cell chronic lymphocytic leukemia; BrdU, 5-bromodeoxyuridine; $(Boc)_2O$, di-*tert*-butyl dicarbonate; DCA, dichloroacetate; DCM, dichloromethane; EEDQ, *N*-ethoxycarbonyl-2-ethoxy-1,2-dihydroquinoline; FCCP, carbonyl cyanide *p*-(trifluoromethoxy)phenylhydrazone; FITC, fluorescein isothiocyanate; IC_{50}, half maximal inhibitory concentration; IMDM, Iscove's modified Dulbecco's medium; IMM, inner mitochondrial membrane; LC−MS, liquid chromatography−mass spectrometry; MPC, mitochondrial pyruvate carrier; MTT, 3-(4,5-dimethylthiazol-2-yl)-2,5-diphenyltetrazolium bromide; OCR, oxygen consumption rate; PBMC, peripheral mononuclear cell; PDH, pyruvate dehydrogenase; PDK, pyruvate dehydrogenase kinase; PI, propidium iodide; RPMI, Roswell Park Memorial Institute; SLC5A8, solute carrier family 5 member 8; TFA, trifluoroacetic acid; TLC, thin-layer chromatoraphy; $\Delta\psi_m$, mitochondrial membrane potential

■ REFERENCES

(1) Abdelmalak, M.; Lew, A.; Ramezani, R.; Shroads, A. L.; Coats, B. S.; Langaee, T.; Shankar, M. N.; Neiberger, R. E.; Subramony, S. H.; Stacpoole, P. W. Long-term safety of dichloroacetate in congenital lactic acidosis. *Mol. Genet. Metab.* **2013**, *109*, 139−143.

(2) Christofk, H. R.; Vander Heiden, M. G.; Harris, M. H.; Ramanathan, A.; Gerszten, R. E.; Wei, R.; Fleming, M. D.; Schreiber, S. L.; Cantley, L. C. The M2 splice isoform of pyruvate kinase is important for cancer metabolism and tumour growth. *Nature* **2008**, *452*, 230−233.

(3) Lu, J.; Tan, M.; Cai, Q. The Warburg effect in tumor progression: mitochondrial oxidative metabolism as an anti-metastasis mechanism. *Cancer Lett.* **2015**, *356*, 156−164.

(4) Elf, S. E.; Chen, J. Targeting glucose metabolism in patients with cancer. *Cancer* **2014**, *120*, 774−780.

(5) Bonnet, S.; Archer, S. L.; Allalunis-Turner, J.; Haromy, A.; Beaulieu, C.; Thompson, R.; Lee, C. T.; Lopaschuk, G. D.; Puttagunta, L.; Bonnet, S.; Harry, G.; Hashimoto, K.; Porter, C. J.; Andrade, M. A.; Thebaud, B.; Michelakis, E. D. A mitochondria-K+ channel axis is suppressed in cancer and its normalization promotes apoptosis and inhibits cancer growth. *Cancer Cell* **2007**, *11*, 37−51.

(6) Bhat, T. A.; Kumar, S.; Chaudhary, A. K.; Yadav, N.; Chandra, D. Restoration of mitochondria function as a target for cancer therapy. *Drug Discovery Today* **2015**, *20*, 635−643.

(7) Michelakis, E. D.; Webster, L.; Mackey, J. R. Dichloroacetate (DCA) as a potential metabolic-targeting therapy for cancer. *Br. J. Cancer* **2008**, *99*, 989−94.

(8) Robey, I. F.; Martin, N. K. Bicarbonate and dichloroacetate: evaluating pH altering therapies in a mouse model for metastatic breast cancer. *BMC Cancer* **2011**, *11*, 235.

(9) Lin, G.; Hill, D. K.; Andrejeva, G.; Boult, J. K.; Troy, H.; Fong, A. C.; Orton, M. R.; Panek, R.; Parkes, H. G.; Jafar, M.; Koh, D. M.; Robinson, S. P.; Judson, I. R.; Griffiths, J. R.; Leach, M. O.; Eykyn, T. R.; Chung, Y. L. Dichloroacetate induces autophagy in colorectal cancer cells and tumours. *Br. J. Cancer* **2014**, *111*, 375−385.

(10) Niewisch, M. R.; Kuçi, Z.; Wolburg, H.; Sautter, M.; Krampen, L.; Deubzer, B.; Handgretinger, R.; Bruchelt, G. Influence of dichloroacetate (DCA) on lactate production and oxygen consumption in neuroblastoma cells: is DCA a suitable drug for neuroblastoma therapy? *Cell. Physiol. Biochem.* **2012**, *29*, 373−380.

(11) Fujiwara, S.; Kawano, Y.; Yuki, H.; Okuno, Y.; Nosaka, K.; Mitsuya, H.; Hata, H. PDK1 inhibition is a novel therapeutic target in multiple myeloma. *Br. J. Cancer* **2013**, *108*, 170−178.

DOI: 10.1021/acs.jmedchem.5b01165
J. Med. Chem. 2016, 59, 147−156

(12) Agnoletto, C.; Melloni, E.; Casciano, F.; Rigolin, G. M.; Rimondi, E.; Celeghini, C.; Brunelli, L.; Cuneo, A.; Secchiero, P.; Zauli, G. Sodium dichloroacetate exhibits anti-leukemic activity in B-chronic lymphocytic leukemia (B-CLL) and synergizes with the p53 activator Nutlin-3. *Oncotarget.* **2014**, *5*, 4347−4360.
(13) Agnoletto, C.; Brunelli, L.; Melloni, E.; Pastorelli, R.; Casciano, F.; Rimondi, E.; Rigolin, G. M.; Cuneo, A.; Secchiero, P.; Zauli, G. The anti-leukemic activity of sodium dichloroacetate in p53mutated/null cells is mediated by a p53-independent ILF3/p21 pathway. *Oncotarget.* **2015**, *6*, 2385−2396.
(14) Kankotia, S.; Stacpoole, P. W. Dichloroacetate and cancer: new home for an orphan drug? *Biochim. Biophys. Acta, Rev. Cancer* **2014**, *1846*, 617−629.
(15) Garon, E. B.; Christofk, H. R.; Hosmer, W.; Britten, C. D.; Bahng, A.; Crabtree, M. J.; Hong, C. S.; Kamranpour, N.; Pitts, S.; Kabbinavar, F.; Patel, C.; von Euw, E.; Black, A.; Michelakis, E. D.; Dubinett, S. M.; Slamon, D. J. Dichloroacetate should be considered with platinum-based chemotherapy in hypoxic tumors rather than as a single agent in advanced non-small cell lung cancer. *J. Cancer Res. Clin. Oncol.* **2014**, *140*, 443−452.
(16) Dunbar, E. M.; Coats, B. S.; Shroads, A. L.; Langaee, T.; Lew, A.; Forder, J. R.; Shuster, J. J.; Wagner, D. A.; Stacpoole, P. W. Phase 1 trial of dichloroacetate (DCA) in adults with recurrent malignant brain tumors. *Invest. New Drugs* **2014**, *32*, 452−464.
(17) Jackson, V. N.; Halestrap, A. P. The kinetics, substrate, and inhibitor specificity of the monocarboxylate (lactate) transporter of rat liver cells determined using the fluorescent intracellular pH indicator, 2′,7′-bis(carboxyethyl)-5(6)-carboxyfluorescein. *J. Biol. Chem.* **1996**, *271*, 861−868.
(18) Babu, E.; Ramachandran, S.; CoothanKandaswamy, V.; Elangovan, S.; Prasad, P. D.; Ganapathy, V.; Thangaraju, M. Role of SLC5A8, a plasma membrane transporter and a tumor suppressor, in the antitumor activity of dichloroacetate. *Oncogene* **2011**, *30*, 4026−4037.
(19) Pathak, R. K.; Marrache, S.; Harn, D. A.; Dhar, S. Mito-DCA: a mitochondria targeted molecular scaffold for efficacious delivery of metabolic modulator dichloroacetate. *ACS Chem. Biol.* **2014**, *9*, 1178−1187.
(20) Biasutto, L.; Mattarei, A.; Marotta, E.; Bradaschia, A.; Sassi, N.; Garbisa, S.; Zoratti, M.; Paradisi, C. Development of mitochondria-targeted derivatives of resveratrol. *Bioorg. Med. Chem. Lett.* **2008**, *18*, 5594−5597.
(21) Zatelli, M. C.; Gagliano, T.; Pelà, M.; Bianco, S.; Bertolasi, V.; Tagliati, F.; Guerrini, R.; degli Uberti, E.; Salvadori, S.; Trapella, C. N-carbamidoyl-4-((3-ethyl-2,4,4-trimethylcyclohexyl)methyl)benzamide enhances staurosporine cytotoxic effects likely inhibiting the protective action of Magmas toward cell apoptosis. *J. Med. Chem.* **2014**, *57*, 4606−4614.
(22) Jubinsky, P. T.; Short, M. K.; Ghanem, M.; Das, B. C. Design, synthesis, and biological activity of novel Magmas inhibitors. *Bioorg. Med. Chem. Lett.* **2011**, *21*, 3479−3482.
(23) Simoni, E.; Bergamini, C.; Fato, R.; Tarozzi, A.; Bains, S.; Motterlini, R.; Cavalli, A.; Bolognesi, M. L.; Minarini, A.; Hrelia, P.; Lenaz, G.; Rosini, M.; Melchiorre, C. Polyamine conjugation of curcumin analogues toward the discovery of mitochondria-directed neuroprotective agents. *J. Med. Chem.* **2010**, *53*, 7264−7268.
(24) Jitschin, R.; Hofmann, A. D.; Bruns, H.; Giessl, A.; Bricks, J.; Berger, J.; Saul, D.; Eckart, M. J.; Mackensen, A.; Mougiakakos, D. Mitochondrial metabolism contributes to oxidative stress and reveals therapeutic targets in chronic lymphocytic leukemia. *Blood* **2014**, *123*, 2663−2672.
(25) Biasutto, L.; Dong, L. F.; Zoratti, M.; Neuzil, J. Mitochondrially targeted anti-cancer agents. *Mitochondrion* **2010**, *10*, 670−681.
(26) Saghir, S. A.; Schultz, I. R. Low-dose pharmacokinetics and oral bioavailability of dichloroacetate in naive and GST-zeta-depleted rats. *Environ. Health Perspect.* **2002**, *110*, 757−763.
(27) Schultz, I. R.; Shangraw, R. E. Effect of short-term drinking water exposure to dichloroacetate on its pharmacokinetics and oral bioavailability in human volunteers: a stable isotope study. *Toxicol. Sci.* **2006**, *92*, 42−50.
(28) Deuse, T.; Hua, X.; Wang, D.; Maegdefessel, L.; Heeren, J.; Scheja, L.; Bolaños, J. P.; Rakovic, A.; Spin, J. M.; Stubbendorff, M.; Ikeno, F.; Länger, F.; Zeller, T.; Schulte-Uentrop, L.; Stoehr, A.; Itagaki, R.; Haddad, F.; Eschenhagen, T.; Blankenberg, S.; Kiefmann, R.; Reichenspurner, H.; Velden, J.; Klein, C.; Yeung, A.; Robbins, R. C.; Tsao, P. S.; Schrepfer, S. Dichloroacetate prevents restenosis in preclinical animal models of vessel injury. *Nature* **2014**, *509*, 641−644.
(29) Zauli, G.; Celeghini, C.; Melloni, E.; Voltan, R.; Ongari, M.; Tiribelli, M.; di Iasio, M. G.; Lanza, F.; Secchiero, P. The sorafenib plus nutlin-3 combination promotes synergistic cytotoxicity in acute myeloid leukemic cells irrespectively of FLT3 and p53 status. *Haematologica* **2012**, *97*, 1722−1730.
(30) Voltan, R.; di Iasio, M. G.; Bosco, R.; Valeri, N.; Pekarski, Y.; Tiribelli, M.; Secchiero, P.; Zauli, G. Nutlin-3 downregulates the expression of the oncogene TCL1 in primary B chronic lymphocytic leukemic cells. *Clin. Cancer Res.* **2011**, *17*, 5649−5655.
(31) Celeghini, C.; Voltan, R.; Rimondi, E.; Gattei, V.; Zauli, G. Perifosine selectively induces cell cycle block and modulates retinoblastoma and E2F1 protein levels in p53 mutated leukemic cell lines. *Invest. New Drugs* **2011**, *29*, 392−395.
(32) Secchiero, P.; Melloni, E.; di Iasio, M. G.; Tiribelli, M.; Rimondi, E.; Corallini, F.; Gattei, V.; Zauli, G. Nutlin-3 up-regulates the expression of Notch1 in both myeloid and lymphoid leukemic cells, as part of a negative feedback antiapoptotic mechanism. *Blood* **2009**, *113*, 4300−4308.
(33) Secchiero, P.; Rimondi, E.; di Iasio, M. G.; Agnoletto, C.; Melloni, E.; Volpi, I.; Zauli, G. C-Reactive protein downregulates TRAIL expression in human peripheral monocytes via an Egr-1-dependent pathway. *Clin. Cancer Res.* **2013**, *19*, 1949−1959.
(34) Zauli, G.; Voltan, R.; Bosco, R.; Melloni, E.; Marmiroli, S.; Rigolin, G. M.; Cuneo, A.; Secchiero, P. Dasatinib plus Nutlin-3 shows synergistic antileukemic activity in both p53 wild-type and p53 mutated B chronic lymphocytic leukemias by inhibiting the Akt pathway. *Clin. Cancer Res.* **2011**, *17*, 762−770.
(35) Tisato, V.; Garrovo, C.; Biffi, S.; Petrera, F.; Voltan, R.; Casciano, F.; Meroni, G.; Agnoletto, C.; Zauli, G.; Secchiero, P. Intranasal administration of recombinant TRAIL down-regulates CXCL-1/KC in an ovalbumin-induced airway inflammation murine model. *PLoS One* **2014**, *9*, e115387.

DOI: 10.1021/acs.jmedchem.5b01165
J. Med. Chem. 2016, 59, 147−156

Psychopharmacology (2016) 233:3685–3709
DOI 10.1007/s00213-016-4402-y

ORIGINAL INVESTIGATION

Effect of the novel synthetic cannabinoids AKB48 and 5F-AKB48 on "tetrad", sensorimotor, neurological and neurochemical responses in mice. In vitro and in vivo pharmacological studies

Isabella Canazza[1] · Andrea Ossato[1] · Claudio Trapella[2] · Anna Fantinati[2] · Maria Antonietta De Luca[3] · Giulia Margiani[3] · Fabrizio Vincenzi[4] · Claudia Rimondo[5] · Fabiana Di Rosa[6] · Adolfo Gregori[6] · Katia Varani[4] · Pier Andrea Borea[4] · Giovanni Serpelloni[7] · Matteo Marti[1,8]

Received: 26 April 2016 / Accepted: 1 August 2016 / Published online: 15 August 2016

Abstract
Rationale AKB48 and its fluorinate derivate 5F-AKB48 are two novel synthetic cannabinoids belonging to a structural class with an indazole core structure. They are marketed as incense, herbal preparations or chemical supply for their psychoactive Cannabis-like effects.
Objectives The present study was aimed at investigating the in vitro and in vivo pharmacological activity of AKB48 and 5F-AKB48 in male CD-1 mice and comparing their in vivo effects with those caused by the administration of Δ^9-THC and JWH-018.
Results In vitro competition binding experiments performed on mouse and human CB_1 and CB_2 receptors revealed a nanomolar affinity and potency of the AKB48 and 5F-AKB48. In vivo studies showed that AKB48 and 5F-AKB48, induced hypothermia, increased pain threshold to both noxious mechanical and thermal stimuli, caused catalepsy, reduced motor activity, impaired sensorimotor responses (visual, acoustic and tactile), caused seizures, myoclonia, hyperreflexia and promoted aggressiveness in mice. Moreover, microdialysis study in freely moving mice showed that systemic administration of AKB48 and 5F-AKB48 stimulated dopamine release in the nucleus accumbens. Behavioural, neurological and neurochemical effects were fully prevented by the selective CB_1 receptor antagonist/inverse agonist AM 251.
Conclusions For the first time, the present study demonstrates the overall pharmacological effects induced by the administration of AKB48 and 5F-AKB48 in mice and suggests that the fluorination can increase the power and/or effectiveness of SCBs. Furthermore, this study outlines the potential detrimental effects of SCBs on human health.

Keywords AKB48 · 5F-AKB48 · JWH-018 · Δ^9-THC · Sensorimotor responses · Cannabinoids · Synthetic cannabinoids · Behavior · Microdialysis

Isabella Canazza and Andrea Ossato are equally contributed to this work.

Electronic supplementary material The online version of this article (doi:10.1007/s00213-016-4402-y) contains supplementary material, which is available to authorized users.

✉ Matteo Marti
m.marti@unife.it

[1] Department of Life Sciences and Biotechnology (SVeB), University of Ferrara, via Fossato di Mortara 17-19, 44121 Ferrara, Italy

[2] Department of Chemistry and Pharmaceutical Sciences, University of Ferrara, Ferrara, Italy

[3] Department of Biomedical Sciences, University of Cagliari, Cagliari, Italy

[4] Department of Medical Sciences, University of Ferrara, Ferrara, Italy

[5] Department of Diagnostic and Public Health, University of Verona, Verona, Italy

[6] Department of Scientific Investigation (RIS), Carabinieri, 00191 Rome, Italy

[7] U.R.I.To.N., Forensic Toxicology Unit, Department of Health Science, University of Florence, Florence, Italy

[8] Center for Neuroscience and Istituto Nazionale di Neuroscienze, , Italy

Abbreviations

AM 251 1-(2,4-Dichlorophenyl)-5-(4-iodophenyl)-4-methyl-*N*-(piperidin-1-yl)-1*H*-pyrazole-3-carboxamide

AKB48	*N*-(1-Adamantyl)-1-pentyl-1*H*-indazole-3-carboxamide
DA	Dopamine
NAc shell	Nucleus accumbens shell
Δ^9-THC	(−)-Δ^9-THC or Dronabinol®
JWH-018	Naphthalen-1-yl-(1-pentylindol-3-yl)methanone
5F-AKB48	*N*-(1-Adamantyl)-1-(5-fluoropentyl)-1*H*-indazole-3- carboxamide

Introduction

During the first half of 2013, AKB48 (*N*-(1-adamantyl)-1-pentyl-1*H*-indazole-3-carboxamide), also known as APINACA, and its derivative fluorinated 5F-AKB48 (*N*-(adamantan-1-yl)-1-(4-fluorobutyl)-1*H*-indazole-3-carboxamide) formed respectively 1.0 and 2.5 % of all synthetic cannabinoids (SCBs) reported by the DEA-operated National Forensic Laboratory Information System in the USA (NFLIS 2013). Toxicological and forensic analysis revealed their presence in seized products or in biological fluids of people subjected to toxicological control (Uchiyama et al. 2012; Karinen et al. 2015; Vikingsson et al. 2015; Odoardi et al. 2016). As described by Santacroce and collaborators (Santacroce et al. 2015), AKB48 and 5FAKB48 may be retrieved in products sold as incense mixtures, as a sole ingredient infused on herbs or as a powder (EMCDDA 2009; EMCDDA 2015). AKB48 and 5F-AKB48 may be added to tobacco or sprayed on leaves and then smoked, inhaled from heated aluminum foil, dissolved in ethanol and finally ingested with lipid-rich foods or vaporized (DrugsForum 2012a; DrugsForum 2012b). AKB48 and 5F-AKB48 bind at nanomolar concentration at CB_1 cannabinoid receptor (Uchiyama et al. 2013; De Luca et al. 2015b), suggesting that they could have similar or more higher in vivo effects as others SCBs. Recent findings showed that the adamantylindazole compounds (i.e. 5F-AKB48) induce DNA damage at the chromosomal level, without causing gene mutations (Koller et al. 2015). AKB48 and 5F-AKB48 do not belong to any of the seven groups commonly used to classify synthetic cannabinoids: cyclohexylphenol (such as cannabicyclohexanol (CCH) and CP-47,497), classical cannabinoids (such as HU-210), naphthoylindoles (such as JWH-018 and JWH-073), phenylacetylindoles (such as JWH-250 and JWH-203), benzoylindoles (such as AM-694 and RCS-4), naphthoylnaphthalenes (such as CB-13) and adamantylindoles (APICA) but are adamantylindazole (Uchiyama et al. 2012). In particular, AKB48 differs from earlier JWH-type SCBs by having an adamantyl group connected to an indazole moiety through a carboxamide linkage. Furthermore, to increase the lipophilicity of AKB48, hence enhancing the absorption through biological membranes/blood–brain barrier (Schifano et al. 2015), a fluorine atom was linked at the 5-pentyl position of the indazole scaffold. This formulation strategy was previously carried out for AM-2201, the fluorinated analog of JWH-018 (Gandhi et al. 2013). The metabolism of AKB48 and 5F-AKB48 has been identified using a hepatocyte model (Gandhi et al., 2013) and human liver microsomal incubation (Holm et al. 2015). In particular, AKB48 was metabolized in 11 major metabolites that included monohydroxylated, dihydroxylated, trihydroxylated, and mono- and dihydroxylated glucuronide conjugates and dihydroxylated with ketone formation at the *N*-pentyl side chain (Gandhi et al., 2013). As reported for other SCBs, this aspect should be considered since a large number of metabolites could maintain agonistic activity at CB_1 receptors, as demonstrated for JWH-018 and other SCBs (Brents et al. 2011; Brents et al. 2012). Despite the presence of these in vitro metabolism studies, there are poor preclinical in vivo evidence on pharmaco-toxicological effects of these SCBs. Recently, it was shown that 5F-AKB48 facilitated dopamine (DA) release in the Nucleus Accumbens shell of rats (De Luca et al. 2015b), suggesting its potential positive role in rewarding mechanisms (Miliano et al. 2016), as already mentioned for other SCBs, as well as JWH-018 (De Luca et al. 2015a), JWH-250 and JWH-073 (Ossato et al. 2016). Moreover, AKB48 depressed spontaneous locomotion in ND4 Swiss-Webster mice and positively substituted for the discriminative stimulus effects of Δ^9-THC in rats (Gatch and Forster, 2015). Therefore, the present study was aimed at investigating the acute effect of AKB48 and 5F-AKB48 (0.01–6 mg/kg i.p.) on body temperature, acute mechanical and thermal analgesia, catalepsy, motor activity, sensorimotor responses (to visual, acoustic and tactile stimulation), neurological changes (convulsion, hyperreflexia, and myoclonia), aggressive response and modulation of DAergic release in mesoaccumbal pathway in CD-1 mice. In vitro binding studies on CD-1 murine and human CB_1/CB_2 receptors have been also performed. Moreover, to better understand the behavioural effects of the AKB48 and 5F-AKB48, their actions were compared with those of JWH-018 and Δ^9-THC and effects were monitored for over 5 h.

Materials and methods

Animals

Male ICR (CD-1®) mice, 25–30 g (ENVIGO Harlan Italy; S. Pietro al Natisone, Italy), were group-housed (8–10 mice per cage; floor area per animal was 80 cm^2; minimum enclosure height was 12 cm) on a 12:12-h light–dark cycle (light period from 6:30 AM to 6:30 PM), temperature of 20–22 °C, humidity of 45–55 % and were provided ad libitum access to food (Diet 4RF25 GLP; Mucedola, Settimo Milanese, Milan, Italy) and water. Experimental protocols performed in the present study were in accordance with the European Communities Council Directive of September 2010 (2010/63/EU) and were

approved by Italian Ministry of Health (license n. 335/2016-PR) and by the Ethics Committee of the University of Ferrara. Moreover, adequate measures were taken to minimize the number of animals used and their pain and discomfort.

Drug preparation and dose selection

AKB48 (Fig. 1a), 5F-AKB48 (Fig. 1b), JWH-018 (Fig. 1c) and (−)-Δ^9-THC (Dronabinol®) were purchased from LGC Standards (LGC Standards S.r.l., Sesto San Giovanni, Milan, Italy), while AM 251 was purchased from Tocris (Tocris, Bristol, UK). Drugs were initially dissolved in absolute ethanol (final concentration was 2 %) and Tween 80 (2 %) and brought to the final volume with saline (0.9 % NaCl). The solution made of ethanol, Tween 80 and saline was also used as the vehicle. Drugs were administered by intraperitoneal injection at a volume of 4 μl/g. The CB_1 receptor-preferring antagonist/inverse agonist AM 251 (6 mg/kg) was administered 20 min before AKB48 and 5F-AKB48 injections. The single dose of AM 251 at 6 mg/kg was chosen based on previous studies that have shown that this dose was able to block the behavioural effects caused by administration of high doses (6 mg/kg) of synthetic cannabinoids such as JWH-018, JWH-018 Cl, JWH-018 Br (Vigolo et al., 2015; Ossato et al., 2015), JWH-073 and JWH-250 (Ossato et al., 2016) in mice. Recently, we reported that the memory impairment in the novel object recognition test in mice caused by JWH-018 (0.01–1 mg/kg) is prevented by administration of AM 251 in a ratio of doses 1:1 (Barbieri et al., 2016). Moreover, in preliminary studies on the visual sensorimotor responses in mice, effects caused by administration of AKB48 and 5F-AKB48 (both at 6 mg/kg) were progressively prevented by administration of AM 251 at 1, 3 and 6 mg/kg (prevented by about ~35, ~56 and ~100 % for AKB48 and ~20, ~35 and ~98 % for 5F-AKB48; data not shown). Therefore, in the present study, we used the full dose of AM 251 (6 mg/kg) in order to completely block the effects caused by higher doses of AKB48 and 5F-AKB48. A novel set of Δ^9-THC and JWH-018 data (stimulated aggressiveness) has been done in the present study. Doses of AKB48 and 5F-AKB48 (0.01–6 mg/kg i.p.) were chosen based on previous studies (Vigolo et al. 2015; Ossato et al. 2015; Ossato et al. 2016).

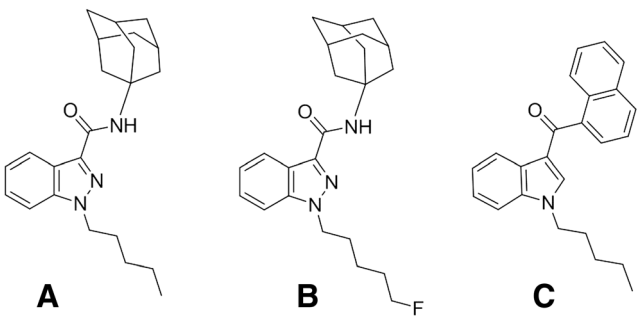

Fig. 1 Chemical structures of **a** AKB48 (*N*-(1-adamantyl)-1-pentyl-1*H*-indazole-3-carboxamide), **b** 5F-AKB48 (*N*-(1-adamantyl)-1-(5-fluoropentyl)-1*H*-indazole-3- carboxamide) and **c** JWH-018 (Naphthalen-1-yl-(1-pentylindol-3-yl)methanone)

Mouse tissues and cell culture membrane preparation

After mice were sacrificed by cervical dislocation, brain and spleen were removed and suspended in 50 mM Tris HCl buffer, pH .4 at 4 °C. The mouse brain suspension was homogenized with a Polytron and centrifuged for 20 min at 40,000×*g*. The mouse spleen was homogenized with a Polytron and centrifuged for 10 min at 2000×*g*. The supernatant was filtered and centrifuged for 20 min at 40,000×*g*. The resulting pellets were used for competition binding experiments (Vincenzi et al. 2013). CHO cells transfected with human CB_1 or CB_2 receptors (Perkin Elmer Life and Analytical Sciences, USA) were grown adherently and maintained in Ham's F12 containing 10 % fetal bovine serum, penicillin (100 U/ml), streptomycin (100 μg/ml) and Geneticin (G418, 0.4 mg/ml) at 37 °C in 5 % CO_2/95 % air. For membrane preparation, the culture medium was removed and the cells were washed with PBS and scraped off plates in ice-cold hypotonic buffer (5 mM Tris HCl, 2 mM EDTA, pH .4). The cell suspension was homogenized with a Polytron and then centrifuged for 30 min at 40,000×*g*. The membrane pellet was suspended in 50 mM Tris HCl buffer (pH .4) containing 2.5 mM EDTA, 5 mM $MgCl_2$, 0.5 mg/ml BSA for CB_1 receptors or in 50 mM Tris HCl (pH .4), 1 mM EDTA, 5 mM $MgCl_2$, 0.5 mg/ml BSA for CB_2 adenosine receptors (Vincenzi et al. 2013).

[^{3}H] CP-55,940 competition binding assays and cyclic AMP assays

Competition binding experiments were performed as previously reported (Vincenzi et al. 2013; Vigolo et al., 2015) using 0.5 nM [^{3}H]-CP-55,940 and different concentrations of the tested compounds with membranes obtained from CHO cells transfected with human CB_1 or CB_2 receptors (2 μg protein/100 μl). Competition binding experiments were also performed in mouse brain membranes (40 μg protein/100 μl) for CB_1 receptors and in mouse spleen membranes (80 μg protein/100 μl) for CB_2 receptors. Non-specific binding was determined in the presence of 1 μM WIN 55,212–2. The filter bound radioactivity was counted using a Packard Tri Carb 2810 TR scintillation counter. Cyclic AMP assays were carried out in CHO cells transfected with human CB_1 or CB_2 receptors which were washed with PBS, detached with trypsin and centrifuged for 10 min at 200×*g* (Vincenzi et al. 2013; Vigolo et al. 2015). The pellet was suspended in 0.5 ml of incubation mixture: 150 mM NaCl, 2.7 mM KCl, 0.37 mM NaH_2PO_4, 1 mM $MgSO_4$, 1 mM $CaCl_2$, 5 mM Hepes, 10 mM $MgCl_2$, 5 mM glucose, pH .4 at

37 °C. Then, 0.5 mM Ro 20–1724 as a phosphodiesterase inhibitor was added and pre-incubated for 10 min in a shaking bath at 37 °C. Different concentrations of cannabinoid agonists were then added and incubated for 10 min before the addition of forskolin 1 μM. After a further 5 min, the reaction was terminated by the addition of cold 6 % trichloroacetic acid and the suspension was centrifuged at 2000×*g* for 15 min at 4 °C. Trichloroacetic acid was extracted with water-saturated diethyl ether, and the final aqueous solution was tested for cyclic AMP levels by a competition protein binding assay. One hundred microliters of samples or cyclic AMP standards (0–10 pmol) were added to each test tube containing the incubation buffer (0.1 M Trizma base, 8.0 mM aminophylline, and 6.0 mM 2-mercaptoethanol, pH .4) and [^{3}H]-cyclic AMP in a total volume of 0.5 ml. The binding protein was prepared by using cortical tissues from beef adrenal glands that were homogenized in 10 vol of buffer consisting of 100 mM Tris HCl, 250 mM NaCl, 10 mM EDTA, 0.1 % 2-mercaptoethanol, 0.25 M sucrose, pH .4 (Nordstedt and Fredholm 1990). The homogenate was filtered and centrifuged at 30,000×*g* for 30 min at 4 °C. The supernatant, opportunely diluted, was added to the samples and incubated at 4 °C for 150 min. After the addition of charcoal, samples were centrifuged at 2000×*g* for 10 min. The clear supernatant (0.2 ml) was mixed with 4 ml of Ultima Gold scintillation cocktail and counted in a Packard Tri Carb 2810 TR scintillation counter.

Behavioural studies

The effect of AKB48 and 5F-AKB48 was investigated using a battery of behavioural tests widely used in studies of "safety-pharmacology" for the preclinical characterization of new molecules in rodents (Irwin, 1968; Mattsson et al. 1996; Porsolt et al. 2002; Redfern et al. 2005; Hamdam et al. 2013; S7A 2001). Those tests have been also validated to describe effects of cannabinoids on the "tetrad", sensorimotor and neurological changes in mice (Compton et al. 1992; Vigolo et al. 2015; Ossato et al. 2015; Ossato et al. 2016). To reduce the number of animals used, the behaviour of mice was evaluated in five consecutive experimental sections (for a detailed information, see Supplementary Material). Moreover, to reduce the animal's stress induced by manipulation, and to confirm the stability and reproducibility over time of the responses of our tests, animals were trained 2 times per week for 2 weeks before the pharmacological treatment. All experiments were performed between 8:30 AM to 2:00 PM. Experiments were conducted in blind by trained observers working together in pairs (Redfern et al. 2005). The behavior of mice (neurologic and sensorimotor responses) was videotaped and analyzed off-line by a different trained operator that gives test scores.

Major neurological changes and aggressive response

As previously described by others studies (Vigolo et al. 2015; Ossato et al. 2015; Ossato et al. 2016), tail elevation, hyperreflexia, myoclonus, convulsions and aggressive responses in mice were observed immediately after SCBs administration (for detailed information see Supplementary Material). The tail elevation was measured during the observation of the freely moving mice in a square area (score 0/4 not tail elevation, score 4/4 Straub tail; for detailed information see Supplementary Material). Spontaneous aggressive response was measured based on the number of bites that the freely moving mouse confers to an object of gray cloth that approaches the front of the snout of the animal, while in the case of stimulated aggressiveness the animal is manually restrained. Moreover, it is held in a supine position following which an object is brought near its mouth. For both spontaneous and stimulated aggressive behavior tests, a gray cloth was placed in front of the mouse's nose for 10 consecutive times (score 0/10 not aggressive, score 10/10 very aggressive).

Sensorimotor studies

We studied the voluntary and involuntary sensorimotor responses resulting from different mouse reaction to visual, acoustic and tactile stimuli (Koch 1999; Marti et al. 2013; Ossato et al. 2015; for detailed information see Supplementary Material).

Visual response was verified by two behavioural tests, which evaluated the ability of the mouse to capture visual information even when the animal is moving (the visual placing response) or when it is stationary (the visual object response). *Visual Placing response* test is performed using a tail suspension modified apparatus able to bring down the mouse towards the floor at a constant speed of 10 cm/s (Ossato et al. 2015). *Visual object response* test was used to evaluate the ability of the mouse to see an object approaching from the front or the side, than inducing the animal to shift or turn the head or retreat it (Ossato et al. 2015).

Acoustic response measures the reflex of the mouse in replay to an acoustic stimulus produced behind the animal (Koch 1999).

The tactile response in the mouse was verified through vibrissae, pinna and corneal reflexes (Ossato et al. 2015).

"*Tetrad*" *paradigm for screening cannabinoid-like effect*

To better assess the effects of the ligands on thermoregulation, we measured both changes in the core (rectal) and surface (ventral fur) temperature (for a detailed information, see Supplementary Material). The *core temperature* was evaluated by a probe (1 mm diameter) that was gently inserted, after lubrication with liquid vaseline, into the rectum of the mouse (to

about 2 cm) and left in position until the stabilization of the temperature (about 10 s; Vigolo et al. 2015). The probe was connected to a Cole Parmer digital thermometer (model 8402). The *surface temperature* was measured by a Microlife FR 1DZ1 digital infrared thermometer, placed at 1 cm from the surface of the abdomen of the mouse (Vigolo et al. 2015).

Acute mechanical and thermal nociception was evaluated respectively using the tail pinch and the tail withdrawal test (Vigolo et al. 2015; for detailed information see Supplementary Material).

Alterations of motor activity induced by AKB48 and 5F-AKB48 were measured using the bar, drag, accelerod tests and the analysis of spontaneous locomotor activity (Marti et al. 2004; Marti et al. 2005; Vigolo et al. 2015; Ossato et al. 2015; for detailed information see Supplementary Material).

In vivo brain microdialysis studies

Male ICR (CD-1®) mice, 25–30 g (ENVIGO. Harlan Italy; S. Pietro al Natisone, Italy) were anaesthetized with Sodium Penthobarbital (50 mg/kg i.p.; Sigma-Aldrich, Italy) and implanted with vertical dialysis probe (1 mm dialyzing portion) prepared with AN69 fibers (Hospal Dasco, Bologna, Italy) in the Nucleus Accumbens shell (NAc shell; A + 1.4, L 0.4 from

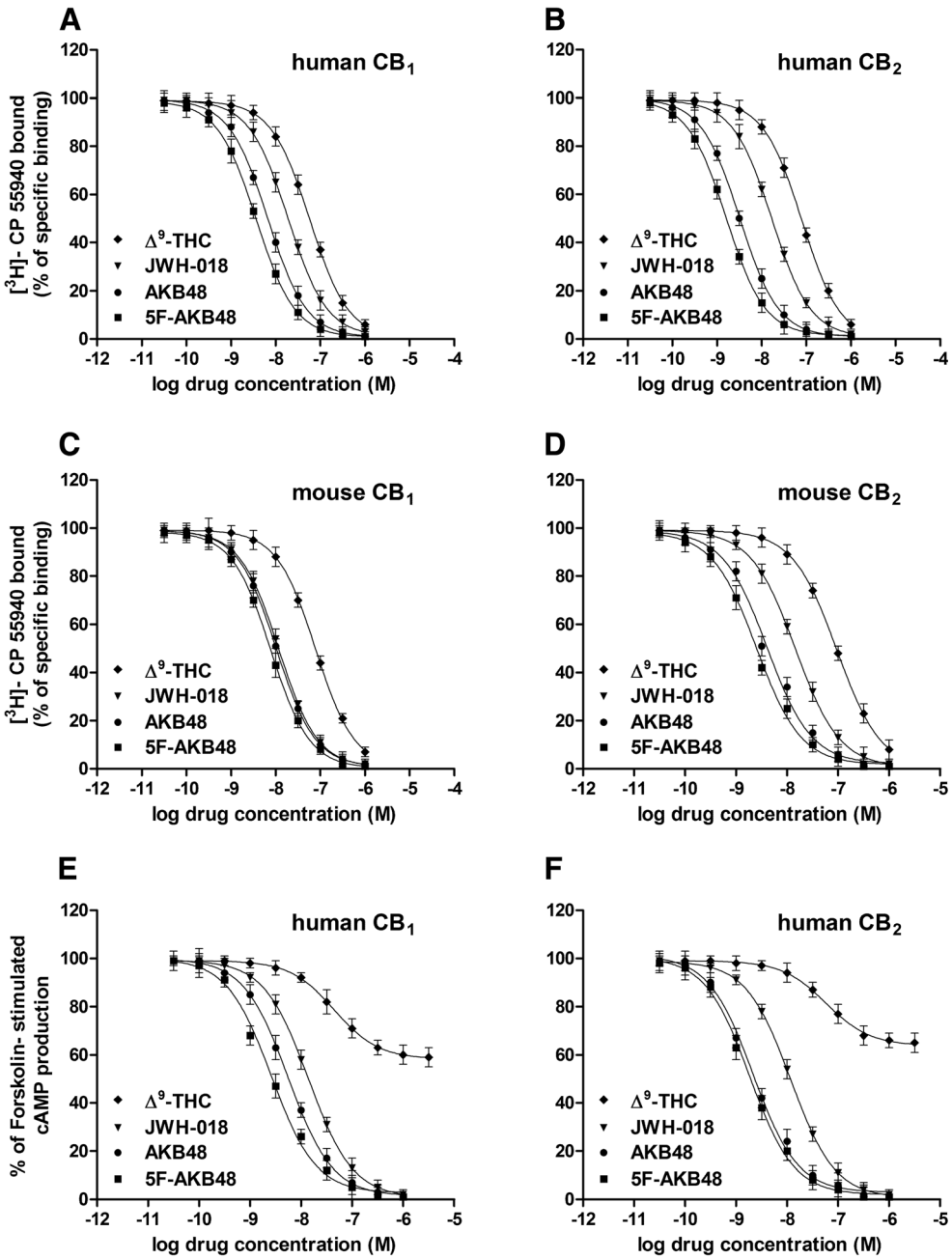

Fig. 2 Competition curves of specific [^{3}H]-CP 55940 binding by AKB48 and 5F-AKB48, in comparison to Δ^9-THC and JWH-018, in CHO cell membranes transfected with human CB_1 receptors (**a**) or human CB_2 receptors (**b**) and to CB_1 receptors expressed in mouse brain membranes (**c**) or CB_2 receptors expressed in mouse spleen membranes (**d**). Inhibition curves of forskolin-stimulated cAMP accumulation by AKB48 and 5F-AKB48, in comparison to Δ^9-THC and JWH-018, in CHO cells transfected with human CB_1 receptors (**e**) or human CB_2 receptors (**f**). Results are given as the mean ± SEM of three independent experiments performed in duplicate

bregma, V-4.8 from dura) according to the mouse brain atlas by Paxinos and Franklin (Second Edition, 2001). On the day following surgery, probes were perfused with Ringer's solution (147 mM NaCl, 4 mM KCl, 2.2 mM $CaCl_2$) at a constant rate of 1 μl/min. Dialysate samples (15 μl) were injected into an HPLC equipped with a reverse phase column (C8 3.5 um, Waters, USA) and a coulometric detector (ESA, Coulochem II) to quantify DA. The first electrode of the detector was set at +130 mV (oxidation) and the second at −175 mV (reduction). The composition of the mobile phase was: 50 mM NaH_2PO_4, 0.1 mM Na_2-EDTA, 0.5 mM *n*-octyl sodium sulfate, 15 % (*v*/*v*) methanol, pH .5. The sensitivity of the assay for dopamine (DA) was 5 fmol/sample. At the end of each experiment, animals were sacrificed and their brains removed and stored in formalin (8 %) for histological examination to verify the correct placement of the microdialysis probe.

Data and statistical analysis

Protein concentrations were determined according to a Bio-Rad method with bovine serum albumin as reference standard. Inhibitory binding constants (Ki) were calculated from the IC_{50} values according to the Cheng and Prusoff equation: $Ki = IC_{50}/(1 + [C^*]/K_D^*)$, where [C*] is the concentration of the radioligand and K_D^* its dissociation constant. Functional experiments were analyzed by non-linear regression analysis using the equation for a sigmoid concentration-response curve using Prism (GraphPad Prism, USA). All data are expressed as the mean ± SEM of 3 independent experiments. Core and surface temperature values are expressed as the difference between control temperature (before injection) and temperature following drug administration (Δ°C). Antinociception (tail withdrawal and tail pinch tests) and catalepsy (bar test) are calculated as percent of maximal possible effect {EMax% = [(test − control latency)/(cutoff time − control)] × 100}. Data are expressed in absolute values (s in neurological changes and immobility time, m for distance travelled, m/s for calculation of maximum speed and n° of bites in the aggressive response test), Δ°C (core and surface temperature), Emax% (tail withdrawal, tail pinch and bar test) and percentage of basal (drag test and accelerod test). In sensorimotor response experiments, data are expressed in arbitrary units (visual objects response, acoustic response, vibrissae, corneal and pinna reflex) and percentage of baseline (visual placing response). In microdialysis experiments, data are expressed as percentage of DA basal values. All the numerical data are given as mean ± SEM. Data were analyzed by utilizing repeated measures ANOVA. Results from treatments showing significant overall changes were subjected to post hoc Tukey tests with significance for $p < 0.05$. The statistical analysis of the effects of the individual substances in different concentrations over time and that of antagonism studies in histograms were performed by two-way ANOVA followed by Bonferroni's test for multiple comparisons. The analysis of the total average effect induced by treatments (expressed in the panels D) was performed with one-way ANOVA followed by Tukey's test for multiple comparisons. The Student's *t* test was used to determine statistical significance ($P < 0.05$) between two groups (see neurological changes). The statistical analysis was performed with the program Prism software (GraphPad Prism, USA). The detailed results of the statistical tests are detailed in the Supplementary Material.

Results

Affinity and potency of AKB48 and 5F-AKB48 for CB_1 and CB_2 cannabinoid receptors

Competition binding experiments performed in CHO cell membranes transfected with human CB_1 or CB_2 (Fig. 2a, b) receptors revealed affinity values of the examined compounds in the nanomolar range. The affinity values of Δ^9-THC and JWH-018, which were used as reference compounds, are reported in Table 1. The introduction of a fluorine group in the structure of AKB48 determined a slightly increase in the

Table 1 Binding and functional parameters of AKB48 and 5F-AKB48 to human and mouse CB_1 and CB_2 receptors, in comparison to Δ^9-THC and JWH-018

Compound	hCB1 CHO membranes[a] Ki (nM)	hCB2 CHO membranes[a] Ki (nM)	Mouse cortex membrane CB1[a] Ki (nM)	Mouse spleen membranes CB2 Ki (nM)	hCB1 CHO cells[b] IC_{50} (nM)	hCB2 CHO cells[b] IC_{50} (nM)
Δ^9-THC	28.35 ± 2.43	37.82 ± 3.14	39.21 ± 2.88	45.57 ± 4.18	44.76 ± 4.68	56.24 ± 5.12
JWH-018	9.62 ± 0.79	8.55 ± 0.73	5.79 ± 0.63	7.24 ± 0.65	13.88 ± 1.19	11.54 ± 1.06
AKB48	3.24 ± 0.28	1.68 ± 0.12	5.34 ± 0.44	1.93 ± 0.14	5.39 ± 0.47	2.13 ± 0.21
5F-AKB48	1.82 ± 0.15	0.82 ± 0.07	3.87 ± 0.27	1.24 ± 0.07	2.57 ± 0.19	1.94 ± 0.14

Data are expressed as mean ± SEM

[a] [^{3}H]-CP-55,940 competition binding experiments

[b] Cyclic AMP experiments

Table 2 Effects of the systemic administration of Δ^9-THC (0.01–100 mg/Kg i.p.), JWH-018, AKB48 and 5F-AKB48 (0.01–6 mg/Kg i.p.) on the neurological changes of the mouse

Elevation tail																						
Compound	Vehicle	Δ^9-THC[a]							JWH-018[a]					AKB48					5F-AKB48				
Doses(mg/Kg)		*0.01*	*0.1*	*1*	*3*	*6*	*30*	*100*	*0.01*	*0.1*	*1*	*3*	*6*	*0.01*	*0.1*	*1*	*3*	*6*	*0.01*	*0.1*	*1*	*3*	*6*
Frequency (%)	–	–	–	–	–	–	10	65	–	–	10	35	80	–	–	–	40	70	–	–	–	30	75
Score	–	–	–	–	–	–	0.6 ± 0.76	1.1 ± 0.8	–	–	0.5 ± 0.41	1.2 ± 0.17	2.4 ± 0.33	–	–	–	2.2 ± 0.6	1.88 ± 0.3	–	–	–	2.6 ± 0.12 *	3.1 ± 0.2 #
Duration (sec)	–	–	–	–	–	–	654.7 ± 82.9	934.7 ± 88.2	–	–	412.6 ± 132.9	1236.8 ± 111.5	1766.6 ± 189.7	–	–	–	1007.7 ± 146	998.5 ± 89 **	–	–	–	1271 ± 122	1436.1 ± 157
Latency (sec)	–	–	–	–	–	–	112.5 ± 33.9	103.6 ± 17.4	–	–	92.5 ± 17.1	94.8 ± 16.3	88.6 ± 13.4	–	–	–	99.7 ± 24	101.2 ± 21	–	–	–	88.2 ± 18	91.2 ± 10
Hyperreflexia																						
Compound	Vehicle	Δ^9-THC[a]							JWH-018[a]					AKB48					5F-AKB48				
Doses (mg/Kg)		*0.01*	*0.1*	*1*	*3*	*6*	*30*	*100*	*0.01*	*0.1*	*1*	*3*	*6*	*0.01*	*0.1*	*1*	*3*	*6*	*0.01*	*0.1*	*1*	*3*	*6*
Frequency (%)	–	–	–	–	–	–	–	–	–	–	–	15	80	–	–	–	–	25	–	–	–	30	75
Duration (s)	–	–	–	–	–	–	–	–	–	–	–	1354.8 ± 67.2	1439.8 ± 45.3	–	–	–	–	1980.2 ± 298	–	–	–	1009 ± 221	1254.2 ± 210
Latency (s)	–	–	–	–	–	–	–	–	–	–	–	124.9 ± 31.7	93.5 ± 21.2	–	–	–	–	143 ± 55	–	–	–	191.2 ± 51	179 ± 61
Myoclonie																						
Compound	Vehicle	Δ^9-THC[a]							JWH-018[a]					AKB48					5F-AKB48				
Doses (mg/Kg)		*0.01*	*0.1*	*1*	*3*	*6*	*30*	*100*	*0.01*	*0.1*	*1*	*3*	*6*	*0.01*	*0.1*	*1*	*3*	*6*	*0.01*	*0.1*	*1*	*3*	*6*
Frequency (%)	–	–	–	–	–	–	–	–	–	–	–	–	80	–	–	–	–	45	–	–	–	90	100
Duration (s)	–	–	–	–	–	–	–	–	–	–	–	–	669.7 ± 36.6	–	–	–	–	1087.6 ± 241	–	–	–	1181.6 ± 224	1593 ± 299 *
Latency (s)	–	–	–	–	–	–	–	–	–	–	–	–	109.7 ± 16.35	–	–	–	–	185 ± 19.7	–	–	–	224 ± 41	210 ± 36 *
Convulsion																						
Compound	Vehicle	Δ^9-THC[a]							JWH-018[a]					AKB48					5F-AKB48				
Doses (mg/Kg)		*0.01*	*0.1*	*1*	*3*	*6*	*30*	*100*	*0.01*	*0.1*	*1*	*3*	*6*	*0.01*	*0.1*	*1*	*3*	*6*	*0.01*	*0.1*	*1*	*3*	*6*
Frequency (%)	–	–	–	–	–	–	–	–	–	–	–	–	70	–	–	–	–	30	–	–	–	30	90
Duration (s)	–	–	–	–	–	–	–	–	–	–	–	–	369.7 ± 32.2	–	–	–	–	454.2 ± 67.1	–	–	–	480.1 ± 59	1821.3 ± 457 ** ##
Latency (s)	–	–	–	–	–	–	–	–	–	–	–	–	109.7 ± 16.3	–	–	–	–	248 ± 79	–	–	–	271.3 ± 47.9	274.7 ± 69.2
Spontaneous aggressiveness																						
Compound	Vehicle	Δ^9-THC[a]							JWH-018[a]					AKB48					5F-AKB48				
Doses (mg/Kg)		*0.01*	*0.1*	*1*	*3*	*6*	*30*	*100*	*0.01*	*0.1*	*1*	*3*	*6*	*0.01*	*0.1*	*1*	*3*	*6*	*0.01*	*0.1*	*1*	*3*	*6*
Frequency (%)	–	–	–	–	–	–	–	–	–	–	–	–	90	–	–	–	–	50	–	–	–	50	100
Score (n° of bites)	–	–	–	–	–	–	–	–	–	–	–	–	8.2 ± 3.1	–	–	–	–	1.60 ± 1.7	–	–	–	1.4 ± 0.31	1.7 ± 2.9
Duration (s)	–	–	–	–	–	–	–	–	–	–	–	–	2750 ± 621	–	–	–	–	2971.1 ± 581	–	–	–	3303 ± 512	3272.6 ± 602
Latency (s)	–	–	–	–	–	–	–	–	–	–	–	–	324.5 ± 76	–	–	–	–	318.2 ± 88	–	–	–	296.2 ± 66	302.2 ± 64
Stimulated aggressiveness																						
Compound	Vehicle	Δ^9-THC[a]							JWH-018[a]					AKB48					5F-AKB48				
Doses (mg/Kg)		*0.01*	*0.1*	*1*	*3*	*6*	*30*	*100*	*0.01*	*0.1*	*1*	*3*	*6*	*0.01*	*0.1*	*1*	*3*	*6*	*0.01*	*0.1*	*1*	*3*	*6*
Frequency (%)	–	–	–	–	–	–	–	–	–	–	–	50	100	–	–	–	35	70	–	–	30	70	100
Score (n° of bites)	–	–	–	–	–	–	–	–	–	–	–	5.1 ± 4.3	10 ± 0.2	–	–	–	1.75 ± 1.7	4.37 ± 3.9	–	–	3.75 ± 4.1	7.3 ± 3.6	4.75 ± 2.9
Duration (s)	–	–	–	–	–	–	–	–	–	–	–	12,316 ± 4	15,286 ± 408	–	–	–	3499 ± 553	7217.1 ± 677 ***	–	–	3051.8 ± 590	14,071 ± 387 ###	14,482 ± 428 ###

Data are expressed as percentage (frequency of animal with neurological signs), seconds (duration and latency of neurological signs) and score (number of bites connected to spontaneous and stimulated aggressiveness and degree of elevation connected to the elevation tail), represent the mean ± SEM of 10 animals for each treatment. Statistical analysis was performed with one-way ANOVA followed by Tukey's test for multiple comparisons, and Student's *t* test was used to determine statistical significance ($P < 0.05$) between two groups

[a] from Vigolo et al. 2015

[b] from Ossato et al. 2016

*$p < 0.05$, **$p < 0.01$, ***$p < 0.001$ versus JWH-018 at the same dosage and #$p < 0.05$, ##$p < 0.01$, ###$p < 0.001$ versus AKB48 at the same dosage

affinity for both CB_1 and CB_2 receptor subtypes. A similar ratio between the Ki value to human CB_2 and the Ki value to human CB_1 for AKB48 and 5F-AKB48 was observed, with values of 0.52 and 0.45, respectively (Table 1). Also in this case, competition binding experiments performed in mouse brain membranes (for CB_1 receptors Fig. 2c) and in mouse spleen membranes (for CB_2 receptors Fig. 2d) showed a better affinity for the fluorinated version of AKB48 for both the receptors (Table 1).

Cyclic AMP experiments were performed to evaluate the potency of the AKB48 and 5F-AKB48 in CHO cells transfected with human CB_1 or CB_2 (Fig. 2e, f) receptors, in comparison with Δ^9-THC and JWH-018. Potency values were in accordance with affinity data obtained in competition binding experiments (Table 1). As expected, the partial agonist Δ^9-THC did not completely inhibit forskolin-stimulated cAMP production showing efficacy values of 41 ± 4 and 35 ± 3 % for CB_1 and CB_2 receptor, respectively. In contrast, JWH-018, AKB48 and 5F-AKB48 behaved as full agonists as demonstrated by the capability to completely inhibit the forskolin-stimulated cAMP production (Fig. 2e, f).

Major neurological changes

Systemic administration of AKB48 and 5F-AKB48 (0.01–6 mg/kg i.p.) caused important neurological changes in mice (Table 2), while in vehicle-treated mice no neurological alterations were observed. In particular, administration of high doses (3 and 6 mg/kg, i.p.) of adamantyl compounds induced spontaneous and handling-induced convulsions, hyperreflexia and myoclonias in mice: Those effects were not observed after the administration of Δ^9-THC (Table 2). AKB48 administered at 6 mg/kg induced convulsions in 30 % of treated animals, while 5F-AKB48 administered at 3 and 6 mg/kg induced convulsions in 30 and 90 % of treated animals, respectively. AKB48 at 6 mg/kg induced convulsions with latency and duration similar to those produced by JWH-018, while

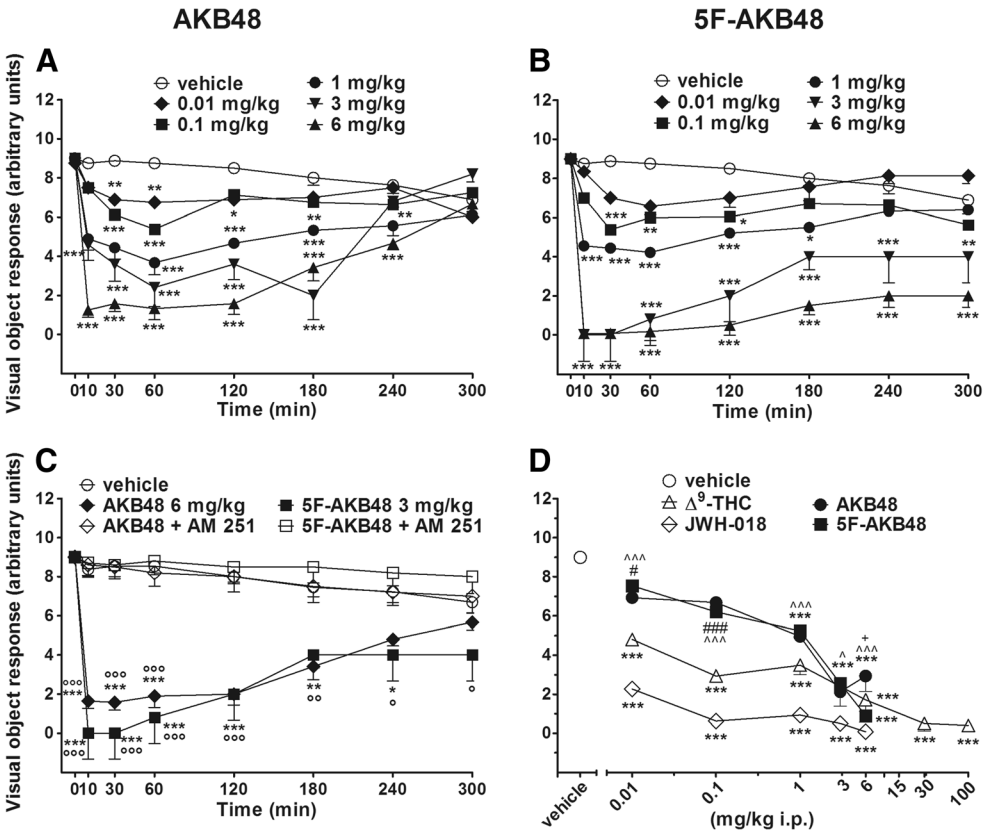

Fig. 3 Effect of the systemic administration (0.01–6 mg/kg i.p.) of AKB48 (**a**) and 5F-AKB48 (**b**) on the visual object test of mice. Interaction of effective dose of AKB48 and 5F-AKB48 (6 mg/kg) with the selective CB_1 receptor antagonist AM 251 (6 mg/kg, i.p., **c**). Comparison of the total average effect observed in 5 h (**d**) with Δ^9-THC (0.01–100 mg/kg)[c] and JWH-018 (0.01–6 mg/kg i.p.)[c]. Data are expressed (see "Materials and methods") as arbitrary units and represent mean ± SEM of 8 animals for each treatment. Statistical analysis was performed by two-way ANOVA followed by the Bonferroni's test for multiple comparisons for both the dose-response curve of each compound at different times (**a**, **b**) and for the interaction with the AM 251 (**c**), while the statistical analysis of the comparison of the total average effect of the compounds (**d**) was performed with one-way ANOVA followed by Tukey's test for multiple comparisons. *$p < 0.05$, **$p < 0.01$, ***$p < 0.001$ versus vehicle; #$p < 0.05$, ###$p < 0.001$ versus Δ^9-THC; ^$p < 0.05$, ^^$p < 0.01$, ^^^$p < 0.001$ versus JWH-018, +$p < 0.05$ versus 5F-AKB48 and °$p < 0.05$, °°$p < 0.01$, °°°$p < 0.001$ versus AM 251+ agonist. [c]From Ossato et al., 2015

5F-AKB48 at 6 mg/kg induced seizures with longer duration but same latency as those produced by AKB48 (Table 2).

AKB48 administered at 6 mg/kg induced hyperreflexia in 25 % of treated animals, while 5F-AKB48 at 3 and 6 mg/kg induced hyperreflexia in 30 and 75 % of mice, respectively (Table 2). AKB48 at 6 mg/kg induced hyperreflexia with same latency and quite longer duration than that produced by 5F-AKB48 and JWH-018.

AKB48 administered at 6 mg/kg induced myoclonias in 45 % of treated mice while 5F-AKB48 at 3 and 6 mg/kg induced myoclonias in 90 and 100 % of treated animals (Table 2). 5F-AKB48 at 6 mg/kg induced myoclonias with longer latency and duration than those produced by AKB48 and JWH-018.

AKB48, 5F-AKB48 and JWH-018 induced tail elevation in mice with comparable frequency, latency and duration at the dose of 3 mg/kg (Table 2). However, 5F-AKB48 at 3 mg/kg greater increased the degree of tail elevation than JWH-018 and AKB48.

Finally, AKB48 (3 and 6 mg/kg), 5F-AKB48 (1, 3 and 6 mg/kg) and JWH-018 (3 and 6 mg/kg) induced spontaneous and stimulated aggressiveness in mice. JWH-018, AKB48 and 5F-AKB48 (6 mg/kg) caused spontaneous aggressiveness in 90, 50 and 100 % of treated animals respectively. While JWH-018, AKB48 and 5F-AKB48 (6 mg/kg) induced aggressive behaviour in 100, 70 and 100 % of treated mice, respectively. 5F-AKB48 at 6 mg/kg induced a stimulated aggressiveness with comparable duration than JWH-018 but higher than AKB48 at the same dose. 5F-AKB48 at 1 and 3 mg/kg, respectively, stimulated aggressive behavior in 30 and 70 % of treated mice. The effect induced at 3 mg/kg was greater than that caused by AKB48 at the same dose.

All neurological changes were prevented by the pre-treatment with the selective CB_1 receptor antagonist AM 251 (6 mg/kg, i.p. injected 20 min before AKB48, 5F-AKB48 and JWH-018 administration; data not shown).

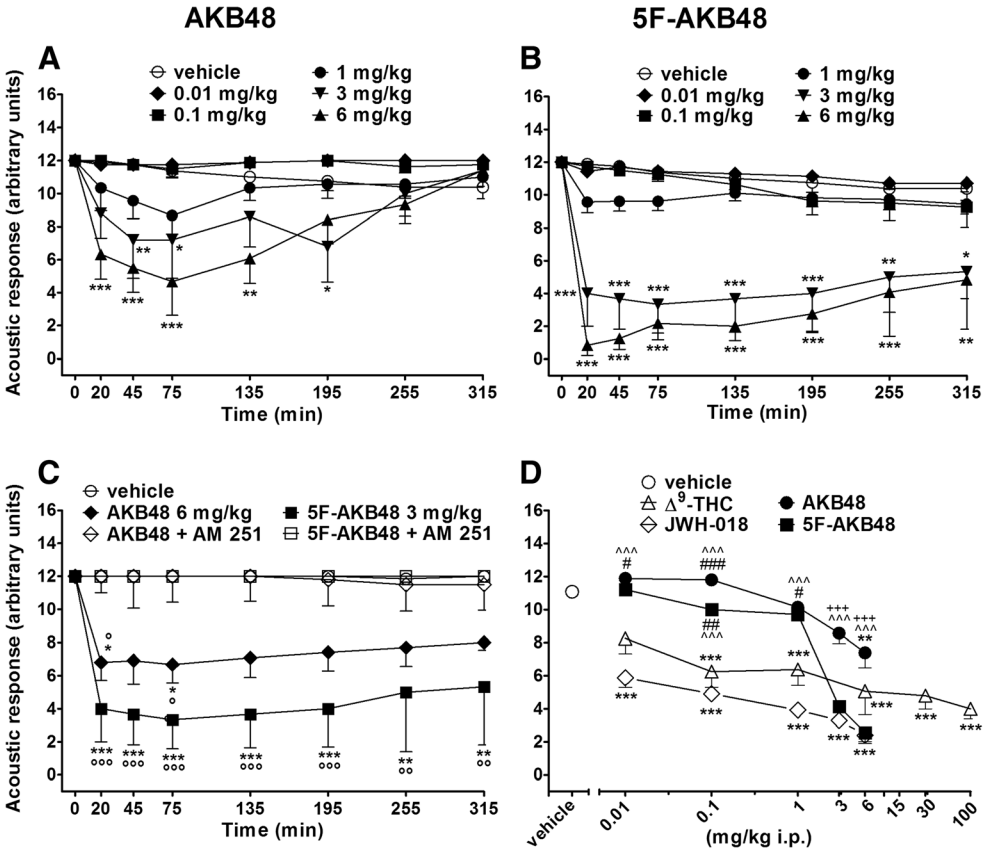

Fig. 4 Effect of the systemic administration (0.01–6 mg/kg i.p.) of AKB48 (**a**) and 5F-AKB48 (**b**) on the acoustic response test of mice. Interaction of effective dose of AKB48 and 5F-AKB48 (6 mg/kg) with the selective CB_1 receptor antagonist AM 251 (6 mg/kg, i.p., **c**). Comparison of the total average effect observed in 5 h (**d**) with Δ^9-THC (0.01–100 mg/kg)[c] and JWH-018 (0.01–6 mg/kg i.p.)[c]. Data are expressed (see "Materials and methods") as arbitrary units and represent mean ± SEM of 8 animals for each treatment. Statistical analysis was performed by two-way ANOVA followed by the Bonferroni's test for multiple comparisons for both the dose-response curve of each compound at different times (**a**, **b**) and for the interaction with the AM 251 (**c**), while the statistical analysis of the comparison of the total average effect of the compounds (**d**) was performed with one-way ANOVA followed by Tukey's test for multiple comparisons. *$p < 0.05$, **$p < 0.01$, ***$p < 0.001$ versus vehicle; #$p < 0.05$, ##$p < 0.01$, ###$p < 0.001$ versus Δ^9-THC; ^^^$p < 0.001$ versus JWH-018, +++$p < 0.001$ versus 5F-AKB48 and °$p < 0.05$, °°$p < 0.01$, °°°$p < 0.001$ versus AM 251+ agonist. [c]From Ossato et al., 2015

Evaluation of the visual object response

Visual object response tended to stay the same in vehicle-treated mice over 5 h observation (Fig. 3a, b), and the effect was similar to that observed in naïve untreated animals (data not shown). Systemic administration of AKB48 (0.01–6 mg/kg i.p.) dose-dependently reduced the visual object response in mice at all doses tested and the effect persisted up to 240 min after injection (Fig. 3a). Systemic administration of 5F-AKB48 (0.01–6 mg/kg i.p.) dose-dependently reduced the visual object response in mice at all doses tested and the effect persisted up to 5 h of observation only for the highest doses of substance 3 and 6 mg/kg i.p. (Fig. 3b). The inhibition of visual object response induced by the highest dose of AKB48 (6 mg/kg i.p.) and 5F-AKB48 (3 mg/kg i.p.) was prevented by the pre-treatment with AM 251 (6 mg/kg i.p., Fig. 3c) which alone did not alter the visual object response in mice. AKB48 and 5F-AKB48 inhibited the visual placing response in a prolonged manner, although the effect appeared to be lower with respect to that induced by JWH-018 and Δ^9-THC at the same doses, while for doses of 3 and 6 mg/kg effects were similar to those induced by Δ^9-THC (Fig. 3d).

Evaluation of the acoustic response

Acoustic response tended to stay the same in vehicle-treated mice over 5 h observation (Fig. 4a, b), and the effect was similar to that observed in naïve untreated animals (data not shown). Systemic administration of AKB48 transiently reduced the acoustic response at 3 and 6 mg/kg doses tested up to 195 min after injection (Fig. 4a). Differently, 5F-AKB48 inhibited the acoustic response in a prolonged manner and the effect appeared to be higher than that induced by AKB48 at the same doses where the inhibitory effect persisted up to 5 h (Fig. 4b). The inhibition of acoustic response induced by AKB48 (6 mg/kg i.p.) and 5F-AKB48 (3 mg/kg i.p.) was prevented by the pre-treatment with AM 251 (6 mg/kg i.p., Fig. 4c) which alone did not alter the

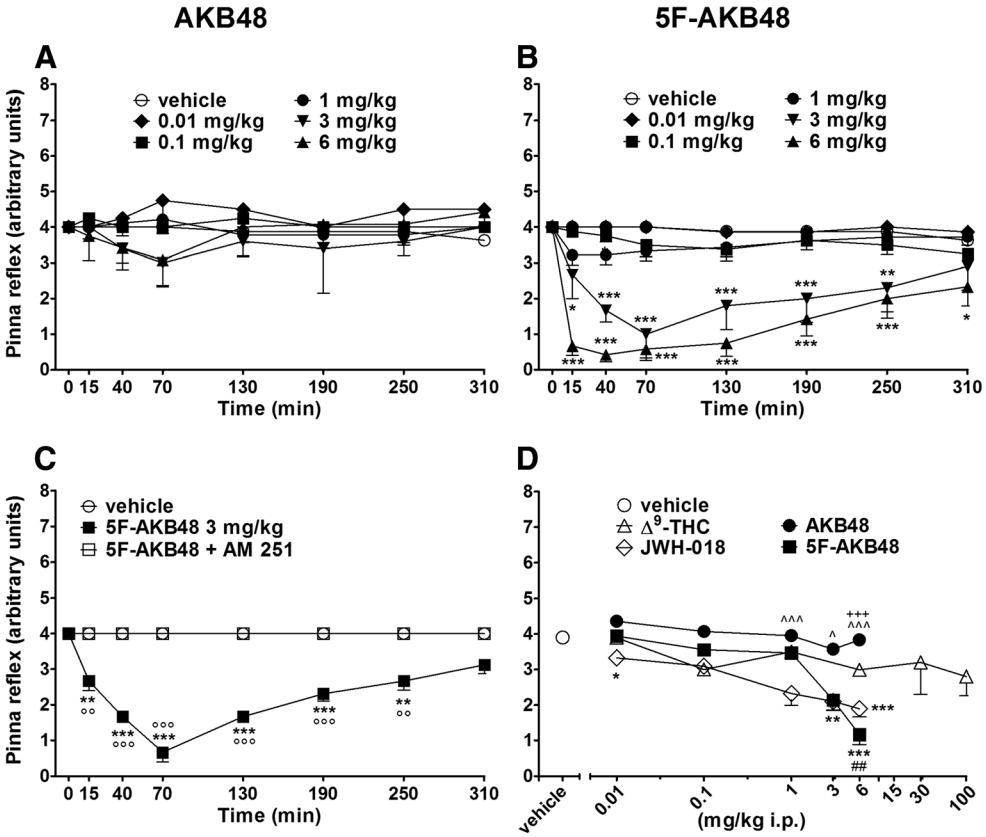

Fig. 5 Effect of the systemic administration (0.01–6 mg/kg i.p.) of AKB48 (**a**) and 5F-AKB48 (**b**) on the pinna reflex of mice. Interaction of effective dose of AKB48 and 5F-AKB48 (6 mg/kg) with the selective CB_1 receptor antagonist AM 251 (6 mg/kg, i.p., **c**). Comparison of the total average effect observed in 5 h (**d**) with Δ^9-THC (0.01–100 mg/kg)[c] and JWH-018 (0.01–6 mg/kg i.p.)[c]. Data are expressed (see "Materials and methods") as arbitrary units and represent mean ± SEM of 8 animals for each treatment. Statistical analysis was performed by two-way ANOVA followed by the Bonferroni's test for multiple comparisons for both the dose-response curve of each compound at different times (**a**, **b**) and for the interaction with the AM 251 (**c**), while the statistical analysis of the comparison of the total average effect of the compounds (**d**) was performed with one-way ANOVA followed by Tukey's test for multiple comparisons. *$p < 0.05$, **$p < 0.01$, ***$p < 0.001$ versus vehicle; ##p < 0.01 versus Δ^9-THC; ^$p < 0.05$, ^^^$p < 0.001$ versus JWH-018, +++$p < 0.001$ versus 5F-AKB48 and °$p < 0.05$, °°°$p < 0.001$ versus AM 251+ agonist. [c]From Ossato et al., 2015

acoustic response in mice (data not shown). AKB48 and 5F-AKB48 inhibited the acoustic response in a prolonged manner at the highest dose tested. Although the effect of AKB48 appeared to be lower than that induced by JWH-018 and Δ^9-THC at the same doses, effects of 5F-AKB48 were similar to those evocated by JWH-018 (Fig. 4d).

Evaluation of the pinnae reflex

Pinnae reflex did not change in vehicle-treated mice over 5 h observation (Fig. 5a, b), and the response was similar to that observed in naïve untreated animals (data not shown). Systemic administration of AKB48 did not alter the pinnae reflex in mice (Fig. 5a), contrarily to that presented after administration of 5F-AKB48 in which the effect was prolonged for the highest dose tested (3 and 6 mg/kg i.p.; Fig. 5b). The inhibition of pinnae reflex induced by 5F-AKB48 (3 mg/kg i.p.) was prevented by the pre-treatment with AM 251 (6 mg/kg i.p., Fig. 5c) which alone did not alter the pinnae reflex in mice (data not shown). 5F-AKB48 dose-dependently reduced the pinnae reflex at 6 mg/kg, and the effect appeared to be higher than that induced by JWH-018 and Δ^9-THC at the same doses (Fig. 5d).

Evaluation of the vibrissae reflex

Vibrissae reflex did not change in vehicle-treated mice over 5 h observation (Fig. 6a, b), and the response was similar to that observed in naïve untreated animals (data not shown). Systemic administration of AKB48 did not alter the vibrissae reflex (Fig. 6a). Contrarily, the effects of 5F-AKB48 were evident after 15 min with the highest dose (6 mg/kg i.p.; Fig. 6b). The inhibition of vibrissae reflex induced by 5F-AKB48 (3 mg/kg i.p.) was prevented by the pre-treatment with AM 251 (Fig. 6c) which alone did not alter the vibrissae reflex in mice (data not shown). 5F-AKB48 impaired the vibrissae reflex at 3 and 6 mg/kg, and the effect appeared to be

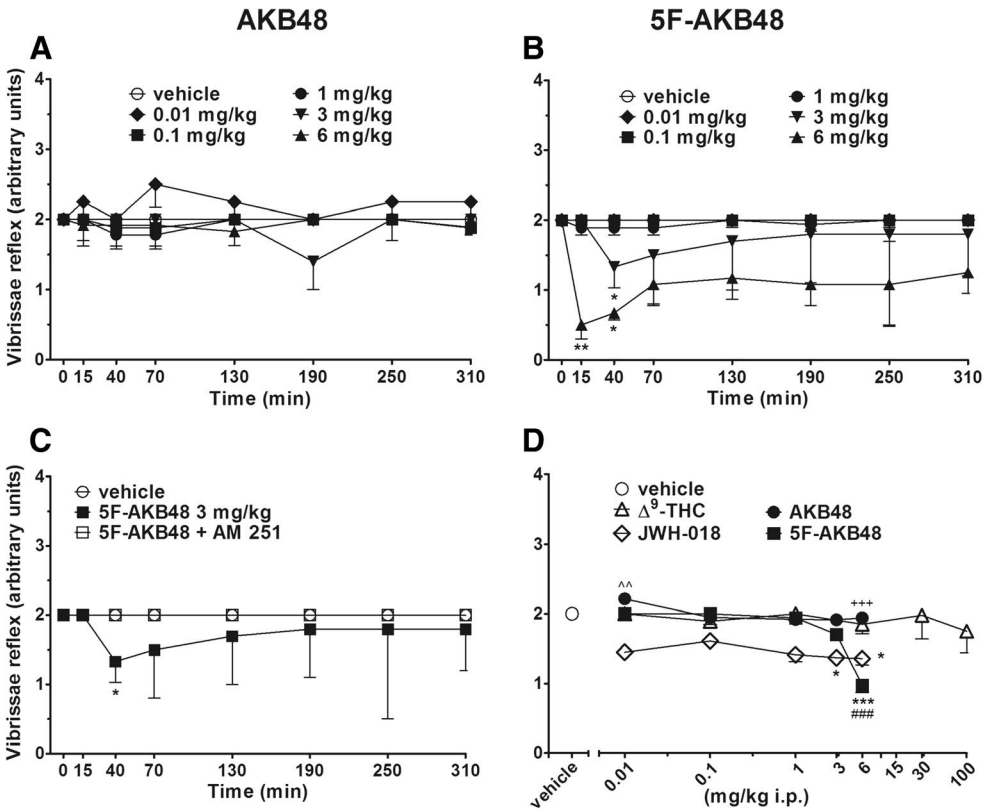

Fig. 6 Effect of the systemic administration (0.01–6 mg/kg i.p.) of AKB48 (**a**) and 5F-AKB48 (**b**) on the vibrissae reflex of mice. Interaction of effective dose of AKB48 and 5F-AKB48 (6 mg/kg) with the selective CB_1 receptor antagonist AM 251 (6 mg/kg, i.p., **c**). Comparison of the total average effect observed in 5 h (**d**) with Δ^9-THC (0.01–100 mg/kg)[c] and JWH-018 (0.01–6 mg/kg i.p.)[c]. Data are expressed (see "Materials and methods") as arbitrary units and represent mean ± SEM of 8 animals for each treatment. Statistical analysis was performed by two-way ANOVA followed by the Bonferroni's test for multiple comparisons for both the dose-response curve of each compounds at different times (**a**, **b**) and for the interaction with the AM 251 (**c**), while the statistical analysis of the comparison of the total average effect of the compounds (**d**) was performed with one-way ANOVA followed by Tukey's test for multiple comparisons. *$p < 0.05$, ***$p < 0.001$ versus vehicle; ###p < 0.001 versus Δ^9-THC; ^^$p < 0.01$ versus JWH-018 and +++$p < 0.001$ versus 5F-AKB48. [c]From Ossato et al., 2015

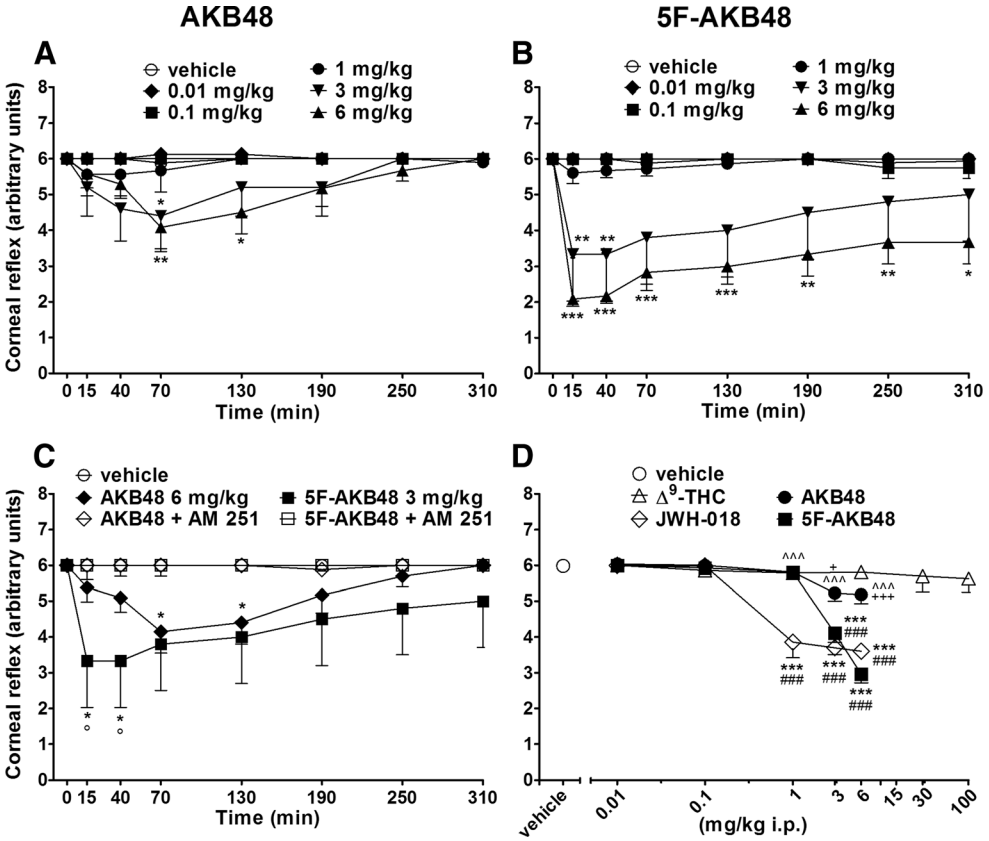

Fig. 7 Effect of the systemic administration (0.01–6 mg/kg i.p.) of AKB48 (**a**) and 5F-AKB48 (**b**) on the corneal reflex of mice. Interaction of effective dose of AKB48 and 5F-AKB48 (6 mg/kg) with the selective CB_1 receptor antagonist AM 251 (6 mg/kg, i.p.; **c**). Comparison of the total average effect observed in 5 h (**d**) with Δ^9-THC (0.01–100 mg/kg)[c] and JWH-018 (0.01–6 mg/kg i.p.)[c]. Data are expressed (see "Materials and methods") as arbitrary units and represent mean ± SEM of 8 animals for each treatment. Statistical analysis was performed by two-way ANOVA followed by the Bonferroni's test for multiple comparisons for both the dose-response curve of each compound at different times (**a**, **b**) and for the interaction with the AM 251 (**c**), while the statistical analysis of the comparison of the total average effect of the compounds (**d**) was performed with one-way ANOVA followed by Tukey's test for multiple comparisons. $*p < 0.05$, $**p < 0.01$, $***p < 0.001$ versus vehicle; $###p < 0.001$ versus Δ^9-THC; $\wedge\wedge\wedge p < 0.001$ versus JWH-018, $+p < 0.05$, $+++p < 0.001$ versus 5F-AKB48 and $°p < 0.05$ versus AM 251+ agonist. [c]From Ossato et al., 2015

similar to that induced by JWH-018 and higher than that induced by AKB48 and Δ^9-THC (Fig. 6d).

Evaluation of the corneal reflex

Corneal reflex did not change in vehicle-treated mice over 5 h observation (Fig. 7a,b), and the response was similar to that observed in naïve untreated animals (data not shown). Systemic administration of AKB48 inhibited transiently at 3 and 6 mg/kg the corneal reflex in mice (Fig. 7a). On the other hand, 5F-AKB48 inhibited deeply the corneal reflex in mice at 3 and 6 mg/kg (Fig. 7b). The inhibition of corneal reflex induced by AKB48 (6 mg/kg i.p.) and 5F-AKB48 (3 mg/kg i.p.) was prevented by the pre-treatment with AM 251 (6 mg/kg i.p. ,Fig. 7c) which alone did not alter the corneal reflex in mice (data not shown). As previously reported, the effects of 5F-AKB48 were higher than those induced by AKB48 at higher doses (3 and 6 mg/kg). Finally, the effects of 5F-AKB48 at 3 and 6 mg/kg i.p. seem to be more similar than those induced by JWH-018 but higher than those induced by Δ^9-THC and AKB48 at same doses (Fig. 7d).

Evaluation of the visual placing response

Visual placing response tended to be reduced in vehicle-treated mice over 5 h observation (~47 % of reduction at 300 min; Fig. 8a, b), and the effect was similar to that observed in naïve untreated animals (data not shown). Systemic administration of AKB48 transiently reduced the visual placing response in mice at 3 and 6 mg/kg i.p., and the effect persisted up to 130 min (Fig. 8a). Systemic administration of 5F-AKB48 reduced the visual placing response in mice at all doses tested (0.01–6 mg/kg i.p.), and the effect persisted up to 5 h only for the highest dose considered (6 mg/kg i.p., Fig. 8b). The visual impairment induced by AKB48 and 5F-AKB48 was prevented by the pre-treatment

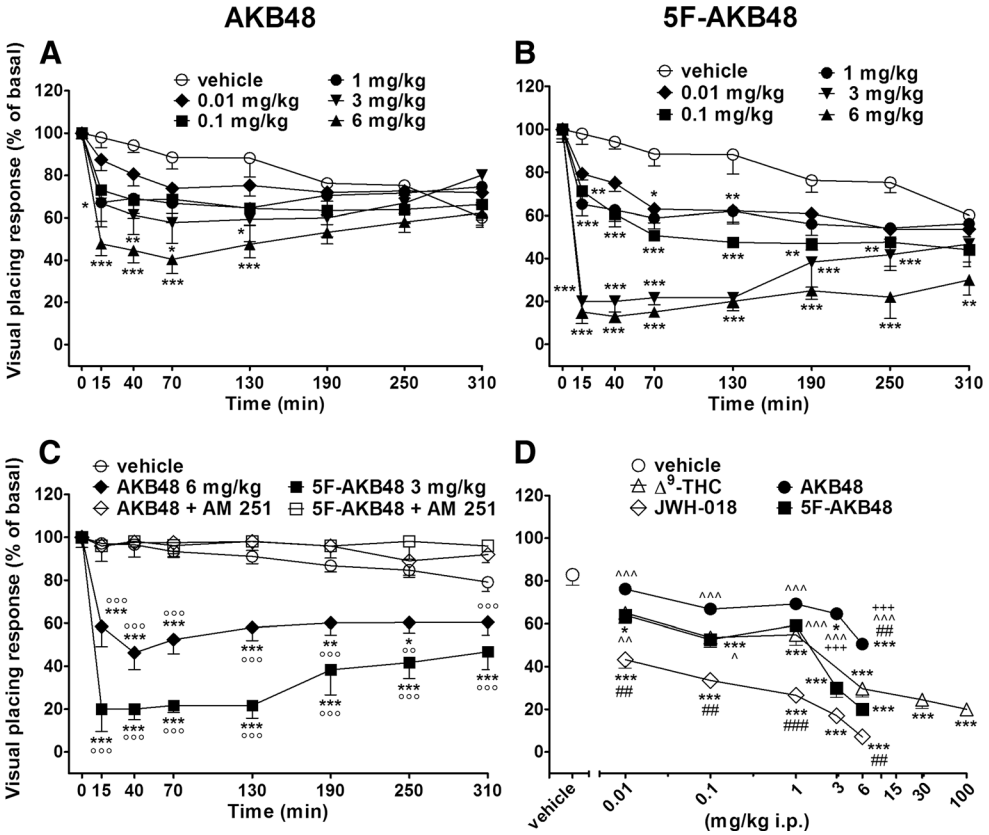

Fig. 8 Effect of the systemic administration (0.01–6 mg/kg i.p.) of AKB48 (**a**) and 5F-AKB48 (**b**) on the visual placing test of mice. Interaction of effective dose of AKB48 and 5F-AKB48 (6 mg/kg) with the selective CB_1 receptor antagonist AM 251 (6 mg/kg, i.p., **c**). Comparison of the total average effect observed in 5 h (**d**) with Δ^9-THC (0.01–100 mg/kg)[c] and JWH-018 (0.01–6 mg/kg i.p.)[c]. Data are expressed (see "Materials and methods") as arbitrary units and represent mean ± SEM of 8 animals for each treatment. Statistical analysis was performed by two-way ANOVA followed by the Bonferroni's test for multiple comparisons for both the dose-response curve of each compound at different times (**a**, **b**) and for the interaction with the AM 251 (**c**), while the statistical analysis of the comparison of the total average effect of the compounds (**d**) was performed with one-way ANOVA followed by Tukey's test for multiple comparisons. $*p < 0.05$, $**p < 0.01$, $***p < 0.001$ versus vehicle; $\#\#p < 0.01$, $\#\#\#p < 0.001$ versus Δ^9-THC; $\hat{}p < 0.05$, $\hat{}\hat{}p < 0.01$, $\hat{}\hat{}\hat{}p < 0.001$ versus JWH-018, $+++p < 0.001$ versus 5F-AKB48 and $^{\circ\circ}p < 0.01$, $^{\circ\circ\circ}p < 0.001$ versus AM 251+ agonist. [c]From Ossato et al., 2015

with AM 251 (6 mg/kg i.p., Fig. 8c) which alone did not alter the parameter. The inhibition of the visual response induced by 5F-AKB48 is more higher than those induced by AKB48 and similar to those induced by Δ^9-THC (Fig. 8d).

Bar test

AKB48 and 5F-AKB48 induced catalepsy in the bar test (Fig. 9a, b). In particular, AKB48 induced a transient increase in the time spent on bar at 3 mg/kg and a marked catalepsy at 6 mg/kg which gradually decreases to baseline levels after 95 min from administration of AKB48 (Fig. 9a). 5F-AKB48 induced a marked catalepsy at 3 and 6 mg/kg, and the effects remained up to 270 min (Fig. 9b). The effects were prevented by the pre-treatment with AM 251 which alone did not induce akinesia and catalepsy (Fig. 9c). The effects of 5F-AKB48 were more intense than those induced by JWH-018, AKB48 and Δ^9-THC at the same doses considered effective (Fig. 9d).

Evaluation of core and surface body temperature

Systemic administration of AKB48 and 5F-AKB48 (0.01–6 mg/kg ip) reduced both core (Fig. 10) and surface (Fig. 11) body temperatures in mice. In particular, AKB48 induced a transient reduction in core temperature at 3 mg/kg (−2 °C at 85 min time point) and a prolonged and significant hypothermia at 6 mg/kg (−5.5 °C at 85 min time point; Fig. 10a) that was maintained up to 140 min. Moreover, 5F-AKB48 induced a prolonged and significant hypothermia at both 3 and 6 mg/kg in mice (Fig. 10b). AKB48 and 5F-AKB48 were ineffective in the range of doses of 0.01–1 mg/kg. Internal body hypothermia was associated by a reduction of the external body temperature which was observed only at the higher dose tested (6 mg/kg for AKB48 and 3–6 mg/kg for 5F-AKB48; Fig. 11a, b). Core and surface temperature changes were prevented by the pre-treatment with AM

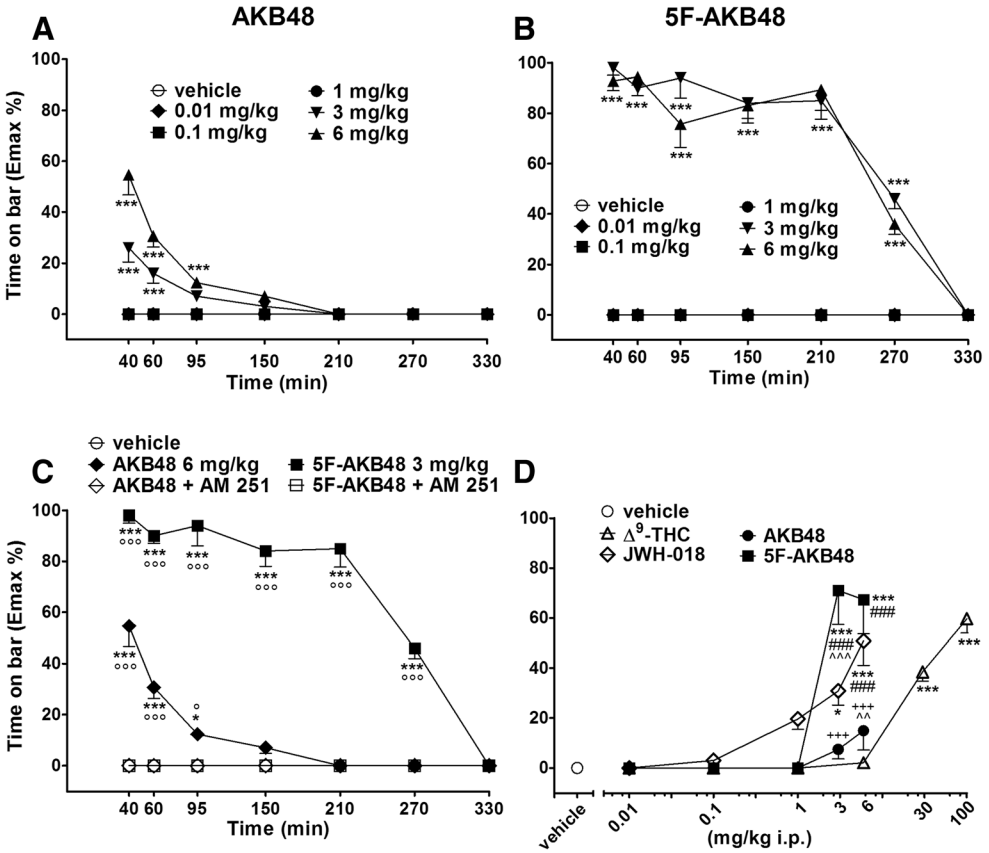

Fig. 9 Effect of the systemic administration (0.01–6 mg/kg i.p.) of AKB48 (**a**) and 5F-AKB48 (**b**) on the bar test of mice. Interaction of effective dose of AKB48 and 5F-AKB48 (6 mg/kg) with the selective CB_1 receptor antagonist AM 251 (6 mg/kg, i.p., **c**). Comparison of the total average effect observed in 5 h (**d**) with Δ^9-THC (0.01–100 mg/kg)[a] and JWH-018 (0.01–6 mg/kg i.p.)[a]. Data are expressed (see "Materials and methods") as arbitrary units and represent mean ± SEM of 8 animals for each treatment. Statistical analysis was performed by two-way ANOVA followed by the Bonferroni's test for multiple comparisons for both the dose-response curve of each compound at different times (**a**, **b**) and for the interaction with the AM 251 (**c**), while the statistical analysis of the comparison of the total average effect of the compounds (**d**) was performed with one-way ANOVA followed by Tukey's test for multiple comparisons. *$p < 0.05$, ***$p < 0.001$ versus vehicle; ###$p < 0.001$ versus Δ^9-THC; ^^$p < 0.01$, ^^^$p < 0.001$ versus JWH-018, +++$p < 0.001$ versus 5F-AKB48 and °$p < 0.05$, °°°$p < 0.001$ versus AM 251+ agonist. [a]From Vigolo et al., 2015

251 which did not affect body temperature when administered alone (Figs 10 and 11c). Furthermore, the effects on core temperature of AKB48 and 5F-AKB48 seem to be similar to those induced by JWH-018, while Δ^9-THC was less effective (Fig. 10d). The effects on surface temperature of AKB48 seem to be less effective than those induced by JWH-018 and 5F-AKB48 (Fig. 11d).

Evaluation of pain induced by a mechanical stimulus

Systemic administration of AKB48 and 5F-AKB48 (0.01–6 mg/kg i.p.) increased the threshold to acute mechanical pain stimulus in mice in the tail pinch test (Fig. 12). In the case of AKB48, only the dose of 6 mg/kg was transiently effective from 55 to 90 min of analysis (Fig. 12a). On the other hand, 5F-AKB48 was active in the all dose range of 0.01–6 mg/kg (Fig. 12b) and the effects were prolonged up to 5 h after injection of the compound. The effects were prevented by the pretreatment with AM 251 which alone did not alter the threshold to acute mechanical pain stimuli (Fig. 12c). 5F-AKB48 produced significantly greater analgesia than AKB48 in the mechanical nociception assay. Even the lowest doses of 5F-AKB48 produced significant analgesia (relative to vehicle) in this assay.

Evaluation of pain induced by a thermal stimulus

Systemic administration of AKB48 and 5F-AKB48 (0.01–6 mg/kg i.p.) increased the threshold to acute thermal pain stimulus in mice in the tail withdrawal test (Fig. 13a, b). In particular, AKB48 induced a robust elevation of the pain threshold at 6 mg/kg which ended after 145 min after administration of the compound (Fig. 13a). Also 5F-AKB48 induced a robust elevation of the pain threshold at 6 mg/kg but the effect persisted up to 5 h

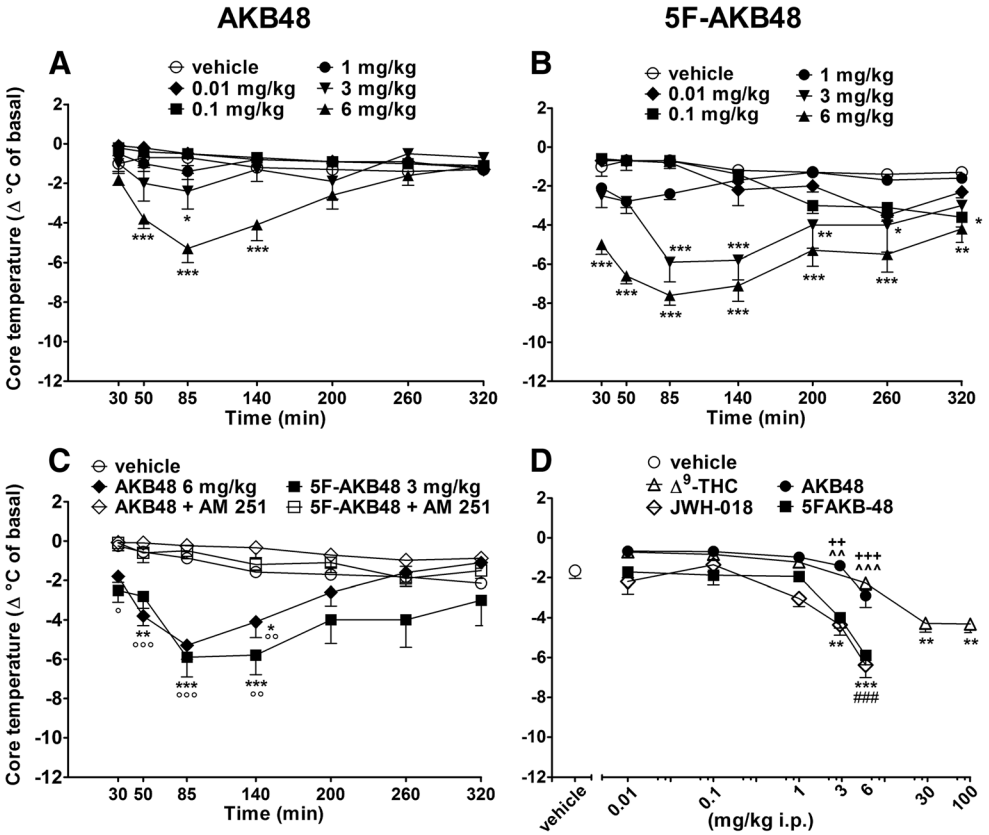

Fig. 10 Effect of the systemic administration (0.01–6 mg/kg i.p.) of AKB48 (**a**) and 5F-AKB48 (**b**) on mouse core temperature. Interaction of effective dose of AKB48 and 5F-AKB48 (6 mg/kg) with the selective CB_1 receptor antagonist AM 251 (6 mg/kg, i.p., **c**). Comparison of the total average effect observed in 5 h (**d**) with Δ^9-THC (0.01–100 mg/kg)[a] and JWH-018 (0.01–6 mg/kg i.p.)[a]. Data are expressed (see "Materials and methods") as arbitrary units and represent mean ± SEM of 8 animals for each treatment. Statistical analysis was performed by two-way ANOVA followed by the Bonferroni's test for multiple comparisons for both the dose-response curve of each compound at different times (**a**, **b**) and for the interaction with the AM 251 (**c**), while the statistical analysis of the comparison of the total average effect of the compounds (**d**) was performed with one-way ANOVA followed by Tukey's test for multiple comparisons. $*p < 0.05$, $**p < 0.01$, $***p < 0.001$ versus vehicle; $\#\#\#p < 0.001$ versus Δ^9-THC; $\wedge\wedge p < 0.01$, $\wedge\wedge\wedge p < 0.001$ versus JWH-018, $++p < 0.01$, $+++p < 0.001$ versus 5F-AKB48 and $°p < 0.05$, $°°p < 0.01$, $°°°p < 0.001$ versus AM 251+ agonist. [a]From Vigolo et al., 2015

(Fig. 13c). The effects were prevented by the pre-treatment with AM 251 which alone did not alter the threshold to acute thermal pain stimuli (Fig. 13c). At 6 mg/kg, AKB48 and 5F-AKB48 induced an increase in the pain threshold similar to that induced by the same dose of Δ^9-THC (Fig. 13d).

Accelerod test

In the accelerod test, AKB48 transiently inhibited stimulated locomotion only at 6 mg/kg (Fig. 14a). Conversely, 5F-AKB48 induced at the highest dose tested (3 and 6 mg/kg i.p.) a prolonged and significant impairment of locomotion (Fig. 14b). The inhibitory effects were prevented by the pre-treatment with the AM 251, which alone did not affect mice performance (Fig. 14c). AKB48 and 5F-AKB48 caused an effect lower than that induced by JWH-018 at 6 mg/kg (Fig. 14d).

Drag test

Systemic administration of AKB48 transiently inhibited the number of steps performed with the front legs of the mice at 3 and 6 mg/kg (Fig. 15a). On the other hand, the effects of 5F-AKB48 were evident also with the dose of 1 mg/kg (Fig. 15b). At 6 mg/kg, the effect of 5F-AKB48 was prolonged and persisted up to 5 h observation. The inhibitory effects were prevented by the pre-treatment with the AM 251 (Fig. 15c). The inhibition induced by 5F-AKB48 was similar to those induced by JWH-018 and greater with respect to those caused by AKB48 and Δ^9-THC at the same doses (Fig. 15d).

Studies on spontaneous locomotor activity in mice

To exclude that the reduction of sensorimotor responses could be due to the inhibition of motor activity, we investigated the effect of AKB48 and 5F AKB48 administration (0.01–6 mg/kg i.p.) on spontaneous locomotor activity in

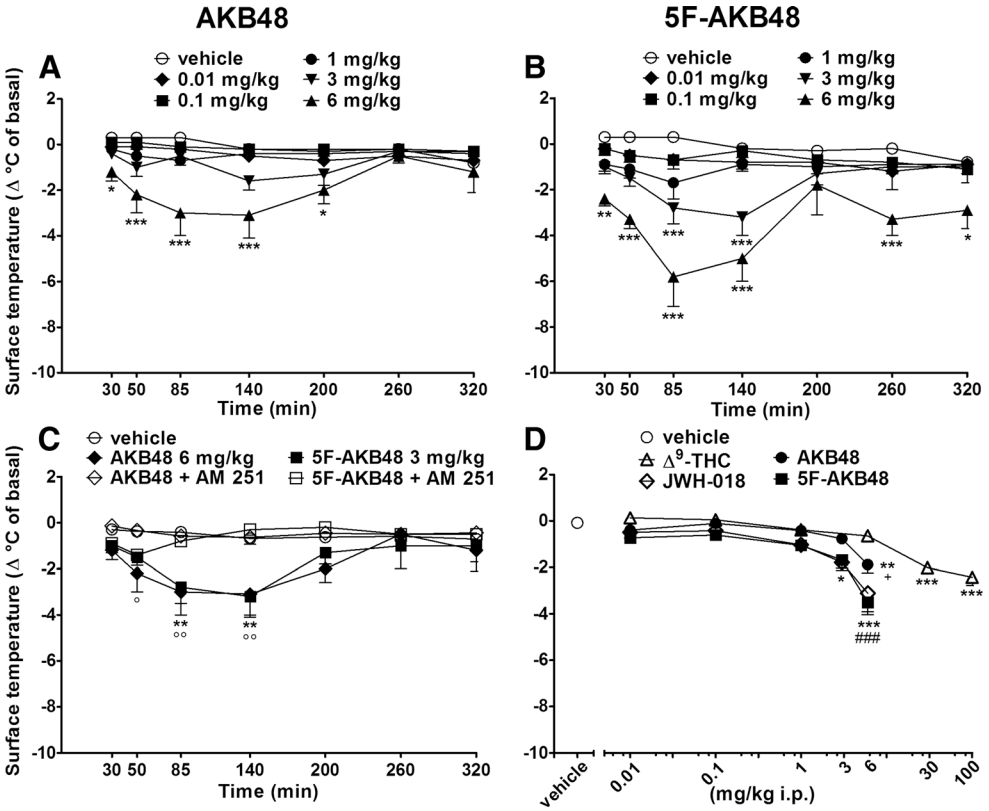

Fig. 11 Effect of the systemic administration (0.01–6 mg/kg i.p.) of AKB48 (**a**) and 5F-AKB48 (**b**) on the surface temperature of mice. Interaction of effective dose of AKB48 and 5F-AKB48 (6 mg/kg) with the selective CB_1 receptor antagonist AM 251 (6 mg/kg, i.p., **c**). Comparison of the total average effect observed in 5 h (**d**) with Δ^9-THC (0.01–100 mg/kg)[a] and JWH-018 (0.01–6 mg/kg i.p.)[a]. Data are expressed (see "Materials and methods") as arbitrary units and represent mean ± SEM of 8 animals for each treatment. Statistical analysis was performed by two-way ANOVA followed by the Bonferroni's test for multiple comparisons for both the dose-response curve of each compound at different times (**a**, **b**) and for the interaction with the AM 251 (**c**), while the statistical analysis of the comparison of the total average effect of the compounds (**d**) was performed with one-way ANOVA followed by Tukey's test for multiple comparisons. $*p < 0.05$, $**p < 0.01$, $***p < 0.001$ versus vehicle; $\#\#\#p < 0.001$ versus Δ^9-THC; $+p < 0.05$ versus 5F-AKB48 and $°p < 0.05$, $°°p < 0.01$ versus AM 251+ agonist. [a]From Vigolo et al., 2015

mice. AKB48 at 6 mg/kg reduced the total distance travelled (Fig. 16a) and increased the immobility time at 1 and 6 mg/kg (Fig. 16d) in mice. To be noted, AKB48 at 1 mg/kg evoked a transient facilitation of spontaneous locomotion (Fig. 16a). Likewise, 5F-AKB48 at 6 mg/kg reduced the total distance travelled (Fig. 16b) and increased at 1 and 6 mg/kg the immobility time (Fig. 16e) in mice. 5F-AKB48 induced a greater inhibition of total distance travelled respect AKB48 administration (Fig. 16c) without changing the total immobility time (Fig. 16f).

In vivo brain microdialysis

Basal values of extracellular DA in NAc shell were 15 ± 5 (mean ± SEM) fmoles/10 μl sample. Systemic administration of AKB48 (0.3 and 1 mg/kg i.p.) and 5F-AKB48 (0.01, 0.03, 0.1 and 0.3 mg/kg i.p.) increased extracellular DA release in NAc shell of awake and freely moving mice (Fig. 17a, b) in a dose-dependent manner. In particular, AKB48 increased DA levels in the NAc shell with a biphasic effect after the administration of the highest dose tested (1 mg/kg i.p.); no effects were observed with the lowest dose as with vehicle. Moreover, the administration of the fluorinated analog, 5F-AKB48, produced a dose-response curve with the dose of 0.03 mg/kg increasing dialysate DA; no effects were observed with the lower and higher doses tested as with vehicle. 5F-AKB48 at 0.03 mg/kg induced a prolonged release of DA (up to 180 min) that reached the maximum at 30–60 min after drug administration (max increase of about +75 %) showing differences at 30, 40 and 60 min samples with respect to basal values.

Discussion

This is the first study showing a comparative analysis of the effects caused by the new third-generation synthetic cannabinoids AKB48 and 5F-AKB48 on "tetrad", sensorimotor, neurological and neurochemical responses in CD-1 male mice.

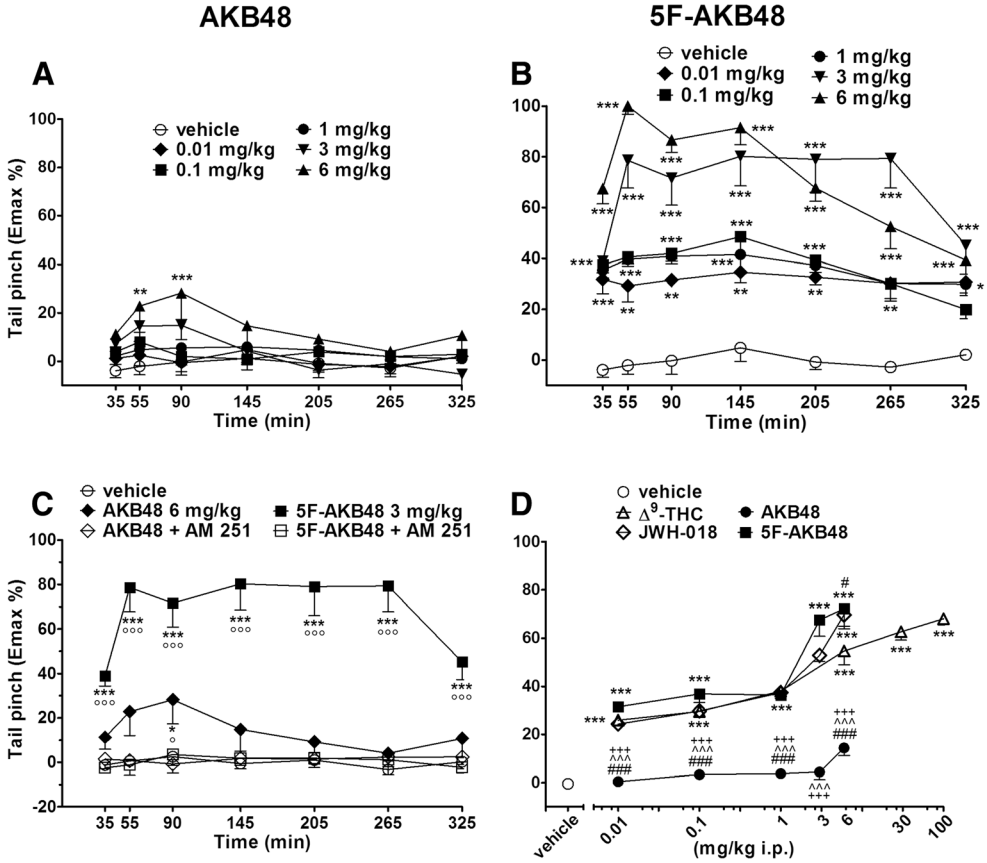

Fig. 12 Effect of the systemic administration (0.01–6 mg/kg i.p.) of AKB48 (**a**) and 5F-AKB48 (**b**) on the tail pinch test of mice. Interaction of effective dose of AKB48 and 5F-AKB48 (6 mg/kg) with the selective CB_1 receptor antagonist AM 251 (6 mg/kg, i.p., **c**). Comparison of the total average effect observed in 5 h (**d**) with Δ^9-THC (0.01–100 mg/kg)[a] and JWH-018 (0.01–6 mg/kg i.p.)[a]. Data are expressed (see "Materials and methods") as arbitrary units and represent mean ± SEM of 8 animals for each treatment. Statistical analysis was performed by two-way ANOVA followed by the Bonferroni's test for multiple comparisons for both the dose-response curve of each compound at different times (**a**, **b**) and for the interaction with the AM 251 (**c**), while the statistical analysis of the comparison of the total average effect of the compounds (**d**) was performed with one-way ANOVA followed by Tukey's test for multiple comparisons. $*p < 0.05$, $**p < 0.01$, $***p < 0.001$ versus vehicle; $\#p < 0.05$, $\#\#\#p < 0.001$ versus Δ^9-THC; $\wedge\wedge\wedge p < 0.001$ versus JWH-018, $+++p < 0.001$ versus 5F-AKB48 and $^{\circ\circ\circ}p < 0.001$ versus AM 251+ agonist. [a]From Vigolo et al., 2015

Firstly, the study shows that the systemic administration of AKB48 and 5F-AKB48 induces the typical "tetrad effect" as reported for other JWH-type SCBs (Wiebelhaus et al. 2012; Wiley et al. 1998; Macri et al. 2013; Vigolo et al. 2015; Ossato et al. 2016) and Δ^9-THC (Compton et al. 1992; Vigolo et al. 2015). In particular, the study shows that AKB48 and 5F-AKB48 cause important alteration of sensorimotor reflexes and they promote spontaneous and stimulated aggressive response in mice.

Furthermore, as previously reported regarding the synthetic cannabinoids JWH-018, JWH-250 and JWH-073, these two adamantylindazoles induce neurological alterations such as convulsions, hyperreflexia and myoclonias that are not observed after administration of Δ^9-THC (Marshell et al. 2014; Vigolo et al. 2015; Ossato et al. 2016).

Finally, by the microdialysis technique in awake and freely moving mice, we demonstrated that systemic administration of AKB48 and 5F-AKB48 transiently facilitates extracellular DA release in the NAc shell. All these behavioural and neurochemical effects were fully dependent on CB_1 receptor stimulation since they are completely prevented by the administration of the selective CB_1 receptor antagonist/inverse agonist AM 251.

The protocol we used in this study was previously validated to describe the effects of other cannabinoids on the "tetrad", sensorimotor and neurological changes in mice (Vigolo et al. 2015; Ossato et al. 2015; Ossato et al. 2016).

In vitro binding studies show that AKB48 and 5F-AKB48 retain nanomolar affinity for both CD-1 murine and human CB_1 and CB_2 receptors with a slight preference for CB_2 receptor. In particular, in CD-1 murine preparation, AKB48 displays an affinity for CB_1 receptors (Ki = 5.34 nM) similar to that of 5F-AKB48 (Ki = 3.87 nM) and JWH-018 (Ki = 5.82 nM; (Vigolo et al. 2015), whereas on human CB_1 receptors, AKB48 shows an affinity (Ki = 3.24 nM) compared to that of 5F-AKB48 (Ki = 1.82 nM) and slightly

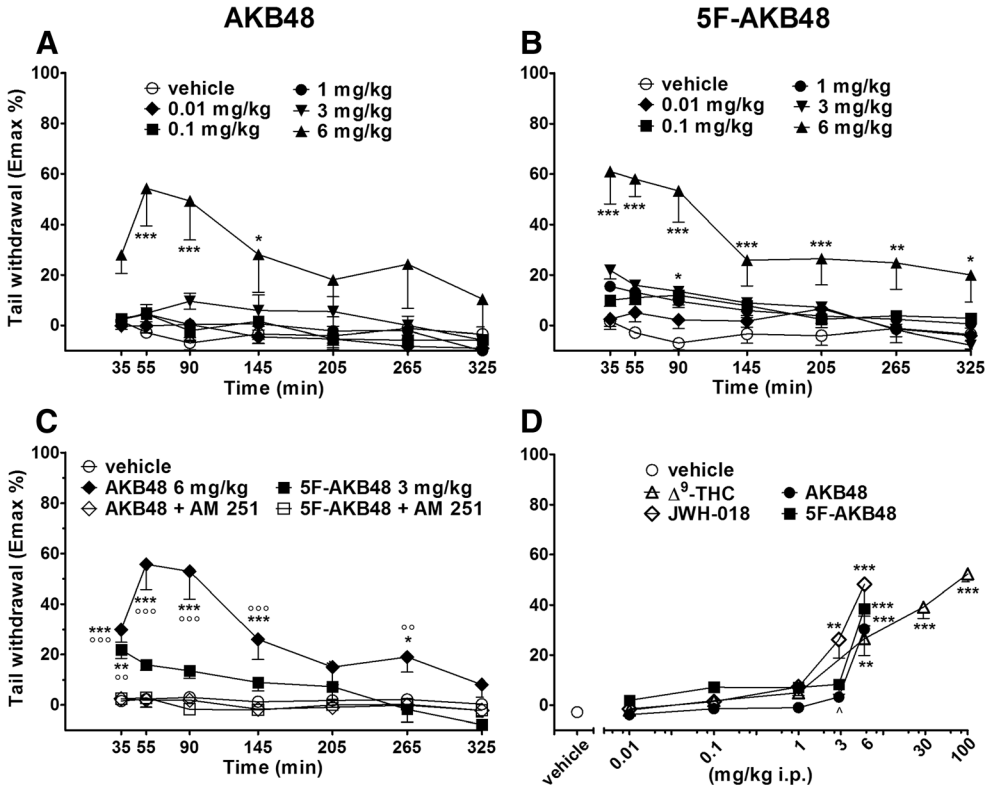

Fig. 13 Effect of the systemic administration (0.01–6 mg/kg i.p.) of AKB48 (**a**) and 5F 5F-AKB48 (**b**) on the tail withdrawal test of mice. Interaction of effective dose of AKB48 and 5F-AKB48 (6 mg/kg) with the selective CB_1 receptor antagonist AM 251 (6 mg/kg, i.p., **c**). Comparison of the total average effect observed in 5 h (**d**) with Δ^9-THC (0.01–100 mg/kg)[a] and JWH-018 (0.01–6 mg/kg i.p.)[a]. Data are expressed (see "Materials and methods") as arbitrary units and represent mean ± SEM of 8 animals for each treatment. Statistical analysis was performed by two-way ANOVA followed by the Bonferroni's test for multiple comparisons for both the dose-response curve of each compound at different times (**a**, **b**) and for the interaction with the AM 251 (**c**), while the statistical analysis of the comparison of the total average effect of the compounds (**d**) was performed with one-way ANOVA followed by Tukey's test for multiple comparisons. $*p < 0.05$, $**p < 0.01$, $***p < 0.001$ versus vehicle; $\hat{}p < 0.05$ versus JWH-018 and $^{\circ\circ}p < 0.01$, $^{\circ\circ\circ}p < 0.001$ versus AM 251+ agonist. [a]From Vigolo et al., 2015

higher to JWH-018 (Ki = 9.53 nM; Vigolo et al. 2015). The increased CB_1 receptor affinity of AKB48 and 5F-AKB48 could justify their potency value (AKB48, IC_{50} = 5.39 nM and 5F-AKB48, IC_{50} = 2.57 nM) in inhibiting cyclic AMP formation respect to JWH-018 (IC_{50} = 14.1 nM; (Vigolo et al. 2015). Despite this in vitro evidence that show AKB48 and 5F-AKB48 have an affinity for the CB_1 receptors equal or slightly greater than JWH-018, in vivo data show a different efficacy and potency between AKB48, 5F-AKB48 and JWH-018. This is suggestive of the fact that the in vivo efficacy of these compounds does not depend exclusively on pharmacodynamic (i.e. receptor affinity) but possibly by pharmacokinetic (i.e. absorption, metabolism) parameters. This is supported by recent studies that have shown that the halogenation in the pentilic side chain of JWH-018 (i.e. JWH-018Cl and JWH-018Br) does not significantly change the binding affinity of the compounds at the cannabinoid CB_1 and CB_2 receptors, but it influences their biological activity in vivo (Vigolo et al. 2015). Therefore, the increased power of 5F-AKB48 compared to AKB48 could be due to the enhanced lipophilicity of the fluorinate compound (Schifano et al. 2015).

Indeed, administration of AKB48 in the dose-range up to 6 mg/kg induces a core and surface hypothermia which is significantly lower respect to that induced by 5F-AKB48 and JWH-018, and it was similar to that induced by administration of Δ^9-THC (Vigolo et al. 2015). Nevertheless, we cannot exclude that administration of AKB48 at higher doses than those tested might induce a greater hypothermia. However, the occurrence of major neurological changes prevents us to increase doses. As reported for others cannabinoid agonists, hypothermia induced by AKB48 and 5F-AKB48 is completely prevented by pre-treatment with AM 251 confirming that this effect is clearly mediated by the stimulation of CB_1 receptors (Marshell et al. 2014; Vigolo et al. 2015; Ossato et al. 2016).

Systemic administration of AKB48 and 5F-AKB48 increases the threshold to acute mechanical and thermal pain stimulus in mice. However, the analgesic effect induced by AKB48 is less intense with respect to that induced by 5F-AKB48, JWH-018 and Δ^9-THC administration (Vigolo et al. 2015), but it is similar to the analgesic profile of other SCBc as JWH-250 and JWH-073 (Ossato et al. 2016). This

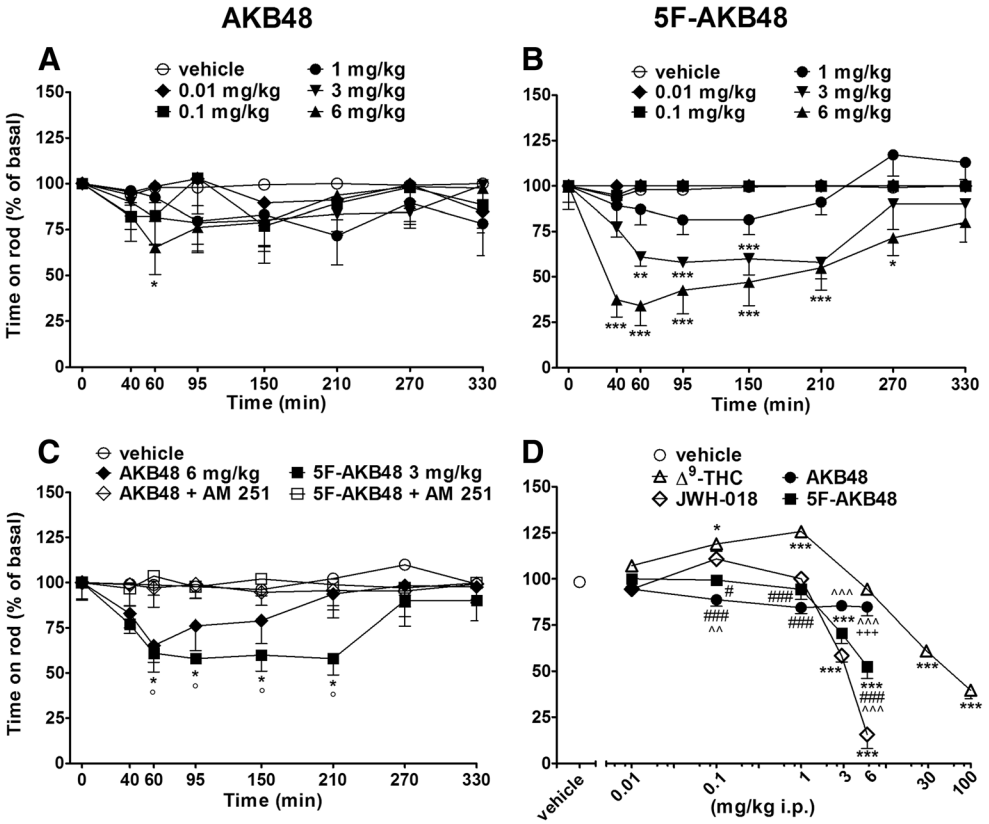

Fig. 14 Effect of the systemic administration (0.01–6 mg/kg i.p.) of AKB48 (**a**) and 5F-AKB48 (**b**) on the accelerod test of mice. Interaction of effective dose of AKB48 and 5F-AKB48 (6 mg/kg) with the selective CB_1 receptor antagonist AM 251 (6 mg/kg, i.p., **c**). Comparison of the total average effect observed in 5 h (**d**) with Δ^9-THC (0.01–100 mg/kg)[a] and JWH-018 (0.01–6 mg/kg i.p.)[a]. Data are expressed (see "Materials and methods") as arbitrary units and represent mean ± SEM of 8 animals for each treatment. Statistical analysis was performed by two-way ANOVA followed by the Bonferroni's test for multiple comparisons for both the dose-response curve of each compound at different times (**a**, **b**) and for the interaction with the AM 251 (**c**), while the statistical analysis of the comparison of the total average effect of the compounds (**d**) was performed with one-way ANOVA followed by Tukey's test for multiple comparisons. $*p < 0.05$, $**p < 0.01$, $***p < 0.001$ versus vehicle; $\#p < 0.05$, $\#\#\#p < 0.001$ versus Δ^9-THC; $\wedge\wedge p < 0.01$, $\wedge\wedge\wedge p < 0.001$ versus JWH-018, $+++p < 0.001$ versus 5F-AKB48 and $^\circ p < 0.05$ versus AM 251+ agonist. [a]From Vigolo et al., 2015

lower response could be due to the fact that AKB48, as well as others SCBs, may be biotransformed into glucuronidated or monohydroxylated metabolites that can act as neutral antagonists at CB_1 receptors dampening the overall activity of the parent compound (Seely et al. 2012; Brents et al. 2012). However, the structural similarity between AKB48 and 5F-AKB48 suggests that the lower efficacy of AKB48 is more likely related to its lower permeation across the blood brain barrier. As previously reported for other JWH-type SCBs (Vigolo et al. 2015), 5F-AKB48 shows a greater efficacy in reducing nociception to mechanical stimulation compared to thermal stimulus, strengthens the hypothesis that cannabinoid agonists exert their analgesic effect by acting on different sensory components of pain generated by a mechanical (Martin et al. 1996) or thermal (Hohmann et al. 1999) stimuli.

Unlike previous studies showing that the analgesic effect caused by JWH-018-R compounds precedes the motor impairment (Vigolo et al. 2015), the analgesic effects induced by AKB48 and 5F-AKB48 overlap almost completely to the motor alterations. This responsiveness is in line with previous studies reporting that small changes in the molecular structure of SCBs induce consistent disparities among potencies and efficacies of in vivo effects (Wiley et al. 1998; Wiley et al. 2014; Ossato et al. 2016).

In our experimental conditions, the possibility that the acute analgesic effect induced by AKB48 and 5F-AKB48 and/or their metabolites (Gandhi et al., 2013; Holm et al. 2015) is due to the activation of peripheral CB_2 receptors (Guindon and Hohmann, 2008) should be ruled out since their analgesic effects are fully prevented by the administration of the selective CB_1 receptor antagonist/inverse agonist AM 251.

Administration of AKB48 and 5F-AKB48 affects, less effectively than JWH-018 and Δ^9-THC, the startle response to visual, acoustic and tactile stimuli in mice (Ossato et al. 2015). A recent study has shown that visual information in mice is elaborated in a subpopulation of neurons selectively localized in the dorsomedial striatum

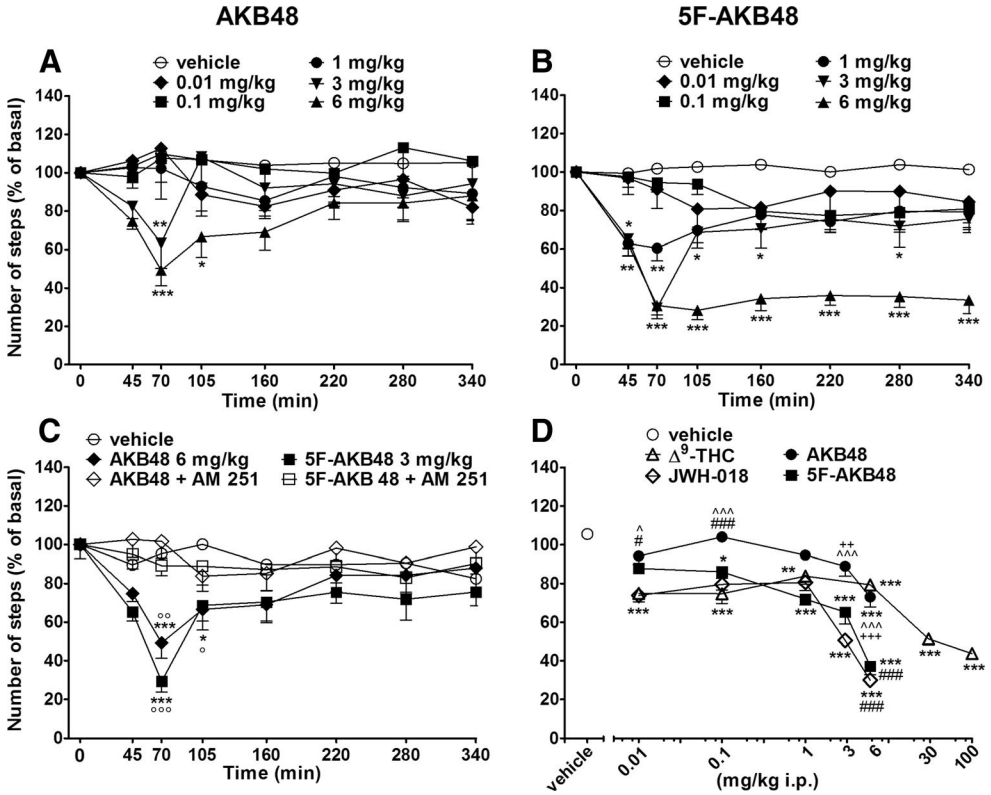

Fig. 15 Effect of the systemic administration (0.01–6 mg/kg i.p.) of AKB48 (**a**) and 5F-AKB48 (**b**) on the drag test of mice. Interaction of effective dose of AKB48 and 5F-AKB48 (6 mg/kg) with the selective CB_1 receptor antagonist AM 251 (6 mg/kg, i.p., **c**). Comparison of the total average effect observed in 5 h (**d**) with Δ^9-THC (0.01–100 mg/kg)[a] and JWH-018 (0.01–6 mg/kg i.p.)[a]. Data are expressed (see "Materials and methods") as arbitrary units and represent mean ± SEM of 8 animals for each treatment. Statistical analysis was performed by two-way ANOVA followed by the Bonferroni's test for multiple comparisons for both the dose-response curve of each compound at different times (**a**, **b**) and for the interaction with the AM 251 (**c**), while the statistical analysis of the comparison of the total average effect of the compounds (**d**) was performed with one-way ANOVA followed by Tukey's test for multiple comparisons. $^*p < 0.05$, $^{**}p < 0.01$, $^{***}p < 0.001$ versus vehicle; $\#p < 0.05$, $\#\#\#p < 0.001$ versus Δ^9-THC; $\hat{}p < 0.05$, $\hat{}\hat{}\hat{}p < 0.001$ versus JWH-018, $++p < 0.01$, $+++p < 0.001$ versus 5F-AKB48 and $°p < 0.05$, $°°p < 0.01$, $°°°p < 0.001$ versus AM 251+ agonist. [a]From Vigolo et al., 2015

(Reig and Silberberg 2014), in which CB_1 receptors are expressed (Tsou et al. 1998; Marsicano and Lutz 1999). Even though in our study we are not able to understand which brain areas and neural mechanisms are responsible for the reduced visual response of the mouse, it is possible to hypothesize that AKB48 and 5F-AKB48 could inhibit visual function through the stimulation of CB_1 receptors expressed in thalamocortical-striatal visual circuitry (Tsou et al. 1998; Marsicano and Lutz 1999; Dasilva et al. 2012; Yoneda et al. 2013). Our study also demonstrates that AKB48 and 5F-AKB48 impair the acoustic startle response in mice by the selective stimulation of CB_1 receptors. This finding is in agreement with previous researches that have demonstrated the effectiveness of acute administration of Δ^9-THC (Malone and Taylor 2006; Nagai et al. 2006; Ossato et al. 2015), CP 55940 (Mansbach et al. 1996; Martin et al. 2003), WIN-55,212–2 (Bortolato et al. 2005), JWH-018 (Ossato et al. 2015), JWH-250 and JWH-073 (Ossato et al. 2016) in reducing the acoustic startle reflex in rodents. Acoustic startle reflex is induced by the activation of three serially connected structures that involve the activation of the dorsal cochlear nucleus (Gomez-Nieto et al. 2014). Therefore, AKB48 and 5F-AKB48 could impair the acoustic startle reflex in mice by stimulating CB_1 receptors expressed on the presynaptic terminals of parallel fibers in the dorsal cochlear nucleus (Tzounopoulos et al. 2007).

Relying on the present study, it is not possible to define whether visual and acoustic alterations induced by AKB48 and 5F-AKB48 in mice are an expression of hallucinatory states, as suggested for the Δ^9-THC in human studies (Winton-Brown et al. 2011). However, our data support the hypothesis that SCBs by stimulating CB_1 receptors could impair the sensorimotor gating in mice similarly to what demonstrated for other cannabinoid agonists such as Δ^9-THC (Malone and Taylor 2006; Nagai et al. 2006), CP 55940 (Mansbach et al. 1996; Martin et al. 2003) and WIN 55,212–2 (Schneider and Koch 2002; Wegener et al. 2008).

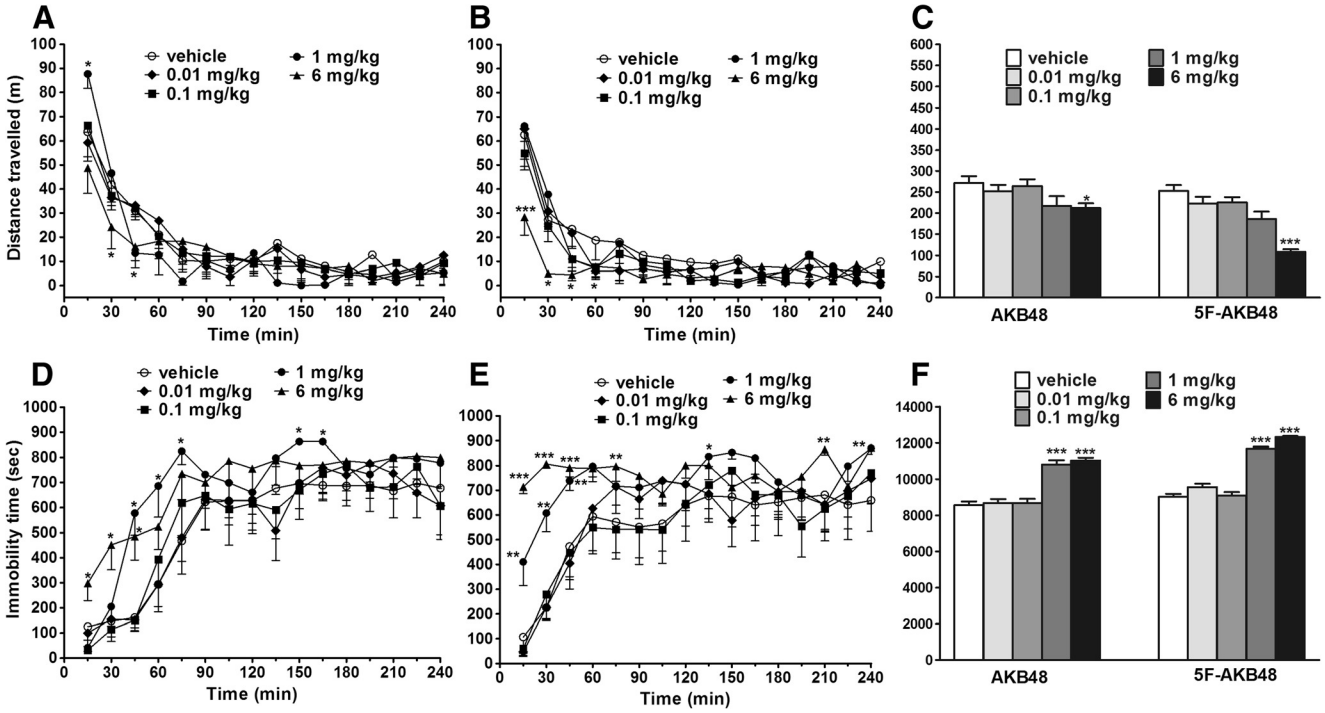

Fig. 16 Effect of the systemic administration (0.01–6 mg/kg i.p.) of AKB48 (**a**, **d**) and 5F-AKB48 (**b**, **e**) on the total distance travelled and the total time immobile of the mouse. The overall effect observed in 4 h (**c**, **f**) was also reported. Data are expressed as meters travelled (total distance travelled; **a**–**c**) and seconds of immobility (total time immobile; **d**–**f**) and represent the mean ± SEM of 10 animals for each treatment. Statistical analysis was performed by two-way ANOVA followed by the Bonferroni's test for multiple comparisons for the dose-response curve of AKB48 (**a**, **d**) and 5F-AKB48 (**b**, **e**) while the analysis of the overall effect (**c**, **f**) was performed with one-way ANOVA followed by Tukey's test for multiple comparisons. $*p < 0.05$, $***p < 0.001$ versus vehicle

We also underline that 5F-AKB48 is more effective than AKB48 in inhibiting the sensorimotor responses in mice in reply to tactile stimuli. The inhibitory effect induced by 5F-AKB48 administration on vibrissae responses is consistent with previous studies showing that endocannabinoid system and exogenous Δ^9-THC or WIN-55,212–2 administration directly modulated whisking activity in rodent (Patel et al. 2002; Pietr et al. 2010; Ho et al. 2010) by activating CB_1 receptors (Tsou et al. 1998; Cristino et al. 2006) expressed in the inferior olive, somatosensory cortex and superior colliculus (Hemelt and Keller 2008). Similarly, 5F-AKB48 might inhibit sensorimotor responses of pinna and cornea through the stimulation of CB_1 receptors directly expressed in trigeminal structures (Herkenham et al. 1991; Tsou et al. 1998; Price et al. 2003) as hypothesized for JWH-018 (Ossato et al. 2015). These results are consistent with previous studies showing that the administration of HU 210 and WIN-55,212–2 suppressed central trigeminal transmission (Jenkins et al. 2004; Papanastassiou et al. 2004) and that topical application of WIN-55,212–2 reduced cornea-evoked trigeminal brainstem activity (Bereiter et al. 2002).

It is interesting to note that both AKB48 and 5F-AKB48 impair visual sensorimotor responses in mice at lower doses (0.1 and 1 mg/kg) that do not cause catalepsy or reduce spontaneous (open field studies) and stimulated motor activity (drag test and accelerod). These findings point out that effects induced by AKB48 and 5F-AKB48 on sensorimotor responses and motor activity are mediated by separate processes and suggest that the decreased sensory responsiveness does not result merely from a disruption of motor function (Ossato et al. 2015).

The present study showing that 5F-AKB48 is more potent in inducing convulsions respect to JWH-018 (Vigolo et al. 2015) probably due to its fluorination which determines a high lipophilicity and a quick pass across the blood-brain barrier (Schifano et al. 2015). These data confirm the proconvulsant effect of SCBs and they are in agreement with the increasing clinical reports showing the occurrence of seizures and hyperreflexia in young people who have smoked "Spice" products containing different SCBs (Gugelmann et al. 2014; Lapoint et al. 2011; McQuade et al. 2013; Schneir and Baumbacher 2012; Simmons et al. 2011).

As previously reported, SCBs promote aggressive response in mice (Ossato et al., 2016). Pharmacological modulation of cannabinoid signal alter spontaneous aggressive behaviour in mice, rats and squirrel monkeys (Ham and De Jong 1975; Miczek 1978; van Ree et al. 1984), and this behaviour was exacerbate in stressful situations in rodents (Carder and Olson

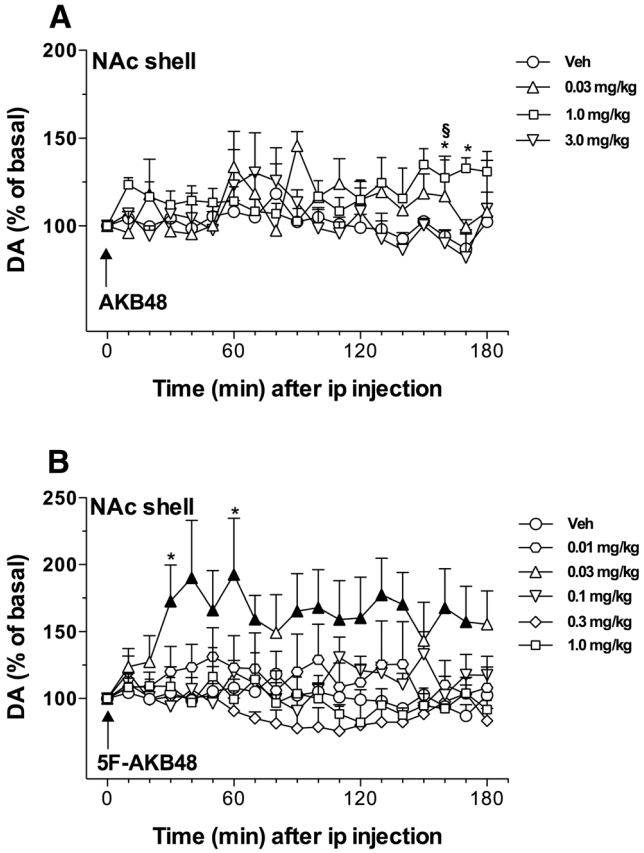

Fig. 17 Effect of the systemic administration of AKB-48 (0.03–3.0 mg/kg i.p., **a**) and 5F-AKB48 (0.01–1.0 mg/kg i.p., **b**) on DA transmission in the NAc shell of mice. Results are expressed as mean ± SEM of change in DA extracellular levels expressed as the percentage of basal values. **a**: the *arrow* indicates the start of AKB48 i.p. injection at the dose of 0.03 mg/kg/ip (*upward-pointing triangles*), 1 mg/kg *(square)*, 3.0 mg/kg/ip (*triangles down)* or vehicle *(circles)* in the NAc shell. *$p < 0.05$ 1.0 vs 3.0 mg/kg/ip; §$p < 0.05$ 1.0 vs veh; (NAc shell $N = 12$). (two-way ANOVA, Tukey's HSD post hoc). **b**: the *arrow* indicates the start of 5F-AKB48 i.p. injection at the dose of 0.01 mg/kg (*hexagon*), 0.03 mg/kg (*upward-pointing triangles*), 0.1 mg/kg (*downward-pointing triangles*), 0.3 mg/kg (*diamonds*), 1 mg/kg/ip (*squares*) or vehicle (*circles*) in the NAc shell. *Solid symbol*: $p < 0.05$ with respect to basal values; *$p < 0.05$ 0.03 vs veh; (NAc shell $N = 13$) (two-way ANOVA, Tukey's HSD post hoc)

1972; Carlini and Gonzales 1972; Carlini et al. 1976). Therefore, despite in our experiment that this behaviour was observed in a simple test that is not fully representative for an overall and accurate assessment of aggressive behavior in mice (Takahashi and Miczek 2014; Miczek et al. 2007), it is possible that the aggressive response caused by the administration of AKB48 and 5F-AKB48 in mice is mainly due to the stressful situation of the animal (sensorimotor alterations and neurological symptoms) rather than a direct effect on neural circuits that control aggressive behaviour.

In order to evaluate whether AKB48 and 5F-AKB48 share with natural and drug rewards the ability to increase DA transmission in the NAc shell, the effect of both drugs was evaluated by means of in vivo brain microdialysis in CD-1 mice. While the AKB48 increased dialysate DA levels in the NAc shell with a biphasic effect after the administration of the highest dose tested (1 mg/kg/i.p.), 5F-AKB48 displayed a bell-shaped dose-response curve with the dose of 0.03 mg/kg increasing DA. The present data confirm the rewarding properties of these third-generation SCBs and are similar to previous observation on the effect of JWH-018 (De Luca et al. 2015a) and BB-22 (De Luca et al. 2015b). Indeed, the specific increase of DA in the shell subdivision of the NAc is a common property of natural (Tanda et al. 1997) and synthetic cannabinoids (Fattore et al. 2005; Lecca et al. 2006), but also of drugs of abuse belonging to the most different pharmacological classes (Pontieri et al. 1995; Tanda et al. 1997; Di Chiara et al. 2004; Miliano et al. 2016). Importantly, this effect was observed at a very low doses compared to Δ^9-THC (Tanda et al. 1997) or to first-generation SCBs such as WIN 55,212–2 (Fattore et al. 2005; Lecca et al. 2006) and JWH-018 (De Luca et al., 2015a). The lack of increase of extracellular DA at high doses might be due to the synthesis of hydroxylated metabolites of the SCBs, thus preventing the effect of the parent drug (Dhawan et al. 2006; Wiebelhaus et al. 2012). Another possible explanation might be a retrograde signaling through presynaptic CB_2 receptors located on DAergic terminals of the NAc (Xi et al. 2011; Morales and Bonci 2012). Interestingly, the inverted U-shaped dose-response curve with an extremely narrow range of doses appears to be peculiar to the SCBs.

Conclusion

For the first time, the present study demonstrates the overall pharmacological effects induced by the administration of novel adamantylindazoles AKB48 and 5F-AKB48 in mice highlighting that the fluorination in the pentilic side chain of the indazolic structure increases the in vivo efficacy of SCBs, enhancing both the pharmacological activity and the adverse effects.

Acknowledgments This research has been funded by the Drug Policies Department, Presidency of the Council of Ministers, Italy (project NS-Drugs to M. Marti) and by local funds from the University of Ferrara to M. Marti. All applicable international, national and/or institutional guidelines for the care and use of animals were followed. All procedures performed in the studies involving animals were in accordance with the ethical standards of the institution or practice at which the studies were conducted.

Conflict of interest The authors have no conflict of interest to declare.

References

Barbieri M, Ossato A, Canazza I, Trapella C, Borelli AC, Beggiato S, Rimondo C, Serpelloni G, Ferraro L, Marti M (2016) Synthetic

cannabinoid JWH-018 and its halogenated derivatives JWH-018-Cl and JWH-018-Br impair novel object recognition in mice: behavioral, electrophysiological and neurochemical evidence. Neuropharmacology 109:254–269

Bereiter DA, Bereiter DF, Hirata H (2002) Topical cannabinoid agonist, WIN55,212-2, reduces cornea-evoked trigeminal brainstem activity in the rat. Pain 99:547–556

Bortolato M, Aru GN, Frau R, Orru M, Luckey GC, Boi G, Gessa GL (2005) The CB receptor agonist WIN 55,212-2 fails to elicit disruption of prepulse inhibition of the startle in Sprague-Dawley rats. Psychopharmacology 177:264–271

Brents LK, Gallus-Zawada A, Radominska-Pandya A, Vasiljevik T, Prisinzano TE, Fantegrossi WE, Moran JH, Prather PL (2012) Monohydroxylated metabolites of the K2 synthetic cannabinoid JWH-073 retain intermediate to high cannabinoid 1 receptor (CB1R) affinity and exhibit neutral antagonist to partial agonist activity. Biochem Pharmacol 83:952–961

Brents LK, Reichard EE, Zimmerman SM, Moran JH, Fantegrossi WE, Prather PL (2011) Phase I hydroxylated metabolites of the K2 synthetic cannabinoid JWH-018 retain in vitro and in vivo cannabinoid 1 receptor affinity and activity. PLoS One 6:e21917

Carder B, Olson J (1972) Marihuana and shock induced aggression in rats. Physiol Behav 8:599–602

Carlini EA, Gonzales C (1972) Aggressive behaviour induced by marihuana compounds and amphetamine in rats previously made dependent on morphine. Experientia 28:542–544

Carlini EA, Lindsey CJ, Tufik S (1976) Environmental and drug interference with effects of marihuana. Ann N Y Acad Sci 281:229–243

Compton DR, Johnson MR, Melvin LS, Martin BR (1992) Pharmacological profile of a series of bicyclic cannabinoid analogs: classification as cannabimimetic agents. J Pharmacol Exp Ther 260: 201–209

Cristino L, de Petrocellis L, Pryce G, Baker D, Guglielmotti V, Di Marzo V (2006) Immunohistochemical localization of cannabinoid type 1 and vanilloid transient receptor potential vanilloid type 1 receptors in the mouse brain. Neuroscience 139:1405–1415

Dasilva MA, Grieve KL, Cudeiro J, Rivadulla C (2012) Endocannabinoid CB1 receptors modulate visual output from the thalamus. Psychopharmacology 219:835–845

De Luca MA, Bimpisidis Z, Melis M, Marti M, Caboni P, Valentini V, Margiani G, Pintori N, Polis I, Marsicano G, Parsons LH, Di Chiara G (2015a) Stimulation OF IN VIVO dopamine transmission and intravenous self-administration in rats and mice by JWH-018, a Spice cannabinoid. Neuropharmacology.

De Luca MA, Castelli MP, Loi B, Porcu A, Martorelli M, Miliano C, Kellett K, Davidson C, Stair LJ, Schifano F, Di Chiara G (2015b) Native CB1 receptor affinity, intrisic activity and accumbens shell dopamine stimulant properties of third generation SPICE/K2 cannabinoids: BB-22, 5F-PB-22, 5F-AKB-48 and STS-135. Neuropharmacology.

Dhawan J, Deng H, Gatley SJ, Makriyannis A, Akinfeleye T, Bruneus M, Dimaio AA, Gifford AN (2006) Evaluation of the in vivo receptor occupancy for the behavioral effects of cannabinoids using a radiolabeled cannabinoid receptor agonist, R-[125/131I]AM2233. Synapse (New York, NY) 60:93–101

Di Chiara G, Bassareo V, Fenu S, De Luca MA, Spina L, Cadoni C, Acquas E, Carboni E, Valentini V, Lecca D (2004) Dopamine and drug addiction: the nucleus accumbens shell connection. Neuropharmacology 47(Suppl 1):227–241

DrugsForum (2012a) AKB-48 (APINACA) drug info. [online] Available at: http://www.drugs-forum.com/forum/showthread.php?t=187522 [Accessed 11 October 2013].

DrugsForum (2012b) Experience with UR-144, 5F-UR-144, AKB-48, & STS-135. [online] Available at: http://www.drugs-forum.com/forum/showthread.php?t=192321 [Accessed 10 October 2013].

EMCDDA (2009) Understanding the 'spice' phenomenon. Thematic papers. European Monitoring Centre for Drugs and Drug Addiction. http://www.emcdda.europa.eu/publications/thematic-papers/spice

EMCDDA (2015) European drug report, trends and developments. Thematic papers. European Monitoring Centre for Drugs and Drug Addiction. http://www.emcdda.europa.eu/attachements.cfm/att_239505_EN_TDAT15001ENN.pdf.

Fattore L, Spano S, Cossu G, Deiana S, Fadda P, Fratta W (2005) Cannabinoid CB(1) antagonist SR 141716 A attenuates reinstatement of heroin self-administration in heroin-abstinent rats. Neuropharmacology 48:1097–1104

Gandhi AS, Zhu M, Pang S, Wohlfarth A, Scheidweiler KB, Liu HF, Huestis MA (2013) First characterization of AKB-48 metabolism, a novel synthetic cannabinoid, using human hepatocytes and high-resolution mass spectrometry. AAPS J 15:1091–1098

Gatch MB, Forster MJ (2015) Delta9-Tetrahydrocannabinol-like effects of novel synthetic cannabinoids found on the gray market. Behav Pharmacol 26:460–468

Gomez-Nieto R, Horta-Junior Jde A, Castellano O, Millian-Morell L, Rubio ME, Lopez DE (2014) Origin and function of short-latency inputs to the neural substrates underlying the acoustic startle reflex. Front Neurosci 8:216

Gugelmann H, Gerona R, Li C, Tsutaoka B, Olson KR, Lung D (2014) 'Crazy monkey' poisons man and dog: human and canine seizures due to PB-22, a novel synthetic cannabinoid. Clin Toxicol (Phila) 52:635–638

Guindon J, Hohmann AG (2008) Cannabinoid CB2 receptors: a therapeutic target for the treatment of inflammatory and neuropathic pain. Br J Pharmacol 153:319–334

Ham MT, De Jong Y (1975) Absence of interaction between delta9-tetrahydrocannabinol (delta-THC) and cannabidiol (CBD) in aggression, muscle control and body temperature experiments in mice. Psychopharmacologia 41:169–174

Hamdam J, Sethu S, Smith T, Alfirevic A, Alhaidari M, Atkinson J, Ayala M, Box H, Cross M, Delaunois A, Dermody A, Govindappa K, Guillon J-M, Jenkins R, Kenna G, Lemmer B, Meecham K, Olayanju A, Pestel S, Rothfuss A, Sidaway J, Sison-Young R, Smith E, Stebbings R, Tingle Y, Valentin J-P, Williams A, Williams D, Park K, Goldring C (2013) Safety pharmacology—current and emerging concepts. Toxicol Appl Pharmacol 273:229–241

Hemelt ME, Keller A (2008) Superior colliculus control of vibrissa movements. J Neurophysiol 100:1245–1254

Herkenham M, Lynn AB, Johnson MR, Melvin LS, de Costa BR, Rice KC (1991) Characterization and localization of cannabinoid receptors in rat brain: a quantitative in vitro autoradiographic study. J Neurosci Off J Soc Neurosci 11:563–583

Ho WS, Patel S, Thompson JR, Roberts CJ, Stuhr KL, Hillard CJ (2010) Endocannabinoid modulation of hyperaemia evoked by physiologically relevant stimuli in the rat primary somatosensory cortex. Br J Pharmacol 160:736–746

Hohmann AG, Tsou K, Walker JM (1999) Cannabinoid suppression of noxious heat-evoked activity in wide dynamic range neurons in the lumbar dorsal horn of the rat. J Neurophysiol 81:575–583

Holm NB, Nielsen LM, Linnet K (2015) CYP3A4 mediates oxidative metabolism of the synthetic cannabinoid AKB-48. AAPS J 17: 1237–1245

Irwin S (1968) Comprehensive observational assessment: Ia. A systematic, quantitative procedure for assessing the behavioral and physiologic state of the mouse. Psychopharmacologia 13:222–257

Jenkins S, Worthington M, Harris J, Clarke RW (2004) Differential modulation of withdrawal reflexes by a cannabinoid in the rabbit. Brain Res 1012:146–153

Karinen R, Tuv SS, Oiestad EL, Vindenes V (2015) Concentrations of APINACA, 5F-APINACA, UR-144 and its degradant product in blood samples from six impaired drivers compared to previous

reported concentrations of other synthetic cannabinoids. Forensic Sci Int 246:98–103

Koch M (1999) The neurobiology of startle. Prog Neurobiol 59:107–128

Koller VJ, Ferk F, Al-Serori H, Misik M, Nersesyan A, Auwarter V, Grummt T, Knasmuller S (2015) Genotoxic properties of representatives of alkylindazoles and aminoalkyl-indoles which are consumed as synthetic cannabinoids. Food and chemical toxicology: an international journal published for the British Industrial Biological Research Association 80:130–136

Lapoint J, James LP, Moran CL, Nelson LS, Hoffman RS, Moran JH (2011) Severe toxicity following synthetic cannabinoid ingestion. Clin Toxicol (Phila) 49:760–764

Lecca D, Cacciapaglia F, Valentini V, Di Chiara G (2006) Monitoring extracellular dopamine in the rat nucleus accumbens shell and core during acquisition and maintenance of intravenous WIN 55,212-2 self-administration. Psychopharmacology 188:63–74

Macri S, Lanuzza L, Merola G, Ceci C, Gentili S, Valli A, Macchia T, Laviola G (2013) Behavioral responses to acute and sub-chronic administration of the synthetic cannabinoid JWH-018 in adult mice prenatally exposed to corticosterone. Neurotox Res 24:15–28

Malone DT, Taylor DA (2006) The effect of Delta9-tetrahydrocannabinol on sensorimotor gating in socially isolated rats. Behav Brain Res 166:101–109

Mansbach RS, Rovetti CC, Winston EN, Lowe JA 3rd (1996) Effects of the cannabinoid CB1 receptor antagonist SR141716A on the behavior of pigeons and rats. Psychopharmacology 124:315–322

Marshell R, Kearney-Ramos T, Brents LK, Hyatt WS, Tai S, Prather PL, Fantegrossi WE (2014) In vivo effects of synthetic cannabinoids JWH-018 and JWH-073 and phytocannabinoid Delta-THC in mice: inhalation versus intraperitoneal injection. Pharmacol Biochem Behav 124C:40–47

Marsicano G, Lutz B (1999) Expression of the cannabinoid receptor CB1 in distinct neuronal subpopulations in the adult mouse forebrain. Eur J Neurosci 11:4213–4225

Marti M, Mela F, Fantin M, Zucchini S, Brown JM, Witta J, Di Benedetto M, Buzas B, Reinscheid RK, Salvadori S, Guerrini R, Romualdi P, Candeletti S, Simonato M, Cox BM, Morari M (2005) Blockade of nociceptin/Orphanin FQ transmission attenuates symptoms and neurodegeneration associated with Parkinson's disease. J Neurosci 25: 9591–9601

Marti M, Mela F, Guerrini R, Calò G, Bianchi C, Morari M (2004) RAPID COMMUNICATION: blockade of nociceptin/orphanin FQ transmission in rat substantia nigra reverses haloperidol-induced akinesia and normalizes nigral glutamate release. J Neurochem 91:1501–1504

Marti M, Ossato A, Trapella C, Seri C, Rimondo C, Serpelloni G (2013) JWH-018 and its N-pentyl-halogenated derivates impair sensory motor functions in mice. First Monothematic Congress of the Italian Society of Pharmacology: "Old and new drugs of abuse, issues and research approaches" Verona, Italy.

Martin RS, Secchi RL, Sung E, Lemaire M, Bonhaus DW, Hedley LR, Lowe DA (2003) Effects of cannabinoid receptor ligands on psychosis-relevant behavior models in the rat. Psychopharmacology 165:128–135

Martin WJ, Hohmann AG, Walker JM (1996) Suppression of noxious stimulus-evoked activity in the ventral posterolateral nucleus of the thalamus by a cannabinoid agonist: correlation between electrophysiological and antinociceptive effects. J Neurosci Off J Soc Neurosci 16:6601–6611

Mattsson JL, Spencer PJ, Albee RR (1996) A performance standard for clinical and functional observational battery examinations of rats. Int J Toxicol 15:239–254

McQuade D, Hudson S, Dargan PI, Wood DM (2013) First European case of convulsions related to analytically confirmed use of the synthetic cannabinoid receptor agonist AM-2201. Eur J Clin Pharmacol 69:373–376

Miczek KA (1978) delta9-tetrahydrocannabinol: antiaggressive effects in mice, rats, and squirrel monkeys. Science (New York, NY) 199: 1459–1461

Miczek KA, de Almeida RMM, Kravitz EA, Rissman EF, de Boer SF, Raine A (2007). Neurobiology of Escalated Aggression and Violence. The Journal of Neuroscience. 27:11803–6

Miliano C, Serpelloni G, Rimondo C, Mereu M, Marti M, De Luca MA (2016) Neuropharmacology of new psychoactive substances (NPS): focus on the rewarding and reinforcing properties of Cannabimimetics and amphetamine-like stimulants. Front Neurosci 10:153. doi:10.3389/fnins.2016.00153

Morales M, Bonci A (2012) Getting to the core of addiction: hooking CB2 receptor into drug abuse? Nat Med 18:504–505

Nagai H, Egashira N, Sano K, Ogata A, Mizuki A, Mishima K, Iwasaki K, Shoyama Y, Nishimura R, Fujiwara M (2006) Antipsychotics improve Delta9-tetrahydrocannabinol-induced impairment of the prepulse inhibition of the startle reflex in mice. Pharmacol Biochem Behav 84:330–336

NFLIS (2013) Annual Report. Thematic paper. U.S. Department Of Justice, D. E. A., Office Of Diversion Control, National Forensic Laboratory Information System. http://www.deadiversion.usdoj.gov/nflis/NFLIS2013AR.pdf

Nordstedt C, Fredholm BB (1990) A modification of a protein-binding method for rapid quantification of cAMP in cell-culture supernatants and body fluid. Anal Biochem 189:231–234

Odoardi S, Romolo FS, Strano-Rossi S (2016) A snapshot on NPS in Italy: distribution of drugs in seized materials analysed in an Italian forensic laboratory in the period 2013-2015. Forensic Sci Int 265: 116–120

Ossato A, Canazza I, Trapella C, Vincenzi F, De Luca MA, Rimondo C, Varani K, Borea PA, Serpelloni G, Marti M (2016) Effect of JWH-250, JWH-073 and their interaction on "tetrad", sensorimotor, neurological and neurochemical responses in mice. Prog Neuro-Psychopharmacol Biol Psychiatry 67:31–50

Ossato A, Vigolo A, Trapella C, Seri C, Rimondo C, Serpelloni G, Marti M (2015) JWH-018 impairs sensorimotor functions in mice. Neuroscience 300:174–188

Papanastassiou AM, Fields HL, Meng ID (2004) Local application of the cannabinoid receptor agonist, WIN 55,212-2, to spinal trigeminal nucleus caudalis differentially affects nociceptive and non-nociceptive neurons. Pain 107:267–275

Patel S, Gerrits R, Muthian S, Greene AS, Hillard CJ (2002) The CB1 receptor antagonist SR141716 enhances stimulus-induced activation of the primary somatosensory cortex of the rat. Neurosci Lett 335:95–98

Paxinos G, Franklin KBJ (2001) The mouse brain in stereotaxic coordinates. Academic Press, San Diego

Pietr MD, Knutsen PM, Shore DI, Ahissar E, Vogel Z (2010) Cannabinoids reveal separate controls for whisking amplitude and timing in rats. J Neurophysiol 104:2532–2542

Pontieri FE, Tanda G, Di Chiara G (1995) Intravenous cocaine, morphine, and amphetamine preferentially increase extracellular dopamine in the "shell" as compared with the "core" of the rat nucleus accumbens. Proc Natl Acad Sci U S A 92:12304–12308

Porsolt RD, Lemaire M, Dürmüller N, Roux S (2002) New perspectives in CNS safety pharmacology. Fundamental & Clinical Pharmacology 16:197–207

Price TJ, Helesic G, Parghi D, Hargreaves KM, Flores CM (2003) The neuronal distribution of cannabinoid receptor type 1 in the trigeminal ganglion of the rat. Neuroscience 120:155–162

Redfern WS, Strang I, Storey S, Heys C, Barnard C, Lawton K, Hammond TG, Valentin J-P (2005) Spectrum of effects detected in the rat functional observational battery following oral administration of non-CNS targeted compounds. J Pharmacol Toxicol Methods 52: 77–82

Reig R, Silberberg G (2014) Multisensory integration in the mouse striatum. Neuron 83:1200–1212

S7A (2001) US Food and Drug Administration Guidance for industry: safety pharmacology studies for human pharmaceuticals (S7 A).

Santacroce R, Corazza O, Martinotti G, Bersani FS, Valeriani G, Di Giannantonio M (2015) Psyclones: a roller coaster of life? Hidden synthetic cannabinoids and stimulants in apparently harmless products. Human psychopharmacology 30:265–271

Schifano F, Orsolini L, Duccio Papanti G, Corkery JM (2015) Novel psychoactive substances of interest for psychiatry. World psychiatry: official journal of the World Psychiatric Association (WPA) 14:15–26

Schneider M, Koch M (2002) The cannabinoid agonist WIN 55,212-2 reduces sensorimotor gating and recognition memory in rats. Behav Pharmacol 13:29–37

Schneir AB, Baumbacher T (2012) Convulsions associated with the use of a synthetic cannabinoid product. J Med Toxicol 8:62–64

Seely KA, Lapoint J, Moran JH, Fattore L (2012) Spice drugs are more than harmless herbal blends: a review of the pharmacology and toxicology of synthetic cannabinoids. Prog Neuro-Psychopharmacol Biol Psychiatry 39:234–243

Simmons JR, Skinner CG, Williams J, Kang CS, Schwartz MD, Wills BK (2011) Intoxication from smoking "spice". Ann Emerg Med 57: 187–188

Tanda G, Pontieri FE, Frau R, Di Chiara G (1997) Contribution of blockade of the noradrenaline carrier to the increase of extracellular dopamine in the rat prefrontal cortex by amphetamine and cocaine. Eur J Neurosci 9:2077–2085

Takahashi A, Miczek KA (2014) Neurogenetics of aggressive behavior: studies in rodents. Curr Top Behav Neurosci 17:3–44

Tsou K, Brown S, Sanudo-Pena MC, Mackie K, Walker JM (1998) Immunohistochemical distribution of cannabinoid CB1 receptors in the rat central nervous system. Neuroscience 83:393–411

Tzounopoulos T, Rubio ME, Keen JE, Trussell LO (2007) Coactivation of pre- and postsynaptic signaling mechanisms determines cell-specific spike-timing-dependent plasticity. Neuron 54:291–301

Uchiyama N, Kawamura M, Kikura-Hanajiri R, Goda Y (2012) Identification of two new-type synthetic cannabinoids, N-(1-adamantyl)-1-pentyl-1H-indole-3-carboxamide (APICA) and N-(1-adamantyl)-1-pentyl-1H-indazole-3-carboxamide (APINACA), and detection of five synthetic cannabinoids, AM-1220, AM-2233, AM-1241, CB-13 (CRA-13), and AM-1248, as designer drugs in illegal products. Forensic Toxicol 30:114–125

Uchiyama N, Kawamura M, Kikura-Hanajiri R, Goda Y (2013) URB-754: a new class of designer drug and 12 synthetic cannabinoids detected in illegal products. Forensic Sci Int 227:21–32

van Ree JM, Niesink RJ, Nir I (1984) Delta 1-Tetrahydrocannabinol but not cannabidiol reduces contact and aggressive behavior of rats tested in dyadic encounters. Psychopharmacology 84:561–565

Vigolo A, Ossato A, Trapella C, Vincenzi F, Rimondo C, Seri C, Varani K, Serpelloni G, Marti M (2015) Novel halogenated derivates of JWH-018: behavioral and binding studies in mice. Neuropharmacology 95:68–82

Vikingsson S, Josefsson M, Green H (2015) Identification of AKB-48 and 5F-AKB-48 metabolites in authentic human urine samples using human liver microsomes and time of flight mass spectrometry. J Anal Toxicol 39:426–435

Vincenzi F, Targa M, Corciulo C, Tabrizi MA, Merighi S, Gessi S, Saponaro G, Baraldi PG, Borea PA, Varani K (2013) Antinociceptive effects of the selective CB2 agonist MT178 in inflammatory and chronic rodent pain models. Pain 154:864–873

Wegener N, Kuhnert S, Thuns A, Roese R, Koch M (2008) Effects of acute systemic and intra-cerebral stimulation of cannabinoid receptors on sensorimotor gating, locomotion and spatial memory in rats. Psychopharmacology 198:375–385

Wiebelhaus JM, Poklis JL, Poklis A, Vann RE, Lichtman AH, Wise LE (2012) Inhalation exposure to smoke from synthetic "marijuana" produces potent cannabimimetic effects in mice. Drug Alcohol Depend 126:316–323

Wiley JL, Compton DR, Dai D, Lainton JA, Phillips M, Huffman JW, Martin BR (1998) Structure-activity relationships of indole- and pyrrole-derived cannabinoids. J Pharmacol Exp Ther 285:995–1004

Wiley JL, Marusich JA, Huffman JW (2014) Moving around the molecule: relationship between chemical structure and in vivo activity of synthetic cannabinoids. Life Sci 97:55–63

Winton-Brown TT, Allen P, Bhattacharyya S, Borgwardt SJ, Fusar-Poli P, Crippa JA, Seal ML, Martin-Santos R, Ffytche D, Zuardi AW, Atakan Z, McGuire PK (2011) Modulation of auditory and visual processing by delta-9-tetrahydrocannabinol and cannabidiol: an FMRI study. Neuropsychopharmacology: official publication of the American College of Neuropsychopharmacology 36:1340–1348

Xi ZX, Peng XQ, Li X, Song R, Zhang HY, Liu QR, Yang HJ, Bi GH, Li J, Gardner EL (2011) Brain cannabinoid CB(2) receptors modulate cocaine's actions in mice. Nat Neurosci 14:1160–1166

Yoneda T, Kameyama K, Esumi K, Daimyo Y, Watanabe M, Hata Y (2013) Developmental and visual input-dependent regulation of the CB1 cannabinoid receptor in the mouse visual cortex. PLoS One 8:e53082